THE JOURNAL
OF
CHEMICAL PHYSICS

VOLUME 18, NUMBER 1 JANUARY, 1950

Diffusional Boundary Value Problems Involving Moving Boundaries, Connected with the Growth of Colloidal Particles

HOWARD REISS* AND VICTOR K. LA MER
Columbia University, New York 27, New York
(Received May 12, 1949)

A method is suggested for treating problems of diffusion which involve moving boundaries. This method is applicable when the flux of material through any surface in the diffusion field is considerably greater than the rate of change of concentration on that surface. The method is applied to two problems dealing with the growth of monodispersed aerosols and hydrosols.

The solution of the first of these problems indicates that, in a naphthalene-like aerosol system growing by means of the diffusion of vapor toward sinks (nuclei) which cannot support supersaturation, spontaneous nucleation will not occur if the number density of nuclei exceeds 100/cc.

The solution of the second problem permits the reproduction from theory of several curves due to Zaiser and La Mer which depict the rate of growth of sulfur hydrosols, therefore lending support to the idea that the particles grow by means of a simple diffusion mechanism rather than by a surface catalyzed deposition. The critical supersaturation concentration for sulfur in aqueous solution is

$$c_0 = 4.7 \times 10^{-6} \text{ g/atom/liter},$$

and the diffusion coefficient of S_8 is

$$D = 2 \times 10^{-6} \text{ cm}^2/\text{sec}.$$

These values are in reasonable agreement with those estimated by independent means, although the diffusion coefficient seems to have about one-half the expected value. This indicates that a unit larger than S_8 may be diffusing, e.g., a polythionate.

I. INTRODUCTION

THE growth of small particles following condensation from a vapor phase or precipitation from a liquid phase involves a diffusion process which is difficult to treat mathematically. The surfaces of the growing particles represent boundaries which are not stationary in time. Consequently, the boundary value problems concerned are not soluble by means of the familiar methods.

It is the purpose of this paper to present a method for obtaining solutions of such problems in certain limiting cases, and to apply this method to two problems which occur in practice.†

II. THE APPROXIMATE EQUATION

The method will be approximate. We shall check its accuracy in several instances where an exact solution is available. The core of the method is the following.

If it is assumed that Fick's law[1] governs the diffusion phenomena, and if we specialize our considerations to sources which are distributed uniformly in space, then the partial differential equation which the concentration of diffusing material, c, must satisfy is

$$\nabla^2 c = (1/D)(\partial c/\partial t) - k(t)/D, \tag{1}$$

where D is the diffusion coefficient, and $k(t)$ is the source function. Now, in certain limiting cases, the flux of diffusing material through any surface in the diffusion field is much greater than the rate of change of concentration on that surface. For example, this is the case when material diffuses from an infinite region toward a single sink.

In such cases, it is evident that Eq. (1) can be approximated by

$$\nabla^2 c \simeq -k(t)/D, \tag{2}$$

since

$$\partial c/\partial t \simeq 0. \tag{3}$$

The most general solution of Eq. (2) can be written in the following form:

$$c(P, t) = \sum_i u_i(P)\psi_i(t) + f(t), \tag{4}$$

where P stands for the positional coordinates, and $u_i(P)$

* Present address: Department of Chemistry, Boston University, Boston, Massachusetts.

† A very brief non-mathematical discussion of some of this material appears in an article by H. Reiss, Trans. N. Y. Acad. Sci. 11, 236 (1949).

[1] L. G. Longsworth, Ann. N. Y. Acad. Sci. 46, 212 (1945).

satisfies the equation

$$\nabla^2 u_i = 0. \tag{5}$$

It is equally simple to obtain the explicit form of (4) independently of whether or not the boundary moves, and it is this fact which serves as the basis of the approximate method. In effect, whenever it is practicable, we try to approximate solutions of (1) with solutions of (2).

III. A MOVING BOUNDARY PROBLEM DEALING WITH THE PREPARATION OF AEROSOLS

The first problem which we shall consider occurs in connection with the preparation of monodispersed aerosols.[2] An important step in this preparation involves the passage of a uniform mixture of air, condensable vapor, and foreign nuclei (sinks) for condensation through a temperature gradient, the pressure of the mixture being maintained constant at atmospheric pressure. At first the mixture is undersaturated with respect to the vapor, but as it cools, it becomes saturated. When this happens, diffusion toward the sinks begins, and liquid particles are formed by condensation. The nuclei are selected so that on their surfaces the saturation concentration of vapor is always maintained.

It is of interest to know whether or not *spontaneous nucleation* can occur in such a system.

This statement requires some explanation. In any supersaturated phase, local transient inhomogeneities (fluctuations) are constantly occurring. A large number of these fluctuations produce embryos of the stable phase, i.e., the phase with respect to which the original phase is supersaturated. Such embryos can serve as nuclei for the growth of the stable phase. The rate at which these embryos are produced increases rapidly with the degree of supersaturation.

Calculations, particularly those of Becker and Döring,[3] indicate that as the supersaturation is increased, a critical point is reached at which the rate of embryo formation (rate of nucleation) undergoes a large and sudden increase. Experimentally, it would appear as though the phase transition occurred at this point. When the supersaturated phase is gaseous, Becker and Döring have called the ratio of the pressure of the supersaturated vapor to the saturation pressure the *supersaturation ratio*. The ratio at the critical point is known as the *critical supersaturation ratio*.

The nuclei formed in this way in large numbers at the critical point are said to be formed *spontaneously*, and the process of formation is called *spontaneous nucleation*.

During the cooling of the air-vapor-nuclei mixture, there is no supersaturation on the surfaces of the nuclei, but some supersaturation will persist in the vapor in the regions between the nuclei. If the rate at which the diffusion process drains material from these regions is slow compared to the rate of cooling, it is conceivable that the supersaturation might exceed the critical value, and nuclei, additional to the foreign ones, originally present, would form spontaneously.

Whether or not spontaneous nucleation will occur can only be decided when the concentration of vapor in the air-vapor-nuclei mixture, as it cools, is known as a function of time and position, for this in turn makes possible the calculation of the supersaturation ratio. Information of this kind can only be obtained from a solution of the diffusional boundary value problem involved.

The boundary value problem, cast into its natural form, is too difficult to solve. It is necessary to consider the diffusion of vapor initially at uniform pressure toward a large number of randomly located sinks which are constantly in relative motion. Furthermore, the temperature in this system is decreasing with time in some specified manner. Consequently, since the total pressure (air and vapor) is being maintained at atmospheric pressure, the volume of the system is undergoing a contraction. This is not the only temperature effect, for the diffusion coefficient of the vapor is a function of the temperature squared, and also the saturation vapor pressure, assumed to be maintained on the surfaces of the growing particles, decreases with temperature. The problem is still further complicated by the fact that the latent heat of condensation, released at the particles, tends to raise the temperature in their neighborhoods above that of the more general environment.

Finally, the particles are growing, so that the boundaries of the boundary value problem are not stationary.

In order to overcome some of these difficulties we will not attempt to solve the natural problem, but will attempt to construct a model, incorporating the important features of the real situation, which will be easier to handle mathematically.

Instead of a large number of sinks, only one will be considered. Instantaneously, it will have the radius, x. It will be surrounded by the air-vapor mixture, and on its surface the concentration of the vapor will always be maintained at the equilibrium value. Condensation begins when the temperature becomes so reduced that the vapor saturates the mixture.

To account for the competition of the other nuclei which are not being considered, the spherical sink of radius, x, will be surrounded by an impermeable shell of radius, h. The magnitude of h will be determined by the fact that the volume, $4\pi h^3/3$, enclosed by the shell is the particulate volume[4] defined by Whytlaw-Gray and Patterson, i.e., the reciprocal of the number density of nuclei.

---

[2] V. K. La Mer and D. Sinclair, O.S.R.D. No. 1857, Department of Commerce, Office of Publication Board, Report No. 944. Chem. Rev. **44**, 245 (1949).

[3] R. Becker and W. Döring, Ann. d. Physik **24**, 719 (1935).

[4] Whytlaw-Gray and Patterson, *Smoke*, (Edward Arnold and Company, London 1932), p. 43.

Although account will be taken of the temperature dependence of the saturation concentration on the boundary of the sink, we will ignore the temperature variation of both the volume of the system and the diffusion coefficient of the vapor. The latter effects are not large, since interest will be focused upon situations in which no more than a fifteen percent variation in temperature occurs. However, we must consider the former effect because of its exponential character. Indeed, it is this effect which is responsible for the initiation of the diffusion process.

The inhomogeneities in temperature produced by the release of the latent heat of condensation will be ignored. Actually, a steady state will set in in which the temperature at the particle will exceed that of the environment by a few degrees.

The movement of the center of mass of the sink can easily be neglected, because during the time of growth in the real case, its movement is negligible. However, the movement of the boundary at x, due to growth, cannot be disregarded. In fact, x may increase 100-fold, resulting in a 10,000-fold increase in the surface area of the sink.

When the problem of diffusion in the above model is solved, the concentration of vapor as a function of time and position in the interval (x, h) will be available. It is convenient to define a ratio, the *cooling ratio*, which is the ratio of the vapor concentration at a given point to the saturation concentration. Since we are interested in spontaneous nucleation, it will be necessary for us to confine our attention to the point where the cooling ratio will always be highest. Since diffusion occurs toward the sink at x, it is evident that any point on the shell at h will serve this purpose.

The cooling ratio at h can be plotted as a function of temperature (time). On the same graph the critical supersaturation ratio, calculated by means of the Becker-Döring theory, can also be plotted. The intersection of these curves, if they should intersect, would mark the temperature at which spontaneous nucleation occurs.

In conclusion, it should be remarked that the information obtained by utilizing the above model can at the best be semi-quantitative, because of the number of real factors which have been eliminated from consideration.

IV. THE SOLUTION

First, the problem will be solved under the assumption that the boundary at x does not move. An exact solution can be obtained for this case. Then the approximate method will be used to solve the same problem, and the two results will be compared. Finally, the approximate method will be applied to the moving boundary problem.

Since the model is spherically symmetric, and there are no sources of diffusing material, Eq. (1) becomes

$$\partial^2 c/\partial r^2+(2/r)(\partial c/\partial r)=(1/D)(\partial c/\partial t), \quad x<r\leqslant h, \quad (6)$$

TABLE I.

$h\alpha_2=$ 4.5
$h\alpha_3=$ 7.7
$h\alpha_4=$10.9
$h\alpha_5=$14.1
$h\alpha_6=$17.2

where r is the magnitude of the radius vector originating at the center of the sink of radius, x. The circumstance that the vapor concentration be at first uniform everywhere leads to the initial condition

$$c(r, 0)=c_0, \quad x\leqslant r\leqslant h, \quad (7)$$

where c_0 is the initial concentration. The boundary condition corresponding to the impermeable shell at h is

$$(\partial c/\partial r)_{r=h}=0. \quad (8)$$

Finally, it is convenient to represent the saturation concentration at x by the form

$$c(x, t)=c_0 e^{-\gamma Bt}, \quad (9)$$

where γB is a constant. This furnishes the other boundary condition. More will be said concerning the origin of the form (9) in a later section.

Although this particular problem has not been solved before, the function, $c(r, t)$ satisfying Eqs. (6), (7), (8), and (9) can be found by standard procedures, i.e., by separating the variables,[5] and applying Sturm-Liouville theory.[6] The only unusual step is the use of a generalization of Duhamel's theorem due to Bartels and Churchill[7] which is valuable in dealing with condition (9). Consequently we shall merely state the result.

The desired function is

$$c(r, t)=c_0 e^{-\gamma Bt}+\frac{c_0 x}{r}$$

$$\times\sum_1^\infty \frac{\gamma B[\exp(-\alpha_n^2 Dt)-\exp(-\gamma Bt)]}{(\gamma B-\alpha_n^2 D)\alpha_n\beta_n^2}\sin\alpha_n(r-x). \quad (10)$$

The α_n in this expression are all the roots of the transcendental equation

$$h\alpha_n=\tan\alpha_n(h-x) \quad (11)$$

exclusive of $\alpha_n=0$. The β_n^2 are given by

$$\beta_n^2=\tfrac{1}{2}[h\sin^2\alpha_n(h-x)-x]. \quad (12)$$

The root α_1 is unique in the fact that it can be very accurately represented by

$$\alpha_1=[3x/(h-x)^3]^{\frac{1}{3}}, \quad (13)$$

[5] H. Margenau and G. M. Murphy, *The Mathematics of Physics and Chemistry* (D. Van Nostrand Company, Inc., New York 1944), p. 213.

[6] Ince, *Ordinary Differential Equations* (Dover Publications, New York 1944). Chapter X.

[7] R. C. F. Bartels and R. V. Churchill, Bull. Am. Math. Soc. **48**, 276 (1942).

so long as $x/h \leqslant 0.1$. Furthermore

$$\sin\alpha_1(r-x)=\alpha_1(r-x) \tag{14}$$

with an error of less than 1 percent when $x/h \leqslant 0.1$.

A few of the values of $h\alpha_n$ for $n \geqslant 2$ are given in Table I. The validity of these is also contingent upon the condition $x/h \leqslant 0.1$.

The functions

$$\sin\alpha_n(r-x)/r\beta_n \tag{15}$$

form a set of Sturm-Liouville characteristics on the interval (x, h). They are ortho-normal with the weight function r^2. Any function, $F(r)$, which is sectionally continuous in (x, h) and has a sectionally continuous derivative can be expanded in terms of the functions (15),

$$F(r)=\sum c_n \frac{\sin\alpha_n(r-x)}{r\beta_n}, \tag{16}$$

where

$$c_n=\int_x^h r^2F(r)\frac{\sin\alpha_n(r-x)}{r\beta_n}dr. \tag{17}$$

It is interesting to investigate the conditions under which the entire solution (10) is accurately represented by the expression which includes only the first term of the series on the right. In the first place, this will be so when t is small since then the series does not figure importantly in comparison to the magnitude of $c_0e^{-\gamma Bt}$.

Consider the situation when

$$\alpha_1^2D>\gamma B \tag{18}$$

which demands that

$$\alpha_n^2D \gg \gamma B, \quad n \geqslant 2. \tag{19}$$

Under these conditions the exponential in α_n can be neglected and the series which must be retained under the summation sign (because its quantities depend upon the index n) can be approximated by

$$\sum_1^\infty \frac{\sin\alpha_n(r-x)}{\alpha_n^3\beta_n^2}. \tag{20}$$

But this is simply the Sturm-Liouville expansion of

$$(h^3/3x^2+x/6)(r-x)-(r^3-x^3)/6x, \tag{21}$$

a fact which can easily be demonstrated by setting (21) equal to the $F(r)$ of (16) and (17).

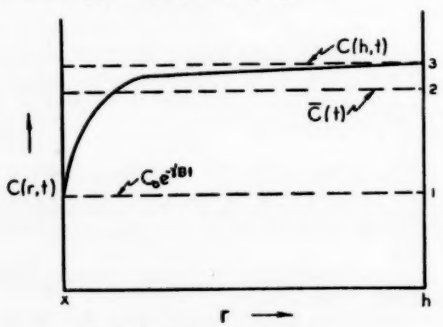

FIG. 1. Plot of $C(r, t)$ *versus* r.

By making use of (13) and (14), the first term of (20) can be written as

$$\sin\alpha_1(r-x)/\alpha_1^3\beta_1^2=2/3[(h-x)^4/x^2(2h+x)](r-x). \tag{22}$$

By subtracting (22) from (20)

$$\sum_2^\infty \frac{\sin\alpha_n(r-x)}{\alpha_n^3\beta_n^2}=\left(\frac{h^3}{3x^2}+\frac{x}{6}\right)(r-x)-\frac{r^3-x^3}{6x}$$
$$-\frac{2}{3}\frac{(h-x)^4}{x^2(2h+x)}(r-x). \tag{23}$$

Consider the ratio of (22) to (21), i.e., the fraction of the whole series which is represented by the first term. This ratio is smallest when $r=h$. When $r=h$, and x/h is as large as 0.05, the ratio is 0.80. In the limit, $x/h \to 0$, the ratio approaches unity.

On the other hand, if

$$\gamma B>\alpha_1^2D, \tag{24}$$

the exponential in γB can be neglected. We are then left with an alternating series containing terms in $e^{-\alpha_n^2Dt}$ and if x/h is small, α_2/α_1 is exceedingly large so that the first term becomes important after the passage of a small interval of time.

We have not yet considered the situation

$$\gamma B=\alpha_1^2D. \tag{25}$$

In this case also

$$\alpha_n^2D \gg \gamma B, \quad n \geqslant 2. \tag{26}$$

The series which must be retained under the summation sign can then be written

$$e^{\gamma Bt}\operatorname*{Lim}_{\gamma B\to\alpha_1^2D}\left\{\frac{[\exp(-\alpha_1^2Dt)-\exp(-\gamma Bt)]}{(\gamma B-\alpha_1^2D)\alpha_1\beta_1^2}\sin\alpha_1(r-x)\right\}$$
$$+\frac{1}{D}\sum_2^\infty \frac{\sin\alpha_n(r-x)}{\alpha_n^3\beta_n^2}=\frac{t}{\alpha_1\beta_1^2}\sin\alpha_1(r-x)$$
$$+\frac{1}{D}\sum_2^\infty \frac{\sin\alpha_n(r-x)}{\alpha_n^3\beta_n^2}. \tag{27}$$

Using (12), (13) and (14)

$$\frac{t}{\alpha_1\beta_1^2}\sin\alpha_1(r-x)=\frac{2t}{[3xh/(h-x)-x]}(r-x) \tag{28}$$

and (23) gives the value of the second member when multiplied by $1/D$. The ratio of (28) to (23) multiplied by $1/D$, i.e. the ratio of the first term to the rest of the series is smallest when $r=h$. If it is assumed that $x/h=0.05$, this ratio, at $r=h$, is

$$tD/500x^2. \tag{29}$$

If now x is chosen to equal 10^{-4} cm and $D=10^{-1}$ cm^2/sec. (typical magnitudes) the ratio will be as high as 20 even when t equals 10^{-3} seconds, a very small interval of time.

These considerations indicate that when x/h is small the first-order approximation to the solution (10) is entirely reasonable.

With the aid of (12), (13) and (14), and the assumption $h-x\simeq h$, this first-term approximation can be written as

$$c(r,t)=c_0e^{-\gamma Bt}+c_0\gamma B\left\{\frac{\exp[-(3xD/h^3)t]-\exp(-\gamma Bt)}{\gamma B-(3xD)/h^3}\right\}\frac{r-x}{r}. \quad (30)$$

Now apply the approximate method to the problem for which (10) is the solution. Equation (2), specialized to the present situation, is

$$\partial^2c/\partial r^2+(2/r)(\partial c/\partial r)=0. \quad (31)$$

To this equation we append the conditions (7) and (9), but we cannot annex (8) because the only solution of (24) satisfying (8) is

$$c(r,t)=f(t). \quad (32)$$

However, it is possible to devise a condition to be valid at h, in place of (8), which will be reasonably consistent with the physics of the situation, so long as x/h is small. In common with a large class of diffusion problems, a plot of $c(r,t)$ *versus* r ought to look like the curve of Fig. 1. There is a steep concentration gradient in the neighborhood of the sink at x. The dotted line, No. 2 in Fig. 1, represents the average concentration, $\bar{c}(t)$, in the interval (x,h) at the time, t. Analytically

$$\bar{c}(t)=\frac{\int_x^h c(r,t)4\pi r^2dr}{4\pi(h^3-x^3)/3}\simeq\frac{\int_x^h c(r,t)4\pi r^2dr}{4\pi h^3/3}, \quad (33)$$

where it has been assumed that $h^3\gg x^3$. Now, because $c(r,t)$ departs appreciably from $c(h,t)$, only in the neighborhood of x

$$c(h,t)\simeq\bar{c}(t), \quad (34)$$

and this is a good approximation, especially when x/h is small. The material which has flowed into the sink at x by the time, t, is measured by

$$[c_0-\bar{c}(t)]4\pi h^3/3\simeq[c_0-c(h,t)]4\pi h^3/3. \quad (35)$$

By differentiation of the right side of (35) with respect to t, the rate at which material flows into the sink at any instant is found to be

$$-(\partial c/\partial t)_{r=h}\cdot 4\pi h^3/3. \quad (36)$$

This rate is also measured by

$$[4\pi r^2D(\partial c/\partial r)]_{r=x} \quad (37)$$

if Fick's law holds.

Now, Eq. (31) can be written in the form

$$\partial/\partial r(r^2(\partial c/\partial r))=0, \quad (38)$$

and this indicates that the value of the expression in brackets, in (37), is independent of r. Consequently

$$4\pi r^2D(\partial c/\partial r)=-Q(t), \quad (39)$$

and by equating the right side of (39) to (36) the condition

$$(\partial c/\partial t)_{r=h}=(3Q(t)/(4\pi h^3) \quad (40)$$

is obtained to be valid at h, in place of (8). This result accounts for the impermeable shell in the following manner. The impermeability of the shell limits the amount of material available for diffusion. On the other hand, (40) through the equality of (37) and (36) expresses this limitation by demanding that the amount of material diffusing through the surface at x equals, exactly, the amount removed from the interval (x,h).

By integrating (39) with respect to r, the expression (see Eq. (4))

$$c(r,t)=[Q(t)/4\pi rD]+f(t) \quad (41)$$

is the result. Differentiation of (41) with respect to t, for $r=h$, yields

$$(\partial c/\partial t)_{r=h}=(1/4\pi hD)(dQ/dt)+df/dt. \quad (42)$$

Equating the right sides of (42) and (40) gives the relation

$$df/dt=-(1/4\pi hD)(dQ/dt)+(3/4\pi h^3)Q. \quad (43)$$

Substitution of (7) into (39) yields

$$Q(0)=0, \quad (44)$$

and substitution of (7) and (44) into (41) yields

$$f(0)=c_0. \quad (45)$$

The integration of (43) subject to (44) and (45) gives

$$f(t)=c_0-\frac{Q}{4\pi hD}+\frac{3}{4\pi h^3}\int_0^t Qdt, \quad (46)$$

and the combination of (46) and (41) leads to the equation

$$c(r,t)=c_0+\frac{Q}{4\pi D}\left(\frac{1}{r}-\frac{1}{h}\right)+\frac{3}{4\pi h^3}\int_0^t Qdt. \quad (47)$$

Differentiation of (47) with respect to t, at $r=x$, gives

$$(\partial c/\partial t)_{r=x}=(1/x-1/h)(1/4\pi D)(dQ/dt)+3Q/4\pi h^3, \quad (48)$$

while by differentiation of (9)

$$(\partial c/\partial t)_{r=x}=-\gamma Bc_0e^{-\gamma Bt}. \quad (49)$$

An ordinary differential equation for Q can be obtained by equating the right sides of (48) and (49). The result is

$$\frac{dQ}{dt}+\frac{3D}{h^3(1/x-1/h)}Q=-\frac{4\pi D\gamma Bc_0}{(1/x-1/h)}e^{-\gamma Bt}. \quad (50)$$

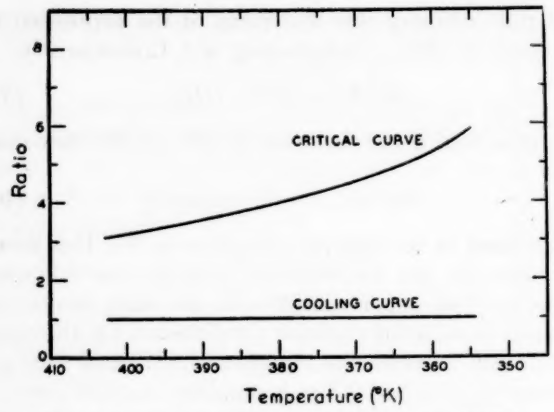

FIG. 2. Concentration of nuclei = 10^6/cc, $T_0 = 403$°K, cooling rate = 53 or 530°K/sec.

This equation is linear, inhomogeneous, and of the first order. Its solution subject to the initial condition (44) is

$$Q(t) = -\frac{\gamma B c_0 4\pi D}{(1/x - 1/h)} \times \left\{ \frac{\exp[-3Dt/h^3(1/x-1/h)] - \exp[-\gamma B t]}{\gamma B - 3D/h^3(1/x-1/h)} \right\}. \quad (51)$$

When this is substituted into (47) and the integral on the extreme right of (47) is evaluated, we obtain with the aid of a somewhat detailed process of regrouping the expression

$$c(r,t) = c_0 e^{-\gamma B t} + \frac{h}{h-x} c_0 \gamma B \times \left\{ \frac{\exp[-3Dt/h^3(1/x-1/h)] - \exp[-\gamma B t]}{\gamma B - 3D/h^3(1/x-1/h)} \right\} \times \left(\frac{r-x}{r} \right). \quad (52)$$

When x/h is small so that x can be ignored in comparison to h, and $1/h$ in comparison to $1/x$, (52) reduces to (30), and so the approximate method has produced the first term of the series solution, obtained by the exact procedure.

This result is not surprising, in the light of the facts that the relation

$$\partial c/\partial t \simeq 0$$

is applicable to the case of diffusion from an infinite region to a single sink, and x/h, small, constitutes an approach to the character of an infinite region.

The approximate method will now be applied to the more real problem in which the value of x increases at a rate controlled by the diffusion of material into the sink. The flux of material into the sink is

$$4\pi x^2 D(\partial c/\partial r)_{r=x} = -Q(t), \quad (53)$$

and this is proportional to the rate of change of volume of the sink

$$4\pi x^2 (dx/dt). \quad (54)$$

The proportionality constant is

$$A\rho/W, \quad (55)$$

where A is Avogadro's number, ρ is the density of the particle, and W is the molecular weight of the diffusing material. Therefore,

$$Q(t) = -(A\rho/W)4\pi x^2 (dx/dt). \quad (56)$$

In the previous analysis, x, or the phenomena occurring at x, were not mentioned before Eq. (47). It is therefore possible to begin the present analysis with

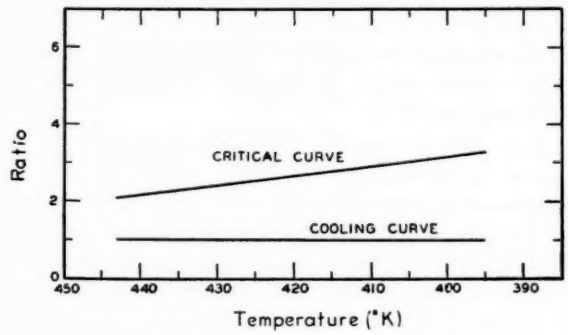

FIG. 3. Concentration of nuclei = 10^6/cc, $T_0 = 443$°K, cooling rate = 530°K/sec.

this equation. Upon the insertion of (53) into (47) the following equation results

$$c(r,t) = c_0 - (A\rho/WD)x^2(dx/dt)(1/r - 1/h) - (A\rho/Wh^3)x^3. \quad (57)$$

The integral on the right of (47) has been evaluated, assuming that $x(0) = 0$. The combination of (9) with (57), specialized to the point $r = x$, yields

$$d(x^2)/dt = (2WDc_0/A\rho)(1 - e^{-\gamma B t}) - (2D/h^3)x^3, \quad (58)$$

where $1/h$ has been ignored in comparison to $1/x$.

Referring to (57), the cooling ratio is

$$\frac{c(h,t)}{c_0 \exp(-\gamma B t)} = \frac{c_0 - (A\rho/Wh^3)x^3}{c_0 \exp(-\gamma B t)}, \quad (59)$$

and this can only be evaluated when x, determined by (58), is known as a function of time. Unfortunately, (58) cannot be integrated in closed form, and it is necessary to resort to numerical methods[8] in order to determine the dependence of x upon t.

V. CALCULATIONS

It will be convenient to begin by discussing the origin of (9). Suppose that the air-vapor-nuclei mixture of

[8] Ford, *Differential Equations*, (McGraw-Hill Book Company, New York 1933), p. 161.

Section III is cooled at a constant rate. Then

$$T=T_0-\gamma t, \tag{60}$$

where T_0 is the temperature at which the mixture becomes saturated with vapor, and γ is a constant, i.e., the cooling rate. At temperatures above room temperature, the saturation concentration of most vapors can be approximated by the following form

$$c=Ae^{BT}, \tag{61}$$

where A and B are constants. This type of approximation can be chosen so that it holds to within a few percent of the true value over ranges of temperature, including as many as seventy or eighty degrees.

Substitution of (60) into (61) yields

$$c=Ae^{BT_0}e^{-\gamma Bt}, \tag{62}$$

but

$$c_0=Ae^{BT_0}, \tag{63}$$

so that (62) is identical with (9). This explains how the latter condition originates.

It will be convenient to choose naphthalene, $C_{10}H_8$, as the substance for which representative calculations will be made. Naphthalene is similar to a number of

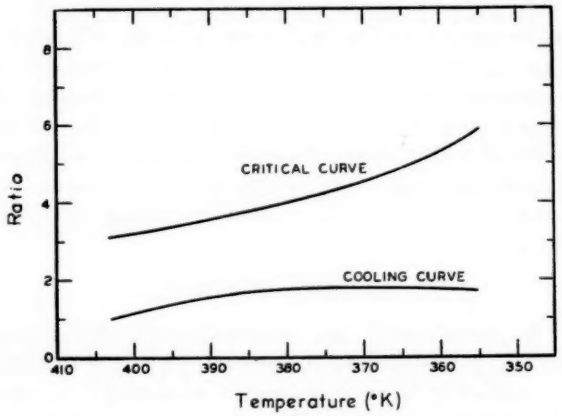

FIG. 4. Concentration of nuclei = 10^3/cc, T_0 = 403°K, cooling rate = 53°K/sec.

substances which have been used in the laboratory for the preparation of monodispersed aerosols, and, in addition, both the temperature dependence of its vapor pressure[9] and the value of its diffusion coefficient in air[10] are known. Furthermore, the value of the surface tension of liquid naphthalene[11] is available for the application of the Becker-Döring theory to the calculation of the critical supersaturation ratio. In accordance with a previous decision to look upon the diffusion coefficient as though it were independent of temperature, we will assign it the value which it has, specially, at T_0.

[9] Lange, *Handbook of Chemistry*, (1944), 5th edition, p. 1431.
[10] International Critical Tables **5**, 63.
[11] International Critical Tables **4**, 459.

We shall deal with two values of γ:

$$\gamma=53°/\text{sec.}, \tag{64}$$

which is considered to be a normal cooling rate, and

$$\gamma=530°/\text{sec.} \tag{65}$$

which is considered to be a high cooling rate. Reasoning qualitatively, it would appear that spontaneous nucleation should be favored by high cooling rates and low concentrations of nuclei.

Cooling curves and *critical* curves were computed for naphthalene in a variety of situations, employing the relation (59) and the results of the Becker-Döring theory. These have been plotted in Figs. 2 through 5.

In Figs. 2 and 3, the concentration of nuclei was chosen to be 10^6/cc, a normal concentration. Figure 2 represents two situations, one in which $\gamma=53°$/sec. and another in which $\gamma=530°$/sec. In both cases T_0 was chosen to be 403°K, and this fixed c_0 at 1.56×10^{18} molecules/cc. The values of A and B necessary for use in (61) were

$$\begin{aligned} A&=1.59\times10^{11}\ \text{mol./cc},\\ B&=3.99\times10^{-2}/\text{degree}. \end{aligned} \tag{66}$$

In neither case do the cooling and critical curves intersect. In fact, throughout the entire temperature range, the cooling ratio is conspicuously unity. On the basis of this result, spontaneous nucleation is not possible for the conditions of Fig. 2.

Figure 3 investigates the effect of using a higher T_0 and, consequently, a higher c_0. Here T_0=443°K and $c_0=5.26\times10^{18}$ molecules/cc. For this new range

$$\begin{aligned} A&=1.32\times10^{12}\ \text{mol./cc},\\ B&=3.43\times10^{-2}/\text{degree}. \end{aligned} \tag{67}$$

The cooling rate was again chosen high, i.e., $\gamma=530°$/sec. The critical and cooling curves still do not intersect. In fact the cooling ratio is again unity.

Figures 4 and 5 investigate the effect of decreasing the concentration of nuclei. T_0 was chosen at the orig-

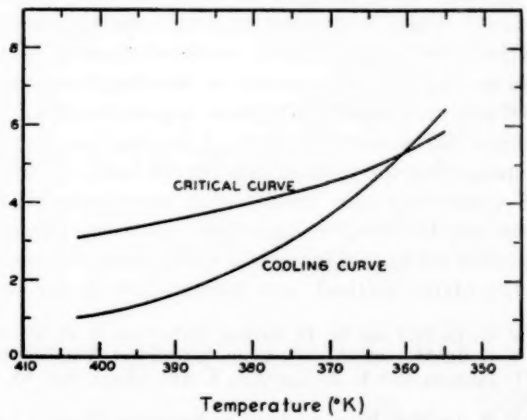

FIG. 5. Concentration of nuclei = 10/cc, T_0 = 403°K, cooling rate = 53°K/sec.

inal value of 403°K, c_0 assumed the original value, and A and B were given by (66). In both figures $\gamma=53°/\text{sec}$.

In Fig. 4, the concentration of nuclei is 10^3/cc. Still the critical and cooling curves do not intersect, but the cooling ratio does depart appreciably from unity. In Fig. 5, where the nuclear concentration is only 10/cc, the curves do intersect. In this case, spontaneous nucleation would be expected, but the number of nuclei is so low that the situation is very unreal.

In the light of these results it may be concluded that spontaneous nucleation does not easily occur when we deal with substances whose critical ratio is similar to that of naphthalene, and when, in addition, there are a few (more than 10^2/cc) nuclei present whose surfaces cannot support supersaturation.

VI. A MOVING BOUNDARY PROBLEM DEALING WITH THE PREPARATION OF HYDROSOLS

Another diffusion problem which is complicated by a moving boundary occurs in connection with the preparation of monodispersed sulfur hydrosols.[12–14] In this case, dilute solutions of sodium thiosulfate and acid are mixed and the following *homogeneous* reaction occurs.

$$2HS_2O_3^- = 2S + 2HSO_3^-.$$

The concentration of dissolved sulfur increases until a critical supersaturation limit of the Becker-Döring type is reached. At this point nuclei are formed spontaneously, and the excess of dissolved sulfur begins to diffuse towards the nuclei, forming droplets of sulfur and lowering the supersaturation below the critical point. This leads to the cessation of rapid nucleation, and the remainder of the process consists of diffusion toward a constant number of sinks. Of course, the homogeneous chemical reaction is still proceeding and if it were rapid enough the diffusion might be unable to reduce the concentration and nucleation would continue.

The physical ideas concerning the steps in the production of monodispersed hydrosols were formulated by La Mer at a meeting of the American Chemical Society.[15] There is a possibility that the homogeneous reaction producing sulfur is accelerated at the droplet surfaces and that the growth of the droplets is mainly ascribable to a locally catalyzed deposition rather than a simple diffusion mechanism. A decision can be made by computing the growth rate on the basis of diffusion and comparing the result with experimental data. Zaiser and La Mer,[16] using a light scattering technique, measured the rate of growth of sulfur droplets produced by the above method, and plotted the square of the radius against time.[17] We shall attempt to reproduce these curves from diffusion theory.

Fortunately, with each of the four curves which these authors present, the number density of the growing particles is given, so that the number of nuclei necessary for the calculation of h is available. In addition, the reaction was slow enough so that during the interval of time involved the concentrations of reactants did not vary appreciably from their initial values. Furthermore, spectrophotometric studies made prior to the point of nucleation indicate that the reaction products do not appreciably alter the rate, at least in the early stages. It is therefore feasible to assume that the rate is a constant, k.

The k corresponding to each curve can be obtained by extrapolating the curve in question to the point of zero radius, thereby marking the time, l_0, at which spontaneous nucleation occurs. If c_0 is the concentration of sulfur at this point, then

$$k = c_0/l_0. \tag{68}$$

Finally, calculations of the Becker-Döring type indicate that the critical supersaturation ratio in the present case is at least one hundred, so that little error is incurred by assuming that the saturation concentration (solubility) of sulfur at the particle surfaces is zero.

Once more it will be convenient to perform the calculation upon a spherically symmetric model, bounded by an impermeable shell of radius h. The radius of the growing particle will be denoted as usual by x. The results of the present calculation are likely to be more quantitative than those of the previous, because not so many real factors have been eliminated from consideration.

VII. THE SOLUTION

The problem will first be solved under the assumption that the boundary at x does not move. Since there is a uniformly distributed source of strength k, where k is independent of time, Eq. (1) assumes the following form.

$$\partial^2 c/\partial r^2 + (2/r)(\partial c/\partial r) = (1/D)(\partial c/\partial l) - k/D, \qquad x < r \leqslant h. \tag{69}$$

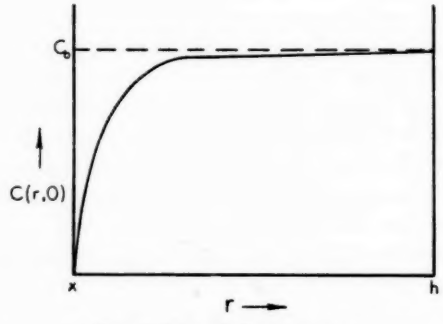

FIG. 6. Plot of $C(r, 0)$ *versus* r.

[12] V. K. La Mer and M. D. Barnes, J. Coll. Sci. **1**, 71, 79 (1946).
[13] V. K. La Mer and A. S. Kenyon, J. Coll. Sci. **2**, 257 (1947).
[14] I. Johnson and V. K. La Mer, J. Am. Chem. Soc. **69**, 1184 (1947).
[15] V. K. La Mer. Paper read before American Chemical Society (September, 1947).
[16] E. Zaiser and V. K. La Mer, J. Coll. Sci. **3**, 571 (1948).
[17] E. Zaiser and V. K. La Mer, J. Coll. Sci. **3**, 571 (1948) Fig. 3.

To this are appended the initial condition

$$c(r, 0)=c_0, \quad x<r\leqslant h, \tag{70}$$

and the boundary conditions

$$(\partial c/\partial r)_{r=h}=0, \tag{71}$$

$$c(x, t)=0. \tag{72}$$

The solution of this problem is

$$c(r, t)=\frac{c_0 x}{r}\sum_1^\infty \exp(-\alpha_n^2 Dt)\frac{\sin\alpha_n(r-x)}{\alpha_n\beta_n^2} + \frac{kx}{r}\sum_1^\infty \frac{[1-\exp(-\alpha_n^2 Dt)]}{\alpha_n^3\beta_n^2 D}\sin\alpha_n(r-x), \tag{73}$$

where the α_n and β_n have the same significance as in Eq. (10). If only the first terms of the series in (73) are retained, and (12), (13) and (14) are used together with the assumption that $h-x\simeq h$, the result is

$$c(r, t)\simeq c_0 x(1/x-1/r)\exp[-(3x/h^3)Dt] + kh^3/3D(1/x-1/r)\{1-\exp[-(3x/h^3)Dt]\}. \tag{74}$$

Now, let us solve the problem using the approximate method. Equation (2) assumes the special form

$$\partial^2 c/\partial r^2+(2/r)(\partial c/\partial r)=-k/D, \tag{75}$$

or

$$\partial/\partial r[r^2(\partial c/\partial r)]=-kr^2/D.$$

Recalling the definition of Q in (39) this can be written

$$\partial Q/\partial r=4\pi kr^2, \tag{76}$$

or by integration

$$Q(r, t)=4\pi r^3 k/3+\varphi(t), \tag{77}$$

where $\varphi(t)$ is an arbitrary function of time. It can be shown that $\varphi(t)$ contains the term

$$-4\pi h^3 k/3. \tag{78}$$

This leads to some difficulty because as $h\to\infty$, $Q\to\infty$. The difficulty, of course, is a result of the approximation. It will be shown, however, that so long as h is not too large, the approximation still leads to a reasonable result. The solution of (75) (see Eq. (4)) can be written in the form

$$c(r, t)=-(kr^2)/6D+\varphi(t)/(4\pi rD)+f(t), \tag{79}$$

where $f(t)$ is a second, arbitrary function of time.

In the exact solution of the problem the conditions (72) and (70) combine to demand that at the zero of time

$$\begin{aligned} &c(r, 0)=c_0, \quad x<r\leqslant h,\\ &c(x, 0)=0. \end{aligned} \tag{80}$$

This requirement involves a discontinuity at $r=x$ which (79) will never be able to satisfy. However, a value for c, defined by (79) can be found which satisfies

$$\begin{aligned} &c(h, 0)=c_0,\\ &c(x, 0)=0, \end{aligned} \tag{81}$$

in such a way that the plot of c *versus* r has the form exhibited in Fig. 6. This approximates the initial condition (80). In fact, it is probably a truer representation of the real state of affairs, because the spontaneous formation of a nucleus at x depletes the solution in the immediate neighborhood of x. In any event, it will be shown that the approximate solution, based on the condition (81), and the exact solution based on (80) tend to coincide after a finite interval of time.

The application of (81) to (79) determines the values of $\varphi(0)$ and $f(0)$. Thus

$$\varphi(0)=\frac{4\pi Dc_0}{(1/h-1/x)}+\frac{4\pi k}{6}\frac{(h^2-x^2)}{(1/h-1/x)}, \tag{82}$$

$$f(0)=c_0+\frac{kh^2}{6D}-\frac{c_0}{(1/h-1/x)h}-\frac{k}{6hD}\frac{(h^2-x^2)}{(1/h-1/x)}. \tag{83}$$

The boundary condition for h is determined by substituting (77) written for $r=h$, into (39). Thus

$$(\partial c/\partial t)_{r=h}=k+3\varphi(t)/4\pi h^3. \tag{84}$$

By differentiating (79) with respect to t at h

$$(\partial c/\partial t)_{r=h}=(1/4\pi hD)(d\varphi/dt)+(df/dt). \tag{85}$$

Equating the right-hand members of (84) and (85) results in the differential equation

$$df/dt=k-(1/4\pi hD)(d\varphi/dt)+3\varphi/4\pi h^3. \tag{86}$$

This can be integrated using the initial conditions (82) and (83), yielding

$$f(t)=c_0+\frac{kh^2}{6D}+kt-\frac{\varphi(t)}{4\pi hD}+\frac{3}{4\pi h^3}\int_0^t \varphi dt. \tag{87}$$

When (79) is specialized to the point $r=x$, and (87) substituted in it, we obtain

$$c(x, t)=0=c_0+kt+\frac{k}{6D}(h^2-x^2) + \frac{\varphi}{4\pi D}\left(\frac{1}{x}-\frac{1}{h}\right)+\frac{3}{4\pi h^3}\int_0^t \varphi dt, \tag{88}$$

and when (88) is differentiated with respect to t, a differential equation for φ is obtained. Thus

$$\frac{d\varphi}{dt}-\frac{3D}{h^3(1/h-1/x)}\varphi=\frac{4\pi Dk}{(1/h-1/x)}. \tag{89}$$

TABLE II.

Curve A	concentration of acid = 0.002 M concentration of thiosulfate = 0.002 M concentration of nuclei = 2.7×10^{6}/cc $k=2.1\times10^{11}$ mol./cc sec.
Curve B	concentration of acid = 0.0015 M concentration of thiosulfate = 0.002 M concentration of nuclei = 2.1×10^{6}/cc $k=1.7\times10^{11}$ mol./cc sec.
Curve C	concentration of acid = 0.006 M concentration of thiosulfate = 0.001 M concentration of nuclei = 1.8×10^{6} cc $k=1.2\times10^{11}$ mol./cc sec.
Curve D	concentration of acid = 0.003 M concentration of thiosulfate = 0.001 M concentration of nuclei = 1×10^{6}/cc $k=0.83\times10^{11}$ mol./cc sec.
For *A*, *B*, *C*, and *D*	$D=2\times10^{-6}$ cm²/sec. $c_0=3.5\times10^{14}$ mol./cc

The solution of (89) subject to (82) is

$$\varphi(t)=\left\{4\pi h^3k/3+\frac{4\pi Dc_0}{(1/h-1/x)}+\frac{2\pi k}{3}\frac{h^2-x^2}{(1/h-1/x)}\right\}\times\exp\left[\frac{3Dt}{h^3(1/h-1/x)}\right]-4\pi h^3k/3. \quad (90)$$

Furthermore

$$\int_0^t\varphi dt=\frac{h^3(1/h-1/x)}{3D}\times\left\{4\pi h^3k/3+\frac{4\pi Dc_0}{(1/h-1/x)}+\frac{2\pi k}{3}\frac{h^2-x^2}{(1/h-1/x)}\right\}\times\left\{\exp\left[\frac{3Dt}{h^3(1/h-1/x)}\right]-1\right\}4\pi h^3kt/3. \quad (91)$$

Substitution of (87) into (79) and of (90) and (91) into the resulting equation yields after considerable rearrangement

$$c(r,t)=\frac{k}{6D}(x^2-r^2)-\left(\frac{1}{x}-\frac{1}{r}\right)\frac{c_0}{(1/h-1/x)}\exp\left[\frac{3Dt}{h^3(1/h-1/x)}\right]+\left(\frac{1}{x}-\frac{1}{r}\right)\frac{kh^3}{3D}\left\{1-\exp\left[\frac{3Dt}{h^3(1/h-1/x)}\right]\right\}-\left(\frac{1}{x}-\frac{1}{r}\right)\frac{k}{6D}\frac{h^2-x^2}{(1/h-1/x)}\exp\left[\frac{3Dt}{h^3(1/h-1/x)}\right]. \quad (92)$$

This can be simplified by making use of the fact that $h\gg x$. Thus we obtain

$$c(r,t)=(k/6D)(x^2-r^2)+(1/x-1/r)c_0x\exp[-(3x/h^3)Dt]+(1/x-1/r)(kh^3/3D)\{1-\exp[-(3x/h^3)Dt]\}+(1/x-1/r)(kh^2/6D)x\exp[-(3x/h^3)Dt]. \quad (93)$$

The first term in (93) is unbounded when r approaches infinity. This effect has been mentioned in connection with (78). However, in every application of the approximate method which we shall make, the following order of magnitude relation shall hold

$$Dc_0/kh^2\approx100. \quad (94)$$

Using this relation together with the fact that $h\geqslant r$, it is possible to show that the ratio of the second to the first term is initially about 100, so that the first term can be ignored. At later times the second term diminishes, but then the third term which has about the same magnitude takes its place. Finally, the ratio of the second to the fourth term at all times is about 100, so that the fourth term can be neglected also. Consequently, the only terms of importance are the second and third, the latter becoming large at later times when the former becomes small. But the expression obtained by using just these terms is identical with (74), the first term of the exact solution.

Because $\alpha_{n+1}>\alpha_n$ this first term becomes a better approximation to the whole solution, after the passage of time, supporting the contention that the exact and approximate solutions coincide with the passage of time, despite the difference in the initial conditions.

Now introduce the moving boundary. In analogy to (56)

$$Q(x,t)=-(A\rho/W)4\pi x^2(dx/dt), \quad (95)$$

and by (77)

$$Q(x,t)=(4/3)\pi x^3k+\varphi(t). \quad (96)$$

The first term on the right of (96) can be ignored in comparison to the $4\pi h^3k/3$ contained in $\varphi(t)$ (See (78)), and so it is possible to write

$$Q(x,t)=\varphi(t)=-(A\rho/W)4\pi x^2(dx/dt). \quad (97)$$

In the present development (79) can be assumed in full since its derivation was independent of the movement or non-movement of the boundary at x. In addition (82) and (83) can be used, and under the condition, $x(0)=0$, these reduce to

$$\varphi(0)=0 \quad (98)$$

and

$$f(0)=c_0+kh^2/6D. \quad (99)$$

It is also permissible to adopt Eq. (86) which when integrated, subject to (98) and (99), yields

$$f(t)=c_0+\frac{kh^2}{6D}+kt-\frac{\varphi(t)}{4\pi hD}+\frac{3}{4\pi h^3}\int_0^t\varphi dt. \quad (100)$$

If (100) is substituted into (79), and the result specialized to $r=x$, we obtain

$$c(x,t)=0=c_0+kt+(k/6D)(h^2-x^2)+\frac{\varphi(t)}{4\pi D}\left(\frac{1}{x}-\frac{1}{h}\right)+\frac{3}{4\pi h^3}\int_0^t \varphi dt. \quad (101)$$

This can be simplified by the use of the condition, $h\gg x$, and in addition, $\varphi(t)$ can be replaced using (97). The integral on the right of (101) is easily evaluated. Thus

$$\int_0^t \varphi dt=-\frac{A\rho}{W}4\pi\int_0^t x^2\frac{dx}{dt}dt=-\frac{A\rho}{W}4\pi\int_0^x x^2dx=-\frac{A\rho}{W}\frac{4}{3}\pi x^3. \quad (102)$$

The entire result for (101) is

$$d(x^2)/dt=(2WD/A\rho)kt-(2D/h^3)x^3+(2WD/A\rho)(c_0+kh^2/6D), \quad (103)$$

and the last term can be simplified by the use of condition (94), $kh^2/6D$ being negligible with respect to c_0. Thus

$$d(x^2)/dt=(2WD/A\rho)kt-(2D/h^3)x^3+(2WD/A\rho)c_0. \quad (104)$$

Equation (104) gives the dependence of x^2 upon t, when it is integrated, subject to the condition $x(0)=0$. This is exactly what is needed to reproduce the curves of Zaiser and La Mer. Unfortunately, like (58), it cannot be integrated in closed form, and it is necessary to resort to numerical methods.

VIII. CALCULATIONS

The four curves of Zaiser and La Mer which we now wish to reproduce by means of (104) seem at first glance to be identical in shape, but this is due to a fortuitous set of circumstances wherein the various factors which determine the dependence of x^2 upon time have in their variations counterbalanced each other. For example, when the source function, k, is larger, the concentration of nuclei is also larger, and h^3 is therefore smaller. The import of these last statements should be carefully regarded, lest it be thought that the fact that we can reproduce one curve renders trivial the reproduction of the remaining three, on the basis that all have identical shapes.

The values of c_0 and D necessary for the application of both (68) and (104) were not independently available. But there are four curves, so that it is possible to fix the values of these two parameters by the use of one of the curves, and it will be significant if the values fixed in this way are adequate for the description of the remaining curves. The significance will be increased if the values so fixed are reasonable in the light of other evidence.

TABLE III.

Curve *A*

Time (sec.)	Calculated x^2 (microns^2)	Observed x^2 (microns^2)
0	0	0
500	0.015	0.015
1000	0.030	0.029
1500	0.042	0.042
2000	0.051	0.052
2500	0.058	0.060
3000	0.064	0.067
3500	0.070	0.075

Curve *B*

Time (sec.)	Calculated x^2 (microns^2)	Observed x^2 (microns^2)
0	0	0
500	0.015	0.016
1000	0.030	0.030
1500	0.041	0.043
2000	0.052	0.053
2500	0.061	0.060
3000	0.068	0.067
3500	0.074	0.075
4000	0.079	0.082
4500	0.085	0.087

Curve *C*

Time (sec.)	Calculated x^2 (microns^2)	Observed x^2 (microns^2)
0	0	0
500	0.015	0.014
1000	0.030	0.029
1500	0.042	0.043
2000	0.052	0.054
2500	0.060	0.062
3000	0.067	0.069
3500	0.072	0.077

Curve *D*

Time (sec.)	Calculated x^2 (microns^2)	Observed x^2 (microns^2)
0	0	0
500	0.015	0.014
1000	0.030	0.027
1500	0.044	0.043
2000	0.057	0.054
2500	0.068	0.062
3000	0.077	0.069
3500	0.085	0.075
4000	0.092	0.080

All four curves can be fitted by using the values

$$c_0=4.7\times10^{-6}\text{ g/atom/liter}=3.5\times10^{14}\text{ mol./cc}, \quad (105)$$

$$D=2\times10^{-6}\text{ cm}^2/\text{sec}. \quad (106)$$

Employing spectrophotometric means, and an extinction coefficient for sulfur in water obtained by taking an average over many organic solvents,[13] Zaiser and La Mer estimate the critical concentration to be

$$3\text{ to }4\times10^{-6}\text{ g/atom/liter}. \quad (107)$$

The value of the diffusion coefficient can also be estimated. Assuming that the diffusing unit contains eight sulfur atoms, i.e., is S_8, it is found from the critical tables [18] that at room temperature in aqueous solution,

[18] International Critical Tables **5**, 63–76.

the values of the diffusion coefficients of most molecules which compare in size with S_8 lie in the range

$$4 \text{ to } 7\times10^{-6} \text{ cm}^2/\text{sec}. \tag{108}$$

It is satisfying to note that (105) and (106) are in reasonable agreement with (107) and (108). This indicates that the simple diffusion picture provides an adequate description of the observed facts.

Table II contains the values of the important experimental parameters, associated with each of the four curves which Zaiser and La Mer have called *A*, *B*, *C*, and *D*, respectively.

In Table III, the values of x^2 obtained for various times from the calculated and observed curves are presented.

The agreement in Table III is better than the experimental accuracy warrants. An error of 5 percent could be expected on the basis of the known precision limit of the experimental procedure. Of course, it must be remembered that two of the parameters were chosen to provide a good fit. During the first thousand seconds, any values of c_0 and D, chosen to satisfy one curve, will tend to satisfy the others, since the initial slope given by (104) is identical for all curves. However, over the interval of time considered in Table III the slopes change by as much as threefold, so that the continued agreement is significant.

The value of D given by (106) is somewhat lower than it should be, according to (108). It is possible that S_8 is not the diffusing unit, and that it is a larger molecule, e.g., a polythionate. There is also some question concerning the choice of the boundary condition at x. Collins and Kimball[19] have discussed this condition from the point of view of kinetic theory, and it is possible that their treatment has a bearing on the present work.

Finally, it is possible and, in fact, probable, that there is some error in the nuclear concentrations quoted by Zaiser and La Mer, since these authors point out that the number of nuclei was not observed to be *strictly* constant during the period of growth.

IX. THE SINGLE-SINK REPRESENTATION

In the preceding work, the diffusion phenomena occurring in the field of many competing sinks have been discussed in terms of a simple spherically symmetric model enclosing a single sink. There is some justification for this procedure.

Consider an infinite region filled with a large number, n, of identical spherical sinks, upon whose surfaces the concentration of diffusing material must remain zero. Suppose that the initial concentration everywhere is uniformly c_0. Then the boundary value problem is

$$\nabla^2 c = (1/D)(\partial c/\partial t), \tag{109}$$

$$c(P, 0) = c_0, \tag{110}$$

$$c = 0, \quad \text{on each sink.} \tag{111}$$

For the moment, imagine that only one sink is present in the infinite region. The solution[20] of the problem is now simple and can be found in standard references. Call this solution w_i. It has the property that, at finite times,

$$w_i \simeq c_0 \tag{112}$$

so long as the value is measured at a point removed more than ten- or fifteen-sink diameters from the surface of the sink. Of course, w_i satisfies (109), (110) and (111). If each sink in turn is isolated, a w_i is obtained for each.

Suppose that the sinks originally are separated by more than ten or fifteen diameters. Then construct the function

$$c = c_0 + \sum_i (w_i - c_0). \tag{113}$$

This function satisfies (109) and (110), since the w_i satisfy these conditions. It almost satisfies (111), for consider the jth sink. On its surface, $w_j = 0$, but all w_i for $i \neq j$ by (112) are equal approximately to c_0. Then

$$\begin{aligned} c &= c_0 + (w_1 - c_0) + \cdots (w_j - c_0) + \cdots (w_n - c_0) \\ &\simeq c_0 + (c_0 - c_0) + \cdots (0 - c_0) + \cdots (c_0 - c_0) \\ &= 0. \end{aligned} \tag{114}$$

Consequently, (113), which is a superposition of identical *spherically symmetric* solutions, one for each sink is almost an adequate solution of the real problem when the sinks are far enough apart.

[19] Collins and Kimball, to be published in J. Coll. Sci. (1949).

[20] R. Fricke, Zeits. Phys. Chemie **104**, 363 (1923).

THE JOURNAL OF CHEMICAL PHYSICS VOLUME 18, NUMBER 1 JANUARY, 1950

An Electron Diffraction Investigation of the Structures of Neopentyl Chloride and Silico-Neopentyl Chloride

The Determination of Intensities through the Use of a Rotating Sector

J. M. HASTINGS* AND S. H. BAUER
Department of Chemistry, Cornell University, Ithaca, New York

(Received April 25, 1949)

Constructional details and operational data on an electron diffraction apparatus, in which a rotating sector has been incorporated, are presented. Its range of application and limitations are listed, and methods for the reduction of microphotometer records are discussed.

Electron diffraction photographs of neopentyl chloride and silico-neopentyl chloride were taken with and without sectors. Their structures were deduced by a combination of the visual and photometric procedures. Attempts were made to estimate quantitatively the equivalent temperature factors for libration about the C−C and Si−C bonds. Best values for the interatomic distances and their possible interpretations are presented in the concluding section.

IN this and in the two papers which follow we shall present structural conclusions based on electron diffraction patterns of gases obtained with and without the use of a rotating sector. An abbreviated description of the apparatus will be given, since the essential conclusions regarding the structures of the compounds discussed do not depend on the sector data. On the other hand, the description will be adequate enough to permit an assessment of the validity of those conclusions which do depend on the sector data. The apparatus utilized in these studies has since been improved; an analysis of the fundamentals and limitations of the sector technic, and of the design features which have been incorporated to reduce some of these limitations, will be published in another journal.†

FUNDAMENTAL EQUATIONS

The ratio of the intensity scattered at an angle θ to the power in the primary beam is given by[1]

$$\frac{I(s)}{P_0}=\left[\frac{8\pi^2me^2}{h^2}\right]^2\frac{N}{R^2s^4}\left\{\sum_i f_i^2+\sum_i G_i+\sum_i{}'\sum_j{}' f_if_j \times\int_0^\infty P(r_{ij})\frac{\sin sr_{ij}}{sr_{ij}}dr_{ij}\right\}, \quad (1)$$

where N = number of scattering units per unit area of beam; R = distance from scattering point to detector; $s=(4\pi/\lambda)\sin\theta/2$; f_i, G_i = coherent, incoherent atom form factors; $f_i=(Z_i-F_i)$; F_i = x-ray atom form factor, coherent; r_{ij} = distance between atoms i and j in the scattering unit; $P(r_{ij})$ = probability distribution in r_{ij} due to interatomic motions within each scattering unit. The other symbols have their usual meanings. The observable range of s extends from about 1.5 to a maximum of 35 for most cameras, while the variation in intensity over this range is roughly 10^4 to 1, due to the $1/s^4$ factor. Since photographic materials are approximately linear over a range of 100/1, photographic recording of electron intensity permits an objective quantitative evaluation of only a small interval of the intensity at any one time. Furthermore, the steep declining slope on which the oscillating term is superposed transforms the maxima and minima to inflections or derivatives of higher order. In Fig. 1 the electron current which might be received by a collector is plotted as a function of s for hexamethylcyclotrisiloxane.

To obtain a photographic record of $I(s)/P_0$, which can be treated quantitatively over the entire range of s, one must *multiply* the pattern, prior to recording, by a function which will reduce the range of electron intensity. Then the maxima and minima of the third term appear as such rather than as inflections. A number of investigators[2] have accomplished this through the use of a sector—a heart-shaped mask which rotates about an axis which lies along the undeflected ray, in a plane in front of and parallel to the photographic plate; the sector in effect, limits the time of exposure as some function of s (see Fig. 2).

The accuracy of the determination of interatomic distances is limited not only by the precision of the evaluation of $I(s)/P_0$, but also by the relative magnitude of the molecular to the atomic terms in the scattering equation. Even if the background term is reduced to unity with an appropriate sector, this limitation is a severe one since the ratio of molecular to atomic contributions

* Present address: Brookhaven National Laboratory, Upton, New York.

† A major portion of this analysis has been presented in a report to ONR by Bauer, Keidel, and Harvey, February 1949, submitted under Contract No. N6 ori-213, Task Order I.

[1] P. J. W. Debye, J. Chem. Phys. **9**, 55 (1941).

[2] (a) F. Trendelenburg, Naturwiss. **21**, 175 (1933); Physik. Zeits. **40**, 727 (1939). (b) P. Debye, Physik. Zeits. **40**, 404 (1939). (c) Finbak, Hassel, and Ottar, Arch. Math. Naturv. **B44**, No. 13 (1941). (d) H. J. Yearian, Phys. Rev. **59**, 926 (1941). (e) S. H. Bauer, Phys. Rev. **64**, 316 (1943). (f) H. Viervoll, Acta Chem. Scand. **1**, 120 (1947). (g) H. J. Yearian and W. M. Barss, J. App. Phys. **19**, 700 (1948).

declines as $\exp(-a^2s^2)/s$, with typical values for a^2 around 0.002. For the case of hexamethylcyclotrisiloxane, if $I(s)/P_0$ were determined to one percent (densitometry rarely leads to values so reliable), then it would be possible to estimate the molecular term to an accuracy of approximately three percent at $s=5$; seven percent at $s=10$; 30 percent at $s=20$; and 100 percent at $s=30$. To increase the precision of these determinations one must either increase the precision of evaluation of $I(s)/P_0$, or *subtract* from the pattern, prior to recording, a major portion of the atomic contribution. The impossibility of performing this subtraction is inherent in photographic recording. Whether it could be successfully done by direct measurement of the diffraction current is being investigated in this laboratory.

To reduce the background term to unity, the fractional opening of the sector should be

$$[\phi/\pi]=\frac{s^4}{\sum_i f_i^2+\sum_i G_i} \qquad (2)$$

then,

$$\left[\frac{I(s)}{P_0}\right]_{\text{sector}}=\left[\frac{8\pi^2me^2}{h^2}\right]^2\frac{N}{R^2}\left\{1+\frac{\sum'\sum' f_if_j}{\sum f_i^2+\sum G_i}\times\int_0^\infty P(r_{ij})\frac{\sin sr_{ij}}{sr_{ij}}dr_{ij}\right\}. \qquad (3)$$

Equations (1) and (3) are idealized relations, for in their derivation one assumed, besides absolute monochromaticity, that the electron beam may be represented by a plane parallel wave of infinitesimal width both at the sector and at the plate; further, that the sample of N molecules extends over a region negligibly small compared to the dimensions of R; finally, that no multiple scattering occurs. In practice none of these is satisfied in the usual experimental arrangements. The beam has finite width at the plate—0.01 to 0.04 cm; the sample diffuses out of the nozzle into the camera section; multiple scattering may remove up to five percent of the primary diffracted rays, if nozzle pressures are as high as

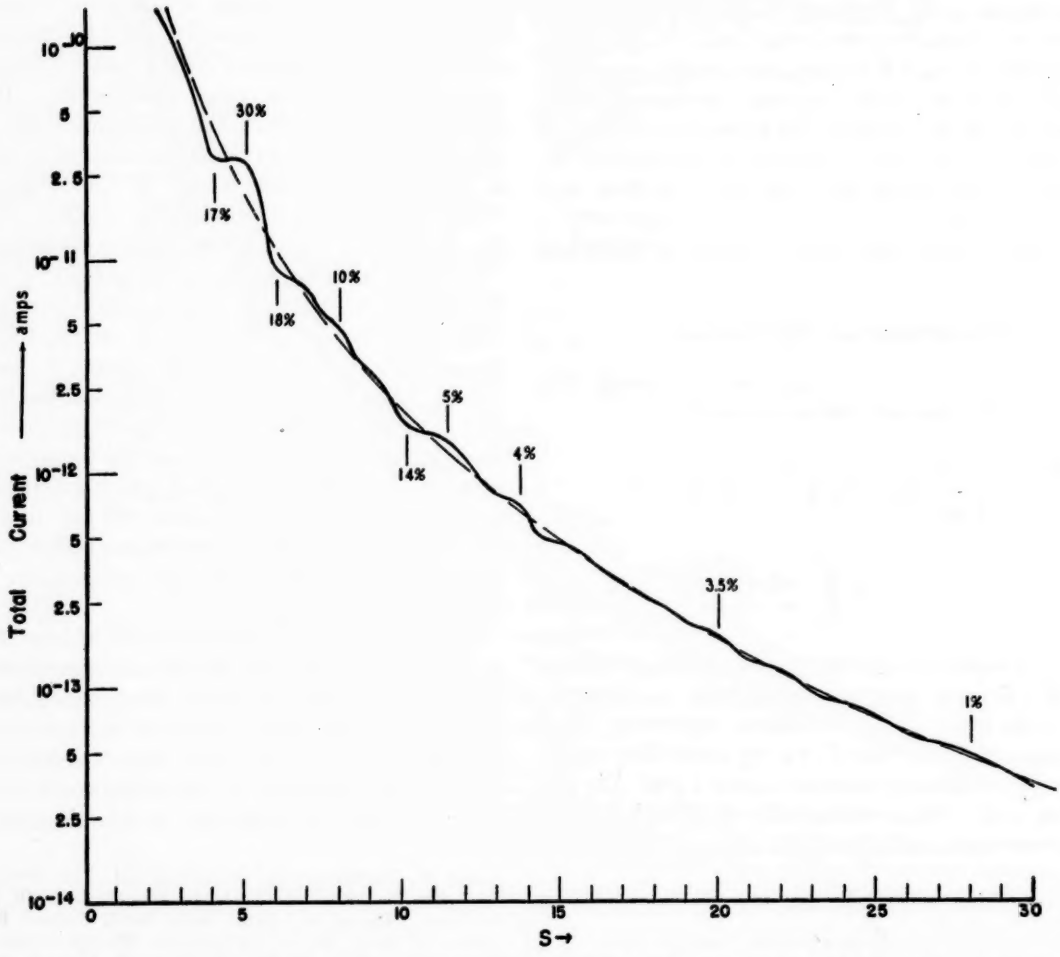

FIG. 1. Collector current expected for electrons diffracted by $[(CH_3)_2SiO]_3$ vapor, under the following conditions: $N=4.09\times10^{14}$; $R=20$ cm; collector 0.01×0.20 cm (narrow dimension equivalent $\Delta s=0.057$ unit); $P_0=1\times10^{-5}$ amp.

three mm Hg. For visual work the loss in resolution introduced by these effects is of no particular consequence except in the estimation of temperature factors. For sector work, however, the fact that the experimental arrangement does not satisfy the conditions implied by the equation must be considered.[3] We have made extensive computations to determine the magnitude of loss in resolution arising from finite extension of the sample, multiple scattering and imperfect focusing of the primary ray; these can be allowed for in the interpretation of the reduced microphotometer records.

THE APPARATUS

In Fig. 3, top and side views of the electron diffraction unit are shown. Items 1, 2, and 3 are the electron gun, biasing cup, and anode, respectively. A set of collimating holes, 0.010 in., 0.050 in., and 0.062 in. follows; 4 is a set of vertical and horizontal deflecting plates across which a controlled potential of 50–150 volts is placed in order to permit the accurate location of the electron beam at the center of rotation of the sector. The horizontal set also serves as a shutter when 2000 volts are impressed across it. Item 5 is a magnetic lens, while 6a, 6b are top and side views, respectively, of a high temperature nozzle. This design permits the interposing of calibrating samples (gold foil, zinc oxide) at the exact position of the slot through which the gas enters. The region through which the gas passes is heated by conduction; unfortunately, due to thermal leaks in the vicinity of the position control, the section around the bellows valve must be kept 5–10°C higher than the temperature of the nozzle itself.

The sample holder is sketched in Fig. 4. The material either may be placed or distilled into the container, which is then evacuated, and sealed off. After connecting it to the electron diffraction unit by means of the compression coupling, the bellows valve is opened for a short interval, and the thin glass partition is broken by actuating a small external coil. Another type of nozzle useful for room temperature studies is shown in Fig. 5. In both nozzles, provision is made for interposing a platinum stop, several thousandths of an inch wider than

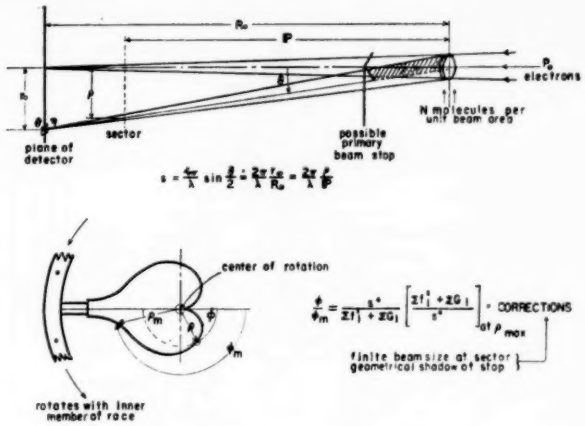

FIG. 2.

the diameter of the primary beam, to remove this beam about 1 cm after the point of maximum gas density.[4]

Returning to Fig. 3, 7 is a gate valve which permits shutting off the main body of the apparatus from the camera section by raising a flap (not shown), actuated through the ground joint, 7a. Thus air may be admitted to the camera, plates changed, and the section prepumped through 12, without cooling down the diffusion pumps. Item 8 is the sector assembly; it consists of a precision race the inner member of which carries the heart-shaped mask (8a), several friction drives, and a Wilson seal[5] through which the rotational motion is introduced into the vacuum. The driving motor is located about three feet from the beam to reduce the effects of stray magnetic fields. Directly behind the sector is another platinum cup (9) on an insulated mount. It is not only useful for setting the beam current so that reproducible exposures may be made, but is essential for the positioning of the front beam stop. The latter is adjusted so that on the most sensitive range, the Vance-type electrometer reading is at a minimum. Item 10 is a hexagonal drum which carries one fluorescent and five photographic plates (spectroscopic VD or microfile for sector work; Eastman Commercial or Panatomic X for visual work). The fluorescent pattern may be observed through the window by means of the front surface mirror, 10a. The drum is rotated by means of gears attached to the flat ground joint, 10b. Various lengths of tubing may be inserted at 11 to allow extension of the sample-plate distance to about 48 cm.

The recent modifications which will be described in a forthcoming paper were made in the construction of the nozzle (6, 6a) sector and camera (8–12) sections.

The accelerating voltage is electronically controlled;[6]

[3] To reduce the magnitude of the extraneous contribution arising from the scattering of the primary beam by the escaped gas and by the residual gas in the camera, a stop was introduced to remove the beam about one cm after the point of maximum gas density. However, this stop also casts a shadow which must be considered in computing the sector shape, as also must be the effect of finite beam size at the sector and extraneous slit and multiple scattering. Consequently, we have replaced (2) by a rather complicated function which formally may be written

$$\left[\frac{\phi}{\pi}\right]_{\text{corr}} = \frac{s^4}{\Sigma f_i^2 + \Sigma G_i} \cdot \frac{1}{\text{shadow function}} \cdot \frac{\text{infinitesimal}}{\text{finite beam}} \cdot \left[\frac{\text{extraneous}}{\text{scattering}}\right]. \quad (3a)$$

Since these computations involve averaging processes, we found it more convenient to compute the scattering intensity distribution to be expected under our operating conditions, assuming an approximate sector opening; then we correct the assumed transmission coefficient (ϕ/π) so that a flat background results.

[4] Since the positioning of this stop is extremely critical, a vertical v-shaped strip, the position of which is controlled by a micrometer operating on a 3/1 lever arm is used on the high temperature nozzle (Fig. 3). The first such stop which we introduced (Fig. 5) was circular and hence had to be accurately positioned both vertically and horizontally. It was controlled through a bellows attachment by means of fine thread screws, as shown in the latter figure.

[5] R. R. Wilson, Rev. Sci. Inst. **12**, 91 (1941).

[6] Bauer, Hastings, and MacMillan, Rev. Sci. Inst. **14**, 30 (1943).

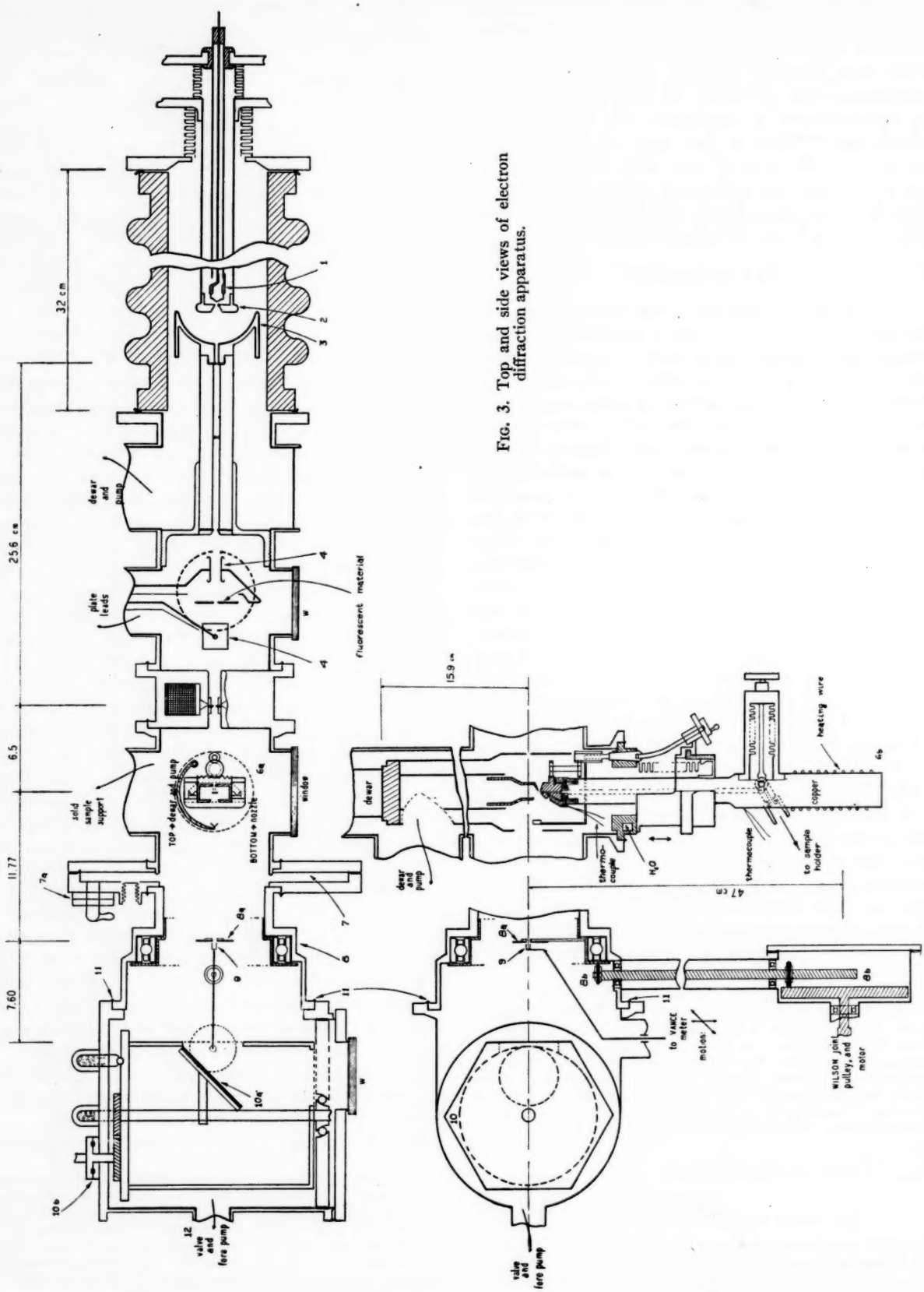

FIG. 3. Top and side views of electron diffraction apparatus.

it may be set at any desired value up to about 55 kv and measured to a precision of several hundredths of a percent by a Type K potentiometer spanning a calibrated potential divider. The beam is space-charge limited.[7] Its current (0.1–25 μa) is determined in a gross manner by the distance of the filament tip from the hole in the self-biased cup; it may be finely controlled by the magnitude of the biasing resistor. Exposures are pre-set by selecting one of a number of resistors across which a capacitor is discharged; when the potential drops to a given point a thyratron fires and switches on 2000 v across the first set of deflecting plates. Periods ranging from 0.07 to 30 sec. are available. For reference, the controlling circuits are given in Fig. 6. The focused spot is observed by means of a long focal length microscope (20× linear magnifications); gold leaf spread on uranium glass affords a low intensity, no-grain screen.

A good vacuum is maintained by two diffusion pumps ($3\frac{1}{2}$ in. diameter) and three liquid-air traps. Low pressures may be measured by McLeod and ion gauges, while for higher pressures and leak hunting a Pyrani gauge was connected to the line at the fore-vacuum end of the diffusion pumps. Between the latter and a Hypervac 20, a baffled liquid-air trap was inserted. This not only keeps the mechanical-pump oil from becoming contaminated by the substances studied, but also allows an increase of about a factor of ten in the sensitivity of the Pyrani gauge measurements due to the elimination of the mechanical-pump oil vapors from the vacuum system.

OPERATIONAL DATA

Regarding the construction of the sector, we need only indicate that the function (3a) (see reference 3) is transferred onto 0.012 in. aluminum foil[8] by means of an indexing head on a milling machine (ϕ *vs.* ρ), and the two halves of the heart-shaped figure cut and filed simultaneously to a precision of better than 0.001 in. The last operation is performed under a microscope, linear magnification approximately 50. Since the fractional error for each atom species arising from our incomplete knowledge of the atomic scattering functions is

$$\frac{d\phi}{\phi}=n_i\frac{2F_i(Z-F)_i}{\sum(Z-F)_i^2+\sum G_i}\frac{dF_i}{F_i}, \qquad (4)$$

it is the region of small ϕ which is most sensitive, Fig. 7. However, the accuracy in that region is also limited by the extraneous slit and multiple scattering, and by the small net opening in the sector. To reduce the magnitude of the latter, it has been customary to use two sectors, covering the ranges $0.5<s<8$; $0.5<s<20$. (In many cases, the use of a beam stop close to the nozzle exit eliminates the need for the 0.5–8 sector.) After filing, the sector is mounted and carefully centered so that its geometrical center is within 0.0015 in. of its center of rotation.

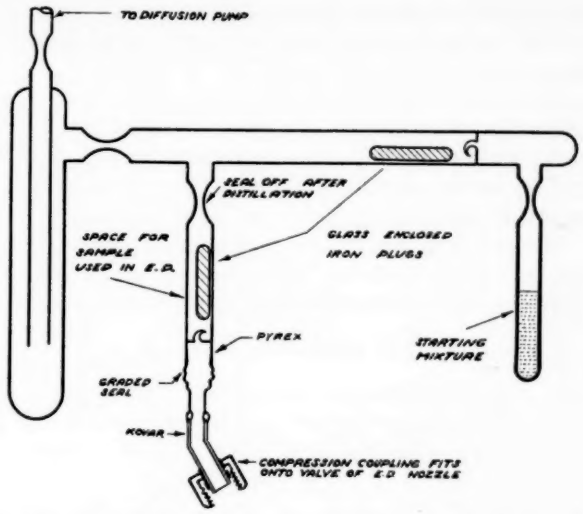

FIG. 4. Sample holder; illustrates manner of handling materials of low volatility without allowing contact with atmosphere of stopcock grease.

Since Eq. (2) implies that a new sector is to be cut for every compound, it is of interest to consider the conditions under which a single sector will serve for a variety of compounds. Inspection of families of reduced atom form factor curves $[(Z-F)/Z]_i$ suggests that a single sector might be satisfactory for all molecules which consist predominantly of elements within one row of the periodic table. The use of quadratic or cubic sectors has also been proposed. Figures 8(a) and 8(b) are curves showing the backgrounds which would result were the sector openings made proportional to s^2 and s^3, respectively, for a variety of compounds. If the useful range of photographic density is 0.05 to 1.5, s^2 or s^3 sectors will bring most of the pattern within this density range. However, it is clear that the "drawing-in" of a background is a highly subjective operation under such conditions.

Typical conditions for gas diffraction photography are:

beam current	0.1–2.5 μa	film	microfile
exposure time	0.2–0.5 sec.	number of exposures	3–6
reservoir pressure	10–50 mm Hg	1-min. interval between spurts	

sector revolves at approximately 1200 r.p.m.

We have calibrated both microfile and spectroscopic VD plates by running a series of unfocused spot exposures for varying intervals, and found that over the range 0.05–1.00 the density is directly proportional to the intensity.

After aligning the beam with the center of the sector, the current is set at the desired level, the front beam stop interposed and the exposures made. The beam position is then checked, for if it had moved during the exposures

[7] S. G. Ellis, J. App. Phys. **18**, 879 (1947) and references cited therein.

[8] Sheet brass or foil of higher atomic number might be preferable; extraneous scattering by edges might thus be reduced.

to the extent of several thousandths of an inch, an incorrect sector function will have been used, particularly for low values of s.[9]

Unretouched microphotometer recordings of electron diffraction photographs of carbon tetrachloride taken under various conditions are reproduced in Fig. 9, while in Fig. 10 the usefulness of the sector in the study of crystallite size in surface layers[10] is demonstrated.

We have now reached the final point, which relates to the manner of reducing the microphotometer data to intensity values. Two objective procedures have been

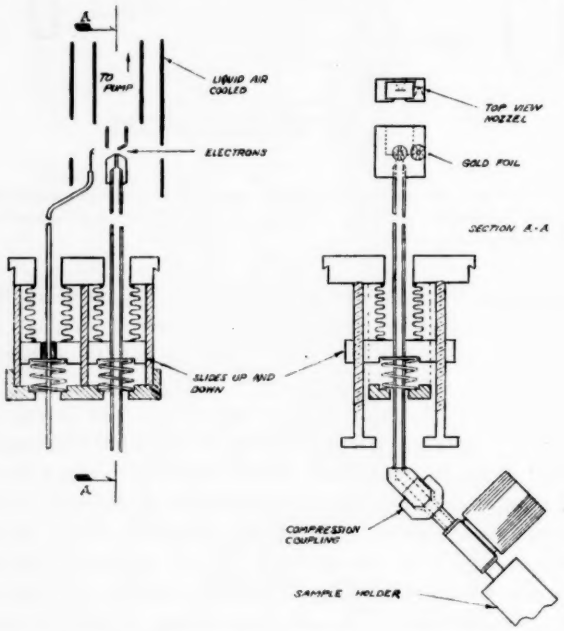

FIG. 5. Room temperature nozzle, with insulated round beam trap.

utilized in drawing in the background, which on the basis of Eq. (3) may be assigned the value unity. Both depend on the availability of theoretical intensity curves (i.e., of the molecular part) for models which are not far from the correct structure.

(A) Average values are computed for the ratios of intensities of adjacent maxima to minima from several theoretical curves. Points are then selected on the microphotometer record for which, if the background were drawn through them, the corresponding ratios for adjacent maxima to minima would result. The best smooth curve through these points is taken as the background.

(B) Average values are computed for the s positions at which the theoretical curves cross from positive to negative values, and vice versa. These are plotted on the microphotometer record and the best smooth curve drawn through them is taken as the background. Experience has shown that the background curves are not sensitive to the selection of models used in the averaging processes when these nearly represent the correct structure, and that the backgrounds deduced by means of procedures (A) and (B) differ very little from each other. Models which depart appreciably from the correct structure will lead to points which scatter badly from a smooth curve. Then, as a first approximation, the intensity of the molecular term relative to the atomic terms (taken as unity) is the ratio of the density indicated by the microphotometer trace to that of the background at each value of s. This is valid only when extraneous scattering and other factors which disturb the theoretical relation (3) between the atomic and molecular terms, are negligible in magnitude.

THE PHOTOGRAPHS

Electron diffraction pictures of neopentyl, and silico-neopentyl chlorides were taken on samples generously given to us by the late Dean F. C. Whitmore. Pictures with and without a sector were taken of both compounds. Three sectors were used for the neopentyl chloride covering the range from $s=0$ to $s=9$, 14, and 20, respectively, while two sectors were used for the silico-neopentyl chloride going out to $s=11$, and 16.5, respectively. A visual estimate of the $I(s)$ curve based on pictures taken with and without a sector for the neopentyl chloride is shown in Fig. 11, curve A, while that for the silico-neopentyl chloride is curve C. The points of inflection of the visual $I(s)$ curves were obtained by direct measurement on a comparator; the hairline being set in each case on the point of apparent maximum or minimum density. The amplitudes of these visual $I(s)$ curves were determined by drawing in a background and arbitrarily setting the most intense peak equal to ten and the least intense equal to a half-unit, above this background. The intermediate region was then estimated on this scale. Curves B and D are the result of microphotometer measurements on sector pictures of neopentyl chloride and silico-neopentyl chloride, respectively. The positions of the maxima and minima for these curves were determined by drawing in a background (as indicated in the previous section), and choosing those points which showed the largest difference from this background.

The s_0 values of the maxima and minima for the visual curves are given in Tables I and II, while those for the sector curves are indicated in Fig. 11. The self-consistency among the individual visually estimated s_0

[9] Slight changes in beam position may be due to fluctuations in the effective electrostatic potential on the deflecting plates due to adsorbed oil films; see A. E. Shaw, Phys. Rev. 44, 1006 (1933). The beam position may also be affected by slight motions of the filament due to mechanical vibrations.

[10] In this connection, we should specify that the resolution obtainable with our instrument is 1/83, an average value of that measured for the (220), (311), (331), and (420) rings of gold. The definition of resolution is the one given by J. Hillier and R. F. Baker, J. App. Phys. 17, 12 (1946):

$$\left(\frac{\Delta d}{d}\right)_{hkl}=\frac{1.73w}{2}\frac{d_{hkl}}{R}, \qquad (4a)$$

wherein w is the observed width at half-maximum of the trace for the corresponding ring.

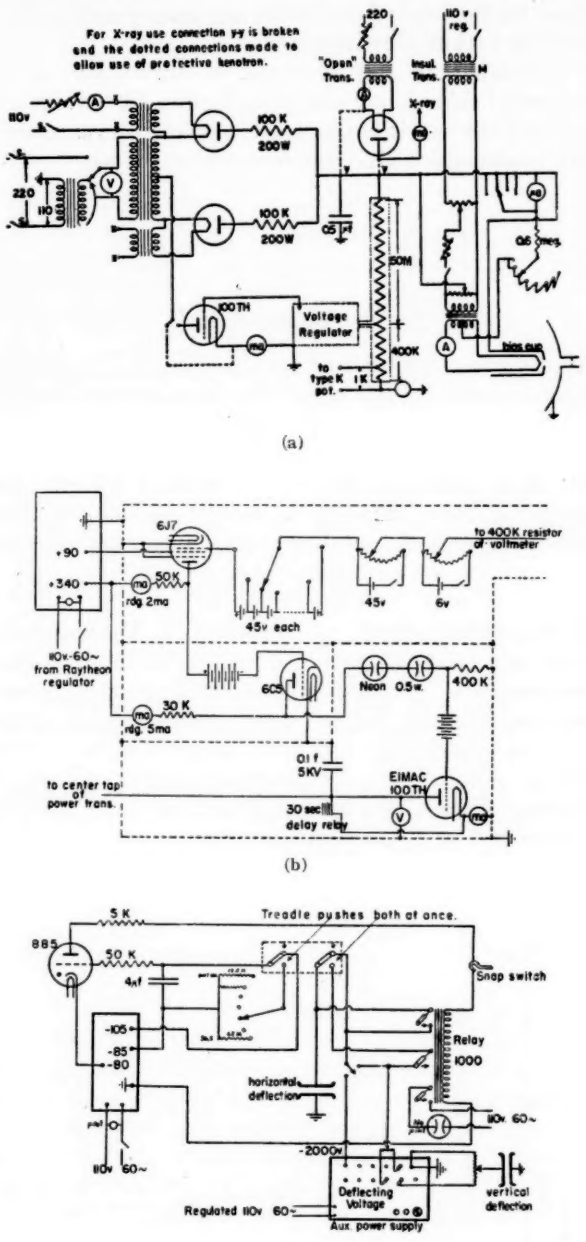

FIG. 6. Electrical circuits, schematic. (a) High voltage, (b) voltage regulator, (c) timer.

values is such that the probable error is of the order of a half of one percent. In the case of the sector curves, the s_0 values were measured to a tenth of an s unit and to this accuracy no deviations were observed among six different microphotometer records. In the case of the neopentyl chloride the sector curve could not be extended beyond $s=14$, even though a sector was cut for $s=20$, because the intensity was so low; at the last observed maximum ($s\simeq 12.5$) the intensity at the peak was only four percent above the background. The amplitudes of the sector $I(s)$ curves are in doubt in the region $s\leqslant 4$ because of the extraneous background introduced by the undeviated beam and by multiple scattering.

A comparison of the visual and sector $I(s)$ curves shows a very good check in the case of the silico-neopentyl chloride. For the neopentyl chloride, however, there is an appreciable difference between the two curves from $s>8$. This difference will be discussed in more detail when a comparison between theoretical and observed $I(s)$ curves is made.

INTERPRETATION OF THE DATA

Radial Distribution Curves

Radial distribution curves computed from the visual $I(s)$ curves are shown in Fig. 12 together with "synthetic" distribution plots. The method used was that of Walter and Beach.[11] The synthetic radial distribution curves are semi-empirical in nature since they are based on an average form of the peaks (arbitrarily terminated for $|r-r_{ij}|=0.325$A) for the several different molecules examined by Walter and Beach. A constant shape has been assumed for all distances between directly and adjacently bonded atoms; the standard curve was then multiplied by the weight factor Z_iZ_j.

For the neopentyl chloride we have been able to match the synthetic curve B to the calculated one A

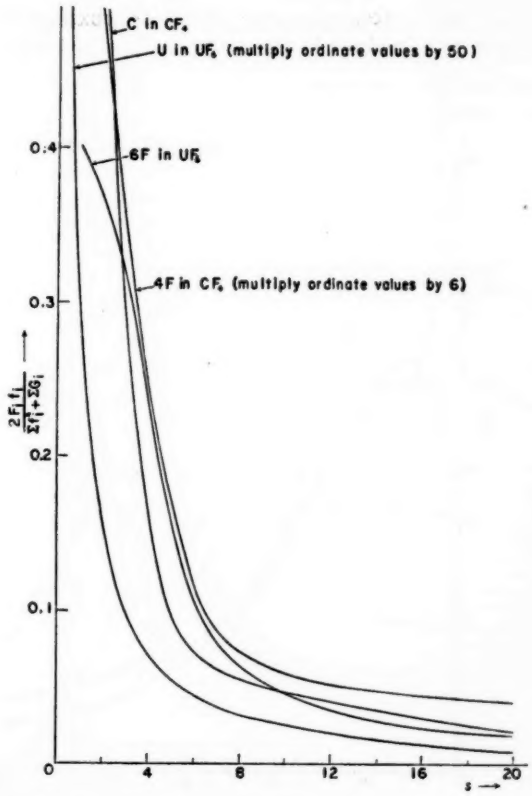

FIG. 7. The fractional error introduced in the sector opening for a given fractional error in x-ray atom form factor.

[11] J. Walter and J. Y. Beach, J. Chem. Phys. 8, 601 (1940).

rather well except for the peak at $r=1.57$A using the model:

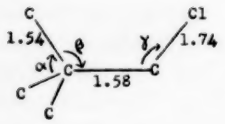

$\alpha=108°$
$\beta=111°$
$\gamma=111°$
C−H=1.09A
$\angle$HCH=109.5°.

The discrepancy at $r=1.57$ might be avoided by lengthening all the C−C bonds, but then other difficulties are introduced. Another possibility would be to widen somewhat the "synthetic" peak shapes. If one assumes the normal C−C distance of 1.54 and C−Cl 1.76, the discrepancy becomes more marked as can be seen from Fig. 12, curve C. The sharpness of the peaks at 3.19 and 4.13 which result from

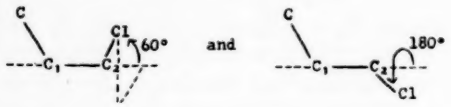

respectively, indicates that the barrier height restricting rotation about the C_1-C_2 bond is relatively large compared to kT. Hence these C⟷Cl (C−C) contributions to the scattering curve can be approximated by constant r_{C-Cl} values in the $\sin sr_{C-Cl}/sr_{C-Cl}$ terms; to allow for the limited oscillation the corresponding temperature factors were increased.

Calculated D and synthetic E curves for siliconeopentyl chloride are also given in Fig. 12. The match between the two is not as good as in the previous case. The model which gives the best agreement has

Si−C	1.88A
C−Cl	1.73A
C−H	1.09A

all angles tetrahedral.

A distortion similar to the one used for neopentyl chloride is not satisfactory. The calculated curve does not show prominent Si−C(H) distance whereas the synthetic curve indicates a strong maximum at this point. This lack of resolution may be due to the influence of the very large Si−C(Cl) contribution. The match for $r>3$ is necessarily poor due to the method of constructing the "synthetic" curve, since no direct allowance was made for rotation about the Si−C bond, which becomes appreciable for these longer distances. This clearly indicates that the barrier to rotation is lower in the case of the silicon compound that the corresponding carbon one, as is to be expected.[12]

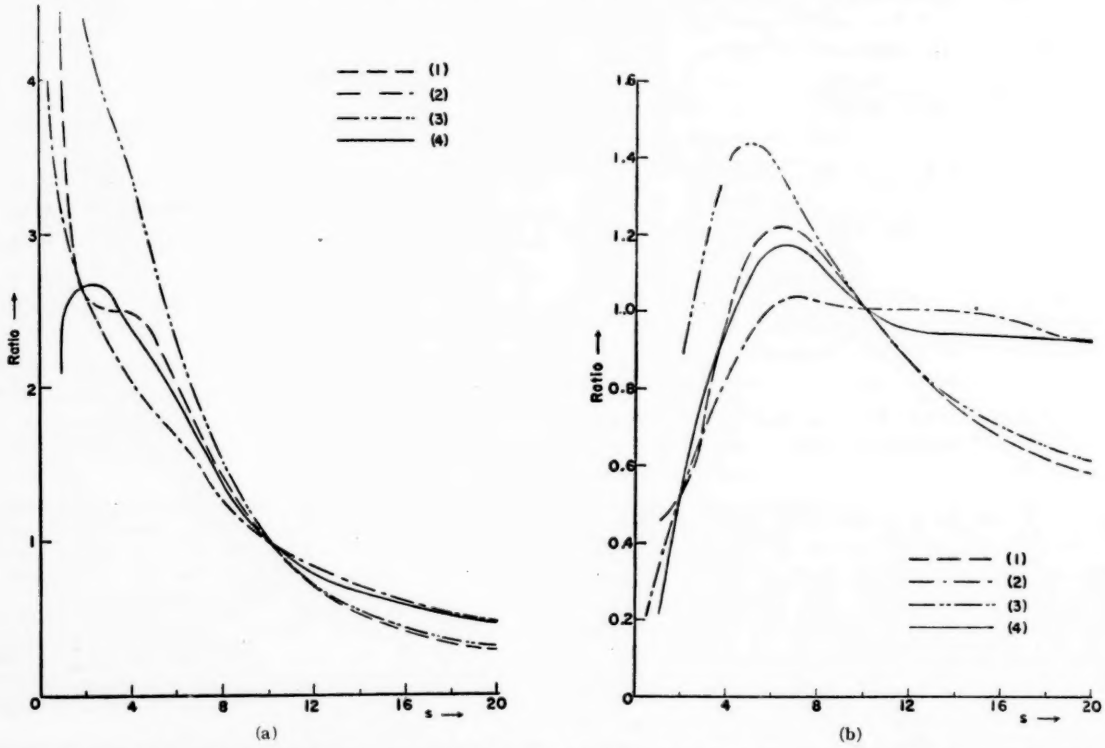

FIG. 8. Backgrounds expected for various compounds when (a) s^2 sectors and (b) s^3 sectors are used. Ordinates are ratios of backgrounds expected to that computed with Eq. (2), for: (1) CF_4, (2) UF_6, (3) H_2CO, (4) CI_4.

[12] Aston, Isserow, Szasz, and Kennedy, J. Chem. Phys. **12**, 336 (1944).

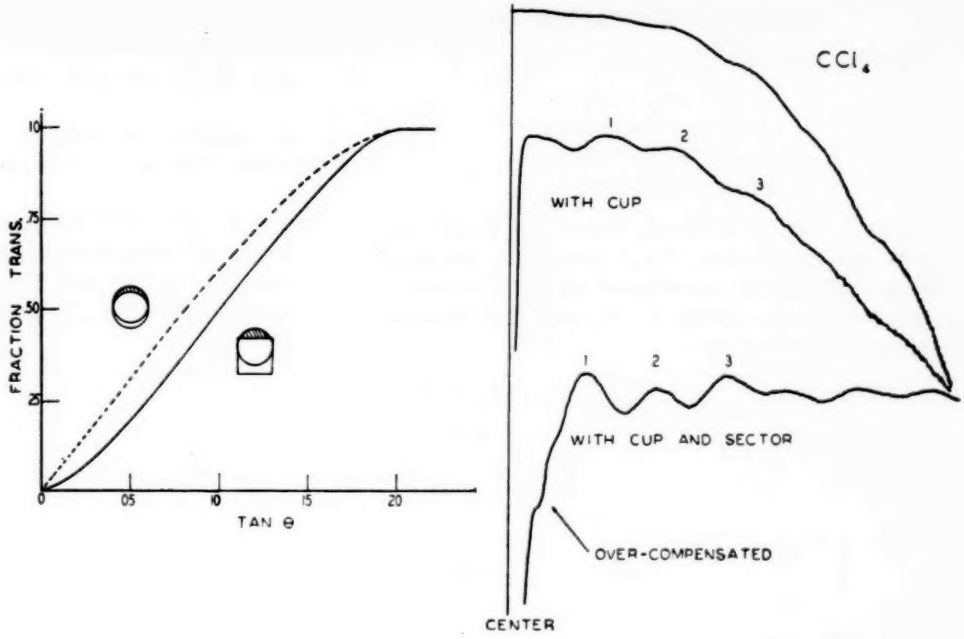

FIG. 9. Left—the geometrical shadow, for an infinitesimal sample, cast by a square and by a round front beam stop. Right—typical unreduced microphotometer records for gas diffraction.

The largest error introduced in the radial distribution curve is due to the improper integration procedure used in the Fourier inversion. It is hoped that a better numerical integration based on the method of Lanczos-Danielson[13] or with an IBM punched card system[14] will be made. When this is carried through, the radial distribution curve will furnish valuable information about internal rotation.

Correlation Method

In order to check the conclusions reached by fitting synthetic radial distribution curves to the radial distribution curves obtained from our intensity data, theoretical $I(s)$ curves for several models for each compound were computed and compared with the patterns observed. In making these comparisons we found that the visual curves, A and C (Fig. 11), correspond fairly well to intensity patterns computed according to the simple expression

$$\sum_{ij}{}' Z_i Z_j \frac{\sin sr_{ij}}{sr_{ij}} \exp(-a_{ij}^2 s^2), \qquad (5)$$

where the a_{ij} is assumed to be zero for all but those pairs whose distances vary due to hindered rotation about single bonds. The microphotometer recordings (B and D of Fig. 11) show considerably less detail than is apparent to the eye. They should be compared to curves computed by means of Eq. (3). In the latter case, not only should one consider the general form of the curves, but also the measured intensities relative to the background taken as unity. Since the maximum deviations from the background are only 12 percent, the structure sensitive features often are only of the order of one percent. But in attempting to realize an accuracy of one percent in the total density (which is equivalent to about eight percent of the molecular contribution at small s), we are approaching the limit of photographic measurements due to grain size, inhomogeneities in the emulsion, and variations in development.

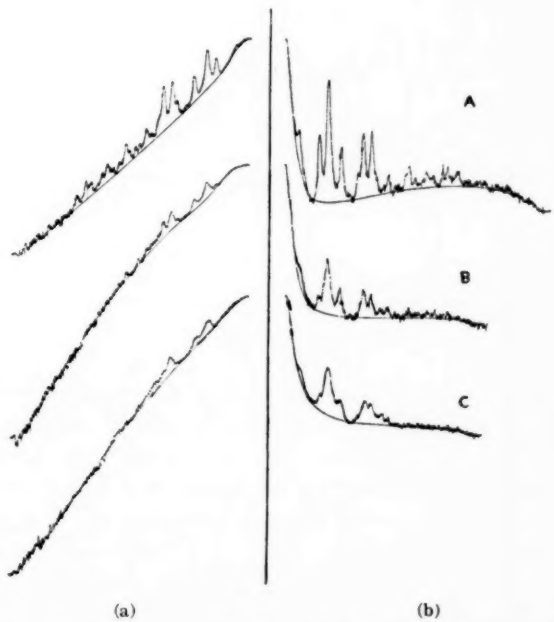

FIG. 10. Microphotometer records of electron diffraction patterns of powders, illustrating the usefulness of the sector as an aid in estimating diffraction line widths. (a) No sector. (b) Empirical sector. Spinels of decreasing size.

[13] Danielson and Lanczos, J. Frank. Inst. **33**, 365, 435 (1942).
[14] Shaffer, Schomaker, and Pauling, J. Chem. Phys. **14**, 659 (1946).

Neopentyl Chloride (Fig. 13)

We considered the following models:

All C−C=1.54A
C−H=1.09A
C−Cl=1.76A
all angles tetrahedral.

In curve A (Eq. (3) was used, wherein the integration over the distribution $P(r_{ij})$ was given the usual $\exp(-a_{ij}^2 s^2)$ form) we included all distances except the variable C−Cl and C−H, with the following temperature factors:

Atom Pair	a_{ij}^2	$\langle\Delta^2\rangle_{Av}=(2a_{ij}^2)^{\frac{1}{2}}$
C−C, C−Cl, C−H	0.0015	0.055A
C(C)(C)−C	0.0022	0.066A
C(Cl)(C)−C	0.0043	0.093A
C(H)(C)−C		
Cl(H)(C)−C		

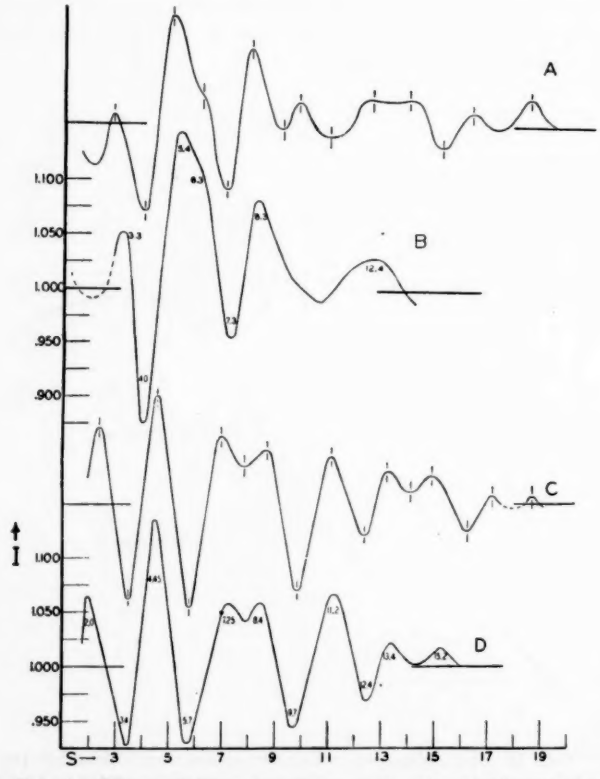

FIG. 11. Observed intensity patterns. A—visual estimates for $(CH_3)_3C-CH_2Cl$, B—microphotometer record $(CH_3)_3C-CH_2Cl$, C—visual estimate for $(CH_3)_3Si-CH_2Cl$, D—microphotometer record $(CH_3)_3Si-CH_2Cl$.

$\langle\Delta\rangle_{Av}$ is equal to the root mean displacement from the equilibrium separation of the particular atom pair, due to zero point energy.

In omitting the variable terms we have, in effect, assumed very large a_{ij}^2 values for these distances.

B and B′. The same distances as in Model A plus a staggered configuration about the C−C bond were assumed, and the following additional temperature factors were used:

Atom Pair	a_{ij}^2	$\langle\Delta^2\rangle_{Av}=(2a_{ij}^2)^{\frac{1}{2}}$
C(C)(C)−C	B 0.0050	0.1A
C(C)(H)−C	B′ 0.0050	0.1A
C(C)(H)−C	B 0.0050	0.1A
C(H)(H)−C	B′ 0.0100	0.142A

D and D′. In Models D and D′ we assumed the distances and angles deduced from our radial distribution analysis. With regard to the temperature factors, D and D′ correspond to B and B′, respectively.

C. In Model C the distances and angles were again those derived from the radial distribution analysis computed, however, according to Eq. (5) with the a_{ij}^2's=0 except for

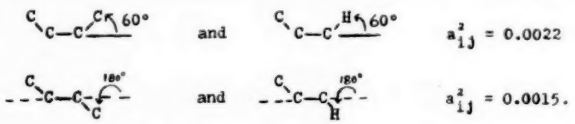

Comparison of the curves in Figs. 11 and 13 shows that the structure sensitive regions are at $s=6.3$ and in the intervals $9<s<12$ and $13.5<s<17.5$. Curves A, B, B′, and D show no distinct hump at $s=6.3$; however, the peaks are definitely asymmetric and the magnitude of the hump as indicated may be exaggerated due to the difficulty of estimating a small fluctuation of intensity in a region of sharply falling intensity ($5.2<s<7$). In curve C there is a strong suggestion of a hump at $s=6.3$ which, if present in a photograph, would appear to the eye as a distinct shelf. The structure apparent visually in the region $9<s<12$ is not properly reproduced by

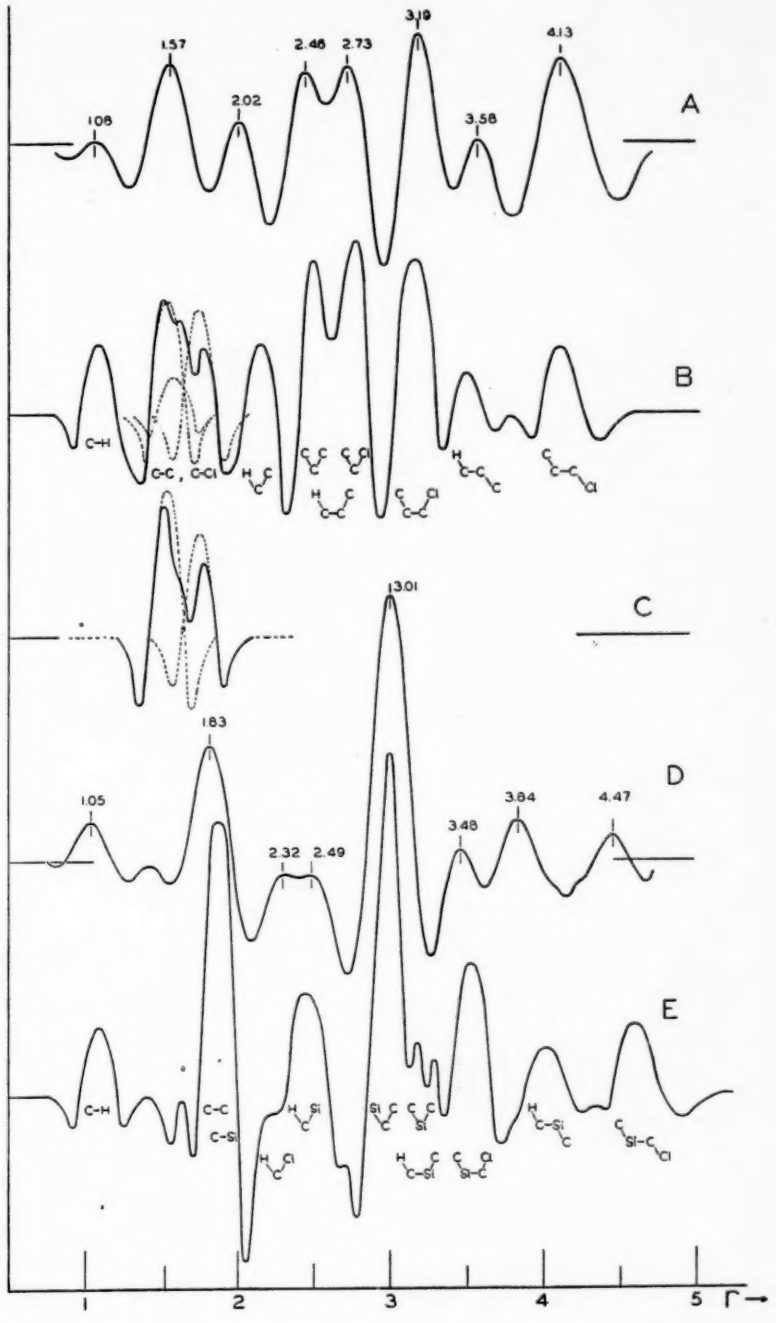

FIG. 12. Radial distribution curves. B, C, and E are synthetic. In these, the widths of peaks arising from terms such as 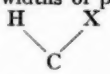 and 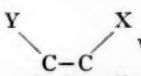 were made 1.5 times the widths of peaks from directly bonded or adjacently bonded pairs, in order that their correspondingly larger temperature factors be matched.

curves A, B, B′, and D′, but fairly well in C and D. The same is true in the region $13.5 < s < 17.5$.

Curve C is in best qualitative agreement with our visually observed $I(s)$ curve. A curve computed in a manner similar to C, but with the distances and angles of model A (undistorted) is not acceptable. Furthermore, D and D′ are more like our visually observed curve than are B and B′. Hence, we conclude that although the distortion is barely outside our experimental error it is probably real.

Unfortunately, our microphotometer record is not sufficiently detailed to permit a more definite selection of a model. The quantitative comparison of the experimental and theoretical $I(s)$ curves is presented in Table I. Our best values for the interatomic distances and angles in neopentyl chloride are:

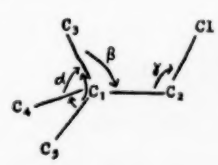

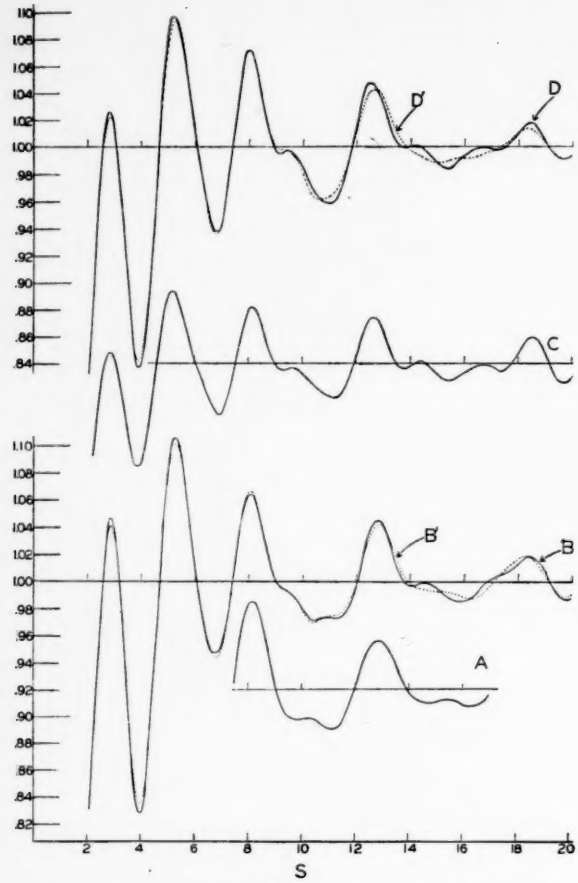

FIG. 13. Computed intensity curves for $(CH_3)_3C-CH_2Cl$.

All other

$C-Cl=1.74A\pm0.03$
$C_1-C_2=1.58A\pm0.04$
$C-C=1.54A\pm0.03$
$C-H=1.09A$ (assumed)

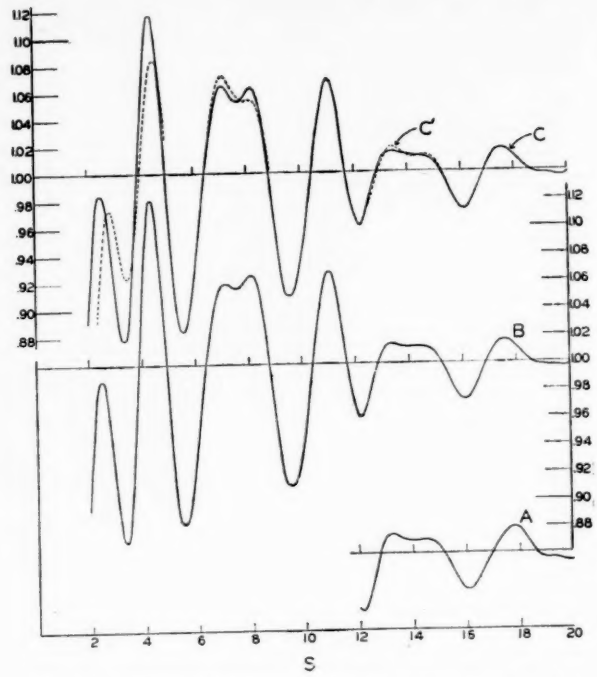

FIG. 14. Computed intensity curves for $(CH_3)_3Si-CH_2Cl$.

$\angle HCH=109.5°$ (assumed)
$\alpha=108°\pm2°$
$\beta=111°\pm2°$
$\gamma=111°\pm2°$.

Silico-Neopentyl Chloride (Fig. 14)

The following models were considered:

A.
$C-Si=1.88A$
$C-Cl=1.73A$
$C-H=1.09A$
all angles tetrahedral.

TABLE I. Neopentyl chloride.

Max.	Min.	s_0 (vis.)	I (vis.)	$\frac{s_0 \text{ comp.}}{s_0 \text{ obs.}}$(C)	$\frac{s_0 \text{ comp.}}{s_0 \text{ obs.}}$(D)	I_{comp}(D)	I_{mpr}(D)	$\frac{I_{comp}}{I_{mpr}}$
1		2.86	+1	0.983	0.986	1.027	(1.107)	
	2	4.04	−8	(0.948)	0.965	0.838	0.875	0.957
2		5.06	+10	1.008	1.029	1.097	1.142	0.960
2*a*		6.02	+3	1.023				
	3	7.11	−6	0.968	0.959	0.938	0.955	0.982
3		8.02	+7	1.006	0.998	1.072	1.080	0.992
	4	8.91	$-\frac{1}{2}$	0.979	1.028	0.995	0.953	1.044
4		9.80	+2	0.979	0.961	0.997		
	5	11.39	−3.5	0.975	0.964			
5		12.62	+4	0.994	0.990	0.958		
	6	13.23		1.034	1.043	1.047	1.045	1.001
6		13.93	+3.5	1.027	1.020			
	7	15.21	−2	1.012	1.009			
7		16.30	+3	1.023	1.030			
	8							
8		18.56	+1	0.992	0.994			
				Average=1.000	0.998			
				Mean deviation=0.018	0.024			

This model corresponds to the one deduced from the radial distribution curve. It was computed using Eq. (5), assuming $a_{ij}^2=0$ for all pairs except for those distances which vary due to rotation. The temperature factors used for the latter were:

Atom Pair	a_{ij}
C–Si–C–Cl (180°) and C–Si–C–H (180°)	0.0015
C–Si–C–Cl (60°) and C–Si–C–Cl (60°)	0.0022 .

B. The same distances and angles were assumed as in model A, but Eq. (3) was used. The varying C–Cl and C–H distances were omitted. The a_{ij}^2's used for curve B were the same as those used for the carbon compound.

C and C′. This model is identical with B, including a staggered configuration about the C–Si bond. The additional temperature factors were:

Atom Pair	a_{ij}^2
C–Si–C–Cl	C 0.0050
C–Si–C–H	C′ 0.0050
C(Cl)–Si–C	C 0.0180
C(H)–Si–C	C′ 0.0100

The regions of comparison for this substance are $6.5<s<8.5$ and $13<s<15$. The visual and microphotometer curves (C and D of Fig. 11) are in complete agreement. In the region $6.5<s<8.5$, A is very similar to model B which reproduces the relative intensities of the visually observed doublet. Model C, having a larger temperature factor for the varying pairs than does C′, is in closer agreement with the relative intensities of the doublet as deduced from the microphotometer record. Neither of the models reproduces exactly the relative intensities of the doublet occurring in the region $13<s<15$. The fluctuation above or below the background, however, is not more than one percent so that the doublet in curves C and D of Fig. 11 may actually not be as prominent as drawn.

Curve C (Fig. 14) is in best agreement with the microphotometer record; the large temperature factors used indicate a relatively low barrier hindering rotation about the C–Si bond as compared with the barrier in neopentyl chloride. This checks the conclusions reached from the radial distribution method. The quantitative comparison is given in Table II. The best values for the interatomic distances and angles in silico-neopentyl chloride are:

C–Si = 1.88A±0.04
C–Cl = 1.73A±0.03
C–H = 1.09A± (assumed)
all angles = 109.5°±2°.

DISCUSSION OF RESULTS

Visual and Sector Methods

Firstly, the introduction of a stop just past the point of diffraction has several advantages. It helps clear up the inner portion of the photograph so that the s_0 values for this region may be obtained more easily. At the same time it enables one to make more reliable intensity estimates of the inner portion of the diffraction pattern. The introduction of a beam stop would probably require

TABLE II. Silico-neopentyl chloride.

Max.	Min.	s_0 (vis.)	I (vis.)	$\frac{s_0 \text{ comp.}}{s_0 \text{ obs.}}$(C)	I_{comp}(C)	I_{mpr}(C)	$\frac{I_{comp}}{I_{mpr}}$
1		2.38	+7	1.046	0.984		
	2	3.47	−9	0.962	0.878	0.927	0.947
2		4.54	+10	0.966	1.117	1.135	0.984
	3	5.87	−10	0.952	0.884	0.930	0.950
3		6.95	+6	1.021	1.064	1.057	1.006
	4	7.81	−½	0.983	1.054	1.043	1.010
4		8.68	+5	0.943	1.063	1.058	1.004
	5	9.81	−8	0.977	0.910	0.945	0.962
5		11.09	+5	0.994	1.068	1.066	1.002
	6	12.33	−3	0.991	0.961	0.970	0.990
6		13.15	+3	1.020	1.015	1.021	0.994
	7	14.06	−½	1.001	1.012	0.988	1.024
7		14.86	+2.5	0.985	1.011	1.017	0.994
	8	16.21	−3	0.993			
8		17.14	+½	1.022			

Average = 0.990
Mean deviation = 0.022

very little redesigning of most existing cameras. However, a serious objection against the use of a beam trap along with a sector is the difficulty of properly allowing for the shadow function in cutting the sector. Another undesirable feature is the extraneous edge scattering when the width of the stop is just a little greater than that of the primary beam.

Secondly, the sector technique is the only reliable method which can be used to obtain intensity data with photographic detection. Its inherent accuracy is limited by the fact that the total electron scattering is recorded, whereas structure determinations depend on the molecular term only. For this reason, the sector method will not displace the visual method for structure determinations; however, it will be of invaluable aid in deciding between parameters on the basis of, which member of a doublet is the more intense, the height and presence of shoulders, etc. It will also be useful for estimating the magnitude of large temperature factors. Use of the sector does provide a means for calibrating the visual method.

With sector data there are three checks on the maximum variation of the parameters which can be allowed. They include the two employed in the visual method; *viz.*, the matching of the synthetic radial distribution curves with the one obtained from the data, and the matching of over-all shape (relative peak heights) as well as the s_0 values of the theoretical $I(s)$ curve with these observed. In addition, one may compare point by point the observed intensity with that of the theoretical $I(s)$ curve.

Reference to the last column of Tables I and II shows that for values of $s>7$ the computed intensities check very well with the measured ones. In the region $s<7$, the drawing-in of the background cannot be performed in a satisfactory manner. Such disturbing effects as arise from finite sample and beam dimensions, multiple scattering and the lack of good atom form factor values are largest for low s values. With regard to the determination of reliable coherent and incoherent atom form factors, a study of a series of diatomic and simple polyatomic molecules is contemplated.

Regarding $(CH_3)_3C-CH_2Cl$ and $(CH_3)_3Si-CH_2Cl$

The two molecules studied permit an assessment of the applicability of electron diffraction technic to the study of internal rotation. For the neopentyl chloride, a very satisfactory fit was obtained between computed and synthetic radial distribution curves. Models without distortion, or those in which normal covalent distances (all C−C 1.54; C−Cl 1.76) were assumed, could not be made to fit. The radial distribution analysis also indicated that the configuration was a staggered one with relatively little motion about the C−C bonds. The correlation procedure confirmed these conclusions rather well. For the silico-neopentyl chloride the radial distribution curve indicated a staggered configuration with a low barrier to rotation about the C−Si bond, as well as a shortening of the C−Cl distance. The correlation method confirmed these conclusions also. The intensity data were valuable in determining the magnitude of the temperature coefficient in the silicon compound. However, the present intensity data for the neopentyl chloride are not sufficiently detailed to enable one to make a clear-cut choice of temperature factors.

One may present plausible interpretations for the deviation of the distances and bond angles in these compounds from the values which are currently considered "normal." He may argue that two effects, both operating in the same directions, introduce distortions in neopentyl chloride. (a) The $-CH_2Cl$ group is sterically larger than the $-CH_3$ group; (b) the $-CH_2Cl$ group is electron seeking ($-I$) compared to the $-CH_3$ group. This tends to draw electron density toward the Me_3C-CH_2Cl bond, making it relatively more p and less s in character compared to hybridized, truly tetrahedral sp^3. As a result, the Me_3C-CH_2Cl bond is longer (1.58±0.04A) than the Me_3C-CH_3 bond (1.54 ±0.02A).[15] Further, the $\angle C_tC_1C_2$ angle is smaller (108±2°) than the corresponding angle in *t*-butyl chloride (111.5±2°);[16] it is rather, more like the nitrogen valence angle in trimethyl amine (108±4°).[17] It is doubtful whether the small apparent departure of the C−Cl distance from the sum of radii[18] (1.76A) or from that found in Me_3C-Cl (1.78±0.03A) is significant.

In the silico-neopentyl chloride no distortion about the silicon atom is observed; the average Si−C distance is equal to the sum of radii[18] (1.88±0.4A), and to that found in hexamethylcyclotrisiloxane (1.88±0.04).[19] The value reported for silicon tetramethyl is somewhat larger (1.93±0.03).[17] In this case, due to the larger $Si-CH_2Cl$ distance, the steric effect does not come into play, nor is the (−I) factor significant, since the Si−C bond has considerably more ionic character than the C−C bond. However, the Me_3SiCH_2-Cl is somewhat shorter (1.73±0.03A) than the C−Cl distance in *t*-butyl chloride.[16] Perhaps it is a consequence of the greater electron-seeking character of Me_3SiCH_2- compared to Me_3C- and Me_3CCH_2-;[20] this would tend to increase the s character of the C−Cl bond, and make it shorter.

ACKNOWLEDGMENTS

We wish to acknowledge the kindness of the late Dean F. C. Whitmore who furnished highly purified samples of the neopentyl chloride and silico-neopentyl chloride. We also wish to express our sincere thanks to Mr. H. S. Bush for his patience and cooperation in the construction of the apparatus.

[15] L. Pauling and L. O. Brockway, J. Am. Chem. Soc. **59**, 1223 (1937). F. Rogowski, Ber. Deut. Chem. Gesel. **72**, 2021 (1939).
[16] J. Y. Beach and D. P. Stevenson, J. Am. Chem. Soc. **60**, 475 (1938).
[17] L. O. Brockway and H. O. Jenkins, J. Am. Chem. Soc. **58**, 2036 (1936).
[18] V. Schomaker and D. P. Stevenson, J. Am. Chem. Soc. **63**, 37 (1941).
[19] Eleanor (Weller) Aggarwal and S. H. Bauer (unpublished).
[20] F. C. Whitmore and L. H. Sommers, J. Am. Chem. Soc. **68**, 481 (1946).

The Structure of Uranium Hexafluoride as Determined by the Diffraction of Electrons on the Vapor*

S. H. BAUER
Department of Chemistry, Cornell University, Ithaca, New York
(Received April 25, 1949)

The structure of uranium hexafluoride has been redetermined by electron diffraction. Special precautions were taken to eliminate sample contamination; both sector and non-sector photographs were analyzed. Even casual inspection of the photographs and microphotometer traces shows that insofar as this type of measurement is concerned, the structure of UF_6 is not a regular octahedron. The model which is in best agreement with the data is a distorted octahedron with three short (1.87A) and three long bonds (2.17A). However, a model with a center of inversion, possessing two short (1.87A), two medium (2.12A), and two long bonds (2.22A) cannot be eliminated.

The disagreement between the structures deduced from various technics is discussed, as are also possible experiments which might be done to resolve these differences.

INTRODUCTION

FROM the observed physical properties of uranium hexafluoride (v.p. of the solid 760 mm at 56.2°C), one would predict its structure to be highly symmetric, with the fluorine atoms arranged to form a protecting shell around the heavy central atom, so that the polarizability of the molecule as a whole is low. The question remains, however, whether all six bonds are equivalent. With an electron configuration for uranium . . . (Radon core) . . . $6d^4 7s^2$, $^5D_0$; it would be unwise to predict that the $7p$ orbitals do not enter in an hybridization scheme on bond formation, say, by promotion of some of the $6d$ or $7s$ electrons. Thus it is possible to make a variety of choices from the seven electron configurations proposed by Kimball[1] for a coordination of six, some requiring equivalent, others non-equivalent, bonds. Only those configurations which have a null magnetic moment are acceptable.

Insofar as the U—F distances are concerned, one could make a rough prediction. The structure of the metal has been found[2] to be a deformed hexagonal close-packed arrangement, with four of the twelve nearest neighbors moved in to appreciably closer distances than the other eight. Thus:

No. of neighbors:	2	2	4	4
Distance	2.76	2.85	3.27	3.36A.

Pauling[3] suggests that since the nearest neighbors are very nearly at four of the five corners of a trigonal pyramid, these bonds may be considered to be essentially covalent in nature, with the non-bonding electron pair ($7s^2$) occupying the fifth corner. Let us then assume that the covalent radius of uranium is approximately 1.4A. Furthermore, since the solid shows a structure not at all typical of a metal, it is safe to assume that its electronegativity is somewhere around 1.5. On hits basis, the smallest U—F distance expected is 1.9A, as computed according to the method of Schomaker and Stevenson.[4]

Broune and Pinnow[5] did investigate the structures of the hexafluorides of uranium, tungsten, and molybdenum. For each of these they report irregular octahedral configurations (holohedral orthorhombic symmetry), the three pairs of metal-fluorine distances having the ratios 1:1.12:1.22. For the uranium compound, this leads to 1.78, 1.99, and 2.17A for the metal-fluorine distances. At first glance such structures seem improbable, since we wish to believe in the equivalence of bonds between like pairs of atoms. Unfortunately, Broune and Pinnow gave no detailed description of the appearance of their photographs, and quote the $[(\sin\theta/2)/\lambda]$ values for the first six maxima only. Were one to accept these as correct, it becomes immediately obvious that the U—F distances cannot be equivalent, since the first differences in their $s_m \equiv (4\pi/\lambda)\sin(\theta_{max}/2)$ values are 3.41, 2.55, 2.20, 3.05, and 3.09; nearly equal differences would be obtained were the U—F distances equivalent.

During the last five years much information has been accumulated regarding the molecular constants of uranium hexafluoride, most of it pointing rather strongly toward a configuration more symmetrical than indicated by the work of Broune and Pinnow. The strongest arguments are, briefly:

(a) In the vapor, uranium hexafluoride has a negligible permanent electric moment.[6]

(b) The available Raman (R) and infra-red (IR) absorption data may be adequately accounted for[7] by assuming only six

* This paper is based on work performed under contract for the AEC. The major portion of this paper was presented as Columbia Report A-1209 (October, 1943), and was declassified on October 14, 1946.

[1] G. E. Kimball, J. Chem. Phys. **8**, 188 (1940).

[2] C. W. Jacob and B. E. Warren, J. Am. Chem. Soc. **59**, 2588 (1937).

[3] L. Pauling, *The Nature of the Chemical Bond* (Cornell University Press, Ithaca, New York, 1940), second edition, p. 413.

[4] V. Schomaker and D. P. Stevenson, J. Am. Chem. Soc. **63**, 37 (1941).

[5] H. Broune and P. Pinnow, Zeits. f. Physik, **B35**, 239 (1937).

[6] (a) C. P. Smyth and N. B. Hannay, Princeton Report A-2130. (b) Amphlett, Mullinger, and Thomas, Trans. Faraday Soc. **44**, 927 (1948).

[7] Bigeleisen, Mayer, Stevenson, and Turkevich, J. Chem. Phys. **16**, 442 (1948). See also, D. F. Heath and J. W. Linnett, Trans. Faraday Soc. **45**, 264 (1949).

TABLE I.

Level	Wave-length	Excitation removes	Min. vel. for excitation	$Z_{eff}(U)$	$\frac{15Z_FZ_F}{2.88}\ \frac{2.00}{6Z_FZ_U}$
				92	0.170
K	0.1066A	$1s$ electron	116.1 kv	90	0.173
L_I	0.5680	$2s$ electron	21.8		
L_{III}	0.7208	$2p$ electron	17.2	82	0.191
M_I	2.228	$3s$ electron	4.57		
M_V	3.491	$3d$ electron	3.55	74	0.210
N_I	8.628	$4s$ electron	1.44		

fundamental frequencies (3 R, 2 IR, 1 inact.). A complete assignment of the recorded lines has been made on the basis of a regular octahedral model. Furthermore, the entropy of the gas computed from the spectroscopic data, assuming a symmetry number of 24, checks the third law entropy[8] to within the experimental error, over the temperature range tested (273°K–348°K).

(c) X-ray diffraction data on the solid[9] (single crystal studies) can be accounted for by assuming a distorted octahedron, possessing a plane of symmetry, with two long U−F distances equal to 2.13±0.10A in that plane (hence in opposed positions), while the other four bonds extend in the girdle perpendicular to that plane with U−F=2.02±0.05A. The trigonal prism configuration was unacceptable on the basis of the electron diffraction data and was definitely excluded by the x-ray study.

We reinvestigated the molecular structure in the vapor with the hope of resolving the existing ambiguity. Two improvements were introduced: (α) To the best of our ability we eliminated possible contamination of the sample, prior and during diffraction, by water and pump-oil vapors; and (β) we employed a rotating sector so that the final patterns could be microphotometered, thus to present objective data. The subjective factor which is always present in the visual method of interpretation of electron diffraction photographs can no longer be cited as a possible source of the discrepancy.

ANALYSIS OF THE OPTIMUM CONDITIONS FOR AN ELECTRON DIFFRACTION INVESTIGATION

The assignment of a unique structure to uranium hexafluoride depends on (1) the determination of the U−F distances, and (2) the location of the F atoms with respect to one another. It is clear that for the first objective the F−F scattering should be reduced to a minimum, whereas for second, the F−F scattering should be made as large as possible, in comparison with that due to U−F. Since the intensity of scattering for a pair of atoms is roughly proportional to the product of their effective atomic numbers, a glance at the critical x-ray absorption wave-lengths of uranium proves very instructive.[10]

It is clear from Table I that the optimum accelerating potential for objective (2) is below 3550 v. Unfortunately, many difficulties are encountered in this low velocity range, most of which have not been investigated. Generally, electron diffraction work has been done utilizing potentials greater than 25 kv.

TREATMENT OF THE SAMPLE

Samples of UF_6 of known purity were submitted to us by Dr. W. L. Roth. The containers were made of nickel and were fitted with (W. Crane) sylphon valves; these were tested for vacuum leaks and "stabilized" prior to insertion of the samples. The samples were connected directly to the nozzle by means of a flared joint;[11] the apparatus was evacuated to about 5×10^{-6} mm Hg and the lead tubes from the valve to the nozzle were flamed. The sample tube was cooled in a dry-ice-acetone bath and the valve opened. No appreciable influx of gas was noted, indicating the absence of leaks in the sample holder, and of reactions which produce products not condensable at −78°C during the transport and storage period. Evacuation was continued for about five minutes; the container was then heated to 10°C and the valve opened for about 15 seconds to permit enough UF_6 vapor to enter the lead tube and nozzle to react with any active surfaces present. The electron diffraction photographs were then taken. During three consecutive runs which extended over a period of about eight hours, the non-condensable pressure in the apparatus as measured by an ion gauge ranged from 3 to 4×10^{-6} mm Hg. At all times liquid-air-cooled surfaces protruded over the pumps and nozzle to keep residual oil and water vapors from getting to the actual diffraction chamber and lead tube in the nozzle. Photographs taken at the beginning and end of these runs are identical except in scale (due to intentional change in wavelength) and density (variation in exposure), in spite of the fact that in the interval about 0.5 g of UF_6 had passed through the valve, lead tubes, and nozzle, and was condensed on a liquid-air-cooled copper surface just above the nozzle.

The above procedure was repeated on four different occasions. In the first two trials an all-brass nozzle was used; in the last two, a nozzle which was made of copper, stainless steel, and brass. In no case did we observe corrosion of the visible sections of the nozzles. In the second trial, 1.7 g of UF_6 were distilled through the diffraction chamber and condensed on the liquid-air-cooled copper surface prior to the taking of the photographs. We noted that during the distillation the condensed material was pure white and crystalline, and that no visible reaction had taken place on the cold surface. Again, the resulting photographs were identical with the photographs previously taken except for intended scale and density factors.

About a year previous to the first of these runs, a series of photographs was taken on a sample of uranium hexafluoride prepared by Dr. E. G. Rochow, to whom we wish to express our sincere appreciation. This material was handled in a glass apparatus without observing all of the detailed precautions enumerated above. Nevertheless, the electron diffraction photographs taken with no sector could not be distinguished from those similarly taken later.

APPARATUS AND PHOTOGRAPHS

The apparatus used in this study has been described in the preceding paper,[11] as have also the mode of operation and the inherent limitations in accuracy. Diffraction patterns taken without a sector were recorded on Eastman Commercial Plates; those with a sector on E.K. spectroscopic VD plates and on 35-mm microfile film. During the runs the sample tube was maintained at temperatures from 6°–11°C. The voltage for the sector pictures

[8] (a) Brickwedde, Hodge, and Scott, J. Chem. Phys. **16**, 429 (1948); calorimetric heat capacities. (b) B. Weinstock and R. H. Crist, J. Chem. Phys. **16**, 436 (1948); vapor pressures. (c) C. B. Amphlett *et al.* [reference 6(b)] also measured vapor pressures. (d) J. F. Masi, J. Chem. Phys. **17**, 755 (1949); heats of vaporization. (e) H. J. Hoge and M. T. Wechsler, J. Chem. Phys. **17**, 617 (1949); liquid densities. (f) J. R. White and A. E. Cameron, Phys. Rev. **71**, 907 (1947); critical ionization potentials.

[9] J. L. Hoard and J. D. Stroupe, Columbia Report A-1242 (March, 1944), declassified on October 7, 1946.

[10] E. Lindberg, Zeits. f. Physik **54**, 632 (1929).

[11] J. M. Hastings and S. H. Bauer, J. Chem. Phys. **18**, 13 (1950), in particular, note Fig. 5.

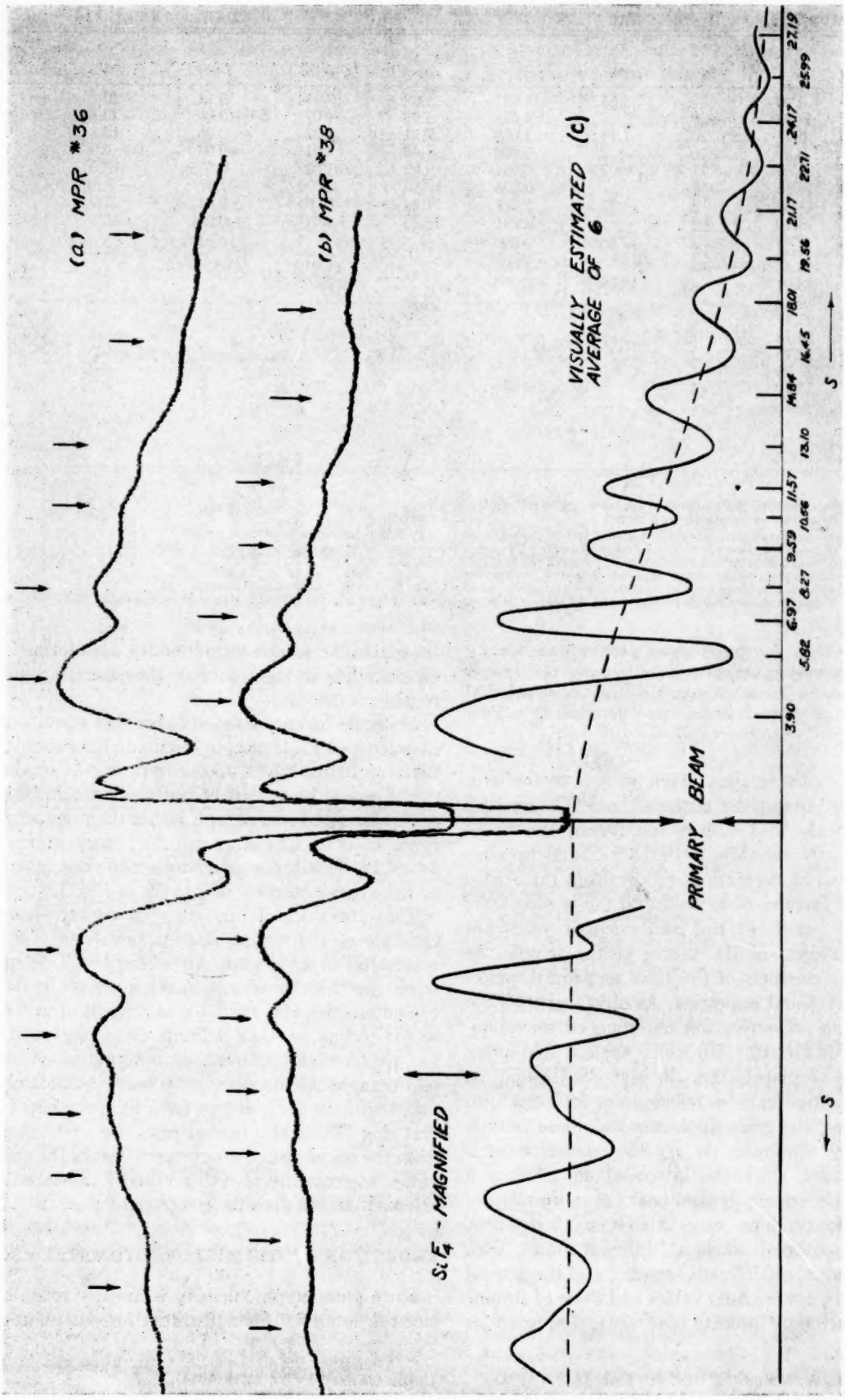

FIG. 1. Observed intensity curves for uranium hexafluoride. (a), (b) Unretouched microphotometer tracings of plates taken with a sector, at different electron accelerating voltages. The lower sketch (c) is the visually estimated pattern of photographs taken without a sector. For comparison, the pattern which would be introduced, were SiF_4 present, is also included.

TABLE II. Summary of peak and valley s values and intensities.

Max.	Min.	s_0^v	I^v	s_0^{BP}	s_0^s/s_0^v	s_0^{mpr}	s_0^{mpr}/s_0^v	I^{mpr}	I_r	Model A_4 s_c/s^{mpr}
1		3.90	30	3.65	(1.047)	3.68	(0.944)	0.13	30	1.014
	2	5.82	−20		1.011	5.95	1.022	−0.09	−20.8	0.951
2		6.97	20	7.14	1.009	7.11	1.020	0.06	13.8	0.989
	3	8.27	−10		1.009	8.40	1.015	−0.03	−6.9	1.002
3		9.59	11	9.67	0.994	9.62	1.003	0.015	3.5	0.997
	4	10.56	−7		0.998	10.50	0.994	−0.015	−3.5	1.000
4		11.57	8	11.86	1.006	11.62	1.005	0.017	3.9	0.990
	5	13.10	−3		1.010	13.23	1.010	−0.020	−4.6	0.985
5		14.84	6	14.89	0.995			0.015	3.5	0.991
	6	16.45	−4		1.004		1.010		−2	1.004
6		18.01	4	18.05	±0.006		±0.008		2	0.998
	7	19.56	−3						−1	0.997
7		21.17	3						1	0.992
	8	22.71	−2						−0.5	0.996
8		24.17	2						0.5	1.007
	9	25.99	−1						−0.25	0.994
9		27.19	1						0.25	1.004
10		(30.16)	½						0.10	1.002
										0.995
										±0.0083

Key to Table II.—
s_0^v—visually estimated peak positions—no sector (average of 6).
I^v—visually estimated intensities—no sector.
s_0^{BP}—visually estimated peak positions (Broune and Pinnow, ×0.993, to allow for difference in voltage scale).
s_0^s/s_0^v—ratio of peak positions for sector (average of four) to non-sector photographs both estimated visually.
s_0^{mpr}—peak positions determined from microphotometer recordings, average of seven.
I^{mpr}—intensities from average recording, relative to unit background.
I_r—I^{mpr} reduced to scale of I^v, and combined with latter for large s values to permit complete R.D. calculation.
s_c/s^{mpr}—ratio of peak positions computed for Model A_4 [Eq. (1)] to those deduced from mpr, or visually estimated for the range $14.78 < s < 30.04$.

ranged from 32–37 kv, for those without a sector in the vicinity of 48 kv. The exact values were determined by means of a Type K potentiometer placed across an accurately calibrated potential divider. The sample-plate distances were determined by calibration with gold foil;[12] assumed for gold, $a_0 = 4.055$A.

To the eye, photographs taken with a sector look much "cleaner" than those taken without. The over-all contrast of peaks and valleys relative to the background is greatly enhanced; the background appears uniform instead of decreasing rapidly from the center outward. The features observed in all the photographs taken over a period of two and one-half years are identical, regardless of the source of the sample. In particular, the closeness of the third and fourth peaks is apparent on casual inspection. As objective evidence we present the accompanying unretouched microphotometer records Fig. 1(a), (b) which are 2.35-fold linear enlargements of plates Nos. 36 and 38. Insofar as electron diffraction can be relied upon for structural determinations, the gross appearance of these records *unquestionably eliminates the regular octahedron as a possible structure*, since the latter would produce a pattern showing equally spaced peaks of uniformly decreasing intensity. The very satisfactory agreement between photographs taken at different times, with different voltages, on different samples, and the general agreement between our final values and those of Broune and Pinnow strongly indicate that whatever impurities (in particular, silicon tetrafluoride) were formed during our handling of the material, they were not sufficient to disturb the data.

Molecule for molecule, SiF_4 scatters about one-sixth as much as UF_6. Hence, to obtain an appreciable effect, twice as many moles of the impurity as of the compound would be required. The result would be a more or less smudged photograph rather than one with sharp rings, equally spaced except for those in the range $8 < s < 12$. This becomes obvious when one attempts to add the curve marked SiF_4 to (c) in Fig. 1.[13]

The remainder of this report is concerned with an estimate of the degree of departure from the regular octahedral arrangement. An attempt will be made to select the "best" model by making use of the quantitative intensities now available as a result of utilizing the sector technique. One point is clear, the positions of the maxima and minima as determined visually on photographs taken with a sector (s_0^s) check closely those taken without (s_0^v), except for a St. John effect on the first ring (Table II); in that case, the s_0^{mpr} value taken from the microphotometer records checks the computed value, whereas the s_0^v value visually measured is considerably larger than the computed value.

REDUCTION OF THE MICROPHOTOMETER RECORDS

Since photographic density is linearly related to the electron intensity (demonstrated for our photographic

[12] C. Lu and E. W. Malmberg, Rev. Sci. Inst. **14**, 271 (1943).

[13] Taken from the data of L. O. Brockway and F. T. Wall, J. Am. Chem. Soc. **56**, 2373 (1934).

materials by Dr. J. M. Hastings in the range of densities employed), and since the background is equal to "unit" intensity,

$$\left[\frac{I(s)}{P_0}\right]_{\text{sector}}=\left[\frac{8\pi^2me^2}{h^2}\right]^2\frac{N}{R^2}\left\{1+\frac{\sum'\sum' f_if_j}{\sum f_i^2+\sum G_i}\exp(-a_{ij}^2s^2)\frac{\sin sl_{ij}}{sl_{ij}}\right\}, \tag{1}$$

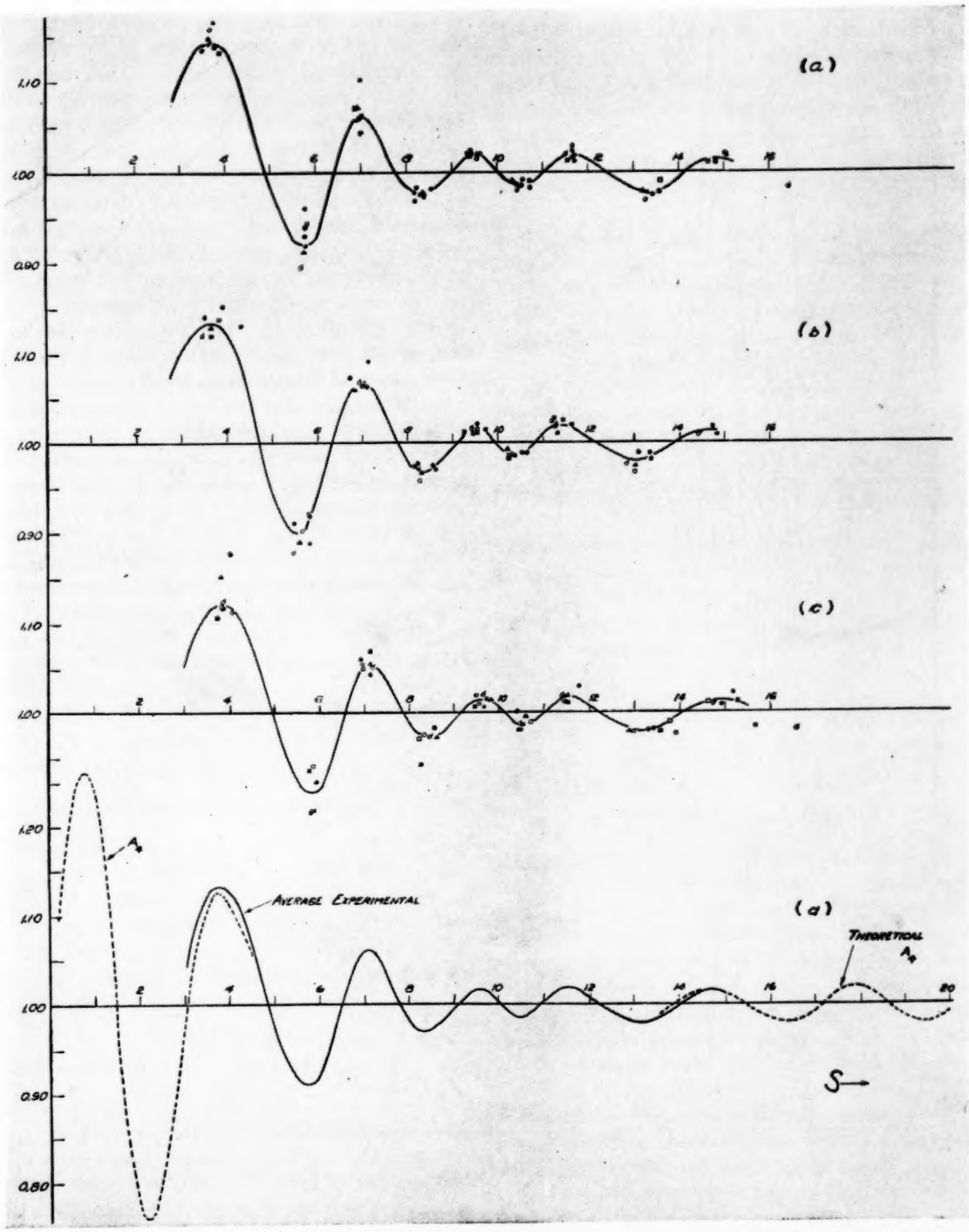

FIG. 2. Experimentally determined intensity curves, as deduced according to the following three methods of reduction. (a) Background curve drawn through "cross-over" points, taken from average s_c's of six models (A_1, A_4, B_1', C_1', C_3, C_4). (b) Background curve, based on average s_c's of four models (A_1, A_2, A_3, A_4). (c) Background adjusted so that the *relative* intensities of adjacent maxima and minima check the average values for four models (A_1, A_4, C_3, C_4). (d) Average of top three curves.

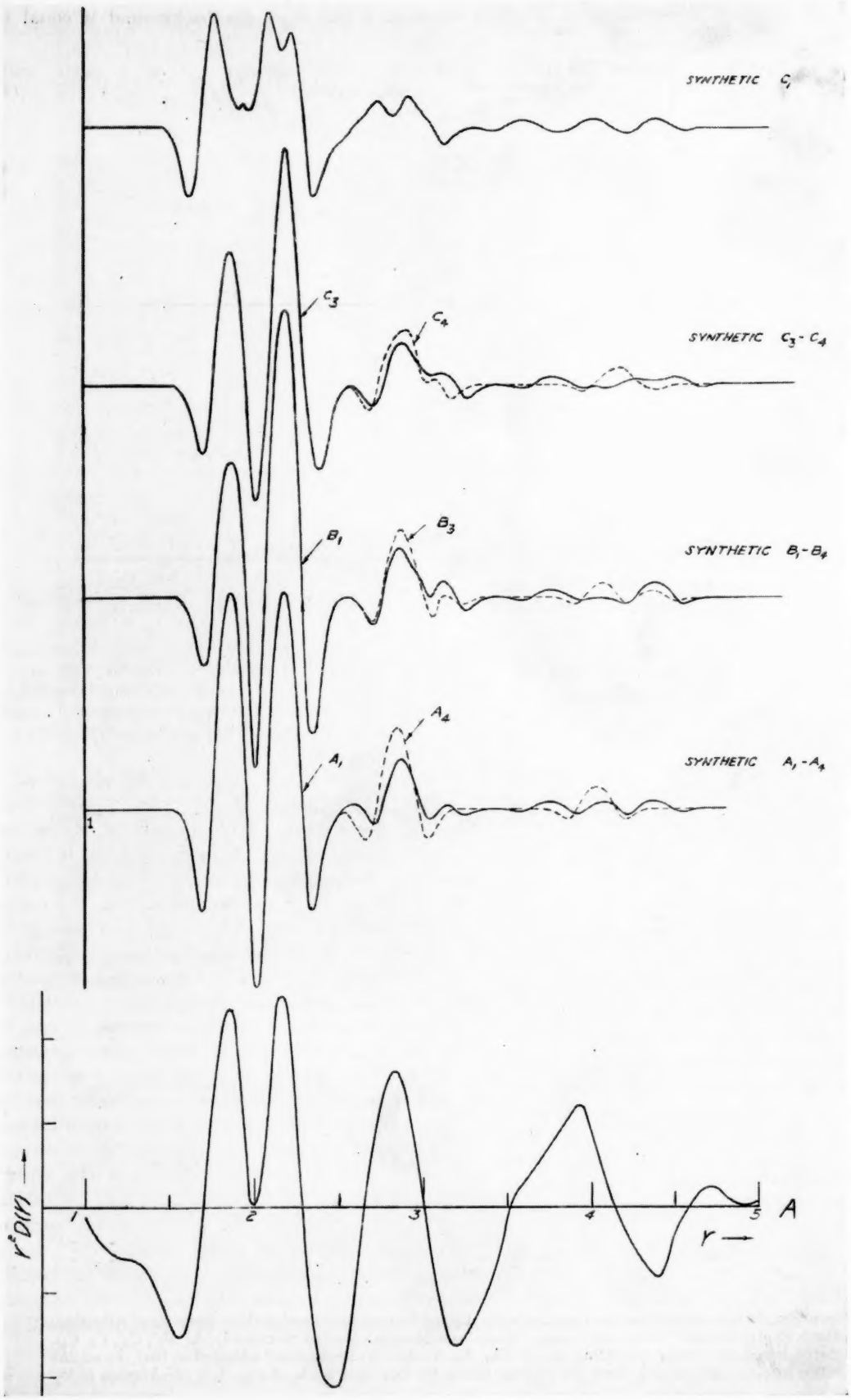

FIG. 3. Radial distribution curves for UF_6. The bottom curve is computed from the average reduced mpr, 2(d), to which the visual curve, 1(c), has been matched to extend the angular range.

the intensity striking any point on the plate in "atomic" units is simply the quotient of the observed density at that point by the density of the background. One only has to draw in the background correctly. Unfortunately, this cannot be performed unambiguously for all values of $s<s_m$. In the present state of development of the sector technique, two procedures may be followed; these are subjective in the sense that they depend on how much information is already available regarding the structure of the molecule being investigated.

In the case of UF_6, it is evident from inspection of the gross microphotometer records that the background is changing slowly except for small values of s, where closely similar curves are predicted for all models anyway; and that such changes in background which are observed do follow a smooth curve. The procedure for the reduction of the microphotometer records has been outlined by Hastings and Bauer;[11] the three experimental curves so obtained are plotted in Fig. 2 with the weighted average curve. From that figure the degree of agreement which is attainable between individual recordings of photographs taken with a variety of voltages, plates, temperatures etc., is evident, as is also the self-consistency which followed from a statistical treatment of the data. The average curves (a), (b), (c) are very much alike; the results seem to be independent of the method used in reducing the data. Reference to Table II illustrates the agreement between the positions and relative intensities of the maxima and minima as deduced from Fig. 2 (average) and those deduced from measurements. In the region $7<s<12$, we estimate the accuracy of intensities of the maxima and minima to be reliable to one-half percent; for $s<7$ our error in intensity is estimated to be one percent. Our final s_0 values we believe are accurate to about one-half percent.

RADIAL DISTRIBUTION FUNCTION, $D(r)$

The molecular part of the intensity of diffraction pattern may be inverted, so that a radial distribution function results, this without the assumption of a specific model. A detailed interpretation of the $D(r)$ function has been given by Debye and Pirenne.[14] The inversion was performed according to the procedure of Walter and Beach[15] using:

$$D(r)=\text{const.}\sum_k \frac{\cos a_k r}{\pi^2-4a_k r^2} a_k I(s_k) s_k^2 \frac{\sin s_k r}{s_k r}, \qquad (2)$$

for which the average intensity curve, Fig. 2(d), was used. The first peak was computed from Model A_4; however, the shape of the diffraction curve in this region is not sensitive to the model selected. For the region $s>15$, the visual data were matched in intensity to those of the microphotometer records, as indicated in Table II. The normalization factor $[\cos a_k r/(\pi^2-4a_k r^2)]$ was computed from experimentally determined a_k values. The resulting $r^2D(r)$ function is shown in Fig. 3.

Peaks of equal height appear at 1.85A and 2.16A. These must be due to two equal sets of directly bonded

U−F distances; the peak at 2.83A arises from U−F scattering, while the one at 3.94A is due to F−U−F scattering. The latter peak is distinctly broader than the first two indicating that possibly not all the separations in that region are of equal length. Without the assumption of a specific model we can nevertheless conclude that insofar as electron diffraction is concerned:

(1) Uranium hexafluoride does not have a symmetric structure; on the basis of such a model a single peak in the vicinity of 2A should appear on the R.D. curve.

(2) This R.D. curve is not compatible with the model suggested by the x-ray data, since for the latter one would expect the first peak to occur at 2.02A, and it should cover twice the area of the second, at 2.12A. Thus Models H_1 and H_2 are eliminated (see Table III).

(3) Models B (Table III) are not compatible with the equal heights of the first two peaks observed in radial distribution curve; some of the C models are also excluded (Fig. 3).

(4) Models A are in best agreement with the electron diffraction data. These possess sufficient planes of symmetry so that the formal space group requirements in the crystal can be satisfied. However, the Fourier projection suggests a structure containing more symmetry elements than are shown by Models A. Further, since such models lack a center of inversion, a finite dipole moment would be expected for the molecule.

(5) The ∠FUF angles are close to 90°, since $\sqrt{2}\langle U-F\rangle_{Av}=2.83$A.

INTENSITY CURVES

As a further check on the acceptability of the A and possibly of the C models, compare the observed intensity curve [Fig. 2(d)] with those computed by means of Eq. (1). This can best be done by placing successively the tracing of the average curve over the computed curves in Fig. 4, A, B···H. It will be obvious that the best check in peak positions and intensities, particularly in the crucial region around the third and fourth peaks, is given by A_4. The quantitative fit in the observed s positions for maxima and minima in the diffraction pattern, as measured by the deviation of the individual s values from those computed, is excellent for A_4; average deviation in s_{calc}/s_{obs} is 0.006.

We wish to emphasize that in reducing the microphotometer curves either average cross-over point or average *ratios* of peak intensities were used. However, remarkably good checks of the values of peak and valley intensities relative to unit background were obtained. This indicates (a) that the disturbing factors

[14] P. Debye and M. R. Pirenne, Ann. d. Physik **33**, 617 (1938).
[15] J. Walter and J. Y. Beach, J. Chem. Phys. **8**, 601 (1940).

such as sample diffusion, multiple scattering etc., enumerated by Hastings and Bauer,[11] have been experimentally minimized, and (b) that the technique devised for drawing in the background is certainly reliable for highly symmetrical molecules. The general scattering Eq. (1) has thus been given a quantitative check. To our knowledge this is the first time the validity of the Born approximation has been directly checked for 30–50-kv electrons scattered by gases.

Reference to Fig. 5 will demonstrate the over-all agreement between the visually observed pattern (vis.) and selected curves computed with

$$I_{\text{approx}}(s)=\sum_i{}' \sum_j{}' Z_i Z_j \frac{\sin r_{ij}s}{r_{ij}s}, \qquad (3)$$

using $Z_{\text{eff}}(U)=90$; $Z(F)=9$. The dashed jagged curves indicate percentage departure from perfect agreement between the visually estimated and computed peak positions. Again A_4 is superior to the other curves. With regard to intensity comparisons, the region $8<s<13$ should be taken with reserve, since the relative heights of the third and fourth peaks apparent to the eye are incorrect. We have found from the inspection of a large number of patterns taken with and without a sector that the eye tends to accentuate variations in the background by making shoulders look like peaks and by introducing valleys for points of inflection; further, one tends to overestimate in adjacent regions the relative intensity of the inner part relative to the outer part of the pattern.

TABLE III.

There are essentially two configurations for coordination 6 from which all others may be derived by slight distortion; looking along the trigonal axis these are:

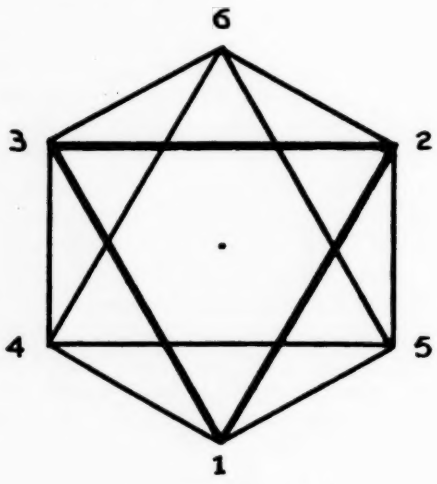

Octahedral angles
(90°, 180°)

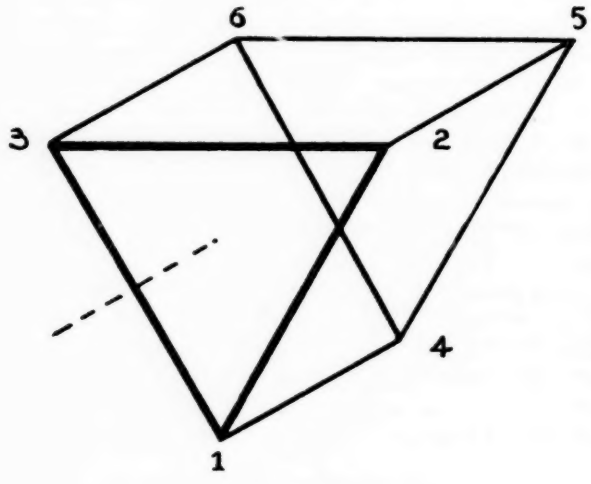

Prismatic angles
(81.786°, 135.583°)

with atoms 1, 2, and 3 in the top plane and 4, 5, and 6 in the bottom plane.

Models A: Three U−F at 1.87A; three U−F at 2.17A.
(1) 1, 2, and 6 short; 3, 4, and 5 long; octahedral angles.
(2) 1, 2, and 6 short; 3, 4, and 5 long; prismatic angles.
(3) 1, 2, and 3 short; 4, 5, and 6 long; prismatic angles slightly distorted to make

1–2=2–3=3–1=4–5=5–6=6–4=2.88A.

The height of the prism is then reduced to 2.25A.
(4) 1, 2, and 3 short; 4, 5, and 6 long; octahedral angles slightly distorted to make

1–2=2–3=3–1=4–5=5–6=6–4=2.88A.

The separation 1–4 etc. then becomes 2.80A.

Models B: Two U−F at 1.87A; four U−F at 2.17A.
(1) 1 and 6 short; 2, 3, 4, and 5 long; octahedral angles.
(2) 1 and 6 short; 2, 3, 4, and 5 long; prismatic angles.
(3) 1 and 5 short; 2, 3, 4, and 6 long; octahedral angles slightly distorted so that

1–5=2–3=3–6=3–4=2.88A.

B_1' 2 U−F 1.88
4 U−F 2.18
octahedral angles } similar to (1).

TABLE III.—(*Continued*)

Models C: Three different U−F distances, in sets of two, were assumed.
(1) 1 and 6 at 1.89; 2 and 4 at 2.09; 3 and 5 at 2.27; octahedral angles (this one corresponds to final structure proposed by Broune and Pinnow).
(2) 1 and 6 at 1.89; 2 and 4 at 2.09; 3 and 5 at 2.24; octahedral angles.
(3) 1 and 6 at 1.87; 2 and 4 at 2.12; 3 and 5 at 2.22; octahedral angles.
(4) 2 and 5 at 1.87; 1 and 6 at 2.12; 3 and 4 at 2.22; octahedral angles. Slightly distorted to make

$$1\text{–}2=2\text{–}3=3\text{–}1=4\text{–}5=5\text{–}6=6\text{–}4=2.88\text{A}$$
$$\text{and } \begin{cases} 1\text{–}4=1\text{–}5=2\text{–}6=3\text{–}6=2.98\text{A} \\ 2\text{–}5=3\text{–}4=2.89\text{A}. \end{cases}$$

C_1' 2 U−F 1.88; 2 U−F 2.12; 2 U−F 2.24; octahedral angles } similar to (1).

Other distortions of Models A, and B, and C were considered but were not treated in detail since these did not lead to R.D. curves which were as good as those of the above models.

Model D: Symmetrical octahedron, U−F=2.00A.

Models H: 2, 3, 4, and 5 short; 1 and 6 long.
H_1 4 U−F 2.02; 2 U−F 2.12; octahedral angles.
H_2 4 U−F 1.87; 2 U−F 2.17; octahedral angles.

DISCUSSION

The model for uranium hexafluoride which is in best agreement with the electron diffraction data is a slightly distorted octahedron with three U−F bond distances equal to 1.86A, and three U−F equal to 2.16A. Each set of three bonds forms a trigonal pyramid, the length of all the base edges being 2.88A. The fact that this model does not have a center of symmetry is not necessarily inconsistent with the fact that the molecule has no dipole moment large enough to be detectable. The short bonds may be considerably more ionic than the longer ones; indeed, some such postulate must be made in order to explain the non-equivalence of six bonds in UF_6. (Expected for a coordination number of 6, the configuration d^2sp^3 gives a symmetrical octahedron; d^3p^3 gives a trigonal antiprism with the possibility of two unequal sets of three bonds.) That this difference in ionic character may be just enough to compensate for the longer U−F extensions on the opposite side of the molecule appears to be fortuitous. The lack of a dipole moment is the sole reason for my suggesting at the present time that Model C_4 still be considered as a possibility.[16] Next to A_4, this model is in adequate agreement with the data both with respect to peak positions and relative intensities; C_4 differs somewhat from the structure proposed by Broune and Pinnow.

The discrepancy of the electron diffraction data on the vapor with the x-ray diffraction studies on single crystals is real. Three possible explanations may be offered.

(1) The molecular structure in the solid differs from that in the vapor. Distortion upon solidification seems to be indicated for several molecules; hexamethylenetetramine[17] and phosphorous pentachloride[18] are examples. One would expect the higher symmetry to occur in the vapor; the reverse is found.

(2) The methods of analysis of the diffraction data are quite different for the two investigations. In x-ray studies reliance is placed on the assumed phase assignments to permit computation of the Fourier projection. This is followed by checking on a statistical basis, the individual spot intensities against those observed. In electron diffraction studies chief reliance is placed in the radial distribution computation, and is followed by a check on general shape of the diffraction pattern. When sector data are available, it is also possible to

[16] An interesting comparison was made by Amphlett *et al.* [reference 6(b)] with respect to the total polarization of the gases at one atmosphere and 20°C for UF_6 (30.7±1.0 cc) and TeF_6 [24.3 cc; Linke, Zeits. f. physik. Chemie **B48**, 193 (1941)]. The latter compound has a regular octahedral structure, per e.d., and has an appreciably lower total polarization.

[17] V. Schomaker and P. A. Shaffer, Jr., J. Am. Chem. Soc. **69**, 1555 (1947). Electron diffraction study of hexamethylenetetramine vapor, report C−N 1.48±0.01A; ∠CNC=∠NCN=109½°±1°. P. A. Shaffer, Jr., J. Am. Chem. Soc. **69**, 1557 (1947). Single crystal study by x-ray diffraction, reports C−N 1.45±0.01A; ∠CNC=107°; ∠NCN=113½°.

On solidification there may thus be a total shrinking of 0.36A in the C−N bonds. Neglecting the energy required for the angular distortion, and assuming a C−N stretching force constant of 5×10^5 dynes/cm, a compression energy of approximately 90 kcal./mole would thus be required.

For the transition $UF_6(A_4)\rightarrow UF_6(H_1)$, there is a total lengthening of three U−F bonds by 0.45A and a shortening of the others by 0.25A, so that the net effect would be considerably smaller in UF_6 than in $N_4(CH_2)_6$. Indeed, it is not unreasonable to expect a change in bond type upon crystallization of a uranium compound, since the energy difference between the various lowest electronic states for the heavy element are small. Polarization forces may be sufficient to shift one bond type to another.

[18] M. Rouault, Comptes Rendus **207**, 620 (1938). Clark, Powell, and Wells, J. Chem. Soc. 642 (1942).

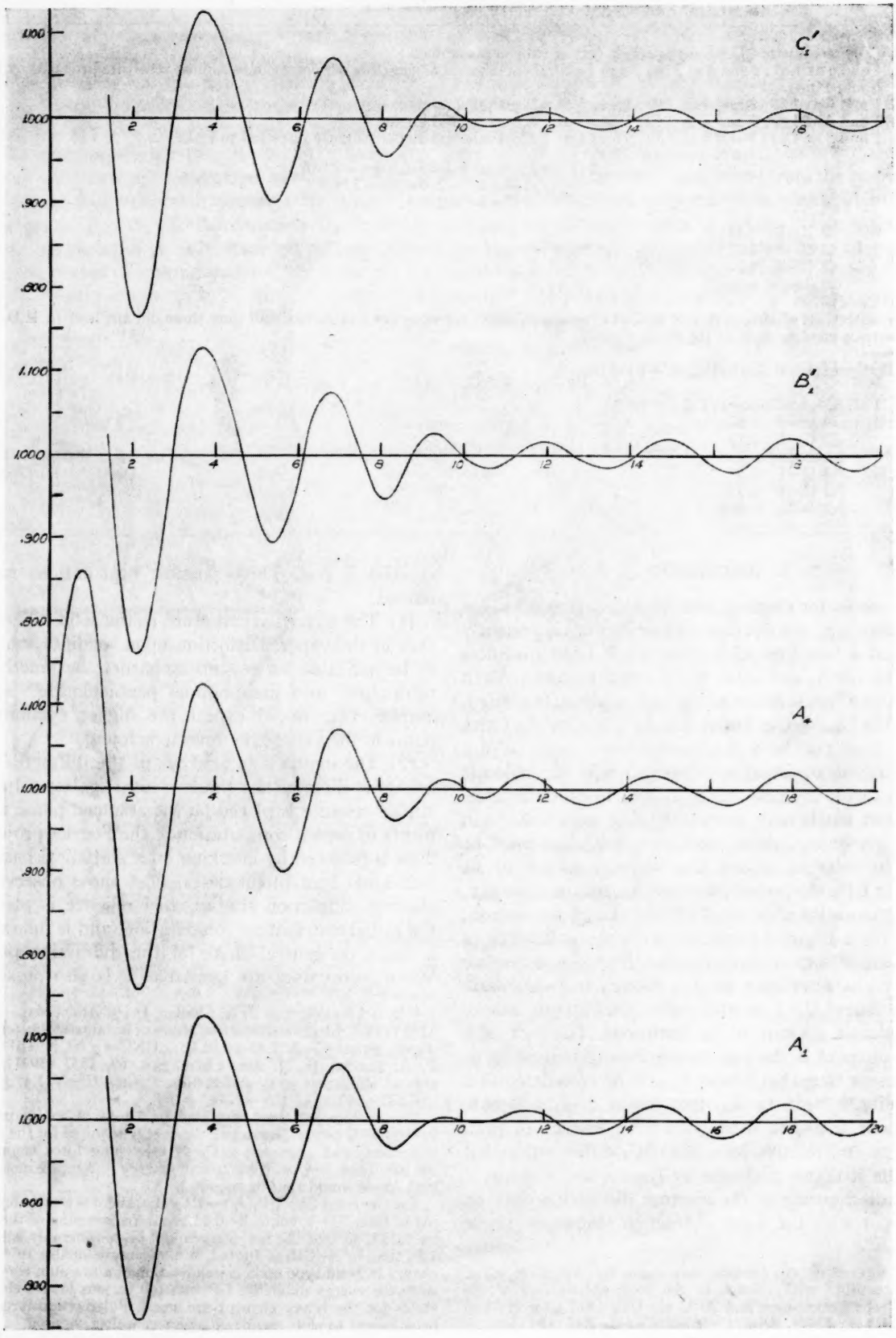

FIG. 4(a). (See caption under Fig. 4(c) on page 38.)

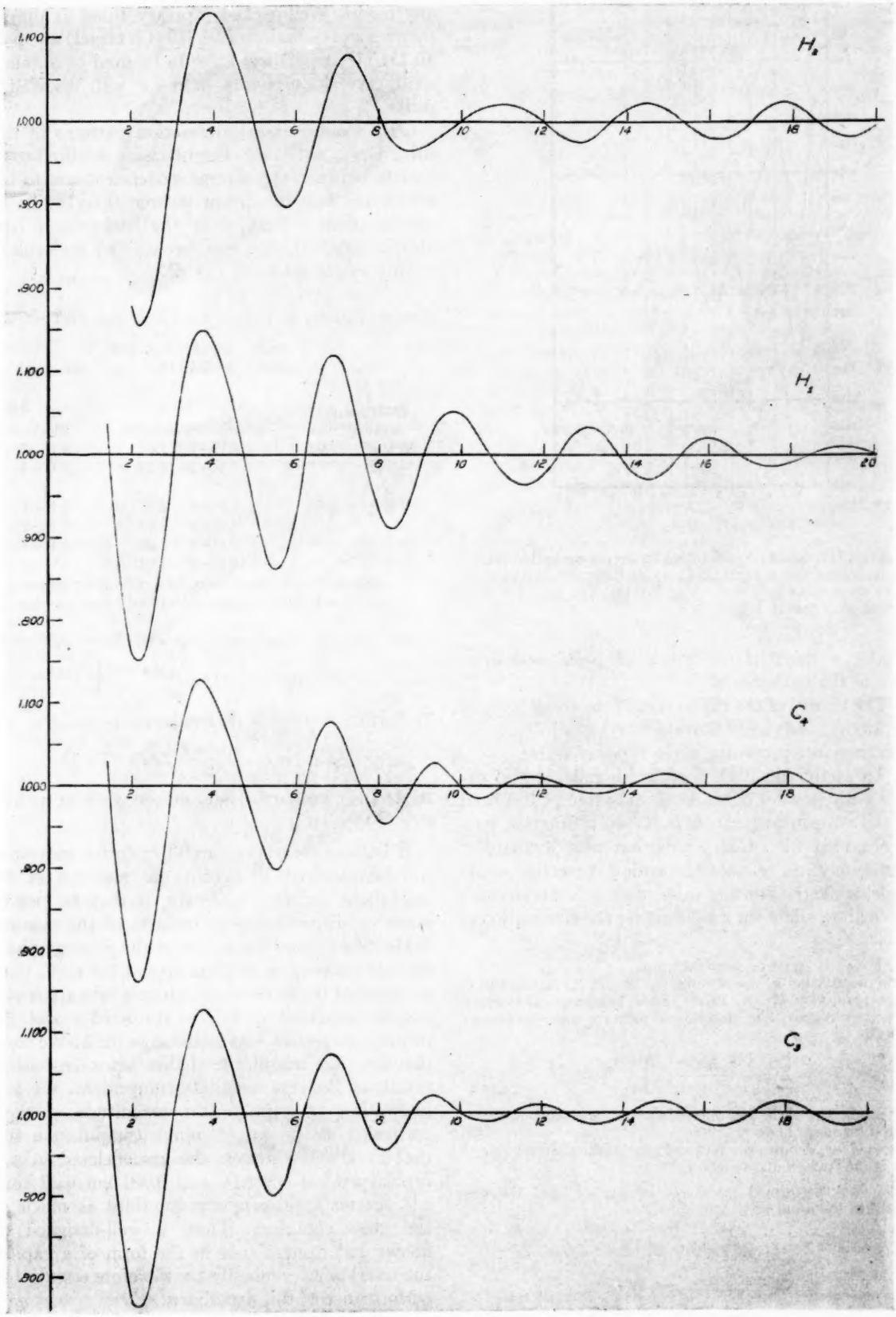

FIG. 4(b). (See caption under Fig. 4(c) on page 38.)

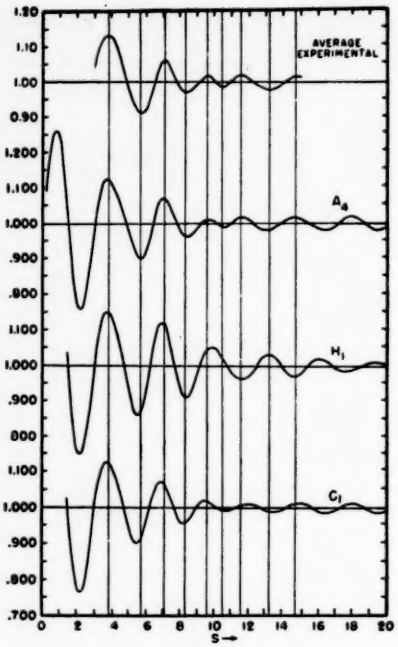

FIG. 4(c).

FIG. 4 (a), (b), (c). $A_1 \cdots C_1'$ Intensity curves computed for the models indicated, using Eq. (1). $C_3 \cdots H_2$ Intensity curves computed for the models indicated, using Eq. (1). The scale for these is identical with that in Fig. 2.

undertake a quantitative check of peak intensities relative to the background.

(3) The theory of the diffraction of electrons by very heavy atoms needs amplification.[19]

I am therefore proposing three types of tests:

(1) To apply the R.D. method to reliable and extensive x-ray powder data. An initial attempt has been made with inconclusive results. Good diffraction patterns obtained with CuK_α radiation were available.[20] Unfortunately, no reliable absorption correction could be made, while the limiting value of sin θ/λ was so small as not to allow sufficient resolution for the elimination of any model. Well-packed capillary tubes as diffracting samples and radiation of λ0.749 (Cb target) and possibly λ0.131 (U target) will have to be used to obtain sufficient crystal diffraction data for well resolved R.D. peaks.

(2) To obtain x-ray diffraction patterns of the gas using CbK_α radiation. The precision required to differentiate between the several models appears to be just within the best of current technic. The results of our computations follow, while the background (sum of atomic coherent plus incoherent) and molecular contributions are shown in Fig. 6.

Molecular, curves D, H, and A_4: $2\sum_i{}' \sum_j{}' F_i F_j \exp(-a_{ij}^2 s^2) \frac{\sin l_{ij} s}{l_{ij} s}$

with $s=(4\pi/\lambda)\sin\theta/2$,
and $\lambda=0.749$A.

D Symmetrical octahedron		H_1 X-ray (crystal) diff.		A_4 Electron diff.	
6 U−F	2.02	4 U−F	2.02	3 U−F	1.87
		2 U−F	2.12	3 U−F	2.17
12 F−F	2.86	4 F−F	2.86	6 F−F	2.80
		8 F−F	2.93	6 F−F	2.88
3 F−F	4.04	2 F−F	4.04	3 F−F	4.02
		1 F−F	4.24		

For the U−F distances $a_{ij}^2=0.0015$ were assumed.
For the F−F distances $a_{ij}^2=0.0022$ were assumed.

Atomic (coherent+incoherent), curve b: $[\Sigma F_i^2+Q\Sigma G_i]$

where $Q=\left[1+\frac{h}{mc}\frac{1-\cos\theta}{\lambda}\right]^{-3}$.

To illustrate the effect of the polarization factor,

curve c: $\frac{1+\cos^2\theta}{2}[\Sigma F_i^2+Q\Sigma G_i]$.

Both b and c were plotted using the scale given on the left of the vertical axis.

It is clear that very careful intensity measurements will be required to permit the reaching of an unambiguous decision. However, it may be possible to prove or disprove the correctness of the symmetrical model from visual inspection of the photographs. If no marked maxima or minima appear for $s>9$, the rapid damping of the molecular pattern would argue strongly but not conclusively for the distorted model. No absorption correction was included in the above computation since the magnitude of this factor depends on the details of the experimental arrangement. We found it interesting to estimate the magnitude of the total scattering of the gas. A rough computation suggests that at about 3 atmos. the gas enclosed in a Pyrex capillary 0.100 cm I.D. and 0.001 cm wall thickness will scatter approximately one-third as much as will the glass container. Thus, a well-designed sample holder and camera (not in the form of a capillary in the usual powder mount) are therefore essential for the performance of this experiment.

(3) As a check on the theory of diffraction of electrons by very heavy atoms, to investigate the structures of

[19] W. F. Libby (private communication).

[20] The preparation of the samples by Mr. P. A. Agron and of the photographs by Mr. R. Palter (SAM Laboratories) is gratefully acknowledged. The diffraction pattern was represented analytically by

$$I(s)=\sum_{k=1}^{83}\frac{i_k}{[1+\alpha^2(s_k-s)^2]^2}\Bigg]_{s_k-\gamma}^{s_k+\gamma}+B(s). \quad \text{(i)}$$

i_k = peak height of the kth diffraction line—arbitrary units.
$\alpha\cong 100$ for sharp lines.
$\gamma=(5.534/\alpha)$, denotes the range of contribution of each line.
$B(s)$ is the background function.

Inversion was performed by direct integration, and the sum evaluated in the usual way.

$$4\pi r^2 D_{\text{solid}}(r)=\frac{2r}{\pi}\sum_k \frac{i_k}{\alpha_k}[s_k \sin s_k r\cdot G_1(r,\alpha)+\cos s_k r\cdot G_2(r,\alpha)]$$
$$+\frac{2r}{\pi}\int_0^\infty sB(s)\sin rs\,ds. \quad \text{(ii)}$$

For large α, $G_1(r)\to 0.567$
$G_2(r)\to 0$.

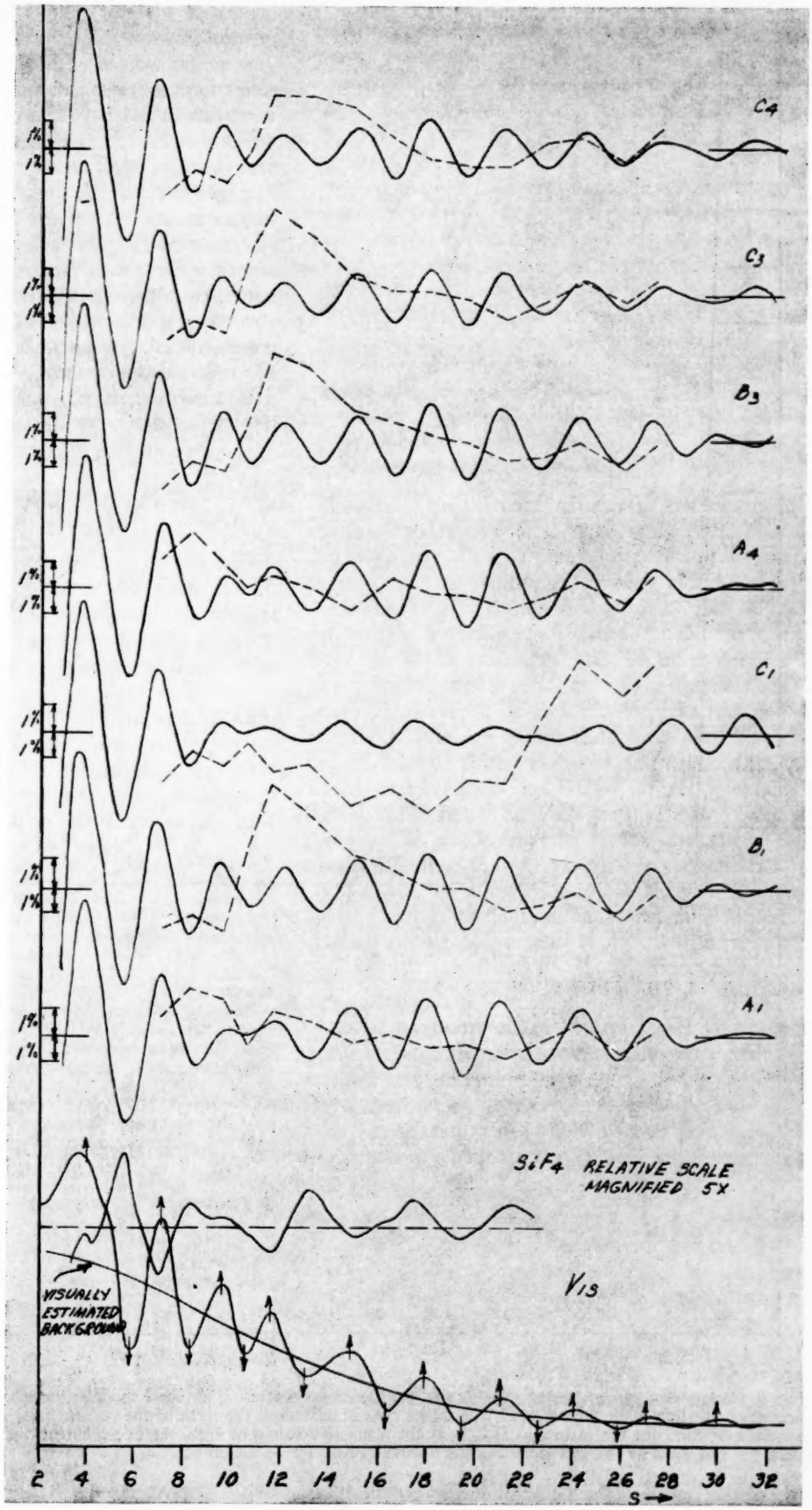

FIG. 5. Relative intensity curves computed for various models, using Eq. (3). The dashed jagged curves indicate percentage departure from perfect agreement between visually estimated and computed peak positions.

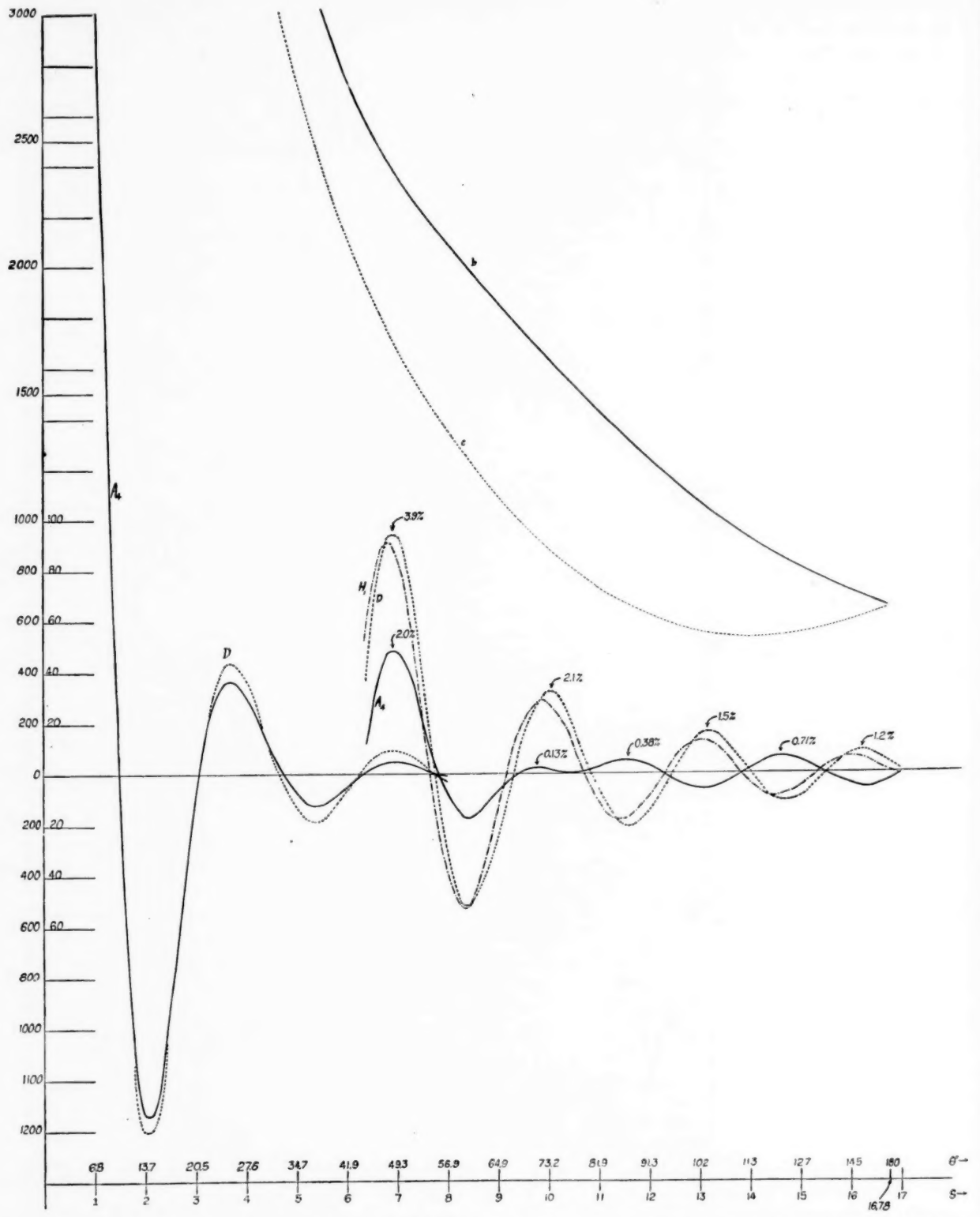

FIG. 6. Computed x-ray scattering by UF_6 gas. (a) Molecular scattering for three models; the scale for the region $1 \leqslant s \leqslant 7.6$ is that indicated on the left, while for $6 \leqslant s \leqslant 17$ it is shown that indicated on the right of the vertical axis. The percentages listed at the maxima were computed for the ratio $I_{\text{mole}}/I_{\text{atmoic}}$ at the respective values of s. (b) Atomic coherent plus incoherent (background)—scale on left. (c) The same as (b), but including the polarization factor—scale on left.

a number of volatile compounds wherein a central uranium atom is bonded to several light-weight groups. The first such study, of $U(BH_4)_4$, is now under way while the preparation and study of other compounds is contemplated. To date, structure determinations of $Pb(CH_3)_4$ and similar compounds have lead to nothing unexpected.[21] We also hope to be able to study the structures of UOF_4 and UCl_6 by electron diffraction.[22]

To reconcile the observed spectra and the measured entropy with the structures which follow from the diffraction data is quite difficult. This difficulty is most pressing for the electron diffraction models, since the x-ray crystal intensities might be forced into agreement with a symmetric octahedral structure. As Bigeleisen *et al.* have shown, there is a close check between the third law entropy and that computed on the assumption of a symmetry number, $\sigma=24$. Our various models require

C_4, H_1	$\sigma=8$; hence add to computed entropy[7]	2.18 e.u.
A_4	$\sigma=3$	4.13.

Discrepancies of this magnitude are outside the experimental error (±0.6 e.u.). However, we wish to call attention to the fact that the computed vibrational contribution to the entropy may be in error by as much as 2.2 e.u. That it is possible to reassign the frequencies in a manner which appreciably reduces their contribution is shown in Table IV. No assumption of accidental degeneracy need be made. Were one to neglect the net effect of splitting on the entropy and to neglect the slight corrections due to differences in moments of inertia, he would find that on the basis of the new

TABLE IV. Possible reassignment of frequencies for UF_6.

Designation	Type	Assign. (Bauer)	Assign. (B.M.S.T.)		Observed frequency	Intensity	State
ν_4	T_{2u}	164	130		Inact.		
ν_2	T_{2g}	208	202		202(R)		soln.
ν_5	T_{1u}	220	200		—(IR)		
$\nu_4+\nu_3$		372	332		—(IR)		
$\nu_5+\nu_3$		428	402		—(IR)		
ν_2	E_g	511	511		511(R)		liq.
ν_6	T_{1u}	630	640	accidental degeneracy	623(IR)	1000	gas
ν_1	A_{1g}	656	656		656–666(R)		liq., soln.
$\nu_4+\nu_2$		675	641		675(IR)	10	gas
$\nu_5+\nu_2$		731	711		713–719(IR)	½	gas
$\nu_6+\nu_3$		838	842		825(IR)	2	gas
$\nu_5+\nu_1$		876	856		850(IR)	¼	gas
$\nu_6+\nu_2$		1141	1151		1163(IR)	4	gas
$\nu_6+\nu_1$		1286	1296		1295(IR)	3	gas

assignment for $\sigma=8$, $S°$ at

Assign.	273°K	348°K
Bauer	88.65 e.u.	95.12 e.u.
B.M.S.T.	87.65	95.22
Measured values	88.21	94.97

Insofar as the thermodynamic and spectroscopic data are concerned, either the C_4 or H_1 models are admissible and one may not argue that a large value (24) must be assumed for the symmetry number of UF_6. Further, the failure of appearance of a spectrum rich in lines is not weighty evidence since either the splittings arising from the lower symmetry may be unresolved or the corresponding dipole moment matrix elements may be small. However, it is difficult to shift the low frequencies to such an extent as to force agreement with the A_4 model. High resolution infra-red data which would permit direct estimation of the moments of inertia, and band contours, would help solve this problem. To check what frequency assignment is the correct one, the infra-red spectrum in the range 200–400 cm^{-1} should be traced. Determination of the gaseous heat capacity would also be useful in resolving the existing ambiguity.

ACKNOWLEDGMENT

I wish to thank sincerely Dr. J. M. Hastings and Miss Miriam Michnik for their aid with the experimental and computational work, respectively; and Dr. Bigeleisen for various discussions. To the Guggenheim Foundation, many thanks for a fellowship, during the tenure of which this paper was completed.

[21] L. O. Brockway and H. O. Jenkins, J. Am. Chem. Soc. **58**, 2036 (1936), regular tetrahedron for $Pb(CH_3)_4$. M. W. Lister and L. E. Sutton, Trans. Faraday Soc. **37**, 393 (1941), regular tetrahedron for $PbCl_4$; similarly for other tetrahalides. Brockway, Ewens, and Lister, Trans. Faraday Soc. **34**, 1350 (1938), regular octahedra for hexacarbonyls of Cr, Mo, W. R. V. G. Ewens and M. W. Lister, Trans. Faraday Soc. **34**, 1358 (1938), regular octahedron for WCl_6. It is also worth while to raise the question that, were the departure from a regular octahedron due merely to the atomic weight of the central atom, why would MoF_6 be distorted (reference 5) whereas TeF_6 is regular [Proc. Nat. Acad. Sci. **19**, 68 (1933)].

[22] W. H. Zachariasen, report to the AEC, No. 2184, declassified July 19, 1948, assigned a regular octahedral structure to UCl_6 in the solid on the basis of powder x-ray diffraction data. See also, Acta Krist. **1**, 285 (1948).

The Structure of Hexamethylcyclotrisiloxane as Determined by the Diffraction of Electrons on the Vapor

ELEANOR H. (WELLER) AGGARWAL AND S. H. BAUER
Department of Chemistry, Cornell University, Ithaca, New York

(Received April 25, 1949)

Hexamethylcyclotrisiloxane vapor has been shown to have a structure incorporating a planar ring with larger oxygen valence angles (125±5°) than silicon valence angles (115±5°); the methyl groups extend above and below the plane of the ring, their equilibrium bond positions making a probable angle of 112±6° with silicon, the temperature motion of the methyl groups allowing an average change in the interatomic distances involved of about 0.09A, as compared with the normal temperature motion change of about 0.03A. The Si−O distances are 1.66±0.04A and the Si−C distances are 1.88±0.04A.

The shortness of the Si−O distance suggests a larger ionic character of the bond than that indicated by the electronegativity table.

HEXAMETHYLCYCLOTRISILOXANE $[(CH_3)_2SiO]_3$, is the lowest isolated member of the polymeric cyclic siloxanes. Frevel and Hunter[1] reported preliminary x-ray diffraction work on several members of this series. They suggested that the structure of the trimer is similar to that found in benitoite,[2] where alternate oxygen and silicon atoms are arranged in a planar six-membered ring, and each silicon is surrounded by four oxygen atoms situated approximately at the corners of a tetrahedron. The octamer and probably all other polymers in this series have puckered rings. X-ray studies by Roth[3] on spiro-siloxane [octamethylspiro (5,5) pentasiloxane] revealed that each molecule consists of two planar six-membered rings linked at 90° through a silicon atom. The interatomic distances and bond angles cited are:

Si−O 1.64±0.03A Si−C 1.88±0.03A
∠CSiC 109±4° ∠OSiO 109±4° ∠SiOSi 130±4°.

The diffraction data reported below confirm the planar six-membered ring structure for the trimeric siloxane as well as the interatomic distances quoted by Roth and Harker,[3(b)] as being typical.

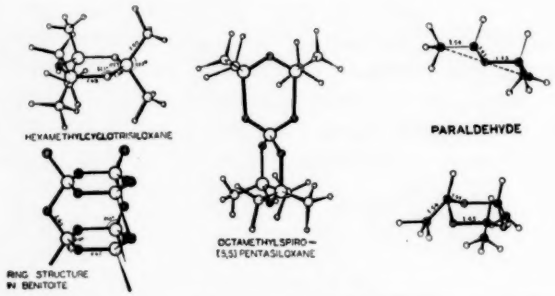

FIG. 1. Structures of hexamethylcyclotrisiloxane and related compounds. Please note that the values given in the drawing for the interatomic distances are not the "best" values quoted in the conclusion of this paper.

Before proceeding with details of the analysis, it will prove interesting to compare the structure and some of the properties of hexamethylcyclotrisiloxane with those of comparable carbon compounds, trioxane and paraldehyde. Their respective geometries are illustrated in Fig. 1. Whereas the silicon analog of trioxane has yet to be prepared, the one directly analogous to paraldehyde, trimethylcyclotrisiloxane, has been synthesized.[4] From both x-ray and spectroscopic evidence[5] the carbon-oxygen compounds have puckered rings, with the chair form predominating as in cyclohexane in contrast to the planar $(Si-O)_3$ rings. Paraldehyde consists of an equilibrium mixture of the *cis-* and *trans-*forms, with the former predominating; the carbon atoms of the methyl groups are roughly coplanar with the oxygen atoms in the ring. Electron diffraction data on this compound indicate[6] that all the bond angles are tetrahedral, and that C−O is 1.43±0.02A, while C−C is 1.54±0.02A. The dipole moment of trioxane, 2.18*D*, is very close to the computed value for the pure chair form, 2.3*D*, as compared to the estimated value for the cradle form, 0.6*D*.[7] On the other hand, the dipole moment of the siloxane trimer is expected to be zero. In general, the carbon analogs are less stable to chemical attack, are more dense, and have higher electric moments. The melting and boiling points are comparable.

One can but speculate at present regarding the structure of hexamethylcyclotrisilazane $[(CH_3)_3SiNH]_3$, the preparation of which has recently been reported,[8] along with that of higher linear and cyclic members. It is probable that the valence angle of the nitrogens is not as large as that of the oxygen atoms, due to the smaller ionic character of the Si−N bonds; if so, the $(Si-N)_3$ rings may prove to be somewhat puckered.

[1] L. K. Frevel and M. J. Hunter, J. Am. Chem. Soc. **67**, 2275 (1945).
[2] *Strukturberichte, II* (1937), p. 128.
[3] (a) W. L. Roth, J. Am. Chem. Soc. **69**, 474 (1937). (b) W. L. Roth and D. Harker, Acta Krist. **1**, 34 (1948).
[4] S. D. Brewer, J. Am. Chem. Soc. **70**, 3962 (1948).
[5] N. F. Moerman, Rec. Trav. Chim. **56**, 161 (1937); H. Gerding and J. Lecomte, Rec. Trav. Chim. **58**, 614 (1939); D. A. Ramsay, Trans. Faraday Soc. **44**, 289 (1948).
[6] D. C. Carpenter and L. O. Brockway, J. Am. Chem. Soc. **58**, 1270 (1936).
[7] A. A. Maryott and S. F. Acree, J. Research Nat. Bur. Stand. **33**, 71 (1944).
[8] S. D. Brewer and C. P. Haber, J. Am. Chem. Soc. **70**, 388 (1948).

EXPERIMENTAL PROCEDURE

The cyclic trimer used in this study was obtained from Dr. Robert O. Sauer of the General Electric Company, to whom we express our sincere thanks. This sample melts at 65°C, and its vapor pressure at 53°C is 30 mm. At this temperature (dp/dt) is 2 mm/°C. An evacuated vial containing the sample was sealed by means of a magnetic breaker joint to a metal high temperature nozzle in the electron diffraction apparatus. The sample was kept at various temperatures between 49° and 66°C during the runs. Electron diffraction pictures, with and without a sector, were taken. The experimental procedure and method of reduction of the photographs has been described by Hastings and Bauer.[9]

A visual intensity curve, showing intensity as a function of scattering angle, was drawn from visual estimation of the ring diameters and relative intensities of maxima and minima for both the sector and nonector pictures (see Table I and Fig. 2). The sectors microdensitometer tracings showed structure only out to about $s=15$, whereas rings out to an s value of almost 32 could be seen on the non-sector films.

ANALYSIS OF DATA

A radial distribution curve was computed following the method of Walter and Beach,[10] using the observed intensities above and below a decreasing background as deduced from the non-sector photographs (see Fig. 3 —R.D.). Significant peaks in the radial distribution function appear at values of r (interatomic distance), summarized in Table II; also included are the interatomic distances with which they have been identified.

The radial distribution curve enables us to eliminate the puckered ring models and also many of the planar structures. We found no acceptable puckered ring models with interatomic distances corresponding completely to those indicated by the radial distribution curve, as can be seen by comparing the "synthetic" α_2-curve with the observed radial distribution curve in Fig. 3. Thus, in model α_2, the heavily weighted C−Si distance across the ring was split up into a number of rather lightly weighted distances because of the dissymmetry introduced by the puckered ring. Furthermore, there is no important distance corresponding to the radial distribution peak at 4.27A. With respect to the planar ring models, it is clear that the Si−O distance is shorter than expected, being in the neighborhood of 1.62A rather than 1.76A. Shortening the Si−O bond also alters the important C−Si distance across the ring. Models incorporating oxygen valence angles outside the range 110°–130° are immediately eliminated because then the important Si/O and C/Si distances across the ring cannot be made to agree with the curve. The models which best fit the radial distribution curve are γ_4 and ζ_3; the first has an oxygen valence angle of 130°, a silicon valence angle of 110°, and the Si−O distance 1.62A, while the second has an oxygen valence angle of 125°, a silicon valence angle of 115°, and the Si−O distance 1.68A. The synthetic curves are based on empirical shapes observed in many radial distribution curves.

TABLE I.

Max.	Min.	Visually estimated s_0 (non-sector)	Visually estimated relative intensity	Visually estimated s_0 (sector)	Microphotometer intensities (relative to unit background)
1		(1.77)	(10)	(1.99)	—
	1	2.28	−10	2.27	—
2		3.20	10	3.24	—
	2	3.95	−20	3.91	−0.109
3		4.84	20	4.79	0.256
	3	5.98	−15	5.84	−0.164
4		6.98	6.5	6.66	—
	4	7.40	5	7.35	—
5		7.96	8	7.85	0.043
	5	8.56	5	8.44	—
6		9.20	7	9.07	—
	6	10.09	−10	9.96	−0.047
7		11.18	7	11.19	0.035
	7	12.61	3	12.62	—
8		13.62	6	13.54	(0.003)
	8	14.49	−5	14.29	(−0.018)
9		15.42	4	14.95	—
	9	16.79	2		
10		17.78	4		
	10	18.81	−3		
11		19.64	3		
	11	20.80	2		
12		21.68	3		
	12	22.85	−2.5		
13		23.97	2		
	13	25.96	−1		
14		26.56	2		
	14	29.58	−0.5		
15		31.61	1		

Diffraction patterns expected for various models were computed and compared with the visual and microphotometer curves. The equation for calculating the scattered intensity as a function of angle is:

$$\left[\frac{I(s)}{I_0}\right]_{\text{sector}}=\left[\frac{8\pi^2 m\epsilon^2}{h^2}\right]^2\frac{N}{R^2}\times\left[1+\frac{\sum_i'\sum_j' f_i f_j}{\sum_i (f_i^2+g_i)}\frac{\sin sr_{ij}}{sr_{ij}}\exp(-a_{ij}^2 s^2)\right]. \quad (1)$$

As a preliminary approximation, some of the theoretical curves were computed using the simplified equation

$$I(s)=\sum_i'\sum_j' Z_i Z_j\frac{\sin sr_{ij}}{sr_{ij}}. \quad (2)$$

Three important parameters determine the structure of this compound; these are the oxygen valence angle, the ratio of the distances C−Si/Si−O, and the C−Si−C angle. The motion of the $Si(CH_3)_2$ groups relative to one another might be taken as a fourth parameter. The effect on the total curve of changing the C−Si−C angle is small, however, when restricted to the reasonable range 108°–118°, whereas the effect of temperature motion of the $Si(CH_3)_2$ groups is to smooth out the sharper features of the pattern, and hence the latter can readily be predicted. Consequently, the essential

[9] J. M. Hastings and S. H. Bauer, J. Chem. Phys. 18, 13 (1950).

[10] J. Walter and J. Y. Beach, J. Chem. Phys. 8, 601 (1940).

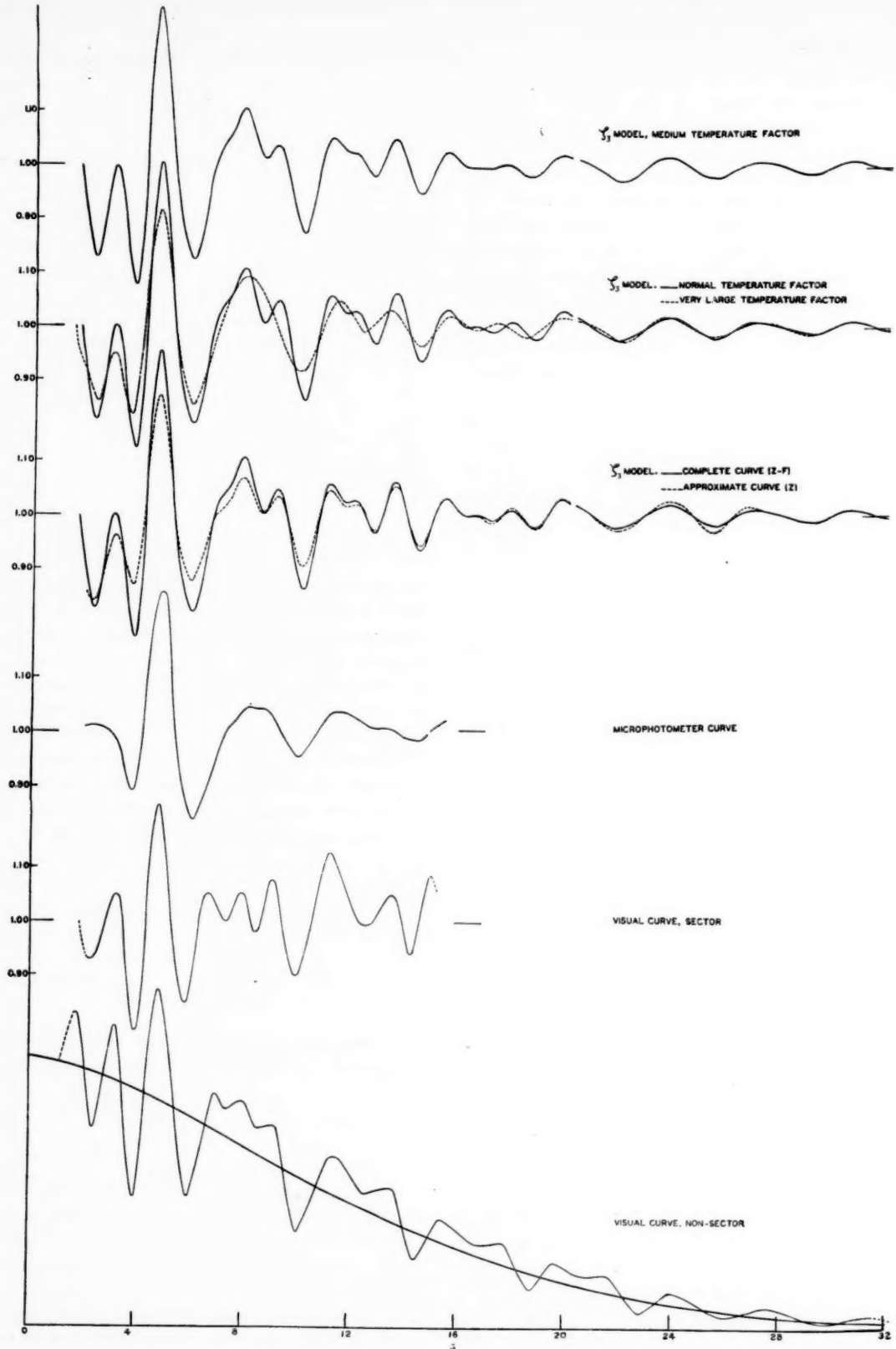

FIG. 2. Theoretical curves based on ζ_3-model: $\angle$Si−O−Si=125°, $\angle$O−Si−O=115°; C−Si=1.90A, Si−O=1.68A. (1) ζ_3-model, medium temperature factor (0.0050). (2) ζ_3-model, normal temperature factor (0.0020). ζ_3-model, large temperature factor (0.0261). (3) ζ_3-model, "complete" curve, calculated from Eq. (1). ζ_3-model, "approximate" curve, calculated from Eq. (3). (Note: The break in each of the theoretical curves appearing here and in Figs. 5 and 6, is caused by the fact that the tabulated values of the function $\sin sr/sr$ were available, beyond $s=20$, only up to the value of $r=3.99$. The interatomic distances exceeding this value were therefore not included in the sum beyond $s=20$. The difference in most cases is not large.)

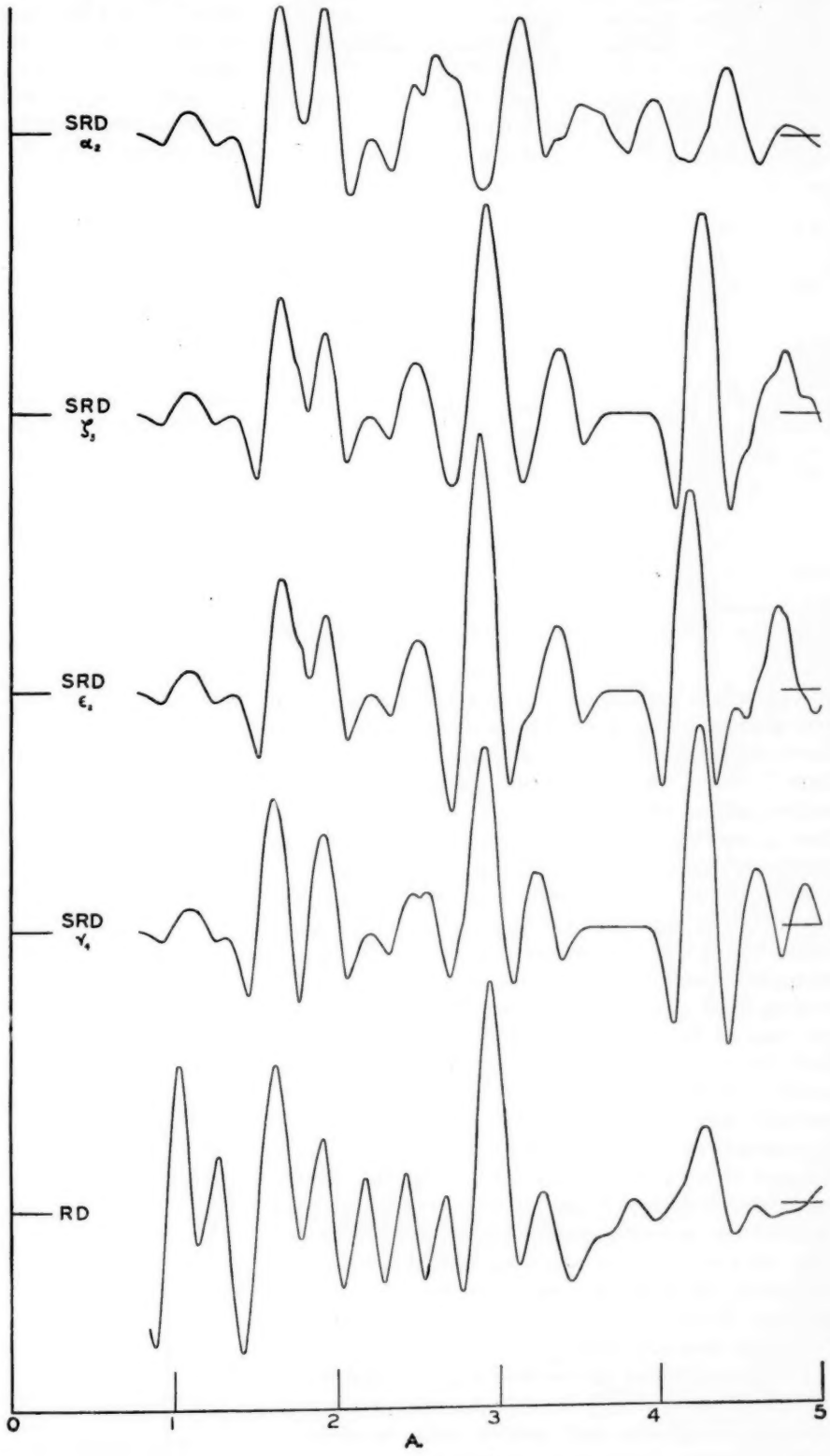

FIG. 3. "Synthetic" radial distribution curves (SRD):

α_2—puckered ring (chair form) model: all angles tetrahedral,
C–Si=1.90A,
Si–O=1.68A.

ζ_3—planar ring model:
∠Si–O–Si=125°,
∠O–Si–O=115°;
C–Si=1.90A,
Si–O=1.68A.

ϵ_2—planar ring model:
∠Si–O–Si=120°,
∠O–Si–O=120°;
C–Si=1.90A,
Si–O=1.68A.

γ_4—planar ring model:
∠Si–O–Si=130°,
∠O–Si–O=110°;
C–Si=1.90A,
Si–O=1.62A.

RD—computed radial distribution curve.

TABLE II.

Radial distribution maxima	Relative intensity	Interatomic distance identified	Distance in best model	Weight	Angle assumed	Distance expected*
1.03A	6	C—H	1.09A	108		1.10
1.27	2	?				
1.62	6	Si—O	1.66	672		1.76
1.91	3	C—Si	1.88	504		1.88
2.17	1	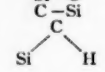				
2.42	1		2.49	252	110°	
2.66	½	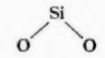	2.84	192	115°	
2.94	10	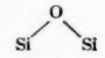	2.98	588	125°	
		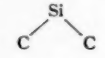	3.12	108	110°	
		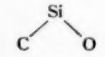	2.90	576		
3.27	½	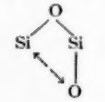	3.36	336	planar	
4.27	3	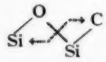	4.26	1008		

* Distances calculated by method of Schomaker and Stevenson; see reference 12.

features of the pattern must be fitted by adjusting the first two parameters listed. The particular models computed are indicated in the field of Fig. 4. For these the angle C—Si—C was assumed to be tetrahedral (with the oxygen valence angle as ordinate and the C—Si/Si—O ratio as abscissa. Puckered ring models, in which all angles were assumed tetrahedral, are not included.

Some of the best theoretical intensity curves are reproduced in Figs. 5 and 6. Comparison of the theoretical curves with the curves drawn from visual and microphotometer data give added evidence for discarding those models which were believed incorrect on the basis of the radial distribution curve. In making these comparisons we must interpret the general impression which our eye receives in terms of our experience, which is based on the observation of many photographs of compounds of known structure. Since the eye accentuates various features in the density curve, we feel that the correct curve may be interpolated between the microphotometer curve which does not show all the necessary resolution and the visual impression of the sector pictures which shows accentuated features. With this in mind, let us now examine the theoretical intensity curves.

The puckered ring models bear little resemblance to the experimental curves, the relative heights and positions of the maxima and minima being incorrect in many instances. These are not shown in the figures.

There are several series of intensity curves in which the ratio C—Si/Si—O is varied but the oxygen valence angle is constant. In the series ζ_2, ζ_3, ζ_4 (see Fig. 5), the oxygen angle is 125° and the Si—O distance varies from 1.72 to 1.64A. ζ_2 is excluded because although the fit is fairly good at low s values, at intermediate s the maxima and minima are shifted, and the structure in the region of $s=15$ and beyond is poor. ζ_3 gives a good fit with the experimental data over the whole s range, with the exception of the eleventh and twelfth maxima in the region $s=20$–23. ζ_4 cannot be excluded, for although the relative intensities of the seventh and eighth maxima are not as good as in the ζ_3-model, and the structure in the region $s=20$–23 is not good, the essential features of the curve are not much altered. In the series γ_3, ϵ_4, and ϵ_2 (see Fig. 6), the oxygen valence angle is 120° and the Si—O distance varies from 1.76 to 1.68A. The γ_3-model is excluded because the match over the whole s range is not good, and there are scarcely any features which the computed and observed curves have in common beyond $s=15$. ϵ_4 is much better, and cannot be excluded on the basis of this comparison with the visual data. All the essential features of the visual curve are present, but the match is not good in the region of the eleventh maximum to the twelfth minimum, from $s=19$–23; beyond this also the match is not as good as in the case of ζ_3. ϵ_2 lies at the limit of acceptable models, the match with the visual curve being poor in the region from $s=18$ to the end. The last series with constant oxygen valence angle of 130°, and Si—O distances 1.72, 1.68, and 1.62A, are Models δ_4, δ_3, and γ_4 (see Fig. 6). The δ_4-model is definitely excluded, for it shows a very poor match throughout the entire s range. Even at low s values the theoretical structure fails to match the observed structure closely, and the fit becomes very poor at larger s values. The δ_3-model, while close to the limit of acceptable models, cannot be ex-

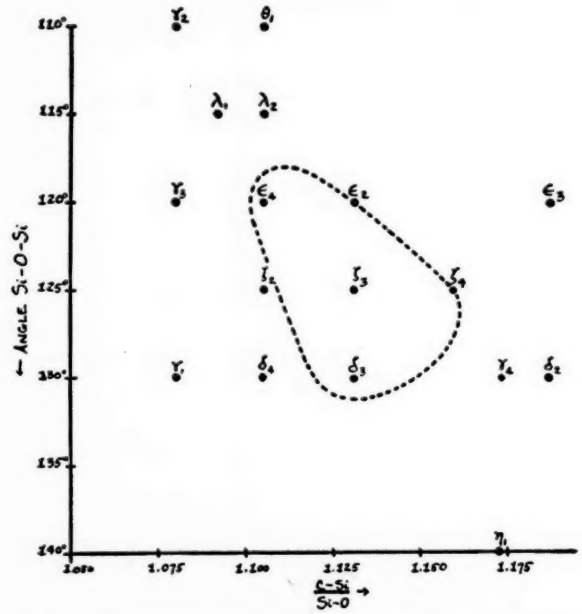

FIG. 4. Field of some of the planar ring models investigated.

cluded, for most of the important features of the observed curve are present, although the relative intensities of the seventh and eighth maxima in the region $s=11$–14 are incorrect, and the match is not particularly good in the region $s=16$–22. The γ_4-model is excluded because of the incorrect relative intensities of the maxima and minima over the region $s=11$–20. The positions of these structural features also are not in good agreement.

Let us now examine the series having constant ratio C−Si/Si−O and varying oxygen valence angle. The members of the series ϵ_2, ζ_3, and δ_3, with distance Si−O=1.68A, and oxygen angle varying from 120° to 130°, have already been discussed separately; ζ_3 is the best model in the series, but neither ϵ_2 nor δ_3 is definitely excluded. The series, ζ_2, ϵ_4, and λ_2, has constant Si−O distance 1.72A and oxygen angles varying from 125° to 115°. ζ_2 and ϵ_4 have been discussed separately; ζ_2 is not

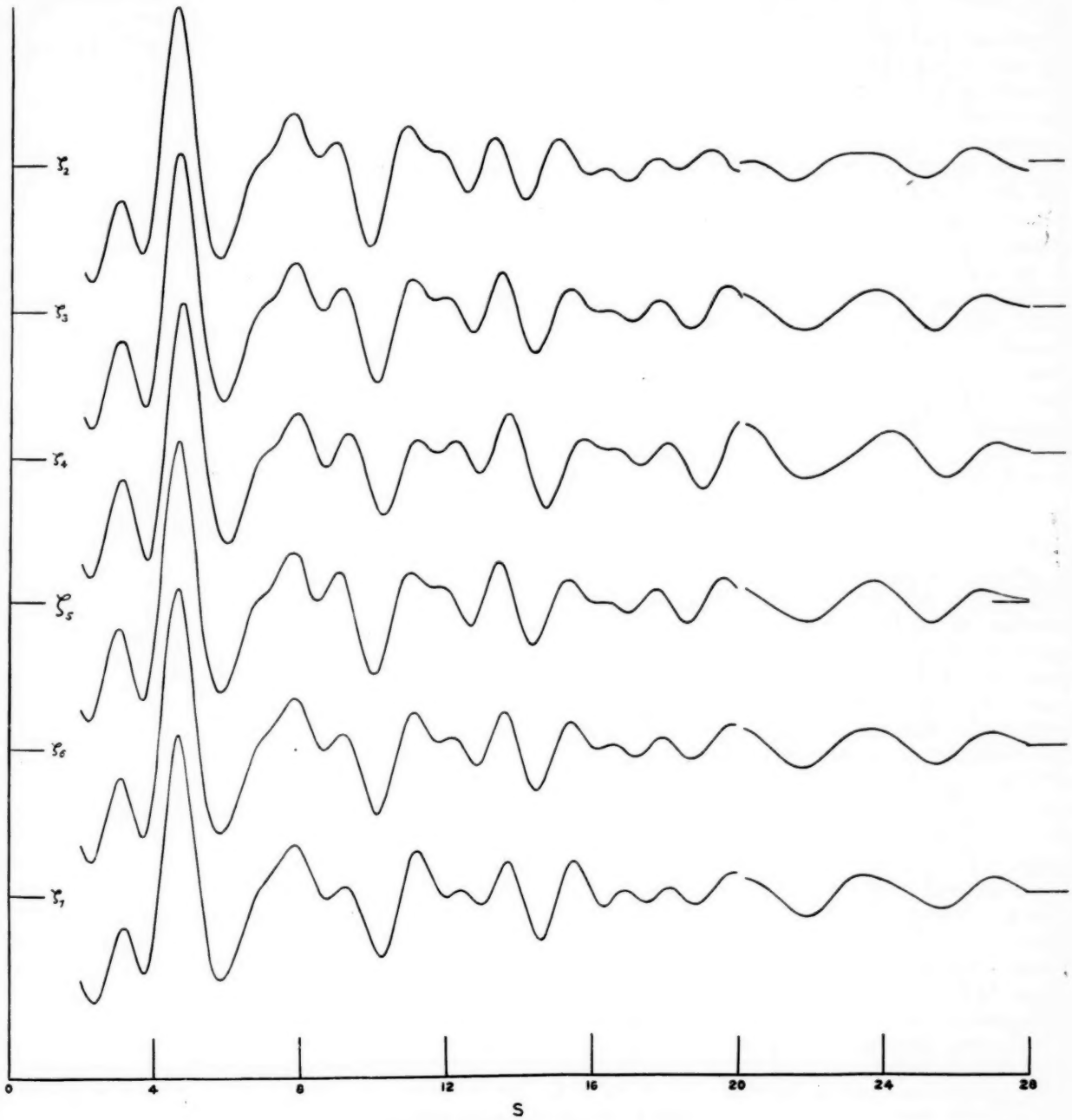

FIG. 5. Theoretical intensity curves.

Model	ζ_2	ζ_3	ζ_4	ζ_5	ζ_6	ζ_7
Si−O	1.72	1.68	1.64	1.68	1.68	1.68A
∠CSiC	110°	110°	110°	108°	115°	120°

All C−Si 1.90A, all ∠SiOSi 125°, all ∠OSiO 115°.

admissible, but ϵ_4 is not excluded. The relative intensities of structural features in the λ_2-model are not very good even at low s values, and the match in the region $s=20$ and beyond is poor, so that this model may also be excluded.

The carbon-silicon-carbon angle is also an important parameter in this molecule. In all the models mentioned above, this angle has been assumed to be 110°. The effect of varying this angle while keeping the other structure of the molecule constant has also been in-

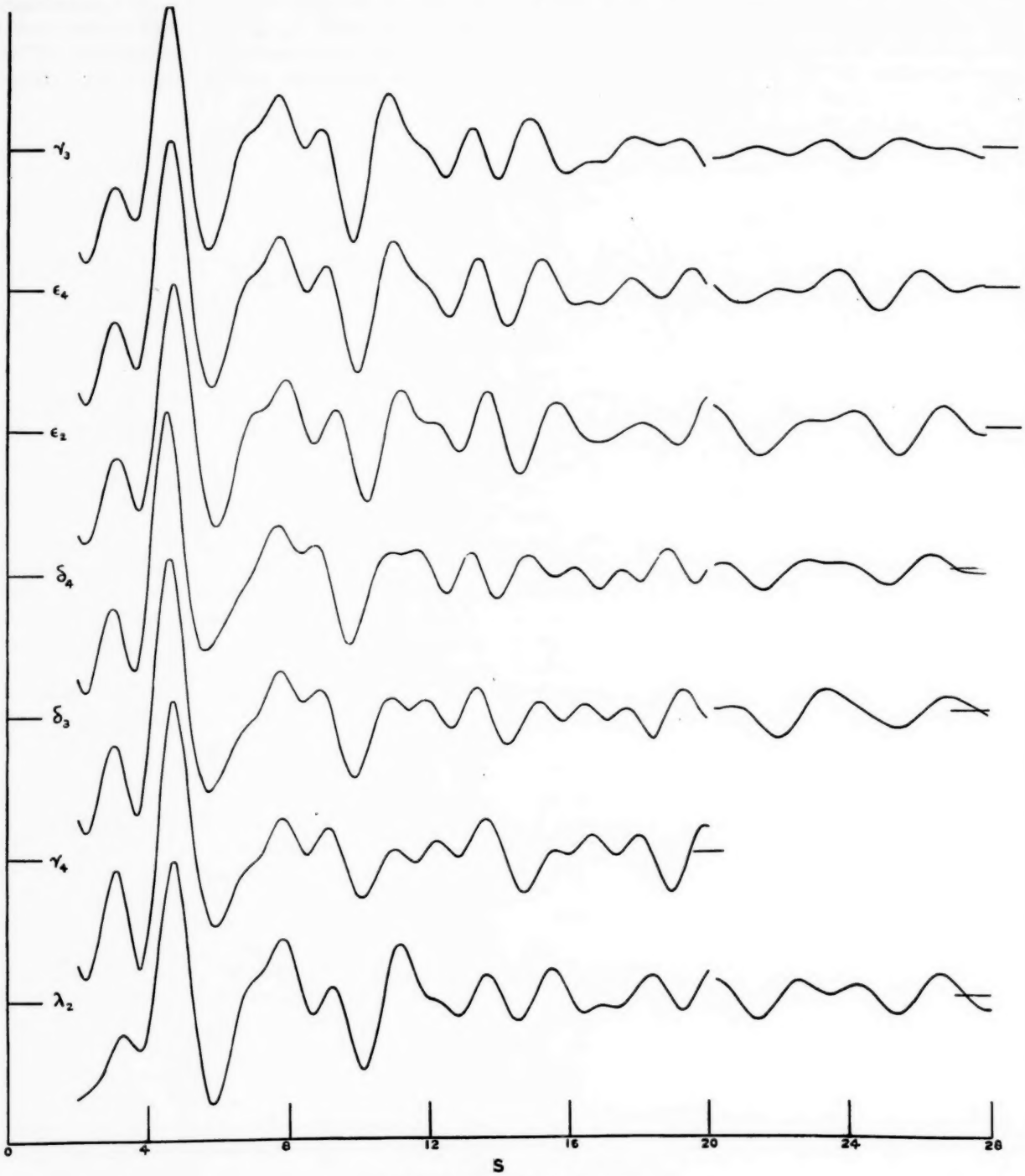

FIG. 6. Theoretical intensity curves.

Model	γ_3	ϵ_4	ϵ_2	δ_4	δ_3	γ_4	λ_2
Si—O	1.76	1.72	1.68	1.72	1.68	1.62	1.72A
∠OSiO	120°	120°	120°	110°	110°	110°	125°
∠SiOSi	120°	120°	120°	130°	130°	130°	115°

All ∠CSiC 110°.

vestigated. The best model of those listed is obviously ζ_3, so the distances and angles found in that model were used and kept constant, while the angle C−Si−C was varied from 108° (ζ_5) to 115° (ζ_6) and 120° (ζ_7); ζ_5 shows most of the structural features of the visual curve, but the relative intensities of the seventh and eighth maxima are incorrect, and the match at fairly large s values is not very good. The ζ_6-curve shows a very good match over most of the s range, as do also the ζ_3- and ζ_7-curves. No quantitative information may be gained from this particular series, since the structural changes in the intensity curves are not large, but we may say that the most probable C−Si−C angle is 112°, with a possible variation of ±6°. The preferred structure on the basis of these curves is the planar ring model with oxygen valence angles 125°, silicon valence angles 115°, and the methyl groups extending above and below the plane of the ring, with C−Si−C angles 112±6°.

Roth[3(a)] found it necessary to assume that the motion of the methyl groups swept out a cone of large volume around the silicon atoms; accordingly, we have calculated, using Eq. (1), an intensity curve corresponding to 30° oscillation of the methyl groups from their equilibrium positions, by adjusting the value of the temperature factor, $\exp(-a_{ij}^2 s^2)$, to allow for such departures from equilibrium. Various other curves assuming different temperature factors were calculated, and compared with the visual and microphotometer curves (see Fig. 2). As would be expected, the greater the temperature factor, the less prominent the features of the pattern become. Interpolations of the absolute intensities of the maxima and minima of the observed microphotometer curve between the complete ζ_3-curves with varying temperature factors were made, in order to estimate the average temperature factor and from this obtain the average departure of the methyl groups from equilibrium position. Because of the inaccuracies inherent in the determination of intensities, we can only be certain of the indication of a large temperature factor, but the value quoted has no real quantitative significance. An average temperature factor between 0.0050 and 0.0261 gives the closest fit; perhaps a value closer to 0.0050 may be assumed. The normal average temperature factor (0.0020) corresponds to a root-mean-square departure of 0.03A from equilibrium interatomic distance, whereas the medium (0.0050) temperature factor corresponds to a departure of 0.05A and the very large one (0.0261) to an average departure of 0.11A. Our interpolated value of 0.0150 corresponds to a root-mean-square motion of 0.09A.

In Table III are listed for comparison the positions, and intensities, for the chief maxima and minima of the microphotometer curve and the best theoretical curve, ζ_3, with normal temperature factor. The subscript m refers to the microphotometer curve, and the subscript c to the computed curve. The positions of the maxima and minima check reasonably well, but in all cases the intensities recorded by the microphotometer are less in absolute value than those of the computed curve.[11] Since in cases of other molecules treated in this way, there is much better agreement between the observed and computed intensities, and the resolution is close to unity, the lack of agreement in this case is interpreted as additional evidence for extensive relative motion of the $Si(CH_3)_2$ groups. Large fluctuations in the equilibrium interatomic distances would produce broader peaks and decrease the deviation from unit background.

TABLE III.

Max.	Min.	Positions s_m	Positions s_c	Intensities (relative to unit background) I_m	Intensities (relative to unit background) I_c
	2	3.80	3.78	−0.109	−0.225
3		4.91	4.68	0.256	0.303
	3	6.06	5.92	−0.163	−0.178
4		8.18	7.82	0.043	0.106
	4	10.04	10.08	−0.047	−0.137

In summary, the quantitative comparison of the computed with the observed data is given in Table IV; ζ_3 is the best computed model, the subscript c refers to the computed data, the subscript O refers to observed data, and a and b refer to the data for ζ_3 with normal and large temperature factors, respectively. The average deviation is acceptable. This indicates that the assumed model is satisfactory.

DISCUSSION OF RESULTS

If the bonds between silicon and oxygen and silicon and carbon were completely covalent in character, we should expect, using the covalent bond radii as given by Schomaker and Stevenson,[12] that the silicon-carbon bond distance would be 1.88A, and the silicon-oxygen bond distance 1.76A. It has been found that the silicon-carbon bond is 1.88A, in agreement with the distance predicted, and with the values 1.88±0.04A in neopentyl chloride[9] and 1.93±0.03A in $Si(CH_3)_4$.[13] However, the silicon-oxygen distance is 1.66A, which agrees with the values 1.60A and 1.65A reported for benitoite.[2] These results indicate the presence of one or both of the following: (1) partial double-bond character arising from resonance, and (2) larger ionic character of the bond than is suggested by the electronegativity table. It is more likely that the ionic contribution is the more important one, in view of the physical and chemical evidence against multiple bonding which will be cited.

Infra-red absorption spectra have been obtained by Wright and Hunter of both the linear and cyclic siloxane

[11] For a discussion of the inherent limitations of electron diffraction as a technic for structure determinations, and a listing of the sources of error, see Hastings and Bauer, reference 9.

[12] V. Schomaker and D. P. Stevenson, J. Am. Chem. Soc. **63**, 37 (1941), and unpublished discussions from a conference on the electron diffraction of gases at Cornell University, August, 1947.

[13] L. O. Brockway and H. O. Jenkins, J. Am. Chem. Soc. **60**, 1836 (1938).

TABLE IV.

Max.	Min.	Average s_0	s_c for ζ_3 a	b	s_c/s_0 a	b
	1	2.28	2.27	2.36	0.996	1.035
2		3.22	3.00	2.97	0.932	0.922
	2	3.93	3.78	3.66	0.962	0.931
3		4.82	4.68	4.67	0.971	0.969
	3	5.91	5.92	5.91	1.002	1.000
4		6.82	[7.05]	—	—	—
	4	7.37	[7.33]	—	—	—
5		7.90	7.82	7.92	0.990	1.003
	5	8.50	8.59	—	1.011	—
6		9.13	9.09	—	0.996	—
	6	10.02	10.08	9.97	1.006	0.995
7		11.18	11.06	—	0.989	—
	7	12.62	12.71	12.28	1.007	0.973
8		13.58	13.49	13.22	0.993	0.973
	8	14.39	14.41	14.42	1.001	1.002
9		15.20	15.38	15.43	1.012	1.015
	9	16.79	17.07	16.42	1.017	0.978
10		17.78	17.80	17.30	1.001	0.973
	10	18.81	18.70	18.32	0.994	0.974
11		19.64	19.72	19.72	1.004	1.004
	11	20.80	—	—	—	—
12		21.68	—	—	—	—
	12	22.85	21.77	21.90	0.953	0.958
13		23.97	23.75	23.58	0.991	0.984
	13	25.96	25.43	25.46	0.980	0.981
14		26.56	26.90	27.20	1.013	1.024
	14	29.58	29.20	29.00	0.987	0.980
15		31.61	30.57	30.57	0.967	0.967
				Average	0.991	0.983
				Average deviation	0.015	0.021

Final values
Si−O = (0.991)(1.68) = 1.66±0.04A
Si−C = (0.991)(1.90) = 1.88±0.04A

series.[14] These records cover the range 2–14μ and show many lines, several of them quite strong. The unusual weakness of the C−H bands has been attributed to rather free angular motion of the $-CH_3$ groups around silicon, which decreases the dipole moment of C−H; also the methyl rocking vibration is much stronger in these compounds than in hydrocarbons. This is in agreement with the assumption proposed by Roth[3] that the $-CH_3$ groups in the spiro compound liberate very freely about the Si−C bond position. Indeed, in order to obtain good checks between the observed and calculated x-ray intensities, he had to assume a radius of precession equal to 0.6A. Lack of any evidence of an absorption band due to Si=O at about 6.5μ confirms the chemical evidence[15] that double bonding in the siloxanes does not exist. The strong band at 9.5μ has been assigned to the Si−O stretching vibration.[16]

The spectrograms of the cyclic trimer and linear dimer, first of their respective series, differ more from other members of each series than do subsequent members. The two series approach congruence at large polymer size. This difference of the trimer confirms the suggestion already made by Scott[17] that cyclic methylpolysiloxanes above the trimer are probably strain-free, but that the trimer might have slight strain, since the equilibrium constants for a series of reactions involving this cyclic series varied in regular manner with number of units four or more.

From data on dipole moments of linear and cyclic dimethylpolysiloxanes, Sauer and Mead[18] have computed a Si−O−Si angle of 160±15°. Although the validity of the conclusions reached by these authors regarding the large oxygen valence angle is seriously questioned by their neglect of the atomic polarization term (as pointed out by Baker, Barry, and Hunter[19]); the dielectric constant data nevertheless suggest that the oxygen valence angle is comparatively large, and the force constant for its deformation comparatively small.

ACKNOWLEDGMENT

We wish to thank Dr. Robert O. Sauer of the General Electric Company for the samples of $[(CH_3)_2SiO]_3$ used in this study. The structures of other interesting silicon-oxygen compounds which Dr. Sauer gave us are now in the process of being investigated.

[14] Wright and Hunter, J. Am. Chem. Soc. **69**, 803 (1947); C. W. Young *et al.*, J. Am. Chem. Soc. **70**, 3758 (1948).

[15] Kipping investigated the possible existence of ketone-like structures such as $R_2Si=O$ [J. Chem. Soc. **79**, 455–6 (1901); **91**, 218 (1907); **93**, 442–4 (1908); **95**, 313 (1909); **101**, 2106 (1912)], but could not confirm their existence. Diols or linear and cyclic polymeric compounds always formed instead of the multiply bonded structures. [J. Chem. Soc. **105**, 484 (1914)]. He finally concluded that double bonding between Si and itself or other atoms never occurred [J. Chem. Soc. **1927**, 104 (1927); **1929**, 1180 (1929)]. See also Hunter, Hyde, Warrick, and Fletcher, J. Am. Chem. Soc. **68**, 671 (1946).

[16] The method used by Wright and Hunter (reference 14) for evaluating the ionic character of the Si−O bond from the intensity of the stretching frequency, is highly questionable.

[17] D. W. Scott, J. Am. Chem. Soc. **68**, 2294 (1946).

[18] R. O. Sauer and D. J. Mead, J. Am. Chem. Soc. **68**, 1794 (1946).

[19] Baker, Barry, and Hunter, Ind. Eng. Chem. **38**, 1117 (1946).

Spectroscopic Studies of Rotational Isomerism. V. The Infra-Red Absorption Spectra of Six Solid Hydrocarbons in the Region 1600–650 cm^{-1}*

D. W. E. Axford and D. H. Rank
Spectroscopy Laboratory, School of Chemistry and Physics, The Pennsylvania State College, State College, Pennsylvania

(Received May 23, 1949)

The infra-red absorption spectra of six hydrocarbons have been measured at low temperatures. As with the Raman spectra, a considerable degree of simplification occurs on freezing, due to the existence of only one rotational isomer in the solid state. It has not proved possible to obtain accurate values of the energy differences between the isomers from this data. The possible ways of obtaining energy difference from spectroscopic data are discussed.

THE detection of rotational isomerism in organic compounds by spectroscopic measurements was first proposed and investigated qualitatively by Kohlrausch[1] and Kohlrausch and Koppl.[2]

The first quantitative study of the phenomenon of rotational isomerism by means of the Raman effect was the work of Langseth and Bernstein[3] in which 1,1,2,2-tetrachloroethane was investigated. Mizushima, Morino and Nakamura[4] have investigated a number of hydrocarbons by obtaining Raman spectra in the liquid and solid states. Qualitatively the results of their researches show that the equilibrium concentration of the rotational isomers is temperature dependent.

Recently[5–8] in this laboratory the Raman spectra of a number of hydrocarbons have been investigated in the liquid and solid states. A quantitative study of the energy differences of the observed rotational isomers has been made.

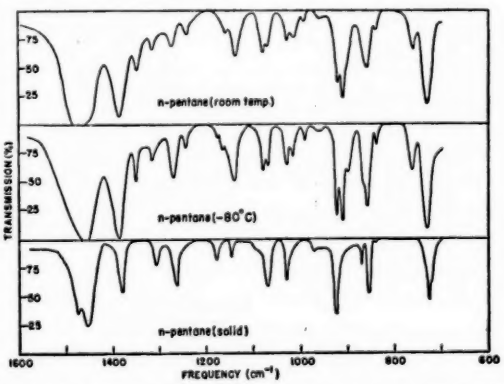

FIG. 1. The infra-red absorption spectrum of *n*-petane at different temperatures. Cell thickness approximately 0.1 mm.

Only a few investigations have been carried out to date on the infra-red spectra of organic compounds at low temperatures. Avery and Ellis[9] have studied ethane, propylene, and 2,2-dimethyl butane at liquid air temperatures and Halford and co-workers[10,11] have studied benzene and cyclohexane. More recently, Thompson and Richards[12] have studied a considerable number of compounds in the solid state.

Recently a paper[13] has appeared by Bernstein in which he has obtained quantitative measurements of the energy differences of the rotational isomers in 1–2 dichloroethane. This is the first demonstration of the spectroscopic method of investigating these isomers by means of infra-red absorption spectra. Gerding[14] has cast some doubt upon measurements of energy differences of rotational isomers by means of observations on spectra produced in the liquid state. To avoid these objections, which may or may not be valid, depending on the behavior of the material under investigation,

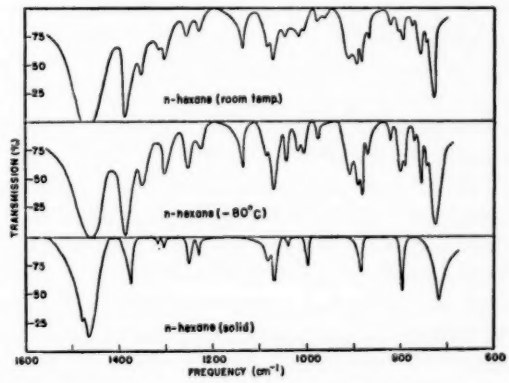

FIG. 2. The infra-red absorption spectrum of *n*-hexane at different temperatures. Cell thickness approximately 0.1 mm.

* This research was carried out on contract N6onr-269, Task V, of the Office of Naval Research.

[1] K. W. F. Kohlrausch, Zeits. f. physik Chemie. **B18**, 61 (1932).
[2] K. W. F. Kohlrausch and F. Koppl, Zeits. f. physik Chemie. **B26**, 209 (1934).
[3] A. Langseth and H. J. Bernstein, J. Chem. Phys. **8**, 410 (1941).
[4] Mizushima, Morino, and Nakamura, Sci. Pap. Inst. Phys. Chem. Res. (Tokyo).
[5] Szasz, Sheppard, and Rank, J. Chem. Phys. **16**, 704 (1948).
[6] Rank, Sheppard, and Szasz, J. Chem. Phys. **17**, 83 (1949).
[7] N. Sheppard, and G. J. Szasz, J. Chem. Phys. **17**, 86 (1949).
[8] G. J. Szasz, and N. Sheppard, J. Chem. Phys. **17**, 93 (1949).
[9] W. H. Avery and C. F. Ellis, J. Chem. Phys. **10**, 10 (1942).
[10] R. S. Halford and G. B. Carpenter, J. Chem. Phys. **15**, 99 (1947).
[11] R. S. Halford and O. A. Schaeffer, J. Chem. Phys. **14**, 141 (1946).
[12] R. E. Richards and H. W. Thompson, Proc. Roy. Soc. (London) **195**, 1 (1948).
[13] H. J. Bernstein, J. Chem. Phys. **17**, 258 (1949).
[14] H. Gerding and P. G. Meerman, Rec. Trav. Chim. **61**, 523 (1942).

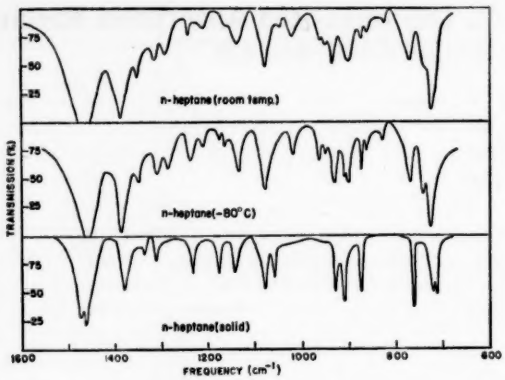

FIG. 3. The infra-red absorption spectrum of *n*-heptane at different temperatures. Cell thickness approximately 0.1 mm.

Bernstein has made his measurements in the vapor phase. It goes without saying that if it is possible to make measurements in the vapor phase, this method is very much more desirable than using measurements made in the liquid state. The complicating phenomena associated with the liquid state do not enter into the results of the experiments with the vapor.

The character of infra-red absorption bands in the gas phase for molecules of more than a very few atoms will often make the determination of energy differences of rotational isomers difficult or impossible when the study is made in the gas phase by means of infra-red absorption spectra. In general, the rotational structure of infra-red absorption bands in the gas phase is so widespread that anything approaching complete resolution of a pair of moderately close bands in the spectrum of even a simple molecule is relatively impossible.

In the Raman spectrum the situation is much more favorable since the bands in general are inherently very much sharper owing to the difference in selection rules for the rotational structure. However, a study of rotational isomerism by means of the variation in intensity of Raman lines obtained by excitation in the gas would be experimentally extremely difficult. With regard to the infra-red spectrum, the difficulties occasioned by rotational structure are not greatly diminished when one proceeds from the gas to the liquid at ordinary temperatures. However, at low temperatures, the bands will become very much sharper. This increased sharpness will allow at least a qualitative study of rotational isomerism. In the case of spectra which are produced by molecules somewhat larger than the molecules investigated by Bernstein, the complicating nature of the rotational structure may not permit quantitative determinations of energy differences of rotational isomers to be made even if temperatures are reduced, producing much sharper absorption bands. The purpose of this research is to investigate the possibility of obtaining energy differences of rotational isomers by means of the infra-red absorption spectra of some simple hydrocarbons. We have also investigated the discontinuous nature of the conversion of rotational isomers when the material is transformed to the solid state, which phenomena has previously been observed in the Raman effect.

EXPERIMENTAL

The absorption cell which was used in the present investigation was based on a design employed by Dr. R. C. Lord at the Massachusetts Institute of Technology. It consists of an ordinary infra-red absorption cell for liquids attached to the end of a copper tube which is sealed at the other end into a Pyrex tube and constitutes the bottom of a Dewar flask. This tube fits by means of a ground joint into an outer jacket with silver chloride windows which can be evacuated. The absorption cell was filled with the liquid under examination, and placed in the jacket which was then flushed with nitrogen. The liquid was then frozen by pouring liquid air into the Dewar flask and the cell evacuated by means of a Hyvac pump. Though the cell is best employed at liquid air temperatures, where it is possible to evacuate the outer jacket, it was found possible to

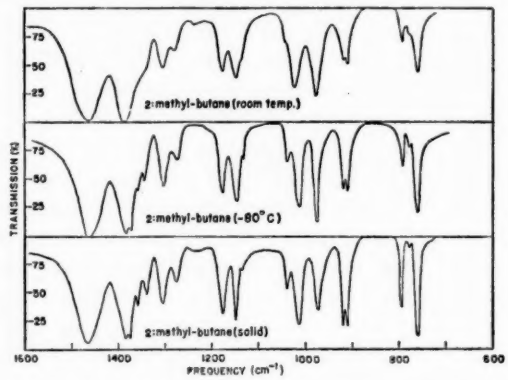

FIG. 4. The infra-red absorption spectrum of 2-methylbutane at different temperatures. Cell thickness approximately 0.1 mm.

get good traces at −80°C using CO_2/acetone as a refrigerant, even though the jacket could not be evacuated at this temperature. The procedure for filling the cell and freezing the sample was straightforward except in the case of *n*-butane. The procedure with this compound has already been described.[15] All traces were run using a constant energy drive on the spectrometer, which was a standard Perkin-Elmer Model 12C instrument. This drive did not yield a perfectly flat I_0 curve and the curves shown later have all been corrected so that they give percent transmissions accurate to approximately 5 percent. Calibration of the instrument and estimates of the scattered light correction were carried out in the usual way. The compounds studied here are the same as those used in the previous Raman investigations from this laboratory; namely: *n*-butane, *n*-pentane, *n*-hexane, *n*-heptane, 2-methylbutane (isopentane) and 2,3-dimethyl butane.

[15] D. W. E. Axford and D. H. Rank, J. Chem. Phys. **17**, 430 (1949).

RESULTS

The absorption curves obtained for the various substances are contained in Figs. 1–5. They show the absorption spectrum of each substance between 1600 and 650 cm^{-1} at room temperature (approximately 25°C), −80°C, and when frozen at approximately liquid-air temperatures.

In Table I are listed the frequencies of absorption maxima observed in the straight-chain hydrocarbons at −80°C and in the solid state. The frequencies given are those quoted in the A.P.I. data on hydrocarbons.[16] They have not been corrected to vacuum. We have noted appreciable shifts in the positions of the maxima of some of the bands when the temperature is lowered, but these are not shown in the tables, which are the positions the bands would have at room temperature. In Table II are listed similar values for the two branched chain hydrocarbons studied.

All spectra become very much sharper on cooling, and accordingly certain bands which are diffuse at room temperatures are split at lower temperatures. This effect is very noticeable in the case of the branched hydrocarbons.

TABLE I. Observed frequencies in hydrocarbon spectra at −80°C and in the solid state.

n-Pentane		*n*-Hexane		*n*-Heptane	
−80°C	Solid	−80°C	Solid	−80°C	Solid
1464	1474	1467	1478	1470	1473
	1452		1456		1467
1379	1379	1379	1379	1377	1377
1342		1341		1342	1342
1308	1308		1307	1300	1300
1265	1265	1293	1293	1278	
1237		1246	1246	1232	1232
	1176	1219	1219	1204	
1162		1137		1176	1176
1138	1138	1066	1066	1166	
1072		1057	1057	1137	1137
1067	1067	1037	1037	1074	1074
1025	1025	1015			1055
1014		1005	1005	1020	
989		973		965	
965	965	905		945	
919	919	890		930	930
907		884	884	908	908
900		869		900	
868	868	825		875	875
861	861	804		863	
840		794	794	833	
763		773		773	773
728	728	759		739	
	721	726	726	723	724
					721

DISCUSSION

We shall briefly discuss the spectrum of *n*-butane reported previously[15] since recently a paper by Gates[17] has appeared which somewhat supplements previous work. In any event *n*-butane is a small enough molecule so that it may be feasible in the near future to obtain a complete and unambiguous analysis of its vibrations.

Previously,[5] making use of available infra-red data and temperature classification and polarization data from the Raman spectrum, an attempt was made to analyze the vibrations of the *trans*-isomer of *n*-butane. At the time this work was done the authors were aware of the necessity for similar temperature classification data from the infra-red spectrum. We have recently obtained this data[15] and made certain changes in assignment necessitated by this new experimental material. In our note mentioned above, owing to a typing error in comment (2), it was stated that both the band at 1340 cm^{-1} and that at 795 cm^{-1} disappear on cooling. Since as can be seen from the published curves, the 1340 cm^{-1} band persists in the solid, the remarks in comment (2) obviously do not apply to this band. There is a reasonable probability that the 1340 cm^{-1} frequency is a combination frequency of the 215 cm^{-1} skeletal torsional vibration found by Gates[17] with one of the CH_3 wagging vibrations around 1140 cm^{-1}. It should be pointed out that from work on the Raman effect of *n*-butane[5] it seems extremely unlikely that the 325 cm^{-1} Raman frequency belongs to the *trans*-isomer as suggested by Gates[17] in his recent assignment of the skeletal vibrations of *n*-butane. From our work it seems to be almost a certainty that the 432 cm^{-1} frequency belongs to the *trans*-isomer and the 325 cm^{-1} frequency belongs to the low energy form. It must be mentioned for the sake of completeness that the statement made by Gates[17] that the infra-red spectrum of *n*-butane gas can be interpreted in terms of only a single rotational isomer seems to rest on a rather insecure foundation in view of our present knowledge of the spectrum of gaseous, liquid, and solid *n*-butane. Furthermore, recent work on molecular vibrations tends to make it obvious that only when complete infrared and Raman spectra with polarizations are available is it possible to approximate correct assignments of molecular vibrations of even the more simple polyatomic molecules.

The traces for the straight-chain hydrocarbons show that there is a considerable degree of simplification on

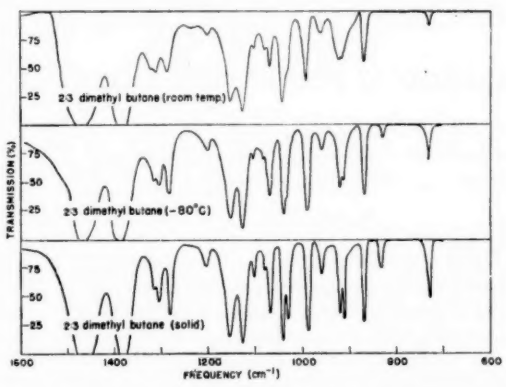

FIG. 5. The infra-red absorption spectrum of 2,3-dimethyl butane at different temperatures. Cell thickness approximately 0.1 mm.

[16] American Petroleum Institute Research Project No. 44.
[17] David M. Gates, J. Chem. Phys. 17, 393 (1949).

TABLE II. Observed frequencies in hydrocarbon spectra at −80°C and in the solid state.

2-Methylbutane		2,3-Dimethyl butane	
−80°C	Solid	−80°C	Solid
1462	1462	1459	1459
1381	1381	1381	1381
1368	1368	1308	1308
1352	1352	1297	1297
1337	1337	1280	1280
1299	1299	1196	1196
1269	1269	1153	1153
1176	1176	1129	1129
1149	1149	1106	1106
1135	1135	1083	1083
1043	1043	1066	1066
1014	1014	1038	1038
974	974	—	1028
920	920	991	991
910	910	958	958
796	796	921	921
779	779	910	910
764	764	870	870
		832	832
		728	728

cooling, paralleling their behavior in the Raman effect. A close study of our curves showed some significant shifts in the positions of the maxima of certain bands on freezing. At the present time we have not studied this effect closely, though its reality is convincing. Not all bands are shifted and one must conclude, as might in any case be expected, that certain vibrations are much more sensitive to change in environment than others.

Attempts to obtain values for the energy differences between the various rotational isomers from the data reproduced here were not very successful. There are variations in the relative intensities of certain line pairs in the straight-chain hydrocarbons, but the behavior is nowhere near as clean-cut as in the case of the Raman spectra. Few, if any, bands appear to decrease in absolute intensity on cooling, though in all cases, a number increase. This is probably because of the greater importance of rotational structure in the case of absorption with its attendant overlapping of bands. No value could be obtained with *n*-butane as it proved too difficult with our cell to obtain a satisfactory spectrum of liquid *n*-butane at temperatures near that of the room.

It appears from our results that the Raman spectra in general are better than the infra-red for obtaining quantitative data on rotational isomerism. On the other hand, the infra-red spectrum shows the existence of the phenomenon convincingly in a relatively simple fashion and should prove of use in further investigations.

The results on the two branched-chain hydrocarbons 2-methylbutane and 2,3-dimethyl butane appear to confirm the results obtained from the Raman spectra. In neither case was there any simplification on freezing; in fact, owing to the sharpening of the bands, the solid spectra are actually more complex than those at room temperature.

There were no significant changes in the relative intensities of the bands on cooling. These branched-chain hydrocarbons showed considerably higher absolute transmissions at liquid-air temperatures than did the straight-chain compounds, though direct observation showed beyond doubt that these liquids were frozen. It seems possible in view of this high transmission, that the branched hydrocarbons formed glasses instead of crystallizing. The absence of changes in the relative intensities of the bands and the lack of simplification on cooling mean that it is still impossible to decide unambiguously between the cases of either a small or relatively large energy difference between the isomers.

ACKNOWLEDGMENT

We wish to thank Miss Thelma Hobaugh for assistance in the preparation of the figures, and the Petroleum Research Laboratory of this College who kindly supplied the hydrocarbons.

THE JOURNAL OF CHEMICAL PHYSICS VOLUME 18, NUMBER 1 JANUARY, 1950

Light Scattering Arising from Composition Fluctuations in Multi-Component Systems

JOHN G. KIRKWOOD AND RICHARD J. GOLDBERG
The Gates and Crellin Laboratories of Chemistry, California Institute of Technology, Pasadena, California
(Received May 6, 1949)

A general theory of Rayleigh scattering due to composition fluctuations in multi-component systems is developed with the aid of the grand canonical ensemble of Gibbs. It reduces to the usual expression for systems of two components, but contains previously neglected terms arising from thermodynamic interactions between solutes in systems of more than two components. The theory is used to interpret the turbidity measurements of polystyrene in benzene-methanol mixtures of Ewart, Roe, Debye, and McCartney.

I

THE utility of light scattering measurements in the determination of molecular weights and in the study of thermodynamic interactions in solutions of macromolecules has been clearly demonstrated in recent years. Correct theoretical interpretation of the measurements has been achieved for two-component systems composed of one macromolecular solute in a solvent of low molecular weight. However, attempts to extend the two-component theory to multi-component systems

have led to certain errors and misconceptions, the correction of which is one of the purposes of the present article.

A general theory of composition fluctuations in multicomponent systems will be developed with the use of the grand canonical ensemble of Gibbs. The theory provides a complete thermodynamic description of Rayleigh scattering without the use of supplementary molecular assumptions, although the latter may be of importance in interpreting the thermodynamic information obtained from the light scattering measurements.

It is found that thermodynamic interaction between a macromolecular solute and a solute of low molecular weight may cause the former to induce composition fluctuations with respect to the latter of the same order of magnitude as composition fluctuations with respect to the macromolecular species itself. This effect, which has been neglected in previous theories, is shown to be of importance in interpreting turbidity measurements of solutions of macromolecules in mixed solvents. To illustrate the use of the theory, an analysis is made of the turbidity measurements of solutions of polystyrene in benzene-methanol mixtures obtained by Ewart, Roe, Debye, and McCartney.[1]

II

The turbidity τ_0 of a fluid arising from Rayleigh scattering of light of wave-length λ is determined by the well-known relation,[2] based on the theory of Einstein,

$$\tau_0=(8\pi^3/3\lambda^4)V\langle\Delta\epsilon^2\rangle_{Av}, \tag{1}$$

where $\langle\Delta\epsilon^2\rangle_{Av}$ is the dielectric constant fluctuation in a region of volume V. We shall be concerned here only with those contributions to $\langle\Delta\epsilon^2\rangle_{Av}$ arising from composition and density fluctuations. If we denote by $m_0, \cdots m_\nu$ the average masses and by $N_0, \cdots N_\nu$ the numbers of molecules of the several components in the region V, and define

$$\begin{aligned} c_i&=m_i/m_0; \quad i=1, \cdots \nu,\\ m_i&=M_i\langle N_i\rangle_{Av}/N,\\ \Delta N_i&=N_i-\langle N_i\rangle_{Av},\\ \xi_i&=\Delta N_i/\langle N_i\rangle_{Av}-\Delta N_0/\langle N_0\rangle_{Av},\\ \xi&=\sum_{k=0}^{\nu}\bar{v}_k\Delta N_k/NV; \end{aligned} \tag{2}$$

where N is Avogadro's number and $\bar{v}_k$ the partial molar volume of component k, we may write,

$$\langle\Delta\epsilon^2\rangle_{Av}=\frac{\langle\xi^2\rangle_{Av}}{\kappa^2}\left(\frac{\partial\epsilon}{\partial p}\right)^2_{T,c} +\sum_{\substack{i,k\\=1}}^{\nu}c_ic_k\langle\xi_i\xi_k\rangle_{Av}\left(\frac{\partial\epsilon}{\partial c_i}\right)_{T,p,c_j}\left(\frac{\partial\epsilon}{\partial c_k}\right)_{T,p,c_j}, \tag{3}$$

where κ is the compressibility of the fluid, and the sum extends over all solute species, $k=1, \cdots \nu$, the subscript zero denoting solvent. The first term of Eq. (3) arises from density fluctuations at constant composition, and the second from composition fluctuations. Except for critical phases, Eq. (3) is exact to terms of statistically negligible order of magnitude. We now define in the customary manner the turbidity τ due to composition fluctuations,

$$\begin{aligned} \tau_0&=\tau+\frac{8\pi^3V}{3\lambda^4}\frac{\langle\xi^2\rangle_{Av}}{\kappa^2}\left(\frac{\partial\epsilon}{\partial p}\right)^2_{T,c}\\ \tau&=\frac{8\pi^3V}{3\lambda^4}\sum_{\substack{i,k\\=1}}^{\nu}c_ic_k\langle\xi_i\xi_k\rangle_{Av}\left(\frac{\partial\epsilon}{\partial c_i}\right)_{T,p,c_j}\left(\frac{\partial\epsilon}{\partial c_k}\right)_{T,p,c_j}, \end{aligned} \tag{4}$$

where the second term of the first of Eqs. (4) is the turbidity arising from pure density fluctuations. In Eqs. (3) and (4), we have anticipated the result, $\langle\xi\xi_i\rangle_{Av}=0$, presently to be proved.

In order to determine the composition fluctuations we employ the theory of the grand canonical ensemble in a manner which has been earlier described by one of us.[3] The probability that an open region V in an infinite mass of fluid contain exactly $N_0, N_1, \cdots N_\nu$ molecules of the several components, considered as an example of a grand canonical ensemble, is

$$\begin{aligned} P&=\exp([\Omega+\sum_{i=0}^{\nu}N_i\mu_i'-A(N_0\cdots N_\nu)]/kT),\\ \Omega&=-pV+kT\log\sigma, \end{aligned} \tag{5}$$

where k is Boltzmann's constant, T the temperature, μ_i' the chemical potential of component i, per molecule, and A is the Helmholtz free energy of the region when it contains the specified numbers of molecules. The term $kT\log\sigma$ is of statistically negligible magnitude relative to pV, but is important for normalization in the order required for the calculation of the composition fluctuations. Expansion of the exponent of the right-hand side of Eq. (5) in the variables $N_i-\langle N_i\rangle_{Av}$ yields, with the neglect of terms of higher degree than quadratic, which, except for critical phases make statistically negligible contributions to mean values,

$$\begin{aligned} P&=\sigma\exp(-\tfrac{1}{2}\sum_{\substack{i,k\\=0}}^{\nu}\beta_{ik}^0\Delta N_i\Delta N_k),\\ \Delta N_i&=N_i-\langle N_i\rangle_{Av},\\ kT\beta_{ik}^0&=\left(\frac{\partial^2A}{\partial N_i\partial N_k}\right)_{T,V,N_j}=\left(\frac{\partial\mu_i'}{\partial N_k}\right)_{T,V,N_j}=\left(\frac{\partial\mu_k'}{\partial N_i}\right)_{T,V,N_j}. \end{aligned} \tag{6}$$

[1] Ewart, Roe, Debye, and McCartney, J. Chem. Phys. **14**, 687 (1946); P. Debye, J. Phys. Coll. Chem. **51**, 18 (1947).

[2] See, for example, Doty, Zimm, and Mark, J. Chem. Phys. **13**, 159 (1945).

[3] J. G. Kirkwood, mimeographed notes, "Lectures on statistical mechanics" delivered at Princeton University (Spring term, 1947).

We now make use of the mathematical relation,

$$\left(\frac{\partial \mu_i'}{\partial N_k}\right)_{T,\,V,\,N_j} = \frac{\bar{v}_i \bar{v}_k}{N^2 \kappa V} + \frac{M_k}{N^2 m_0}\left(\frac{\partial \mu_i}{\partial c_k}\right)_{T,\,p,\,c_j}, \quad (7)$$

where N is Avogadro's number, $\bar{v}_i$ the partial molar volume of component i, M_i the molecular weight, and μ_i is the chemical potential per mole of that component. The coefficients $\beta_{ik}{}^0$ may then be expressed in the form,

$$\beta_{ik}{}^0 = \frac{\bar{v}_i \bar{v}_k}{N^2 \kappa V k T} + \frac{N m_0}{2}\frac{\beta_{ik}}{\langle N_i\rangle_{Av}\langle N_k\rangle_{Av}},$$

$$\beta_{ik} = \frac{c_i c_k}{M_i R T}\left(\frac{\partial \mu_i}{\partial c_k}\right)_{T,\,p,\,c_j} = \frac{c_i c_k}{M_k R T}\left(\frac{\partial \mu_k}{\partial c_i}\right)_{T,\,p,\,c_j}, \quad (8)$$

$$\sum_{k=0}^{\nu} \beta_{ik} = 0; \quad \beta_{00} = \sum_{\substack{i,\,k\\=1}}^{\nu} \beta_{i0}\beta_{k0},$$

where the sum rules for the coefficients β_{ik} follow from the Gibbs-Duhem equation. Introducing the composition fluctuation variables ξ_i and the reduced density fluctuation variable ξ, of Eq. (2)

$$\xi_i = \Delta N_i/\langle N_i\rangle_{Av} - \Delta N_0/\langle N_0\rangle_{Av},$$
$$\xi = \sum_{k=0}^{\nu} \bar{v}_k \Delta N_k / NV; \quad (9)$$

we obtain from Eqs. (6) and (8) the fluctuation distribution function,

$$P(\xi_1 \cdots \xi_\nu, \xi) = \frac{(2\pi)^{-(\nu+1/2)}(\kappa V k T)^{-\frac{1}{2}}}{|\beta|^{\frac{1}{2}}} \times \exp\left(-(N m_0/2)\sum_{\substack{i,\,k\\=1}}^{\nu} \beta_{ik}\xi_i\xi_k - V\xi^2/2\kappa k T\right) \quad (10)$$

$$|\beta| = |\beta_{ik}|,$$

where $|\beta|$ is the determinant of the thermodynamic coefficients β_{ik}. It will be remarked that the transformation, Eq. (9), has eliminated non-diagonal terms in the Gaussian distribution involving the composition fluctuations ξ_i and the density fluctuation ξ.

The distribution function, Eq. (10), yields with the aid of the theory of quadratic forms the following mean values,

$$V\langle \xi_i \xi_k\rangle_{Av} = (V/N m_0)(|\beta|_{ik}/|\beta|); \quad i, k = 1 \cdots \nu,$$
$$V\langle \xi^2\rangle_{Av} = \kappa k T, \quad (11)$$
$$\langle \xi \xi_i\rangle_{Av} = 0,$$

where $|\beta|_{ik}$ is the appropriate co-factor of the determinant $|\beta|$. Substitution of the density and composition fluctuations of Eq. (11) into Eqs. (1) and (3) yields the following expressions for the turbidity,

$$\tau_0 = \tau + (8\pi^3/3\lambda^4)(kT/\kappa)(\partial\epsilon/\partial p)^2_{T,c},$$

$$\tau = \frac{8\pi^3}{3\lambda^4}\frac{1}{N\rho_0}\sum_{\substack{i,\,k\\=1}}^{\nu} c_i c_k \frac{|\beta|_{ik}}{|\beta|}\left(\frac{\partial \epsilon}{\partial c_i}\right)_{T,\,p,\,c_j}\left(\frac{\partial \epsilon}{\partial c_k}\right)_{T,\,p,\,c_j}, \quad (12)$$

where ρ_0 is the mass of solvent in unit volume. Equations (12) give a complete description of Rayleigh scattering arising from density and composition fluctuations in terms of thermodynamically defined quantities and the derivatives $(\partial\epsilon/\partial c_i)_{T,\,p,\,c_j}$. The non-diagonal terms in which have previously been neglected in the analysis of Rayleigh scattering in multi-component systems, make it possible for a solute of high molecular weight to induce significant composition fluctuations with respect to a second solute of low molecular weight as the result of strong thermodynamic interaction between the two.

III

We shall now present several applications of Eq. (12), which illustrate the manner in which the turbidity of a multi-component fluid may be used to obtain thermodynamic information relating to the dependence of the chemical potentials of the components on composition. For the case of two components, Eq. (12) of course reduces to the expression,

$$\tau = \frac{8\pi^3 RT}{3\lambda^4 N\rho_0}\left(\frac{\partial \epsilon}{\partial c_1}\right)^2_{T,\,p} M_1 \Big/ \left(\frac{\partial \mu_1}{\partial c_1}\right)_{T,\,p}, \quad (13)$$

given by the elementary theory of composition fluctuations and which has been extensively used in light scattering studies. In order to simplify Eq. (12) in the multi-component case, we suppose all solutes to be non-electrolytes and expand the excess chemical potentials in power series in the concentrations c_i,

$$\mu_i = RT\log\gamma_i c_i + \mu_i{}^0(T, p),$$
$$\mu_i{}^0 = \lim_{c_1 \cdots c_\nu} [\mu_i - RT\log c_i], \quad (14)$$
$$\log\gamma_i = \sum_{k=1}^{\nu} A_{ik}c_k + 0(c_k c_j),$$

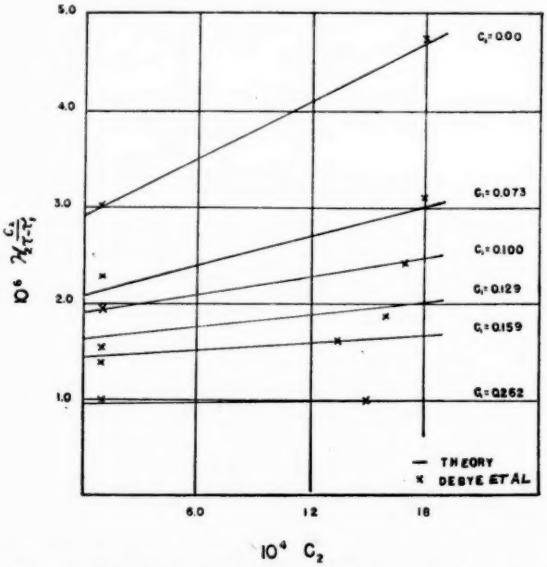

FIG. 1. Turbidity-composition curves of solutions of polystyrene in benzene-methanol mixtures.

retaining only linear terms in the expansions of $\log\gamma_i$. In this approximation, we may write,

$$(\partial\mu_i/\partial c_k)=(RT/c_i)\delta_{ik}+A_{ik},$$
$$M_kA_{ik}=M_iA_{ki}, \tag{15}$$

where, as henceforth, we abbreviate the derivatives $(\partial\mu_i/\partial c_k)_{T,\,p,\,c_j}$ as $\partial\mu_i/\partial c_k$. Using Eq. (15), we find

$$|\beta|_{ik}/|\beta|=M_i\delta_{ik}/c_i-M_iA_{ki},$$
$$\tau=\frac{8\pi^3}{3N\rho_0\lambda^4}\left\{\sum_{k=1}^{\nu}M_kc_k\left(\frac{\partial\epsilon}{\partial c_k}\right)^2-\tfrac{1}{2}\sum_{\substack{i,\,k\\=1}}^{\nu}M_kA_{ik}\frac{\partial\epsilon}{\partial c_i}\frac{\partial\epsilon}{\partial c_k}c_ic_k\right\}, \tag{16}$$

where we abbreviate $(\partial\epsilon/\partial c_i)_{T,p,c_j}$ by $\partial\epsilon/\partial c_i$. In the case of a polymer with a molecular weight distribution, where it is appropriate to treat $\partial\epsilon/\partial c_i$ as independent of i in first approximation, we obtain

$$\frac{Hc}{\tau}=\frac{1}{\langle M\rangle_{Av}}+\frac{c}{\langle M\rangle_{Av}^2}\sum_{\substack{i,\,k\\=1}}^{\nu}M_kA_{ik}f_if_k,$$
$$c=\sum_{k=1}^{\nu}c_k;\quad\langle M\rangle_{Av}=\sum_{k=1}^{\nu}f_kM_k, \tag{17}$$
$$H=(8\pi^3/3N\rho_0\lambda^4)(\partial\epsilon/\partial c)^2,$$

where f_i is the weight fraction of component of molecular weight M_i. In a previous attempt to adapt two-component fluctuation theory to this case,[4] the non-diagonal terms in the sum of Eq. (17) were overlooked.

We now turn our attention to the system of three components. In this case Eq. (12) may be put in the form,

$$\Delta\tau=\frac{H_2M_2RT}{\partial\mu_2/\partial c_2}\frac{1-2\alpha\omega_1+\alpha^2\omega_1^2}{1-(M_2/M_1)\omega_1\omega_2},$$
$$\Delta\tau=\tau-\tau_1;\quad H_2=\frac{32\pi^3n^2}{3N\rho_0\lambda^4}\left(\frac{\partial n}{\partial c_2}\right)^2;\quad\epsilon=n^2, \tag{18}$$
$$\omega_1=(\partial\mu_1/\partial c_2)/(\partial\mu_1/\partial c_1),$$
$$\omega_2=(\partial\mu_1/\partial c_2)/(\partial\mu_2/\partial c_2),$$
$$\alpha=(\partial n/\partial c_1)/(\partial n/\partial c_2),$$

where τ_1 is given by Eq. (13). If all components are non-electrolytes, and we employ the power series,

$$\log\gamma_i=\sum_{k=1}^{2}A_{ik}c_k+\sum_{\substack{j,\,k\\=1}}^{2}B_{ijk}c_jc_k+\cdots,$$
$$\alpha=\alpha_0+\alpha_1c_1+\alpha_2c_2, \tag{19}$$

for the activity coefficients, γ_i, and the refractive index ratio, α, we obtain the following expansion of Eq. (19),

$$H_2c_2/\Delta\tau=1/M_2\{1+G_{10}c_1+G_{01}c_2+G_{20}c_1^2+G_{11}c_1c_2+G_{02}c_2^2\};$$
$$G_{10}=2\alpha_0A_{12};\quad G_{01}=A_{22};\quad G_{02}=2B_{222};$$
$$G_{20}=4\alpha_0B_{112}-2\alpha_0A_{11}A_{12}+2\alpha_1A_{12}+3\alpha_0^2A_{12}^2; \tag{20}$$
$$G_{11}=2(1+2(M_1/M_2)\alpha_0)B_{212}-(M_2/M_1)A_{12}^2+2\alpha_0A_{12}A_{22}+2\alpha_2A_{12}.$$

We have analyzed the light scattering data of Ewart, Roe, Debye, and McCartney[1] on solutions of polystyrene in benzene-methanol mixtures, by means of Eq. (20), supplemented by an additional cubic term of the order $c_1^2c_2$, the coefficient of which we do not interpret theoretically, although this could easily be done. The curves from which the coefficients are determined are compared with experiment in Fig. 1. It will be observed that the measurements are reasonably well reproduced. The coefficients of the refractive index increment ratio α were estimated to be $\alpha_0=-1.9$; $\alpha_1=4.8$; $\alpha_2=0$. The values of the thermodynamic interaction coefficients, A_{ik} and B_{ijk}, of Eq. (20), calculated from the experimentally determined coefficients G_{ik} of Eq. (20) are presented in Table I. The coefficients A_{ik} and B_{ijk} are, of course, dimensionless, but it should be remembered that the numerical values are appropriate to concentrations c_i expressed in grams of solute per gram of benzene.

The calculations which have been presented exhibit the manner in which turbidity measurements may be used in conjunction with the present theory to obtain thermodynamic data in multi-component systems containing at least one macromolecular component. The positive value of the interaction coefficient A_{12} for polystyrene and methanol, when interpreted from the molecular standpoint, means, as Debye surmised, that a polystyrene molecule exhibits a preference for benzene molecules in its statistical environment. Such qualitative considerations should, however, be regarded as supplementing the thermodynamic theory presented here, rather than the basis for an exact analysis of turbidity.

TABLE I. Thermodynamic interaction coefficients in benzene-methanol-polystyrene solutions.*

A_{12}	A_{22}	B_{212}	B_{222}
1.1	340	5100	0.0

* Subscript 1, methanol; subscript 2, polystyrene; $M_2=3.45\times10^5$.

[4] B. Zimm, and P. Doty, J. Chem. Phys. **12**, 203 (1944).

THE JOURNAL OF CHEMICAL PHYSICS VOLUME 18, NUMBER 1 JANUARY, 1950

Light Scattering in Multi-Component Systems*

W. H. STOCKMAYER
Department of Chemistry, Massachusetts Institute of Technology, Cambridge, Massachusetts
(Received May 31, 1949)

A general equation is developed for the fluctuation of refractive index in multi-component systems, thus permitting the interpretation of turbidities for such systems in the absence of angular dissymmetry. Applications to several special cases of interest are presented.

1. INTRODUCTION

MEASUREMENTS of light scattering from polymer solutions have yielded much valuable information concerning average molecular weights, molecular dimensions, and thermodynamic interaction-constants.[1] These measurements have been largely restricted to one- or two-component systems. Multi-component systems have thus far received scant attention, but existing data, such as those of Ewart, Roe, Debye, and McCartney[2] on polymers in mixed solvents, indicate that the theoretical equations developed for binary systems cannot be used without amendment for the interpretation of measurements on ternary or more complex mixtures. The latter authors gave a theory only for the special case of an infinitely dilute polymer solution in a mixed solvent.

General equations for multi-component systems would be desirable for a number of reasons. For example, strict interpretation of the data for polymers in pure solvents requires recognition of the fact that even "sharp" polymer fractions are composed of many components. Also, certain polymers of interest are appreciably soluble only in mixed solvents. Finally, interpretation of the data for multi-component systems affords a relatively rapid and simple method of evaluating certain thermodynamic quantities of interest.

In this paper, equations are derived for fluctuations of refractive index in multi-component systems, permitting the interpretation of turbidity in cases for which the angular dissymmetry of the scattered light is negligible. Systems displaying angular dissymmetry could be treated by an extension of the theory of Zimm,[3] but will not be considered here.

2. FLUCTUATION THEORY

In the absence of angular dissymmetry, the turbidity, τ, of a liquid is given by the equation

$$\tau=(32\pi^3n^2/3\lambda^4)V\langle(\Delta n)^2\rangle_N, \qquad (2.1)$$

where λ is the wave-length, n the refractive index, and $\langle(\Delta n)^2\rangle_N$ is the fluctuation of refractive index in a region of volume V.

There are several ways in which the fluctuation of refractive index could be evaluated, corresponding to different choices of independent thermodynamic variables. Physically, it is perhaps easiest to visualize fluctuations in the quantities of all components in a small constant volume of the solution. However, in view of the set of thermodynamic variables ultimately to be used, we have preferred to consider the fluctuation of index in a portion of solution containing a constant mass of some one component. The choice of this component, which we shall call the first, is arbitrary, but for dilute solutions it is obviously convenient to choose the solvent, and to fix its quantity as one kilogram; the numbers of moles of the other $(C-1)$ components are then their weight-molalities.

We express the refractive index as a function of temperature T, pressure p, and quantities of components $m_2, m_3, \cdots, m_C$. An infinitesimal variation in index is thus given by

$$dn=(\partial n/\partial T)_{p,m}dT+(\partial n/\partial p)_{T,m}dp+\sum_2^C{}_i\,(\partial n/\partial m_i)_{T,p,m}dm_i. \qquad (2.2)$$

The quantities m_i of the components may be measured in grams, moles, molecules, or any desired units, the definitions of their chemical potentials varying accordingly. The subscript m, as is customary, denotes constancy of all the m_i not specifically indicated as variable in the derivative to which it is subscribed.

For all wave-lengths of interest, the refractive index depends on pressure and temperature, at constant composition, sensibly only through the density ρ. Hence Eq. (2.2) may be written

$$dn=(-\alpha dT+\kappa dp)(\partial n/\partial\ln\rho)_m+\sum_2^C{}_i\,\psi_i dm_i$$

with

$$\alpha=(\partial\ln V/\partial T)_{p,m},\quad \kappa=-(\partial\ln V/\partial p)_{T,m},\quad \psi_i=(\partial n/\partial m_i)_{T,p,m}. \qquad (2.3)$$

Since fluctuations of extensive variables are more simply treated, we make use of the thermodynamic relation

$$dV=\alpha V dT-\kappa V dp+\textstyle\sum_i\bar v_i dm_i, \qquad (2.4)$$

* A similar investigation has been independently carried out by J. G. Kirkwood and R. J. Goldberg (J. Chem. Phys. **18**, 54 (1949)), but was not known to the author until this manuscript had been substantially completed. See also H. C. Brinkman and J. J. Hermans, J. Chem. Phys. **17**, 574 (1949).

[1] For reviews, see G. Oster, Chem. Rev. **43**, 319 (1948); H. Mark, *Frontiers in Chemistry* (Interscience Publishers, Inc., New York, 1948), Vol. 5, Chap. 5.

[2] Ewart, Roe, Debye, and McCartney, J. Chem. Phys. **14**, 687 (1946).

[3] B. H. Zimm, J. Chem. Phys. **13**, 141 (1945); *ibid.* **16**, 1093 (1948).

where $\bar{v}_i=(\partial V/\partial m_i)_{T,p,m}$, to rewrite Eq. (2.3) in the form

$$dn=(\partial n/\partial \ln\rho)_m(\sum_2^C{}_i \bar{v}_i dm_i-dV)/V+\sum_2^C{}_i \psi_i dm_i. \quad (2.5)$$

From the above equation, it is clear that fluctuations of volume and of the m_i are desired for a system in statistical equilibrium with surroundings in which constant values of T, p and chemical potentials μ_i are maintained, the quantity m_1 in the system being fixed. This state is described by a modified grand canonical ensemble,[4,5] for which the expression

$$\Omega(E, V, \{m_i\})\exp[-\beta(E+pV-\sum_2^C{}_i \mu_i m_i)]dEdVd\{m_i\},$$

with

$$\beta=1/kT,$$

is proportional to the probability that the system has energy, volume, and quantities of components in an infinitesimal range about the given values. Here $\{m_i\}$ represents the set of variables $m_2, m_3, \cdots, m_C$, and $d\{m_i\}=dm_2dm_3\cdots dm_C$. The function $\Omega(E, V, \{m_i\})$ is the density of quantum states of the system at the given values of the variables. The partition-function corresponding to the above expression is

$$Z(\beta, p, \{\mu_i\})=\exp(-\beta\mu_1 m_1)=\int\cdots\int\Omega \times\exp[-\beta(E+pV-\sum_2^C{}_i \mu_i m_i)]dEdVd\{m_i\}. \quad (2.6)$$

The desired fluctuations are found simply by appropriate differentiation of Z. For example,

$$(\partial Z/\partial\mu_i)_{T,p,\mu}=\int\cdots\int\beta m_i\Omega\exp[-\beta(E+pV-\sum_2^C{}_i \mu_i m_i)]dEdVd\{m_i\}=\beta Z\langle m_i\rangle_{Av}, \quad (2.7)$$

the subscript μ denoting constancy of all potentials except μ_i and μ_1. A second differentiation of the integral gives

$$(\partial^2 Z/\partial\mu_i\partial\mu_j)_{T,p,\mu}=\beta^2 Z\langle m_i m_j\rangle_{Av}. \quad (2.8)$$

But from the last member of Eq. (2.7) we also obtain

$$\begin{aligned}(\partial^2 Z/\partial\mu_i\partial\mu_j)_{T,p,\mu}&=\beta(\partial Z\langle m_i\rangle_{Av}/\partial\mu_j)_{T,p,\mu}\\&=\beta\langle m_i\rangle_{Av}(\partial Z/\partial\mu_j)_{T,p,\mu}+\beta Z(\partial m_i/\partial\mu_j)_{T,p,\mu,m_1}\\&=\beta^2 Z\langle m_i\rangle_{Av}\langle m_j\rangle_{Av}+\beta Z(\partial m_i/\partial\mu_j)_{T,p,\mu,m_1}. \quad (2.9)\end{aligned}$$

In this expression, the last derivative is actually $(\partial\langle m_i\rangle_{Av}/\partial\mu_j)_{T,p,\mu}$, but is written in the given form because $\langle m_i\rangle_{Av}$ is to be identified with the *thermodynamic* variable m_i. Also, the constancy of m_1 has been expressly noted in writing the thermodynamic derivative. Comparison of Eqs. (2.8) and (2.9) yields

$$\begin{aligned}\beta\langle\Delta m_i\Delta m_j\rangle_{Av}&=\beta\langle m_i m_j\rangle_{Av}-\beta\langle m_i\rangle_{Av}\langle m_j\rangle_{Av}\\&=(\partial m_i/\partial\mu_j)_{T,p,\mu,m_1}=(\partial m_j/\partial\mu_i)_{T,p,\mu,m_1}. \quad (2.10)\end{aligned}$$

By similar procedures, the other desired fluctuations are found to be

$$\begin{aligned}\beta\langle(\Delta V)^2\rangle_{Av}&=-(\partial V/\partial p)_{T,\mu,m_1}\\&=\kappa V-\sum_2^C{}_i \bar{v}_i(\partial m_i/\partial p)_{T,\mu,m_1} \quad (2.11)\end{aligned}$$

$$\begin{aligned}\beta\langle\Delta m_i\Delta V\rangle_{Av}&=(\partial V/\partial\mu_i)_{T,p,\mu,m_1}\\&=-(\partial m_i/\partial p)_{T,\mu,m_1}. \quad (2.12)\end{aligned}$$

Thus, squaring Eq. (2.5) and averaging, using Eqs. (2.10) to (2.12) for the fluctuations, we obtain

$$\beta\langle(\Delta n)^2\rangle_{Av}=[\kappa(\partial n/\partial\ln\rho)_m{}^2/V]+\sum_2^C{}_i\sum_2^C{}_j\psi_i\psi_j(\partial m_i/\partial\mu_j)_{T,p,\mu,m_1}. \quad (2.13)$$

As could have been expected, the contribution from density-fluctuations at constant composition is independent of the concentration-fluctuations, and is given by the familiar Einstein-Smoluchowski formula. Since it is of secondary interest, this term is omitted from now on.

The thermodynamic quantities in the last term of Eq. (2.13) are still relatively unfamiliar. However, at constant T, p, and m_1 we have the set of differential equations

$$d\mu_k=\sum_2^C{}_i a_{ik}dm_i;\quad k=2, 3, \cdots, C,$$

with

$$a_{ik}=(\partial\mu_i/\partial m_k)_{T,p,m}=(\partial\mu_k/\partial m_i)_{T,p,m}. \quad (2.14)$$

Letting all the $d\mu_k$ except $d\mu_j$ equal to zero, and solving for dm_i, we find

$$(\partial m_i/\partial\mu_j)_{T,p,m_1,\mu}=A_{ij}/|a_{ij}|, \quad (2.15)$$

where $|a_{ij}|$ represents the determinant of all the a_{ij} (omitting the first component), and A_{ij} is the co-factor, $\partial|a_{ij}|/\partial a_{ij}$, of the element a_{ij} in this determinant. Thus finally we write

$$\tau'=H'V\sum_2^C{}_i\sum_2^C{}_j\psi_i\psi_j A_{ij}/|a_{ij}|, \quad (2.16)$$

where

$$H'=32\pi^3 n^2 kT/3\lambda^4,$$

[4] J. W. Gibbs, *Elementary Principles in Statistical Mechanics* (Yale University Press, New Haven, 1902), Chapter 15.
[5] E. A. Guggenheim, J. Chem. Phys. 7, 103 (1939).

the prime indicating that the term due to density-fluctuations has been omitted. The volume V must be chosen to correspond to the constant quantity m_1 of the first component that is assumed in evaluating the a_{ij}. The quantity $VA_{ij}/|a_{ij}|$ is then an intensive property.

In the vicinity of a critical point, Eq. (2.16) is inadequate, predicting too large a turbidity. In fact, an infinite value is obtained at the critical point, where $|a_{ij}|$ vanishes.[6] This circumstance is due to neglect of the coupling (through the conditions of conservation of matter) between the fluctuations in different regions of a finite closed system, and more elaborate treatments[7,8] are required. However, the absence of angular dissymmetry is a sufficient criterion for the validity of Eq. (2.16).

3. APPLICATIONS

In this section, Eq. (16) will be applied to several cases of interest, involving non-electrolytes exclusively. Electrolyte solutions are to be considered in more detail elsewhere, but one remark is worthy of mention here. In the theory of equilibrium across semipermeable membranes, the requirement of electroneutrality leads to the familiar Donnan conditions and contributes to the osmotic pressure. If electroneutrality is invoked in limiting the number of components, Eq. (2.16) also yields contributions corresponding to "Donnan terms" in the osmotic pressure, although no semipermeable membrane is considered to be present. In other words, the fluctuations have then been restricted to those producing no net charge in the region V considered. If this restriction is seriously violated only for regions with dimensions small compared to the wave-length of the light, Eq. (2.16) will be valid. Thus, the thickness of the Debye-Hückel ion atmosphere furnishes the necessary criterion. It may be mentioned that turbidity measurements on saline solutions of human serum albumin[9] are in satisfactory agreement with Eq. (2.16).

In the applications to follow, the quantity of the first component (always chosen as the principal solvent) will be taken as one kilogram, and those of the other components, m_i, will be measured in moles. For non-electrolytes, following the notation of Scatchard,[10] we may then write

$$\begin{aligned}(\mu_i-\mu_i^0)/RT&=\ln m_i+\ln\gamma_i,\\ a_{ii}/RT&=(1+\beta_{ii}m_i)/m_i,\\ a_{ij}/RT&=\beta_{ij}\ (i\neq j)\end{aligned}\qquad(3.1)$$

where

$$\beta_{ij}=(\partial\ln\gamma_i/\partial m_j)_{T,p,m}.$$

It is seen that the reference state of unit activity coefficient, for all these components, is the infinitely dilute solution in component 1. In general, the quantities β_{ij} will not be independent of composition, although in many cases some of them may adequately be represented by constants.

A. One Polymer and Two Solvents

This is the case treated by Ewart, Roe, Debye, and McCartney[2] at infinite dilution of polymer. Let component 1 be the principal solvent, component 2 the polymer, and component 3 a second solvent. We are interested in the difference, $\Delta\tau$, between the turbidity of the three-component system and that of the solvents mixed in the same proportion without polymer. From Eq. (2.16),

$$\Delta\tau/H'V=\frac{\psi_2^2a_{33}-2\psi_2\psi_3a_{23}+\psi_3^2a_{22}}{a_{22}a_{33}-a_{23}^2}-\frac{\psi_3^2}{a_{33}^0},\qquad(3.2)$$

where the superscript zero in the last term denotes a solution containing no polymer. This may be rewritten in the form

$$\Delta\tau/H'V=\frac{[\psi_2-(a_{23}/a_{33})\psi_3]^2}{a_{22}-a_{23}^2/a_{33}}+\psi_3^2\left(\frac{1}{a_{33}}-\frac{1}{a_{33}^0}\right).\qquad(3.3)$$

As the concentration of polymer is indefinitely decreased, at a fixed value of m_3, a_{23} and a_{33} approach finite limits with finite slopes, while a_{22} becomes inversely proportional to m_2. Thus, in the limit, $\Delta\tau$ becomes directly proportional to the polymer concentration m_2. With the exception of the last term, which also becomes proportional to m_2 at low polymer concentrations, but which is probably negligible for most systems, Eq. (3.3) agrees with the result of Ewart, Roe, Debye, and McCartney, when allowance is made for the different concentration units employed. The correspondence is better seen when the equality

$$\frac{a_{23}}{a_{33}}=\frac{(\partial\mu_3/\partial m_2)_{T,p,m_3}}{(\partial\mu_3/\partial m_3)_{T,p,m_2}}=-\left(\frac{\partial m_3}{\partial m_2}\right)_{T,p,\mu_3}\qquad(3.4)$$

is examined. It is clear that the ratio a_{23}/a_{33}, here expressed in terms of thermodynamic quantities, is the analog of their adsorption constant α.

To indicate more clearly the dependence on polymer concentration, Eqs. (3.1) may be employed in Eq. (3.3) to yield (with omission of the final term)

$$\Delta\tau(RT/H'V)=\frac{m_2[\psi_2-(m_3\beta_{23}\psi_3/1+\beta_{33}m_3)]^2}{1+m_2[\beta_{22}-(m_3\beta_{23}^2/1+\beta_{33}m_3)]}.\qquad(3.5)$$

It is interesting to observe that the denominator of this expression is proportional to the derivative of the osmotic pressure with respect to polymer concentration,[11] just as for the simple two-component case. It is also seen at once that the two-component result is obtained when m_3 vanishes.

[6] J. W. Gibbs, *Collected Works* (Longmans, Green and Company, New York, 1928), Vol. I. pp. 129–134.
[7] L. S. Ornstein and F. Zernike, Physik. Zeits. **27**, 761 (1926).
[8] M. Klein and L. Tisza, Phys. Rev. **75**, 1303 (1949).
[9] J. T. Edsall and H. Edelhoch, private communication.
[10] G. Scatchard, J. Am. Chem. Soc. **68**, 2315 (1946).
[11] See reference 10, Eqs. (30) and (35).

A restatement of the above result in terms of the more conventional concentration units for non-electrolyte solutions would be practically desirable, but will not be undertaken here.

B. Two Polymers and One Solvent

Reserving the designation 3 for a second solvent, we designate the two polymers as components 2 and 4. In this case, we consider the difference between the turbidity of the three-component system and the sum of those for the two binary polymer-solvent systems, each at the same polymer concentration as in the ternary mixture. One obtains

$$\Delta\tau/H'V=\frac{\psi_2^2a_{44}-2\psi_2\psi_4a_{24}+\psi_4^2a_{22}}{a_{22}a_{44}-a_{24}^2}-\frac{\psi_2^2}{a_{22}^0}-\frac{\psi_4^2}{a_{44}^0};\quad(3.6)$$

$$\Delta\tau(RT/H'V)=-2m_2m_4\psi_2\psi_4\beta_{24},$$

correct to quadratic terms in the polymer concentrations. In this case, translation to more familiar terminology is simple, the result for high polymers being

$$V\beta_{24}=(1+\mu_{24}'-\mu_{12}'-\mu_{14}')M_2M_4/\bar{v}_1\rho_2\rho_4 \quad (3.7)$$

where ρ_2, ρ_4 are the densities and M_2, M_4 the molecular weights of the polymers, and the μ_{ij}' are the familiar interaction constants of the Flory-Huggins theory. Thus, light scattering affords a convenient means of studying interactions between unlike polymer molecules in solution.

C. Heterogeneous Polymer and One Solvent

We consider a polymer sample containing a large number of species of different molecular weight, though of uniform chemical composition. If the polymer concentration remains low, this multi-component system can be simply discussed. From Eqs. (3.1), we obtain

$$\begin{aligned}RTA_{ii}/|a_{ij}|&=m_i-\beta_{ii}m_i^2+\cdots;\\ RTA_{ij}/|a_{ij}|&=-\beta_{ij}m_im_j+\cdots;\quad i\neq j.\end{aligned}\quad(3.8)$$

Substitution in Eq. (2.16) yields

$$RT\tau'/H'V=\sum_2^C{}_i\,\psi_i^2m_i-\sum_2^C{}_i\sum_2^C{}_j\,\beta_{ij}m_im_j\psi_i\psi_j+\cdots. \quad (3.9)$$

We now change to weight concentrations, $w_i=m_iM_i$, expressed as grams of solute per kilogram of solvent, and note that in these units the specific refractive-index increment is independent of molecular weight. Defining $w_2=\sum_i w_i$, the total polymer concentration, we then have

$$\psi_i=M_i(\partial n/\partial w_i)_{T,p,w}=M_i(\partial n/\partial w_2)_{T,p}. \quad (3.10)$$

Furthermore, except for very high molecular weights,[12] the interaction parameter β_{ij} is proportional to the product of molecular weights M_iM_j. If the osmotic pressure is expressed by the formula

$$PV=RT\sum_i(w_i/M_i)+Bw_2^2+\cdots, \quad (3.11)$$

in which V is the volume of solution containing one kilogram of solvent, then

$$\beta_{ij}=2BM_iM_j/RT. \quad (3.12)$$

With Eqs. (3.10) and (3.12), Eq. (3.9) becomes

$$RT\tau'/H'V=\left(\frac{\partial n}{\partial w_2}\right)_{T,p}^2\times\left[\sum_i w_iM_i-\frac{2B}{RT}\sum_i\sum_j w_iw_jM_iM_j+\cdots\right]. \quad (3.13)$$

In terms of the weight-average molecular weight, $M_w=\sum_i w_iM_i/w_2$, and in the more familiar reciprocal form, this equation is

$$Hw_2/\tau=\frac{1}{M_w}+\frac{2B}{RT}w_2+\cdots, \quad (3.14)$$

where H is the usual constant.[1] Thus, the turbidity formula is not sensitive to molecular weight distribution, as had originally been supposed.[1]

ACKNOWLEDGMENT

The author is deeply grateful to Drs. J. G. Kirkwood and R. J. Goldberg for the opportunity to examine their manuscript on the same subject in advance of its publication. He is also pleased to acknowledge stimulating discussions with Drs. G. Scatchard, L. Tisza, and P. M. Doty.

[12] B. H. Zimm, J. Chem. Phys. 14, 146 (1946).

Solubility Relations in Ternary Solid Solutions of Ionic Compounds

CARL WAGNER*
Eduard Zintl Institut für anorganische und physikalische Chemie der Technischen Hochschule, Darmstadt, Germany
(Received May 15, 1949)

The variation of the solubility of a solute due to the presence of a second solute in a solid ionic compound as solvent is investigated theoretically with the aid of the ideal law of mass action. Ions of the solvent in interstitial positions, cation and anion vacancies, quasi-free electrons, and electron holes are to be taken into account in the same manner as the constituents of conventional chemical systems. The theoretical conclusions are illustrated by experimental data, however, qualitatively rather than quantitatively.

The solubility of lead chloride in solid silver chloride is decreased by presence of cadmium chloride. The solubility of iodine (or cupric iodide) in cuprous iodide is likewise decreased by presence of cadmium iodide. The behavior of the corresponding bromide system is analogous. Conversely, gallium oxide increases the solubility of zinc in zinc oxide. The phenomena to be expected in lead sulfide as solvent are more complicated, since this substance can dissolve both excessive lead and excessive sulfur.

The oxidation rate of nickel is increased by presence of chromium and manganese, whereas the chlorination rate of silver is decreased by presence of lead and cadmium chloride.

I. INTRODUCTION

IT is a well-known fact that in general the solubility of an ionic compound in water is considerably diminished when another soluble salt with common ion is added. For example, the solubility of silver chloride is decreased when sodium chloride is added. In sufficiently dilute solutions these effects can be interpreted quantitatively with the aid of the ideal law of mass action. In solid solutions similar effects are to be expected. The logical application of the law of mass action requires that ions of the solvent in interstitial positions, cation or anion vacancies, quasi-free electrons, and electron holes are to be taken into account in the same manner as the normal constituents of aqueous solutions. Thus consequences result which at first sight are somewhat surprising to a chemist familiar with relations in dilute aqueous solutions. In this paper a general outline of the effects to be expected from a theoretical point of view is given, and experimental results are communicated as illustrations. Unfortunately, most of the experimental investigations were untimely discontinued so that the existence of the theoretically predicted effects is shown qualitatively rather than quantitatively. More thorough investigations, involving application of other experimental methods and wider variations of conditions, are desirable.

The law of mass action yields primarily statements in terms of concentrations. The concentrations of quasi-free electrons and electron holes in turn determine the electronic conductivity. Therefore, in many cases, a change in the electrical conductivity can be taken as a measure of the change of the composition which can be determined directly only by cumbersome procedures of chemical analysis. Measurements of the electrical conductivity are also frequently of immediate interest because the so-called semiconductors are used for many technical purposes and the development of methods to prepare reproducibly semiconductors of specified properties plays an important part in the research of our day.

Furthermore, conclusions drawn from the law of mass action may be used to interpret the oxidation rate of alloys. Problems of chemical catalysis are considered in a following paper.

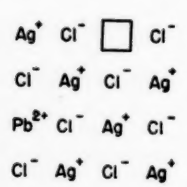

FIG. 1. Silver chloride with lead chloride.

II. SOLUBILITY OF LEAD CHLORIDE IN SILVER CHLORIDE IN THE PRESENCE OF CADMIUM CHLORIDE

In silver halides, electricity is transported mainly by cations as shown by Tubandt.[1] This fact is accounted for by a model suggested by Frenkel,[2] according to which there are cations in interstitial positions and cation holes, the respective concentrations being determined by a thermodynamic equilibrium.

Koch and Wagner[3] have shown that the electrical conductivity of silver chloride and likewise that of silver bromide is greatly increased by addition of lead and cadmium halides. Hence, the authors have concluded that chlorides of divalent metals are solved in monovalent silver chloride according to a scheme shown in Fig. 1. Divalent cations substitute silver ions and simultaneously one cation hole appears for each divalent cation because there is only one cation for each two anions in one molecule of the additive. The con-

* Present address: Department of Metallurgy, Massachusetts Institute of Technology, Cambridge, Massachusetts.

[1] C. Tubandt, Zeits. f. anorg. allgem. Chemie **115**, 105 (1921).
[2] J. Frenkel, Zeits. f. Physik **35**, 652 (1926).
[3] E. Koch and C. Wagner, Zeits. f. physik. Chemie **B38**, 295 (1937).

centration of cations in interstitial positions becomes negligible if the concentration of the additive is much greater than the concentration of cations in interstitial positions in pure silver chloride. Then, the equation of the dissolution of lead chloride in silver chloride reads

$$PbCl_2\,(\text{crystal}) = Pb^{2+} + h(Ag^+) + 2Cl^-. \quad (1)$$

Here the symbol $h(Ag^+)$ represents a cation hole, the symbol Pb^{2+} a lead ion in a normal cation position in the silver chloride phase, substituted for a silver ion, and the symbol Cl^- a chlorine ion in a normal anion position, not distinguishable from those of the solvent.

In the presence of excessive solid lead chloride, the equilibrium condition derived from the ideal law of mass action reads

$$N_{Pb^{2+}} \cdot N_{h(Ag^+)} = K_1, \quad (2)$$

where the symbols $N_{Pb^{2+}}$ and $N_{h(Ag^+)}$ represent the respective mole fractions referred to chlorine, and K_1 is a constant. This relation corresponds to the equation of the solubility product of a uni-univalent electrolyte in aqueous solution, the anion concentration being replaced by the concentration of cation holes.

The constitution of a solid solution of cadmium chloride in silver chloride is completely analogous. Consequently, in a ternary solution, the number of cation holes equals the sum of lead ions and cadmium ions,

$$N_{h(Ag^+)} = N_{Pb^{2+}} + N_{Cd^{2+}}, \quad (3)$$

and thus exceeds the number of cation holes in silver chloride with the same content of lead chloride but without cadmium chloride. Accordingly, the saturation concentration of lead chloride in the presence of cadmium chloride must decrease so that equilibrium condition (2) is satisfied, as recently shown by Wagner and Zimens.[4] The mole fractions referring to equilibrium with solid lead chloride without presence of cadmium chloride are marked by the superscript °. Thus, according to Eq. (3),

$$N^\circ_{h(Ag^+)} = N^\circ_{Pb^{2+}}, \quad (4)$$

and upon substitution in Eq. (2),

$$N^\circ_{Pb^{2+}} \cdot N^\circ_{h(Ag^+)} = (N^\circ_{Pb^{2+}})^2 = K_1. \quad (5)$$

Hence, the ratio of the saturation concentration of lead chloride in a ternary system to that in a binary system free from cadmium chloride, calculated from Eqs. (2), (3), and (5), equals

$$\frac{N_{Pb^{2+}}}{N^\circ_{Pb^{2+}}} = \frac{1}{\frac{1}{2}N_{Cd^{2+}}/N^\circ_{Pb^{2+}} + [1 + (\frac{1}{2}N_{Cd^{2+}}/N^\circ_{Pb^{2+}})^2]^{\frac{1}{2}}}. \quad (6)$$

In case the cadmium chloride concentration is much greater than the saturation concentration of lead chloride in the binary system, the Eq. (6) becomes approximately

$$N_{Pb^{2+}}/N^\circ_{Pb^{2+}} \cong N^\circ_{Pb^{2+}}/N_{Cd^{2+}} \text{ if } N_{Cd^{2+}} \gg N^\circ_{Pb^{2+}}. \quad (7)$$

Thus, the solubility of lead chloride turns out to be inversely proportional to the concentration of cadmium chloride under the indicated limiting conditions. This result is analogous to the fact that the solubility of silver chloride in water is inversely proportional to the concentration of another soluble chloride, provided the concentration of the additive is much greater than that of silver chloride in pure water and formation of complex ions $AgCl_2^-$ can be disregarded.

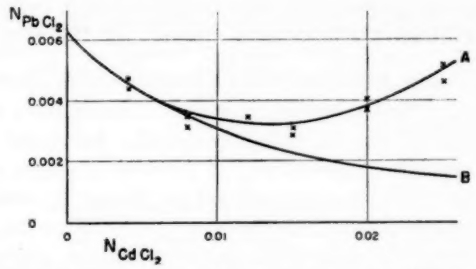

FIG. 2. Solubility of lead chloride in silver chloride as a function of the concentration of cadmium chloride at 270°C. Curve A: observed values; curve B: calculated values according to Eq. (6).

It must be pointed out that in the case of solid solutions the common anion is unimportant. The salient point is that there is an increase of the concentration of cation holes due to the additive involving cations with a greater valency than that of silver ions. Consequently, no significant change of the solubility of lead chloride in silver chloride is to be expected when a small amount of sodium chloride is added.

Figure 2 shows the experimental values of the saturation concentration of lead chloride in silver chloride-cadmium chloride mixed crystals as a function of the composition. At low concentrations of cadmium chloride, the experimental values are close to values calculated from Eq. (6). At higher concentrations, considerable deviations occur and finally the saturation concentration of lead chloride even increases. Similar effects are known in aqueous solutions. In part they are due to the formation of complex ions. However, an increase of the solubility at higher concentrations of an additive with common ion may also be interpreted by electrostatic interionic action as Schaerer[5] has shown on the basis of the theory of Debye and Hueckel.[6] Electrostatic interionic action in solid solutions involving a low dielectric constant must be considerably greater than that in aqueous solutions of the same concentration, but correction factors cannot be calculated theoretically, since the limiting formulas of Debye and Hueckel do not apply when the deviations from the behavior of ideal solutions are large.

[4] C. Wagner and E. K. Zimens, Acta Chem. Scand. **1**, 539 (1947).

[5] O. Schaerer, Physik. Zeits. **25**, 145 (1924).

[6] P. Debye and E. Hueckel. Phvsik. Zeits. **24**, 185 (1923).

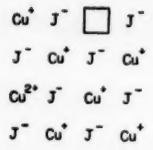

FIG. 3. Cuprous iodide with excess of iodine.

Although the application of the ideal law of mass action may sometimes lead to conclusions even qualitatively faulty, this relation may be introduced tentatively in order to predict effects which subsequently are to be checked experimentally.

III. THE ELECTRICAL CONDUCTIVITY OF CUPROUS HALIDES CONTAINING CADMIUM HALIDES

Baedecker[7] has shown that the electrical conductivity of solid cuprous iodide is mainly electronic and its amount depends on small deviations from the ideal stoichiometric composition. In general, cuprous iodide contains a certain excess of iodine. However, there are no excessive iodine molecules or atoms. Instead, it is fairly correct to describe cuprous iodide containing excessive iodine as a solid solution of the hypothetical compound cupric iodide, CuJ_2, in cuprous iodide, CuJ. Nagel and Wagner[8] have suggested a model shown in Fig. 3, which is completely analogous to the model in Fig. 1 for silver chloride containing lead chloride. The qualitative conclusions drawn from this model have been confirmed experimentally by Nagel and Wagner and more recently by Maurer,[9] but quantitatively there are deviations which can be ascribed to the inconsistency of the ideal law of mass action under the given conditions, or possibly to an "association" of divalent copper ions and cation holes as discussed for other systems by Schottky.[10]

If there are divalent copper ions, surrounded by monovalent copper ions also called electron holes, electrons can be exchanged and accordingly the electrical conductivity may be set proportional to the concentration of divalent copper ions, since the concentration of monovalent copper ions is practically constant. The concentration of divalent copper ions can be given a well-defined value by the equilibrium with iodine molecules in an adjacent gas phase according to the equation

$$\tfrac{1}{2}J_2(\text{gas})+Cu^+=Cu^{2+}+h(Cu^+)+J^-. \qquad (8)$$

Upon application of the ideal law of mass action, it follows that

$$N_{Cu^{2+}}\cdot N_{h(Cu^+)}=K_2\cdot p_{J_2}^{\frac{1}{2}}, \qquad (9)$$

where p_{J_2} represents the partial pressure of iodine molecules in the gas phase and K_2 is a constant.

In the case of the binary system copper iodine, the concentration of divalent copper ions equals that of cation holes. Addition of the iodide of another divalent metal, e.g., cadmium iodide, causes an increase of the cation-hole concentration, and accordingly, the concentration of divalent copper ions must decrease as well as the electrical conductivity. In analogy to Eq. (7), it follows that

$$\frac{\kappa}{\kappa^o}=\frac{N_{Cu^{2+}}}{N^o_{Cu^{2+}}}\cong\frac{N^o_{Cu^{2+}}}{N_{Cd^{2+}}} \quad \text{if} \quad \frac{N_{Cd^{2+}}}{N^o_{Cu^{2+}}}\gg 1, \qquad (10)$$

where κ and κ^o represent the electrical conductivities of samples with and without cadmium iodide, respectively.

Experiments were carried out in collaboration with Karl Steffes. First, the solubility of cadmium iodide in cuprous iodide was investigated by determining the cadmium content of cuprous iodide tablets in contact with cadmium iodide tablets. At 300°C a solubility of about six mole percent was obtained. Second, thin sheets of pure copper and sheets of copper electrolytically coated with cadmium were placed in glass tubes with iodine and transformed into iodide by heating. Measurements of the electrical conductivity were performed at 225 and 300°C in the same manner as described by Nagel and Wagner.[8] The iodine pressure was varied from 0.01 to 300 mm Hg. In accordance with theoretical considerations, the conductivity of samples containing cadmium iodide was less than that of samples free of cadmium iodide. The greatest effect was observed at 300°C and an iodine pressure of 0.02 mm Hg; under these conditions the electrical conductivity of samples containing five mole percent of cadmium iodide was found to be 0.2 $ohm^{-1}cm^{-1}$, whereas the conductivity of samples free of cadmium was 0.8 $ohm^{-1}cm^{-1}$. At an iodine pressure of 300 mm Hg, however, the electrical conductivity of samples containing cadmium iodide was practically the same as that of samples free of cadmium iodide.

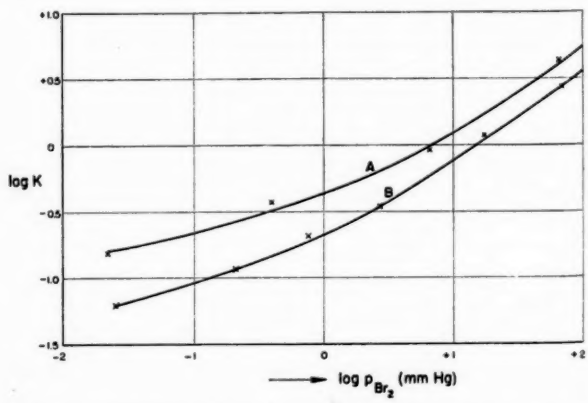

FIG. 4. Conductivity of cuprous bromide (curve A) and cuprous bromide containing five mole percent of cadmium bromide (curve B) as a function of the bromine pressure of 300°C.

[7] K. Baedecker, Ann. d. Physik (4) **22**, 749 (1907); **29**, 566 (1909). Physik. Zeits. **9**, 431 (1908); **13**, 1080 (1912). Nernst-Festschrift, p. 62 (1912). G. O. Greiner, dissertation Jena, Germany (1912). G. Rudert, Ann. d. Physik (4) **31**, 559 (1910). K. Steinberg, Ann. d. Physik (4) **35**, 1009 (1911).

[8] K. Nagel and C. Wagner, Zeits. f. physik. Chemie **B25**, 71 (1934).

[9] R. J. Maurer, J. Chem. Phys. **13**, 321 (1945).

[10] W. Schottky, Zeits. f. Elektrochemie **45**, 33 (1939).

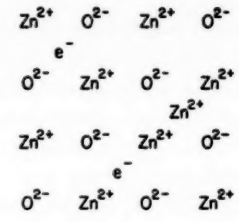

FIG. 5. Zinc oxide with excess of zinc.

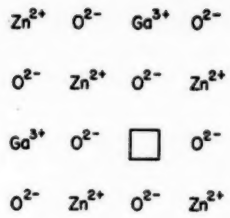

FIG. 6. Zinc oxide with gallium oxide.

The decrease of the electrical conductivity due to the presence of cadmium iodide is far less than that calculated from Eq. (10). From measurements reported by Maurer,[9] a value of $N^{o}_{Cu^{2+}}=2\cdot10^{-5}$ for 300°C and an iodine pressure of 0.02 mm Hg can be extrapolated. Thus, Eq. (10) leads to a decrease of the conductivity by a factor of 2500 for $N_{Cd^{2+}}=0.05$, whereas experimentally, a factor of only four has been found. It is open to question whether this discrepancy is due to the inconsistency of the ideal law of mass action only, or also to association of divalent ions and cation holes, since only non-associated cation holes count in the law of mass action.

Similar experiments were performed on the corresponding bromide system which according to transference measurements of Frers[11] and Geiler[12] seems to be a close analog to the iodide system. First, the electrical conductivity of cuprous bromide at 300°C was determined as a function of the bromine pressure, which was always kept lower than the equilibrium pressure over cuprous bromide and cupric bromide so that the latter phase could not be formed. Results are shown in Fig. 4. The general character of the dependency on the halogene pressure is similar to that in the iodide system. Second, the electrical conductivity of a sample containing five mole percent of cadmium bromide was measured. The observed conductivities, which are also shown in Fig. 4, are somewhat less than those of the sample free of cadmium. The sample with cadmium bromide was heterogeneous because the solubility of cadmium bromide was found to be only two mole percent. Under all conditions, the content of cadmium bromide was considerably greater than the concentration of divalent copper, which was found to be about 0.5 mole percent at a bromine pressure of 170 mm Hg and 300°C, according to analyses carried out in the same manner as those of cuprous oxide reported by Wagner and Hammen.[13] Also in this system there is a wide gulf between observations and values calculated from an equation analogous to Eq. (10).

IV. THE ELECTRICAL CONDUCTIVITY OF ZINC OXIDE CONTAINING GALLIUM OXIDE

The dependency of the electrical conductivity of zinc oxide, ZnO, on the pressure of its electronegative component is reverse to the behavior of the monovalent copper compounds. The higher the oxygen pressure of the ambient gas, the lower is the electrical conductivity of zinc oxide as shown by Skaupy,[14] von Baumbach and Wagner,[15] Kroeger,[16] Fritsch,[17] and Miller.[18] Under all oxygen pressures applied so far, zinc oxide contains a certain excess of zinc in form of zinc ions, probably in interstitial positions, and quasi-free electrons, which carry the electrical current (see Fig. 5). Thus the reaction between zinc oxide and the gas phase can be formulated as follows,

$$ZnO=Zn^{2+}(i)+2e^{-}(i)+\tfrac{1}{2}O_2(gas). \qquad (11)$$

Here the symbol $Zn^{2+}(i)$ represents a zinc ion in an interstitial position and the symbol $e^{-}(i)$ a quasi-free electron, which can also be called an electron in an interstitial position. Hence the equilibrium condition reads

$$N_{Zn^{2+}(i)}\cdot N^{2}_{e^{-}(i)}\cdot p_{O_2}^{\frac{1}{2}}=K_3. \qquad (12)$$

We may anticipate that the solubility of zinc and, accordingly, the electrical conductivity will increase when the excessive zinc ions are offered positions of a lower energy level than that of interstitial positions where the repulsive energy is high. Low energy positions for cations are, of course, cation holes which can be expected to occur in solid solutions consisting of zinc oxide as solvent and the oxide of another metal of higher valency as solute, e.g., gallium oxide, Ga_2O_3, as shown in Fig. 6.

Conductivity measurements on mixtures of zinc oxide and gallium oxide were performed in collaboration with Ruth Hauffe. The experimental procedure was essentially the same as that described by von Baumbach and Wagner.[15] At 600°C and an oxygen pressure of 1 atmos., the following resistances of porous slabs, about 1 cm in diameter and 2 cm in length, were obtained.

Weight percent of gallium oxide:	0;	0.1;	0.3;	1.0;	3.0.
Resistance:	10,000;	4200;	460;	200;	450 ohms.

It is remarkable that the effects observed in this system are far greater than those reported previously for other systems.

[11] I. N. Frers, Ber. d. D. chem. Ges. **61**, 377 (1928).
[12] J. Geiler, dissertation, University of Halle, Germany (1928).
[13] C. Wagner and H. Hammen, Zeits. f. physik. Chemie **B40**, 197 (1938).
[14] F. Skaupy, Zeits. f. Physik **1**, 259 (1920).
[15] H. H. von Baumbach and C. Wagner, Zeits. f. physik. Chemie **B22**, 199 (1933).
[16] M. Kroeger, *Grenzflaechenkatalyse* (S. Hirzel, Leipzig, Germany, 1933).
[17] O. Fritsch, Ann. d. Physik (5) **22**, 375 (1935).
[18] P. H. Miller, Phys. Rev. **60**, 890 (1941).

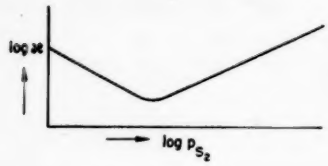

FIG. 7. Schematic representation of the conductivity κ of lead sulfide as a function of the sulfur pressure.

The opposite effect, decrease of the solubility of zinc in zinc oxide and thus decrease of the electrical conductivity, can be expected when the oxide of a metal of lower valency, e.g., silver oxide, is added. Since silver oxide, Ag_2O, contains only one oxygen atom for each two cations, the sum total of cations in such a solution exceeds the number of anions. Consequently, either anion vacancies must appear if all cations occupy normal lattice positions, or some cations must occupy interstitial positions if all anion positions are filled up.

Assuming tentatively the second scheme, we conclude from Eq. (11) that the presence of silver oxide in zinc oxide, causing a greater concentration of zinc ions in interstitial positions, should decrease the concentration of quasi-free electrons and accordingly the electrical conductivity. The same effect is to be expected if anion vacancies instead of interstitial cations are present. No noticeable effect, however, was found, probably because the solubility of silver oxide in zinc oxide is too low.

V. SOLID SOLUTIONS INVOLVING LEAD SULFIDE AS SOLVENT

Investigations on solid solutions with lead sulfide as solvent seem to be very interesting, for, according to Eisenmann,[19] Hintenberger,[20] and Morton,[21] lead sulfide can be provided with an excess of sulfur by heating in sulfur vapor, and conversely with an excess of lead by heating in vacuum or in contact with metallic lead.

FIG. 8. Lead sulfide with excess of sulfur.

FIG. 9. Lead sulfide with excess of lead involving anion vacancies.

[19] L. Eisenmann, Ann. d. Physik (5) **38**, 121 (1940).
[20] H. Hintenberger, Zeits. f. Physik **119**, 1 (1942); Zeits. f. Naturforschung **1**, 13 (1946).
[21] M. C. Morton, Trans. Faraday Soc. **43**, 194 (1947).

Under all conditions the conduction is mainly electronic. Conduction through electron holes prevails in lead sulfide with excess of sulfur, and conversely conduction through quasi-free electrons prevails in lead sulfide with excess of lead as indicated by the sign of thermoelectric effects and the sign of the Hall effect. A schematic representation of the electrical conductivity as a function of the sulfur pressure of the ambient gas is shown in Fig. 7.

Anderson and Richards[22] have shown that the self-diffusion coefficient of lead ions increases with excess of sulfur. This behavior has been accounted for by the assumption that lead sulfide with excess of sulfur contains cation vacancies in the same manner as cuprous oxide, nickel oxide etc. In view of the monotonic decrease of the self-diffusion coefficient of lead ions with decreasing sulfur-lead ratio, Anderson and Richards have inferred that lead sulfide with excess of lead contains no interstitial lead ions but anion vacancies. Thus lead sulfide is considered as an analog to potassium chloride in which, according to Schottky,[23] only cation and anion vacancies but no interstitial ions occur. This conclusion holds true only if, in the aforementioned experiments, the sulfur content was decreased so far that a sufficient excess of lead was present. This presupposition, however, has not been ascertained so that the Frenkel disorder type, involving interstitial cations and cation vacancies, cannot be ruled out at the time being. Therefore, both the Frenkel disorder model and the Schottky disorder model shall be taken into consideration.

Lead sulfide with excess of sulfur may tentatively be described as a solid solution of PbS_2 in PbS. A model involving tetravalent lead ions and cation vacancies is shown in Fig. 8, analogous to the model of cuprous iodide with excess of iodine shown in Fig. 3. In addition, there will be a few trivalent lead ions which exchange electrons with neighboring divalent ions in the same manner as in other cases of conduction through electron holes. The dissolution of sulfur in lead sulfide can then be formulated as follows

$$\tfrac{1}{2}S_2(\text{gas}) + Pb^{2+} = Pb^{4+} + h(Pb^{2+}) + S^{2-}. \qquad (13)$$

Accordingly, the equilibrium condition reads

$$N_{Pb^{4+}} \cdot N_{h(Pb^{2+})} = K_4 \cdot p_{S_2}^{\frac{1}{2}}. \qquad (14)$$

Lead sulfide with excess of lead involving anion vacancies and free electrons is shown in Fig. 9. The corresponding stoichiometric equation of the dissolution of lead in lead sulfide reads

$$Pb(\text{metal}) = Pb^{2+} + h(S^{2-}) + 2e^-(\text{i}). \qquad (15)$$

The resulting equilibrium condition is

$$N_{h(S^{2-})} \cdot N^2_{e^-(\text{i})} = K_5. \qquad (16)$$

[22] J. S. Anderson and J. R. Richards, J. Chem. Soc. London **1946**, 537 (1946).
[23] W. Schottky, Zeits. physik. Chemie **B29**, 335 (1935).

FIG. 10. Lead sulfide with excess of lead involving cations in interstitial positions.

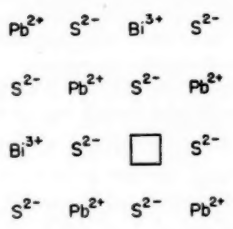

FIG. 11. Lead sulfide with bismuth sulfide.

On the other hand, occurrence of interstitial cations instead of anion vacancies may be assumed as illustrated in Fig. 10. Then the dissolution process is described by the stoichiometric equation

$$\mathrm{Pb(metal)} = \mathrm{Pb^{2+}(i)} + 2e^-(\mathrm{i}), \qquad (17)$$

whence the equilibrium condition is derived as

$$N_{\mathrm{Pb^{2+}}} \cdot N^2_{e^-(\mathrm{i})} = K_6. \qquad (18)$$

Preliminary investigations were made in collaboration with Ruth Hauffe. It was found that lead sulfide dissolves about 0.3 percent of bismuth sulfide at 300°C. Since the cation-anion ratio of bismuth sulfide, Bi_2S_3, is less than that of lead sulfide, PbS, the sum total of cations in the solid solution is less than the number of anions. Occupation of interstitial positions by anions can practically be disregarded because of their large diameter. Therefore, a structure involving cation holes is very likely (see Fig. 11).

We then derive theoretically the behavior of a solid solution of bismuth sulfide in lead sulfide when heated either in sulfur vapor, or in contact with metallic lead.

(a) The greater the content of bismuth sulfide and likewise the concentration of cation holes, the less is the sulfur excess, equivalent to tetravalent lead ions, in view of equilibrium condition (14). Consequently, addition of bismuth sulfide to lead sulfide under a given sulfur pressure of 10 mm Hg or so should decrease the electrical conductivity as far as it is due to exchange of electrons between lead ions of different valencies. Moreover, it is possible that there is no excess of sulfur but an excess of lead, since a crystal of this kind has a strong tendency to fill up cation holes according to the equation

$$\mathrm{Pb(metal)} + h(\mathrm{Pb^{2+}}) = \mathrm{Pb^{2+}} + 2e^-(\mathrm{i}). \qquad (19)$$

In the latter case a shift from prevalent conduction through electron holes to prevalent conduction through quasi-free electrons would occur. This shift could be recognized by a change of the sign of the Hall effect, the sign of thermoelectric effects, or the direction of rectification which takes place when alternating current flows from a platinum pin to lead sulfide.

(b) When a solid solution of bismuth sulfide in lead sulfide is brought in contact with metallic lead, a greater amount of lead will be dissolved than in pure lead sulfide because cation holes represent lower energy levels than interstitial positions. Accordingly, the electrical conductivity should be higher than that of lead sulfide free of bismuth sulfide. The conditions are completely analogous to those in the zinc oxide-gallium oxide system.

Preliminary measurements were performed with samples heated in sulfur vapor at 400°C and samples heated in contact with metallic lead at 300°C. The electrical conductivity was measured at 20°C because of experimental difficulties at higher temperatures. The following values were obtained.

	PbS;	99 percent PbS + one percent Bi_2S_3
Heated in sulfur vapor:	70;	0.02 $\mathrm{ohm^{-1}cm^{-1}}$
Heated in contact with lead:	1;	10 $\mathrm{ohm^{-1}cm^{-1}}$.

These values are ill-defined because of possible changes in the composition due to precipitation of secondary phases during the cooling process, but they are qualitatively in accordance with theoretical considerations and demonstrate impressively the great influence of small amounts of additives.

Reverse conditions are to be expected in the case of additives which contain cations of lower valency such as Cu_2S, Ag_2S, or Tl_2S and accordingly possess a cation-anion ratio greater than unity. If the lead-sulfur ratio is unity, silver sulfide may be dissolved either under formation of anion vacancies (see Fig. 12), or under occupation of interstitial positions by cations (see Fig. 13). Since the number of lead ions exceeds the number of silver ions by far, it is likely that in the latter case preponderately lead ions are in interstitial positions as indicated in Fig. 13.

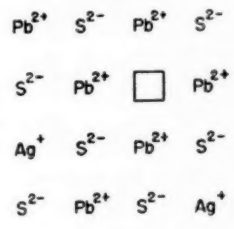

FIG. 12. Lead sulfide with silver sulfide involving anion vacancies.

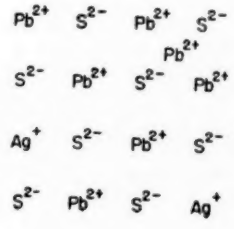

FIG. 13. Lead sulfide with silver sulfide involving cations in interstitial positions.

The following effects are to be expected.

(a) When a solid solution of silver sulfide in lead sulfide is heated in sulfur vapor of a pressure of 10 mm Hg or so, more excessive sulfur than in pure lead sulfide should enter the lattice because either anion vacancies are filled up,

$$\tfrac{1}{2}S_2(\text{gas})+Pb^{2+}+h(S^{2-})=Pb^{4+}+S^{2-}, \qquad (20)$$

or lead ions in interstitial positions are removed,

$$\tfrac{1}{2}S_2(\text{gas})+Pb^{2+}(\text{i})=Pb^{4+}+S^{2-}. \qquad (21)$$

Accordingly one should expect a higher conductivity through electron holes due to the greater number of lead ions of higher valency than in pure lead sulfide.

(b) When a solid solution of thallium sulfide in lead sulfide is heated in contact with metallic lead, the excess of lead should be less than in lead sulfide free of additives. In the case of anion vacancies, the concentration of electrons must decrease by increase of the concentration of anion vacancies in view of equilibrium condition (16). On the other hand, in the case of cations in interstitial positions, the concentration of electrons must also decrease in view of equilibrium condition (18). Possibly, even an excess of sulfur, formation of cations of higher valency, and conduction through electron holes may result as a consequence of reactions (20) and (21), respectively, with sulfur molecules whose partial pressure equals the equilibrium pressure over lead sulfide in contact with metallic lead.

Decisive experiments on solutions of sulfides of monovalent metals in lead sulfide are still missing.

It is remarkable that the conductivity effects due to additives such as bismuth sulfide and silver sulfide do not depend on whether the Frenkel or the Schottky disorder type holds true. A decision between these two possibilities, however, can be reached from self-diffusion measurements in lead sulfide containing the aforementioned additives. Addition of bismuth sulfide, increasing the number of cation vacancies, should no doubt increase the self-diffusion coefficient of lead ions. Addition of silver sulfide should decrease the self-diffusion coefficient of lead ions if the model involving anion vacancies shown in Fig. 12 holds true, because the concentration of cation vacancies is inversely proportional to the number of anion vacancies in view of the stoichiometric equation

$$h(Pb^{2+})+h(S^{2-})=\text{undisturbed crystal}, \qquad (22)$$

and the corresponding equilibrium condition

$$N_{h(Pb^{2+})}\cdot N_{h(S^{2-})}=K_7. \qquad (23)$$

On the other hand, if the model involving cations in interstitial positions, shown in Fig. 13, is true, addition of silver sulfide should increase the self-diffusion coefficient of lead ions owing to the motion of lead ions in interstitial positions. Thus the determination of the self-diffusion coefficient of lead ions in lead sulfide with dissolved silver sulfide or a sulfide of another monovalent metal represents a crucial experiment so as to discriminate between the Schottky and the Frenkel disorder model provided there is a sulfide of a monovalent metal whose solubility in lead sulfide is sufficiently high.

VI. CONCLUSIONS

The foregoing considerations can also be used to interpret the change of the oxidation rate of metals by alloying components when the respective oxides are soluble in each other. Wagner and Zimens[24] have reported a decrease of the oxidation rate of nickel by addition of manganese and chromium. Himmler[25] has found that the chlorination rate of silver is decreased by the presence of lead chloride and cadmium chloride, respectively. Both effects are in accordance with theoretical considerations.

In a subsequent paper,[26] the behavior of mixed oxides as catalyst is considered.

[24] C. Wagner and K. E. Zimens, Acta Chem. Scand. **1**, 547 (1947).
[25] W. Himmler, Zeits. f. Metallkunde (in press).
[26] C. Wagner, J. Chem. Phys. **18**, 69 (1950).

The Mechanism of the Decomposition of Nitrous Oxide on Zinc Oxide as Catalyst

CARL WAGNER*
Eduard Zintl Institut für anorganische und physikalische Chemie der Technischen Hochschule Darmstadt, Germany
(Received May 19, 1949)

For the decomposition of nitrous oxide on metals and oxides, a tentative mechanism is indicated which involves quasi-free electrons as reactants and adsorbed oxygen ions as intermediate product. This mechanism is in accordance with experimental facts such as retardation by oxygen, a fractional order of the reaction with respect to nitrous oxide in the case of indium oxide as catalyst, and the decrease of the electrical conductivity of zinc oxide due to the presence of nitrous oxide. A mixture of zinc oxide and gallium oxide, however, has about the same catalytic activity as pure zinc oxide, although the electrical conductivity of the mixed catalyst is about fifty times greater than that of pure zinc oxide. This finding can be accounted for by the assumption that the reaction between nitrous oxide and electrons of the catalyst takes place in the vicinity of an adsorbed zinc ion or an anion vacancy.

INTRODUCTION

ACCORDING to Volmer and associates[1] and Hunter,[2] nitrous oxide decomposes in the gas phase at high pressures according to a first-order reaction. At low pressures transition to a second-order reaction has been observed which is accounted for by a bimolecular reaction necessary for the accumulation of activation energy. Disregarding the latter reaction and eventual complications,[3] we have the following consecutive reactions

$$N_2O = N_2 + O, \tag{1}$$

$$O + N_2O = N_2 + O_2. \tag{2}$$

Hinshelwood and Prichard,[4] Cassel and Glueckauf,[5] Schwab and Eberle,[6] Steacie and McCubbin,[7] and Steacie and Folkins[8] have investigated the heterogeneous decomposition of nitrous oxide on surfaces of platinum, gold, and silver. In all investigations a first-order reaction with respect to nitrous oxide has been found. In some cases the reaction is retarded by oxygen; under certain conditions oxygen produced by decomposition of nitrous oxide retards the reaction to a higher extent than oxygen initially added. Thus the catalytic reaction can be interpreted essentially in a manner analogous to the homogeneous reaction but with adsorbed oxygen atoms instead of free oxygen atoms.

The phenomenon of catalysis is understandable because the energy content of an adsorbed oxygen atom is less than that of a free oxygen atom and accordingly the activation energy of a reaction leading to an adsorbed oxygen atom can be supposed to be lower than that involving a free oxygen atom. The designation "adsorbed" indicates only the locus of an oxygen atom but implies no statement concerning the binding forces. In the case of metallic catalysts we may suppose that the state of an adsorbed oxygen atom is similar to that of an oxygen atom in oxides which can, in general, be described approximately as lattices consisting of ions. Hence, we have the following tentative scheme on metallic catalysts,

$$\text{catalyst} + 2e^- + N_2O = N_2 + O^{2-}(\text{ads.}), \tag{3}$$

$$O^{2-}(\text{ads.}) + N_2O = N_2 + O_2 + \text{catalyst} + 2e^-. \tag{4}$$

The assumption of exchange of electrons between gaseous reactants and solid catalysts within an adsorption layer is novel and must be examined in further investigations. For the decomposition of formic acid on alloys with systematically varied electron concentrations, Schwab[9] has recently shown that transition of electrons from formic acid to the metallic catalysts is seemingly the rate-determining step.

The heterogeneous decomposition of nitrous oxide on various oxides has been investigated widely by Schwab and associates.[10] Kinetic relations have been reported particularly by Schwab, Staeger, and von

* Present address: Department of Metallurgy, Massachusetts Institute of Technology, Cambridge, Massachusetts.

[1] M. Volmer and H. Kumerow, Zeits. f. physik. Chemie **B9**, 141 (1930); N. Nagasako and M. Volmer, Zeits. f. physik. Chemie **B10**, 414 (1930); N. Nagasako, Zeits. f. physik. Chemie **B11**, 420 (1930); M. Volmer and H. Froehlich, Zeits. f. physik. Chemie **B19**, 85, 89 (1931); M. Volmer and M. Bogdan, Zeits. f. physik. Chemie **B21**, 257 (1933); M. Volmer and H. Briskee, Zeits. f. physik. Chemie **B25**, 81 (1934).

[2] E. Hunter, Proc. Roy. Soc. (London) **A144**, 386 (1934).

[3] R. M. Lewis and C. N. Hinshelwood, Proc. Roy. Soc. (London) **A168**, 441 (1938). R. N. Pease, *Equilibrium and Kinetics of Gas Reactions* (Princeton University Press, Princeton, New Jersey, 1942), pp. 129–134.

[4] C. N. Hinshelwood and C. R. Prichard, Proc. Roy. Soc. (London) **A108**, 211 (1925); J. Chem. Soc. **127**, 327 (1925).

[5] H. Cassel and E. Glueckauf, Zeits. f. physik. Chemie **B9**, 428 (1930); **17**, 380 (1932).

[6] G. M. Schwab and H. Eberle, Zeits. f. physik. Chemie **B19**, 102 (1931).

[7] E. W. R. Steacie and J. W. McCubbin, J. Chem. Phys. **2**, 585 (1934); Can. J. Research **14B**, 84 (1936).

[8] E. W. R. Steacie, Can. J. Research **15B**, 237 (1937).

[9] G. M. Schwab, Trans. Faraday Soc. **42**, 689 (1946).

[10] G. M. Schwab and H. Schultes, Zeits. f. physik. Chemie **B9**, 265 (1930); Schwab, Staeger, and von Baumbach, Zeits. f. physik. Chemie **B21**, 65 (1933); G. M. Schwab and H. Schultes, Zeits. f. physik. Chemie **B25**, 411 (1934); G. M. Schwab and R. Staeger, Zeits. f. physik. Chemie **B25**, 418 (1934); G. M. Schwab and H. Nakamura, Ber. d. D. chem. Ges. **71**, 1755 (1938); G. M. Schwab and G. Driskos, Zeits. f. physik. Chemie **A186**, 348 (1940).

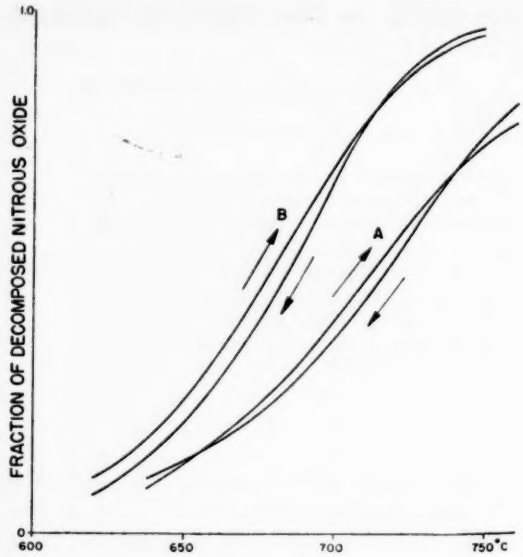

FIG. 1. Decomposition of nitrous oxide as a function of temperature on pure zinc oxide (curve A) and zinc oxide containing one percent of gallium oxide (curve B).

Baumbach. In general, the reaction is of first order with respect to nitrous oxide. On zinc oxide and cadmium oxide, retardation by oxygen has been observed, and on indium oxide a fractional order of the reaction with respect to nitrous oxide has been found. Results have been interpreted by means of the consecutive reactions (1) and (2) involving adsorbed oxygen atoms, and the Langmuir adsorption isotherm to account for the retardation effects.

We may interpret results by means of a more detailed description of the state of the catalyzing surface. It is known that the electrical conductivity of many oxides at high temperatures depends on the oxygen pressure of the ambient gas. In some oxides, e.g., zinc oxide and cadmium oxide, we have conduction through quasi-free electrons due to the presence of a small excess of metal. The higher the oxygen pressure over zinc oxide, the lower are the electrical conductivity and the concentration of quasi-free electrons.[11] Thus, we may tentatively describe the mechanism of the decomposition of nitrous oxide on electron-excess semiconducting oxides by the scheme given in Eqs. (3) and (4). Assuming that the reaction in Eq. (3) is rate-determining, we infer that the decomposition rate must decrease with increasing oxygen pressure in accordance with the dependency of the electrical conductivity on oxygen pressure.

The mechanism suggested above needs further examination. To this end, the following investigations have been made.

[11] H. H. von Baumbach and C. Wagner, Zeits. f. physik. Chemie **B22**, 199 (1933); M. Kroeger, *Grenzflaechenkatalyse* (S. Hirzel, Leipzig, Germany, 1933); O. Fritsch, Ann. d. Physik (5) **22**, 375 (1935); P. H. Miller, Phys. Rev. **60**, 890 (1941).

CONDUCTIVITY MEASUREMENTS ON ZINC OXIDE CATALYZING THE DECOMPOSITION OF NITROUS OXIDE

If electrons are involved in the elementary reactions of the decomposition of nitrous oxide, a correlation between electrical conductivity and catalytic activity should be found. First, it is to be expected that the steady-state concentration of quasi-free electrons in zinc oxide in a mixture of oxygen and nitrous oxide is lower than in oxygen alone because the rate constant of reactions (2) and (4), respectively, are finite and thus an excessive surface concentration of adsorbed oxygen must prevail. Analogous observations have been reported and discussed by Wagner and Hauffe[12] and Doehlemann.[13] In particular, it has been shown with the aid of measurements of the electrical conductivity that the oxygen excess of nickel oxide catalyzing the decomposition of nitrous oxide exceeds that of nickel oxide under the same given oxygen pressure in absence of nitrous oxide.

The electrical conductivity of zinc oxide catalyzing the decomposition of nitrous oxide was measured in collaboration with Inge Eisele after the method indicated by von Baumbach and Wagner.[11] Results are compiled in Table I. In accordance with theoretical considerations, the electrical resistance of zinc oxide at a given oxygen pressure is increased by presence of nitrous oxide, and accordingly the concentration of electrons in zinc oxide is decreased by presence of nitrous oxide. Thus, in view of the tentative scheme given in Eqs. (3) and (4) involving free electrons as reactants, it is understandable that under certain conditions the decomposition rate of nitrous oxide is proportional only to a fractional power of its concentration as it has been reported in the case of indium oxide by Schwab, Staeger, and von Baumbach.[10]

TABLE I. Electrical resistance of a porous slab of zinc oxide in mixtures of oxygen and nitrous oxide.

Gas % O_2	Composition % N_2O	Flow rate (liters/hour)	Resistance (ohms)
100	0	1.0	12,200
91	9	1.1	18,800
100	0	1.0	12,300
91	9	1.1	18,550
100	0	1.0	12,100
80	20	1.25	20,600
95	5	1.05	16,800
100	0	1.00	12,200
70	30	1.50	24,000
0	100	0.25	28,300
0	100	0.50	29,100
100	0	1.00	12,500

[12] C. Wagner and K. Hauffe, Zeits. f. Elektrochemie **44**, 172 (1938); **45**, 409 (1938).

[13] E. Doehlemann, Zeits. f. Elektrochemie **44**, 178 (1938).

DECOMPOSITION OF NITROUS OXIDE ON ZINC OXIDE-GALLIUM OXIDE

In the foregoing paper,[14] it has been shown that the electrical conductivity of a solid solution of gallium oxide in zinc oxide is much higher than that of pure zinc oxide. According to the tentative scheme given in Eqs. (3) and (4), it is to be expected that also the catalytic decomposition of nitrous oxide on such catalysts is much faster than that on zinc oxide. Experiments were made in collaboration with Inge Eisele and Karl Steffes. Catalyst samples were prepared by precipitation from a solution of the nitrates with sodium hydroxide and dehydration at successively increased temperatures up to 900°C. All factors possibly determining the specific surface area were the same for the preparations of samples without and with gallium oxide so that it may be assumed that the specific surface areas of the samples did not differ widely. A steady stream of a mixture of 10 mole percent of nitrous oxide and 90 percent of oxygen was led over the catalyst and the temperature was slowly increased. The degree of decomposition was determined from measurements of the heat conductivity of the gas leaving the catalyst. Results are shown in Fig. 1.

The decomposition rate of nitrous oxide on a catalyst containing 0.01 gram atom of gallium per one gram atom of zinc is indeed somewhat higher than that on pure zinc oxide, but the observed differences of the decomposition rate are much less than the differences in the electrical conductivity corresponding to a factor of about 50.[14]

Likewise, no substantial change of the catalytic activity was found in the case of two other reactions on the same catalysts, (1) oxidation of carbon monoxide and (2) decomposition of methanol.

Hence, Eq. (3) involving free electrons as reactants seems to be disapproved. However, it must be borne in mind that introduction of gallium oxide changes not only the concentration of electrons but also the concentration of interstitial cations, or that of anion vacancies as explicated in the foregoing paper.[14]

[14] C. Wagner, J. Chem. Phys. 18, 62 (1950).

For instance, we may assume that reaction (3) takes place not equally at all points of the surface of the catalyst but only at specified points, namely, either in the vicinity of an adsorbed zinc ion or at an anion vacancy and thus an oxygen ion beside an isolated zinc ion is formed.

In the case of thermodynamic equilibrium, the surface concentration of adsorbed zinc ions is proportional to that of interstitial zinc ions provided each concentration is relatively small. In view of the considerations presented in the foregoing paper,[14] especially Eq. (12), the product of the concentration of adsorbed zinc ions and the square of the concentration of electrons is proportional to the partial pressure of zinc and independent of the content of gallium oxide.

Possibly, there are anion vacancies rather than interstitial zinc ions. From the stoichiometric equation $Zn^{2+}(i)+O^{2-}=Zn^{2+}+h(O^{2-})$ and the law of mass action, it follows that the concentration of anion vacancies is proportional to the concentration of interstitial zinc ions. Thus, the product of the concentration of anion vacancies and the square of the electron concentration is also proportional to the partial pressure of zinc and independent of the content of gallium oxide.

Thus, if reaction (3) takes place preponderately in the vicinity of an adsorbed zinc ion or an anion vacancy, the reaction rate should be independent of the presence of gallium oxide which is nearly in accordance with the experimental finding.

CONCLUSIONS

For the time being, no definite mechanism of the decomposition of nitrous oxide on zinc oxide can be indicated. Further experimental investigations are necessary.

The present attempt to develop a mixed catalyst with an outstanding activity has been a failure. However, it seems worth while to investigate other systems and to examine whether there is a correlation between catalytic activity and the concentrations of disorder centers such as interstitial ions, and anion vacancies, quasi-free electrons, and electron holes.

Determination of the Concentrations of Cation and Anion Vacancies in Solid Potassium Chloride

CARL WAGNER* AND PAUL HANTELMANN
Eduard Zintl Institut für anorganische und physikalische Chemie der Technischen Hochschule Darmstadt, Germany
(Received May 19, 1949)

The mobility of cation vacancies and the equilibrium concentration of cation and anion vacancies in solid potassium chloride are calculated from measurements of the electrical conductivity of pure potassium chloride and solid solutions of strontium chloride in potassium chloride.

INTRODUCTION

IT has been shown by Phipps and Leslie,[1] Joffe,[2] Jost and Schweitzer,[3] and Tubandt, Reinhold, and Liebold[4] that in solid potassium chloride and likewise in sodium chloride both cations and anions participate to a comparable extent in the transport of electricity, whereas in most other halides, within the limits of error, only either cations or anions have been found to be mobile. The behavior of the alkali halides can be accounted for by the Schottky disorder model[5] according to which there are equal number of cation and anion vacancies whose concentrations are determined by a thermodynamic equilibrium. Ionic conduction is due to jumping of ions from normal positions to adjacent vacancies. Interstitial cations and anions in alkali halides can be disregarded according to calculations of energy levels carried out by Jost and Nehlep[6] and Mott and Littleton.[7] Koch and Wagner[8] have indicated a method to determine (1) the mobilities and (2) the concentration of "disorder centers" from measurements of the electrical conductivity of a pure salt and that of suitable solutions involving known concentrations of disorder centers due to the presence of ions whose valency differs from that of the ions of the solvent. In this way, silver chloride and silver bromide with the corresponding lead and cadmium compounds as additives have been investigated. Moreover, Croatto and associates[9] have used this method in order to determine mobilities and concentrations of disorder centers in cerium oxide and in strontium fluoride.

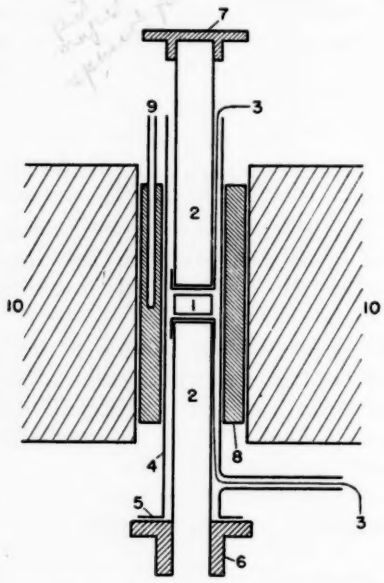

FIG. 1. Set-up for conductivity measurements. 1: Specimen. 2: Rods of ceramic material with platinum caps. 3: Platinum wires. 4: Quartz tube. 5: Plane ground joint resting on counterpart of brass. 6: Brass ring holding ceramic rod. 7: Brass cap for applying additional load. 8: Insert of high temperature resistant steel to equalize temperature. 9: Boring for thermocouple. 10: Electrical furnace, 25 cm high.

To obtain a known concentration of cation vacancies in potassium chloride, one can try to prepare solid solutions consisting of potassium chloride, KCl, as solvent and lead chloride, $PbCl_2$, or strontium chloride, $SrCl_2$, as solute. Since the solute contains only one cation for each two anions, either cation vacancies or interstitial anions must occur. The latter possibility is unlikely because of the large diameters of the anions and can be ruled out because of exclusively cationic conduction in such solutions.[10]

The preparation of such solutions implies that the solubility of the additive is sufficiently high. The existence of a solid solution of lead chloride in potassium chloride can be inferred from the observation of Lehfeldt[11] that the conductivity of potassium chloride containing some lead chloride exceeds considerably that of pure potassium chloride. Initially, the present authors also used lead chloride. However, results were not satisfactorily reproducible because lead chloride volatized during the runs. The main measurements

* Present address: Department of Metallurgy, Massachusetts Institute of Technology, Cambridge, Massachusetts.

[1] T. E. Phipps and R. T. Leslie, J. Am. Chem. Soc. **50**, 2412 (1928).

[2] A. Joffe, Zeits. f. Physik **62**, 730 (1930).

[3] W. Jost and A. Schweitzer, Zeits. f. physik. Chemie **B10**, 159 (1930).

[4] Tubandt, Reinhold, and Liebold, Zeits. f. anorg. allgem. Chemie **197**, 225 (1931).

[5] W. Schottky, Zeits. f. physik. Chemie **B29**, 335 (1935).

[6] W. Jost and G. Nehlep, Zeits. f. physik. Chemie **B32**, 1 (1936).

[7] N. F. Mott and M. J. Littleton, Trans. Faraday Soc. **34**, 485 (1938).

[8] E. Koch and C. Wagner, Zeits. f. physik. Chemie **B38**, 295 (1937).

[9] U. Croatto, Ricerca Scient. **13**, 830 (1942); U. Croatto and A. Mayer, Gazz. Chim. Ital. **73**, 199 (1943); U. Croatto and M. Bruno, Gazz. Chim. Ital. **78**, 83, 95 (1948).

[10] G. Ronge and C. Wagner, J. Chem. Phys. **18**, 74 (1950).

[11] W. Lehfeldt, Zeits. f. Physik **85**, 717 (1933).

TABLE I. Conductivity of solid potassium chloride and solutions of strontium chloride in potassium chloride.

Temp. °C	0%	0.1%	0.2%	0.4%	0.8% $SrCl_2$
600	···	2.6	4.8	9.8	23×10^{-4} ohm^{-1}cm^{-1}
625	···	3.5	6.4	13.4	30×10^{-4} ohm^{-1}cm^{-1}
650	0.14	4.6	8.3	17.5	38×10^{-4} ohm^{-1}cm^{-1}
675	0.24	5.9	10.6	22.0	$(55) \times 10^{-4}$ ohm^{-1}cm^{-1}
700	0.43	7.5	13.4	28.0	$(84) \times 10^{-4}$ ohm^{-1}cm^{-1}
725	0.80	9.4	16.8	38.0	$(172) \times 10^{-4}$ ohm^{-1}cm^{-1}

were performed with strontium chloride as solute. The strontium ion has a radius of 1.27A which is close to 1.33A characteristic of potassium ion. Thus the strontium ions fit well into the lattice of potassium chloride.

EXPERIMENTAL

Weighed quantities of potassium chloride and strontium chloride, freed of water by heating in a stream of nitrogen and hydrogen chloride, were melted together. From the solidified product, pulverized in an agate mortar, cylindrical tablets, about 0.5 cm high and 1 cm thick, were formed under a pressure of about 3000 kg/cm^2, and simultaneously gold foils, 0.005 cm thick, were attached to the circular faces as electrodes according to a recommendation of Seith.[12]

The installation of the specimen in an electrical furnace is shown in Fig. 1. During the runs a gentle current of purified nitrogen was led through the quartz tube surrounding the specimen. After annealing at 725°C for one hour or more, the electrical resistance was measured in a Wheatstone bridge with alternating current of 800 and 2100 cycles per second, respectively, at descending and ascending temperatures.

Results are compiled in Table I. Values for pure potassium chloride at 600 and 625°C are omitted because the minimum of sound in the earphones in the diagonal circuit of the Wheatstone bridge was indistinct and a considerable influence of the frequency of the alternating current was noticed. Measurements of solid solutions of strontium chloride in potassium chloride were free of such disturbances, probably because of the far higher conductivity of these specimens.

The conductivity of the specimens with strontium chloride is much higher than that of pure potassium chloride and is essentially proportional to the concentration of strontium chloride. At 675, 700, and 725°C, the increase of the conductivity between 0.4 and 0.8 mole percent is excessive, possibly because some liquid phase was present. These values are set in parentheses and are disregarded in the following evaluation.

CONCLUSIONS

The electrical conductivity due to potassium ions, i.e., the product of the over-all conductivity κ and the transference number of potassium ions t_{K^+}, equals

$$\kappa t_{K^+} = 96500 c x_{h(K^+)} u_{h(K^+)} \quad (1)$$

[12] W. Seith, Zeits. f. Physik **56**, 802 (1929).

Table II. Conductivity κ° and transference number $t^\circ_{K^+}$ in pure potassium chloride, mobility $u_{h(K^+)}$ of cation vacancies, and concentrations $x^\circ_{h(K^+)} = x^\circ_{h(Cl^-)}$ in pure potassium chloride.

Temp. °C	κ° ohm^{-1}cm^{-1}	$t^\circ_{K^+}$	$u_{h(K^+)}$ cm^{2}volt^{-1}sec.$^{-1}$	$x^\circ_{h(K^+)} = x^\circ_{h(Cl^-)}$
600	0.23×10^{-5}	0.88	1.0×10^{-4}	0.8×10^{-5}
625	0.48×10^{-5}	0.87	1.4×10^{-4}	1.2×10^{-5}
650	1.06×10^{-5}	0.85	1.7×10^{-4}	2.1×10^{-5}
675	2.0×10^{-5}	0.83	2.2×10^{-4}	3.0×10^{-5}
700	3.7×10^{-5}	0.80	2.8×10^{-4}	4.1×10^{-5}
725	6.8×10^{-5}	0.77	3.6×10^{-4}	5.7×10^{-5}

where c represents the over-all concentration of cations, in mole/cm^3, $x_{h(K^+)}$ the fraction of cation vacancies (holes), and $u_{h(K^+)}$ the mobility of a cation vacancy in cm^{2}volt^{-1}sec.$^{-1}$.

Since all specimens with strontium chloride have a conductivity much higher than that of pure potassium chloride, it can be concluded that the presence of anion vacancies in these specimens can be disregarded and the mole fraction y of strontium chloride can be equated to the fraction of cation vacancies. According to the following paper by Ronge and Wagner,[10] the transference number of potassium equals unity. Hence, the mobility of cation vacancies can be calculated from the conductivity of the specimens with strontium chloride as follows:

$$u_{h(K^+)} = \kappa / 96500\, cy. \quad (2)$$

Applying Eq. (1) to pure potassium chloride, the specific values of which are marked by the superscript $^\circ$, we can calculate the fraction $x^\circ_{h(K^+)}$ of cation vacancies, which according to the Schottky disorder model also equals the fraction $x^\circ_{h(Cl^-)}$ of anion vacancies. Thus,

$$x^\circ_{h(K^+)} = x^\circ_{h(Cl^-)} = \kappa^\circ t^\circ_{K^+} / 96500\, c u_{h(K^+)}. \quad (3)$$

The required transference numbers can be extrapolated from measurements of Tubandt, Reinhold, and Liebold[4] at lower temperatures, ranging from 425 to 600°C.

The conductivity κ° of pure potassium chloride has previously been determined by Benrath and associates,[13] Tammann and Veszi,[14] Phipps and Partridge,[15] Lehfeldt,[11] and Brennecke.[16] Single crystals were investigated by Phipps and Partridge and by Lehfeldt. Their values check satisfactorily in the temperature range under consideration. Values obtained on pressed tablets by Phipps and Partridge are four percent higher at 700°C, and 60 percent higher at 600°C. Values listed in Table I coincide with the latter values within 10

[13] A. Benrath and J. Wainoff, Zeits. f. physik. Chemie **77**, 257 (1911); A. Benrath and H. Tesche, Zeits. f. physik. Chemie **96**, 474 (1920).

[14] G. Tammann and G. Veszi, Zeits. f. anorg. allgem. Chemie **150**, 355 (1926).

[15] T. E. Phipps and E. G. Partridge, J. Am. Chem. Soc. **51**, 1331 (1929).

[16] C. G. Brennecke, J. App. Phys. **11**, 202 (1940).

percent. Since measurements on tablets may be distorted by a certain contribution of surface ions, it seems reasonable to use the values obtained on single crystals for evaluation of Eq. (3).

Table II lists the conductivity values of Phipps and Partridge, transference numbers, mobilities of cation vacancies calculated from Eq. (2), and the fractions of cation vacancies in pure potassium chloride calculated from Eq. (3).

The mobilities of cation vacancies in potassium chloride are about five times less than those in silver halides at the same ratio of measuring temperature to melting point. The dependence of the mobility of cations on temperature corresponds to an activation energy of 18 kcal./mole in accordance with a value of 0.78 ev= 18 kcal./mole derived from frequency-dispersion measurements by Breckenridge.[17]

From a plot of the logarithms of the fractions of cation vacancies *versus* the reciprocal of the absolute temperature, it follows that the energy required for the creation of one mole of cation vacancies and one mole of anion vacancies amounts to 48 kcal. This is within 1 kcal. the same value as calculated theoretically by Mott and Littleton.[7] This close agreement between theory and experiment, however, is fortuitous, for the limits of error of each method are far higher than 1 kcal.

[17] R. G. Breckenridge, J. Chem. Phys. **16**, 959 (1948).

THE JOURNAL OF CHEMICAL PHYSICS VOLUME 18, NUMBER 1 JANUARY, 1950

Transference Numbers of Solid Potassium Chloride with Strontium Chloride, Potassium Oxide, and Sodium Sulfide as Additives

GRETE RONGE AND CARL WAGNER*
Eduard Zintl Institut für anorganische und physikalische Chemie der Technischen Hochschule Darmstadt, Germany
(Received May 19, 1949)

The transference number of cations in solid potassium chloride at 600°C has been found to be 0.88 in accordance with previous experiments of Tubandt, Reinhold, and Liebold. Addition of strontium chloride causes increase of the transference number approaching unity. Addition of potassium oxide and sodium sulfide, respectively, lowers somewhat the transference number of cations and accordingly increases the transference number of anions. These results are in accordance with the Schottky disorder model, but the presence of interstitial cations apart from cation and anion vacancies cannot be ruled out.

I. INTRODUCTION

TO support the conclusions drawn in the foregoing paper,[1] transference experiments were made on solutions of strontium chloride in solid potassium chloride. In accordance with the Schottky disorder model,[2] virtually only potassium ions were found to be mobile.

In addition, experiments were made with potassium chloride containing small amounts of potassium oxide and sodium sulfide, respectively. If the solubilities of the additives were sufficient, transition to anionic conduction should be expected as expounded by Koch and Wagner.[3] Since the additives K_2O and Na_2S contain only one anion for each two cations, there should be one cation vacancy for each molecule of K_2O and Na_2S provided the Schottky model is correct. On the other hand, if potassium chloride contains interstitial cations as well as cation and anion vacancies, addition of K_2O and Na_2S, respectively, should result in formation of both interstitial cations and anion vacancies. Thus, even large concentrations of these additives should lead to conduction through both cations and anions. Consequently, if the solubilities of the additives are sufficiently high, the determination of transference numbers of these mixed crystals represents a crucial experiment to rule out noticeable concentrations of interstitial cations and thus to confirm the Schottky disorder model. The experiments described in Section II, however, do not lead to decisive conclusions because of the low solubility of the additives.

II. EXPERIMENTAL

Transference experiments were made on both pressed tablets and single crystals at 600°C after the method previously used by Tubandt, Reinhold, and Liebold.[4] To avoid metallic conduction through potassium filaments evolving from the cathode, experiments were made on piles consisting of a platinum foil cathode, three barium chloride tablets, three potassium chloride tablets, three barium chloride tablets, and a platinum foil anode. The tablets and likewise the single crystals, which were used in some runs, were provided with small oblique faces at the edges so that after the electrolysis

* Present address: Department of Metallurgy, Massachusetts Institute of Technology, Cambridge, Massachusetts.
[1] C. Wagner and P. Hantelmann, J. Chem. Phys. **18**, 72 (1950).
[2] W. Schottky, Zeits. f. physik. Chemie, **B29**, 335 (1935).
[3] E. Koch and C. Wagner, Zeits. f. physik. Chemie **B38**, 295 (1937).
[4] Tubandt, Reinhold, and Liebold, Zeits. f. anorg. allgem. Chemie **197**, 225 (1931).

TABLE I. Transference measurements on pure potassium chloride. (Q electrical equivalents according to titrations of solutions in silver coulometers; Δm_C weight change of KCl sample facing cathode and adjacent $BaCl_2$ tablet; Δm_M weight change of middle KCl sample; Δm_A weight change of KCl sample facing anode and adjacent $BaCl_2$ tablet; Δm_S total weight loss due to sublimation; weight changes corrected for sublimation are primed; all weight changes are given in mg; t_{K+} transference number of potassium ions.)

	KCl tablets		Single crystals of KCl		
$Q\times10^4$	8.02	7.33	5.09	6.42	4.14
Δm_C	+51.5	+46.3	+34.7	+39.8	+24.5
Δm_M	− 1.9	−49.4	− 1.6	− 2.2	+ 0.7
Δm_A	−52.6		−35.2	−43.3	−28.0
Δm_S	3.0	3.1	2.1	5.7	2.8
$\Delta m'_C$	+52.3	+47.2	+35.4	+42.1	+25.5
$\Delta m'_M$	− 0.7	−47.2	− 0.9	− 1.0	+ 1.3
$\Delta m'_A$	−51.6		−34.5	−41.1	−26.8
t_{K^+} from $\Delta m'_C$	0.875	0.865	0.932	0.880	0.827
t_{K^+} from $\Delta m'_A$	0.862	0.865	0.909	0.869	0.868

they could easily be pried apart with a razor blade. The piles were mounted in a furnace described in the foregoing paper.[1] The quantity of electricity applied was determined with the aid of two silver titration coulometers.

Since conduction in barium chloride is exclusively anionic,[4] the weight of each potassium chloride tablet should remain constant during electrolysis if conduction in potassium chloride is also exclusively anionic. In the case of exclusively cationic conduction in potassium chloride, the weight increase of a potassium chloride tablet facing the cathode would be equal to the product of electrical equivalents sent through the pile and the molecular weight of potassium chloride, because potassium ions in potassium chloride and chlorine ions in barium chloride migrate toward the interface between the two salts. Conversely, the weight of the potassium chloride tablet facing the anode would decrease by the same amount. The weight of the middle tablet should remain constant.

Consequently, the transference number of potassium ions is to be calculated by dividing the actual weight increase of the potassium chloride tablet facing the cathode by the weight increase calculated for exclusively cationic conduction.

Actually, the potassium chloride tablets adjacent to barium chloride tablets could not be isolated and were therefore weighed together with the adjacent barium chloride tablets. The foregoing conclusions remain unaltered as expounded by Tubandt, Reinhold, and Liebold.[4]

In all runs the weight increase of the cathodic potassium chloride tablet and the adjacent barium chloride tablet was found to be less than the weight decrease of the corresponding anodic tablets. Moreover, it was found that the weight of the middle potassium chloride tablet had decreased. Obviously some substance was lost by vaporization. Therefore, corrections had to be provided which were calculated in the same manner as used by Tubandt, Reinhold, and Liebold.[4]

TABLE II. Transference measurements on potassium chloride containing strontium chloride.

	KCl tablets with 0.4 mole percent of $SrCl_2$		Single crystals of KCl drawn from melt with 0.3 mole percent of $SrCl_2$		
$Q\times10^4$	8.93	9.78	8.87	9.87	6.84
Δm_C	+63.1	+69.2	+64.7	+71.1	+46.5
Δm_M	− 1.2	−72.6	− 1.0	− 1.0	− 0.1
Δm_A	−66.3		−64.9	−74.2	−52.5
Δm_S	4.4	3.4	1.2	4.1	6.1
$\Delta m'_C$	+64.5	+70.3	+65.1	+72.3	+48.8
$\Delta m'_M$	+ 0.4	−70.3	− 0.5	+ 0.4	+ 1.0
$\Delta m'_A$	−64.9		−64.6	−72.7	−49.8
t_{K^+} from $\Delta m'_C$	0.970	0.964	0.984	0.984	0.958
t_{K^+} from $\Delta m'_A$	0.976	0.964	0.978	0.989	0.979

It was assumed that potassium chloride vaporized preponderately because of its higher vapor pressure and the weight losses were proportional to the quantities of potassium chloride of the respective tablets. These corrections are, of course, not exact and thereby the accuracy of all results is limited. The corrected weight change of the middle potassium chloride tablets should be zero, and the absolute amounts of the corrected weight changes of tablets facing cathode and anode, respectively, should be equal to each other. Actually, there are deviations up to about 1 mg as shown in Tables I and II. Since the weight increases of potassium chloride tablets facing the cathode range from 40 to 75 mg, errors of the resulting transference numbers are between 0.012 and 0.025. This is also the magnitude of deviations between parallel runs.

Since in the first runs with single crystals of potassium chloride it was observed that the crystals adjacent to barium chloride tablets had split, further runs were made with five potassium chloride crystals one above the other. The first and the second potassium chloride crystal were weighed together with the adjacent barium chloride tablet in order to obtain the weight change of the potassium chloride crystal facing the cathode; correspondingly, the fourth and the fifth potassium chloride crystal were weighed together with the adjacent barium chloride tablet. In spite of these precautions, many runs were failures so that the number of results given in this paper is rather small.

Data referring to runs with pure potassium chloride are compiled in Table I. In the average, a transference number of cations equal to 0.88 at 600°C has been obtained in accordance with Tubandt, Reinhold, and Liebold.[4]

Further runs were made with pressed tablets consisting of potassium chloride with 0.4 mole percent of strontium chloride, and with single crystals obtained from Professor R. Hilsch at Göttingen. These crystals were drawn from a melt with 0.3 mole percent of strontium chloride. Their specific electrical conductivity ranged from 2×10^{-5} to 8×10^{-5} $ohm^{-1}cm^{-1}$ at 600°C, whereas the conductivity of pure potassium chloride is only 2.3×10^{-6} $ohm^{-1}cm^{-1}$ according to Phipps and

Partridge.[5] Since the conductivity of the mixed crystals was 10 to 40 times greater than that of pure potassium chloride, transition to exclusively cationic conduction was to be expected. Upon comparison with the conductivities measured by Wagner and Hantelmann[1] on samples of known composition, there follows a concentration of 0.01 to 0.03 mole percent of strontium chloride in the single crystals.

Results obtained with samples containing strontium chloride are compiled in Table II. In the average, a transference number of cations of 0.975 at 600°C has been found.

In addition, the influence of additives such as K_2O and Na_2S was investigated. Single crystals of potassium chloride with some potassium oxide were also obtained from Professor Hilsch at Göttingen. They were prepared from crystals drawn from a melt of potassium chloride with 0.02 mole percent of potassium nitrate by heating in an atmosphere of potassium vapor. Potassium oxide was formed by the reactions $10K+2KNO_3=6K_2O+N_2$ and $6K+2KNO_2=4K_2O+N_2$, respectively.[6] The concentration of dissolved potassium oxide, however, was only of the order of the concentration of cation and anion vacancies in pure potassium chloride, for the electrical conductivity of the crystal containing potassium oxide deviated less than 20 percent from that of pure potassium chloride between 600 and 725°C. In a single run at 600°C, a transference number of cations of 0.56 to 0.60 was obtained.

Further experiments were made with sodium sulfide as additive. This substance was prepared by reaction of cadmium sulfide with sodium vapor at 500°C and then added to molten potassium chloride, care being taken to exclude water vapor and oxygen. Tablets were pressed from the solidified product, in which a content of 0.11 mole percent of sodium sulfide was found by titration with iodine solution. The electrical conductivity between 600 and 675°C was found to be about the same as that of tablets without additive. Here too, the concentration of anion vacancies did not deviate substantially from that in pure potassium chloride. A single run at 600°C yielded a transference number of cations of 0.69.

[5] T. E. Phipps and E. G. Partridge, J. Am. Chem. Soc. **51**, 1331 (1929).

[6] K. Korth, Göttingen Nachrichten N.F. **1**, 221 (1935).

CONCLUSIONS

The transference number of cations obtained on potassium chloride with strontium chloride equals 0.975. This value is slightly less than the value of 1.00 inferred from the Schottky disorder model. The difference is of the order of experimental errors.

The solubilities of the additives K_2O and Na_2S in solid potassium chloride seem to be not greater than the order of the concentrations of cation and anion vacancies in pure potassium chloride, since the conductivity is changed only slightly by these additives. In accordance herewith, the transference numbers of cations in crystals containing these additives were found to be somewhat less than that in pure potassium chloride. This decrease is due to an increase of the concentration of anion vacancies. However, no transition to preponderately anionic conduction has been observed; nor was such a transition to be expected, because the conductivity of these samples was about the same as that of pure potassium chloride. Thus presence of noteworthy concentrations of interstitial cations apart from cation vacancies cannot be ruled out on the basis of experiments but is unlikely for theoretical reasons.

The Thermodynamic Functions of Methyl Mercaptan and Dimethyl Sulfide

JOHN L. BINDER*
Akron, Ohio

(Received May 23, 1949)

The entropies, free energies, heat capacities and heat contents of methyl mercaptan and dimethyl sulfide have been calculated from 298.16°K to 1500°K at 100°K intervals. The free energies of formation of these compounds have also been calculated for this temperature range based both on sulfur gas and rhombic sulfur as the standard states of sulfur.

I. INTRODUCTION

THE entropy of methyl mercaptan and dimethyl sulfide at the boiling point has been measured by Russell, Osborne, and Yost,[1] and by Osborne, Doescher, and Yost,[2] respectively. From these values and values calculated using spectroscopic data they determined the hindered rotation potential of the methyl groups. Their value for dimethyl sulfide agrees with the potential calculated by Thompson[3] who obtained the infrared spectrum of this compound. In view of the growing commercial importance of these compounds it seemed desirable to complete the thermodynamic calculations and tabulate them in much the same way as has been done by the National Bureau of Standards and the American Petroleum Institute for hydrocarbons.

II. CALCULATIONS

Entropy, Free Energy, Heat Capacity, Heat Content

The entropy, free energy, heat capacity and heat content of methyl mercaptan and dimethyl sulfide were computed, at 100°K intervals, from 298.16°K to 1500°K by calculating the translational, classical rotational, vibrational and hindered rotational contributions at each temperature and summing. The equations and tables used were those given in Taylor's and Glasstone's *Treatise on Physical Chemistry*.[4]

In calculating the restricted rotation contribution a potential of 1460 cal. was used for methyl mercaptan and 1900 cal., rather than 2000 cal., given by Osborne, Doescher, and Yost,[2] for dimethyl sulfide, because with our graphs this gave a more exact fit with the measured entropy. The difference, 100 cal., can scarcely be regarded as significant.

Since the equations and tables used were based on the old value of the gas constant R, the values obtained for the entropy, free energy, heat capacity, and heat content were corrected to the new value by multiplying by 1.00014. This was done only for the total entropy, free energy, heat capacity, and heat content, not for the individual contributions of translation, rotation, etc. The results of the calculations are given in Tables I and II. The entropy values were adjusted, where necessary,

TABLE I. Summary of thermodynamic functions of methyl mercaptan.

T°K	298.16	300	400	500	600	700	800	900	1000	1100	1200	1300	1400	1500
S°	60.86	60.94	64.66	68.08	71.13	73.96	76.59	79.06	81.38	83.58	85.64	87.60	89.47	91.25
$-\left(\frac{F^\circ-H_0^\circ}{T}\right)$	51.16	51.23	54.09	56.60	58.76	60.73	62.55	64.25	65.85	67.37	68.80	70.17	71.49	72.75
C_p°	12.12	12.15	14.11	15.96	17.62	19.08	20.38	21.53	22.54	23.43	24.21	24.89	25.49	26.00
$\left(\frac{H^\circ-H_0^\circ}{T}\right)$	9.70	9.71	10.57	11.48	12.37	13.23	14.04	14.81	15.53	16.21	16.84	17.43	17.98	18.50
$H^\circ-H_0^\circ$	2892	2913	4228	5740	7422	9261	11232	13329	15530	17831	20208	22659	25172	27750

TABLE II. Summary of thermodynamic functions of dimethyl sulfide.

T°K	298.16	300	400	500	600	700	800	900	1000	1100	1200	1300	1400	1500
S°	68.25	68.36	73.75	78.55	82.99	87.18	91.15	94.91	98.47	101.84	105.03	108.02	110.88	113.61
$-\left(\frac{F^\circ-H_0^\circ}{T}\right)$	55.69	55.77	59.64	62.92	65.90	68.65	71.23	73.69	76.01	78.23	80.34	82.33	84.28	86.13
C_p°	17.00	17.15	20.25	23.27	26.07	28.56	30.76	32.68	34.35	35.82	37.10	38.22	39.17	40.01
$\left(\frac{H^\circ-H_0^\circ}{T}\right)$	12.56	12.59	14.11	15.63	17.09	18.53	19.92	21.22	22.46	23.61	24.69	25.69	26.60	27.48
$H^\circ-H_0^\circ$	3745	3777	5644	7815	10254	12971	15936	19098	22460	25971	29628	33397	37240	41220

* Present address: Firestone Tire and Rubber Company, Akron, Ohio.

[1] Russell, Osborne, and Yost, J. Am. Chem. Soc. **64**, 165 (1942).
[2] Osborne, Doescher, and Yost, J. Am. Chem. Soc. **64**, 169 (1942).
[3] H. W. Thompson, Trans. Faraday Soc. **37**, 38 (1941).
[4] H. S. Taylor and S. Glasstone, *Treatise on Physical Chemistry* I. *Atomistics and Thermodynamics* (D. Van Nostrand Company, Inc., New York, 1942).

TABLE III. Free energies of formation.

	CH_3SH		CH_3SCH_3	
T°K	$\Delta F_f°$ S_2(gas)	$\Delta F_f°$ S(rh)	$\Delta F_f°$ S_2(gas)	$\Delta F_f°$ S(rh)
298.16	−8919	+760	−5344	+4335
300	−8865	778	−5244	4399
400	−5723	1989	+ 448	8160
500	−2442	3391	6431	12264
600	+ 973	4978	12589	16594
700	4469	6701	18861	21091
800	8010	8519	25212	25721
900	11599	10441	31603	30495
1000	15207	12437	38038	35268
1100	18833	14506	44489	40162
1200	22471	16642	50959	45130
1300	26100	18825	57463	50191
1400	29717	21052	63913	55248
1500	33345	23345	71780	61780

to satisfy the equality $S°=(H°-H_0°/T)-(F°-H_0°/T)$. This adjustment amounted to 0.06 in two cases but in general it was 0.00 or ±0.01.

Free Energy of Formation

With the free energy tables given here and those given in "Selected values of chemical thermodynamic properties"[5] it was most convenient to calculate the free energy of formation of methyl mercaptan and of dimethyl sulfide, as a function of temperature, by using the relation

$$F°=H_0°+(F°-H_0°/T)T. \quad (1)$$

This involves determining $\Delta H_0°$ for the reactions of the formation of the compounds in their standard states from the elements in their standard states. Since the free energy functions were not available for rhombic sulfur, which is generally taken to be the standard state of sulfur,[6] and since they were for diatomic sulfur gas, the free energies were calculated for the reactions

$$C_s(\text{graphite})+2H_2(\text{gas})+\tfrac{1}{2}S_2(\text{gas})=CH_3SH(\text{gas}) \quad (2)$$

and

$$2C_s(\text{graphite})+3H_2(\text{gas})+\tfrac{1}{2}S_2(\text{gas})=CH_3SCH_3(\text{gas}). \quad (3)$$

These were converted to rhombic sulfur using the free energy data given by Kelley[7] for the reaction

$$2S(rh)=S_2(\text{gas}). \quad (4)$$

The quantity $\Delta H_0°$ was found for reactions (2) and (3) by determining the free energy change at 298.16°K using the relation

$$\Delta F°=\Delta H°-T\Delta S° \quad (5)$$

and also evaluating $\Delta(F°-H_0°/T)$ at 298.16°K. $\Delta H_{298.16}°$ was obtained, for each reaction, by using heat content values given in reference 5 for CH_3SH, $\Delta H_f°=-2.97$ kcal./mole;[8] CH_3SCH_3, $\Delta H_f°=-6.90$ kcal./mole;[9] $S_2(g)$, $\Delta H_f°=+29.86$ kcal./mole.[10] For reaction (2) $\Delta H°=-17.90$ kcal./mole and for reaction (3) $\Delta H°=-21.830$ kcal./mole. From the same source and the entropies given here $\Delta S°=-30.128$ e.u. for reaction (2) and $\Delta S°=-55.278$ e.u. for reaction (3), using 54.41 e.u. for the entropy of $S_2(g)$.[7] Therefore $\Delta F_{298.16}°=-8914$ cal. for reaction (2) and $\Delta F_{298.16}°=-5339$ for reaction (3). From values of $(F°-H_0°)/T$ given here, in the tables of reference 5 and by Kelley[7] $\Delta(F°-H_0°)_{298.16}=6506$ cal. for reaction (2) and $\Delta(F°-H_0°)_{298.16}=12596$ cal. for reaction (3). Combining the $\Delta F°$ and $\Delta(F°-H_0°)$ values $\Delta H_0°=-15423$ cal. for reaction (2) and $\Delta H_0°=-17935$ cal. for reaction (3).

With these values of $\Delta H_0°$ the free energy changes at several temperatures were calculated for reactions (2) and (3) and the results are given in Table III. The free energies of formation based on rhombic sulfur as the standard state are also given. It will be noted that there is some change in these values from those given in the previous note on this subject.[11] This is due to the different values for the heats of formations of CH_3SH and CH_3SCH_3 used here.

ACKNOWLEDGMENT

It is a pleasure to acknowledge my indebtedness to Doctors F. D. Rossini and D. D. Wagman of the Bureau of Standards and Professors Gibson and Brewer of the University of California for their suggestions regarding this work.

[5] "Selected values of chemical thermodynamic properties," Nat. Bur. Stand. (1947).

[6] G. N. Lewis and M. Randall, *Thermodynamics and Free Energy of Chemical Substances* (McGraw-Hill Book Company, Inc., New York, 1923).

[7] K. K. Kelley, "Thermodynamic properties of sulfur and its inorganic compounds," Bureau of Mines Bulletin 406, 1937.

[8] Selected values of chemical thermodynamic properties, Nat. Bur. Stand., Series I, table 23–12 (1947).

[9] See reference 8, table 23–42.

[10] See reference 8, table 14–2.

[11] J. Chem. Phys., **17**, 499 (1949).

Quantitative Studies of Radiation-Induced Reactions in Aqueous Solution. I. Oxidation of Ferrous Sulfate by X- and γ-Radiation

NICHOLAS MILLER
Department of Natural Philosophy, University of Edinburgh, Edinburgh, Scotland
(Received May 24, 1949)

A study has been made of the oxidation of ferrous ions in 0.8N sulfuric acid solution by x- and γ-radiation in different types of system and using different energies of incident radiation. The conclusion is reached that simple modes of dosimetry, such as have been used in previous determinations of the ionic yields for a number of reactions induced by radiation in aqueous systems, are adequate if accuracy within 20 percent is all that is required. For greater precision, more rigorous methods have to be adopted, and using such a method, the ferrous sulfate system has been calibrated with a view to its possible use as a mode of integral dosimetry for aqueous media. Some speculations as to the mechanism of this particular reaction are included.

I. INTRODUCTION

Statement of the Problem

THE mechanism of the indirect action of high energy radiation on aqueous solutions, in which the observed chemical change in the solute is attributed to reactive entities produced by the radiation in the solvent, was first discussed by Risse[1] and later by Allen,[2] Allsopp,[3] Dainton,[4] Dainton and Miller,[5] Lea,[6] Weiss[7] and others. It is proposed here to direct attention to experimental techniques available for estimating the amount of chemical change produced per unit of energy absorbed in such systems, and to present the results of some further studies of the oxidation of ferrous ions in 0.8N sulfuric acid solution by x- and γ-radiation.

Quantitative assessment of the amount of chemical change as a function of energy absorbed in such systems has been carried out in the past by examining the relation between the ionization current observed in an air-filled chamber and the chemical change in a cell containing the solution under study, both being exposed to the same field of radiation. The basis of this method is that the mass absorption coefficients of water and air are very similar even for x-rays of 50 kev and lower energy, so that it suffices as an approximation to multiply the observed energy loss per unit volume of air by the ratio of the densities of water and air in order to obtain the energy loss per unit volume of water in the same radiation field. The energy loss per unit volume of air can be computed from the ionization current observed in suitable air-filled chambers following well-established methods.

If greater accuracy is required, however, certain objections may be raised to this procedure, depending largely on the geometry of the irradiation cell used. If its volume is too large, the absorption of the beam of radiation in the solution will be appreciable. If it is too small and, as commonly is the case, the wall of the cell consists of glass or some medium with a linear absorption coefficient for the incident radiation very different from that of water, the ionization produced within the solution by secondary electrons generated within the wall may not be negligible. These effects will both become more marked the softer is the primary beam of radiation. The former difficulty has been recognized by certain workers[8–10] who have applied correction factors to their results accordingly. Many workers on the other hand either made no such correction,[11] compared their results with those obtained in other systems which had been calibrated previously,[12–14] or computed the dose from a formula whose validity was not tested.[15] In a number of cases[16–18] no mention is made of the method of dosimetry used.

In the work described in this paper the quantitative results obtained by Fricke and Morse[8] and Shishacow[18] in the case of the oxidation of Fe^{++} ions in 0.8N sulfuric acid solution have been compared with those obtained by a somewhat more rigorous approach to the problem. The figures are in fair agreement, but those obtained by the more rigorous procedure are significantly higher than the others.

Theoretical Approach

The difficulties encountered in the quantitative study of these systems are similar to those met with in the

[1] O. Risse, Strahlentherapie **34**, 78 (1929).
[2] A. O. Allen, J. Phys. Coll. Chem. **52**, 479 (1948).
[3] C. B. Allsopp, Trans. Faraday Soc. **40**, 79 (1944); Brit. J. Radiology, Supp. No. 1, 43 (1947).
[4] F. S. Dainton, J. Phys. Coll. Chem. **52**, 490 (1948).
[5] F. S. Dainton and N. Miller, XI International Chemical Congress (in press).
[6] D. E. Lea, *Actions of Radiations on Living Cells*, (Columbia University Press, New York, 1946).
[7] J. Weiss, Nature **153**, 748 (1944); **157**, 584 (1946); Trans. Faraday Soc. **43**, 314 (1947).
[8] H. Fricke, Am. J. Roent. Rad. Ther. **18**, 430 (1927); H. Fricke and S. Morse, Phil. Mag. **7**, 129 (1929).
[9] G. L. Clark and W. S. Coe, J. Chem. Phys. **5**, 97 (1937).
[10] V. E. Kinsey, J. Biol. Chem. **110**, 551 (1935).
[11] W. M. Dale, Biochem. J. **34**, 1367 (1940); **36**, 80 (1942); J. Physiol. **102**, 50 (1943).
[12] H. Fricke and E. R. Brownscombe, J. Am. Chem. Soc. **55**, 2358 (1933).
[13] W. Stenstrom and A. Lohmann, J. Biol. Chem. **79**, 673 (1928).
[14] Fricke, Hart, and Smith, J. Chem. Phys. **6**, 229 (1938).
[15] Liechti, Minder, and Wegmuller, Radiol. Clin. **14**, 167 (1945).
[16] R. S. Anderson and B. Harrison, J. Gen. Physiol. **27**, 69 (1944).
[17] B. E. Proctor and S. A. Goldblith, Nucleonics **3**(2), 32 (1948).
[18] N. A. Shishacow, Phil. Mag. **14**, 198 (1932).

TABLE I. Relative ionization within small air-filled cavities in various materials on exposure to radiation of (i) 41 kev, (ii) 92 kev, (iii) 820 kev.

	41 kev	92 kev	820 kev
Water	100	100	100
Lucite	71	92	99
Polystyrene	52	87	99
Graphite	54	84	92
0.8N Sulfuric acid	111	102	99
Air	102	95	92
Aluminum	520	216	87
Typical soft glass	495	208	88

1920's in the establishment of a satisfactory definition of the roentgen. The theoretical approach of Bragg[19] used by Gray[20] in resolving the earlier problem can also be used in this case.

The relation we seek is one between the ionization per unit volume of air in a given system, which can readily be measured, and the energy release per unit volume of an aqueous system exposed to the same intensity of radiation.

Let us suppose that an ionization chamber can be constructed of a medium which is "water-wall" for the type of radiation being used, i.e., in which the atmosphere of secondary electrons induced by the radiation can be regarded as identical with that which would be induced in a similar body of water. If the linear dimensions of the effective volume of the chamber are small compared with the range of the secondary electrons in air, we shall obtain the relationship we seek directly, using the reasoning of Gray, thus:

If E_m = energy released per unit volume of medium in unit time, E = incident γ-ray energy flux, J_m = number of single ionizations per unit volume of air within the chamber in unit time, W = energy required to produce one ionization in air, S_m = stopping power of medium relative to that of air for secondary electrons, σ_a = part of the Compton scattering coefficient relating to the transference of energy to the secondary electron, τ = photoelectric absorption coefficient, and the subscript $_m$ denote the values of these quantities for the medium,

$$E_m = J_m W \cdot S_m = E(\sigma_a + \tau)_m. \tag{1}$$

For a water-wall chamber E_m will clearly be equal to the energy released per unit volume of water in unit time in the same γ-ray flux.

The solutions normally studied under the influence of radiation are dilute (e.g. up to 1N in acid, $<10^{-3}$N in other solutes), so that the energy released per unit volume within them can be regarded as very similar to that released in water in the same radiation field. We have therefore only to construct a cell of identical geometry to the chamber out of the same material, fill it with the solution, and examine the chemical change taking place on exposure to the same source of radiation, in order to assess the chemical change as a function of energy absorbed in the solution. This is true provided that the cell is sufficiently small to ensure that the absorption of the primary radiation can be regarded as negligible within the aqueous medium.

We will see how well these conditions can be met in practice.

If a chamber is water-wall, the ionization per unit volume of air in a small cavity within the wall material will be identical with that which would be observed in a small cavity in a body of water exposed to the same radiation field. Thus, from Eq. (1),

$$J_m = (E/W) \times (\sigma_a + \tau)_m / S_m,$$

and a water-wall chamber is one for which

$$(\sigma_a + \tau)_m / S_m = (\sigma_a + \tau)_w / S_w, \tag{2}$$

where the subscripts $_m$ and $_w$ relate to the medium and water, respectively.

The relative values of the quantity $(\sigma_a + \tau)_m / S_m$ for various practical media whose chemical composition is known can be evaluated for different types of radiation, as follows:

If n_{em} be the number of electrons per gram of medium, S_{em} the average stopping power per electron in the medium, and ρ the density of the material, $S_m \sim n_{em} \rho S_{em}$, and $(\sigma_a + \tau)_m / S_m \sim (\sigma_a + \tau)_m / n_{em} \rho S_{em}$. The quantities n_{em} and $(\sigma_a + \tau)/\rho$ can be evaluated for various media using tables provided by Lea (see reference 6, pp. 345–9), and the values for the electronic stopping power as a function of atomic number given by Gray[20] can be used to give figures for S_{em} assuming a value for the "effective atomic number" of the material given to a sufficiently close approximation by

$$Z_1 N_1 + Z_2 N_2 + \cdots + Z_x N_x / N_1 + \cdots + N_x,$$

where N_1, N_2, are the relative numbers of atoms of Z_1, Z_2, etc. In this way the values of the quantities in Eq. (2) can be compared for various media. The results of such calculations are given in Table I for a number of materials of practical interest in this connection, for incident radiation of 41 kev, 92 kev, and 820 kev energy. They are expressed as values of the quantity $(\sigma_a + \tau)_m / S_m$ relative to that for water as 100, and illustrate how wide the discrepancies between these quantities become as the transition is made from absorption largely by Compton scattering (820 kev) to absorption largely by photoelectric effect (41 kev).

Consideration of these figures leads to the conclusion that, using radiation of 820 kev and greater energy where τ is negligible, and apparatus made of, for instance, polystyrene, it should be possible to make a system which will satisfy these requirements quite closely. In this case the weakening of the primary beam of radiation in passing through a layer of a few mm of water can be regarded as negligible. To provide electrodes in the ionization chamber a thin layer of graphite

[19] W. H. Bragg, *Studies in Radioactivity* (MacMillan, Ltd., London, 1912), p. 94ff.

[20] L. H. Gray, Proc. Roy. Soc. (A) **122**, 647 (1929); **156**, 578 (1936).

can be used, painted on to the inside surfaces of the polystyrene in the form of an alcohol-base "dag," and the production of secondary electrons in the graphite with radiation of this energy can be neglected.

With monochromatic 92 kev radiation a fair approximation to these requirements can evidently be made, but with unfiltered x-radiation produced, say, at 200 kev peak the presence of the softer components will make the matter more difficult. In this case, (i) absorption within the water will be appreciable even in a few mm depth of solution, (ii) the electron atmosphere cannot be regarded as identical within the medium and the water. It may be noted here that chambers constructed of air-wall materials having aluminum electrodes, as were used by Clark and Pickett[21] in their studies of the reduction of potassium nitrate by 105-kev x-rays, are unsuitable for use with this type of radiation. The writer, for instance, observed an increase by a factor 2.3 in the ionization current observed in a Lucite chamber (see Fig. 3) when the "dag" electrodes were replaced with ones of 2 mg/cm^2 aluminum under 200-kev x-radiation, although this substitution had no detectable effect in the case of γ-radiation from radium. The results of Clark and Pickett are therefore probably in error.

An attempt to put these principles into practice in the study of the oxidation of Fe^{++} ions in 0.8N sulfuric acid solution will now be described. The results will be compared with those obtained using methods similar to those of earlier workers in this field. Before discussing these experiments, however, it will be as well to review our knowledge with respect to this particular radiation-induced reaction.

Requirements of Chemical Process for Studies in Dosimetry

In testing various methods for estimating the chemical change induced by the absorption of a given amount of radiant energy, a system is required in which this change is a linear function of the energy absorbed independently of the spatial distribution of the sites of ionization and excitation formed by the radiation. Thus we require for this purpose a reaction induced by radiation in aqueous solution, the rate constant of which is reproducible over a wide range of wave-length and intensity of the incident radiation, and constant over a sufficient range of solute concentration, i.e., of zero order with respect to the solute.

Study of the existing literature on the indirect action of radiation in aqueous solutions and the results of preliminary experiments carried out with a view to finding a useful system of this type indicated to the writer that the oxidation of ferrous ions in 0.8N sulfuric acid solution came close to filling these requirements, although the mechanism of the reaction was not clear. The independence of the measured radiation yield (this being defined as the amount of chemical change per unit of energy absorbed) on the initial concentration of Fe^{++} ions between 10^{-1} and 10^{-3} had been noted by Fricke and Morse[8] and confirmed by Shishacow[18] and Liechti, Minder, and Wegmuller.[15] A degree of independence of the spatial distribution of the ionization had been shown by Fricke's experiments in which the quality of the incident x-radiation was varied by the use of filters,[8] and also by the fact that the figures of Fricke and Morse,[8] Fricke and Hart,[22] and Shishacow[18] for the radiation yield were in agreement despite the fact that it was highly improbable that the wave-length and intensities of radiation used in these various experiments were identical. Further work by the writer showed that the independence of wave-length appeared to be continued into much shorter wave-lengths, when solutions irradiated with γ-rays from radium filtered by 0.5 mm of platinum gave figures for radiation yield agreeing with those of previous workers.

Kinetics of the Radiation-Induced Oxidation of Fe^{++}

As stated above, this reaction has the typical characteristics of an indirect radiation-induced reaction in that the yield is unchanged over a wide range of the concentration of the solute and the wave-length of the incident radiation.[23] The lower limit of the concentration-independent region for solutions containing dissolved oxygen (see below) has been studied by Dewhurst and Krenz,[24] who find that at concentrations below 8×10^{-5} M Fe^{++} the radiation yield falls off with decreasing concentration. The upper limit of this region is not at present of interest, as in solutions of concentrations greater than M/10 large doses have to be administered to cause chemical changes which can be measured with accuracy. The wave-length independence, as has been stated, appears to be maintained from 100 kev x-rays (Fricke and Morse) to Ra γ-rays, a supposition which has been tested more exactly as will be described below. There are, however, complicating factors which have so far prevented the establishment of a satisfactory mechanism for the process. These are:

(i) *Dependence on acid concentration.*—Sulfuric acid solutions only have so far been studied, but it is clear from the work of Fricke and Hart[22] that the yield increases with acid concentration in the range 1/1000 to 1/10N. That this increase is largely due to the hydrogen ions was also shown by these workers, who found that the addition of sodium sulfate to the solution was without detectable effect. In addition, at low acidities the reaction, according to Gray and Weigert,[25] becomes irreproducible, probably due to the simultaneous reduction of the ferric ions produced and the formation of colloidal ferric hydroxide.

[21] G. L. Clark and L. W. Pickett, J. Am. Chem. Soc. **52**, 465 (1930).

[22] H. Fricke and E. J. Hart, J. Chem. Phys. **3**, 60 (1935).

[23] N. Miller, Nature **162**, 448 (1948).

[24] H. Dewhurst and F. H. Krenz, private communication; see F. H. Krenz, Can. J. Research **B26**, 647 (1948).

[25] L. H. Gray and F. Weigert, unpublished work.

(ii) *Presence of dissolved oxygen.*—While the concentration of dissolved oxygen in the solution exceeds a certain critical value the radiation yield is about 2.5 times that found in solutions of oxygen content below this value. If a solution initially containing dissolved oxygen be irradiated in a closed system, this oxygen is used up until its concentration falls below the critical value, when the radiation yield falls sharply. Further work by the writer has established that similar radiation yields are shown in solutions boiled in vacuum or saturated with pure hydrogen or nitrogen, and confirmed the observation of Fricke and Hart[22] that in oxygen-containing solutions about one equivalent of oxygen is used up for each ferrous ion oxidized. The induction periods reported by Shishacow at the start of the reaction in oxygen-free solution have never been observed by the writer in freshly made-up solutions, but have occasionally appeared in solutions which have stood in glass vessels for periods longer than a week.

(iii) *Intensity of the incident radiation.*—Preliminary experiments by the writer using a two million-volt x-ray generator, which will not be discussed further in the present communication, indicate that the radiation yield falls off at high intensities in excess of 100 r/sec. Nevertheless it remains constant in the useful region from $\frac{1}{10}$ to 1 r/sec.

(iv) *Temperature.*—According to Minder and Liechti,[26] changes in ionic yield due to temperature within the region 4–50°C are not significant, but it would be of interest to extend observations over a wider region of temperature.

The limits are thus defined within which the chemical change in this system appears to be a linear function of the radiant energy absorbed. The experiments carried out in order to provide an accurate estimate of the radiation yield in this process will now be described. Later an account will be given of some further experiments on the kinetics of the reaction as induced by γ-rays from radium, and some speculation included as to the mechanism of the process.

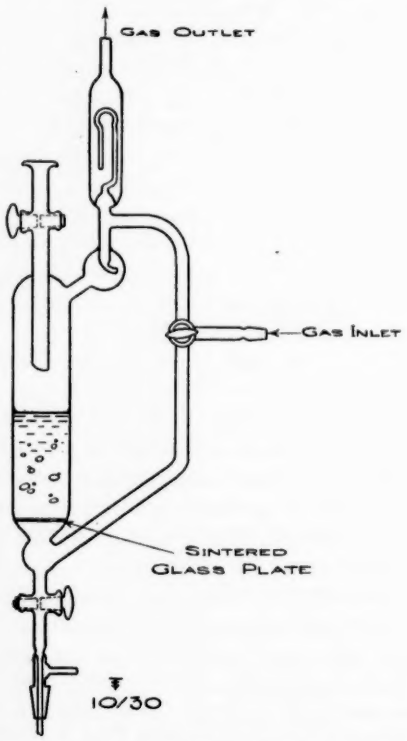

FIG. 1. Apparatus used in equilibration of solutions with gases.

[26] W. Minder and A. Liechti, Experientia **2**, 410 (1946).

II. EXPERIMENTAL

Preparation of Solutions

It was found advisable in order to secure reproducible results to use water as free as possible from organic impurities, and to use freshly made-up solutions. In practice the water was distilled from alkaline permanganate solution and then from alkaline manganous hydroxide to remove traces of volatile oxidizing impurities arising from a chlorinated water supply. When solutions were used which had been standing for periods longer than a week, the results became less reproducible and induction periods similar to those found by Shishacow were occasionally noted, which were never found in hundreds of irradiations using fresh solutions.

The studies of radiation yield were all made in solutions containing dissolved oxygen, and the initial concentrations both of ferrous ion and of oxygen were decided in each case by the dose to be administered. Greatest accuracy was obtained when the ferrous ion concentration was reduced to half of its initial value by the exposure. In order to insure a linear fall of ferrous concentration with dose it was necessary to make sure that this concentration remained at all times within the region of concentration independence of the reaction, i.e., $>8\times10^{-5}$ M, and that the dissolved oxygen concentration did not fall below the critical value at the end of the exposure. The latter condition was satisfied for a dose up to about 5000 r by initial equilibration of the solution with nitrogen containing a few percent of oxygen, up to $\sim$50,000 r with air, and up to $\sim$200,000 r with oxygen. The equilibration was carried out in a special apparatus (Fig. 1) by means of which the irradiation cell could also be swept out with the gas concerned before filling.

The solutions were all made 0.8N in sulfuric acid to provide comparison with the earlier work of Fricke and Morse and Shishacow, and were made up from ferrous ammonium sulfate crystals. The effect of the ammonium ions at this acidity was found by experiment to be negligible.

Analytical Methods

The first method used for assessing the concentration of ferrous ions in solution was potentiometric titration with N/5000 ceric ammonium sulfate in 1N sulfuric acid solution using a commercial *p*H meter equipped with

redox and calomel electrodes. This method was later abandoned in favor of a photometric method using 1:10 phenanthroline, which was quicker, more sensitive, and more reliable. The details of this method were adapted from an ASTM pamphlet on the determination of iron in industrial waters. Using these methods it was found that the ferrous ion concentration of these solutions remained constant for periods much longer than the duration of the irradiations when stored in cells of glass, polystyrene or Lucite.

Preliminary Work with Gamma-Rays from Radium

A small set of brass stands was constructed on lines suggested by Professor W. V. Mayneord, on one of which was placed a capsule containing 600 mc of radium in a 0.5 mm-wall platinum container and on another, which could be at a center-to-center distance from the source varying between 3.7 and 7 cm, a small Pyrex weighing bottle containing the solution. The whole was enclosed in a "castle" of lead 18-in. square. The γ-ray intensity at the various positions was estimated using a 100-r Victoreen R-meter with a 5 mm Lucite cap placed over the sensitive zone to ensure equilibration of the radiation with the secondary electrons produced. The figures for the intensity at the positions nearer the source agreed well with those calculated by the inverse square law using the figures of Mayneord and Roberts[27] but at the more distant positions the values were somewhat higher, presumably due to radiation scattered from the walls of the castle. The solutions used were all saturated with nitrogen containing a few percent of oxygen and irradiated in the presence of an atmosphere of this gas. For the doses used this procedure was sufficient to provide effective saturation with oxygen during the irradiation.

In a number of experiments carried out using this apparatus with radiation intensities of 96, 175, and 295 r/hr., and ferrous ion concentrations ranging from 1.0 to 4×10^{-4}M, the average value for the change in Fe^{++} concentration induced by 1000 r was 17.5 μM/1, in good agreement with the values obtained by Fricke and Morse and Shishacow (see Table III). The interpretation of this value as an "ionic yield," i.e. in equivalents oxidized per ion pair, involves the assumption of a value for the constant W, the energy expended by a secondary electron in forming an ion pair in the solution. It is of course known that the value of W for different gases remains independent of the ionization potential of the material under irradiation, the balance of the energy being used up in excitation, and such experimental evidence as is available on the ionization of other materials in the liquid and gaseous phases[28,29] seems to support the conclusion that the value of W for any material is similar in these phases. In any event such discussion can well be left for the moment, as the present objective, that of assessing various modes of dosimetry in aqueous systems, is not affected. For the purposes of this communication the ionic yield will be defined as the number of equivalents of ferrous iron oxidized per 32.5 ev expended in the solution,[30] and on the above definition the average ionic yield observed using this type of apparatus was 5.95.

TABLE II. Results using radium γ-rays and polystyrene cell and chamber.

Dose, r	Initial Fe^{++} concn., $M\times10^4$	Fe^{++} concn. change $M\times10^4$	Concn. change per 1000 r, μM/1
11860	3.47	2.16	18.2
10380	3.57	2.09	20.2
12930	5.08	2.54	19.6
12820	9.84	2.64	20.6
12760	9.84	2.60	20.4
10850	9.74	2.08	19.2
Temp. = 23°C		Average value	19.7
Intensity of radiation = 5620 r/hr.		M/32.5 ev =	6.7

Later Work with Radium Gamma-Rays Using Polystyrene Apparatus

An attempt was made to apply the principles discussed above using an ionization chamber and irradia-

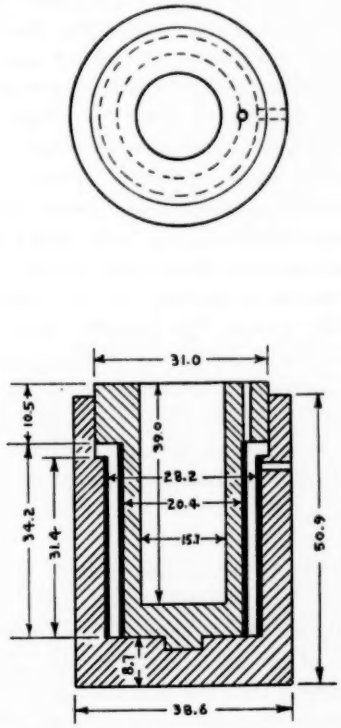

FIG. 2. Polystyrene chamber used in work with radium γ-rays.

[27] W. V. Mayneord and J. E. Roberts, Brit. J. Radiol. **10**, 365 (1937).
[28] F. L. Mohler and L. S. Taylor, J. Res. Nat. Bur. of Stand. **13**, 659 (1934).
[29] G. W. Hutchinson, Nature **162**, 610 (1948).
[30] Reference 6, p. 34.

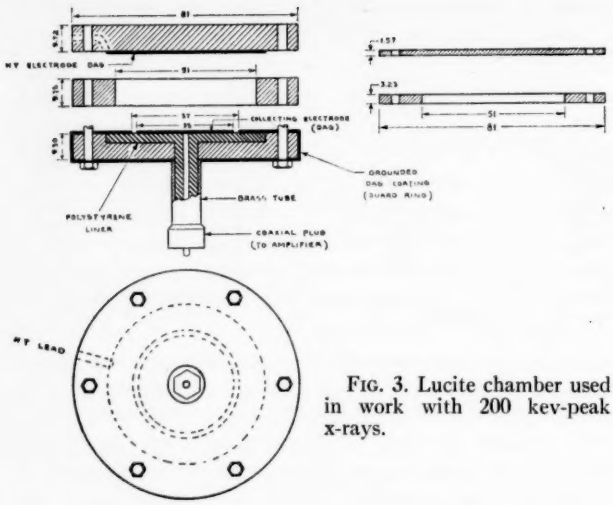

FIG. 3. Lucite chamber used in work with 200 kev-peak x-rays.

tion cell constructed of polystyrene and of identical geometry (see Fig. 2). These were part of an irradiation system designed by Dr. A. J. Cipriani. Both chamber and cell could be placed in turn in the center of a large block of lead by withdrawing a removable section of the block. A two-g radium bomb on the end of a brass rod could be inserted in the central cavity of the cell or chamber through a cylindrical hole in the block at right angles to the first. The cylindrical inside surfaces of the ionization chamber were coated with alcohol-base "dag" and leads taken from the two opposite surfaces to a potentiometer circuit using a Lauritsen type quartz-fiber electroscope as a null instrument. In measuring the ionization current due to the radium one surface was connected to a source of 200 volts or greater, a potential sufficient for saturation, and the other through a Victoreen standard resistor to ground. The voltage above ground of this second surface was measured using the potentiometer circuit. Measurements were made using different resistors, which were found to give variations of a few percent from their stated values, and a mean value for the ionization current taken. By means of a reversing switch the polarity of the electrodes could be changed to nullify the effect of stray ionization currents. These proved in fact to be negligible. In finding values for the radiation yield in solution, the ionization current was measured in the chamber at a known temperature and barometric pressure, and the chamber was then replaced with the cell filled with solution and the irradiation carried out.

The experiments using this system which were reported earlier[23] have since been repeated with solutions saturated with air rather than with nitrogen containing a few percent of oxygen, and the results are significantly higher, indicating that the doses of about 12,000 r used in the earlier experiments were sufficient to reduce the oxygen concentration to too low a figure during the irradiations. These new results are presented in Table II, and illustrate the consistency obtained.

Work with X-Rays Using Lucite Cell and Ionization Chamber

From the discussion above it will be recalled that assessing the ionic yield quantitatively is more difficult when x-rays are used. Nevertheless an attempt was made to measure this quantity using 200-kvp x-rays in apparatus similar to that used with Ra γ-rays (see preceding section).

The ionization chamber used in these experiments is depicted in Fig. 3. Owing to the critical factor of absorption of the x-rays in the solution, it was decided to make an interchangeable system of Lucite plates whereby the depth of the effective volume could be either 9.75 or 3.23 mm. The effect of filtering some of the softer components of the beam could also be studied by changing the thickness of the wall of the chamber facing the x-ray tube (upper wall in Fig. 3) between 9.72 and 1.57 mm. In each case an irradiation cell was available having identical geometry to the chamber. A brass stand was constructed so that cell and chamber could be placed successively in the same position with reference to the tube. The chamber was constructed of Lucite, but had a polystyrene inset on which the collecting electrode of "dag" was painted, this precaution being necessary owing to the poor insulating qualities of Lucite. The gap between the collecting electrode and the guard ring was as small as could be reliably obtained, about 1 mm in width, and the collecting electrode and guard ring were

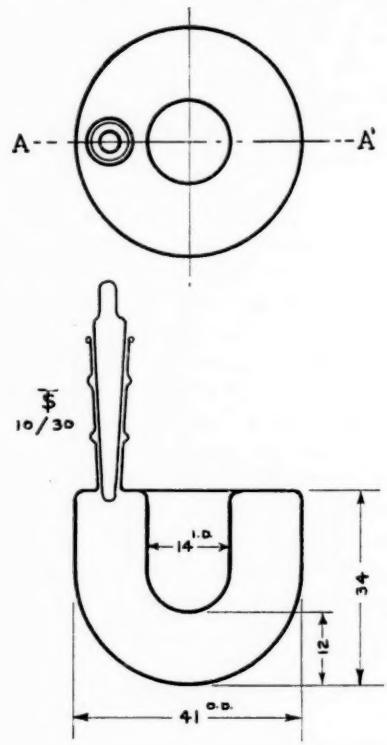

FIG. 4. Apparatus used in kinetic studies on irradiation of solutions in a closed system (Cell No. 1).

painted on the lower surface of the chamber by placing this in a lathe and applying the "dag" suspension with a fine camel hair brush. As a check on stray ionization currents, four different electrodes were used successively in the same radiation field, having diameters of 34.9, 30.2, 25.4 and 18.7 mm, a gap of 1 mm between the electrode and guard ring being used in each case. The ionization currents observed were proportional to the area of the electrode within four percent.

A high tension voltage of 200 v positive, sufficient to obtain saturation, was applied to the upper electrode during measurement and the collecting electrode connected to ground through a Victoreen standard resistor. The voltage at the collecting electrode was impressed on the grid of a Victoreen VW41B electrometer tube connected to a circuit in which the observed voltage could

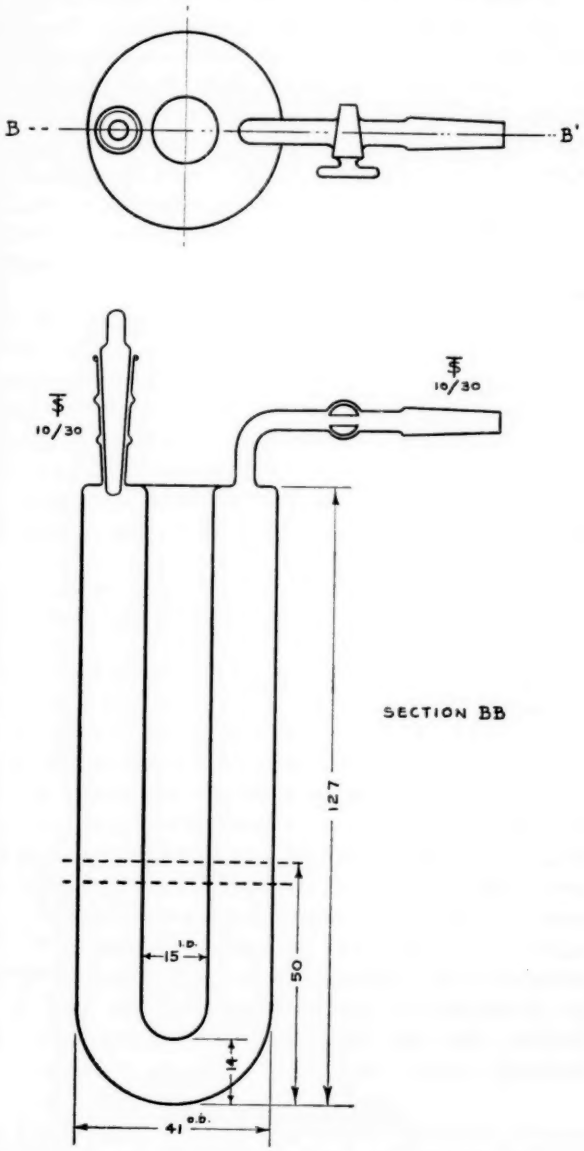

FIG. 5. Apparatus used in kinetic studies using evacuated solutions (Cell No. 2).

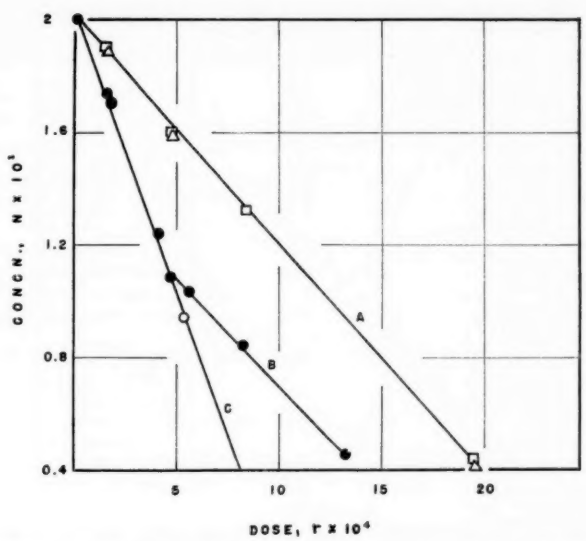

FIG. 6. Concentration-dose curves obtained using Cell No. 1 with solutions equilibrated with various gases and irradiated in a closed system. Dark circles—solutions initially air-saturated. Hollow circle—solutions initially oxygen-saturated. Squares—solutions initially nitrogen-saturated. Triangles—solutions initially hydrogen-saturated.

be compared using a null method with known voltages applied from an external circuit.

Dose rates from 3990 to 6340 r/hr. and Fe^{++} concns. from 1.36 to 4.89×10^{-4} M were used in this system. There was more spread in the results, chiefly due to the difficulty in maintaining the output of the x-ray tube constant during the periods up to two hours required. For the most part the experiments were carried out with solutions saturated with nitrogen containing a few percent of oxygen, the doses used being sufficiently low (<3600 r) to make this procedure satisfactory, but in two cases, where higher doses, of 6000–7000 r, were being studied, oxygen-saturated solutions were used.

It appeared that there was a significant difference between the ionic yields observed in the cells of 9.75 mm- and 3.23 mm-depth, but not between those observed with oxygen and oxygen-in-nitrogen saturated solutions, or between those observed in cells of different front wall thickness (see Table III).

If the average results for ionic yield using the cells of different depth were plotted against depth, and the plot extrapolated to zero depth, an ionic yield of 6.6 was obtained. A linear variation of ionic yield with cell depth, however, is hardly to be expected, and having regard to the other possible sources of error in this method discussed earlier, the only significant conclusion which can be reached from this work is that the ionic yield shows no marked dependence on the wave-length of the incident radiation.

Kinetic Studies

The ionic yields for Fe^{++} oxidation in solutions saturated with oxygen, nitrogen, air, and hydrogen, and in

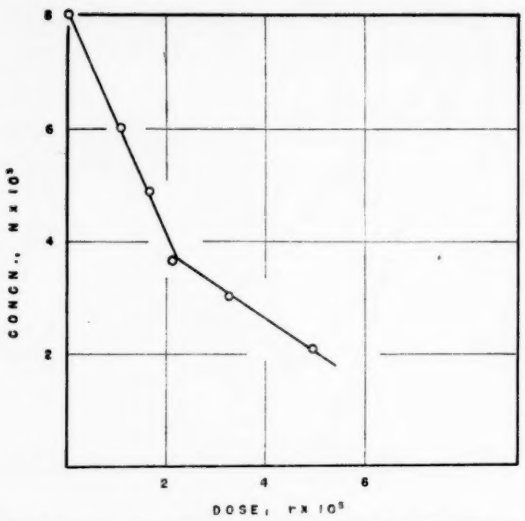

FIG. 7. Concentration-dose curve obtained using Cell No. 1 with oxygen-saturated solutions irradiated in a closed system.

solutions boiled in vacuum, were compared in two types of cell represented in Figs. 4 and 5. No dosimetry was attempted in these cases. The cells could be filled from the equilibration apparatus described previously (Fig. 1), with solutions in equilibrium with various gas phases, and were designed to take radium sources up to 1.2 c in strength in the central cavity. Cell No. 1 was used in studies on irradiations in a closed system. In this case the cell was completely filled and the stopper inserted in such a way as to leave no gas bubbles during irradiation. Cell No. 2 was used in comparisons between solutions boiled in vacuum and solutions in equilibrium with various gases. In the former case the cell was filled to the upper mark with solution, and then evacuated, using a Hyvac pump protected by a liquid air trap, until the volume was reduced to the lower mark. After irradiation water was added to bring the volume to the upper mark again before analysis. This procedure was justifiable, as the ionic yield was independent of the Fe^{++} concentration, and the effect of the slight increase in acidity during evacuation could be neglected. When solutions containing dissolved gases were studied in this cell it was filled to the lower mark to ensure a comparable radiation field in both cases.

Typical concentration-dose curves obtained using Cell No. 1 are shown in Figs. 6 and 7. The dose scale is given in roentgens, the average doses over the whole body of solution being computed by assuming a value of 6.7 for the ionic yield in oxygenated solution, which is the value obtained using the polystyrene apparatus and since taken as the basis for dosimetry measurements.

It will be seen that whereas both oxygen-saturated and air-saturated solutions irradiated in a closed system in the absence of a gas phase showed the same value of the ionic yield, a lower yield (curve *A*, Fig. 6), was shown by solutions initially saturated with (i) nitrogen containing less than one-half percent of oxygen, and (ii) hydrogen. When solutions initially saturated with air at 25° were irradiated, a sharp break in oxidation rate occurred at 45,000 r, as had been noted by Fricke and Morse[8] and Shishacow,[18] the ionic yield then dropping to 2.6 (curve *B*), whereas with solutions saturated with oxygen at the same temperature (Fig. 7), the break appeared at 218,000 r and the subsequent yield was 2.0. Using the known concentrations of oxygen in oxygen-saturated and air-saturated water at 25°C, and assuming that the break occurred at the point at which all the oxygen had been removed by the radiation, it was computed that the ratio eqvts. oxygen removed/eqvts. Fe^{++} oxidized up to the break point in both air-saturated and oxygen-saturated solution was about 1.1. This provides further proof that the increase in slope is attributable to dissolved oxygen.

In Cell No. 2 comparisons were made between deoxygenated solutions and solutions saturated with oxygen irradiated in an oxygen atmosphere. The ionic yields in the former case were on the average a factor 1/2.5 lower than in the latter, although they tended to be less reproducible, a fact evident in the work of earlier investigators.[8,18] Using this system also the ionic yields observed for doses up to 10,000 r with solutions saturated with nitrogen containing a few percent of oxygen and irradiated in an atmosphere of this gas were found to be within a few percent of those found in oxygen-saturated solutions.

The process of boiling in vacuum cannot be expected to remove the last traces of oxygen from a solution, however, and it may be that the lack of good reproducibility in ionic yield shown in solutions treated in this way and solutions initially saturated with nitrogen or hydrogen may be due to small residual differences in initial oxygen content. If this is the case, different behavior again may be expected in solutions which have been rigorously freed from oxygen.

A further point studied in Cell No. 2 was the behavior of the solution after all the ferrous ions had been oxidized. In this case it was found that hydrogen peroxide developed, and could be detected by the formation of the well-known yellow-colored pertitanic acid on addition of titanium sulfate. The formation of peroxide in this way explains the anomalous apparent reduction of ferric iron by radiation observed by Fricke and Morse.[8] In this case, potentiometric titration with sodium dichromate solution was the method of analysis used. The writer has never observed the reduction of ferric iron by x- or γ-radiation in solutions of this acidity. The formation of hydrogen peroxide in the presence of ferric ions, which are well known to catalyze its decomposition, may appear surprising until it is realized that the ferric solutions concerned are exceedingly dilute.

Summary of Results

The most accurate index of the ionic yield for solutions of Fe^{++} in 0.8N sulfuric acid containing oxygen is con-

sidered to be provided by the latest results (Table II) using γ-rays and the polystyrene apparatus. The results provided by the other systems are considered to be of a lower order of accuracy. From the average ratio of the ionic yields in oxygen-containing and deoxygenated solutions observed in all experiments using Cells 1 and 2, the values for the ionic yield in deoxygenated solutions given in columns 3 and 4 of Table III were obtained. The table summarizes the results of the writer and earlier workers.

The previous results using the polystyrene apparatus and solutions saturated with nitrogen containing a few percent of oxygen, which led to an average yield in systems (i), (ii), and (iii) of 5.5,[23] are not included in Table III.

TABLE III. Ionic yields for oxidation of ferrous ions in 0.8N sulfuric acid solution.

	Fe^{++} concn. change, μM/1 kr	M/32.5 ev	Fe^{++} concn. change, μM/1 kr	M/32.5 ev
	Aerated		Deaerated	
Fricke *et al**	17.3	5.9	6.8	2.3
Shishacow**	15.3	5.2	5.9	2.0
Present work:				
(i) Polystyrene apparatus γ-rays	19.7	6.7	7.6	2.6
(ii) Pyrex cells γ-rays	17.5	5.95		
(iii) Lucite apparatus x-rays, cells of 3.23-mm depth	16.7	5.68		
(iv) Ditto, cells of 9.75-mm depth	11.7	3.98		
(v) Ditto, extrap. to zero depth	19.4	6.6		

* See references 8 and 22.
** See reference 18.

III. DISCUSSION

The evaluation of the results for ionic yield using different methods of dosimetry leads to the conclusion mentioned earlier, that simple procedures of dosimetry such as have been used in previous investigations of this type are adequate if accuracy within about 20 percent is all that is required. For greater precision recourse must be had to more rigorous procedures such as those described above. In the use of ferrous sulfate solutions for dosimetry, the conditions described under "Preparation of Solutions" have to be followed, and the dose worked out on the basis of 19.7 μM/1. Fe^{++} concn. change per 1000 r absorbed in the solution.

The mechanism of the radiation-induced oxidation is still not clear, but some speculations on this matter may be made.

It is assumed that the primary radiochemical action is the disruption, by ionization and excitation, of water molecules to give hydrogen atoms and hydroxyl radicals which escape recombination in the excited zones about the electron tracks.[1-7] The fate of the hydrogen atoms will be determined by the concentration of molecular oxygen in the solution. If oxygen is absent, the majority of the hydrogen atoms will recombine to give molecular hydrogen; if the oxygen concentration is appreciable, on the other hand, the reaction of hydrogen atoms with molecular oxygen will predominate:

$$H+O_2 \rightarrow HO_2.$$

That reaction of the hydrogen atoms with ferric ions is not significant in the over-all picture is shown by the linearity of the Fe^{++} concn.-dose curves observed with solutions initially containing very little ferric iron (Figs. 6 and 7). Since a hydroperoxide (HO_2) radical is ultimately capable of oxidizing three ferrous ions, and a hydroxyl radical of oxidizing one, the maximum yield of ferrous ions oxidized per water molecule disrupted will be four if this interpretation is correct.

This over-all yield will be lowered, however, if reactions of H atoms with HO_2 and H_2O_2 or of OH radicals with HO_2 are significant in removing radicals. Side reactions of this type may well be more frequent in less acid solutions, as equilibria of the type:

$$Fe^{++}+HO_2 \rightleftharpoons Fe^{+++}+HO_2^-,$$

which is familiar from studies of the catalytic decomposition of H_2O_2 by Fe^{+++},[31] imply a higher steady-state concentration of HO_2 in less acidic media during irradiation.

The fact that the yield of ferric ions per 32.5 ev absorbed in acid solutions rises above four when oxygen is present leads to one of two conclusions: (i) that the value of W, the energy dissipated in causing an ionization, is markedly different in liquid water from that in water vapor; or (ii), that water molecules are disrupted during irradiation by processes other than ionization. On the basis of the information at present available, the second conclusion would appear to be the more likely, and this is consistent with modern views on the radiation chemistry of gases.[32]

The dependence of the ionic yield on pH observed in solutions whose oxygen content has been reduced below the critical value[22] implies, if the hypothesis just presented is correct, that molecular oxygen is still present in small quantities even in these solutions. More rigorous methods of deaeration should therefore be applied before any statements are made about the behavior in strictly oxygen-free solution.

The full elucidation of the very complicated interplay between the reactive entities formed on irradiation must await the advent of analytical methods for HO_2 and H_2O_2 formed during irradiation and a general advance in our knowledge of the radiation chemistry of water.

The writer wishes to record his gratitude to the National Research Council of Canada for the use of experimental facilities, and to Dr. F. S. Dainton and Mr. F. H. Krenz for many helpful discussions.

[31] F. Haber and J. Weiss, Proc. Roy. Soc. (A) **147**, 332 (1934).
[32] Eyring, Hirschfelder, and Taylor, J. Chem. Phys. **4**, 479, 570 (1936); C. Smith and H. Essex, J. Chem. Phys. **6**, 188 (1938); P. Gunther and H. Theobald, Zeits. f. physik Chemie **B40**, 1 (1938).

The Infra-Red Spectrum of Hydrogen Peroxide*

PAUL A. GIGUÈRE**
Gates and Crellin Laboratories of Chemistry, California Institute of Technology, Pasadena, California
(Received May 31, 1949)

The absorption spectrum of hydrogen peroxide vapor was examined under low dispersion in the range 2–15μ. Four bands were observed at 3590, 2630, 1255, and 877 cm^{-1}. The spectrum of the liquid also was measured between 2 and 21μ; it showed five bands at about 3400, 2780, 1350, 880, and 550 cm^{-1}. The last one, which seems very diffuse, is presumably the torsional oscillation of the OH groups; as such it corresponds to a potential energy barrier of the order of 4 kcal./mole. New assignments are proposed in agreement with the model of Penney and Sutherland. Under high dispersion the second harmonic O—H frequency was found to consist of two identical hybrid bands at 7036.6 and 7041.8 cm^{-1}, of which the rotational constant for the ground state is in perfect agreement with that already found for the third harmonic band. The explanation given previously for the doublet character of the vibrational levels of hydrogen peroxide is further substantiated by the present results. From both vibrational and rotational data the O—H distance in hydrogen peroxide appears to be slightly greater than that in water.

INTRODUCTION

THE molecular configuration of hydrogen peroxide is now well established as the result of theoretical[1] and experimental[2] investigatons; however, the absorption spectrum of this substance has not so far been accounted for satisfactorily. The problem is of great interest because of the question of torsional oscillation or hindered rotation. According to theory, a tetratomic molecule with point-group symmetry C_2 should have six fundamental vibrations, none of them degenerate. In their investigation of the infra-red spectrum of hydrogen peroxide between 2 and 13μ Bailey and Gordon[3] observed four bands in the vapor as well as in the liquid. Because of experimental difficulties they were unable to locate accurately the center of the bands. On the other hand, the Raman spectrum, studied by a number of authors,[4, 5, 6] seemed also to consist of four bands. These results were interpreted by Bailey and Gordon who made tentative assignments of the observed frequencies (Table I). In a later investigation, however, Fehér[7] could find only three definite frequencies in the Raman spectrum of both hydrogen and deuterium peroxides. From the measured shifts in the isotopic molecule he questioned some of the assignments shown in Table I. Finally an investigation of the fine structure of two photographic bands of hydrogen peroxide[8] did not lead to a unique interpretation of the bands on account of multiple overlapping. Therefore it seemed desirable to study further the infra-red spectrum of this molecule.

EXPERIMENTAL PROCEDURE

The low dispersion spectra were obtained with a Beckman IR-2 spectrometer. For the region beyond 15μ a special model of this instrument, with potassium bromide optics, was made available by courtesy of the manufacturer. All the spectra were recorded at rather high speed (20 minutes for complete scanning) with the two-second response. The slit width was automatically controlled so as to offset partly the intensity distribution of the Nernst glower. The near coincidence of some of the water bands with those of hydrogen peroxide made it necessary to dry thoroughly the spectrometer case.[9] Because of the low vapor pressure and of the reactivity of hydrogen peroxide, the absorption cells supplied with the instrument could not be used. Instead the liquid was distilled under constant pressure through a 50-cm Pyrex tube, 25-mm diameter, surrounded by a heating jacket to prevent condensation. The windows were silver chloride plates five-mm thick (Harshaw Chemical Company) held against the tube by means of stainless steel collars and Koroseal gaskets. This material was not affected by the hot peroxide vapor except for a slight leaching of the plasticiser which did not seem to affect the measurements. Previous to a run the entire system was cleaned with hot fuming nitric acid and rinsed re-

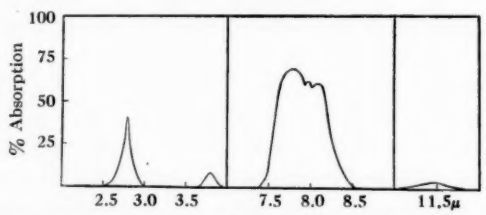

FIG. 1. Absorption spectrum of hydrogen peroxide vapor. Equivalent path length, 0.5 cm; temperature, 90°C.

* Contribution No. 1306 from the Gates and Crellin Laboratories of Chemistry.
** Professor of Physical Chemistry, Laval University, Quebec, Canada.
[1] W. G. Penney and G. B. B. M. Sutherland, Trans. Faraday Soc. **30**, 898 (1934); J. Chem. Phys. **2**, 492 (1934).
[2] Lu, Hughes, and Giguère, J. Am. Chem. Soc. **63**, 1507 (1941).
[3] C. R. Bailey and R. R. Gordon, Trans. Faraday Soc. **34**, 1133 (1938).
[4] S. Venkateswaran, Nature **127**, 406 (1931); Phil. Mag. **15**, 263 (1933).
[5] I. Damaschun, Zeits. f. physik. Chemie **B16**, 81 (1932).
[6] A. Simon and F. Fehér, Z. Elektrochem. **41**, 290 (1935).
[7] F. Fehér, Ber. d. d. chem. Ges. **72**, 1778 (1939).
[8] L. R. Zumwalt and P. A. Giguère, J. Chem. Phys. **9**, 458 (1941).
[9] P. A. Giguère and R. M. Badger, J. Opt. Soc. Am. **38**, 987 (1948).

peatedly. The decomposition in one operation amounted to less than one percent. Some difficulty was encountered in obtaining the spectrum of the liquid. A film, a few microns thick, was obtained by pressing one drop between highly polished silver chloride plates. Due to the large interface, decomposition invariably set in after a few minutes, and the oxygen formed interfered with the transmission of the sample. The cell had to be refilled periodically and a number of spectra were run for a good check.

The vacuum spectrometer used for the high dispersion investigation of the 1.4μ-band has been described elsewhere.[10] The grating, an échelette replica with 7500 lines to the inch, was used in the first and second orders. Wave-length determinations were based on the higher orders of the red and near infra-red lines of argon as observed in the discharge of an ordinary sodium Lab-arc. The effective slit width was about 0.8 cm^{-1} in the region covered. The absorption cell, one meter long, was made so as to allow continuous recycling of the vapor through the absorption path.

The hydrogen peroxide was prepared from Becco's 90 percent commercial solution by fractionation at low pressure; its purity was of the order of 99.5 percent.

RESULTS

Vibrational Structure

The spectrum of the vapor at 90°C and 15 mm pressure is shown in Fig. 1. Similar tracings were made at five and ten mm to obtain the "apparent" absorption coefficients α given in Table II. Attempts to operate at higher pressures in order to bring out weak overtones and combination bands were unsuccessful due to increased decomposition of hydrogen peroxide on raising the temperature. The present data are somewhat different from those of Bailey and Gordon both as regards location and relative intensities of the bands. On the other hand the spectrum of the liquid, in Fig. 2, is quite similar to theirs. As a matter of fact there was hardly any difference between their published spectra of the liquid and of the vapor, contrary to what should be expected. This may have been caused by some fogging of the windows due to the action of hydrogen peroxide on rock salt. The band at 18.3μ has not been reproduced here because of the uncertainty as to its exact shape; on account of the low transmission of the sample in that region a higher amplifier gain was required, which resulted in a rather confused recording of the spectrum. Under these conditions, it was not possible to estimate the intensity or the width of that band. The existence of a very weak band at 2.1μ in the liquid is uncertain as it did not show on all tracings.

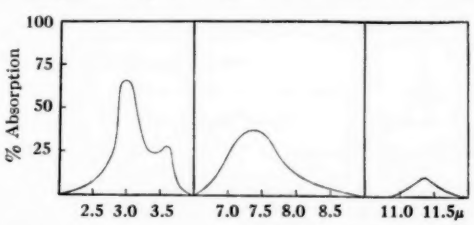

FIG. 2. Absorption spectrum of liquid hydrogen peroxide between two and 15μ.

[10] Badger, Zumwalt, and Giguère, Rev. Sci. Inst. **19**, 861 (1948).

TABLE I. Previous data on infra-red and Raman spectra of hydrogen peroxide.

Infra-red: Vapor (cm^{-1})	Infra-red: Vapor Relative intensity	Infra-red: Liquid (cm^{-1})	Infra-red: Liquid Relative intensity	Raman: Liquid (cm^{-1})	Assignment (Bailey and Gordon)	Ref.
870	18	877	33	877	ν_4*	(3–6)
1370	22	1341	87		ν_6	(3)
				1408	ν_3*	(6)
				1435	ν_2	(6)
2870	15	2869	55		ν_1	(3)
3418	59	3418	78	3407	ν_5	(3–6)
10,283.68 10,291.08		9900				(8, 14)

* In this assignment ν_4 corresponds to the vibrational mode designated below (Fig. 3) as ν_3, and *vice versa*.

TABLE II. Vibrational spectrum of hydrogen peroxide.

Infra-red: Vapor $\nu_{vac.}$ (cm^{-1})	Infra-red: α*	Infra-red: Liquid $\nu_{vac.}$ (cm^{-1})	Slit width cm^{-1}	Raman† Liquid ν (cm^{-1})	Assignment
(490)		550(?)			ν_4 (a)
877	0.025	880	6	877 (v.s.)	ν_3 (a)
1255	0.70	1350	6		ν_6 (b)
				1421 (w.)	ν_2 (a)
2630	0.05	2780	10		$\nu_2+\nu_3+\nu_4$ (A)
				3395 (m.)	ν_1 (a)
3590	0.35	3400	13		ν_5 (b)
		4720 (?)			$\nu_5+\nu_6$ (A)
7036.6 7041.8	0.085		0.8		$\nu_1+\nu_5$ (B)
10,283.68 10,291.08		9900			$\{2\nu_1+\nu_5$ (B) $\{$or $3\nu_5$ (B)

* $\alpha=(1/pl)\log T_0/T$, with p in atm. and l in cm.
† See reference 7.

Assignment of the observed bands with respect to the vibrational modes of the molecule (Fig. 3) was made as follows: The 3590 cm^{-1} frequency is obviously an O—H stretching vibration as confirmed by its proximity to the corresponding bands in water[11] and by the isotopic shift in deuterium peroxide (Table III). Only one O—H stretching frequency has been observed in all previous spectroscopic investigations of hydrogen peroxide. It has been argued[7] that because of the loose coupling between the two OH groups the symmetric and asymmetric frequencies are accidentally degenerate. Support of this view may be seen in the exact coincidence, to within the accuracy of the measurements, of the Raman and infra-red bands at 3400 cm^{-1} in the liquid. It is logical to think that the former corresponds to the symmetric, and the latter mostly to the antisymmetric vibration. However, this question can be decided only by a high dispersion study of the spectrum in that region.

[11] Cross, Burnham, and Leighton, J. Am. Chem. Soc. **59**, 1134 (1937).

TABLE III. Isotopic shifts in the Raman spectra of liquid water* and hydrogen peroxide.**

	H_2O ν (cm^{-1})	D_2O ν (cm^{-1})	H_2O_2 ν (cm^{-1})	D_2O_2 ν (cm^{-1})
ν_1	3440	2515	3395	2510
ν_2	1656	1208	1421	1009

* See reference 11.
** See reference 7.

Leaving for the moment the 2630 cm^{-1} band, that at 1255 cm^{-1} is taken as an O—H bending frequency again by comparison with water. Because it occurred in the region of maximum dispersion of the prism instrument its contour was more clearly discernible; thus it appeared to consist of a double maximum at 1280 and 1240 cm^{-1}, the latter being roughly four-fifths as intense as the former. In as much as they are real they must very likely correspond to the P and R branches of the ν_6 band since ν_2 should be rather weak in the infra-red. This is further confirmed by indications, on some of the tracings, of a prominent Q branch as should occur in the case of an oscillating dipole parallel to the top axis. Then the Raman band at 1420 cm^{-1} is the symmetric bending vibration ν_2, as evidenced by the isotopic shift (Table III).

No doubt exists regarding the origin of the 877 cm^{-1} frequency since its remains unchanged in the spectra of both deuterium and hydrogen peroxides. Badger's rule gives 1.48A for the O—O bond length, very nearly the same value as found by electron diffraction.[12] The fact that ν_3 is the strongest Raman band but fairly weak in the infra-red (it was hardly noticeable in the spectrum of the vapor) is further evidence for the C_2 point-group model for hydrogen peroxide.

Lastly, the 550 cm^{-1} band in the liquid is of the right order of magnitude for ν_4, the torsional oscillation; in hydrazine, where the oscillating mass is double, this vibration is believed to occur at 360 cm^{-1}.[13] Certainly the present experimental evidence for the torsional oscillation would not carry much weight by itself were it not for the fact that it allows an unambiguous assignment of the 2780 cm^{-1} band as a combination of $\nu_2+\nu_3+\nu_4$. No satisfactory interpretation had been given previously for the occurrence of that band. Fehér[7] believed that it was due to the O—H vibration shifted to longer wave-length by hydrogen bond formation. The present data render such an explanation untenable for the following reasons: First, the band appears not only in the spectrum of the liquid but in that of the vapor as well, where there is known to be no appreciable association. Second, the frequency shift on going from vapor to liquid has been observed in the fundamental as well as in the second overtone[14] of the O—H frequency (Table II), and it corresponds to the right magnitude for the energy of hydrogen bonds in hydrogen peroxide, as calculated by other methods.[15] The hypothetical value, 490 cm^{-1}, for ν_4 in the vapor was obtained indirectly from the combination band. Therefore the shift due to molecular association is in the same direction as that of the O—H bending but opposite to that of the O—H stretching vibration, which seems reasonable.

On the basis of this frequency the height V_0 of the barrier restricting free rotation in hydrogen peroxide would be of the order of 4 kcal./mole according to the equation

$$\nu_t = 2n(V_0 A)^{\frac{1}{2}}$$

where n is the symmetry number and A is the rotational constant corresponding to the small moment of inertia of the molecule. Obviously this is only a rough estimate since the shape of the potential energy curve is not very well known.

Rotational Structure of the 1.4 μ-Band

As may be seen from Fig. 4, the second harmonic of the O—H vibrations is strikingly similar in appearance

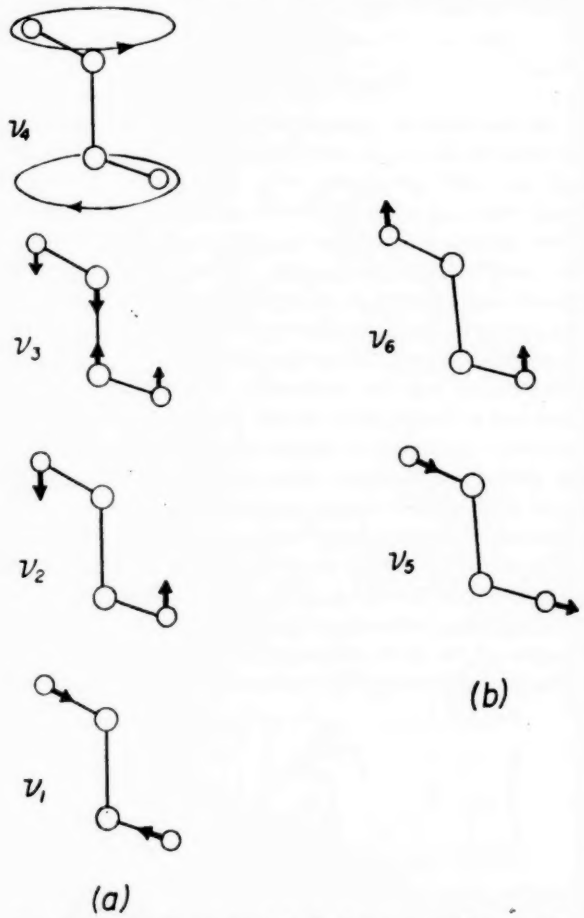

FIG. 3. Normal vibrations of the hydrogen peroxide molecule.

[12] P. A. Giguère and V. Schomaker, J. Am. Chem. Soc. **65**, 2025 (1943).
[13] Scott, Oliver, Gross, Hubbard, and Huffman, J. Am. Chem. Soc. **71**, 2293 (1949).
[14] P. A. Giguère, Trans. Roy. Soc. (Canada) 3 (III) **35**, 1 (1941).
[15] L. Pauling, *Nature of Chemical Bond* (Cornell University Press, Ithaca, New York, 1939).

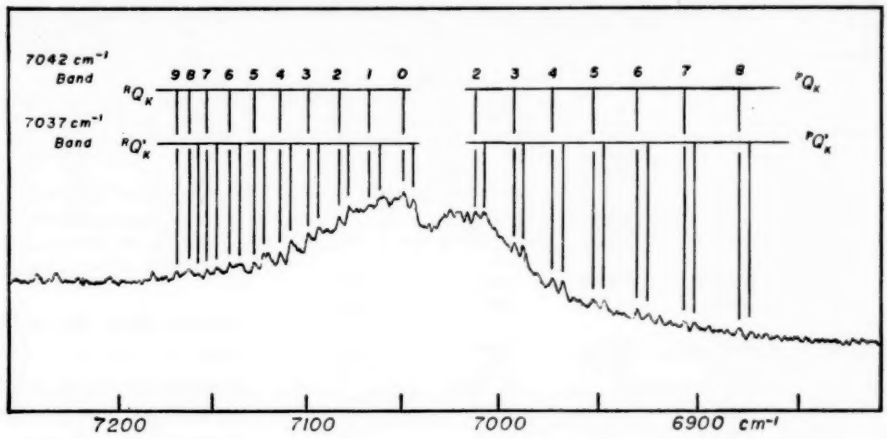

FIG. 4. High dispersion structure of the overtone bands of hydrogen peroxide at 1.4μ. Equivalent path length, 2.7 cm.

to the third harmonic; it shows a doublet structure with the two components of about equal intensity and a separation very closely two-thirds of that found in the latter case.

Considered separately neither of these harmonic bands could be given a unique interpretation. But if it is assumed, as is most probable, that their great resemblance is not a pure accident, then they should be explained similarly. Granted this, a number of otherwise plausible interpretations can be eliminated. Judging from the width of the bands and the relative weakness of the P and R branches, the over-all intensity distribution in both cases is more nearly that to be expected of a parallel type rather than a perpendicular type band. Consequently both bands are primarily due to vibrational transitions in which the upper level is unsymmetrical. In the third harmonic band both the parallel type and the weaker perpendicular type structures center on the same origin and clearly belong to one and the same hybrid band doublet. Therefore this band must be assigned to one of the two possible transitions, $3\nu_5$ (B) or $2\nu_1+\nu_5$ (B). Since the two doublet components have essentially equal intensity it seems highly improbable that they could originate respectively from these two vibrational levels. Indeed, if the intensities were equalized by "borrowing" then the interaction would cause a much larger doublet separation than is observed. At any rate the hybrid band $\nu_1+\nu_5$ (B) is definitely the only possibility in the 1.4μ-region; both $2\nu_1$ and $2\nu_5$ would be purely perpendicular. Thus the present results provide additional support of the explanation previously given for the doublet character, namely that it arises from the presence of a double minimum in the torsional oscillation potential.

The average value of the frequencies obtained from measurements on three different tracings are listed in Table IV together with the calculated rotational constants; the nomenclature used is the same as that of Zumwalt and Giguère.[8] Using these rotational constants the position of the Q branches were calculated and from these, in turn, the center of the two bands were found to occur at 7036.6 and 7041.8 cm^{-1}, respectively. The accuracy of these determinations is somewhat inferior to those in the photographic infra-red because of the limited resolving power of the replica grating. In that connection it should be mentioned at this point that the published microphotometer trace of the 0.927μ-band of hydrogen peroxide shows far less detail than was easily visible on the original photographic plates.

The number of P and R branches measured in the 1.4μ-band is too limited to make an accurate estimate of $X_{02}{}^0$ the rotational convergence constant; but if one takes the same value as obtained from the third harmonic band, the rotational constant for the ground state $X_{01}{}^0$ is in perfect agreement for the two bands. Furthermore the constants for the various vibrational levels show a systematic trend which is strong evidence for the significance of the analyses.

It is interesting to compare the above rotational constants with those corresponding to calculated moments of inertia of the hydrogen peroxide molecule. These quantities are related as follows:

$$X_{01}{}^0=A_0-\tfrac{1}{2}(B_0+C_0);\quad X_{10}{}^0=\tfrac{1}{2}(B_0+C_0),$$

where

$$A_0=h/8\pi^2cI_A{}^0;\quad B_0=h/8\pi^2cI_B{}^0;$$

$$C_0=h/8\pi^2cI_C{}^0;\quad A_0\gg B_0\simeq C_0.$$

Using a set of equations derived for the hydrogen persulfide molecule[16] the calculations were done for various values of ϕ the azimuthal angle, and the following structural data: 1.48A for the O−O distance, 0.98A for the O−H distance, both from the corresponding vibrational frequencies reported above (Badger's rule), and 102° for the H−O−O angle, a decrease of some 3° from the apex angle in H_2O to account for the reduced repulsion of the hydrogen atoms. As could be expected the rotational constant $X_{10}{}^0$ corresponding to the harmonic mean of the two large moments of inertia, $2I_B{}^0I_C{}^0/(I_B{}^0+I_C{}^0)$, is very insensitive to changes of the azimuthal angle (cf. Table V); on the other hand the constant $X_{01}{}^0$, which depends mainly on the small

[16] M. K. Wilson and R. M. Badger, J. Chem. Phys. **17**, 1232 (1950).

TABLE IV. Frequency of principal maxima in the 1.4μ-band of hydrogen peroxide.

	$^{P}Q_K$	$^{R}Q_K$	$\frac{^{R}Q_K - {}^{P}Q_K}{4K}$	$\frac{^{R}Q_{(K-1)} - {}^{P}Q_{(K+1)}}{4K}$
0		7050.6		
0′		7045.8		
1		7068		
1′		7063		
2	7014.1	7084.3	8.77	9.37
2′	7009.3	7078.7	8.67	9.37
3	6993.3	7099.9	8.88	9.26
3′	6988.3	7094.7	8.87	9.13
4	6973.2	7114.6	8.84	9.19
4′	6968.2	7109.1	8.74	9.19
5	6952.8	7128.8	8.80	9.18
5′	6947.7	7123.3	8.78	9.18
6	6930.9	7142.4	8.81	9.17
6′	6925.5	7135.8	8.76	9.16
7	6908.6	7154.7	8.79	
7′	6903.5	7149.2	8.77	
8	6880	7164.2		
8′	6875	7158.8		

Rotational constants for the various vibrational levels.
$X_{02}^{0} = -0.0008_6$* cm^{-1} $X_{01}^{0} = 9.23 = 9.23_1$* cm^{-1}.
($X_{02}^{2} = -0.0008_5$ cm^{-1}) $X_{01}^{2} = 8.83$ cm^{-1}
$X_{02}^{3} = -0.0008_6$* cm^{-1} $X_{01}^{3} = 8.66_8$* cm^{-1}

* From the third harmonic band.

moment of inertia, increases by about five percent from the *cis-* to the *trans*-configuration. However, this quantity cannot give any definite information about the azimuthal angle because it also varies as the square of the O—H distance, which is not known accurately from other sources. Calculations show that if this latter parameter is given the same value, 0.957A, as in H_2O, then the rotational constant X_{01}^{0} becomes greater than the spectroscopic value for the ground state, even in the extreme case of a *cis*-model. Therefore the O—H distance in hydrogen peroxide is probably slightly greater than that in water.

The doublet character is certainly the most remarkable feature of these hybrid bands. In particular, the fact that the doublet splitting in the second and in the third harmonics are almost exactly in the ratio two to three is significant. In other molecules where inversion doubling has been observed so far the magnitude of splitting usually shows a strong dependence on the vibrational level.[17] It appears, from the configuration of hydrogen peroxide, that its normal vibrations are not considerably affected by internal rotation in the molecule, except, of course, ν_4. The situation here is intermediate between pure inversion doubling, as in ammonia, and torsional oscillation, as in methanol. Because the potential energy curve hindering free rotation of the OH groups contains two maxima of unequal height the energy levels first go over into those of an oscillator of greater amplitude, above the lower barrier, then into those of a rotator. A further difference in the case of hydrogen peroxide is the existence of two distinguishable isomeric forms as shown in the crystal structure of the addition compound $CO(NH_2)_2 : H_2O_2$.[2]

[17] G. Herzberg, *Infrared and Raman Spectra of Polyatomic Molecules* (D. Van Nostrand Company, Inc., New York, 1945).

TABLE V. Calculated moments of inertia and rotational constants for the hydrogen peroxide molecule.

Azimuthal angle	Moments of inertia (g cm^2 × 10^{40}) I_A	I_B	I_C	Rotational constants (cm^{-1}) X_{10}^{0}	X_{01}^{0}
0°	2.89	32.0	35.0	0.83_5	8.83
45°	2.88	32.5	34.6	0.83	8.88
90°	2.83	33.6	33.7	0.83	9.03
135°	2.78	34.7	32.8	0.83	9.21
180°	2.76	35.1	32.4	0.83	9.29

The shape of the potential energy curve restricting free rotation in molecules such as hydrogen peroxide and hydrazine will depend on the cause of the hindering potential. According to the quantum mechanical calculations of Penney and Sutherland[1] this arises mostly from the directional properties of the central bond with steric repulsion and ion or dipole interactions contributing only slightly. In this connection it is surprising that the overtone band of hydrogen persulfide shows no sign of doubling under the same dispersion.[16] The use of a lead sulfide cell in the vacuum spectrometer prevented extension of the present investigation beyond 2.7μ. It is hoped that the fundamental frequencies of hydrogen peroxide will be studied soon under high dispersion in order to provide more information on the phenomenon of internal rotation. In particular, it would be interesting to know the equilibrium position of the OH groups and the height of the potential barriers restricting free rotation. Further study of the torsional oscillation is also desirable although it would no doubt involve considerable experimental difficulties.

ACKNOWLEDGMENT

This work was carried out during the tenure of a Fellowship of the John Simon Guggenheim Memorial Foundation. The author is deeply grateful to Professor Richard M. Badger for his continued interest and invaluable advice, specially in connection with the rotational analysis.

Valence Force Displacement Coordinates for Systems in Which the Angles Deviate from the Ideal

P. TORKINGTON
Physical Chemistry Laboratory, Oxford University, Oxford, England
(Received May 18, 1949)

Sets of valence force displacement coordinates are given which are applicable to practically any system. The coordinates for ideal bonding-angles arise as special cases. The derived symmetry coordinates for a few typical systems are obtained, and it is shown how the force constants can be corrected for small deviations of the angles from their ideal hybrid-bond values.

INTRODUCTION

IN carrying out normal coordinate analyses of molecular vibrations ideal values for the angles have often to be assumed; this is unavoidable in polyatomic molecules where the number of independent structural parameters is large. It would be useful to have available a method for the estimation of errors likely to be introduced with such assumptions. Further, where it is desired to use an exact value for an angle, it is often easier to employ coordinates for the ideal system and correct for small deviations. In this paper, general valence force displacement coordinates are given, which can be applied to practically any system. The coordinates for ideal bonding angles arise as special cases. The derived symmetry coordinates for a few typical systems are obtained, and it is shown how the force constants can be corrected for small deviations of the angles from their ideal hybrid-bond values.

DISPLACEMENT COORDINATES FOR SUBSTITUTED METHANES WITH NON-TETRAHEDRAL ANGLES

These may all be derived from the system in Fig. 1. The various angles are related as:

$$\cos\theta_{ij}=\cos\theta_{i4}\cos\theta_{j4}+\sin\theta_{i4}\sin\theta_{j4}\cos\phi_{ij}, \qquad (1)$$

where θ_{ij} is the angle between the bonds r_i and r_j, and ϕ_{ij} is the angle between the planes σ_{i54}, σ_{j54} containing atoms i, 5, 4 and j, 5, 4, respectively. The coordinates for bond-stretching can be written as:[1]

$$\Delta r_i=(\mathbf{s}r_i)_i+(\mathbf{s}r_i)_5, \qquad (2)$$

where the two $\mathbf{s}$ vectors are the components from the two terminal atoms i, 5 of the bond r_i. In terms of the unit vectors $\mathbf{v}_i$ directed along the bonds r_i as in Fig. 1,

$$\left.\begin{aligned}(\mathbf{s}r_i)_i&=\mathbf{v}_i\\(\mathbf{s}r_i)_5&=-\mathbf{v}_i\end{aligned}\right\}. \qquad (3)$$

For each of the displacement coordinates $r_i\Delta\theta_{ij}$ there are three $\mathbf{s}$ vectors, which can be expressed in terms of the unit vectors $\mathbf{v}_i$ as:[1]

$$\left.\begin{aligned}&\text{Terminal atoms:}\begin{cases}\mathbf{s}_i=(\mathbf{v}_i\cot\theta_{ij}-\mathbf{v}_j\csc\theta_{ij})\\ \mathbf{s}_j=a_{ij}(\mathbf{v}_j\cot\theta_{ij}-\mathbf{v}_i\csc\theta_{ij})\end{cases}\\ &\text{Apex atom:}\quad \mathbf{s}_5=[\mathbf{v}_i(a_{ij}\csc\theta_{ij}-\cot\theta_{ij})\\ &\qquad\qquad +\mathbf{v}_j(\csc\theta_{ij}-a_{ij}\cot\theta_{ij})]\end{aligned}\right\} \qquad (4)$$

[1] E. B. Wilson, Jr., J. Chem. Phys. **7**, 1047 (1939); **9**, 76 (1941); A. G. Meister and F. F. Cleveland, Am. J. Phys. **14**, 13 (1946).

where $(r_i/r_j)=a_{ij}$. For tetrahedral angles, $\cos\theta_{ij}=-(\frac{1}{3})$, $\sin\theta_{ij}=(\frac{2}{3})\sqrt{2}$, $\cos\phi_{ij}=-(\frac{1}{2})$, $\sin\phi_{ij}=(\sqrt{3}/2)$, for all values of i and j. Equations (4) then become

$$\left.\begin{aligned}\mathbf{s}_i&=-1/(2\sqrt{2})(\mathbf{v}_i+3\mathbf{v}_j)\\ \mathbf{s}_j&=-(a_{ij}/2\sqrt{2})(\mathbf{v}_j+3\mathbf{v}_i)\\ \mathbf{s}_5&=1/(2\sqrt{2})[(3a_{ij}+1)\mathbf{v}_i+(3+a_{ij})\mathbf{v}_j]\end{aligned}\right\}. \qquad (5)$$

For deviations from the ideal tetrahedral configuration,

$$\Delta\theta_{ij}+(\tfrac{1}{2})(\Delta\theta_{i4}+\Delta\theta_{j4})=(\tfrac{2}{3})^{\frac{1}{2}}\Delta\phi_{ij}, \quad (i,\ j\neq 4). \qquad (6)$$

Since $\sum\Delta\phi_{ij}=0$, therefore $\sum\Delta\theta_{ij}=0$ (taken over all values of i and j).

The coordinates for the system X_3YZ, of symmetry C_{3v}, are readily derived from Eqs. (4) and (5). For r_4 to coincide with the axis C_3, the atoms 1, 2, and 3 must be identical and the following conditions hold:

$$\left.\begin{aligned}&\theta_{12}=\theta_{13}=\theta_{23}(=\alpha);\quad \theta_{14}=\theta_{24}=\theta_{34}(=(\pi-\beta));\\ &a_{12}=a_{13}=a_{23}=1;\quad a_{14}=a_{24}=a_{34}(=a)\end{aligned}\right\}. \qquad (7)$$

The geometry of the system then requires that

$$\left.\begin{aligned}2\sin(\alpha/2)&=\sqrt{3}\sin\beta\\ 4\cos^2(\alpha/2)&=1+3\cos^2\beta\end{aligned}\right\}. \qquad (8)$$

For the angles α, with coordinates $r_1\Delta\theta_{ij}$:

$$\left.\begin{aligned}\mathbf{s}_i&=(\mathbf{v}_i\cot\alpha-\mathbf{v}_j\csc\alpha)\\ \mathbf{s}_j&=(\mathbf{v}_j\cot\alpha-\mathbf{v}_i\csc\alpha)\\ \mathbf{s}_5&=(\csc\alpha-\cot\alpha)(\mathbf{v}_i+\mathbf{v}_j)\end{aligned}\right\} \qquad (9)$$

and for the angles $(\pi-\beta)$, with coordinates $r_1\Delta\theta_{i4}$:

$$\left.\begin{aligned}\mathbf{s}_i&=-(\mathbf{v}_i\cot\beta+\mathbf{v}_4\csc\beta)\\ \mathbf{s}_4&=-a(\mathbf{v}_4\cot\beta+\mathbf{v}_i\csc\beta)\\ \mathbf{s}_5&=[(a\csc\beta+\cot\beta)\mathbf{v}_i+(\csc\beta+a\cot\beta)\mathbf{v}_4]\end{aligned}\right\}. \qquad (10)$$

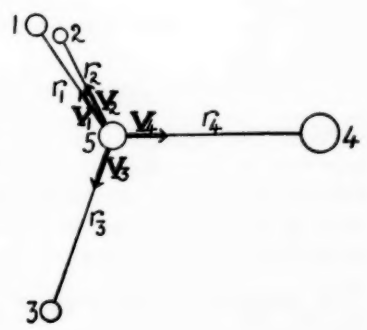

FIG. 1. Coordinates and displacement vectors for asymmetrically substituted non-tetrahedral methanes.

TABLE I. Variation of the force constants with the angle for triatomic molecules.

	H_2O		ClO_2		SO_2		NO_2		
	(a)	(b)	(a)	(b)	(a)	(b)	(a)	(b)	
$100(\Delta d_{11}/d_{11})$	0.102	0.101	0.578	0.427	0.656	0.564	1.387	0.929	
$100(\Delta d_{22}/d_{22})$	−0.102	−0.102	−0.578	−0.485	−0.656	−0.602	−1.387	−1.085	
$100(\Delta d_{12}/d_{12})$	—	−0.468	—	−1.872	—	−1.049	—	−1.464	(For $\Delta\theta=+1°$)
$100(\Delta d_{33}/d_{33})$	−0.098		−0.304		−0.426		−0.531		

With tetrahedral angles, Eqs. (9) and (10) become:

$$\left.\begin{aligned}\mathbf{s}_i&=-1/(2\sqrt{2})(\mathbf{v}_i+3\mathbf{v}_j)\\ \mathbf{s}_j&=-1/(2\sqrt{2})(\mathbf{v}_j+3\mathbf{v}_i)\\ \mathbf{s}_5&=\sqrt{2}(\mathbf{v}_i+\mathbf{v}_j)\end{aligned}\right\}, \tag{11}$$

$$\left.\begin{aligned}\mathbf{s}_i&=-1/(2\sqrt{2})(\mathbf{v}_i+3\mathbf{v}_4)\\ \mathbf{s}_4&=-(a/2\sqrt{2})(\mathbf{v}_4+3\mathbf{v}_i)\\ \mathbf{s}_5&=1/(2\sqrt{2})[(3a+1)\mathbf{v}_i+(3+a)\mathbf{v}_4]\end{aligned}\right\}. \tag{12}$$

For deviations from the tetrahedral, maintaining symmetry C_{3v}, $\Delta\phi_{ij}=0$, and $\Delta\alpha-\Delta\beta=0$.

The coordinates for systems X_2YZ_2 of symmetry C_{2v} are also readily derived from Eqs. (4) and (5). If the axis C_2 is taken as bisecting $\theta_{12}(=\alpha_1)$ and $\theta_{34}(=\alpha_2)$, atoms 1, 2 and 3, 4 being each an identical pair, the conditions are:

$$\left.\begin{aligned}&\theta_{13}=\theta_{23}=\theta_{14}=\theta_{24}(=\beta);\quad a_{12}=a_{34}=1;\\ &a_{13}=a_{23}=a_{14}=a_{24}(=a)\end{aligned}\right\}. \tag{13}$$

The various angles are related as:

$$\cos\beta=-\cos(\alpha_1/2)\cos(\alpha_2/2). \tag{14}$$

The **s** vectors for the coordinates $r_1\Delta\theta_{12}$, $r_3\Delta\theta_{34}$ are identical with those in Eqs. (9) and (11), with α_1 and α_2 in place of α and i, $j=1, 2$, and 3, 4, respectively. Those for the coordinates $r_1\Delta\theta_{14}$ etc. are:

$$\left.\begin{aligned}\mathbf{s}_i&=(\mathbf{v}_i\cot\beta-\mathbf{v}_j\csc\beta)\\ \mathbf{s}_j&=a(\mathbf{v}_j\cot\beta-\mathbf{v}_i\csc\beta)\\ \mathbf{s}_5&=[(a\csc\beta-\cot\beta)\mathbf{v}_i+(\csc\beta-a\cot\beta)\mathbf{v}_j]\end{aligned}\right\} \tag{15}$$

where $i=1$ or 2, $j=3$ or 4. With tetrahedral angles, Eqs. (15) reduce to Eqs. (12), with the subscript 4 taking values 3 or 4. For deviations from the tetrahedral, maintaining symmetry C_{2v}, the angular displacements are related as:

$$\Delta\alpha_1+\Delta\alpha_2+4\Delta\beta=0. \tag{16}$$

APPLICATIONS

From the general formulas obtained, symmetry coordinates for practically any system are readily written down. The derived kinetic energy matrix can then be set up, and the secular equation for the molecular vibrations obtained.[1,2] For a system of coordinates Δ_1 to Δ_n defined in terms of N subsidiary displacement coordinates or vectors $\mathbf{z}_1$ to $\mathbf{z}_N$, as:

$$\Delta_i=\sum_{j=1}^{N} a_{ij}\mathbf{z}_j \tag{17}$$

the elements of the modified kinetic energy matrix **A**, of order n, are:

$$A_{ij}=A_{ji}=\sum_{k=1}^{N} a_{ik}a_{jk}(M/m_k), \tag{18}$$

where m_k is the mass of the atom whose subsidiary displacement coordinate or vector is $\mathbf{z}_k$ and M is an arbitrary mass (conveniently chosen to be one of the m_k's), introduced in order that the elements A_{ij} shall be dimensionless quantities of convenient magnitude. If the coordinates Δ_i are chosen to satisfy any symmetry requirements, the nth order symmetry factor of the secular equation can be written as:

$$|\mathbf{dA}-\lambda\mathbf{I}|=0, \tag{19}$$

where the elements of the nth order matrix **d** are force constants in the potential function:

$$2V=\sum_{i=1}^{n}\sum_{j=1}^{n} d_{ij}\Delta_i\Delta_j, \tag{20}$$

I is the unit matrix of order n, and the function λ is:

$$\lambda=4\pi^2\nu^2c^2M, \tag{21}$$

where ν is a fundamental vibration frequency of the system in cm^{-1} and c is the velocity of light in cm $sec.^{-1}$. If the equation is written in the expanded form:

$$\lambda^n-c_1\lambda^{n-1}+c_2\lambda^{n-2}\cdots+(-1)^{n-1}c_{n-1}\lambda+(-1)^n c_n=0, \tag{22}$$

the coefficients c_1 to c_n are related to the matrix $\mathbf{B}=\mathbf{dA}$ as:

$$c_i=sp_i|\mathbf{B}|, \tag{23}$$

where sp_i stands for the sum of all principal minors of the determinant $|\mathbf{B}|$ of order i.

For small variations in the coefficients c_i, the corresponding variations in any root λ_k are given by[2]

$$(\partial\lambda_k/\partial c_i)=(-1)^{i+1}\lambda_k^{n-i}\prod_p(\lambda_k-\lambda_p)^{-1},\quad(p\neq k). \tag{24}$$

Since the determinant of the matrix product **dA** is the product of the determinants of the matrices **d** and **A**, and similarly for minors of **dA**, the frequency-shifts

[2] P. Torkington, J. Chem. Phys. **17**, 1279 (1949); Nature **162**, 370, 607 (1948).

caused by small variations in the elements of **A**, and the balancing increments to the force constants d_{ij} required to eliminate these shifts, are readily calculated. The solution will be unambiguous only when the number of constants to be adjusted is not greater than the number of frequencies. To correct for deviations from standard valence angles θ, therefore, all that is required is to express the elements A_{ij} generally, so that the derivatives $(\partial A_{ij}/\partial\theta)$ and the corresponding derivatives of $|\mathbf{A}|$ and of its minors, can be obtained. The method will be illustrated in the following examples.

A. The Class A_1 Vibrations of the Symmetric Triatomic Molecule

The required coordinates are identical with those for either half of the non-tetrahedral system X_2YZ_2 of symmetry C_{2v}. Taking the left-hand side, they are:

$$\left.\begin{aligned}\Delta_1&=\Delta r_1+\Delta r_2\\ \Delta_2&=r_1\Delta\theta_{12}\end{aligned}\right\}, \tag{25}$$

the combination of stretching coordinates being such as to satisfy the symmetry requirements of the Class A_1 vibrations. With these coordinates, the matrix **A**, $(M=m_2)$, has the form:

$$\begin{bmatrix}2\{(m_2/m_1)+2\cos^2\alpha\} & -2\sin 2\alpha\\ -2\sin 2\alpha & 2\{(m_2/m_1)+2\sin^2\alpha\}\end{bmatrix} \tag{26}$$

where $2\alpha=\theta$ is the angle of the triatomic molecule, m_1 is the mass of the terminal atom, m_2 that of the apex atom. For a solution for the constants satisfying a given angle,

$$\left.\begin{aligned}[\partial(\lambda_1+\lambda_2)/\partial\theta]&=-2\{(d_{11}-d_{22})\sin\theta+2d_{12}\cos\theta\}\\ [\partial(\lambda_1\lambda_2)/\partial\theta]&=0\end{aligned}\right\}. \tag{27}$$

If the interaction constant d_{12} is zero, the following relations hold for the increments in the force constants necessary to balance a given increment $\Delta\theta$ in the valence angle:

$$\begin{aligned}(\Delta d_{11}/d_{11})&=-(\Delta d_{22}/d_{22})\\ &=2[(d_{11}-d_{22})/(A_{11}d_{11}-A_{22}d_{22})]\sin\theta\Delta\theta.\end{aligned} \tag{28}$$

TABLE II. Variation of the force constants with the angle, for the methylene halides CH_2X_2, treated as three-particle systems.

X	F	Cl	Br	I	
$100(\Delta d_{11}/d_{11})$	1.03	1.38	1.74	1.88	
$100(\Delta d_{22}/d_{22})$	−1.17	−1.54	−1.95	−2.12	
$100(\Delta d_{12}/d_{12})$	−0.62	−0.62	−0.62	−0.62	(For $\Delta\theta=+1°$)
$100(\Delta d_{33}/d_{33})$	−0.79	−0.95	−1.09	−1.13	

For the solution corresponding to ν_1 being a vibration in which the displacement vectors of the terminal atoms lie along the valence bonds, and ν_2 being a pure deformation, in which the stretching coordinate does not take part,[2,3] the relations are:

$$\left.\begin{aligned}(\Delta d_{12}/d_{12})&=\cot\theta\Delta\theta\\ (\Delta d_{11}/d_{11})&=(2/A_{11})[\sin\theta+2(d_{12}/d_{11})\cos\theta]\Delta\theta\\ (\Delta d_{22}/d_{22})&=-(2/A_{11})\sin\theta\Delta\theta\end{aligned}\right\}. \tag{29}$$

The data obtained with four triatomic molecules are summarized in Table I. Solution (*a*) is with the interaction constant zero, and solution (*b*) is for ν_2 being a pure deformation, as described above; for comparison, the results for the asymmetrical stretching vibration ν_3 are also included. Solution (*b*) for the four methylene halides, treated as three-particle systems, is given in Table II for deviations from the tetrahedral angle.

B. The Class A_1 Vibrations of the Methyl Halides

The required coordinates have already been obtained; the combinations satisfying the symmetry requirements of the Class A_1 vibrations are:

$$\left.\begin{aligned}\Delta_1&=\Delta r_1+\Delta r_2+\Delta r_3\\ \Delta_2&=r_1(\Delta\theta_{12}+\Delta\theta_{13}+\Delta\theta_{23}-\Delta\theta_{14}-\Delta\theta_{24}-\Delta\theta_{34})\\ \Delta_3&=\Delta r_4\end{aligned}\right\}. \tag{30}$$

The matrix **A** is then

$$\begin{bmatrix}3(\mu_1+3\cos^2\beta) & -9[\sqrt{3}\sec(\alpha/2)\cos\beta+1]\sin\beta\cos\beta & -3\cos\beta\\ & 3(\mu_1+3\sin^2\beta)[\sqrt{3}\sec(\alpha/2)\cos\beta+1]^2 & 3[\sqrt{3}\sec(\alpha/2)\cos\beta+1]\sin\beta\\ & & (1+\mu_3)\end{bmatrix} \tag{31}$$

where $\mu_1=(m_C/m_H)$, $\mu_3=(m_C/m_X)$, X being the halogen atom. With tetrahedral angles,

$$\mathbf{A}=\begin{bmatrix}(1+3\mu_1) & -4\sqrt{2} & -1\\ & 4(8+3\mu_1) & 4\sqrt{2}\\ & & (1+\mu_3)\end{bmatrix}, \tag{32}$$

$$\text{adj. }\mathbf{A}=\begin{bmatrix}4[3\mu_1(1+\mu_3)+8\mu_3] & 4\sqrt{2}\mu_3 & 12\mu_1\\ & [3\mu_1(1+\mu_3)+\mu_3] & -12\sqrt{2}\mu_1\\ & & 36\mu_1(3+\mu_1)\end{bmatrix} \tag{33}$$

and

$$|\mathbf{A}|=36\mu_1[\mu_1(1+\mu_3)+3\mu_3]. \tag{34}$$

[3] P. Torkington, J. Chem. Phys. **17**, 357 (1949).

The matrix of derivatives $(\partial A_{ij}/\partial\alpha)$, for deviations from the tetrahedral, is

$$\begin{bmatrix} -4\sqrt{2} & 20 & 2\sqrt{2} \\ & -2\sqrt{2}(9\mu_1+16) & -4 \\ & & 0 \end{bmatrix} \tag{35}$$

and the corresponding derivatives of the adjugate:

$$\begin{bmatrix} -2\sqrt{2}[9\mu_1(1+\mu_3)+16\mu_3] & -20\mu_3 & -42\sqrt{2}\mu_1 \\ & -4\sqrt{2}\mu_3 & 12\mu_1 \\ & & -54\sqrt{2}\mu_1(3+\mu_1) \end{bmatrix}. \tag{36}$$

Finally,

$$(1/|\mathbf{A}|)(\partial|\mathbf{A}|/\partial\alpha) = -(3/\sqrt{2}). \tag{37}$$

From the diagonal elements of the above two matrices and from the derivative $(\partial|\mathbf{A}|/\partial\alpha)$, the hypothetical frequency-shifts caused by deviations from the tetrahedral are readily calculated; the balancing increments Δd_{ij} can then be obtained. For the standard solution[2] corresponding to the coordinates Δ_1 to Δ_{i-1} remaining rigid in ν_i, the subscripts being ordered so that Δ_i is the approximate normal coordinate for ν_i, and $\nu_1 > \nu_2 \cdots > \nu_n$, the following matrix is obtained for $(1/d_{ij})(\partial d_{ij}/\partial\alpha)$:

$$\begin{bmatrix} \{[2\sqrt{2}/(1+3\mu_1)][2-7\sqrt{2}(d_{12}/d_{11})-2(d_{13}/d_{11})]\} & -\sqrt{2} & -2\sqrt{2} \\ & [(3/\sqrt{2})-(d_{12}/d_{22})] & \sqrt{2} \\ & & 0 \end{bmatrix}. \tag{38}$$

Application of these formulas to the four methyl halides shows that the deformation constant d_{22} increases by 3.5 percent and the C−H stretching constant d_{11} by 0.25 percent, for a positive increment of 1° in the angle HCH. The C−X stretching constant d_{33} is independent of the angle. The interaction constants d_{12} and d_{23} decrease and increase, respectively, by 2.5 percent, and d_{13} decreases by 4.9 percent. The results are independent of the halogen atom except for variations in the second decimal place for the percentage derivatives for d_{11} and d_{22}.

C. Pyramidal XY_3 Molecules of Symmetry C_{3v}

The required coordinates are analogous to those for the methyl halides:

$$\begin{matrix} A_1 \begin{cases} \Delta_1 = \Delta r_1 + \Delta r_2 + \Delta r_3 \\ \Delta_2 = r_1(\Delta\theta_{12} + \Delta\theta_{13} + \Delta\theta_{23}) \end{cases} \\ E \begin{cases} \Delta_3 = \Delta r_1 + \Delta r_2 - 2\Delta r_3 \\ \Delta_4 = r_1(\Delta\theta_{13} + \Delta\theta_{23} - 2\Delta\theta_{12}) \end{cases} \end{matrix}. \tag{39}$$

The matrix **A** is:

$$A_1 \quad \begin{bmatrix} 3(\mu_1+3\cos^2\beta) & -18\cos^2\beta\tan(\alpha/2) \\ & 9(\mu_1+3\sin^2\beta)\sec^2(\alpha/2)\cos^2\beta \end{bmatrix} \tag{40}$$

$$E \quad \begin{bmatrix} 3(2\mu_1+3\sin^2\beta) & 9\tan(\alpha/2)\sin^2\beta \\ & \{(9/4)[2\mu_1(1+\cos^2\beta)+3\sin^4\beta]\sec^2(\alpha/2)\} \end{bmatrix}. \tag{41}$$

For tetrahedral angles,

$$\mathbf{A} = \left[\begin{array}{cc:c} (1+3\mu_1) & -2\sqrt{2} & \\ & (8+3\mu_1) & \mathrm{O} \\ \hdashline & & \\ & & \end{array}\right] \begin{matrix} A_1 \\ \\ \hdashline \\ \end{matrix}$$
$$\left[\begin{array}{cc:c} & & \\ & & \mathrm{O} \\ \hdashline 2(4+3\mu_1) & 8\sqrt{2} & \\ & (16+15\mu_1) & \end{array}\right] \begin{matrix} \\ \\ \hdashline E \end{matrix} \tag{42}$$

and for deviations from the tetrahedral,

$$(\partial A_{ij}/\partial\alpha) = \left[\begin{array}{cc:c} -4\sqrt{2} & 13 & \\ & -(20+9\mu_1)\sqrt{2} & \mathrm{O} \\ \hdashline & & \\ & & \end{array}\right] \begin{matrix} A_1 \\ \\ \hdashline \\ \end{matrix}$$
$$\left[\begin{array}{cc:c} & & \\ & & \mathrm{O} \\ \hdashline 4\sqrt{2} & 20 & \\ & (32+9\mu_1)\sqrt{2} & \end{array}\right] \begin{matrix} \\ \\ \hdashline E \end{matrix}. \tag{43}$$

In Table III are summarized the results for the symmetrically tri-substituted methanes CHX_3, treated as four-particle systems.

TABLE III. Variation of the force constants with the angle in tri-substituted methanes CHX_3 treated as four-particle systems.

	X	F	Cl	Br	
	$100(\Delta d_{11}/d_{11})$	2.65	3.18	4.68	
A_1	$100(\Delta d_{22}/d_{22})$	4.17	2.73	0.79	
	$100(\Delta d_{12}/d_{12})$	−0.62	−0.62	−0.62	(For $\Delta\theta_{XCX}=+1°$)
	$100(\Delta d_{33}/d_{33})$	−0.41	−0.58	−0.68	
E	$100(\Delta d_{44}/d_{44})$	−2.39	−2.44	−2.46	
	$100(\Delta d_{34}/d_{34})$	−0.12	−0.32	−0.47	

CONCLUSION

The methods described in this paper are quite general, and the results obtained by their application to simple systems of the type treated may be carried over, generally, to a first approximation. Examination of the results summarized reveals one or two features worthy of mention. First, in the triatomic molecules (see Table II), the results for the two solutions (*a*) and (*b*) are sufficiently similar to justify using the analog of (*b*) in other systems where it is not possible to obtain an unambiguous solution. Then, in general, it may be noted that the variations in the constants for a given increment in the valence angle involved increase with the masses of the atoms taking part in the vibration whose normal coordinate approximates to the coordinate going with the constant, in the potential energy expression. Regarding the absolute magnitudes of the increments, it may be observed that, in terms of the nomenclature employed here, an error of one percent in a vibration frequency ν_i leads to an error of approximately two percent in the constant d_{ii}. It may also be noted that the conventionally calculated absolute angular displacements for bending vibrations are of the order of 5° to 10° (20° for hydrogen-displacements).

THE JOURNAL OF CHEMICAL PHYSICS VOLUME 18, NUMBER 1 JANUARY, 1950

Chemical Effects Accompanying the Decay of Mn^{51}

W. H. BURGUS* AND J. W. KENNEDY
Washington University, St. Louis, Missouri

(Received June 7, 1949)

An investigation has been made of the chemical forms assumed by Cr^{51} when it is produced by positron decay of Mn^{51} under a variety of conditions. The data have shown that the oxidation state of the parent Mn^{51} plays an important role in determining the oxidation state of daughter Cr^{51}. By variation of experimental conditions some information has been obtained regarding the types of chemical reactions undergone by the Cr^{51}. These reactions have also been shown to play important roles in determining the ultimate chemical form of daughter Cr^{51}.

The complexity of the factors determining the chemical forms of Cr^{51} after Mn^{51} decay has been pointed out, and possible explanations of some of the observed phenomena have been suggested. We believe the results are consistent with the hypothesis that appreciable ionization in the valence shell accompanies the beta-decay process.

Incidentally it has been demonstrated that the manganese isotope of 44-min. half-life (Mn^{51}) decays to the chromium isotope of 26-day half-life (Cr^{51}).

INTRODUCTION

STUDIES of chemical phenomena accompanying nuclear transformations have been carried on, for the most part, with induced nuclear reactions, while studies with spontaneous reactions (decay processes) have received a somewhat smaller amount of attention. In the latter group the most successful and best explained work has been associated with the process of isomeric transition, particularly as accompanied by internal conversion. Only a very small amount of work has been reported in the literature dealing with the chemical consequences of beta-decay.[1,2] With this process little is currently understood concerning the relative importance of each of the several factors which might be expected to determine observed chemical phenomena. With positron decay, no work at all has been reported.

Of factors which may influence chemical properties of atoms involved in nuclear processes, one of the more important is the kinetic energy imparted to an atom by a departing particle or photon arising in the nuclear process. Often the recoil energy is of sufficient magnitude to cause severance of chemical bonds holding the atom in a molecule. Thus the atom may be endowed with unusual chemical properties and by virtue of its remaining kinetic energy may be able to initiate chemical reactions which do not ordinarily occur. In beta-decay two particles are emitted, the electron or positron, and the neutrino or antineutrino respectively. In these cases calculations of recoil energies are difficult because for a given radioactive species, the energies

* This paper is abstracted from the Ph.D. thesis of W. H. Burgus, Washington University, 1949. Present address of Mr. Burgus is P.O. Box 882, Los Alamos, New Mexico. The work was supported by a research grant from the Standard Oil Development Company which we gratefully acknowledge.

[1] T. H. Davies, J. Phys. and Colloid Chem. **52**, 595 (1948).

[2] Burgus, Davies, Edwards, Gest, Stanley, Williams, and Coryell, J. Chim. Phys. **45**, 165 (1948).

TABLE I. Cr^{51} extractions made during decay of Mn^{51}.

Elapsed time since previous Cr extraction	% of total Cr^{51} in fraction	Theoretical % Cr^{51} in fraction
51 min.	(59.2±1.0)	55.3
45 min.	(21.0±0.5)	22.7
18 hr.	(19.8±0.5)	22.0

TABLE II. Exchange of chromium between Cr(III) and Cr(VI) forms.

Sol. I, pH 1.50		Sol. II, 8.45f HNO_3		Sol. III, 2.38f NaOH	
Time of exchange	Percent exchange	Time of exchange	Percent exchange	Time of exchange	Percent exchange
18.4 hr.	1.1±0.2	18.2 h.	1.4±0.2	18.2 h.	2.0±0.2
122.0 hr.	2.7±0.2	120.8 h.	2.5±0.2	120.8 h.	3.3±0.2
289.2 hr.	8.6±0.3	289.0 h.	2.2±0.1	289.0 h.	4.7±0.2

of the individual particles are not fixed, but lie between zero and a definite maximum value. In addition the energy distribution may be complicated by the existence of a complex beta-spectrum, and in the case of positron decay electron capture may compete with positron emission. Energy distributions and decay schemes may be experimentally determined, but even with a known energy distribution for a simple beta-spectrum, recoil momentum calculations are difficult because of the present lack of knowledge of electron-neutrino angular correlations.

A second factor which may influence the chemical properties of atoms produced by negatron or positron decay is the behavior of the orbital electrons during and after the decay process. Theoretical calculations[3,4] have been made which predict that electronic excitation and ionization may occur as a result of change in nuclear charge. While it has been impossible to predict accurately the probability of ionization for all shells, the calculations have shown that there is only a rather small probability of ionization in the inner shells. Migdal[4] has estimated that for negatron decay of an atom of large atomic number Z, the probability of ionization in the K shell is $0.6/Z^2$, in the L shell is $6.8/Z^2$, and in the M shell is $14/Z^2$. For the outermost shells the probability of ionization is much greater and is predicted to be of the order of unity. Numerical calculations for the case of positron decay were not carried out, but Migdal has shown that in rough approximation the probability of ionization in the K shell is the same for negatron or positron decay. Numerical calculations for probabilities of processes leading to various excited states were not carried out.

An additional factor which may play a role in determining chemical properties of atoms resulting from negatron or positron decay is the chemical oxidation state of the parent species. If the parent atoms were in a given oxidation state, and no serious kinetic or electronic disturbances were to occur, then the daughter of a negatron emitter might be expected to exhibit an oxidation number one higher than that of the parent, while the daughter of a positron emitter might be expected to have an oxidation number one lower.

In addition to the above factors which may directly influence the chemical properties of daughter atoms of negatron or positron emitters, there may also be secondary or indirect factors which can play important roles in determining final chemical forms. A secondary process of great importance in determining final chemical form of a daughter of a negatron or positron emitter, is chemical reaction of daughter atoms with molecules of the surrounding medium. This may occur as a result of one or more of the primary processes of ionization, electronic excitation, or high recoil energy, or as a result of the appearance of the daughter in a nonstable chemical oxidation state. By variation of experimental conditions such as temperatures, composition of solutions, etc., it may be possible for the experimenter to learn something about these chemical reactions which occur.

As a consequence of the primary decay process, the daughter atoms may result at tracer concentrations in a chemical form not ordinarily encountered at macro concentrations. Studies of such phenomena have been meager and little is known about the subject which has been called "tracer solution chemistry." However, such a chemical species could conceivably undergo further reactions which would then determine the final chemical state of the daughter. One of these reactions might be exchange with another chemical form of the element added as a carrier. Thus the bulk of the daughter atoms might ultimately exhibit the chemistry of the added carrier, although not originally formed in the oxidation state of that carrier.

From the preceding considerations it is clear that the final chemical forms in which daughter atoms of negatron or positron emitters are found are determined by one or more of several important and possibly competing factors. The object of the present investigation was to determine the chemical forms assumed by chromium when it is formed by positron decay of manganese. By adjustment of variables such as the oxidation state of the manganese, the temperature, the composition of the medium in which decay occurs, etc., it was hoped to learn something of the nature and importance of two of the factors which may determine the chemical form of the chromium, *viz.* the oxidation state of the parent, and subsequent reactions with other molecules.

EXPERIMENTAL

For determination of the chemical forms of chromium grown from manganese, the manganese isotope of 46±2 min. half-life was employed. It decays by emission of positrons of 2.0-Mev maximum energy and has been

[3] E. L. Feinberg, J. Phys. U.S.S.R. 4, 424 (1941).
[4] A. Migdal, J. Phys. U.S.S.R. 4, 449 (1941).

assigned[5] mass number 51. The use of this particular isotope was dictated by the requirement that the daughter chromium must also be radioactive to make possible its detection. The chromium isotope to which the mass number 51 has been assigned[6] decays by electron capture with a half-life of 26.5 days. About 3–5 percent of the transitions[6] to V^{51} are accompanied by emission of 0.32-Mev[7] gamma-rays of which less than 0.5 percent are converted.[6] However the production of Cr^{51} from positron decay of Mn^{51} had not been reported at the time of the present experiments and it was first necessary to demonstrate the parent-daughter relationship of these two nuclides. This genetic relationship was established in an experiment in which a sample of Mn^{51} was prepared, was initially freed of its daughter Cr^{51}, and was allowed to decay. Manganese-chromium separations were then made at measured time intervals and the percentage of Cr^{51} activity found in each chromium daughter fraction was compared with the percentage calculated to arise from decay of a parent of the half-life of Mn^{51}.

To prepare Mn^{51}, a target of metallic chromium plate was bombarded with deuterons in the Washington University cyclotron. The chromium isotope of mass number 50, isotopic abundance 4.49 percent, was transmuted to Mn^{51} by the nuclear reaction $Cr^{50}(d, n)Mn^{51}$. To isolate Mn^{51} from the target, the chromium plate was dissolved in hydrochloric acid, and manganous carrier and appropriate holdback carriers were added. The hydrochloric acid was removed by fuming with concentrated nitric acid, and manganese dioxide was precipitated from boiling 16f nitric acid solution by addition of potassium chlorate. The precipitated manganese dioxide was centrifuged out, washed once with 0.1f nitric acid, and redissolved in a small quantity of 1f nitric acid by the addition of bisulfite. Chromic and vanadate holdback carriers were added and the precipitation of manganese dioxide was carried out as before. This cycle was repeated a third time. Tests of this procedure with dummy solutions "spiked" with Cr^{51} showed that each manganese dioxide precipitate carried less than 0.5 percent of the chromium present. After three such precipitations of manganese dioxide, the Cr^{51} initially present in the target should have been diminished by a factor of at least 10^5. Because of the relatively short half-life of Mn^{51}, the removal of other contaminating activities could not be carried out at this point without a prohibitive loss of Mn^{51} through decay. Consequently the removal of these contaminants was deferred until later when they were removed from the individual Cr^{51} daughter fractions.

From the prepared source of Mn^{51} free of Cr^{51} a small aliquot was removed for determination of the Mn^{51} half-life. A value of 44.3±0.5 min. was obtained in a measurement extending over 8 half-lifes. The remainder of the Mn^{51} sample was allowed to decay. At measured time intervals manganese-chromium separations were effected with the aid of carriers by precipitation of manganese dioxide in the manner described above. Because it was found necessary to count the weak

TABLE III. Distribution of Cr^{51} grown from Mn^{51}(II).

Expt. No.	Mn^{++} conc. f×10^4	Cr(III) conc. f×10^3	Cr(VI) $Cr_2O_7^=$ f×10^3	pH	Distribution of daughter Cr^{51} Cr(III) fraction (%)	Cr(VI) fraction (%)	Other experimental conditions
1	1.04	3.84	1.92	4.56	(99.1±1.9)	(0.9±0.1)	0.86f acetic acid and 0.86f sodium acetate
2	2.00	7.68	3.84	4.50	(98.8±2.5)	(1.2±0.5)	0.86f acetic acid and 0.86f sodium acetate
3	1.85	3.84	1.92	4.65	(98.7±2.8)	(1.3±0.4)	0.86f acetic acid and 0.86f sodium acetate
4	1.85	3.84	1.92	2.95	(97.7±2.1)	(2.3±0.5)	
5	1.85	3.84	1.92	1.18	(99.7±1.2)	(0.3±0.4)	
6	1.00	3.84	1.92	1.13	(98.6±1.9)	(1.4±0.8)	Solution cooled to 0°C. during decay.
7	1.04	3.84	1.92	1.40	(98.6±1.3)	(1.4±0.9)	
8	1.85	3.84	1.92	0.25	(98.2±2.0)	(1.8±0.4)	
9	1.04	3.84	1.92	(8.0f HNO_3)	(97.0±1.2)	(3.0±0.2)	
10	1.04	3.84	1.92	~2	(94.7±1.9)	(5.3±0.3)	Dioxane−H_2O solution mole fraction dioxane =0.29.
11	1.04	3.84	1.92	~2	(89.7±2.3)	(10.3±1.3)	Dioxane−H_2O solution mole fraction dioxane =0.56.
12	1.00	3.84	1.92	~2	(88.2±2.2)	(11.8±0.9)	Acetone−H_2O solution mole fraction acetone =0.60.
13	1.85	3.84	1.92	~2	(83.4±1.8)	(16.6±1.0)	Acetone−H_2O solution mole fraction acetone =0.60.
14	6.62	24.9	12.45	~1	(95.4±1.5)	(4.6±0.2)	Frozen in liquid air.
15	6.62	24.9	12.45	~1	(95.1±1.4)	(4.9±0.1)	Frozen in dry ice-acetone mixture.
16	6.54	24.9	12.45	~1	(94.8±1.5)	(5.2±0.2)	Frozen in dry ice-acetone mixture during decay and kept frozen for 6 days after decay.
17	Solid $MnCO_3$				(70.2±1.6)	(29.8±0.6)	Dissolved in 1.0f HNO_3 containing Cr(III) and Cr(VI) carriers.
18	Solid $MnCO_3$				(71.1±1.8)	(28.9±1.4)	Dissolved in 0.1f HNO_3 containing Cr(III) and Cr(VI) carriers.

[5] J. J. Livingood and G. T. Seaborg, Phys. Rev. **54**, 391 (1938).
[6] Walke, Thompson, and Holt, Phys. Rev. **57**, 171 (1940).
[7] L. C. Miller and L. F. Curtiss, Phys. Rev., **70**, 983 (1946).

TABLE IV. Distribution of Cr^{51} grown from $Mn^{51}O_4^-$ decay

Expt. No.	MnO_4^- conc. f×10⁴	Cr(III) conc. f×10³	Cr(VI) $Cr_2O_7^=$ f×10³	*p*H	Distribution of daughter Cr^{51} Cr(III) fraction (%)	Cr(VI) fraction (%)	Other experimental conditions
19	2.50	3.84	1.92	1.17	(48.4±1.9)	(51.6±1.8)	Cooled to 0°C.
20	2.00	3.84	1.92	1.17	(47.0±1.8)	(53.0±1.8)	
21	2.50	3.84	1.92	1.23	(50.1±2.0)	(49.9±1.7)	
22	15.8	3.84	1.92	1.23	(52.5±2.7)	(47.5±1.8)	
23	1.69	3.84	1.92	0.28	(51.2±1.6)	(48.8±1.3)	
24	2.50	1.92	1.92	1.23	(49.9±2.0)	(50.1±1.8)	
25	2.00	0	1.92	6.66	(4.6±0.6)	(95.4±2.5)	Solution brought to *p*H 1 after decay and Cr(III) added.
26	9.77	3.84	1.92	0.29	(53.0±2.6)	(47.0±1.4)	
27	7.70	14.4	7.20	~1	(43.7±0.9)	(56.3±0.8)	Frozen in liquid air.
28	6.52	14.4	7.20	~1	(42.9±0.8)	(57.1±0.9)	Frozen in dry ice-acetone mixture.
29	~7	14.4	7.20	~1	(44.1±0.9)	(55.9±1.2)	Frozen in dry ice-acetone mixture and kept frozen for 6 days after decay.
30	Solid $CsMnO_4$				(0.4±1.3)	(99.6±2.4)	After decay solid dissolved in cold 1f nitric acid containing Cr(III) and Cr(IV) carriers.

vanadium x-rays (and conversion electrons) accompanying the decay of Cr^{51}, complete removal of all other radioactive species was essential. Each Cr^{51} fraction was therefore subjected to a stringent purification process. The purified chromium samples were finally converted to chromic oxide, and chemical recoveries were determined gravimetrically. The samples were transferred to standard cardboard mounting cards and were covered with cellophane. The Cr^{51} activities were measured under standard geometric conditions using a Geiger counter with a thin mica end-window. No other absorber was interposed between samples and the counter. The average weight of chromic oxide samples mounted for counting was 10.5 mg with a maximum deviation of ±0.5 mg in individual samples. Each sample was uniformly spread over a circular area of 2.00 cm.² corresponding to an average thickness of 5.25 mg/cm². The close agreement between duplicate experiments run throughout the present studies indicated that counting errors introduced by differences in sample weight and uniformity were negligibly small.

The percentages of the total Cr^{51} daughter activity associated with each sample, corrected for chemical losses, are shown in Table I. The percentage of total daughter activity calculated to be present in a given fraction, assuming growth from a 44-min. parent, is also shown. Comparison of observed and calculated percentages confirms the parent-daughter relationship of these two nuclides, although the amount of Cr^{51} in the first sample is seen to be too large by several percent. (This discrepancy may have been due to incomplete removal of Mn^{51} from the Cr^{51} fraction or to growth of Cr^{51} during the ~2 min. required for the precipitation, washing, and centrifugation of the manganese dioxide.) The errors shown in Table I are those attributable only to standard deviations in counting.

The radioactivity in each daughter fraction was identified as Cr^{51} by following the x-ray (and conversion electron) decay curve. Also the gamma-ray decay curve of the first Cr^{51} extract was followed through 1.0 g/cm² of aluminum. Half-lives of 24.5 to 26 days were observed for all samples, in agreement with published values. Absorption curves were obtained consistent with a decay scheme involving vanadium *K* x-rays and 0.3-Mev gamma-rays.

Exchange of Chromium between Cr(III) and Cr(VI)

The chemically stable oxidation states of chromium and therefore the states in which chromium daughter might ultimately be found, are those with formal oxidation numbers +2, +3, and +6. In order to determine the relative amounts of daughter Cr^{51} appearing in each state, chemical separations with the aid of carriers were employed. Because of the ready oxidation of Cr(II) by Cr(VI) in aqueous solutions, and because exchange might be expected to occur between Cr(II) and Cr(III), investigation of Cr^{51} appearing as Cr(II) was not undertaken. Decay-product Cr^{51} was therefore separated into only two fractions, the first containing Cr^{51} formed directly in, or entered by exchange, the Cr(VI) state, and the second containing Cr^{51} formed directly in, exchanged with, or oxidized or reduced to the Cr(III) state. Obviously it was necessary to establish that no rapid exchange occurs between the Cr(III) and Cr(VI) forms.

Investigation of the exchange between Cr(III) and Cr(VI) was carried out with Cr^{51} tracer obtained from the U. S. Atomic Energy Commission. The tracer, carefully purified, was converted to chromic nitrate solution and "diluted" with additional inactive chromic nitrate before use in the exchange experiments. Exchange was studied at room temperature in three different solutions, one strongly acidic, the second at measured pH 1.50, and the third strongly basic. In all solutions equivalent amounts of Cr(III) and Cr(VI) carriers were present. The final concentration of Cr(III) was in each case 0.0358f; final concentrations of other reagents are shown in Table II. In brief, the experiments consisted of addition of equivalent amounts of Cr*(III) nitrate and inactive $Cr_2O_7^=$ to the solution in which

exchange was to be studied. At chosen time intervals, given in Table II, aliquots of the mixtures were withdrawn and the *p*H of each adjusted to 2.0. The Cr(VI) was then separated from Cr(III) by precipitation as lead chromate. The Cr(VI) fractions were converted to chromic oxide, and the specific activities of the samples were determined by measurements of the 0.32-Mev gamma-rays through an aluminum absorber of 1000 mg/cm^2.

Data of the Cr(III)–Cr(VI) exchange experiments are presented in Table II. Errors shown are those calculated to result from standard deviations in counting. A somewhat larger error due to co-precipitation of Cr(III) with the lead chromate, estimated at about 0.5 percent is not included. The results show that no rapid exchange occurs under the conditions of the experiments. These results are consistent with those reported by Muxart *et al.*,[8] who found essentially no exchange beginning either with active Cr(VI) or Cr(III). Because the concentrations of Cr(III) and Cr(VI) carriers employed in Cr^{51} daughter experiments were usually a factor of ten smaller than the concentrations used in the above exchange experiments, only very small errors should have resulted due to exchange between the two forms.

Oxidation States Assumed by Cr^{51} Grown from Mn^{51}(II)

To determine Cr^{51} distribution between Cr(III) and Cr(VI) fractions when grown from decay of Mn^{51} present as divalent manganese, the following general procedure was employed. The Mn^{51} samples were produced by deuteron irradiation of chromium targets and were isolated from the irradiated targets by the procedure already described. The irradiation of 1.5 hours at a beam current of about 120 microamperes gave enough Mn^{51} for division into six to eight samples each producing sufficient Cr^{51} for convenient measurement. After isolation of the Mn^{51} in 10 mg of carrier manganese dioxide as previously described, the final manganese dioxide precipitate was dissolved in 3–4 ml of 1f nitric acid by addition of a few milligrams of solid sodium bisulfite. The resulting Mn(II) solution was then boiled to remove excess sulfite and was diluted with water. This solution, filtered through a fine sintered glass filter to remove dust particles, served as a stock solution. Aliquots were withdrawn, added to previously prepared solutions, and the Mn^{51}(II) allowed to decay under various conditions.

The final composition of each solution, after addition of an aliquot of Mn^{51}(II) stock solution, is shown in Table III. In preparing all solutions water distilled from alkaline permanganate solution was used. In some early experiments nitrogen was bubbled through the solutions to remove dissolved oxygen, but this precaution was abandoned after it was shown to make no difference in the distribution of daughter chromium. (As the solutions were all quite acidic, this result might have been expected.) In all solutions, 10.0 mg of Cr(III) and 10.0 mg of Cr(VI) carriers were present during decay of the parent Mn^{51}.

After decay of Mn^{51}, Cr(III) and Cr(VI) fractions were separated for determination of their Cr^{51} content. The separations were made by precipitation of lead chromate from the solutions adjusted to a *p*H of 2.3–2.4. Each of the chromium fractions was carefully purified of contaminating activities and was finally mounted as chromic oxide for counting. As in the experiment demonstrating the parent-daughter relationship, it was necessary for sensitivity to count the V^{51} x-rays and thin samples were therefore required.

To check on the recovery of Cr^{51} in the Cr(III) and Cr(VI) fractions, an aliquot of Mn^{51} stock solution after decay was analyzed for total Cr^{51} content. It was found that from about 97 to 102 percent of Cr^{51} was always recovered in the two fractions.

In addition to decay of Mn(II) ions in solution, experiments were carried out in which Mn(II) was incorporated into solid manganous carbonate before decay. To prepare microcrystalline manganous carbonate into which Mn^{51} was incorporated, an aliquot of Mn^{51}(II) stock solution was mixed with a few milligrams of Mn(II) carrier. The mixture was diluted about tenfold with 95 percent alcohol and then manganous carbonate was precipitated by addition of a small amount of aqueous sodium carbonate solution. The precipitate was centrifuged out and washed once with alcohol and then with ether. Titration experiments showed that only about 2 percent of the manganese was oxidized by air to higher valence forms.

To separate Cr^{51} which had grown in solid manganous carbonate, the solid was dissolved in nitric acid solution containing 10 mg each of Cr(III) and Cr(IV) carriers. In one experiment the nitric acid concentration was 0.1f and in another was 1.0f. After solution, Cr(III)–Cr(VI) separations were carried out in the standard manner.

Table III shows the distribution of Cr^{51} between Cr(III) and Cr(VI) fractions when the Cr^{51} arises from decay of Mn^{51}(II) under various conditions. In the second, third, and fourth columns of Table III are shown the concentrations of Mn(II), Cr(III), and Cr(VI) carriers present in solutions during decay. When solutions were frozen before decay, these columns give concentrations before freezing. In the fifth column are shown the *p*H values of solutions, as measured with a Beckman *p*H meter where two decimal places are given. In the sixth and seventh columns are shown the distributions of daughter Cr^{51} between the Cr(III) and Cr(VI) fractions. Errors shown are those attributed only to standard deviations in counting; they do not include co-precipitation errors or errors due to weighing.

[8] Muxart, Daudel, Daudel, and Haissinsky, Nature **159**, 538 (1947).

The eighth column shows other important experimental conditions.

Oxidation States of Cr^{51} Grown from Mn^{51}(VII)

To learn whether the chemical oxidation state of parent Mn^{51} plays an important role in determining the oxidation state of daughter Cr^{51}, experiments were run in which Mn^{51} was prepared in the form of permanganate, allowed to decay, and then Cr^{51} distributions determined and compared with the distributions previously observed when the Cr^{51} had grown from Mn(II) under similar conditions.

In order to prepare Mn^{51} as permanganate the irradiation and isolation procedures of the preceding experiments were followed. After isolation, the final manganese dioxide precipitate was dissolved in 10 ml of 4.0f nitric acid by addition of a few milligrams of solid sodium bisulfite. To this solution about 1 g of solid sodium bismuthate was added to oxidize the manganous ions to permanganate. The suspension was thoroughly stirred and was allowed to stand at room temperature for about one minute. The excess sodium bismuthate was filtered off on a fine sintered glass filter funnel, and was washed free of permanganate with several ml of 0.1f nitric acid. The washings were collected with the filtrate. The clear permanganate solution was diluted to about 20 ml and bismuth was precipitated as the hydroxide by addition of 4f sodium hydroxide solution until the solution was slightly basic to litmus; the bismuth precipitate was centrifuged out. In the removal of bismuth at this point, some loss of permanganate could not be avoided. Tests showed that the bismuth hydroxide carried chromium and thus eliminated Cr^{51} grown during the bismuthate oxidation.

The permanganate solution remaining after removal of the bismuth hydroxide was made slightly acidic with nitric acid and again quickly passed through a fine sintered glass filter to remove a small amount of manganese dioxide. The filtered permanganate solution served as a stock solution. Aliquots were withdrawn, added to previously prepared solutions, and allowed to decay to Cr^{51} under various conditions simulating the conditions of previous experiments with Mn^{51}(II). Analysis of inactive stock solution prepared in this manner showed that greater than 99.4 percent of the manganese present was in the form of permanganate.

The final composition of each solution after addition of an aliquot of active permanganate stock solution is shown in Table IV. Procedures followed in the preparation of these solutions and separation of the daughter Cr^{51} into Cr(III) and Cr(VI) fractions were those used in the preceding experiments with growth from Mn(II). Purification, mounting, and counting procedures were likewise those of the previous experiments. In all cases of decay in solution 10.0 mg of Cr(III) and 10.0 mg of Cr(VI) carriers were present. Unless otherwise indicated in Table IV solutions were kept at room temperature and in the dark.

Because it is thermodynamically possible for permanganate to be reduced by both chromium and water under the conditions of some of the experiments in which both permanganate and chromic carriers were present in solution, tests were made to determine how rapidly the reduction occurs. Dummy solutions were made up in which concentrations of nitric acid, chromic, dichromate, and permanganate carriers were approximately equal to the concentrations of these constituents in some of the actual decay experiments of Table IV. The rate of reduction of permanganate in these solutions (stored in the dark at room temperature) was then followed spectrophotometrically. The results showed that the rate of reduction of permanganate was very slow compared to the rate of decay of Mn^{51} so that in the permanganate decay experiments only about 2 percent of the total Mn^{51} decay occurred with the parent in reduced forms.

In addition to experiments in which permanganate was allowed to decay in solution, an experiment was carried out in which Mn^{51} was incorporated into solid cesium permanganate and then allowed to decay. After complete decay, the solid cesium permanganate was dissolved in a cold solution 1f in nitric acid containing 10.0 mg each of Cr(III) and Cr(VI) carriers. Separation of fractions was then made in the standard manner. To prepare solid cesium permanganate, a few milligrams of potassium permanganate carrier were added to an aliquot of active permanganate stock solution, the solution was quickly cooled to 0°C, and a large excess of saturated cesium nitrate solution was added. The mixture was allowed to stand in an ice bath for about one minute, and the solid cesium permanganate crystals were removed by centrifugation, and washed once with a few milliliters of cold acetone containing a small quantity of permanganate. The precipitate was recentrifuged, and the acetone removed by decantation and evacuation. This left dry crystals of cesium permanganate, contaminated with a little cesium nitrate.

Table IV shows the distribution of Cr^{51} between Cr(III) and Cr(VI) fractions when the Cr^{51} arises from decay of permanganate under various conditions. In the second, third, and fourth columns of Table IV are shown the concentrations of permanganate, Cr(III) and Cr(VI) carriers present in solutions during decay. When solutions were frozen before decay, these columns give concentrations before freezing. In the fifth column, pH values of the various solutions are shown as before. In the sixth and seventh columns are shown the distribution of Cr^{51} between the Cr(III) and Cr(VI) fractions. As in the experiments with decay of Mn(II), Cr^{51} analyses of other aliquots of parent manganese solutions showed that the sum of activities in the two fractions totaled from 97 percent to 102 percent of the Cr^{51}. Errors shown are those attributed to standard deviations in counting. Errors arising from co-precipita-

tion of Cr(III) with lead chromate (estimated at about 0.5 percent) and errors resulting from reduction of permanganate are not included. The last column of Table IV gives other important experimental conditions.

Oxidation States of Cr^{51} Grown from Mn^{51}(IV)

In addition to the experiments with parent Mn^{51} in states with formal oxidation numbers II and VII, an experiment was also carried out with the Mn^{51} in the IV state as manganese dioxide. Because of the insolubility of manganese dioxide, experiments in solution were impossible. Further, if experiments were conducted in which Cr^{51} grew from Mn^{51} incorporated into manganese dioxide, complete separation of Cr^{51} daughter into Cr(III) and Cr(VI) fractions would necessitate solution of the manganese dioxide and addition of chromium carriers. Because procedures available for putting manganese dioxide into aqueous solution require changing the oxidation state of the manganese, risk of also changing the oxidation state of the chromium daughter would be involved. The procedure actually followed was to prepare a sample of solid active manganese dioxide, and to suspend it in a solution containing Cr(III) and Cr(VI) carriers, with the expectation that some of the recoil Cr^{51} daughter atoms might be ejected from the surface of the manganese dioxide and thus escape into solution.

The solution chosen for suspension of manganese dioxide consisted of 10 mg each of Cr(III) and Cr(VI) carriers in 50 ml of 1.030f nitric acid cooled to 0°C in an ice bath. Under these conditions the rate of reduction of the solid manganese dioxide by Cr(III) carrier in solution was found to be negligibly slow. A 10-mg sample of active manganese dioxide was prepared in the usual way. The fresh precipitate was then stirred in the solution described until all the Mn^{51} had decayed. The manganese dioxide was then removed by centrifugation, and examined for Cr^{51} content, and the liquid phase was divided into Cr(III) and Cr(VI) fractions in the standard manner. Of the total Cr^{51} produced from decay of Mn^{51}, (61.0±0.6) percent remained trapped in the solid phase. Of Cr^{51} which made its way into solution (43.8±0.6) percent was included in the Cr(III) fraction, and (56.2±0.7) percent was in the Cr(VI) fraction. The errors are those due to standard deviation in counting.

DISCUSSION

Discussion of Experimental Observations

Referring first to Table III, experiments 1 through 9, in which Cr^{51} was produced by decay of Mn^{51} in the form of manganous ion in aqueous solution, we see that in each experiment almost all of the Cr^{51} appeared in a form which followed the chemistry of Cr(III) carrier. Comparison of experiment 6 with experiment 5 shows that there was no determinable difference in Cr^{51} distribution between 0°C and room temperature.

Reference is now made to experiments 17 and 18 of Table III. In these experiments the parent Mn^{51} was again in the form of Mn(II) but was incorporated into solid dry manganous carbonate and allowed to decay. The data show that unlike the cases of aqueous solutions where nearly all of the Cr^{51} appeared in reduced forms, about 30 percent now appeared in the form of Cr(VI) or a form exchangeable with it.

Because it was suspected that the observed absence of highly oxidized Cr^{51} in aqueous solution (experiments 1 through 9) was due in part to chemical reduction by water, experiments 10 through 16 were designed to reduce this effect of the water. In experiments 10 through 13, organic reagents were added to the aqueous solutions to reduce the mole fraction of water. While it was expected that these compounds, acetone and dioxane, could also act as reducing agents, the results show that they were effective to some degree in decreasing the chemical reduction effect of water.

Experiments 19 through 24 inclusive, and experiment 26, show that in aqueous solution about one-half of the Cr^{51} grown from permanganate appeared in reduced forms, and one-half appeared in oxidized forms. Comparison of experiments 19 and 20 shows that there is no effect on distribution when the temperature of the solution is lowered from room temperature to 0°C. If permanganate were responsible for the oxidation of Cr^{51} to the Cr(VI) state, a dependence of Cr^{51} distribution on permanganate concentration should be observable. There is no significant dependence on permanganate concentration.

In the single experiment in which Mn^{51} was incorporated into manganese dioxide and the dioxide suspended in a nitric acid solution of carriers of Cr(III) and Cr(VI), it was found that of the Cr^{51} recoils that escaped into solution, about 56 percent were in the oxidized form and 44 percent in the reduced form. Again it is seen that an increase in oxidation number was involved.

Possible Explanations of Observed Phenomena

Because the phenomena observed in the present experiments clearly result from a number of complex and competing factors, some of which are not understood at the present time, it is difficult to explain all of the experimental results. However certain ideas do present themselves and these will be discussed in the following paragraphs. It should be pointed out, however, that the suggestions offered may not be the correct ones, and alternative explanations are certainly possible.

One of the more interesting experiments is that in which Mn^{51}(II) was incorporated into solid manganous carbonate and allowed to decay to Cr^{51}. After decay the solid was dissolved in an acidic solution and the Cr^{51} was separated with the aid of carriers into Cr(III) and Cr(VI) fractions. Approximately 30 percent of the

total Cr^{51} was separated as Cr(VI) or a form rapidly exchangeable with this state. The appearance of Cr^{51} in a considerably higher oxidation state than its parent is in agreement with the hypothesis that ionization accompanies the decay.

If no electronic loss were to occur, the decay reaction could be written: $Mn^{++} \rightarrow Cr^{+} + \beta^{+}$. How a singly charged chromium ion would behave in the crystal lattice of manganous carbonate cannot be stated. However, if it were possible for the Cr^{51} ion to lose its recoil energy and still remain singly, or become doubly or triply charged, dissolution of the solid in an acidic solution of Cr(VI) carrier would likely result in formation of Cr^{51}(III). On the other hand should considerable ionization accompany decay, a more highly charged Cr^{51} ion could be produced. If this ion were to lose its recoil energy in the solid without losing its charge, then upon solution of the solid, hydration of the ion to some stable form might occur. An equation for an over-all hydration reaction could be written $Cr^{+6} + 4H_2O = HCrO_4^{-} + 7H^{+}$. Reactions of this type have been proposed by Libby.[9] It should be pointed out that ionization to Cr^{+6} may not be necessary. Although stable chromium compounds of oxidation numbers IV and V are unknown in macro quantities, their existence on a tracer scale might be possible. If such ions existed, they might be transformed to Cr(VI) through rapid exchange with chromate carrier, in a manner analagous to the exchange of manganate and permanganate. It might also be possible that chromium in one of these forms could be oxidized to Cr(VI) by some other mechanism. This seems less likely because the bulk of the experiments indicate that aqueous solutions act as reducing agents rather than oxidizing agents for the Cr^{51}. Of course it is possible that such unknown species might simply have co-precipitated with lead chromate. Regardless of what mechanisms may be in operation to stabilize the Cr^{51} in solution, its appearance in a form higher than Cr(III) implies that considerable ionization must occur, leaving Cr^{51} trapped in the crystal lattice with formal charge of at least IV.

In the experiments in which Mn^{51}(II) ions were allowed to decay in aqueous solutions, the question arises as to why almost all of the Cr^{51} daughter was found in lower oxidation forms. In view of the assumption that considerable ionization occurs, it might be expected that the higher charged Cr^{51} ions would be stabilized in solution through the same mechanisms operating for ions introduced into solution by dissolving solid manganous carbonate. However there is at least one very significant difference between these two kinds of experiments. In the solid manganous carbonate experiment, the Cr^{51} ions had lost their recoil energy before being introduced into solution. In the experiments where decay occurred in solution, such was not the case. This suggests that the recoil energy of the Cr^{51} ions is responsible for their reduction in aqueous solutions. Such reduction reactions, occurring as a result of high recoil energy, have been observed in a large number of cases where the momentum was supplied by gamma-emission following neutron capture.[9]

The question of how much energy a highly charged Cr^{51} ion must have in order to undergo chemical reduction is difficult to answer. For the sake of an estimate it might be assumed that a reaction such as the following is involved: $Cr^{+6} + 3H_2O = Cr^{+3} + \frac{3}{2}H_2O_2 + 3H^{+}$, and a rough idea of the energy required might be obtained from available thermochemical data[10] for ΔH. If an equation for hydration of Cr^{+6} and its subsequent dissociation to $HCrO_4^{-}$ is subtracted from the above equation, a third equation is obtained for which ΔH is known:

$$HCrO_4^{-} + 4H^{+} = \tfrac{3}{2}H_2O_2 + Cr^{+3} + H_2O; \qquad \Delta H = 8 \text{ kcal. mole}^{-1}.$$

Because ΔH for the hydration of Cr^{-6} is likely to be a large negative quantity, ΔH for the first reaction must have a value much smaller than 8 kcal. $mole^{-1}$. This would correspond to <0.35 ev per ion. Should the energy from recoil considerably exceed this approximate value then it may be assumed that the reduction might occur. As the experiments indicate, reduction is the common result.

It may be shown that E_r, the kinetic energy imparted to the Cr^{51} by a positron of energy E_β and an antineutrino of energy E_ν, is given by the equation

$$E_r = 10.5[E_\beta^2 + 1.02E_\beta + E_\nu^2 + 2E_\nu(E_\beta^2 + 1.02E_\beta)^{\frac{1}{2}}\cos\theta]$$

when E_β and E_ν are in millions of electron volts and θ is the angle between directions of emission of positron and antineutrino. The positrons have energies between zero and a maximum energy of 2.0 Mev. The positron spectrum of Mn^{51} has not been determined, but a spectrum may be calculated from the Fermi theory of beta-decay. Then calculation of the recoil energy distribution could be carried out if information about the angular correlation of positrons and antineutrinos were available. Experimental determinations of the correlation for beta-particles and neutrinos have been made, but the results are said by the authors to be somewhat inconclusive.[11–15].

We have calculated recoil spectra of Cr^{51} atoms for several different values of the angle θ. The mass of the neutrino was taken as zero. The distributions are strongly dependent on the value of θ. For the case of parallel directions of positron-antineutrino emission ($\theta = 0°$), all recoils have energies above 43 ev. For

[9] W. F. Libby, J. Am. Chem. Soc. **62**, 1930 (1940).

[10] F. R. Bichowsky and F. D. Rossini, *Thermochemistry of Chemical Substances* (Reinhold Publishing Corporation, New York, 1936), pp. 20 and 95.

[11] J. C. Jacobsen, and O. Kofoed-Hansen, Kgl. Danske Vid. Sels. Math.-Fys. Medd. **23**, No. 12, 1–34 (1945).

[12] Christy, Cohen, Fowler, Lauritsen, and Lauritsen, Phys. Rev. **72**, 698 (1947).

[13] C. W. Sherwin, Phys. Rev. **73**, 216 (1948).

[14] C. W. Sherwin, Phys. Rev. **73**, 1173 (1948).

[15] Allen, Paneth, and Morrish, Phys. Rev. **75**, 570 (1949).

$\theta=180°$ a large share of the recoils have energies over 5 ev, and for $\theta=135°$ (the most probable angle in one theory) all recoils have energies above 8.9 ev. For any case the maximum recoil energy is 63.5 ev. For any of the distributions it seems likely that a large fraction of recoil Cr^{+6} ions would be able to oxidize water readily.

When a comparison is made of the decay of Mn^{51}(II) ions in solution with the decay of permanganate ions in solution, an apparent anomaly is encountered. In the former case all Cr^{51} daughters were reduced, while in the later only about one-half were reduced. If no molecular disruption were to occur, an equation for the decay reaction of permanganate might be written, $MnO_4^-=CrO_4^=+\beta^+$, and in that case all the daughter atoms would initially have the oxidation number VI. As it has been assumed that highly oxidized Cr^{51} ions are produced by the ionization accompanying decay of Mn^{51}(II), the question arises as to why all of these were usually completely reduced whereas only a part of the Cr^{51}(VI) ions from permanganate decay were reduced. To answer this question is difficult but a possible explanation may be as follows. In the case of Mn(II) decay it was assumed that highly charged chromium ions were produced. These ions in almost all cases were assumed to have sufficient kinetic energy to undergo chemical reduction reactions with water. In the case of decay of permanganate, momentum may be conserved not by Cr^{51} alone, but by motion of the whole chromate ion. The suggestion that a large fraction of recoil energy may appear as translational energy for a whole molecule (or ion) with a small fraction as "internal" energy, has been made by Suess.[16] As the mass of chromate is greater than the mass of a bare chromium ion by a factor of 2.24, the recoil kinetic energy of chromate could be at most 0.44 that of the bare Cr^{51} ion. This could partially account for the observation that some of the Cr^{51} grown from permanganate is not chemically reduced. A further consideration involves the assumption that bare highly charged Cr^{51} ions result from Mn(II) decay whereas Cr(VI) resulting from permanganate decay is initially bonded to some oxygen atoms. A non-oxygenated Cr(VI) ion would probably be a much better oxidizing agent than one bound to oxygen atoms.

The preceding argument takes little account of the effect of the ionization on the stability of chromate. Cooper[17] has calculated that the acquisition of positive charge by a bromine atom in bromate can result in formation of excited vibrational states in the ion. In the bromine case the positive charge was assumed to be built up by Auger processes following internal conversion. In the present experiments if ionization of Cr^{51} in chromate were to occur, a similar effect might be expected. As a result one or more oxygen ions might be split out of the chromate ion leaving fragments such as CrO_3, CrO_2^{+2}, etc. The rupture of chromium-oxygen bonds could also occur in cases with high initial recoil energy. If such fragments were produced by either process they could undergo two competing types of reactions.[9] The first is hydration to stable acid chromate ion by over-all reactions such as:

$$CrO_3+H_2O=HCrO_4^-+H^+$$
$$CrO_2^{++}+2H_2O=HCrO_4^-+3H^+$$

The second-type reaction is chemical reduction to Cr(III) as has already been mentioned.

Of course if singly charged or neutral oxygen is split out of the chromate ion this could account for reduction in such cases. From all of the considerations it is evident that the factors which can determine chemical forms are quite complex and the tentative descriptions offered are probably over simplified.

[16] H. Suess, Zeits. f. physik. Chemie **B45**, 312 (1939).

[17] E. P. Cooper, Phys. Rev. **61**, 1 (1942).

THE JOURNAL OF CHEMICAL PHYSICS VOLUME 18, NUMBER 1 JANUARY, 1950

The Magnetic Susceptibility of Potassium Ferrate*

HENRY J. HROSTOWSKI AND ALLEN B. SCOTT
Chemistry Department, Oregon State College, Corvallis, Oregon

(Received June 10, 1949)

A method of preparation of potassium ferrate of 97 percent purity is described. Although the product contained an inseparable ferromagnetic impurity, the susceptibility of the ferrate was determined by extrapolation to infinite field strength of data obtained by the Gouy method. The observed effective magnetic moment of the ferrate ion agrees approximately with that expected for hexavalent iron.

INTRODUCTION

THE difficulty of preparing pure salts of hexavalent iron has resulted in a scarcity of reliable physical data regarding its compounds. No magnetic data are available with the exception of qualitative measurements made on solutions containing ferrate.[1] A method for preparing potassium ferrate has been developed in this laboratory, resulting in a product of sufficient purity to make possible the determination of the magnetic susceptibility of the ferrate ion. This investigation

* Based on a thesis submitted by H. Hrostowski in partial fulfillment of the requirements for the M.S. degree at Oregon State College; published with the approval of the Oregon State College Monographs Committee, Research Paper No. 141, Department of Chemistry, School of Science.

[1] O. Liebknecht and A. P. Wills, Ann. d. Physik. (4) **1**, 380 (1900).

was undertaken in an attempt to verify the moment expected of hexavalent iron.

PREPARATION OF K_2FeO_4

In concentrated sodium hydroxide solution Na_2FeO_4 is very soluble[2] whereas sodium chloride is quite insoluble.[3] Since chloride was expected as the main impurity in the synthesis of K_2FeO_4, the ferrate ion was prepared by treatment of $Fe(OH)_3$ with sodium hypochlorite in very concentrated sodium hydroxide solution and then precipitated as K_2FeO_4 by addition of KOH after filtration.[4] This procedure eliminates most of the chloride without resorting to repeated reprecipitations. The equation may be written

$$2Fe(OH)_3+3ClO^-+4OH^-=2FeO_4^{--}+3Cl^-+5H_2O$$

although the ferrite ion is probably an intermediate.

A paste of 32 g of $FeCl_3$ and 40 g of NaOH in 100 ml of water was added to 350 ml of an aqueous solution containing 17 percent each of NaClO and NaOH. With continual stirring 300 g of NaOH were added while the temperature was kept between 50 and 55°C. After having been maintained in this temperature range for one or two hours, the mixture was allowed to cool below 40°C and was filtered through a fritted glass funnel into a flask containing 30 g of KOH. The solid K_2FeO_4, which formed immediately as the KOH dissolved, was filtered off and redissolved in 500 ml of 20 to 40 percent KOH solution. Decomposition, which is minimized by rapid filtration, occurred quite noticeably on the surface of the filter funnel and $Fe(OH)_3$ present, but to a lesser degree on the container walls. The filtrate was saturated with potassium hydroxide and the recrystallized K_2FeO_4 separated by filtration. Three thorough washings with 300 to 400 ml of 95 percent ethanol cooled to −5°C and subsequent washing with small amounts of ether[2] left the product free of all traces of NaCl, NaOH, and C_2H_5OH. The product was a stable, homogeneous, black powder which was stored for long periods of time over P_2O_5 without noticeable decomposition.

Yields ranging from 10 to 15 percent of the theoretical were obtained, while deviation from this procedure decreased the yield substantially. The sample used for magnetic measurements consisted of three thoroughly mixed batches.

TABLE I. Variation of χ_M with H.

H (oersteds)	Determinations	$\chi_M \times 10^5$ (c.g.s. units)
1750	3	815±3
4670	6	666±4
6460	2	607±2
8150	2	569±0

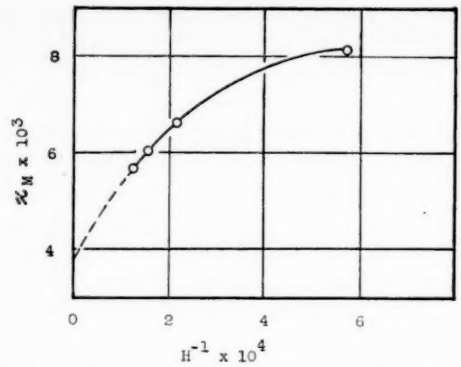

FIG. 1. Variation of χ_M with reciprocal field strength for potassium ferrate sample.

Analysis for carbonate by absorption of CO_2 on ascarite[5] showed the presence of 2.94±0.06 percent K_2CO_3 if the CO_2 is assumed present in this form. Volumetric iron determination** proved the iron content to be 27.52±0.08 percent. The theoretical percent K_2FeO_4 calculated from this was 97.6 with a probable error of ±0.1 percent while that calculated from the percent K_2CO_3 impurity was 97.1 percent. Incompatibility of these figures indicated the presence of an iron compound having a higher proportion of iron than K_2FeO_4. Assuming the foreign iron compound to be ferric oxide, the composition of the sample was calculated to be 96.9 percent K_2FeO_4, 2.9 percent K_2CO_3, and 0.2 percent Fe_2O_3. It is doubtful whether the undesired iron compound can be removed, since further reprecipitations showed the strongly alkaline ferrate solutions to be unstable to some degree.

EXPERIMENTAL

Apparatus

A Gouy magnetic balance[6] employing a Christian Becker micro-analytical balance was used for all susceptibility measurements although weights were taken only to the nearest milligram except for the calibrations with water. Small permanent magnets produced the weaker fields while the stronger ones were obtained with the electromagnet from the apparatus of Scott and Cromwell.[7] To avoid lateral motion of the samples in the field, the mass of the sample tubes was increased by adding glass rod to the lower ends.

Calibration

Water and an approximately 29 weight percent $NiCl_2$ solution were used as calibrating agents. The latter was prepared by dissolving "Baker's Analyzed" $NiCl_2 \cdot 6H_2O$

[2] J. M. Schreyer, Ph.D. thesis, Oregon State College, 1948. Part of this thesis was presented at the 114th meeting of the American Chemical Society, September 16, 1948, at Portland, Oregon by W. E. Caldwell.

[3] A. H. Hooker, Chem. and Met. Eng. **23**, 961 (1920).

[4] Suggestion of J. Schulein and J. Miller, Chem. Eng. Dept., Oregon State College.

[5] H. H. Willard and N. H. Furman, *Elementary Quantitative Analysis* (D. Van Nostrand Company, Inc., New York, 1940), third edition, pp. 402–406.

** Iron was determined by titration of the reduced sample with potassium bichromate.

[6] L. G. Gouy, Comptes Rendus **109**, 935 (1889).

[7] A. B. Scott and T. M. Cromwell, Am. Chem. Soc. **70**, 3981 (1948).

in distilled water. Nickel was determined gravimetrically by precipitation with dimethylglyoxime. The gram susceptibility of the solution at the experimental temperature of 26°C was calculated from the data given by Selwood.[8]

Since each tube was filled to the same mark, first with $NiCl_2$ solution and then with K_2FeO_4, the apparatus was calibrated in terms of the quantity $A(H_1^2-H_2^2)/2g$, H_1 and H_2 being the field strengths acting on the ends of the sample, A the cross-sectional area of the sample tube, and g the gravitational constant. Simultaneous measurements of susceptibility and density were accomplished by this procedure.

Because the experimental method permitted determination only of relative field strength, an absolute measurement of one magnetic field was made using a flip coil and a ballistic galvanometer of known sensitivity. The value found was 1750±40 oersteds.

MEASUREMENTS

The molar susceptibility of the K_2FeO_4 sample was determined at four different field strengths. Results are recorded in Table I. The errors indicated are errors of observation only. Values of χ_M were calculated from the equation

$$\chi_M = M\kappa_N \Delta W/d\Delta W_N,$$

where M and d are the formula weight and density of the K_2FeO_4 sample, and ΔW and ΔW_N the apparent weight changes respectively of the solid ferrate and the $NiCl_2$ solution in the field. The density of the sample was quite reproducible and varied only within a few percent during the measurements justifying the assumption of homogeneous packing of the powder in the sample tube. All determinations except three at 4670 oersteds were made using $NiCl_2$ solution for calibration. For these three, water was used for calibration.

DISCUSSION

Although the sample of potassium ferrate showed marked field strength dependence, there is no evidence for assuming a ferrate to be ferromagnetic. The analytical data indicate the presence of an amount of iron-containing impurity sufficient to account for this behavior. The ferromagnetic contaminant may be a ferrite or, more likely, a ferromagnetic form of ferric oxide.

When the Gouy method is employed, the volume susceptibility at any field strength, κ_H, of a sample containing a small amount of ferromagnetic impurity is given by the equation[9]

$$\kappa_H = \kappa_\infty + 2c'\sigma_s/H,$$

where κ_∞ is the true volume susceptibility in an extremely high field; c' is the concentration of the ferromagnetic impurity in g/cc of sample, and σ_s its saturation specific magnetization. In terms of χ_M the equation retains its linear form. Plotting χ_M at any field strength as a function of reciprocal field strength yields the true molar susceptibility on extrapolation to $H^{-1}=0$.

Figure 1 shows the experimental variation of χ_M with H^{-1} for the K_2FeO_4 sample.

It is difficult to extrapolate this curve to infinite field strength accurately since the slope has not yet become exactly linear. More points at higher field strengths would increase the accuracy of the extrapolation. However, at field strengths greater than 8150 oersteds the lateral forces exerted on the sample tubes became so great that little confidence could be placed in weighings made in the field.

No simple function of $1/H$ was found which yielded a linear curve throughout this region. Consideration of possible limits of the intercept introduces a possible error of about seven percent in the value 380×10^{-5} obtained by extrapolation of the actual curve. The error of extrapolation is the limiting error of the experiment and is large enough so that corrections for ionic diamagnetism would merely exaggerate the accuracy of the results. However, correction for the estimated purity of the sample seems justified. The value, $(392\pm26)\times10^{-5}$, is effectively the susceptibility of the ferrate ion.

The effective magnetic moment calculated from the relation $\mu_{eff.}=2.83(\chi_M T)^{\frac{1}{2}}$ is 3.06±0.08 Bohr magnetons. Iron in an oxidation state of six should have two $3d$ electrons not used in bond formation; these would be expected to be unpaired, leading to a theoretical magnetic moment of 2.83 Bohr magnetons.

It is not possible to arrive at a structure for the ion by consideration of its moment. Since in any case three $3d$ orbitals are available for bond formation, the most likely structure is tetrahedral.[10] This configuration is further indicated by the suggestion of Retgers,[11] based on an examination of microscopic crystals, that K_2FeO_4, K_2SO_4, and K_2CrO_4 should be isomorphous.

ACKNOWLEDGMENTS

We wish to acknowledge the helpful discussions with Professors J. L. Huston and H. Freund and the valuable assistance of Mr. T. M. Cromwell.

[8] P. W. Selwood, *Magnetochemistry* (Interscience Publishers, Inc., New York, 1943), pp. 29, 46.

[9] L. F. Bates, *Modern Magnetism* (Cambridge University Press, London, 1948), second edition, pp. 115–117.

[10] O. K. Rice, *Electronic Structure and Chemical Binding* (McGraw-Hill Book Company, Inc., New York, 1940), pp. 268, 275.

[11] J. W. Retgers, Zeits. f. physik. Chemie **10**, 529 (1892).

THE JOURNAL OF CHEMICAL PHYSICS VOLUME 18, NUMBER 1 JANUARY, 1950

Statistical Mechanics of Swelling of Network Structures

PAUL J. FLORY
Department of Chemistry, Cornell University, Ithaca, New York

(Received May 18, 1949)

Inaccuracies in previously published theories dealing with the swelling of network polymers in solvents are pointed out. The treatment of Flory and Rehner, based on the tetrahedral model, is overly restrictive and leads to an entropy of swelling which is too small. A more recent treatment of Kuhn, Pasternak, and Kuhn introduces an error in the opposite direction. In the present paper the entropy of swelling a network of any degree of connectivity, or functionality f, is derived in a manner which avoids these inaccuracies. Corrected relationships are given for the partial molal-free energy of dilution, swelling equilibrium and the influence of deformation on swelling equilibrium. These differ appreciably from those previously given when the degree of interlinking (i.e., concentration of cross linkages if $f=4$) is large and the equilibrium degree of swelling therefore is small. Previous expressions for elastic deformation at constant volume are unaffected.

INTRODUCTION

THE entropy of isotropic swelling of cross-linked network structures calculated several years ago by Rehner and the writer[1] through consideration of the (hypothetical) formation of the network structure from ν-independent linear chain molecules, (represented by —) and $\nu/2$-cross linkages as follows:

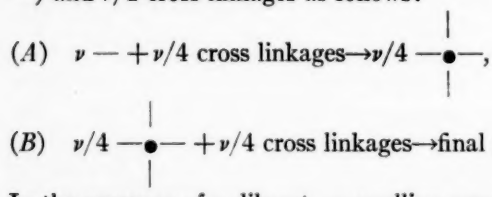

(A) ν — + $\nu/4$ cross linkages→$\nu/4$ —•—,

(B) $\nu/4$ —•— + $\nu/4$ cross linkages→final network.

In the presence of a diluent, or swelling agent, an additional process consisting of dilution of the ν-chains prior to cross linking and designated as "(D)" in the preceding paper,[1,2] must be included. The entropy of swelling, calculated as the difference between the entropies involved in these three processes when carried out in the presence and in the absence of diluent, was given as

$$\Delta S_s = -k[n \ln(1-v_2) + (3/2)\nu(v_2^{-\frac{1}{3}} - 1)] \qquad (1)$$

where v_2 is the volume fraction of polymer in the swollen network and n is the number of molecules of the swelling agent or solvent. Use of the tetrahedral model[3] in this derivation led to the assignment of half of the cross linkages to definite positions in space, a restriction which obviously is artificial and should be expected to cause ΔS_s as given by Eq. (1) to be too low.[4] Kuhn, Pasternak, and Kuhn[5] recently criticized this treatment on the grounds that it neglects the "permutation entropy."[6] The tetrahedral model considers the structure to be comprised of the four-chain elementary units formed in process (A). Equation (1) was derived on the assumption that each such unit may be replaced by an average unit, and that the total entropy is simply the sum of the entropies of each of these unit systems. In the actual network the states of these systems will be subject to fluctuations, and this situation gives rise to an entropy of permutation of the systems which was not taken into account. However, the permutation entropy will be smaller in this model than in those in which the individual chains are taken as the elementary units, or "sub-systems." This term added to Eq. (1) would further increase ΔS_s.

Kuhn, Pasternak, and Kuhn,[5] and also Hermans,[5] have arrived at an expression for the entropy of swelling merely by considering the isotropic dilation of a system of independent chains. Their result may be written

$$\Delta S_s = -k[n \ln(1-v_2) + (3/2)\nu(v_2^{-\frac{1}{3}} - 1) + \nu \ln v_2] \qquad (2)^7$$

where the volume fraction v_2 of polymer in the system may be looked upon as the reciprocal of the "swelling volume."[1] Equation (2) differs from (1) by the inclusion of the last term. Whereas Eq. (1) underestimates the entropy of swelling, it is readily evident that Eq. (2) must lead to values which are too large, for it has been derived on the assumption that the chains are independent elements. In a cross-linked network structure the ends of each set of four chains must meet within the same volume element. This stipulation becomes more severe as the system is diluted and hence must be taken into account in formulating the entropy of swelling.

In this paper a derivation of the entropy of swelling will be given which includes both the entropy arising from fluctuations of the sub-systems (chains) and the non-independence of the chains. A general treatment will be given for a network of any connectivity $f>2$ which represents the functionality of the junctions between chains.

[1] P. J. Flory and J. Rehner, Jr., J. Chem. Phys. **11**, 521 (1943).
[2] Process (C) of the previous papers (see references 1 and 3) is omitted here as it is not required in the calculation of the swelling entropy.
[3] P. J. Flory and J. Rehner, Jr., J. Chem. Phys. **11**, 512 (1943).
[4] This fault of the previous treatment is of consequence only when volume changes are involved; it does not vitiate the calculations (see reference 3) of entropy of elastic deformation at constant volume.
[5] Kuhn, Pasternak, and Kuhn, Helv. Chim. Acta **30**, 1705 (1947). A similar, though less detailed, treatment has been given by J. J. Hermans, Trans. Faraday Soc. **43**, 591 (1947).
[6] W. Kuhn and F. Grün, J. Polymer Sci. **1**, 183 (1946); W. Kuhn and H. Kuhn, Helv. Chim. Acta **29**, 1615, 1634 (1946).
[7] See Eq. (33) of Kuhn, Pasternak, and Kuhn (reference 5).

THE ENTROPY OF SWELLING

Consider the following cycle:

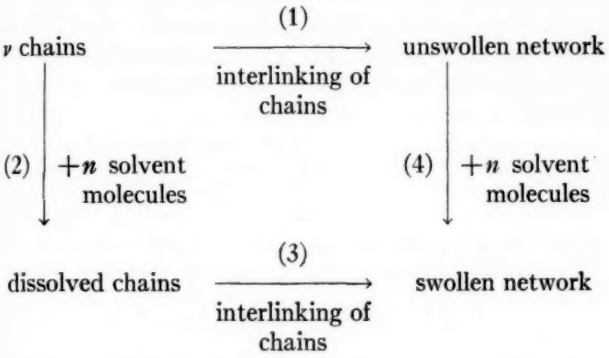

Process (3) differs from process (1) in that the interlinking process occurs in the presence of diluent. We wish to calculate the entropy change associated with process (4), or ΔS_s, which is given by

$$\Delta S_s = S_2 + S_3 - S_1. \tag{3}$$

Interlinking of the chains entails no alteration of the distribution of chain displacement lengths (i.e., the lengths of the vectors leading from beginning to end of each chain). All that is involved in step (1), therefore, is the assemblage of the chain elements in $2\nu/f$ groups of f-ends each. The probability that a given chain-end is surrounded by $f-1$ other chain-ends, each within the proper volume element $\Delta\tau$, can be written

$$[2\nu\Delta\tau/V]^{f-1},$$

where V is the volume of the system. The probability for the second such grouping becomes

$$[(2\nu-f)\Delta\tau/V]^{f-1},$$

and so forth. The probability that all chain-ends are thus disposed in $2\nu/f$ groups is

$$(f\Delta\tau/V)^{2\nu(f-1)/f}[(2\nu/f)!]^{f-1}.$$

Introducing Stirling's approximation and making use of the Boltzmann relation, the entropy change associated with step (1) can be written

$$S_1 = [2k\nu(f-1)/f]\ln(2\nu\Delta\tau/Ve). \tag{4}$$

The entropy change on mixing the ν-chains with n solvent molecules in step (2) is

$$S_2 = -k[n\ln(1-v_2) + \nu\ln v_2]. \tag{5}^{8,9}$$

The distribution of chain displacement lengths is assumed to be undistorted by dilution with solvent.[10]

Process (3) can be accomplished therefore in two steps: dilation of the most probable chain displacement length distribution by the factor $\alpha_s = 1/v_2^{\frac{1}{3}}$, followed by joining of the chain-ends in a fashion analogous to step (1) in order to reproduce an equivalent network structure. The initial chain displacement length distribution is assumed to be Gaussian in accordance with custom. Thus, the number of chains having displacement lengths between r_i and r_i+dr_i can be expressed as

$$\nu_i dr_i = \nu W(r_i) dr_i,$$

where

$$W(r_i) = (\beta/\pi^{\frac{1}{2}})^3 \exp(-\beta^2 r_i^2) 4\pi r_i^2.$$

After dilation by the linear factor α_s

$$\nu_i' dr_i = \nu W(r_i/\alpha_s) dr_i/\alpha_s.$$

The relative number of configurations, or probability of the system in a state specified by the ν_i's, is therefore

$$\Omega = \nu!\Pi\{[W(r_i)]^{\nu_i'}/\nu_i'!\} \cong \Pi[W(r_i)/W(r_i/\alpha_s)]^{\nu_i'}.$$

Taking the logarithm and converting the resulting summation to an integral which can be evaluated after substituting from the above expressions for the quantities involved, there is obtained

$$\ln\Omega = \nu[\ln\alpha_s^3 - 3(\alpha_s^2-1)/2].$$

On multiplying by Boltzmann's constant and replacing α_s^3 with v_2^{-1}, this expression yields the "elastic entropy" S_{el} given by

$$S_{el} = -(3/2)k\nu(v_2^{-\frac{2}{3}}-1) - k\nu\ln v_2. \tag{6}$$

Addition of the entropy of mixing of solvent and *network* (not the separate chains), which is given by the first term of Eq. (5), yields Kuhn's result, Eq. (2), for the entropy of swelling.

To proceed with the evaluation of S_3, we have now to consider the process of joining the ends of chains precisely as in step (1) except that the volume V must be replaced by V' where $V/V' = v_2$. Hence,

$$S_3 = 2k\nu[(f-1)/f]\ln(2\nu\Delta\tau/V'e) + S_{el}. \tag{7}$$

Finally, substituting these various expressions in Eq. (3),

$$\Delta S_s = -k[n\ln(1-v_2) + (3\nu/2)(v_2^{-\frac{2}{3}}-1) + (2\nu/f)\ln v_2] \tag{8}$$

For a tetrafunctionally connected network ($f=4$), this expression reduces to

$$\Delta S_s = -k[n\ln(1-v_2) + (3\nu/2)(v_2^{-\frac{2}{3}}-1) + (\nu/2)\ln v_2], \tag{8.1}$$

which is the mean of Eqs. (1) and (2). As f goes to infinity, Eq. (8) reduces to Eq. (1), which is to be expected according to the nature of the errors introduced in the derivation of the latter.

[8] M. L. Huggins, J. Phys. Chem. **46**, 151 (1942); Ann. N. Y. Acad. Sci. **43**, 1 (1942).

[9] P. J. Flory, J. Chem. Phys. **10**, 51 (1942).

[10] This assumption is somewhat in error if the dilution is so great that the chains do not overlap one another extensively in the solution; see J. Chem. Phys. **17**, 303 (1949). Under these same conditions Eq. (5) also becomes inaccurate; see J. Chem. Phys. **13**, 453 (1945). The errors involved affect ΔS_s in opposite directions, but the latter is likely to be much larger than the former.

If, subsequent to isotropic swelling, the network is elastically deformed without further change in volume, the second term of Eq. (8) must be modified; specifically, $v_2^{-\frac{1}{3}}$ must be multiplied by a factor which depends on the macroscopic deformation. If this deformation is an elongation by a factor α expressing the ratio of the stretched-swollen length to the unstretched-swollen length, the entropy of swelling and subsequent deformation is

$$\Delta S_{s,d} = -k\{n\ln(1-v_2)+(3\nu/2) \times[v_2^{-\frac{1}{3}}(\alpha^2+2/\alpha)/3-1]+(2\nu/f)\ln v_2\}. \quad (9)^{11}$$

PARTIAL MOLAL FREE ENERGY OF DILUTION AND SWELLING EQUILIBRIUM

A heat of mixing of the van Laar form will be used in accordance with current custom. Then

$$\Delta H_s = \mu kTn v_2, \quad (10)$$

where $\mu = BV_1/RT$; V_1 is the molar volume of the solvent and B is a parameter characteristic of the polymer-solvent pair. The partial molal-free energy of dilution for the elastically undeformed ($\alpha=1$) network obtained by differentiating Eqs. (8) and (10) is then

$$\Delta\bar{F}_1 = RT[\ln(1-v_2)+v_2(1-2/Zf)+v_2^{\frac{1}{3}}/Z+\mu v_2^2] \quad (11)$$

where Z represents the ratio of the volume of a chain to the volume of a solvent molecule, i.e., $v_2 = Z\nu/(n+Z\nu)$. Equation (11) supersedes Eq. (8) of reference (1); Z of course may be replaced by $M_c/\rho V_1$, ρ being the density of the polymer and M_c the molecular weight per chain. Equation (11) differs from the previous equation in that it contains the additional term $-2v_2/Zf$. At equilibrium between swollen network and pure solvent $\Delta\bar{F}_1=0$, giving

$$Z = -(v_2^{\frac{1}{3}}-2v_2/f)/[\ln(1-v_2)+v_2+\mu v_2^2], \quad (12)^{12}$$

where v_2 represents the reciprocal of the equilibrium swelling volume ratio. Series expansion converts this relationship between the equilibrium swelling volume and the degree of interlinking, as embodied in Z, to

$$Z = \frac{v_2^{\frac{1}{3}}(1-2v_2^{\frac{1}{3}}/f)}{v_2^2[(\frac{1}{2}-\mu)+v_2/3+v_2^2/4+\cdots]}, \quad (12.1)$$

which can be approximated for large swelling volumes with

$$Z \cong 2/(1-2\mu)v_2^{5/3} \quad (12.2)$$

or

$$v_2 \cong [2/Z(1-2\mu)]^{3/5}. \quad (13)$$

These approximate equations are identical to Eqs. (12) and (13) of reference (1), but the degree of approximation generally is somewhat greater than was indicated by the previous theory. Equations (12.2) and (13) become increasingly inaccurate as the degree of swelling ($1/v_2$) decreases.

[11] Equation (9) replaces Eq. (17) of reference 1.
[12] Compare Eq. (11) of reference 1.

The revised relationship between the equilibrium force of retraction τ for the stretched, *unswollen* network and the equilibrium swelling volume in the absence of elastic deformation, which is obtained by eliminating $M_c(=Z\rho V_1)$ from Eq. (12) and the theoretical stress-strain relationship of rubber elasticity theory, may be written[13]

$$\tau = -(RT/V_1)(\alpha^2-1/\alpha)\left[\frac{\ln(1-v_2)+v_2+\mu v_2^2}{v_2^{\frac{1}{3}}-2v_2/f}\right] \quad (14)$$

where τ is expressed in force per unit initial cross section. To the same approximation introduced above,

$$\tau \cong (RT/V_1)(\alpha^2-1/\alpha)(1-2\mu)v_2^{5/3}/2, \quad (14.1)$$

which is identical with Eq. (24) of reference 13. Equation (14) provides a most useful means for arriving at a value of μ from measurements of equilibrium swelling volume and of equilibrium force of retraction.[14]

INFLUENCE OF DEFORMATION ON SWELLING EQUILIBRIUM

The influence of elastic deformation at fixed length on the swelling capacity[15] of the network structure may be deduced by equating to zero the partial molal-free energy obtained from Eqs. (9) and (10) subject to the condition that $\alpha' = \alpha/v_2^{\frac{1}{3}}$ is constant. This partial molal-free energy is

$$\Delta\bar{F}_1(\alpha' \text{ const.}) = RT[\ln(1-v_2)+v_2(1-2/Zf) +1/\alpha' Z+\mu v_2^2]=0. \quad (15)^{16}$$

On equating to zero and introducing the approximations used above

$$v_2 \cong [2/\alpha' Z(1-2\mu)]^{\frac{1}{3}}. \quad (16)$$

Hence, the swelling volume ratio ($1/v_2$) at constant length should increase approximately as the square root of the length, as previously reported.[15]

The theoretically predicted influence of swelling on elastic properties[1,17] is unaltered by the present revision.

NETWORKS FORMED IN THE PRESENCE OF A DILUENT

We have assumed that the actual formation of the network structure takes place in an undiluted polymer system, the chains or molecules involved being in random configurations. If the network is formed in the presence of a diluent, the elastically relaxed state will no longer correspond to the polymer at $v_2=1$, but to the

[13] P. J. Flory, Chem. Rev. **35**, 51 (1944).
[14] Flory, Rabjohn, and Shaffer, J. Polymer Sci. **4**, 225 (1949). J. R. Schaefgen and P. J. Flory, J. Am. Chem. Soc. (in press).
[15] P. J. Flory and J. Rehner, Jr., J. Chem. Phys. **12**, 412 (1944). The influence of a generalized homogeneous strain of any type on swelling has been treated recently by Treloar, "Royal Society discussion on Physical and Chemical Properties of Hydrocarbon Gels," (in press). The author is indebted to Dr. Treloar for furnishing a copy of his manuscript in advance of publication.
[16] Compare Eq. (2) of reference 15.
[17] H. M. James and E. Guth, J. Chem. Phys. **11**, 455 (1943).

semi-swollen polymer containing a proportion of diluent equal to that present at the time of formation of the network structure. The above derivation is easily modified to take into account dilution to a volume fraction v_2^0 of polymer at formation of the network. The resulting modification is the same as was found by Hermans[5] in connection with his derivation of Eq. (2). The partial molal-free energy according to the present theory is given as

$$\Delta\bar{F}_1 = RT[\ln(1-v_2)+v_2(1-2/Zf) + (v_2^0)^{\frac{1}{3}}v_2^{\frac{1}{3}}/Z+\mu v_2^2] \quad (17)$$

which reduces to Eq. (11) for $v_2^0=1$. The separation of the chains with diluent present during the interlinking process will encourage the formation of "intramolecular" connections which do not contribute to the elastic retraction of the network structure.[1] The ν occurring in Eqs. (8) and (9) should refer therefore to the effective number of chains in the network, appropriately corrected for intramolecularly wasted cross linkages.

IMPERFECT NETWORK STRUCTURES

Actual polymer networks invariably will possess imperfections in the form of unattached ends of molecules. In terms of the cycle employed in the primary derivation given in this paper, the number of interlinkages will be insufficient to combine with all chain ends. If the number of f-functional linkages is $2\nu_0/f$ and the number of pairs of unattached ends of chains is ν', the total number of chains is $\nu_0+\nu'$. The ratio ν'/ν_0 is then an index of the degree of imperfection of the network structure. When ν'/ν_0 is not negligible, a revision of the previous treatment is in order as follows.

It is easily shown that under these circumstances

$$S_3-S_1=2k\nu_0[(f-1)/f]\ln v_2+S_{el}.$$

The ν occurring in Eq. (6) for S_{el} must be replaced by the elastically effective number ν_e of chains, which can be deduced by a generalization of the previous derivation[13] of the effective number of network elements in an imperfect cross-linked system. For this purpose it is convenient to consider the formation of the network from the separate $\nu_0+\nu'$-chains to take place in two steps. In the first step let these chains be combined into ν'-linear molecules through the introduction of ν_0-bifunctional connections between chain-ends. The network will then be formed by introducing $2\nu_0/f$ interlinkages each of which binds together $2/f$ of the linear molecules. The effective number of these interlinkages, in accordance with the previous deduction, is taken to be equal to the number of them in excess of the minimum number $\nu'/(f/2-1)$ required to join the linear molecules into a single structure. Hence

$$\begin{aligned}\nu_e &= (f/2)[2\nu_0/f-\nu'/(f/2-1)] \\ &= \nu_0[1-(\nu'/\nu_0)f/(f-2)],\end{aligned} \quad (18)$$

which must replace ν in Eq. (6). Any network must contain a number of interlinkages in excess of that required to combine all of the chains in a continuous structure. The number of chains being $\nu_0+\nu'$ and the number of f-functional linkages $2\nu_0/f$, it follows that

$$(2\nu_0/f)(f-1)>(\nu_0+\nu')$$

or

$$(\nu'/\nu_0)<(f-2)/f.$$

Hence, the factor in brackets in Eq. (18) will always exceed zero.

Finally, ν of Eq. (5) for the entropy of mixing with solvent molecules is to be replaced by the total number of chains $\nu_0+\nu'$. Making these substitutions,

$$\Delta S_s = -k[n\ln(1-v_2)+(3\nu_e/2)(v_2^{-\frac{1}{3}}-1) + (2\nu_e/f)\ln v_2] \quad (8.2)$$

which is identical with Eq. (8) except for the substitution of ν_e for ν, where ν_e is defined by Eq. (18). It should be noted that $\nu'/\nu_0=M_c/M$ where M is the "primary molecular weight," or molecular weight of the system composed of ν' linear molecules, and M_c is the molecular weight per interlinked unit in the network formed from these molecules.[13] The expression for ν_e then assumes the form

$$\nu_e=\nu_0[1-(M_c/M)f/(f-2)] \quad (18.1)$$

which is analogous to that previously given for cross-linked systems.

CONCLUSIONS

The above treatment of the interaction of solvent with a network polymer is believed to be accurate within the limits of current theories of polymer solutions and rubber-like elasticity. Inaccuracies in these theories must be expected to limit the quantitative validity of the relationships given above. Further refinements are to be expected only through improvements in these basic theories, particularly in the treatment of the mixing of polymer with solvent in the moderately dilute range.

Note on the Influence of Structure on Internal Pressure in Polymeric Systems

PAUL J. FLORY
Department of Chemistry, Cornell University, Ithaca, New York
(Received May 18, 1949)

The development of the preceding paper is applied to the calculation of the internal pressure contribution arising from the nature of the polymer structure. A network structure imposes a positive (compressive) internal pressure which increases with the degree of interlinking. In polymers composed of finite molecules the internal pressure should, of course, decrease in proportion to the reciprocal of the molecular weight. A general formula for the dependence of the internal pressure on polymer structure is given which embraces both of these extreme cases and includes also imperfect network structures possessing unattached terminal groups. Magnitudes of the calculated internal pressure contributions are sufficient to alter the specific volumes perceptibly.

THE treatment given in the preceding paper[1] may be adapted at once to the calculation of the internal pressure in polymeric systems, and its dependence on the constitution of the polymer. To this end the previous cycle of four steps may be reconsidered, omitting the solvent molecules. Processes (1) and (3) are to be carried out at volumes of the system V^0 and V, respectively, where V^0 is the volume at which the actual network was formed and V is some other volume. V^0/V will replace v_2 in the formulas of the preceding paper. No solvent being present, the first term of Eq. (5)[1] for S_2 is to be omitted since it arises from mixing of the two components; the second term, representing a gas-like entropy of ν-particles distributed at random in space, is to be retained. With these revisions, the entropy corresponding to ΔS_s given by Eqs. (8) or (8.2) is replaced by

$$\Delta S=-k\nu_e\{3[(V/V^0)^{\frac{1}{3}}-1]/2-(2/f)\ln(V/V^0)\} \quad (19)$$

which represents the configurational entropy associated with change in volume from V^0 to V, the network having been formed from chains of random configurations in the volume V^0.

The contribution of the polymer structure to the internal pressure, given by $-T(\partial\Delta S/\partial V)_T$, is

$$P_i=RT(\nu_e/V^0)[(V^0/V)^{\frac{1}{3}}-(2/f)(V^0/V)] \quad (20)$$

where ν_e is expressed in moles rather than in numbers as above. The network structure ($f>2$) exerts a positive (compressive) pressure for all values of V such that

$$(V/V^0)>(2/f)^{\frac{3}{2}}.$$

Unless the network was formed in the presence of a diluent, this condition necessarily will be fulfilled. If the network is formed in the presence of a diluent which is subsequently removed, V^0 may exceed V at the same temperature and pressure by a factor depending on the dilution. The internal pressure for such a network will be diminished and may in fact be negative if the above condition is not fulfilled.

The internal pressures in structures formed in the absence of diluent and maintained at or near the same volume would seem to be of primary interest, and the remainder of this communication will be concerned with this case. Letting $V=V^0$

$$P_i=(RT\nu_e/V^0)(f-2)/f \quad (21)$$

or, substituting from Eq. (18) for ν_e

$$P_i=(RT\nu_0/V^0)[(f-2)/f-\nu'/\nu^0]. \quad (21.1)$$

Recalling that (ν'/ν^0) must be less than $(f-2)/f$ for any network structure,[1] P_i is seen to be positive for any functionality $f>2$ when $V=V^0$. Uncombined ends of chains ("flaws") in the network, represented by ν', decrease P_i as is to be expected.

These relationships may also be applied to linear systems. If $f=2$, corresponding to the combination of the chains into ν'-linear species, Eq. (21.1) reduces to

$$P_i=-RT\nu'/V^0.$$

If the linear molecules are infinite in length, $\nu'=0$ and the internal pressure is zero. The internal pressure for linear polymers is obtained in a more direct fashion by setting $f=1$. Then steps (1) and (3) vanish from the cycle used in the derivation of Eq. (19); only the second term of Eq. (5) enters. According to Eq. (21) or (21.1)

$$P_i=-RT\nu/V^0 \quad (21.2)$$

where ν has been written for $\nu_e=\nu_0+\nu'$, the basis for differentiation between ν_0 and ν' having vanished. The same relationship should apply to non-linear polymers in which no network structure is formed; ν will then refer to the number of molecules.

For high degrees of interlinking the internal pressure may become appreciable. If $\nu/V=10^{-3}$ cc^{-1}, and $f=4$, for example, $P_i=12$ atmospheres at $T=300$°K. The corresponding change $\Delta\bar{v}$ in the specific volume $\bar{v}=\rho^{-1}$ is given by

$$\Delta\bar{v}=-\rho^{-1}\kappa P_i$$
$$=-\kappa(RT/M_c)[(f-2)/f-M_c/M] \quad (22)$$

where M_c is the molecular weight per interlinked unit of the network as defined in the preceding paper,[1] M is the "primary" molecular weight, $M_c/M=\nu'/\nu_0$, and κ is the compressibility. Disregarding the correction for net-

[1] P. J. Flory, J. Chem. Phys. 108, (1950).

work imperfections,

$$\Delta\bar{v} = -(\kappa RT/M_c)(1-2/f) \qquad (22.1)$$

where M_c is equal to the molecular weight per chain. If $f=1$, M_c represents the molecular weight of the polymer. Taking $\kappa \sim 10^{-4}$ atmos.$^{-1}$, an M_c of 10^3 leads to volume changes of the order of 10^{-3} as compared to the infinite linear polymer. For finite linear (or finite non-linear) molecules $\Delta\bar{v}$ is positive; for network structures ($f>2$), it is negative and depends according to Eq. (22) not only on the degree of interlinking (ν_0 or $1/M_c$) but also on the proportion of free ends of chains (ν' or $1/M$).

The above relationships cannot be expected to account for the entire dependence of the specific volume on molecular weight in the case of linear (or non-network) polymers, or on the network structure in the case of infinite networks. Other factors, such as the abnormal volume occupied by terminal groups or by the interlinking groups, may outweigh the effect of the change in internal pressure.

The theoretical relationships of the preceding paper expressing the influence of expansion of the network structure on the activity of the solvent mixed with the network may, of course, be derived by considering the alterations in the activity brought about by the internal pressure of the network acting on the solvent. The two procedures obviously are fully equivalent.

THE JOURNAL OF CHEMICAL PHYSICS VOLUME 18, NUMBER 1 JANUARY, 1950

Ultrasonic Measurements in Metallic Beryllium at Low Temperatures*

W. C. Overton, Jr.**
The Rice Institute, Houston, Texas
(Received June 9, 1949)

Using the ultrasonic pulse method, the velocity of longitudinal waves in metallic beryllium has been measured from 300°K to 23°K, and transverse waves from 300°K to 3°K. The adiabatic moduli and compressibility have been computed from the velocities. A new technique for affixing the quartz transducer to the solid for ultrasonic measurements, in suitable solids, below 100°K, has been successfully employed for the measurements in beryllium.

INTRODUCTION

THE ultrasonic pulse method described by Pellam and Squire[1] for sound ranging in liquid helium and by Huntington[2] for velocity measurements in solids has been applied to measure the longitudinal and transverse velocities of 10 Mc/sec. sound pulses in metallic beryllium. The usual technique is to apply the electrical pulse from a transmitter to a quartz crystal which is rigidly affixed to the solid sample. The quartz transducer then generates a sound pulse which is propagated through the material, reflects from the surface opposite the quartz and then returns to produce an echo. Direct measurements are made on the echoes of the pulses displayed on an oscilloscope such as the DuMont A/R 256-D. The velocities are determined from the round trip distance traveled by the sound pulse and the timing of the corresponding echoes.

The selection of beryllium as the initial material of a series of proposed echo ranging experiments was guided by several factors, one of which was to develop a material for affixing the quartz crystal to the solid that would hold at low temperatures. These compounds and techniques of application could then be used in the measurements on the more fragile materials which might be damaged by thermal contraction at the low temperatures. In addition beryllium has certain interesting properties. Simon and Critescu[3] have observed a hump in the specific heat between 10°K and 14°K. Although the specific heat is small in that range, the hump is about twice the value one would obtain if an extrapolation, according to the Debye T^3 law, were made from about 18°K to 0°K. Simon and Critescu attribute the hump to electronic causes; however Squire[4] has measured the resistivity of beryllium and observed no anomaly in the 10 to 14°K region. The resistivity curve in itself is peculiar in that it does not approach zero near the absolute zero, as do most ordinary metals, but levels off to about three-tenths of the room temperature value. Because of the specific heat hump one might expect a slight change in the ultrasonic attenuation[1] and possibly a measurable change in the velocity.

The difficulties in making ultrasonic measurements in solids at low temperatures are mainly due to the different thermal contraction rates of the quartz crystal and the solid. The organic film used as a cement to hold the quartz and solid together must provide a continuous sound transmission path. Organic materials such as stopcock grease, salol, natural rubber with Vaseline and

* This work has been supported by the ONR, Navy Contract N6onr-224.
** This paper represents a portion of a thesis submitted to the Rice Institute Faculty in partial fulfillment for the M.A. degree.
[1] J. R. Pellam and C. F. Squire, Phys. Rev. **71**, 477 (1947).
[2] H. B. Huntington, Phys. Rev. **72**, 321 (1947).
[3] F. Simon and S. Critescu, Zeits. f. physik. Chemie Ab.B. **25-26**, 276 (1934).
[4] C. F. Squire, M.I.T. Research Laboratory of Electronics, Quarterly Progress Report (April 15, 1947), p. 22.

TABLE I.

Temp. °K	Longitudinal velocity $V_l \times 10^{-3}$ meters/sec.	Percent error	Temp. °K	Transverse velocity $V_t \times 10^{-3}$ meters/sec.	Percent error
300	12.55	±0.2	300	8.83	±0.3
280	12.56	±0.2	280	8.84	±0.3
260	12.59	±0.3	260	8.86	±0.3
240	12.63	±0.3	240	8.88	±0.3
220	12.65	±0.3	220	8.89	±0.3
200	12.65	±0.3	200	8.89	±0.3
180	12.65	±0.3	180	8.90	±0.3
160	12.66	±0.3	160	8.90	±0.3
140	12.66	±0.3	140	8.90	±0.3
120	12.66	±0.3	120	8.90	±0.3
100	12.66	±0.3	100	8.90	±0.3
80	12.66	±0.2	80	8.90	±0.3
60	12.66	−0.4±0.1	60	8.90	−0.4±0.1
40	12.66	−0.3±0.1	40	8.90	−0.3±0.1
23	12.66	±0.2	20	8.90	−0.3±0.1
			3	8.90	±0.3

others have worked with varying success in the relatively high temperature regions. These materials may work very well even as low as 80°K, but the differential contraction usually sets in strains sufficient to cause the quartz to break away from the solid or to fracture the solid if measurements are made in a fragile material such as an alkali halide crystal. Galt[5] encountered this difficulty in his measurements on KBr.

By using a mixture of ether, isopentane and ethyl alcohol (EPA)[6] in amounts by volume of 5–6–2, as a cement, it has been possible to obtain measurements in beryllium as low as 3°K. The technique is to apply a liquid film of the EPA after the sample has already been cooled to about 120°K and has already undergone a considerable amount of its thermal contraction. For the ultrasonic measurements in beryllium the additional thermal contraction that takes place between 100°K, where the EPA begins to solidify, and the liquid helium range did not set in sufficient strains to break the quartz-to-solid bind. However the EPA cement is not suitable for all materials, for measurements in pure metallic tin were unsuccessful below 40°K due to the quartz breaking away from the solid at that temperature.

VELOCITY MEASUREMENTS

In the first longitudinal velocity measurements, an ordinary stopcock grease cement was applied as a very thin layer between the quartz crystal and the beryllium specimen. This worked very well down to about 130°K, but the thermal contraction between the quartz and the specimen caused the bind to break so that sharp echoes could not be obtained. Using the EPA mixture the longitudinal velocities could be measured from the very low temperatures to 250°K. This mixture served as a liquid transmission medium from 100°K to 250°K and as a solid cement below 100°K. There is less chance of the quartz-to-solid bind breaking in the low temperature range if the selected solid material undergoes the major portion of its thermal contraction before the low melting point cement is applied.

A comparison of the longitudinal velocities in beryllium above 130°K using the liquid EPA against the values obtained using stopcock grease cement indicated no measurable difference. The transverse velocities were measured using stopcock grease which worked satisfactorily down to 112°K, and using solid EPA from 100°K to 3°K.

To obtain the longitudinal velocities a time average was taken over eight echoes in the 100 microsecond sweep range of the DuMont oscilloscope. For the transverse velocities an average was taken over five echoes. The accuracy of measurement on the leading edge of any echo was ±0.03 microseconds or better. However there was distortion of some of the echoes caused by reflections from the walls of the beryllium sample and by multiple reflections in the thin cement film or transmission medium between the quartz and the sample. This distortion reduced the desirable over-all accuracy considerably and the various factors caused the over-all error to vary with the temperature. A small amount of error may occur in calibrating the oscilloscope but this can be partly corrected by making a calibration correction curve and by using a consistent technique of measurement.

In making the velocity measurements at low temperature the beryllium specimen was properly adjusted in its carrier and surrounded by an external container. After an initial cooling by liquid air to about 120°K, a liquid EPA film was placed on the solid and the quartz crystal and contact arrangement were properly adjusted. The apparatus was then cooled to about 100°K and then transferred to the experimental chamber of the Rice Institute Collin's type helium cryostat. The cryostat cooling could be stopped at any desired temperature below 100°K and careful measurements could be made after the beryllium sample came to equilibrium with the surrounding helium. Since the EPA cement held down to

TABLE II.

Temp. °K	Shear modulus $\mu \times 10^{-12}$ dyne/cm²	Compressibility $K_s \times 10^{12}$ cm²/dyne
300	1.41	1.03
280	1.42	1.02
260	1.43	1.02
240	1.44	1.01
220	1.44	1.00
200	1.44	1.00
180	1.44	1.00
160	1.45	1.00
140	1.45	0.099
120	1.45	0.099
100	1.45	0.099
80	1.45	0.099
60	1.45	0.099
40	1.45	0.099
23	1.45	0.099

[5] J. K. Galt, Phys. Rev. **73**, 1460 (1948).

[6] G. N. Lewis and M. Kasha, J. Am. Chem. Soc. **66**, 2100 (1944). The writer wishes to express his gratitude to Dr. E. S. Lewis of the Rice Institute Chemistry Department for suggesting this material.

the very low temperatures, further careful measurements could be obtained during the very slow warm-up period of the cryostat. Temperatures were measured with vapor pressure and constant volume thermometers. The thermometer bulbs were placed next to the beryllium sample. The longitudinal and transverse velocities are given in Table I.

By considering the $\frac{3}{4}$-in. quartz crystal as a vibrating piston in a plane wall and following the analyis due to Morse,[7] the approximate intensity distributions in the longitudinal and transverse sound beams have been obtained. The computed angular width of 3.6° between the half-intesnsity points of the longitudinal beam accounts for pulse distortion only after the second echo. In the transverse case, a 3° beam width introduced pulse distortion after the third echo. In both cases, however, the intensities of the second echoes were very small because of effects apparently due to flaws in the beryllium sample. Because of this only a qualitative measure of the ultrasonic attenuation could be obtained. Nevertheless, any appreciable change in attenuation would manifest itself in a noticeable change in the relative amplitudes of the echoes. No such change in attentuation was observed in the region of the specific heat hump of beryllium between 10°K and 14°K.

ELASTIC MODULI

The adiabatic elastic moduli and compressibility are computed directly from the measured velocities. The longitudinal waves are propagated with a velocity $[1/\rho(1/K_s+4\mu/3)]^{\frac{1}{2}}$ where K_s is the adiabatic compressibility and μ is the shear modulus. The transverse waves are propagated with a velocity $(\mu/\rho)^{\frac{1}{2}}$. The length of the beryllium sample was assumed to vary with the temperature according to the linear coefficient of expansion down to 80°K. In the low temperature range below 80°K an extrapolation of the length was made assuming that the coefficient of expansion became zero at 0°K according to the Nernst thermodynamic theory. The density ρ was corrected on the basis of this extrapolation. Although some small error is introduced by this approximation, it is considerably less than the experimental error in the velocity measurements. The shear modulus and adiabatic compressibility are given in Table II. Since these quantities involve the squares of the velocities, the uncertainty in their values is at least twice as great as the velocity errors in Table I.

The Poisson's ratio was computed from

$$\sigma=\frac{(v_l/v_t)^2-2}{2(v_l/v_t)^2-2}.$$

The value came out to be extremely small because of the relatively high transverse velocity. The value over the whole temperature range was only 0.01 ± 1.0 percent, and the variation from 23°K to 300°K was 2 percent of the value.

CONCLUSIONS

The velocity measurements in beryllium are interesting because of the high longitudinal velocity of 12,600 meters per second. Only a few materials propagate a sound velocity higher than beryllium. The velocity in diamond has been computed from the elastic constants to be about 16,000 meters per second although we believe no direct measurements have been published.

The inaccuracies caused by pulse distortion suggest measurements at a frequency higher than 10 Mc/sec. so as to obtain a narrower sound beam and to reduce wall reflection effects that cause the pulse distortion.

The adiabatic compressibility values are accurate to 1 percent or better. Knowledge of the grain structure of the particular beryllium sample used was not available but the assumption of isotropy does not appear unreasonable in view of Roth's[8] findings that there is negligible velocity dependence on the grain structure. Nevertheless the adiabatic compressibility value at 300°K in Table II is 15 percent higher than the isothermal value of 8.85×10^{-13} cm²/dyne, measured by Bridgman[9] at 30°C. Bridgman's specimen may not have been as pure as the 99.2 percent purity beryllium used in the present experiments for he states that in his sample there were occlusions of the salt from which the sample had been formed. However the 15 percent difference warrants further investigation, perhaps on a different frequency and with different samples.

There was no noticeable change in the attenuation or velocity in the region of the specific heat hump between 10°K and 14°K. We may conclude that, if the specific heat hump is caused by lattice changes, then such changes must leave the velocity of sound unaffected to within the error of our measurements (1 percent). On the other hand, if the specific heat hump is caused by electronic transitions, then the attenuation of sound must be unaffected by such effects.

ACKNOWLEDGMENTS

The writer wishes to express his thanks to Professor C. F. Squire, who suggested the problem and under whose direction this research was carried out. He also wishes to express his gratitude to the several members of the Rice Institute Low Temperature Physics Laboratory who were very helpful during the experiments. He especially wishes to thank Professor W. V. Houston for his interest in the problem and for many helpful discussions.

[7] P. M. Morse, *Vibration and Sound* (McGraw-Hill Book Company, Inc., New York, 1948), p. 326.

[8] W. Roth, J. App. Phys. **19**, No. 10 (1948).

[9] P. W. Bridgman, Proc. Am. Acad. **62**, 207 (1927).

Raman Spectrum of Liquid Ethylene and Methane*

D. H. RANK, E. R. SHULL, AND D. W. E. AXFORD
Spectroscopy Laboratory, School of Chemistry and Physics, The Pennsylvania State College, State College, Pennsylvania
(Received June 13, 1949)

A search was made for the missing frequencies in the Raman spectrum of liquid methane. $\nu_2(e)$ was found and the harmonic of $\nu_4(f_2)$. Intense plates were obtained of the Raman spectrum of liquid ethylene. The polarizations of the lines in this spectrum were obtained. ω_6, the only missing Raman active fundamental, was found in the position predicted by Arnett and Crawford.

AMONG the first polyatomic molecules investigated in both the gas and the liquid states by means of the Raman effect were the very simple organic molecules methane and ethylene.

The experimental work of Dickinson, Dillon, and Rasetti[1] on these two gases would be hard to improve upon to any appreciable extent. The frequencies observed by the above-mentioned authors for methane have been checked quantitatively by MacWood and Urey[2] in the course of their investigations of the deutero methanes. Bhagavantam[3] has measured the degree of polarization of the strongest Raman lines of gaseous ethylene and found three highly polarized lines which is in agreement with theoretical predictions.

Liquid methane has been investigated by McLennan, Smith, and Wilhelm[4] and by Daure,[5] using very small dispersion. Liquid ethylene has been investigated most recently by Glockler and Renfrew[6] under good dispersion.

Herzberg[7] has summed up the state of affairs and given the analysis of the vibrational spectrum of methane and ethylene. The Raman spectrum of methane is quite incomplete since only two of the four theoretically allowed fundamental frequencies have been observed directly in the Raman effect. In addition, measurements made under good dispersion would show whether an appreciable frequency shift occurs between liquid and gas for the high frequencies.† While the investigation of the methane spectrum was in progress, one of us (D.H.R.) received a private communication from Dr. Jules Duchesne of the Institut D'Astrophysique, Université de Liége, Belgium, suggesting that certain aspects of the vibrational analysis of ethylene might be wrong and suggesting further work on the Raman spectrum of this molecule. It was decided that the depolarizations of certain lines in the spectrum might clear up some of the doubtful points. We obtained the polarizations of all but the two weakest lines in the spectrum of ethylene and the polarizations agreed with those predicted by Herzberg[7] in all cases.

Upon completion of the work mentioned above, a preliminary report on the preceding paper by Arnett and Crawford came to our attention through private communication.‡ This completely new assignment based on very sound new experimental evidence required the depolarizations of the two weakest lines to settle some doubtful points in the analysis. Furthermore, Arnett and Crawford predicted ω_6 the only Raman active frequency which had not been experimentally observed, to occur at 1236 cm^{-1}. As a result of the Arnett and Crawford communication, we repeated our experimental determinations, obtaining very much stronger plates.

EXPERIMENTAL

Excitation of the Raman spectrum of ethylene was accomplished by means of the low temperature apparatus described previously.[8] The apparatus was suitably modified so as to use liquid air directly for cooling the methane. The temperature of the sample was controlled by means of a jacket on the scattering tube which could be made heat-conducting or isolated at will by evacuation. Polarization measurements were made using the method of polarized incident light described previously.[9] Three cameras were available for use with the spectrograph, $F=2$, $F=4$, and $F=8$. The dispersion produced by the $F=8$ camera was 19A/mm at λ4600. Exposure times varied from 15 min. with the $F=2$ camera to 8 hr. with the $F=8$ camera. The spectrum of methane was photographed with all three cameras. Suitable filters were used with the $F=2$

* This research was carried out on Contract N6onr-269, Task Order V of the ONR.

[1] Dickinson, Dillon, and Rasetti, Phys. Rev. **34**, 582 (1929).

[2] G. E. MacWood and H. C. Urey, J. Chem. Phys. **4**, 402 (1936).

[3] S. Bhagavantam, Nature **138**, 1096 (1936).

[4] McLennan, Smith, and Wilhelm, Trans. Roy. Soc. Can. **23**, 279 (1929).

[5] P. Daure, Comptes Rendus **188**, 61, 1492 (1929).

[6] G. Glockler and M. M. Renfrew, J. Chem. Phys. **6**, 170, 410 (1938).

[7] G. Herzberg, *Infra-Red and Raman Spectra of Polyatomic Molecules* (D. Van Nostrand Company, Inc., New York, 1945), pp. 306, 325.

† The material given in this paper was reported at the Washington Meeting of the American Physical Society by D. H. Rank [Phys. Rev. **76**, 161 (1949)]. In the discussion Mr. J. Harrold reported he had also investigated liquid methane confirming our findings. He stated that he had obtained more intense spectra than those obtained in the present work with a consequent increase in spectroscopic information. We are awaiting the publication of his paper for further details.

‡ Raymond L. Arnett and Bryce L. Crawford, Jr., "The vibrational frequencies of ethylene," ONR Technical Report (March 1, 1949), Contract N5ori-147, Task Order II.

[8] Szasz, Sheppard, and Rank, J. Chem. Phys. **16**, 704 (1948).

[9] A. E. Douglas and D. H. Rank, J. Opt. Soc. Am. **38**, 281 (1948).

camera to make certain of the origin of the lines observed. The polarization measurements were made with the $F=2$ camera.

Since a search was to be made for very weak lines in the methane spectrum, it was necessary to make use of a very pure sample. The methane was obtained from sewer gas (anaerobic fermentation) which process is known to produce only products which are easily removed by simple treatment, leaving pure methane. After treatment, the infra-red spectrum of the gases used did not show the slightest trace of any impurity.

The intensity of the spectra of methane was such that the 2904-cm^{-1} frequency shift was observed excited by λ4358, λ4047, λ4078, and λ3984 of Hg. The strongest line in the ethylene spectrum was excited by λ3906 in addition to the exciting lines mentioned above.

Results obtained are summarized in Tables I and II. The frequency measurements should be accurate to ±3 cm^{-1} or better.

ETHYLENE

The measurements of Glockler and Renfrew[6] show clearly that the high frequency lines in the spectrum of liquid ethylene are shifted to lower frequencies by 10 cm^{-1} when compared to measurements made on the spectrum of the gas. The line at 3075 cm^{-1} which appears only in the liquid, has been ascribed by the above-mentioned authors to a forbidden transition caused by a breakdown of the selection rules by virtue of complications introduced by the liquid state.

The results obtained on the Raman spectrum of liquid ethylene are summarized in Table II. When the values of the frequency shifts in the gas are known, the gas values are quoted in Table II. The frequency assignment compiled by Herzberg[7] is included for comparison purposes. The work of Arnett and Crawford in "observing" the torsional frequency ω_4 by virtue of the isotopic ethylenes, and the assignments directly following from the torsional assignment plus prediction of ω_6 and subsequent observation of this frequency by us, completely verifies their assignment in all major details.

The 3075-cm^{-1} frequency shift, which definitely and unequivocally appears only in the liquid in the Raman spectrum, in our opinion should be assigned to ω_9 as quoted by Herzberg.[7] The polarizations of 3272-cm^{-1} and 3240-cm^{-1} frequency shifts also seem to indicate the correctness of the previous assignments of these frequencies to ω_5 and $2\omega_2$, respectively, especially since an alternative assignment would yield incorrect polarization for one of these frequencies.

The assignments given in Table II in the column marked R.S.A. seem to be in complete agreement with all the experimental data now available on the vibrational spectra of the ethylene molecule. A quite convincing argument for this assignment arises from the finding of the last remaining unobserved Raman active fundamental 1236-cm^{-1} ω_6 at the position predicted by Crawford and Arnett.

TABLE I. The Raman spectrum of liquid and gaseous methane.

Liquid	Methane Gas[a]	Designation
1513		
1529 v.w.		$v_2(e)$
1547		
2570 w.		$2v_4(f_2)$
2904 v.s.	2914.8	$v_1(a_1)$
3011 s.	3022.1	$v_3(f_2)$
3052 s.	3071.5	$2v_2(e)$

[a] Measurements taken from reference 1.

TABLE II. Vibrational frequencies of ethylene.

Frequency	Species	Herzberg[a]	R.S.A.	Activity	Pol.[b]	Raman[c]
ω_1	A_{1g}	3019.3	3019.3	R	P	G.L.
ω_2	A_{1g}	1623.3	1623.3	R	P	G.L.
ω_3	A_{1g}	1342.4	1342.4	R	P	G.L.
ω_4	A_{1u}	825	1027*	In		
ω_5	B_{1g}	3272.3	3272.3	R	Dep.	G.L.
ω_6	B_{1g}	1050	1236*	R	Dep.?	L.
ω_7	B_{1u}	949.2	949.2	I		
ω_8	B_{2g}	943	943	R	Dep.	L.
ω_9	B_{2u}	3105†	3105†	I		
ω_{10}	B_{2u}	995	810.3	I		
ω_{11}	B_{3u}	2989.5	2989.5	I		
ω_{12}	B_{3u}	1443.5	1443.5	I		
$2\omega_{10}$	A_g	$2\omega_4$	1656	R	P	G.L.
$2\omega_2$	A_g	3240.0	3240.0	R	P	G.L.
$2\omega_{12}$	A_g	2880.0	2880.0	R	P	G.L.
$2\omega_7+\omega_8$			2831*	R	Dep.	L.

[a] Assignments of ethylene vibrations given by Herzberg (see reference 7).
† Indicates the origin of this frequency from the depolarized 3075-cm^{-1} Raman line which occurs only in the liquid.
* This assignment incorporates the new data observed by the authors and by Arnett and Crawford.
[b] A list of the authors' observations of the state of polarization of all the observed Raman frequencies.
[c] Indicates whether the Raman line in question is observed in the liquid state alone or in both the gas and the liquid.

METHANE

Our Raman results for the liquid are given in the first column of Table I. We have observed three very weak diffuse lines at 1513 cm^{-1}, 1529 cm^{-1}, and 1547 cm^{-1} which have a separation comparable to the lines in the rotation-vibration band observed by Dickinson, Dillon, and Rasetti[1] in the spectrum of methane gas. The center of this band 1529 cm^{-1} agrees very closely with the predicted value of $v_2(e)$, i.e., 1526 cm^{-1} obtained from infra-red combination bands. The harmonic of $v_4(f_2)$ was also obtained in the Raman spectrum of the liquid. However, no trace of the fundamental $v_4(f_2)$ was found in spite of favorable experimental conditions for its observations. In the spectrum of methane, the unique situation occurs that the harmonics of $v_4(f_2)$ and $v_2(e)$ are very much stronger than the allowed fundamental frequencies themselves.

It is also definitely shown that the high frequency lines in the spectrum of liquid methane are shifted to lower values by about 10 cm^{-1} compared to the gas.

The Vibrational Frequencies of Ethylene*

RAYMOND L. ARNETT† AND BRYCE L. CRAWFORD, JR.
School of Chemistry, University of Minnesota, Minneapolis, Minnesota

(Received June 13, 1949)

The infra-red spectrum of a mixture of deuterated ethylenes has been obtained, and the non-planar fundamentals analyzed. The assignment establishes the twisting frequency as 1027 cm^{-1} (C_2H_4). This result leads to a new and more satisfactory assignment of the fundamental vibrational frequencies of ethylene.

INTRODUCTION

THROUGH an attempt to prepare *cis*-dideutero-ethylene for another purpose, we obtained a mixture of all seven deutero-isotopic ethylenes. To our pleased surprise, the infra-red absorption spectrum of this mixture proved to be analyzable with regard to the non-planar vibrations. The most significant result of our analysis is the location of the twisting frequency of ethylene (C_2H_4) at 1027 cm^{-1}. With this information and the remeasurement of the low frequency band in C_2H_4, we found it possible to make a most satisfactory assignment of all fundamentals and all observed frequencies for C_2H_4 and C_2D_4.

EXPERIMENTAL

The deuterated ethylenes were prepared by passing heavy water (D_2O) vapor over calcium carbide and subjecting the resulting dideutero-acetylene to catalytic hydrogenation (H_2 on Pd) to convert it to the olefin. The heavy water used contained 99.9 percent D_2O and the usual precautions were taken to remove H_2O from the apparatus and from the carbide.

The gas resulting from the hydrogenation reaction contained both ethane and unchanged acetylene as impurities. The latter component was effectively removed by bubbling the gas through a solution of alkaline mercuric cyanide. Chemical analysis of the final product revealed the composition: acetylene two percent, ethylene 85 percent, and ethane 13 percent.

After the spectrum of this sample was obtained, the gas was completely hydrogenated (H_2 on Pt) to ethane. This product was 98±2 percent pure. The spectrum of this ethane was used to locate the ethane bands which were expected in the ethylene spectra. The records made at several pressures revealed that only one region

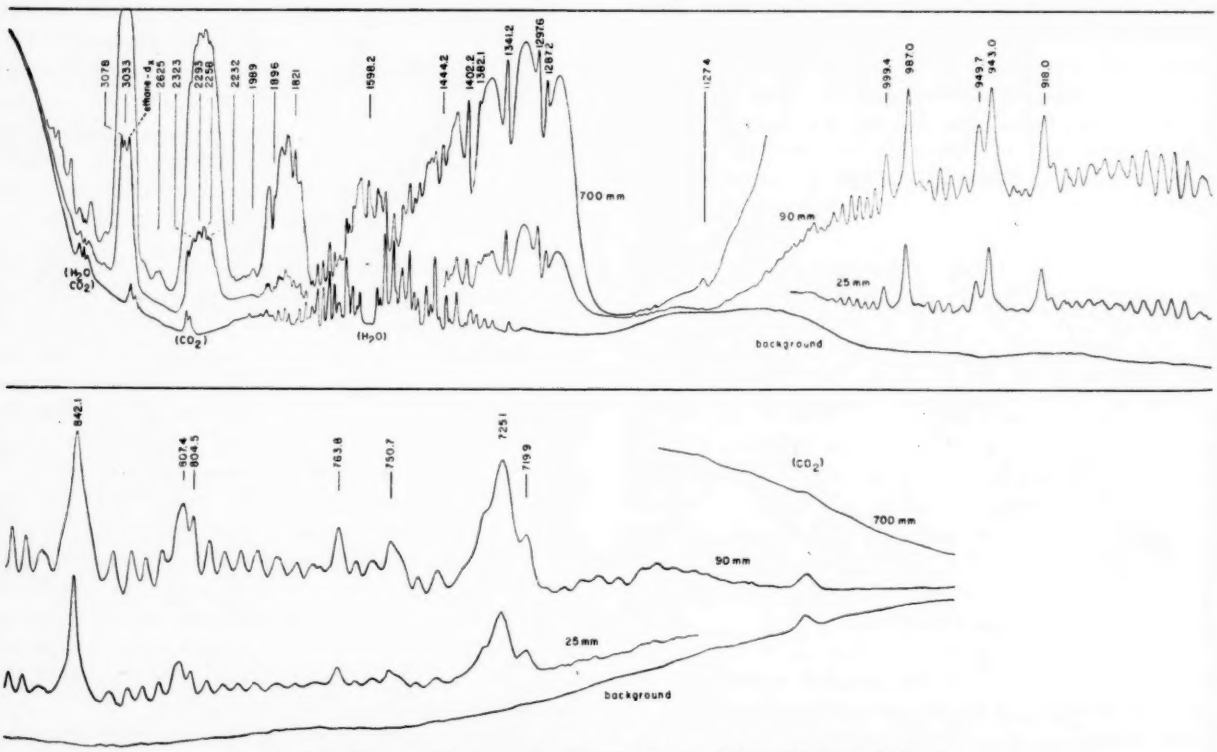

FIG. 1. Spectrum of deuterated ethylene mixture (NaCl). Cell length 10 cm.

* From a dissertation submitted by Raymond L. Arnett to the Graduate Faculty of the University of Minnesota in partial fulfillment of the requirement for the degree of Doctor of Philosophy.

† Present Address: National Bureau of Standards, Washington, D.C.

of absorption of the paraffin was sufficiently intense to be observed in the olefin spectrum.

The qualitative composition of the ethylene as to the isotopic molecules present was deduced from the mass spectrum of the ethane. The appearance of mass number 34 ($C_2H_2D_4$) makes it almost certain (in view of the method of preparation) that all the isotopic ethylenes were present in the olefin sample. This received confirmation through the analysis of the non-planar vibrational frequencies.

The infra-red absorption spectra were obtained from Model 12-C (for the rocksalt region) and Model 12-B (for the potassium-bromide region) Perkin-Elmer recording spectrometers. The 12-C instrument was fitted with a continuous slit drive adjusted to give approximately constant incident energy as the spectrum was traversed. The degree to which this is achieved can be seen from the lowest curves (marked "background") in Figs. 1 and 3. The 12-B spectrometer was not so equipped and its background changes rapidly with wave-length (Fig. 2).

For the deuterated ethylene, records in the rocksalt region were obtained at 25, 90, 135, and 700 mm Hg pressure. Traces obtained at each of these pressures (save 135 mm) are reproduced in Fig. 1; the 135-mm record is omitted for the sake of clarity. As many of the weak bands are seen only at the highest pressure, records at 700 mm were obtained in triplicate. All observations appearing in Tables I and II are thus the means of at least three measurements. Frequencies are corrected to vacuum conditions.

TABLE I. Ethylene-d_x absorption maxima below 1100 cm^{-1} (Figs. 1 and 2).

Line	Assignment	Line	Assignment	Line	Assignment
637		802.3		899.0$^+$	
644		804.5Q	$2\omega_7$–ω_7 C_2H_3D	902.8	
694.6		807.4Q	ω_7 C_2H_3D	905.9$^+$	
697.5		809.5$^+$		908.3	
702.0		812.0$^+$		913.0	
705.9		814.1		918.0Q	ω_8 C_2HD_3
709.6		817.2$^+$		921.9$^+$	
712.5		819.3		926.6	
719.9Q	ω_7 C_2D_4	823.8		929.9	
725.1Q	ω_7 t-$C_2H_2D_2$	829.8		932.5	
729.0		838.2$^+$		943.0Q	ω_8 a-$C_2H_2D_2$
739.1		842.1Q	ω_7 c-$C_2H_2D_2$	949.7Q	ω_7 C_2H_4
744.1		845.3$^+$		957.0	
750.7Q	ω_7 a-$C_2H_2D_2$	853.0$^+$		964.3	
753.9		855.1		969.7	
755.9$^+$		860.2		975.4	
759.4		865.3		980.7	
761.9$^+$		870.3		987.0Q	ω_4 t-$C_2H_2D_2$
763.8Q	ω_4 C_2HD_3	875.5		999.4Q	ω_4 C_2H_3D
785.7		880.7		1005.9	
788.0$^+$		884.8$^+$		1011.1	
790.8		886.8		1015.9	
793.0$^+$		892.1		1020.8	
794.7		894.1$^+$		1026.0	
799.6		897.1		1031.2	

Note.—Frequencies marked with Q are the labeled Type C bands in Fig. 1; those marked (+) do not appear in Fig. 1 as they are so weak or so close to a neighbor that the compression of the scale does not permit their showing.

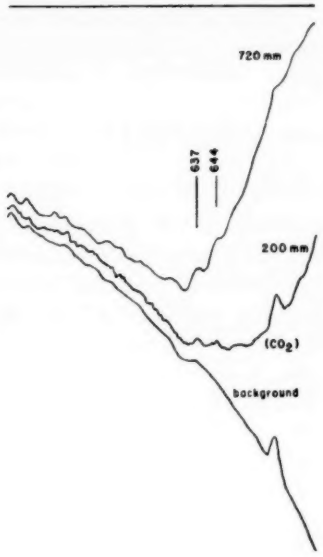

FIG. 2. Spectrum of deuterated ethylene mixture (KBr). Cell length 10 cm.

The material is transparent in the KBr region except for a very feeble absorption near 640 cm^{-1}. Two weak maxima appear here at 637 and 644 cm^{-1} (Fig. 2).

Since the ethylene sample contained an appreciable amount of ethane, the spectrum of the latter was obtained to identify the ethane bands which might appear in the ethylene spectrum. The deuterated ethane spectrum was obtained at three pressures, 16, 104, and 480 mm. Only the highest pressure is recorded here (Fig. 3), for the records at the lower pressures were blank except for a strong absorption at 3.4μ and a feeble one at 5.0μ. Duplicate runs were made at the highest pressure; the observed frequencies are listed in Table III.

The ethane proved to be completely transparent in the KBr region event at the highest pressure (480 mm). Only one ethane band, then, appears in the ethylene spectrum. This band is marked in Fig. 1.

Ohio Chemical Company ethylene (99.5–99.7 percent) was used to obtain the record of the 810.3-cm^{-1} band shown in Fig. 4; the line positions are listed in

TABLE II. Ethylene-d_x absorption bands above 1100 cm^{-1} (Fig. 1).

ω	Maxima	ω	Maxima
1127.4		1802	P(?)
1269	P	1821	Q
1287.2	Q	1847	R
1297.6	Q	1868	P
1314	R, P	1896	Q
1341.2	Q	1920	R
1362	R, P	1989	
1382.1	Q	2232	
1402.2	Q	2258	
1419	R, P	2293	
1444.2	Q	2323	
1464	P	2625	
1515(?)		2972	(ethane-d_x)
1577	P	3033	
1598.2	Q	3078	
1618	R		

Note.—Frequencies marked with Q and those unmarked as to branch are labeled in Fig. 1. Region from 1400 to 1800 cm^{-1} uncertain due to H_2O absorption.

Table IV. Records were obtained at six pressures from 12 to 700 mm. Evidence of the band is faintly observable at 50 but not at 12 mm.

MATHEMATICAL MACHINERY

Normal Coordinates

For our analysis we shall need the mathematical relations among the frequencies. The method employed in obtaining these is that of Wilson.[1] As valence-force coordinates, R, we select the five interatomic distances between bonded atoms plus the following seven angles: α_i=HC$_i$H angle; β_i=angle between C−C bond and bisector of the C$_i$H$_2$ angle; η_i=angle between C−C bond and C$_i$H$_2$ plane; δ=angle between the two CH$_2$ planes caused by rotation about a common axis which includes the C atoms. The numbering of the atoms is shown in Fig. 5.

Symmetry coordinates, S, obtained from these valence-force coordinates by the matric transformation, $S=UR$, are identified by use of the orthogonal U matrix shown.

U	r_{12}	r_{13}	r_{15}	r_{24}	r_{26}	$r_0\alpha_1$	$r_0\alpha_2$	$r_0\beta_1$	$r_0\beta_2$	$\Gamma r_0\eta_1$	$\Gamma r_0\eta_2$	$\Sigma r_0\delta$
A_{1g}: S_1	0	$\frac{1}{2}$	$\frac{1}{2}$	$\frac{1}{2}$	$\frac{1}{2}$	0	0	0	0	0	0	0
S_2	1	0	0	0	0	0	0	0	0	0	0	0
S_3	0	0	0	0	0	$1/\sqrt{2}$	$1/\sqrt{2}$	0	0	0	0	0
A_{1u}: S_4	0	0	0	0	0	0	0	0	0	0	0	1
B_{1g}: S_5	0	$\frac{1}{2}$	$-\frac{1}{2}$	$-\frac{1}{2}$	$\frac{1}{2}$	0	0	0	0	0	0	0
S_6	0	0	0	0	0	0	0	$1/\sqrt{2}$	$-1/\sqrt{2}$	0	0	0
B_{1u}: S_7	0	0	0	0	0	0	0	0	0	$1/\sqrt{2}$	$1/\sqrt{2}$	0
B_{2g}: S_8	0	0	0	0	0	0	0	0	0	$1/\sqrt{2}$	$-1/\sqrt{2}$	0
B_{2u}: S_9	0	$\frac{1}{2}$	$-\frac{1}{2}$	$\frac{1}{2}$	$-\frac{1}{2}$	0	0	0	0	0	0	0
S_{10}	0	0	0	0	0	0	0	$1/\sqrt{2}$	$1/\sqrt{2}$	0	0	0
B_{3u}: S_{11}	0	$\frac{1}{2}$	$\frac{1}{2}$	$-\frac{1}{2}$	$-\frac{1}{2}$	0	0	0	0	0	0	0
S_{12}	0	0	0	0	0	$1/\sqrt{2}$	$-1/\sqrt{2}$	0	0	0	0	0

Following Wilson's procedure, we obtain the following factored F and G matrices ($\bar{F}, \bar{G}$) arranged for study of the hydrogen-deuterium isotopic molecules. The original F matrix included all interaction terms; the zeros in $\bar{F}$ are required by symmetry if our valence-force coordinates are used in defining the potential.

In addition to the elements in the $\bar{G}$ matrix in Table V, there are certain off-diagonal "perturbation" terms. All of these elements vanish for V_h symmetry (C_2H_4, C_2D_4) but some will not for the ethylenes having less symmetry. Whenever such an element does not vanish, the two (or more) so "linked" species of V_h combine to form one species of the new point group (C_{2v}, C_{2h}, or C_s). These off-diagonal sub-matrices are given in Table VI.

In our calculations, we took $\alpha=119°55'$, $r_{12}^0=1.353$A, $r_{13}^0=1.071$A; we used atomic weights on the chemical scale, and the Birge 1941 values of the physical constants.[2]

Anharmonic Correction

Because of the lack of agreement of the isotopic relations for species B_{3u} where the frequencies of both C_2H_4 and C_2D_4 are precisely known, and the good agreement in species B_{1u} (also B_{2g}) where frequencies are also precisely known, we felt that an anharmonic correction was necessary but that it should be applied only to the C−H (C−D) bond-stretching vibrations. We used the following arbitrary procedure: (i) Assume all the anharmonicity arises from bond-stretching vibrations

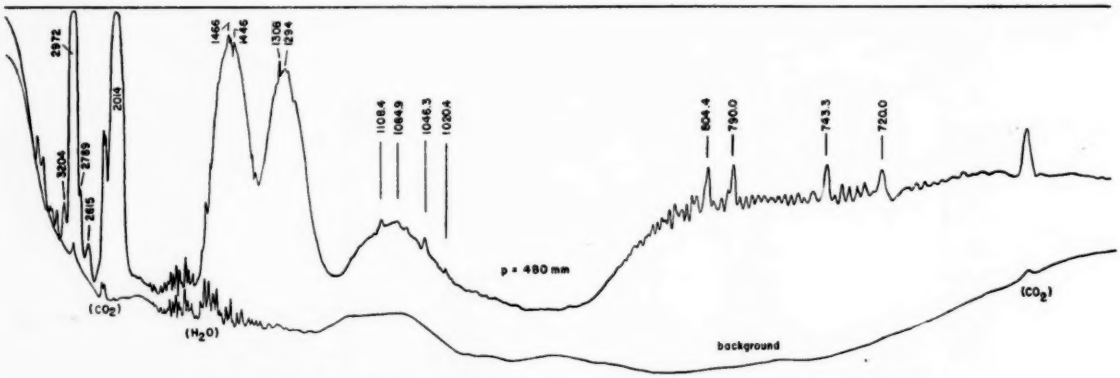

FIG. 3. Spectrum of deuterated ethane mixture (NaCl). Cell length 10 cm.

[1] E. B. Wilson, Jr., J. Chem. Phys. **7**, 1047 (1939); **9**, 76 (1941).
[2] R. T. Birge, Rev. Mod. Phys. **13**, 233 (1941).

TABLE III. Ethane-d_x absorption maxima (Fig. 3).

720.0Q	766.3	804.4Q	1046.3Q
726.9	769.8	810.9	1084.9Q
730.1	773.5	813.6	1108.4Q
733.7	776.9	816.4	1294Q
736.6	779.8	819.5	1308Q
739.8	783.0	823.7	1446Q
743.3Q	786.6	826.9	1466Q
749.9	790.0Q	831.7	2014Q
754.2	792.8	834.7	2615Q
756.9	796.1	837.7	2789Q
759.8	801.1	1020.4Q	2972Q
763.1			3204Q

Note.—Frequencies marked with Q are positions of maxima labeled in Fig. 3.

involving H or D atoms. (ii) For the anharmonic vibrations so defined, we use the relation between observed, ω_0, and harmonic, ω_e, frequencies found to hold for diatomic molecules; i.e. (for fundamentals), $\omega_0=\omega_e-2x_e\omega_e$. (iii) Assume the anharmonic correction, x_e, is constant for all defined anharmonic vibrations.

The constant, x_e, may be found with the aid of isotopic molecules. If we let primes refer to the heavier molecule and let ρ be the mass function relating ω_e and $\omega_e'(\omega_e'=\rho\omega_e)$, we have for the two isotopic molecules[3]

$$\omega_0'=\rho\omega_e(1-2\rho x_e);\quad \omega_0=\omega_e(1-2x_e)$$

and from the ratio ω_0'/ω_0,

$$x_e=(\rho-r)/2(\rho^2-r),$$

where $r=\omega_0'/\omega_0$. On applying this to species B_{3u} of C_2H_4 and C_2D_4, we find $x_e=0.0445$.

INTERPRETATION OF OUR DATA

Previous work on C_2H_4 and C_2D_4[4] has established eight of the twelve fundamentals beyond question (see Table IX). The values of the twisting frequency $\omega_4(A_{1u})$, the planar rocking frequencies $\omega_{10}(B_{2u})$ and $\omega_6(B_{1g})$, and the CH stretching frequency $\omega_5(B_{1g})$ were still far from certain.

Deuterated Ethylenes

In the sample prepared here, all seven isotopic ethylenes are present: C_2H_4, C_2H_3D, *cis-*, *trans-*, and *asymmetric-* $C_2H_2D_2$, C_2HD_3, and C_2D_4. A convincing detailed interpretation of the spectrum obtained is possible only for those bands lying in the range 700 cm^{-1} to 1000 cm^{-1}. There are twelve bands observed in this region, all with prominent Q branches. Also, the rotational spacings are such as to enable the positive identification of each as a Type C band. (Since the moments of inertia of the less symmetric isotopic ethylenes are intermediate between those of C_2H_4 and C_2D_4, their absorption bands may be expected to be similar to those known for C_2H_4 and C_2D_4) No other Type C bands were observed in the range investigated, 420 cm^{-1} to 3300 cm^{-1}. Our analysis is therefore limited to the Type C bands.

TABLE IV. Line positions in the 810.3-cm^{-1} C_2H_4 band (Fig. 4).

K	$^rQ(K)$	K	$^rQ(K)$
1	805.7		744.9
2	796.2	8	738.6
3	786.8	9	728.7
4	777.7	10	718.4
5	767.9	11	708.2
6	758.4		696.6
7	748.7		

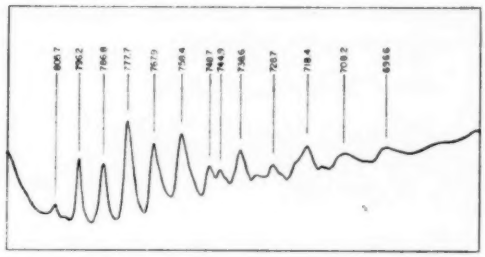

FIG. 4. The 810.3-cm^{-1} band in C_2H_4. Cell length 10 cm ($p=700$ mm Hg.)

The use of measured rotational spacings to identify the molecular species causing an observed band is impractical for the spectra presented here. Firstly, the bands are so close together that identification of the subbands is impossible; secondly, the expected differences among the spacings are so small as to be almost within the precision of the measurements. We turn then to the secular equations for aid in the interpretation.

Type C bands correspond, for all the isotopic molecules, to the non-planar vibrations, ω_4, ω_7, ω_8. Not all are allowed in every case, of course, but it appears reasonable that our twelve observed bands are due to these vibrations. Consequently, they should be related through the mass factors and three potential constants, one of which is already known accurately from the known value of ω_7 in C_2H_4 and C_2D_4. Another is known approximately from the Raman observation of ω_8, but liquid frequencies may be shifted somewhat. We should therefore be able to account for these 12 observed bands in terms of (say) one-and-a-half adjustable parameters, the force constants. We proceed along this line.[5]

The equations which relate the frequencies of the several isotopic molecules to the appropriate masses and force constants are obtained from the $\bar{F}$ and $\bar{G}$ matrices. On substituting numerical values in the $\bar{G}$ matrix, these equations for the non-planar frequen-

[3] G. Herzberg, *Diatomic Molecules* (Prentice-Hall, Inc., New York, 1939), pp. 152.

[4] Thoroughly discussed and summarized by G. Herzberg, *Infrared and Raman Spectra* (D. Van Nostrand Company, Inc., New York, 1945), p. 325.

[5] We may note that, since we use the most general potential function, there is no question here of "estimated" or "transferred" force constants. The only neglect here is of anharmonic corrections.

cies are:

C_2H_4	C_2D_4
A_{1u}: $(\omega_4)^2=16.844148\Delta$	A_{1u}': $(\omega_4)^2=8.428463\Delta$
B_{1u}: $(\omega_7)^2=9.835438H_1$	B_{1u}': $(\omega_7)^2=5.627595H_1$
B_{2g}: $(\omega_8)^2=12.963655H_2$	B_{2g}': $(\omega_8)^2=8.755812H_2$.

In these equations as in all the subsequent numerical work, the square of the frequency is in units of 10^5 cm^{-2} and the force constants are in units of 10^5 dynes/cm.

From the accurate values of ω_7 for C_2H_4 and C_2D_4 (949.85 and 720.30 cm^{-1}, respectively) we find $H_1=0.918996$ as the arithmetic mean of (B_{1u}) and (B_{1u}').

This value of H_1 is put into the equations of the other molecules so that only the constants Δ and H_2 appear as undetermined. These remaining equations follow with the selection rules indicated:

trans-$C_2H_2D_2(A_uIR;\ B_gR)$

A_u: $(\omega_4)^2+(\omega_7)^2=12.636305\Delta+7.105232$
$(\omega_4)^2(\omega_7)^2=81.648039\Delta$
B_g: $(\omega_8)^2=10.859731H_2$

cis-$C_2H_2D_2(B_2IR;\ A_2R)$

A_2: $(\omega_4)^2+(\omega_8)^2=12.636305\Delta+10.859731H_2$
$(\omega_4)^2(\omega_8)^2=128.373904\Delta H_2$
B_2: $(\omega_7)^2=7.731516H_1=7.105232$

asym.-$C_2H_2D_2(B_2IR;A_2R)$

A_2: $(\omega_4)^2=12.636305\Delta$
B_2: $(\omega_7)^2+(\omega_8)^2=7.105232+10.859731H_2$
$(\omega_7)^2(\omega_8)^2=73.092987H_2$

C_2H_3D $(A''IR,\ R)$

A'': $(\omega_4)^2+(\omega_7)^2+(\omega_8)^2=14.740227\Delta+11.911689H_2+8.071980$
$(\omega_4)^2[(\omega_7)^2+(\omega_8)^2]+(\omega_7)^2(\omega_8)^2=116.948856\Delta+95.133934H_2+173.367757\Delta H_2$
$(\omega_4)^2(\omega_7)^2(\omega_8)^2=1355.923353\Delta H_2$

$C_2HD_3(A''IR,\ R)$

A'': $(\omega_4)^2+(\omega_7)^2+(\omega_8)^2=10.532384\Delta+9.807768H_2+6.138485$
$(\omega_4)^2[(\omega_7)^2+(\omega_8)^2]+(\omega_7)^2(\omega_8)^2=62.618920\Delta+59.187856H_2+101.085936\Delta H_2$
$(\omega_4)^2(\omega_7)^2(\omega_8)^2=594.133947\Delta H_2$.

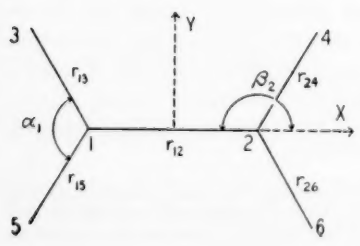

FIG. 5. Coordinates for ethylene.

Now ω_7 of *cis*-$C_2H_2D_2$ is immediately given; we find $\omega_7=842.93$ cm^{-1}. A strong band is observed at 842.1 cm^{-1} and we unhesitatingly assign it to ω_7 (*cis*-$C_2H_2D_2$).

To make any further assignments it is necessary to know the constants Δ and H_2. Let us examine the equations for species A_u of *trans*-$C_2H_2D_2$, where only Δ enters. There are here two independent relations in the three unknown quantities ω_4, ω_7, and Δ. By eliminating Δ we obtain one relation containing the symmetric pair ω_4 and ω_7,

$$(\omega')^2=6.461385(\omega^2-7.105232)/(\omega^2-6.461385)$$

where one member of the pair is designated by ω' and the other by ω. We may now take an observed frequency as one member of the pair and calculate its companion. If we do this for all observed frequencies (Table I) of the appropriate magnitude, then only the ones whose calculated companions fall reasonably near an observed band are eligible for assignment to the A_u species of *trans*-$C_2H_2D_2$.

In like manner the constant, H_2 may be eliminated from the equations for species B_2 of *asym.*-$C_2H_2D_2$ to obtain an equation relating ω_7 and ω_8 for that molecule. The equation so obtained is used to assign the two frequencies for this species.

Having now tentative assignments for A_u (*trans*-$C_2H_2D_2$) and B_2 (*asym.*-$C_2H_2D_2$), the force constants Δ and H_2 are calculated and used in turn in the equation for species A'' of C_2HD_3 and C_2H_3D as a check on the previous work and to complete the assignment. The resulting assignment of all the observed Type *C* bands is shown in Table I, while the calculated frequencies for the non-planar vibrations of all the ethylenes are compared with observed values, where this is possible, in Table VII.

It is apparent from the calculated values that the frequencies ω_8 of C_2H_3D and *asym.*-$C_2H_2D_2$ are very close together, perhaps within a few tenths of a wave number. The same can be said for ω_7 of C_2HD_3 and *trans*-$C_2H_2D_2$. Thus with the resolution obtained in these measurements, the 943.0 band may represent both C_2H_3D and *asym.*-$C_2H_2D_2$, while the broad (as it appears on our records) 725.1 band may also break into two *Q* branches under better resolution. We feel that the intensity of bands from the di-deuterium molecules will be greater than those from the mono- and tri-deuterium compounds,[6] therefore the 725.1 cm^{-1} band is assigned to ω_7

[6] According to an intensity sum rule derived by B. L. Crawford, Jr. (in press) for isotopic molecules, the sum of the integrated intensities of all ethylene bands in a given symmetry species is equal to the same quantity for an isotopic molecule of the same total symmetry; the integrated intensities being weighted by the inverse squares of the frequencies of the bands involved. In C_2H_4 and C_2D_4 (point group V_h) this intensity is concentrated in one band (ω_7); in *trans*-$C_2H_2D_2$ and in *asym.*-$C_2H_2D_2$, this intensity is distributed among two bands (ω_4, ω_7 for the former and ω_7, ω_8 for the latter), while the mono- and tri-deuterated compounds have three active bands to absorb the intensity. Although overlapping of the observed bands and lack of knowledge as to the composition of the gas mixture prevent a quantitative application of the intensity rule, one may base qualitative arguments on it leading to the conclusion stated in the text.

TABLE V.[a]

Species	Coordinate	$\bar{F}$	$\bar{G}$
A_{1g}	S^1 S^2 S^3	$\begin{bmatrix} K_1 & 2k_2^1 & \sqrt{2}k_1 \\ & K_0 & \sqrt{2}k_6^1 \\ & & A_1 \end{bmatrix}$	$\begin{bmatrix} (\mu_1'+\mu_2')/4+c/M & -2\Gamma/M & -\sqrt{2}s/M \\ & 2/M & 2\sqrt{2}\Sigma/M \\ & & (\mu_1'+\mu_2')/2-2c/M \end{bmatrix}$
A_{1u}	S^4	$[\Delta]$	$[(m_1'+m_2')/4]$
B_{1g}	S^5 S^6	$\begin{bmatrix} K_2 & 0 \\ & B_1 \end{bmatrix}$	$\begin{bmatrix} (\mu_1'+\mu_2')/4-c/M & -\sqrt{2}(2\rho+\Gamma)\Sigma/M \\ & (m_1'+m_2')/8+(2\rho+\Gamma)^2/M \end{bmatrix}$
B_{1u}	S^7	$[H_1]$	$[(m_1'+m_2')/8+1/M]$
B_{2g}	S^8	$[H_2]$	$[(m_1'+m_2')/8+(1+2\rho\Gamma)^2/M]$
B_{2u}	S^9 S^{10}	$\begin{bmatrix} K_3 & 0 \\ & B_2 \end{bmatrix}$	$\begin{bmatrix} (\mu_1'+\mu_2')/4-c/M & -\sqrt{2}s/2M \\ & (\mu_1'+\mu_2')/8+c/2M \end{bmatrix}$
B_{3u}	S^{11} S^{12}	$\begin{bmatrix} K_4 & \sqrt{2}k_2 \\ & A_2 \end{bmatrix}$	$\begin{bmatrix} (\mu_1'+\mu_2')/4+c/M & -\sqrt{2}s/M \\ & (\mu_1'+\mu_2')/2-2c/M \end{bmatrix}$

[a] Symbols are defined under Table VI.

of *trans*-$C_2H_2D_2$ (rather than C_2HD_3) and 943.0 cm^{-1} to ω_8 of *asym.*-$C_2H_2D_2$ (rather than C_2H_3D).

The sample of C_2D_4 used by Gallaway and Barker[7] contained some C_2HD_3. The Type *C* band measured by them to be 919.0 cm^{-1} and assigned to C_2HD_3 is unquestionably the same band we observed at 918.0 cm^{-1}. The band they observed at 723.38 cm^{-1} was assigned by them to $2\omega_7-\omega_7$ of C_2D_4, but in the light of the additional data of this research we assign it to ω_7 of C_2HD_3 and so enter it in Table VII. Indeed, the presence of the two bands (723.38 and 763.8 cm^{-1}) of C_2HD_3 within the structure of the 720.30 band of C_2D_4 would adequately account for the complex structure of the latter observed by Gallaway and Barker.

One other observed frequency listed in Table VII needs comment here, namely, ω_8 of *trans*-$C_2H_2D_2$. The value given here is that of a Raman shift reported by deHemptinne, Jungers, and Delfosse[8] in a mixture of partially deuterated ethylenes.

The force constants used in this frequency computation are given in Table VIII together with the coordinates appropriate to these numerical values.

TABLE VI. Perturbation sub-matrices of the $\bar{G}$ matrix.

	B_{1g}	B_{2u}	B_{3u}
A_{1g}	$\begin{bmatrix} (m_1''-m_2'')/4 & 0 \\ 0 & 0 \\ 0 & -(m_1''-m_2'')/4 \end{bmatrix}$	$\begin{bmatrix} (m_1''+m_2'')/4 & 0 \\ 0 & 0 \\ 0 & -(m_1''+m_2'')/4 \end{bmatrix}$	$\begin{bmatrix} (m_1'-m_2')/4 & 0 \\ 0 & 0 \\ 0 & (m_1'-m_2')/2 \end{bmatrix}$

	B_{1u}	B_{2g}
A_{1u}	$[\sqrt{2}s(m_1''-m_2'')/8]$	$[\sqrt{2}(m_1''+m_2'')/8]$

	B_{2u}	B_{3u}
B_{1g}	$\begin{bmatrix} (m_1'-m_2')/4 & 0 \\ 0 & (m_1'-m_2')/8 \end{bmatrix}$	$\begin{bmatrix} (m_1''+m_2'')/4 & 0 \\ 0 & -(m_1''+m_2'')/4)) \end{bmatrix}$

	B_{2g}
B_{1u}	$[(m_1'-m_2')/8]$

	B_{3u}
B_{2u}	$\begin{bmatrix} (m_1''-m_2'')/4 & 0 \\ 0 & -(m_1''-m_2'')/4 \end{bmatrix}$

Note.—

α = equilibrium value of H−C−H angle.
$\Gamma = \cos\alpha/2$, $c = \cos\alpha$.
$\Sigma = \sin\alpha/2$, $s = \sin\alpha$.
ρ = ratio of equilibrium C−H to C−C distance.
m_i = mass of i'th hydrogen atom.
M = mass of carbon atom.
$1/\mu_i = 1/m_i + 1/M$.

$m_1' = 1/m_3 + 1/m_5$.
$m_1'' = 1/m_3 - 1/m_5$.
$m_2' = 1/m_4 + 1/m_6$.
$m_2'' = 1/m_4 - 1/m_6$.

$\mu_1' = 1/\mu_3 + 1/\mu_5$.
$\mu_1'' = 1/\mu_3 - 1/\mu_5$.
$\mu_2' = 1/\mu_4 + 1/\mu_6$.
$\mu_2'' = 1/\mu_4 - 1/\mu_6$.

[7] W. S. Gallaway and E. F. Barker, J. Chem. Phys. **10**, 88 (1942).
[8] deHemptinne, Jungers, and Delfosse, J. Chem. Phys. **6**, 319 (1938).

The 810.3-cm^{-1} C_2H_4 Band

We have reexamined the low frequency C_2H_4 band reported by Rasmussen and Brattain[9] and by Thompson and Harris.[10] In general contour, this band (Fig. 4) has the appearance of one branch (the P) of a Type B band; particularly when compared with the resolved curve of this species (ω_9 at 3105.5 cm^{-1}) obtained by Gallaway and Barker. Through this comparison we make the assignment of the observed lines given in Table IV. The distinct alternating intensity of the subbands leaves no choice as to which lines have an even value of K so that a comparison of the contour of this band with that of its species companion makes the assignment given almost unavoidable.

The position of the band center, ω_0, is found from the equation

$$^PQ(K)=\omega_0+(A'-\bar{B}')-2(A'-\bar{B}')K+[(A'-\bar{B}')-(A''-\bar{B}'')]K^2 \quad (1)$$

given by Herzberg[11] for asymmetric tops. Here A, B, and C are $(h/8\pi^2c)$ times the reciprocals of the principal moments of inertia I_a, I_b, and I_c, respectively; primes refer to the upper and double primes to the lower vibrational states and $\bar{B}$ is the arithmetic mean of B and C. By taking the difference $^PQ(K)-{}^PQ(K+1)$ the rotational spacing is given as a linear function of K. The data in Table IV were fitted to this function by the method of least squares yielding $A'-\bar{B}'=4.555$ and $A''-\bar{B}''=4.609$. On substituting these values in (1), the band center is determined from each line. The arithmetic mean of these is 810.3 cm^{-1}.

TABLE VII. Non-planar vibrational frequencies of all the ethylenes.

	C_2H_4	C_2H_3D	*l*-$C_2H_2D_2$	*c*-$C_2H_2D_2$	*a*-$C_2H_2D_2$	C_2HD_3	C_2D_4
ω_4(obs.)	—	999.4	987.0	(—)	(—)	763.8	—
(calc.)	1026.9	1001.8	990.0	981.6	889.4	759.8	726.4
ω_7(obs.)	949.85	807.4	725.1	842.1	750.7	723.38	720.30
(calc.)	950.7	804.5	722.2	842.9	747.9	722.1	719.2
ω_8(obs.)	(943)		(863.4)	(—)	943.0	918.0	(780.0)
(calc.)	942.0	945.8	862.2	755.7	945.9	919.7	774.2

Note.—Values in parenthesis are liquid-phase Raman observations. The root-mean-square deviation is 2.7 cm^{-1} for the 15 instances where comparison is possible.

TABLE VIII. Force constants involved in the non-planar vibrations ($\Delta=0.6260$; $H_1=0.9190$; $H_2=0.6846$).

Coordinate	$\Sigma r_0\delta$	$\Gamma r_0\eta_1$	$\Gamma r_0\eta_2$
$\Sigma r_0\delta$	0.6260	0	0
$\Gamma r_0\eta_1$	0	0.8018	0.1172
$\Gamma r_0\eta_2$	0	0.1172	0.8018

Note.—Values in units of 10^5 dynes/cm.

[9] R. W. Rasmussen and R. Robert Brattain, J. Chem. Phys. **15**, 120 (1947).
[10] H. W. Thompson and G. P. Harris, Trans. Faraday Soc. **40**, 295 (1944).
[11] G. Herzberg, reference 4, p. 424.

FINAL ASSIGNMENTS FOR C_2H_4 AND C_2D_4

As pointed out earlier, the assignments of eight C_2H_4 fundamentals have been unquestionably correct and need no further comment here. Of the four uncertain frequencies, one, Raman active ω_5, is not settled by this research. The other three are ω_4 (twisting, inactive), ω_6 (Raman-active but unobserved), and ω_{10} (infra-red-active). The twisting frequency has now been established by our work at 1027 cm^{-1} and is most probably correct to within three wave numbers.

There have been two observed bands vying for ω_{10}. Gallaway and Barker[7] assigned 995 cm^{-1} as the frequency of this vibration while Rasmussen and Brattain[9] would have it at 800 cm^{-1} (our work fixes the band center at 810.3 cm^{-1}). Both these bands are perpendicular and both must be fundamentals. Specifically, one must be ω_{10} and the other ω_4 made weakly active by Coriolis interaction[12] with ω_{10} and ω_{12}. Having the frequency of $\omega_4(=1027$ cm$^{-1})$, it is possible to choose Gallaway and Barker's 995 band[13] as resulting from Coriolis perburbation and the 810.3-cm^{-1} band as ω_{10}. Knowing ω_{10}, the frequency of ω_6 is fixed from the certain combination band, $\omega_6+\omega_{10}$ at 2046.5 cm^{-1}; we find $\omega_6=1236$ cm^{-1}.[14]

All the C_2D_4 fundamentals (save ω_6, ω_{10}) are satisfactorily assigned for reasons entirely analogous to the C_2H_4 molecule. The frequency of the heavier isotopic molecule corresponding to 810.3 cm^{-1} in C_2H_4 has not been observed; from the product rule we predict that it will be detected in the KBr region centering near 586 cm^{-1}. As a matter of fact, Conn and Sutherland's[15] sylvine-prism curves covering this region do show faint

TABLE IX. New fundamental frequency assignment for C_2H_4 and C_2D_4.

Species	Activity*	Number	C_2H_4	C_2D_4
A_{1g}	R, p	ω_1	3019.3	2251
		ω_2	1623.3	1515
		ω_3	1342.4	981
A_{1u}	In	ω_4	1027	726
B_{1g}	R, d	ω_5	3272.3	2304
		ω_6	1236[a]	1009[b]
B_{1u}	IR, C	ω_7	949.2	720.0
B_{2g}	R, d	ω_8	943	780
B_{2u}	IR, B	ω_9	3105.5	2345
		ω_{10}	810.3	586[c]
B_{3u}	IR, A	ω_{11}	2989.5	2200.2
		ω_{12}	1443.5	1077.9

* R=Raman, IR=infra-red, In=inactive; p, d=polarized, depolarized; A, B, C, refer to band type.
[a] Calculated from $\omega_6+\omega_{10}=2046.5$ for C_2H_4.
[b] Calculated from $\omega_6+\omega_{10}=1595.1$ for C_2D_4.
[c] Calculated from product rule.

[12] See G. Herzberg, reference 4, p. 467.
[13] The most prominent maximum in this band occurs at 1028 cm^{-1} (private communication from Professor Barker).
[14] This assignment was transmitted to Professor D. H. Rank who was making polarization measurements on the Raman shifts of C_2H_4. He found a hitherto unreported line at 1236±3 cm^{-1} (see preceding paper, Rank, Shull, and Axford, J. Chem. Phys. **18**, 116 (1950).
[15] G. K. T. Conn and G. B. B. M. Sutherland, Proc. Roy. Soc. **A172**, 172 (1939).

TABLE X. Isotopic check on the assignment.

Species	Observed	Theoretical	% difference
A_{1g}	0.4952	0.5004	1.03
A_{1u}	0.7069	0.7074	—
B_{1g}	0.5606	0.6046	7.28
B_{1g} (ω_6 only)	0.8163	0.8107	0.69
B_{1u}	0.7585	0.7564	0.28
B_{2g}	0.8271	0.8218	0.64
B_{2u}	0.5351	0.5351	—
B_{3u}	0.5351	0.5351	—

indications of the existence of a band here. In the KBr records of the spectrum of our isotopic mixture, we found indications of this ω_{10} in two faint maxima near 637 cm^{-1}. The spacing is about that expected for a dideuteroethylene.

With ω_{10} set at 586 cm^{-1}, we may use the combination band $\omega_6+\omega_{10}(=1595.1$ cm$^{-1})$ to establish ω_6 at 1009 cm^{-1}.

This leaves only ω_5 unaccounted for. The Raman line given by C_2D_4 at 2304 cm^{-1} is the only one available for this assignment, but there are two, 3075 and 3272.3 cm^{-1}, possibilities for C_2H_4. Originally we favored 3075 as the fundamental, assigning the higher frequency to a resonance form of species A_{1g}. Rank,[16] however, has recently shown that both the 3075 and 3272.3 lines are depolarized. Since there is no binary combination which would give a depolarized Raman line of this frequency and a ternary (or higher) combination showing in the Raman effect is not likely, we must accept the 3272.3 line as the fundamental, ω_5, even though the product rule is not well satisfied. The 3075 line could then be ω_9 appearing in the Raman effect due to a phase-change breakdown of the selection rules as suggested by Glockler and Renfrew.[17]

The complete assignments are shown in Table IX and the isotopic check in Table X. In making the computations for Table X, the anharmonic correction was applied. The frequencies ω_6, in B_{1g}, were not obtained using the isotopic relation for this species so that the product rule serves as an independent check. The difference between theory and observation is not readily accounted for. It might appear that the ω_6 assignment is bad. In order to check this, we factored off the high frequency and so obtained a "reduced" product rule[1] for B_{1g} involving ω_6 only; this is also listed in Table X and it is seen that the agreement is good.

We have yet to discover what disposition is to be made of the remaining observed infra-red and Raman

TABLE XI. Assignment of infra-red absorption bands of C_2H_4 and C_2D_4.

		C_2H_4					C_2D_4		
Type	Intensity	Coblenz* (1905)	L.+M.* (1928)	G.+B.* (1942)	Calc.	Assignment	C.+S.* (1939)	G.+B.* (1942)	Calc.
?	w.	847				$\omega_{10}{}^bB_{2u}$			
C	v.s.	952	949.5	949.20+		ω_7B_{1u}	721.4	720.00+	
C	s.					t-$C_2H_2D_2$	726.7		
B, C	v.w.			995		ω_4A_{1u}			
C						C_2HD_3		919.0+	
A	s.		1443.5			$\omega_{12}B_{3u}$	1080.3	1077.9	
A						C_2HD_3	1291.5	1289.1	
B		1724		1766		impurity			
A	m.	1887	1889.2	1889.6+	1892	$\omega_7+\omega_8B_{3u}$	1496.9	1495.7+	1500
A	w.		2046.5		a	$\omega_6+\omega_{10}B_{3u}$		1595.1+	a
?	w.	2315				impurity			
					2263	$\omega_4+\omega_6B_{1u}$			
A	s.	3049	2987.4	2989.5+		$\omega_{11}B_{3u}$	2198	2200.2+	
B	s.		3106.6	3105.5+		ω_9B_{2u}	2353	2345	
C	s.					$\omega_1+\omega_7B_{1u}$	2969		2971
						C_2HD_3		3049.0	
A	w.					$2\omega_6+\omega_{12}B_{3u}$			3096
						$\omega_2+\omega_7+\omega_8$			3015
B	w.		4206.7		4226	$\omega_6+\omega_{11}B_{2u}$		3204.3	3209
A	m.	4329	4323.1		4303	$\omega_2+\omega_6+\omega_{12}B_{2u}$			
A	m.					$\omega_6+\omega_9B_{3u}$		3345.3	3354
						$\omega_1+\omega_{12}B_{3u}$			3329
B	m.		4514.3		4510.3	$\omega_2+2\omega_{12}B_{2u}$			
B	v.w.		4727.7		4715.8	$\omega_5+\omega_{12}B_{2u}$		3387.8	3382
					4729	$\omega_2+\omega_9B_{2u}$		3862.8	3860
A	w.					$\omega_1+\omega_{11}B_{3u}$		4429.5	4451
B	w.					$\omega_5+\omega_{11}B_{2u}$		4478.6	4504
A	w.					$\omega_5+\omega_9B_{3u}$		4628.0	4649

Note.—Values marked (+) indicate positions of band centers calculated from rotational structure rather than positions of minima or Q branch maxima.

* G.+B., Gallaway and Barker, reference 7; W. Coblenz, "Investigations of Infrared Spectra," Carn. Inst. Wash. Pub. No. 35, p. 45 (1905); L.+M., A. Levin and C. F. Meyer, J. Opt. Soc. Am. **16**, 137 (1928); C.+S., G. K. T. Conn and G. B. B. M. Sutherland, Proc. Roy. Soc. **A172**, 172 (1939).

[a] Used to calculote ω_6.

[b] Although most workers ascribe this band of Coblenz to an impurity, it is more than likely that it is the absorption band whose center was fixed at 810.3 cm^{-1} by this work. As stated in the text, the band center has also been set at 770 cm^{-1} and at 800 cm^{-1} by Thompson and Harris and by Rasmussen and Brattain, respectively.

[16] See Rank, Shull, and Axford, reference 14.

[17] George Glockler and M. M. Renfrew, J. Chem. Phys. **6**, 170, 409 (1938).

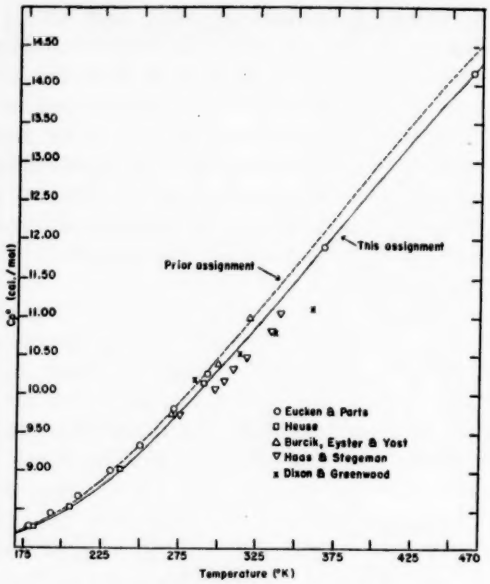

FIG. 6. Heat capacity of C_2H_4.

frequencies in the light of the new assignment of fundamentals. The only Raman line whose assignment needs changing from that given by Herzberg[18] is the 1656 line. Obviously it can no longer be $2\omega_4$; however it can be $2\omega_{10}$ if we allow a small positive anharmonicity so that $2\omega_{10}$ is not $1620.6(=2\times810.3)$, but some value greater than 1623.3 cm^{-1}. With this, the Fermi resonance between the strong 1623.3 level and $2\omega_{10}$ may be expected to cause the latter to appear at the still higher frequency, 1656 cm^{-1}.

There are several changes necessary in the infra-red-active combination bands, most of these resulting in a reduction from quaternary to binary tones. Table XI gives the complete assignment of observed infra-red bands.

[18] G. Herzberg, reference 4, p. 326.

It is interesting to make a comparison of the torsional frequencies in ethylene (1027 cm^{-1}) and allene (820 cm^{-1}). It seems reasonable to us that the greater separation (with one more intervening atom) and perpendicular configuration of the CH_2 groups in allene should result in a lower vibrational frequency than that for ethylene. The old assignment for C_2H_4 had them at the same level and made a perplexing problem for interpretation; the assignment given in Table IX removes the difficulty.

We turn now to heat-capacity data as extra-spectroscopic evidence in support of our assignment. In Fig. 6, the dotted line is the result of calculations to the harmonic-oscillator approximation using the old assignment as given by Herzberg,[4] while the full curve results from similarly calculated values using our assignment (Table IX). The points represent the existing thermal measurements.[19] The better fit over the whole temperature range is at once apparent.

ACKNOWLEDGMENTS

Financial aid throughout most of this research was supplied by the ONR through contract N5ori-147, Task Order II.

We are indebted to the Minnesota Mining and Manufacturing Company for the use of their spectrometer in obtaining spectra in the potassium-bromide region; in particular we wish to thank Mr. D. G. Weiblen for his assistance in supervising the work there.

We are indebted also to Professor A. O. C. Nier for obtaining and interpreting the mass spectra for us. Without this information, the method of attack on the infra-red spectrum would not have been so immediately clear.

[19] Wilhelm Heuse, Ann. d. Physik **59**, 86 (1919); A. Eucken and A. Parts, Zeits. f. physik. Chemie **B20**, 184 (1933); Burcik, Eyster, and Yost, J. Chem. Phys. **9**, 118 (1941); Harold B. Dixon and Gilbert Greenwood, Proc. Roy. Soc. **A105**, 199 (1924); Matthias E. Haas and Gebhard Stegeman, J. Phys. Chem. **36**, 2127 (1932).

The Compressibility of, and an Equation of State for Gaseous Isobutane

JAMES A. BEATTIE, STANLEY MARPLE, JR., AND DAVID G. EDWARDS
Department of Chemistry, Massachusetts Institute of Technology, Cambridge, Massachusetts

(Received July 12, 1949)

The volumetric behavior of gaseous isobutane from 150° to 300°C and from 1.0 to 8.0 moles per liter has been studied. The constants of the Beattie-Bridgeman equation of state for gaseous isobutane are $R=0.08206$, $A_0=16.6037$, $a=0.11171$, $B_0=0.23540$, $b=0.07697$, $c=300\times10^4$ in units of normal atmospheres, liters per mole, degrees Kelvin.

THE determinations of the vapor pressures, orthobaric liquid densities, and critical constants of isobutane have been reported in an earlier paper.[1] The same loading of isobutane was used to study the volumetric behavior in the region above the critical temperature by the method employed for other hydrocarbons.[2] The compressibility of isobutane (liquid and gas) from 21° to 121°C has been studied by Sage and Lacey,[3] and from 38° to 238° by Morris, Sage, and Lacey.[4]

TABLE I. Values of the constants of the Beattie-Bridgeman equation of state for gaseous isobutane.

$$p=[RT(1-\epsilon)/V^2][V+B]-A/V^2$$
$$A=A_0(1-a/V)$$
$$B=B_0(1-b/V)$$
$$\epsilon=c/VT^3$$

Units: normal atmospheres, liters per mole, °K(T°K$=t$°C (Int.)$+273.13$)

$R=$ 0.08206	$b=0.07697$
$A_0=16.6037$	$c=300\times10^4$
$a=$ 0.11171	Mol. wt. $=58.077$
$B_0=$ 0.23540	

The isobutane used in the present investigation was furnished by the Linde Air Products Company through the courtesy of Dr. L. I. Dana. Its high degree of purity was indicated by the small change of vapor pressure with decrease in vapor volume. The mass of the sample of isobutane was 7.0074 g. After the completion of the 0.300° isotherm, we redetermined the pressure for densities 1.0, 2.0, and 3.0 moles per liter at 150°C. These checked with the pressures measured at the beginning of the investigation to better than 0.005 atmos., indicat-

TABLE II. Comparison of the pressures calculated from the equation of state with the observed pressures for gaseous isobutane (C_4H_{10}).

Density, moles/liter → Temp., °C (Int.) ↓	1.0	1.5	2.0	2.5	3.0	3.5	4.0	4.5	5.0	6.0	7.0	8.0
	Pressure, normal atmospheres											
150 obs	25.70	33.05	37.84	40.89	42.85	44.29	45.60	47.20	49.70	63.08	106.66	224.71
obs—calc	−0.14	−0.14	0.00	+0.30	+0.56	+0.46						
175 obs	28.45	37.63	44.49	49.75	54.04	57.92	61.95	66.77	73.34	98.41	160.44	303.79
obs—calc	−0.07	−0.04	+0.08	+0.22	+0.18	−0.34						
200 obs	31.13	42.06	50.93	58.36	65.02	71.51	78.52	86.85	97.67	134.54	214.22	
obs—calc	−0.04	−0.02	+0.08	+0.10	−0.09	−0.72						
225 obs	33.78	46.44	57.27	66.86	75.93	85.12	95.22	107.20	122.42	171.25	269.05	
obs—calc	−0.02	0.00	+0.08	+0.04	−0.17	−0.73						
250 obs	36.39	50.75	63.48	75.23	86.73	98.66	111.94	127.65	147.36	208.05		
obs—calc	−0.02	0.00	+0.03	−0.01	−0.15	−0.51						
275 obs	38.99	55.02	69.66	83.58	97.52	112.27	128.78	148.35	172.59	245.51		
obs—calc	−0.02	0.00	+0.03	+0.04	+0.03	+0.03						
300 obs	41.51	59.24	75.77	91.86	108.25	125.80	145.61	169.00	197.85			
obs—calc	−0.08	−0.03	+0.01	+0.10	+0.29	+0.68						
Average deviation, atmos.**	0.056	0.033	0.044	0.116	0.210	0.496						
Average % deviation**	0.181	0.090	0.083	0.224	0.353	0.656						

* For each temperature the first line gives the observed pressure and the second line gives the observed minus calculated pressure. The critical constants of isobutane are: $t_c=134.98$°C (Int.), $p_c=36.00$ normal atmos., $v_c=0.263$ liters per mole, $d_c=3.80$ moles per liter.
** Total average deviation, 0.159 atmos.; total average % deviation, 0.265%.

[1] J. A. Beattie, D. G. Edwards, and Stanley Marple, Jr., J. Chem. Phys. **17**, 576 (1949).
[2] For the last report on this work see Beattie, Ingersoll, and Stockmayer, J. Am. Chem. Soc. **64**, 546, 548 (1942). For a description of the apparatus and method see J. A. Beattie, Proc. Am. Acad. Arts. and Sci. **69**, 389 (1934).
[3] B. H. Sage and W. N. Lacey, Ind. Eng. Chem. **30**, 673 (1938).
[4] Morris, Sage, and Lacey, Am. Inst. Mining and Met. Eng., Tech. Pub. 1128, Petroleum 2, Nov. 1939.

ing that no decomposition had occurred throughout the entire series of measurements.

The measurements are reported in Table II. In Table I are given the constants of the Beattie-Bridgeman equation of state for isobutane determined from the isometrics below the critical density (3.80 moles per liter). The comparison of the pressures computed from this equation with the observed pressures is given in Table II. The total average percent deviation is 0.27 percent.

The pressures of Morris, Sage, and Lacey were at different temperatures and densities from our values. Their pressures were first interpolated to our densities by suitable treatment of their isotherms, and then smoothed to our temperatures along isometrics. The agreement of the pressures so obtained with our observed pressures is excellent. From a density of 1 through 5 moles per liter and a temperature of 150 to 225°C the average percentage deviation (without regard to sign) is 0.23 percent, the largest positive deviation being 0.52 percent and the largest negative −0.57 percent. The algebraic average is 0.05 percent. For the ten points of densities 6, 7 and 8 moles per liter the average percentage deviation is 0.94 percent and the algebraic average +0.13 percent.

THE JOURNAL OF CHEMICAL PHYSICS VOLUME 18, NUMBER 1 JANUARY, 1950

Hexacovalent Bond Orbitals II

GEORGE H. DUFFEY
Chemistry Department, South Dakota State College, Brookings, South Dakota
(Received July 11, 1949)

Further calculations are reported on the set of trigonal prism orbitals introduced in paper one of this series. The strongest orbitals found have a strength equal to 2.989. The results are used in discussing the difference in stability between these orbitals and the octahedral orbitals in structures of the following types: $Fe(CN)_6^{\equiv}$, $Fe(CN)_6^{=}$, and SF_6.

IN the first paper[1] of this series, s, p, and d orbitals were hybridized to give a set of trigonal prism orbitals more general than the set previously[2] obtained. Some calculations were reported on the new set.

In this paper further calculations are reported. In Table I m was[3] set equal to one. Then θ_1, the angle between the axis and the maximum in ψ_1, and S, the maximum value of ψ_1, were calculated. In Table II values were assigned m. Then n was chosen so as to obtain the strongest orbitals for each m, and the corresponding values of θ_1 and S were obtained. As in paper one[1] θ_1 and S are called the angle between the axis and bond one and the strength of the bond respectively.

The strongest bonds were found when m equals 0.5972 and n equals 0.8464. These bonds have a strength equal to 2.989. Thus these bonds are slightly stronger than cylindrical trigonal prism bonds, which were discussed by Hultgren.[2]

The configuration sp^3d^2 is of especial interest. This configuration in general yields the octahedral structure.[4] The strength of an octahedral bond equals 2.923. The strength of the corresponding trigonal prism bond equals 2.737. However, trigonal prism bonds stronger than 2.923 may result if less of the p orbitals, the same amount or less of the s orbital, and more of the d orbitals are used in forming the bonds. In structures of the $Fe(CN)_6^{\equiv}$ and the $Fe(CN)_6^{=}$ types there are three unshared electron pairs, or two unshared electron pairs and one unshared electron, respectively, in the valence shells of the central atom. In structures of these types the energy obtainable in passing from the octahedral structure to a trigonal prism structure where the strength is greater than 2.923 apparently does not equal the energy needed for the excitation of the required number of unshared electrons. Some energy is required since the interaction energy of a shared electron is less than that of an unshared electron.

Consider the following rough estimates.[5] Suppose the $d-p$ separation is 50 kcal./mole and the $d-s$ separation is 0 kcal./mole (i.e., a valence shell, unshared electron in a p orbital is 50 kcal./mole less stable than when it is in a d or s orbital). Assume that the bond energy equals 100 kcal./mole and that the bonds are 100 percent covalent.

TABLE I. Results of calculations on trigonal prism orbitals of type $s^n p^3 d^{3-n}$.

n	S, Strength of a bond	θ_1, Angle between axis and bond 1
1.0000	2.737	47° 5′
0.9600	2.771	44° 20′
0.9000	2.789	42° 44′
0.8000	2.807	40° 57′
0.5070	2.825	37° 37′
0.3000	2.815	35° 57′
0.1000	2.771	34° 37′
0.0000	2.667	34° 1′

[1] G. H. Duffey, J. Chem. Phys. **17**, 1328 (1949).
[2] R. Hultgren, Phys. Rev. **40**, 891 (1932).
[3] The orbitals are of type $s^n p^{1+2m} d^{5-2m-n}$.
[4] L. Pauling, *The Nature of the Chemical Bond* (Cornell University Press, Ithaca, 1940).
[5] See H. Kuhn, J. Chem. Phys. **16**, 727 (1948).

TABLE II. Results from orbitals of type $s^n p^{1+2m} d^{5-2m-n}$ with n chosen to obtain the strongest orbitals for each m.

m	n	S, Strength of a bond	θ_1, Angle between axis and bond 1
1.0000	0.5070	2.825	37° 37′
0.9000	0.6565	2.937	42° 11′
0.8000	0.7327	2.968	44° 14′
0.7000	0.7941	2.984	45° 51′
0.5972	0.8464	2.989	47° 16′
0.4000	0.9124	2.971	49° 16′
0.3000	0.9272	2.947	49° 47′
0.2000	0.9258	2.908	49° 44′
0.1000	0.8954	2.843	48° 43′
0.0400	0.8417	2.776	47° 9′
0.0000	0.7094	2.645	43° 37′

Also assume that the bond energy is proportional to the strength of the bond orbital. Assume that the interaction energy of a shared pair equals the energy of a single unshared electron. Also assume that if the trigonal prism orbitals of configuration sp^3d^2 had bonds of strength 2.923, they would be as stable as the octahedral orbitals.

In the first case, three electron pairs in the valence shells are unshared. In changing m from one to m_1 two of the unshared electron pairs pass from d levels to hybrid levels[6] containing some p. Simultaneously the shared pairs pass to hybrid levels containing less p. In effect, $2(1-m_1)$ unshared electron pairs are promoted and $2(1-m_1)$ shared electron pairs are demoted. The energy required for this exchange is given by $2(1-m_1)50$ kcal./mole. This is represented by the straight line a of Fig. 1. Curve c gives the energy released in kcal./mole when S is changed from 2.923 to the best value corresponding to m_1. These "best" values are obtained from Table II. Points on the curve were calculated using the expression $600(S-2.923)/2.923$ kcal./mole. The curve was plotted only to its maximum.

In the second case, two electron pairs and an unpaired electron in the valence shells are unshared. Now in changing m from one to m_1, one unshared electron pair and a single unshared electron pass from d levels to hybrid levels[6] containing some p. The energy required now is given by $(1-m_1)50$ kcal./mole. This is represented by the straight line b in Fig. 1.

We note that both lines a and b lie above curve c. This means that under the assumptions more energy is required to make more of the d orbitals available for the bond orbitals than is released from the formation of the stronger bonds. Hence the octahedral structure is more stable than the trigonal prism structures.

The conclusion should not be altered if the partially ionic character of the bonds is considered. As a rule the attached groups are electronegative[7] with respect to the central atom. When this is true, the interaction energy of a shared pair is approximately equal to P times that of a single unshared electron. Here $1-P$ is the degree of ionic character of a bond. The lines a and b of Fig. 1 will be steeper and will hence lie higher when P does not equal one. Also, when P does not equal one, the curve c may lie somewhat lower.

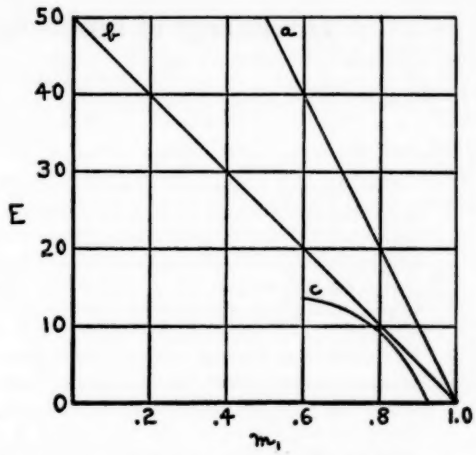

FIG. 1. Energy relations (E in kcal./mole) for the transition from the octahedral structure to the trigonal prism structure chosen as in Table II with $m=m_1$. The straight line a represents the energy required for the transition when there are three unshared electron pairs in the valence shells. The straight line b represents the energy required when there are two unshared electron pairs and one unshared electron in the valence shells. The curve c represents the energy obtained from the transition if the bond energy is 100 kcal./mole. The $d-s$ separation is assumed to be 0 kcal./mole and the $d-p$ separation 50 kcal./mole.

The conclusion is not altered if the bond energy is lowered, since this will lower curve c. If the $d-p$ and/or the $d-s$ separations are increased above the values 50 and 0 kcal./mole, the conclusion is not altered as these changes will raise lines a and b.

Now consider structures of the SF_6 type. In these structures there are no unshared electrons in the valence shell and the d orbitals are less stable than the s or p orbitals. Assume the $p-d$ separation is 50 kcal./mole and assume the amount of s does not change. Then curve b in Fig. 1 represents the energy required to excite the shared electrons if the bonds are 50 percent covalent. If the bond energy equals 100 kcal./mole, the energy obtainable in increasing S above 2.923 will be given by a curve lying below curve c. Thus under the assumptions the theory predicts that the octahedral structure is more stable. The conclusion should not be changed if the amount of s is allowed to change and if the s orbital is most stable. Increasing the $p-d$ separation does not alter the conclusion. Also making the bonds less ionic does not alter the conclusion.

[6] See Eqs. (18), (19), and (20) of reference 1.

[7] L. Pauling, J. Chem. Soc. **1948**, 1461.

The Energy of Interaction between Two Hydrogen Atoms[1]

J. O. HIRSCHFELDER AND J. W. LINNETT
University of Wisconsin Naval Research Laboratory, Madison, Wisconsin, and Queen's College, Oxford, England
(Received July 1, 1949)

The energy of interaction between two hydrogen atoms at intermediate to large separations is determined by the use of the variational principle applied to a wave function in which both ionic and polarization terms are included. The binding energy is known accurately in the neighborhood of the equilibrium separation from Rydberg's analysis of the experimental vibrational spectrum. At very large separations the van der Waals' energy has been calculated accurately by Pauling and Beach. Our calculations extend from the smallest to the largest internuclear distances. For the normal hydrogen molecule we compute a binding energy of 4.25 ev as compared to the experimental value of 4.74 ev. By comparing our calculations at small separations with Rydberg and at large separations with Pauling and Beach we obtain a *most likely* potential energy curve for all separations. Similarly we obtain a *most likely* potential energy curve for the $^3\Sigma$ excited state of hydrogen by comparing with the accurate results of James, Coolidge, and Present. Many new molecular integrals were evaluated and old ones were recalculated to obtain greater accuracy. Convenient tables of these integrals together with all of the calculational detail is given.

THE energy of interaction between two hydrogen atoms at intermediate to large separations is determined by the use of the variational principle applied to a wave function in which both ionic and polarization terms are included. The binding energy is known quite accurately in the neighborhood of the equilibrium separation from Rydberg's[2] analysis of the experimental vibrational spectrum. At very large separations, the van der Waals' energy has been calculated accurately by Pauling and Beach.[3] Our calculations extend from the smallest to the largest internuclear separations. By comparing our calculations at small distances with the experimental Rydberg potential energy, and at large distances with the Pauling and Beach calculations, we obtain a *most likely* potential energy curve for all separations. The potential energy curve for the $^3\Sigma$ state for excited H_2 is calculated in much the same manner as for the normal H_2 and a *most likely* potential energy curve is obtained by comparing our calculations with the very accurate calculations of James, Coolidge, and Present[4] for three separations ($R/a_o = 1.5$, 1.6, and 1.87).

For the normal hydrogen molecule, we compute a binding energy of 4.25 ev as compared to the experimental value of 4.74 ev. From the behavior of our polarization parameters it would appear that the principal error arises from not letting the electrons spend sufficient time in the region between the two nuclei. Acting upon this suggestion, Gurnee and Magee[5] have made calculations which show that considerable improvement in the binding energy can be obtained by using atomic orbitals centered at points lying slightly closer together than the actual nuclei.

TABLE I. Maximum binding energy normal H_2.[a]

Function	Binding energy ev	kcal./mole	R/a_o	z	α	β	γ
Calculated varying z							
$W+I+P$	+4.25	+98.0	1.44	1.195	−0.05735	−0.06944	0.3334
$W+I$	+3.98	+91.9	1.47	1.178	0	0	0.1647
$W+P$	+3.92	+90.5	1.44	1.146	−0.04624	−0.04496	0
W	+3.75	+86.5	1.45	1.159	0	0	0
Calculated with $z=1$							
$S+I+P$	3.52	81.3	1.68	1	−0.05444	−0.11031	0.2450
$S+I$	3.22	74.2	1.69	1	0	0	0.1607
$S+P$	3.38	78.0	1.65	1	−0.04341	−0.07035	0
S	3.14	72.4	1.66	1	0	0	0
Experimental	4.74	109.3	1.40				

[a] S = Sugiura, W = Wang, I = Ionic, P = Polarization.

I. QUANTUM-MECHANICAL CALCULATIONS

It is necessary to use the variational method in order to calculate the energy of interaction of two hydrogen atoms at intermediate to large separations. The first-order perturbation method can be used for small separations and the second-order perturbation method can be used for large separations. However, London, and Eisenschitz[6] have shown that a combination of the first- and second-order perturbations may not be reliable. Such uncertainty is eliminated by the use of the variational method. Thus James and Coolidge[7] succeeded in calculating the binding energy of normal H_2 at the equilibrium separation to within a probable error of 0.001 ev by applying the variational principle to a wave function containing thirteen adjustable parameters.

We selected the following approximate wave function:

$$\Psi_{HL}=a_o(1)b_o(2)[1+(\alpha z^2)(x_{a1}x_{b2}+y_{a1}y_{b2}) +(\beta z^2)(z_{a1}z_{b2})]+\rho a_o(2)b_o(1)[1+ (\alpha z^2)(x_a\, x_{b1}+y_{a2}y_{b1})+(\beta z^2)(z_{a2}z_{b1})] +\gamma[a_o(1)a_o(2)+b_o(1)b_o(2)]. \quad (1)$$

[1] This work was carried out under Contract NOrd 9938 between the U. S. Navy Bureau of Ordnance and the University of Wisconsin.
[2] R. Rydberg, Zeits. f. Physik **73**, 376 (1931); see also H. Beutler, Zeits. f. physik. Chemie **B27**, 287 (1934).
[3] L. Pauling and J. Y. Beach, Phys. Rev. **47**, 686 (1935); see also H. Margenau, Rev. Mod. Phys. **11**, 32 (1939).
[4] James, Coolidge, and Present, J. Chem. Phys. **4**, 187 and 193 (1936).
[5] E. F. Gurnee and J. Magee, J. Chem. Phys. **18**, 142 (1950).
[6] F. London and R. Eisenschitz, Zeits. f. Physik **60**, 491 (1930).
[7] H. M. James and A. S. Coolidge, J. Chem. Phys. **1**, 825 (1933).

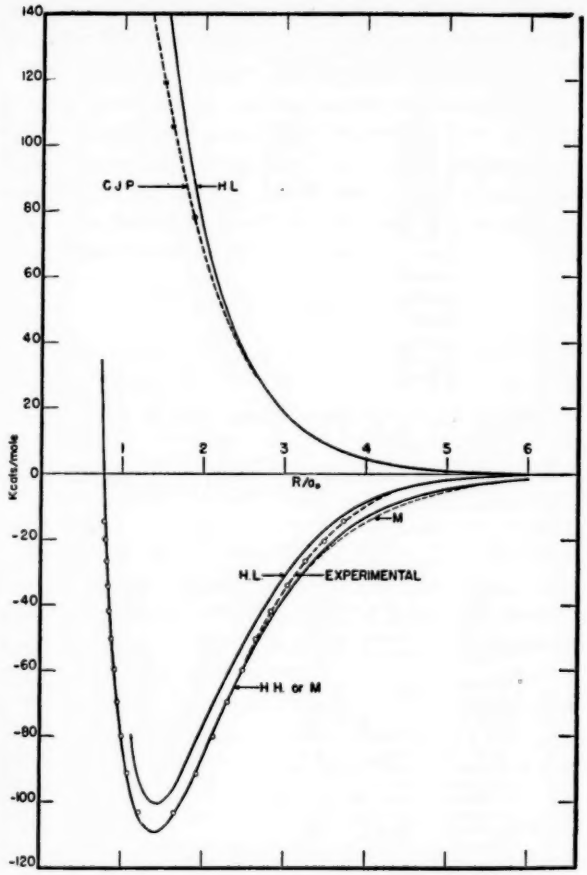

FIG. 1. Energy of hydrogen molecule as function of internuclear separation.

H.L. = Hirschfelder-Linnett calculations given in this paper.
C.J.P. = Coolidge, James, and Present calculations.
M. = Usual Morse curve.
H.H. = Hulburt-Hirschfelder modification of Morse curve.
Experimental = Rydberg determination from experimental vibrational energies.

Here $a_o(1)$ and $b_o(1)$ are the $1s$ hydrogen-like atomic orbitals with centers located respectively on atoms "a" and "b" with effective nuclear charge, z:

$$a_o(1)=(z^3/\pi)^{\frac{1}{2}}\exp(-zr_{a1}), \tag{2}$$

$$b_o(1)=(z^3/\pi)^{\frac{1}{2}}\exp(-zr_{b1}). \tag{3}$$

In these expressions, r_{a1} and r_{b1} are the distances of electron "1" from nuclei "a" and "b" respectively; x_{a1}, y_{a1}, z_{a1} and x_{b1}, y_{b1}, z_{b1} are the Cartesian coordinates of electron "1" measured with respect to "a" and to "b" respectively as origins. The X and Y axes are perpendicular to the line of nuclei, and Z axis is taken along the line of nuclei. We adopt the convention that z_{a1} becomes increasingly positive in the direction of "a" towards "b," and z_{b1} becomes increasingly negative in the direction of "b" towards "a." Thus:

$$x_{a1}=x_{b1},\quad y_{a1}=y_{b1},\quad z_{a1}=z_{b1}+R. \tag{4}$$

Here R is the separation between the nuclei. For the normal $^1\Sigma$ state of the H_2 molecule, the four parameters α, β, γ and z are varied so as to give the lowest energy; the parameter ρ is taken to be one, $\rho=1$. For the excited $^3\Sigma$ state of the H_2 molecule, the three parameters α, β, and z are varied so as to give the lowest energy while ρ is set equal to minus one, $\rho=-1$, and gamma is set equal to zero, $\gamma=0$.

This wave function satisfies the following requirements: (1) It gives good values of the binding energy at small separations. (2) It gives good values of the van der Waals' energy at large separations. (3) It is sufficiently simple that we were able to evaluate all of the exchange and Coulombic integrals at a large number of internuclear separations in a finite length of time.

By varying different combinations of parameters we can obtain a number of individually interesting approximations (designated by the symbols at the left):

W This is the Wang atomic orbital obtained by setting α, β, and γ equal to zero but varying z.

S This is the Sugiura or Heitler-London atomic orbital function obtained by setting α, β, and γ equal to zero and setting $z=1$.

$W+I$ and $S+I$ These are the Weinbaum[8] atomic orbital plus ionic states approximations obtained by setting α and β equal to zero but varying γ. In the $W+I$, z is varied whereas in the $S+I$, z is set equal to one.

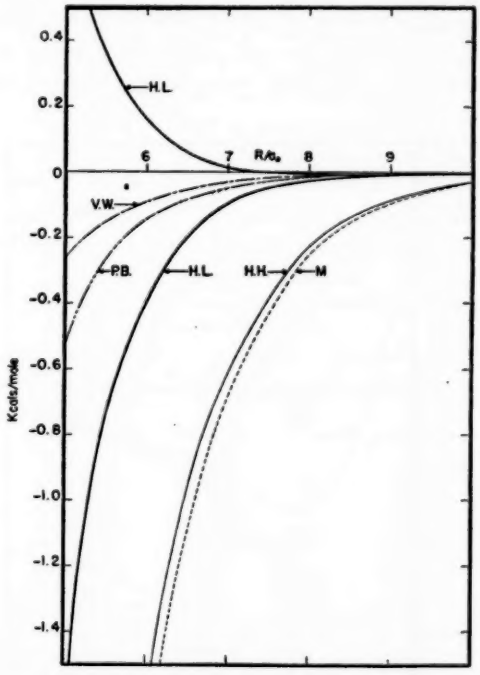

FIG. 2. Energy interaction between two hydrogen atoms at intermediately large separations.

P.B. = Pauling-Beach calculations of van der Waals' energy of attraction.
V.W. = van der Waals' energy using only inverse sixth power energy of attraction.

[8] S. Weinbaum, J. Chem. Phys. **1**, 593 (1933).

TABLE II. Calculated binding energy[a] normal H_2.[b]

$q=zR/a_o$	(Kcal./mole) $W+I+P$	$W+I$	$W+P$	W
1.0	−41.16	−60.28	+5.97	−57.70
1.5	+91.72	+85.15	+88.56	+83.00
1.75	97.90	91.81	89.63	85.85
2.0	88.16	83.28	80.52	74.83
2.5	56.55	54.54	53.57	46.06
3.0	31.35		27.61	26.14
3.5	16.71		14.70	14.05
4.0	8.348		7.380	7.117
4.5	3.983		3.572	3.405
5.0	1.858		1.696	1.584
6.0	0.3995		0.3765	0.318
7.0	0.09190		0.08860	0.060
8.0	0.02510		0.02471	0.0109
10.0	0.004380		0.004371	0.000621
12.0	0.001268		0.001266	0.0000082

[a] Binding energies for q equal or larger than 3.5 are calculated with $z=1$ in order to obtain greatest computational accuracy.
[b] W=Wang, I=Ionic, P=Polarization.

TABLE III. Variation of z with internuclear separation, normal H_2.

$q=zR/a_o$	$W+I+P$	$W+I$	$W+P$	W
1.0	1.3626	1.3976	1.0620	1.3911
1.5	1.2398	1.2411	1.1442	1.2145
1.75	1.1880	1.1746	1.1452	1.1388
2.0	1.1126	1.1195	1.1353	1.0823
2.5	1.0344	1.0472	1.1038	1.0151
3.0	1.0028			
3.5	0.9942			
4.0	0.9932			
4.5	0.9945			
5.0	0.9901			
6.0	0.9957			
7.0	0.9980			
8.0	0.9953			
10.0	0.9979			

TABLE IV. Variation of α, β, and γ for normal H_2.

$q=zR/a_o$	$W+I+P$			$W+I$	$W+P$	
	α	β	γ	γ	α	β
1.0	−0.0555	−0.0440	0.272	(−0.01603)*	−0.04575	−0.05349
1.5	−0.05878	−0.06489	0.3421	+0.1361	−0.04705	−0.04741
1.75	−0.05706	−0.07013	0.3308		−0.04552	−0.04357
2.0	−0.05330	−0.07746	0.2912	0.1780	−0.04303	−0.04081
2.5	−0.04321	−0.06188	0.2100	0.1681	−0.03617	−0.03270
3.0	−0.03269	−0.03534	0.1424		−0.02774	−0.02834
3.5	−0.02345	−0.01376	0.09937		−0.02080	−0.01189
4.0	−0.01642	−0.001845	0.06498		−0.01520	−0.001687
4.5	−0.01151	+0.004034	0.04050		−0.01106	+0.003813
5.0	−0.008131	+0.006575	0.02483		−0.008148	+0.006359
6.0	−0.004707	0.006756	0.008968		−0.004690	0.006681
7.0	−0.002985	0.005233	0.003205		−0.002928	0.005219
8.0	−0.001951	0.003774	0.001147		−0.001955	0.003771
10.0	−0.000998	0.001994	0.000149		−0.000999	0.001994
12.0	−0.000574	0.001157	0.000020		−0.000579	0.001157

* Probably not reliable since γ was calculated on assumption that $z=1$.

$W+P$ and $S+P$ These are the atomic orbital plus polarization approximations obtained by setting γ equal to zero and varying α and β. In the $W+P$, z is varied whereas in the $S+P$, z is set equal to one.

$W+I+P$ and $S+I+P$ These are the full treatments with and without the variation of z. In Figs. 1–3, the $W+I+P$ is referred as the H.L. (Hirschfelder-Linnett).

The maximum binding energies for normal H_2 and the corresponding values of the parameters are given in Table I. Details of the calculations are given in the Appendix. The numerical values are estimated on the basis of $e^2/a_o=27.206$ ev$=627.23$ kcal./mole* and the Bohr radius, $a_o=0.52915$A. The Wang+Ionic+Polarization wave function gives a maximum binding energy of 4.25 ev as compared with the experimental value of 4.74 ev. The Wang function which includes neither ionic nor polarization terms gives 3.75 ev. Thus the inclusion of ionic and polarization terms reduces the discrepancy between calculated and observed binding energies from 20 percent to 10 percent. The minimum for the Wang +Ionic+Polarization theoretical potential energy curve occurs at 0.7610A instead of the experimental value of $R_e=0.7395$A. The binding energy for normal H_2 and the four parameters: z, α, β, and γ are given in Tables II, III, and IV as a function of $q=zR/a_o$. When zR/a_o is greater than 3.0, the value of z is essentially unity. The greatest computational accuracy for the energy is obtained by setting z exactly equal to one. However in Table III where interest centers on the best value of z, we indicate the exact values which we obtained by an arduous process discussed in the Appendix.

In a similar manner, the energy and parameters of the excited $^3\Sigma$ hydrogen molecule are given in Table V as a function of $q=zR/a_o$. Only two approximations $W+P$

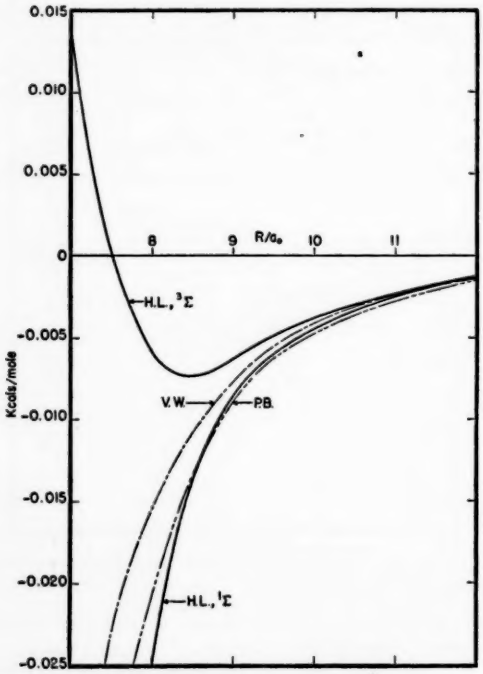

FIG. 3. Van der Waals' energy of interaction of two hydrogen atoms.

* Here we have used the constants of V. W. Dumond and E. R. Cohen (Rev. Mod. Phys. **20**, 82 (1948). By kcal./mole is meant the 15° kcal./mole.

and S are considered. In Figs. 1–3 the $W+P$ is referred to as the H.L. (Hirschfelder-Linnett) approximation.

The functional form of the wave functions which may be used to calculate binding energy at intermediate to large separations is severely limited by the following requirement—the variational principle should yield good values for the van der Waals' energy of attraction when the hydrogen atoms are far apart. For example, the Heitler-London type functions:

$$\Psi=\psi_\alpha(1)\psi_\beta(2)+\psi_\alpha(2)\psi_\beta(1) \qquad (5)$$

would not suffice, since they give zero van der Waals' energy of attraction regardless of the specific form of the one electron orbitals $\psi_\alpha(1)$ and $\psi_\beta(1)$. Here the "1" refers to the electron. Rosen's wave function[9] takes polarization into account but has essentially the form of Eq. (1). Similarly, the Weinbaum[8] function with a combination of polar and homo-polar terms does not give van der Waals' energy. Actually, in order to get van der Waals' energy, there must be statistical correlation between the coordinates of the two electrons, as in the classical theory of van der Waals' attraction—at any instant the electron and proton of atom, "a," induces a dipole moment in atom, "b," by affecting the statistical distribution of the electron on "b"; the interaction between the instantaneous and the induced dipole moments results in the energy of attraction.

The parameters in our wave function have physical significance and the manner in which they vary with internuclear separation gives clues which should be of considerable value in the further development of molecular quantum mechanics.

A. The "Effective Nuclear Charge," z

The parameter, z, is called the "effective nuclear charge" since the atomic orbitals $a_o(1)$ and $b_o(1)$ are solutions to the Schrödinger equation for an electron in the Coulombic field of a nucleus of charge ze. Increasing the value of z contracts the size of the orbitals. Increasing the value of z for a fixed internuclear separation R also has the effect of decreasing the ratio of the average potential to the average kinetic energy of the electrons. However, Hirschfelder and Kincaid[10] (and also Coulson and Bell[11]) have shown that "If the approximate charge distribution is expanded or contracted, the size which corresponds to the lowest energy gives the proper ratio between the potential and kinetic energies." Thus the Wang type variations in z, which we use, automatically establish the correct average distribution of energy between potential and kinetic in accordance with the quantum mechanical virial theorem.[12]

The numerical results in Table I show that the maximum binding energies calculated with z kept equal to unity are all very low, even when ionic and polarization terms are included in the wave function.

In Table III, the change of z with internuclear separation is given for normal hydrogen. When R is zero (Rosen has shown that), z is approximately 1.68. As the internuclear separation increases, z decreases until at $R=3a_o$, z is approximately unity. For larger internuclear separations, where the electron clouds do not appreciably overlap, z remains essentially unity. Actually, careful calculations show for R greater than $3a_o$, z becomes very slightly less than unity. Rosen found the same effect and remarked that "as the atoms approach each other, there is first an expansion of the charges and then, for smaller distances, a contraction." The contraction implies that the two nuclei behave as if they have an increased effective nuclear charge at small values of R. This is due to the mutual repulsion of the two electrons. The expansion at large values of R must arise because the nucleus a exerts more effect than its attendant electron on the electron near b, and vice versa. This results in the charges being pulled towards the nucleus of the approaching atom (cf. Hirschfelder and Kincaid). It is presumably a consequence of the mutual

TABLE V. Excited H_2, $^3\Sigma$.

	$W+P$ Including polarization (varying z)				S Heitler-London ($z=1$)
$\rho=zR/A_o$	E (kcal./mole)	z	α	β	E (kcal./mole)
1.0	232.00	0.8140	−0.0415	0.456	442.30
1.5	107.50	0.8698	−0.0332	0.2581	200.17
1.75	75.20	0.8870	−0.02970	0.2138	138.43
2.0	55.80	0.9132	−0.02652	0.1775	96.60
2.5	30.45	0.9511	−0.02126	0.1288	47.62
3.0	16.35	0.9758	−0.01697	0.09300	23.50
3.5	8.45	0.9893	−0.01351	0.06518	11.47
4.0	4.300	0.9956	−0.01074	0.04449	5.515
4.5	2.008	(0.9981)	−0.008535	0.03009	2.603
5.0	0.9074	(0.9977)	−0.006791	0.02047	1.206
6.0	0.1558	(0.9982)	−0.004340	0.01048	0.247
7.0	+0.01393	(0.9986)	−0.002848	0.006111	+0.048
8.0	−0.00586	(0.9960)	−0.001937	0.003963	+0.00867
10.0	−0.003800	(0.9979)	−0.000999	0.002001	+0.000035
12.0	−0.001252		−0.000579	0.001157	+0.000006

TABLE VI. Rydberg experimental potential energy for normal hydrogen.

Vibrational level	Energy above potential minimum (kcal./mole)	Minimum separation Angstrom	Minimum separation Atomic units (a_o)	Maximum separation Angstrom	Maximum separation Atomic units (a_o)
0	6.12	0.652	1.23	0.887	1.68
1	18.00	0.576	1.09	1.028	1.94
2	29.19	0.536	1.01	1.138	2.15
3	39.75	0.506	0.96	1.228	2.32
4	49.62	0.486	0.92	1.318	2.49
5	58.86	0.466	0.88	1.409	2.66
6	67.48	0.451	0.85	1.504	2.84
7	75.41	0.441	0.83	1.614	3.05
8	82.64	0.431	0.82	1.734	3.28
9	89.18	0.416	0.79	1.855	3.51
10	94.94	0.411	0.78	1.975	3.73
∞	109.32				

[9] N. Rosen, Phys. Rev. **38**, 2099 (1931).

[10] J. Hirschfelder and J. Kincaid, Phys. Rev. **52**, 658 (1937).

[11] C. Coulson, Trans. Faraday Soc. **33**, 1479 (1937); C. Coulson and R. Bell, Trans. Faraday Soc. **41**, 141 (1945).

[12] J. Slater, J. Chem. Phys. **1**, 687 (1933).

TABLE VII. Van der Waals' energy.

	$^3\Sigma$ HL	$^1\Sigma$ HL	PB	vW	HH	M
6	+0.1560	−1.673	−0.1457	−0.0874	−1.673	−1.912
7	+0.0139	−0.0919	−0.0507	−0.0347	−0.6125	−0.6847
8	−0.0059	−0.0251	−0.0209	−0.0156	−0.2261	−0.2448
10	−0.0038	−0.0044	−0.0049	−0.0041	−0.0303	−0.0312
12	−0.0013	−0.0013	−0.0016	−0.0014	−0.0039	−0.0040

TABLE VIII. Most likely potential energy.

A. Normal hydrogen, $^1\Sigma$

1. $R/a_o<4$, Rydberg experimental values given in Table VI
2. $R/a_o=4$, $-E=+10.0$ kcal./mole
3. $4.5\leqslant R/a_o\leqslant 8.5$, Hirschfelder-Linnett, $W+I+P$ values given in Table II
4. $8.5\leqslant R/a_o$ Pauling-Beach values given in Table VII as computed from Eq. (11)

B. Excited hydrogen, $^3\Sigma$

1. $R/a_o<2.5$ James, Coolidge, and Present according to Eq. (12)
2. $2.5\leqslant R/a_o$ Hirschfelder-Linnett, $W+P$ as given in Table V

polarization of the two atoms at large separations. The effect is however small and not of the same magnitude as the change in z that occurs at small values of R.

When z is kept equal to unity the minimum in the potential energy curve occurs at values of R which are much greater than the true value of R_e (see Table I). This is the natural result of failing to contract the hydrogen atom wave functions away from each other as R is decreased, for then the repulsion of the two electrons is exaggerated and this causes the minimum of the curve to be displaced to larger values of R. This result is actually found for all the functions in which $z=1$. For these the minimum is at $(1.67\pm0.03)a_o$ instead of $1.4a_o$. Whereas when z is adjusted to its best value the minimum is at $(1.455\pm0.02)a_o$ whatever the detailed nature of the function used. It is interesting that the calculated potential energy minimum for all these functions is at a nuclear separation which is greater than the true R_e. This implies, perhaps, that all these functions tend to exaggerate the repulsion forces between the electrons even though the introduction of the polarization terms is an attempt to allow further for this interelectronic repulsion.

Table V shows that for the $^3\Sigma$ excited state of the hydrogen molecule, the value of z is always less than unity but that at distances greater than $R=3a_o$, as in the case of the normal hydrogen, z becomes substantially equal to unity.

B. The Ionic Parameter, γ

The parameter γ determines the contribution of the ionic terms, $\gamma[a_o(1)a_o(2)+b_o(1)b_o(2)]$, in the approximate wave function for normal hydrogen. Such terms were first used by Weinbaum.[8] The variation of γ with internuclear separation is given in Table IV. If there were no mutual repulsion between the electrons, the wave function would be expressible in terms of molecular orbitals and γ would be equal to unity. Because mutual electron repulsion does exist, the electrons prefer to be near different nuclei at the same instant rather than near the same nucleus and the value of γ is considerably less than unity. The value of γ is zero for large separation and increases as the nuclei approach one another. As R decreases, the electrons pass more readily from the region of one nucleus to the region of the other and the probability becomes appreciable that at any instant both electrons will be in the vicinity of the same nucleus. It is interesting that γ has a maximum value at about the value of R for which the calculated binding energy is a maximum. There seems to be no easy explanation for this. As the nuclei become closer and closer it becomes less likely that any wave function formed by combining the atomic orbitals of the separated hydrogen atoms will form the basis of a good approximation. Therefore, the various coefficients, like γ, may lose all physical significance when R is small.

C. The Polarization Parameters, α and β

The inclusion of the polarization terms characterized by the parameters α and β enables us to calculate the energy at intermediate to large internuclear separations. For very large separation, γ becomes zero, z becomes unity, and $-\alpha=\beta/2=(R/a_o)^{-3}$. Our wave function then reduces to the simplest function which Hassé[13] used in his determination of the van der Waals' energy by the variational method. These parameters are given as a function of separation in Table IV for normal H_2, and in Table V for excited H_2.

The value of α is negative for all values of R. Reference to the expression for the wave function shows that, for given absolute values of x_{a1} and x_{b2}, this means that the wave function is greater when x_{a1} and x_{b2} have opposite signs than when they have the same sign. The term involving α therefore also allows for the mutual repulsion of the two electrons. Or, in other words, for the instantaneous mutual polarization of the two hydrogen atoms. This mutual polarization increases as the two atoms are brought closer together, as is shown by the increase in the value of $(-\alpha)$ as R decreases. However, like γ, $-\alpha$ is a maximum for a value of R which is near the theoretical equilibrium separation. As with γ there seems to be no reason why there should be a maximum, or why this maximum should be near the theoretical equilibrium separation.

The value of β is positive for values of R greater than $4.1a_o$. For values of R less than this it is negative, and its negative value is also a maximum in the neighborhood of the equilibrium separation. The positive value of β means that, for a given pair of absolute values of z_{a1} and z_{b2}, the wave function is bigger when z_{a1} and z_{b2} are both positive, or both negative, than when one is positive and

[13] H. Hassé, Proc. Camb. Phil. Soc. **26**, 542 (1930); **27**, 66 (1931).

the other negative. The positive value of β at large separations therefore takes account of the instantaneous mutual polarization of the two hydrogen atoms which arises because the electrons repel one another. The negative value of β for R less than $4.1a_o$ means that the wave function is bigger when z_{a1} is positive and z_{b2} negative than when they are both the same sign. So the negative value of β favors the configuration in which both electrons are simultaneously in the region between the nuclei as compared with the configuration in which only one is in that region. It is believed that there is a lowering of the potential energy of the system because of this concentration of negative charge into the region between the nuclei, where the potential energy due to the nuclear fields is low because, at small R, they are both exerting a considerable effect over the whole region between them. The virial theorem, which holds when there is a variable scale factor z, demands that, at the minimum, the relation between the energy, E, the mean potential energy, $\bar{V}$, and the mean kinetic energy, $\bar{T}$, is

$$E=(1/2)\bar{V}=-\bar{T}. \tag{6}$$

Therefore, the electronic potential energy must be low, compared with that in the separated atoms, at values of R near R_e. This low potential energy is achieved by concentrating the negative electronic charge in between the positive nuclei. In our function, therefore, β has a negative sign when R is close to R_e.

A fault of the present function at small values of R is that it treats the configuration in which z_{a1} is positive and z_{b2} is negative in the same term and with the same coefficient as the configuration in which z_{a1} is negative and z_{b2} positive. It is unfortunate that this function gives these two configurations the same weight.

Rosen introduced polarization, parallel to the line of the nuclei, into the Heitler-London function in a different way. He gave each electron cloud a distortion parallel to the nuclear axis but the form of the function was such that it was unable to take account of the instantaneous mutual polarization of the two atoms at large separations. It did, however, lead to the same picture at small separations: namely, that the negative electronic charge tended to migrate to the region between the nuclei. Thus Rosen found that his σ was positive throughout (this positive value of his σ corresponds to our negative value of β). As R increased σ does not change sign, as our β does, because his function is of such a form that it is unable to take account of the mutual polarization of the two atoms that lead to van der Waals' attraction, which is the cause of the change in sign of our β. Like our β Rosen's σ has a maximum absolute value when R is near R_e.

The polarization parameters for the $^3\Sigma$ state of hydrogen are given in Table V. It will be seen that for this state, α is negative for all values of R and increases steadily as R is decreased; and β is positive for all values of R and increases steadily as R is decreased. For both, this is entirely what would be expected if the terms take account of interelectronic repulsion, that is, of the instantaneous mutual polarization of the electron clouds of the two hydrogen atoms (cf. the discussion of the sign and magnitude of α and β for the $^1\Sigma$ state). It appears that, for this state, the terms involving α and β do, in fact, take account of the mutual repulsion throughout. On simple molecular orbital theory one electron would be in a level associated with the function $(a_o(1)+b_o(1))$ while the other was in a level associated with a function $(a_o(2)-b_o(2))$. For the first level there tends to be an increase of the probability of finding the electron in the region between the two nuclei. For the other level there tends to be a decrease in the electron probability in the region between the two nuclei. The general deduction is independent of the exact molecular orbital function used. The result is that, unlike the $^1\Sigma$ state, there is not a considerable concentration of electron density in the region between the nuclei. Therefore, even at values of R/a_o in the neighborhood of 1 or 2 the terms involving α and β seem to retain the significance they had at large values of R of taking account of mutual polarization. It is worth remarking however, that β assumes a much larger value than α in the region of R equals a_o and $2a_o$ which may mean that it has an additional significance. Alternatively it may only mean that the mutual polarization is greater in the z direction than in the x and y directions.

II. ENERGY OF INTERACTION BETWEEN TWO HYDROGEN ATOMS

The *best* or *most likely* potential energy curves for normal and excited hydrogen molecules can be obtained by comparing various experimental and theoretical calculations. This is done in Figs. 1, 2, and 3 for small, intermediate, and large internuclear separations respectively and the results are given in Table VIII.

The most reliable experimental data for normal H_2 up to separations as large as $3.7a_o$ is obtained by Rydberg's[2] analysis (using the Klein method) of the first ten

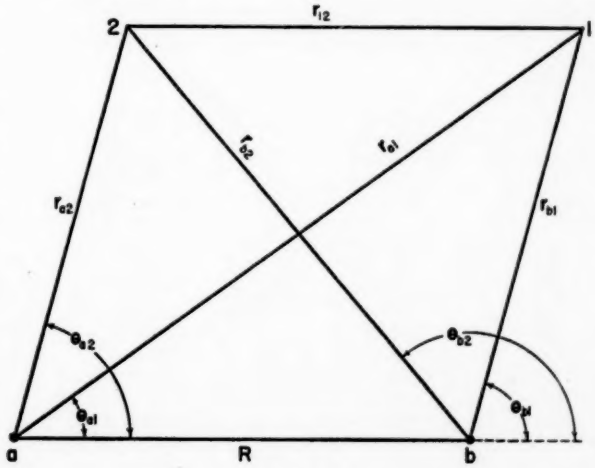

FIG. 4.

vibrational levels of molecular hydrogen. His results are given in Table VI and are labeled "experimental" in Fig. 1. The separations are given with an accuracy of 0.005A or 0.01 atomic unit.

It is interesting to compare the Rydberg experimental values with the usual Morse curve which is very frequently used because of its simplicity.

$$E_{\text{Morse}}=109.46[-2\exp(-x)+\exp(-2x)]\ \text{kcal./mole}, \quad (7)$$

where

$$x=1.0298((R/a_o)-1.401). \quad (8)$$

The Morse curve agrees nicely with Rydberg's up to $R/a_o=2.5$ but for larger separations it gives too much binding energy.

Hulburt and Hirschfelder[14] suggested a modification of the Morse potential which contains five in place of three constants and should therefore be somewhat more accurate.

$$E_{\text{HH}}=109.46\left[\begin{matrix}-2\exp(-x)+\exp(-2x)\\ -0.1145x^3\exp(-2x)(1-0.704x)\end{matrix}\right]\ \text{kcal./mole}. \quad (9)$$

However, a comparison with Rydberg shows that this potential is not appreciably more accurate than the original Morse curve.

The potential energy curve we have obtained is compared in Fig. 1 with the curve deduced by Rydberg. The same figure also shows a curve drawn using a formula of the Hulbert-Hirschfelder type. The energy difference between the experimental points of Rydberg and our theoretical curve is about 10 percent in the region of the minimum. The energy difference between the theoretical curve and the experimental points decreases as R increases but the percentage separation increases to about 20 percent near $3.5a_o$. It will be seen that the experimental points lie close to the Hulbert-Hirschfelder line from about $R/a_o=1$ to 2.5. Beyond this, however, the experimental points are above the Hulbert-Hirschfelder line and for R greater than $3.5a_o$ the present theoretical line seems to lie closer than the Hulbert-Hirschfelder line to the true potential energy curve.

One reason for choosing the function that we have used was that the terms involving α and β took account of the mutual instantaneous polarization of the two hydrogen atoms and so the function was designed so that it would lead to a van der Waals' attraction between the H atoms at large values of R. Other functions, like that of Rosen, are such a form that they cannot lead to a van der Waals' attraction either because they do not contain atomic polarization terms at all or because the atomic polarization terms that they do include are not properly dependent on one another.

TABLE IX. Basic integrals.

$q=ZR$	I_{oo}	I_{cc}	I_{ss}	$G_{o/Z}$	$G_{c/Z}$
0.0	1.000000	1.000000	2.000000	1.000000	0.500000
1.0	0.858385	0.735759	1.646880	0.729329	0.548950
1.5	0.725173	0.482519	1.308467	0.583688	0.536304
2.0	0.586453	0.225559	0.965275	0.472527	0.492661
2.5	0.458308	$0.^{3}5130$	0.668203	0.390567	0.435666
3.0	0.348509	−0.159319	0.438045	0.330028	0.378482
3.5	0.259194	−0.264856	0.274051	0.284542	0.327590
4.0	0.189262	−0.318692	0.164675	0.249581	0.284908
4.5	0.136085	−0.332576	$0.^{1}95545$	0.222071	0.250068
5.0	$0.^{1}96577238$	−0.3189295	$0.^{1}5376360$	0.19994552	0.22185876
6.0	$0.^{1}47096292$	−0.2503540	$0.^{1}1574933$	0.16665949	0.180181700
7.0	$0.^{1}2218913$	−0.1714338	$0.^{2}4235616$	0.142856193	0.151539775
8.0	$0.^{1}1017569971$	−0.107191492	$0.^{2}10632933$	0.124999873	0.1308487433
10.0	$0.^{2}2012730219$	$-0.^{1}34912546$	$0.^{4}570751761$	$0.^{1}999999977$	0.1029997191
12.0	$0.^{2}3747969535$	$-0.^{2}9652558$	$0.^{5}26064767$	$0.^{1}83333333$	$0.^{1}850694374$
1.75	0.6552725786	+0.3514849529	1.133534347	0.5239755402	0.5172387306

$q=ZR$	$G_{s/Z}$	$J_{o/Z}$	$J_{c/Z}$	$J_{s/Z}$	$K_{oo,\,oo/Z}$
0.0	1.000000	1.000000	0.500000	1.000000	0.625000
1.0	0.894694	0.735759	0.306566	0.778930	0.554521
1.5	0.804017	0.557826	0.153402	0.586554	0.490338
2.0	0.714289	0.406006	$0.^{1}22556$	0.407421	0.425974
2.5	0.633281	0.287298	$-0.^{1}701144$	0.264909	0.368388
3.0	0.563267	0.199148	−0.124468	0.163102	0.319804
3.5	0.503922	0.135888	−0.147841	$0.^{1}95946$	0.279944
4.0	0.453937	$0.^{1}91578$	−0.149578	$0.^{1}54308$	0.247554
4.5	0.411796	$0.^{1}61100$	−0.138168	$0.^{1}29744$	0.221192
5.0	0.3760937	$0.^{1}4042768$	−0.1201601	$0.^{1}1583449$	0.19956908
6.0	0.3194558	$0.^{1}1735126$	$-0.^{1}8055943$	$0.^{2}4179292$	0.16659267
7.0	0.2769694	$0.^{2}7295056$	$-0.^{1}4848173$	$0.^{2}1021136$	0.142844724
8.0	0.244140805	$0.^{3}3019163651$	$-0.^{1}27116562$	$0.^{3}234625836$	0.124997956
10.0	0.197000003	$0.^{3}4993992274$	$-0.^{2}7316955$	$0.^{4}107521224$	$0.^{1}99999472$
12.0	0.164930556	$0.^{4}7987476059$	$-0.^{2}1729596$	$0.^{5}427866198$	$0.^{1}83333332$
1.75	$0.^{1}7583760654$	0.4778783446	$+0.^{1}8371921757$	0.4933150199	0.4576042080

[14] H. Hulburt and J. Hirschfelder, J. Chem. Phys. 9, 61 (1941).

TABLE IX.—*Continued.*

$q=ZR$	$K_{cc,\,cc/Z}$	$K_{ss,\,ss/Z}$	$K_{os,\,os/Z}$	$K_{cs,\,cs/Z}$	$K_{oc,\,oc/Z}$	$L_{oo,\,oo/Z}$
0.0	0.391406	0.825000	0.145833	$0.^{1}42188$	$0.^{1}72916$	0.625000
1.0	0.37433	0.773402	0.123914	$0.^{1}1898$	$0.^{1}42717$	0.436651
1.5	0.360048	0.719081	0.103043	$0.^{2}8325$	$0.^{1}18936$	0.296835
2.0	0.345879	0.657139	$0.^{1}81725$	$-0.^{2}1432$	$-0.^{4}30$	0.184156
2.5	0.331183	0.594686	$0.^{1}62773$	$-0.^{2}8268$	$-0.^{1}11818$	0.106622
3.0	0.314537	0.536225	$0.^{1}47309$	$-0.^{1}11760$	$-0.^{1}17301$	$0.^{1}58508$
3.5	0.295358	0.483922	$0.^{1}35359$	$-0.^{1}12569$	$-0.^{1}18497$	$0.^{1}30766$
4.0	0.274176	0.438333	$0.^{1}26430$	$-0.^{1}11690$	$-0.^{1}17316$	$0.^{1}15627$
4.5	0.252151	0.399107	$0.^{1}19880$	$-0.^{1}10003$	$-0.^{1}15112$	$0.^{2}7714$
5.0	0.2305073	0.365497910	$0.^{1}1511295$	$-0.^{2}8107280$	$-0.^{1}1268642$	$0.^{2}371704$
6.0	0.1917270	0.311778878	$0.^{2}9097311$	$-0.^{2}4846741$	$-0.^{2}8510270$	$0.^{2}814027$
7.0	0.1610067	0.271296778	$0.^{2}5801824$	$-0.^{2}2741192$	$-0.^{2}5669731$	$0.^{2}167600$
8.0	0.137725185	0.239903208	$0.^{2}39011236$	$-0.^{2}1544918$	$-0.^{2}3873036$	$0.^{4}328960$
10.0	0.106504961	0.194539121	$0.^{2}19998488$	$-0.^{3}535527$	$-0.^{2}1998731$	$0.^{5}113835$
12.0	$0.^{1}87020932$	0.163411431	$0.^{2}11574032$	$-0.^{3}216840$	$-0.^{2}1157364$	$0.^{7}354839$
1.75	0.352943470	0.688560847	$0.^{1}922190597$	$+0.^{2}3171535$	$+0.^{2}86000949$	0.23611543

$q=ZR$	$L_{ee,\,ee/Z}$	$L_{ss,\,ss/Z}$	$L_{os,\,os/Z}$	$L_{cs,\,cs/Z}$	$L_{oc,\,oc/Z}$
0.0	0.391406	0.825000	0.145833	$0.^{1}42188$	$0.^{1}72916$
1.0	0.2035	0.66567	0.11119	$0.^{2}845$	$0.^{1}4625$
1.5	$0.^{1}93613$	0.51691	$0.^{1}8153$	$-0.^{1}1550$	-0.114956
2.0	$0.^{1}4395$	0.37095	$0.^{1}54758$	$-0.^{1}3114$	-0.144307
2.5	$0.^{1}43284$	0.24907	$0.^{1}34269$	$-0.^{1}3629$	-0.138115
3.0	$0.^{1}61445$	0.15813	$0.^{1}20260$	$-0.^{1}3367$	-0.112495
3.5	$0.^{1}75931$	$0.^{1}95715$	$0.^{1}11433$	$-0.^{1}2715$	$-0.^{1}82014$
4.0	$0.^{1}78505$	$0.^{1}55647$	$0.^{2}6206$	$-0.^{1}1987$	$-0.^{1}55077$
4.5	$0.^{1}70531$	$0.^{1}31249$	$0.^{2}3261$	$-0.^{1}1350$	$-0.^{1}34701$
5.0	$0.^{1}569410$	$0.^{1}17028$	$0.^{2}166632$	$-0.^{2}8656$	$-0.^{1}208652$
6.0	$0.^{1}294102$	$0.^{2}4688$	$0.^{3}40649$	$-0.^{2}3105$	$-0.^{2}66051$
7.0	$0.^{1}121820$	$0.^{2}1188$	$0.^{4}92185$	$-0.^{3}9711$	$-0.^{2}18605$
8.0	$0.^{2}43184$	$0.^{3}283$	$0.^{4}1973$	$-0.^{3}275$	$-0.^{3}47860$
10.0	$0.^{3}392491$	$0.^{4}137$	$0.^{6}7952$	$-0.^{4}175$	$-0.^{4}25982$
12.0	$0.^{4}265330$	$0.^{6}568$	$0.^{7}2822$	$-0.^{5}89$	$-0.^{5}116873$
1.75	$0.^{1}675754$	0.441865	$0.^{1}674753$	$-0.^{1}246928$	-0.1348339

$q=ZR$	$L(a_o, a_o; a_o, b_o)$	G_{co}	$L(a_o, a_c; a_o, b_c)$	$L(a_o, a_s; a_o, b_s)$
0.0	0.625	0.0	$0.^{1}7291666667$	0.145833
1.0	0.50704485	0.187988301	$0.^{1}4063749$	0.122314
1.5	0.40536896	0.1816793613	$0.^{1}1559917$	0.10013
2.0	0.30803646	0.1538428958	$-0.^{2}4239108$	$0.^{1}77650$
2.5	0.22559548	0.1232108094	$-0.^{1}16473472$	$0.^{1}57715$
3.0	0.16074246	$0.^{1}967894319$	$-0.^{1}21943231$	$0.^{1}41534$
3.5	0.1121558092	$0.^{1}7602178750$	$-0.^{1}22678274$	$0.^{1}29146$
4.0	$0.^{1}7698167$	$0.^{1}6029852650$	$-0.^{1}20684210$	$0.^{1}20042$
4.5	$0.^{1}5215030051$	$0.^{1}4851960921$	$-0.^{1}174718272$	$0.^{1}10373$
5.0	$0.^{1}34953043$	$0.^{1}3966222452$	$-0.^{1}140023272$	$0.^{2}9057$
6.0	$0.^{1}15311456$	$0.^{1}2772640534$	$-0.^{2}80856288$	$0.^{2}3921$
7.0	$0.^{2}6537867888$	$0.^{1}2040042496$	$-0.^{2}424690746$	$0.^{2}1653$
8.0	$0.^{2}27387379$	$0.^{1}1562384476$	$-0.^{2}209458666$	$0.^{3}673$
10.0	$0.^{3}4610930366$	$0.^{2}9999974833$	$-0.^{3}450608960$	$0.^{3}108$
12.0	$0.^{4}74658581$	$0.^{3}6944443909$	$-0.^{4}872422396$	$0.^{4}18$
1.75	0.3552642088	0.1689187589	$+0.^{2}4775861$	$0.^{1}887086$

At sufficiently large distances, the energy of interaction of two hydrogen atoms becomes:

$$E_{vW} = -6.5(e^2/a_o)(a_o/R)^6 = -4078/(R/a_o)^6 \text{ kcal./mole.} \quad (10)$$

For slightly smaller separations, according to Pauling and Beach[3] (see Margenau)[15] the energy arising from van der Waals' attraction is

$$E_{PB} = -4{,}076(R/a_o)^{-6} - 78{,}027(R/a_o)^{-8} - 712{,}038(R/a_o)^{-10} \text{ kcal./mole.} \quad (11)$$

Table VII gives the values of E obtained from this equation for large values of R/a_o together with our calculated values. The figures calculated using the present function lie above those of Pauling and Beach at $R/a_o=10$ and 12 (less binding) but below theirs at $R/a_o=7$ and 8 (more binding than theirs). The above formula of Pauling and Beach only takes into account van der Waals' attraction—van der Waals' repulsion and exchange attraction are not included. It therefore appears that, for $R/a_o=10$ and 12 exchange attraction is negligible but that there may be some van der Waals' repulsion so that our figures, which include this, are above those of Pauling and Beach. But for $R/a_o=8$ and 7 it seems that exchange binding is beginning to contribute. From this it would appear that "valency binding" becomes really apparent when R is reduced to

[15] R. Margenau, Rev. Mod. Phys. **11**, 32 (1939).

TABLE X. $H(m, n, q)$.

$q=ZR$	$H(0, 0)$	$H(0, 2)$	$H(0, 4)$	$H(0, 6)$	$H(2, 2)$
0.5	0.5263850	3.98818	113.9415	9297.92	38.92130
1.0	$0.^{1}7399640$	0.2603651	2.158613	44.4104	1.037840
1.5	$0.^{1}1506423$	$0.^{1}3771799$	0.1691903	1.595013	0.1014602
2.0	$0.^{2}2596218$	$0.^{2}741510$	$0.^{1}2315777$	0.1303981	$0.^{1}1600342$
2.5	$0.^{3}9394238$	$0.^{2}1707954$	$0.^{2}4223066$	$0.^{1}1659601$	$0.^{2}3203706$
3.0	$0.^{3}2601366$	$0.^{3}4329912$	$0.^{3}911993$	$0.^{2}2767152$	$0.^{3}7371268$
3.5	$0.^{4}7504706$	$0.^{3}1170097$	$0.^{3}2195736$	$0.^{3}5507173$	$0.^{3}1855502$
4.0	$0.^{4}2231940$	$0.^{4}3308974$	$0.^{4}5695507$	$0.^{3}1237927$	$0.^{4}49705840$
4.5	$0.^{5}6795924$	$0.^{5}9680117$	$0.^{4}1558726$	$0.^{4}3035326$	$0.^{4}1393324$
5.0	$0.^{5}2108426$	$0.^{5}2907023$	$0.^{5}4440395$	$0.^{4}7934455$	$0.^{5}4042300$
6.0	$0.^{6}2119386$	$0.^{6}2780161$	$0.^{6}3928707$	$0.^{6}6201958$	$0.^{6}3668542$
7.0	0.72225164	0.72814819	0.73767454	0.75471039	0.73576132
8.0	$0.^{8}241277$	$0.^{8}296886$	$0.^{8}381835$	$0.^{8}522611$	$0.^{8}366513$
10.0	$0.^{10}304105$	$0.^{10}359743$	$0.^{10}438190$	$0.^{10}555118$	$0.^{10}426439$
12.0	$0.^{12}409213$	$0.^{12}471318$	$0.^{12}554237$	$0.^{12}669494$	$0.^{12}543616$
1.75	$0.^{2}7256391$	$0.^{1}16297041$	$0.^{1}59709541$	0.4245939	$0.^{1}38733375$
$q=ZR$	$H(2, 4)$	$H(2, 6)$	$H(4, 4)$	$H(4, 6)$	$H(6, 6)$
0.5	1330.860	116706.9	53769.80	5207849.0	$5491396^{2}.0$
1.0	9.74306	214.2362	105.3940	2552.528	67400.34
1.5	0.4950293	4.948347	2.691098	29.36522	348.9554
2.0	$0.^{1}5295265$	0.3131766	0.1895836	1.207843	8.330912
2.5	$0.^{2}825198$	$0.^{1}3374799$	$0.^{1}2250316$	$0.^{1}977478$	0.4551916
3.0	$0.^{2}1599594$	$0.^{2}5010642$	$0.^{2}3619242$	$0.^{1}1189016$	$0.^{1}4140596$
3.5	$0.^{3}3560849$	$0.^{3}916073$	$0.^{3}7049874$	$0.^{2}1882640$	$0.^{2}5271534$
4.0	$0.^{4}870468$	$0.^{3}1930795$	$0.^{3}1561040$	$0.^{3}3565483$	$0.^{3}8459180$
4.5	$0.^{4}2274380$	$0.^{4}4502060$	$0.^{4}3781830$	$0.^{4}766141$	$0.^{3}1599926$
5.0	$0.^{5}6242628$	$0.^{4}1130463$	$0.^{5}9783058$	$0.^{4}1804683$	$0.^{4}3411056$
6.0	$0.^{6}5222953$	$0.^{6}832081$	$0.^{6}7508516$	$0.^{5}1210936$	$0.^{5}1984362$
7.0	$0.^{7}4812131$	0.77033889	0.76519462	$0.^{7}961071$	$0.^{6}1432282$
8.0	$0.^{8}473274$	$0.^{8}650905$	$0.^{8}614181$	$0.^{8}84988$	$0.^{7}118517$
10.0	$0.^{10}520703$	$0.^{10}661567$	$0.^{10}637678$	$0.^{10}81305$	$0.^{9}104113$
12.0	$0.^{12}640300$	$0.^{12}77493$	$0.^{12}755625$	$0.^{12}91656$	$0.^{11}111473$
1.75	0.15212236	1.1416611	0.65540465	5.3355808	47.191982

about 5 or 4.5A. The Rydberg figures indicate that the theoretical curve obtained in this paper is quite good beyond $R=5a_o$ and probably, on the whole, the best available at the present time for this region.

The potential energy curve for the $^3\Sigma$ state has been discussed by James, Coolidge, and Present.[4] Using a highly flexible variational function and applying certain corrections, they calculated that for $R/a_o=1.5$, 1.6, and 1.87 the energies of repulsion were 119.3, 105.6, and 77.9 kcal./mole respectively. By fitting a formula to their results we obtain:

$$E_{JCP}=349.7(R/a_o)^{-4/3} \times\exp(-0.357(R/a_o)) \text{ kcal./mole.} \quad (12)$$

Our theoretical curve is 33, 24, and 10 kcal./mole above the James, Coolidge, and Present calculations at their calculated points. This is shown graphically in Fig. 1. Our calculated energy is 28 percent above that of James, Coolidge, and Present at $1.5a_o$; 23 percent above at $1.6a_o$; and 13 percent above at $1.87a_o$. So both the percentage difference and the absolute difference between the two sets of calculated values is decreasing as R increases. Since the energies calculated by James, Coolidge, and Present are calculated using a much more flexible variation function, there is no doubt that their calculated energies are much more reliable than ours. It seems that ours provide a good approximation to the $^3\Sigma$ potential energy curve beyond $2.5a_o$ and that the best over-all curve would be that through the three points given by James *et al.* and taking up the course of our curve at $R=2.5a_o$ and following it for values of R greater than this.

According to Fig. 3, the $^3\Sigma$ state has a minimum energy of -0.0074 kcal./mole when $R/a_o=8.45$; when $R/a_o=7.51$, the energy of interaction is zero; at smaller separations, the energy of interaction is positive.

To summarize, the wave function we have used contains a scale factor, polar terms and polarization terms which are of such a form that the position of one electron is to some extent affected by the position of the other electron. This wave function gives a better calculated binding energy for the ground state of the hydrogen molecule than any other function so far used which is formed by combining orbitals based on those of the separated atoms. The changes in the function, as represented by changes in the coefficients of various terms, can be related to physical concepts and this helps our understanding of the causes of binding in this molecule. Because of the way in which the mutual polarization of the two atoms is included the function leads to van der Waals' attraction at large separations and therefore probably gives a good reproduction of the potential energy curve at intermediate and large values of R. Calculations have also been made for the $^3\Sigma$ state and

the energies obtained are probably good for R greater than 1.5A. For R less than this the calculated energies are high. For this state, as well as the ground state, the changes in the function as R changes can be related to physical concepts.

The calculations of the basic integrals was an extremely difficult job. The authors wish to express their utmost thanks to the following persons who assisted in the algebraic developments of the integrations: Charles Curtiss, Wallace Spaulding, Robert Buehler, Robert Wentorf, Robert Bird, and Ellen Spotz. Moreover, the authors are very grateful to the able computational group of Phyllis Rood, Phyllis Rhoades, Marjorie Leikvold, and Mary Nordling under the direction of Ruth Shoemaker for carrying out the large volume of numerical calculations accurately and efficiently.

APPENDIX

I. Integrals

There are thirty-two basic integrals which must be considered in this treatment. If we let:

$$a_o(1)=(z^3/\pi)^{\frac{1}{2}}\exp(-zr_{a1}), \tag{13}$$

$$a_c(1)=(z^5/\pi)^{\frac{1}{2}}r_{a1}\cos\theta_{a1}\exp(-zr_{a1}), \tag{14}$$

$$a_s(1)=(z^5/\pi)^{\frac{1}{2}}r_{a1}\sin\theta_{a1}\exp(-zr_{a1}). \tag{15}$$

Here the "1" refers to electron one, the "z" refers to the screening constant, the "r_{a1}" is the distance of electron one from the

TABLE XI. $S(m, n, q)$.

$q=ZR$	$S(1,0)$	$S(1,2)$	$S(1,4)$	$S(1,6)$
0.5	2.943036	19.12973	335.5061	12959.66
1.0	0.1691691	0.4905904	2.554453	25.26541
1.5	$0.^{1}2212759$	$0.^{1}4589425$	0.1363169	0.6474368
2.0	$0.^{2}4006546$	$0.^{2}6939910$	$0.^{1}1518553$	$0.^{1}4625638$
2.5	$0.^{3}8624572$	$0.^{2}1336809$	$0.^{2}2433509$	$0.^{2}5596519$
3.0	$0.^{3}2065627$	$0.^{3}2970932$	$0.^{3}4798545$	$0.^{3}9174188$
3.5	$0.^{4}5317096$	$0.^{4}7248613$	$0.^{3}1077991$	$0.^{3}1816493$
4.0	$0.^{4}1441441$	$0.^{4}1887796$	$0.^{4}2644604$	$0.^{4}4074248$
4.5	$0.^{5}4062874$	$0.^{5}5158011$	$0.^{5}6908310$	$0.^{5}9964394$
5.0	$0.^{5}1180398$	$0.^{5}1461878$	$0.^{5}1890889$	$0.^{5}2594631$
6.0	$0.^{6}1066704$	$0.^{6}1273130$	$0.^{5}1566062$	$0.^{6}2004298$
7.0	$0.^{7}1030320$	$0.^{7}1197917$	0.71423912	0.71740970
8.0	$0.^{8}1044027500$	$0.^{8}1190414579$	$0.^{8}1380407891$	$0.^{8}1634692317$
10.0	$0.^{10}1185163333$	$0.^{10}1315273655$	$0.^{10}1475376339$	$0.^{10}1676355629$
12.0	$0.^{12}1474661932$	$0.^{12}1607601491$	$0.^{12}1765506727$	$0.^{12}1955701477$
1.75	$0.^{2}9156057947$	$0.^{1}1714784479$	$0.^{1}4281519718$	0.1586289491
$q=ZR$	$S(3,0)$	$S(3,2)$	$S(3,4)$	$S(3,6)$
0.5	104.4778	985.9169	26771.32	1520631.0
1.0	1.843943	6.919016	51.79112	742.1449
1.5	0.1327655	0.3302747	1.293781	8.539822
2.0	$0.^{1}1667009$	$0.^{1}3296457$	$0.^{1}8857552$	0.3439041
2.5	$0.^{2}2802986$	$0.^{2}4799402$	$0.^{1}1018046$	$0.^{1}2899745^{*}$
3.0	$0.^{3}5623095$	$0.^{3}8734286$	$0.^{2}1583860$	$0.^{2}3574092$
3.5	$0.^{3}1267422$	$0.^{3}1836336$	$0.^{3}2986398$	$0.^{3}5722014$
4.0	$0.^{4}3099917$	$0.^{4}4264689$	$0.^{4}6410831$	$0.^{3}1092018$
4.5	$0.^{5}8050510$	$0.^{4}1064298$	$0.^{4}1508563$	$0.^{4}2356295$
5.0	$0.^{5}2188277$	$0.^{5}2803391$	$0.^{5}3798059$	$0.^{5}5556497$
6.0	$0.^{6}1786728$	$0.^{6}2185508$	$0.^{6}2776835^{*}$	$0.^{6}3711228$
7.0	$0.^{7}1603613$	$0.^{7}1899404$	$0.^{7}2311980$	$0.^{7}2915260$
8.0	$0.^{8}1537278979$	$0.^{8}1778424593$	$0.^{8}2099888341$	$0.^{8}2544228628$
10.0	$0.^{10}1614140930$	$0.^{10}1808463918$	$0.^{10}2051891017$	$0.^{10}2363945525$
12.0	$0.^{12}1906478446$	$0.^{12}2092316477$	$0.^{12}2315882423$	$0.^{12}2589136545$
1.75	$0.^{1}4486037182$	$0.^{1}9805955309$	0.3108223462	1.556176689
$q=ZR$	$S(5,0)$	$S(5,2)$	$S(5,4)$	$S(5,6)$
0.5	9076.321	103352.1	3673865.0	$2740601^{2}.0$
1.0	42.27536	186.0437	1783.837	33447.50
1.5	1.459601	4.148877	20.12753	171.4878
2.0	0.1132744	0.2501610	0.8026585	4.036441
2.5	$0.^{1}1356818$	$0.^{1}2545015^{*}$	$0.^{1}6235846$	0.2164749
3.0	$0.^{2}2120455$	$0.^{2}3551447$	$0.^{2}7235439$	$0.^{1}1925211$
3.5	$0.^{3}3953873$	$0.^{3}6098411$	$0.^{2}1089742$	$0.^{2}2389482$
4.0	$0.^{4}8343824$	$0.^{3}1209482$	$0.^{3}1963094$	$0.^{3}3731746$
4.5	$0.^{4}1927218$	$0.^{4}2662464$	$0.^{4}4019349$	$0.^{4}6865007$
5.0	$0.^{5}4764813$	$0.^{5}6336574$	$0.^{5}9045776$	$0.^{4}1423928$
6.0	$0.^{6}3373203$	$0.^{6}4241522$	$0.^{5}5592882$	$0.^{5}7861367$
7.0	$0.^{7}2736064$	$0.^{7}3309544$	$0.^{7}4140033$	$0.^{7}5411842$
8.0	$0.^{8}2433638244$	$0.^{8}2862015571$	$0.^{8}3450336709$	$0.^{8}4293467522$
10.0	$0.^{10}2306546843$	$0.^{10}2612074028$	$0.^{10}3002485691$	$0.^{10}3514852418$
12.0	$0.^{12}2549948109$	$0.^{12}2819537319$	$0.^{12}3148456221$	$0.^{12}3557080279$
1.75	0.3790780474	0.9356389908	3.606043864	23.04086594

TABLE XII.

	X_1	X_2	X_3	X_4	X_5	X_6	X_7	X_8	X_9	X_{10}	X_{11}	X_{12}
$S(1,0,q)$	+1	3	9	−7	0		0	0	39	2	−2/5	0
$S(1,2,q)$	−3	−24	−81	6	6		36	96	−234	−12	7/5	39/4
$S(1,4,q)$		35	135	25	−25		−120	−320	195	10	−1	−117/2
$S(1,6,q)$		−14	−63	0	21		84	224	0	0	0	195/4
$S(3,0,q)$		−3	−38	0	6		0	0	−45	−10	1	39/4
$S(3,2,q)$		87	342	30	−18	51	−138	−690	270	60	−1	−279/4
$S(3,4,q)$		−245	−570	−50	0	−240	460	2300	−225	−50		465/4
$S(3,6,q)$		161	266		0	217	−322	−1610				−225/4
$S(5,0,q)$		0	21		−7	0	0	0				−45/4
$S(5,2,q)$		−63	−189		21	−63	126	630				135/2
$S(5,4,q)$		210	315			315	−420	−2100				−225/4
$S(5,6,q)$		−147	−147			−294	294	1470				

TABLE XIII.

	Y_1	Y_2	Y_3	Y_4	Y_5	Y_6	Y_7	Y_8	Y_9	Y_{10}	Y_{11}	Y_{12}
$H(0,0,q)$	+1	3	1	−7	0	0			9/2	1	−1/5	0
$H(0,2,q)$	−6	−36	−18	42	9	0			−54	−12	7/5	9/4
$H(0,4,q)$	0	30	30	0	−20	0			45	10	−1	−27/2
$H(0,6,q)$	0	0	−14	0	7	0			0	0	0	45/4
$H(2,2,q)$	9	117	81	−54	−27	27	−27	−135	162	36	−6/5	−27/2
$H(2,4,q)$		−240	−270	−30	60	−135	180	900	−270	−60	1	369/4
$H(2,6,q)$		42	126	0	−21	63	−126	−630	0	0		−135/2
$H(4,4,q)$		175	225	25		225	−300	−1500	225/2	25		−135/2
$H(4,6,q)$		−140	−210			−315	420	2100				225/4
$H(6,6,q)$		49	49			147	−147	−735				

nucleus "a," and the "θ_{a1}" is the angle which r_{a1} makes with the line of nuclei as shown in Fig. 4. Similarly with respect to nucleus "b," we define the functions:

$$b_o(1)=(z^3/\pi)^{\frac{1}{2}}\exp(-zr_{b1}), \tag{16}$$

$$b_c(1)=(z^5/\pi)^{\frac{1}{2}}r_{b1}\cos\theta_{b1}\exp(-zr_{b1}), \tag{17}$$

$$b_s(1)=(z^5/\pi)^{\frac{1}{2}}r_{b1}\sin\theta_{b1}\exp(-zr_{b1}). \tag{18}$$

And likewise we define another six functions: $a_o(2)$, $a_c(2)$, $a_s(2)$, $b_o(2)$, $b_c(2)$, and $b_s(2)$ which involve electron "2" instead of electron "1." The basic integrals can be written:

1. $I_{oo}=\int a_o(1)b_o(1)$ (19)

2. $I_{cc}=\int a_c(1)b_c(1)$ (20)

3. $I_3=\int\int(a_s(1)b_s(2)\cos(\phi_2-\phi_1))^2=2$ (21)

4. $I_{ss}=\int\int a_s(1)b_s(1)a_s(2)b_s(2)\cos^2(\phi_2-\phi_1)$ (22)

5. $F_o=\int(a_o(1))^2/r_{a1}=z$ (23)

6. $F_c=\int(a_c(1))^2/r_{a1}=z/2$ (24)

7. $F_s=\int\int(a_s(1)b_s(2)\cos(\phi_2-\phi_1))^2/r_{a1}=z$ (25)

8. $G_o=\int(a_o(1))^2/r_{b1}$ (26)

9. $G_c=\int(a_c(1))^2/r_{b1}$ (27)

10. $G_s=\int\int(a_s(1)b_s(2)\cos(\phi_2-\phi_1))^2/r_{b1}$ (28)

11. $J_o=\int a_o(1)b_o(1)/r_{a1}$ (29)

12. $J_c=\int a_c(1)b_c(1)/r_{a1}$ (30)

13. $J_s=\int\int a_s(1)b_s(1)a_s(2)b_s(2)\cos^2(\phi_2-\phi_1)/r_{a1}$ (31)

14. $K_{oo,oo}=\int\int(a_o(1)b_o(2))^2/r_{12}$ (32)

15. $K_{cc,cc}=\int\int(a_c(1)b_c(2))^2/r_{12}$ (33)

16. $I_{co}=-I_{oc}=\int a_c(1)b_o(1)=(q/2)I_{oo}$ (34)

17. $J_{co}=-J_{oc}=\int a_c(1)b_o(1)/r_{a1}=(q/3)J_o$ (35)

18. $J_{co}'=-J_{oc}'=\int a_c(1)b_o(1)/r_{b1}=(2q/3)J_o$ (36)

19. $K_{ss,ss}=\int\int(a_s(1)b_s(2)\cos(\phi_2-\phi_1))^2/r_{12}$ (37)

20. $K_{os,os}=\int\int a_o(1)a_s(1)b_o(2)b_s(2)\cos(\phi_2-\phi_1)/r_{12}$ (38)

21. $K_{cs,cs}=\int\int a_c(1)a_s(1)b_c(2)b_s(2)\cos(\phi_2-\phi_1)/r_{12}$ (39)

22. $K_{oc,oc}=\int\int a_o(1)a_c(1)b_o(2)b_c(2)/r_{12}$ (40)

23. $L_{oo,oo}=\int\int a_o(1)b_o(1)a_o(2)b_o(2)/r_{12}$ (41)

24. $L_{cc,cc}=\int\int a_c(1)b_c(1)a_c(2)b_c(2)/r_{12}$ (42)

25. $L_{ss,ss}=\int\int a_s(1)b_s(1)a_s(2)b_s(2)\cos^2(\phi_2-\phi_1)/r_{12}$ (43)

26. $L_{os,os}=\int\int a_o(1)b_s(1)a_o(2)b_s(2)\cos(\phi_2-\phi_1)/r_{12}$ (44)

27. $L_{cs,cs}=\int\int a_c(1)b_s(1)a_s(2)b_c(2)\cos(\phi_2-\phi_1)/r_{12}$ (45)

28. $L_{oc,oc}=\int\int a_o(1)b_c(1)a_c(2)b_o(2)/r_{12}$ (46)

29. $G_{co}=-G_{oc}=\int a_o(1)a_c(1)/r_{b1}$

30. $L(a_o,a_o;a_o,b_o)=\int\int a_o(1)a_o(1)a_o(2)b_o(2)/r_{12}$

31. $L(a_o,a_c;a_o,b_c)=\int\int a_o(1)a_c(1)a_o(2)b_c(2)/r_{12}$

32. $L(a_o,a_s;a_o,b_s)=\int\int a_o(1)a_s(1)a_o(2)b_s(2)\cos(\phi_2-\phi_1)/r_{12}$

The following integrals were taken directly from the work of Rosen:[16] I_{oo}, I_{cc}, F_o, F_c, G_o, G_c, G_{co}, J_o, J_c, $K_{oo,oo}$, $K_{cc,cc}$, $K_{oc,oc}$, $L_{oo,oo}$, and $L_{cc,cc}$. Note that our definition of θ_b is minus Rosen's definition of θ_b. As a consequence, our I_{cc} is minus Rosen's I_{11}; our J_c is minus Rosen's J_{11}; and our $K_{oc,oc}$ is minus Rosen's $K_{o1,o1}$.

The integral, I_3, was readily evaluated. From the work of Coulson,[17] we obtained expressions for I_4 and J_s (in terms of Coulson's K_{25} and K_{29}). From Hellmann,[18] we obtained G_s (see Hellmann's equation, 63.22). From Bartlett,[19] we obtained expressions for $K_{cs,cs}$, $L_{ss,ss}$, and $L_{cs,cs}$. From Kemble and Zener,[20] we obtained good starting points for determining $K_{os,os}$ and $L_{os,os}$. The integral $L(a_o,a_o;a_o,b_o)$ was given in Hirschfelder's Doctor's thesis.

The remaining integrals required a considerable amount of work, but yielded to the standard methods of integration as developed by Rosen and Bartlett. The greatest difficulty arose in the determination of $K_{ss,ss}$ and $L_{oc,oc}$. In this work we were very fortunate to have the use of some unpublished tables of integrals which were loaned to us by Nathan Rosen. His tables of $H(m,n,\alpha)$ and $S(m,n,\alpha)$ are given (with his permission) in Tables X and XI together with our extensions to $q=8$, 10, and 12.

The numerical values of all of these integrals are given in Table IX for values of $q=zR$ ranging from zero to seven. Analytical expressions for all except the exchange integrals are given in the following equations:

1. $I_{oo}=[(q^2/3)+q+1]\exp(-q)$ (47)

2. $I_{cc}=[-(q^4/15)-(2q^3/15)+(q^2/5)+q+1]\exp(-q)$ (48)

3. $I_{ss}=2[(q^3/15)+(2q^2/5)+q+1]^2\exp(-2q)$ (49)

4. $G_o/z=q^{-1}-(1+q^{-1})\exp(-2q)$ (50)

5. $G_c/z=q^{-1}+3q^{-3}-[q^2+3q+(11/2)+7q^{-1}+6q^{-2}+3q^{-3}]\exp(-2q)$ (51)

6. $G_s/z=2q^{-1}-3q^{-3}+[1+4q^{-1}+6q^{-2}+3q^{-3}]\exp(-2q)$ (52)

7. $J_o/z=(q+1)\exp(-q)$ (53)

8. $J_c/z=[-(q^3/6)+(q/2)+(1/2)]\exp(-q)$ (54)

9. $J_s/z=[(q^3/30)+(q^2/5)+(q/2)+(1/2)]\times[(q^2/3)+q+1]\exp(-2q)$ (55)

10. $K_{oo,oo}/z=q^{-1}-[(q^2/6)+(3q/4)+(11/8)+q^{-1}]\exp(-2q)$ (56)

11. $K_{cc,cc}/z=q^{-1}+6q^{-3}+54q^{-5}-\exp(-2q)\begin{bmatrix}+(q^6/140)+(141q^5/2520)+(19q^4/70)\\+(893q^3/840)+(23809q^2/6720)\\+(6411q/640)+(30731/1280)+49q^{-1}\\+84q^{-2}+114q^{-3}+108q^{-4}+54q^{-5}\end{bmatrix}$ (57)

12. $K_{ss,ss}/z=2q^{-1}-6q^{-3}+54q^{-5}-\exp(-2q)\begin{bmatrix}+(q^4/70)+(13q^3/84)+(709q^2/840)\\+(63q/20)+(373/40)+26q^{-1}+60q^{-2}\\+102q^{-3}+108q^{-4}+54q^{-5}\end{bmatrix}$ (58)

13. $K_{os,os}/z=2q^{-3}-\exp(-2q)\begin{bmatrix}+(q^3/30)+(4q^2/15)+(25q/24)\\+(121/48)+4q^{-1}+4q^{-2}+2q^{-3}\end{bmatrix}$ (59)

14. $K_{cs,cs}/z=-54q^{-5}+\exp(-2q)\begin{bmatrix}+(613q^5/67200)+(9253q^4/134400)\\+(201q^3/560)+(201q^2/140)\\+(1547q/320)+(9243/640)+36q^{-1}\\+72q^{-2}+108q^{-3}+108q^{-4}+54q^{-5}\end{bmatrix}$ (60)

15. $K_{oc,oc}/z=-2q^{-3}+\exp(-2q)\begin{bmatrix}+(q^4/30)+(q^3/5)+(77q^2/120)\\+(71q/48)+(263/96)+4q^{-1}+4q^{-2}+2q^{-3}\end{bmatrix}$ (61)

16. $G_{co}/z=q^{-2}-\exp(-2q)[q+2+2q^{-1}+q^{-2}]$

17. $L(a_o,a_o;a_o,b_o)/z=(1/16)[(2+16q+5q^{-1})\times\exp(-q)-(2+5q^{-1})\exp(-3q)]$

18. $L(a_o,a_c;a_o,b_c)/z=\exp(-q)[Ei(-2q)-\ln(q)-C]\times[2q+10+30q^{-1}+60q^{-2}+60q^{-3}]\times\exp(+q)[Ei(-2q)-Ei(-4q)]\times[2q-10+30q^{-1}-60q^{-2}+60q^{-3}]\times\exp(-q)(q^{-3}/64)[412q^4+1186q^3+2527q^2+5054q-2626]\times\exp(-3q)(q^{-3}/64)[-12q^6-42q^3+297q^2+198q+2626]$ (Here $C=0.5772156649$).

The remaining integrals can be expressed most easily in terms of Rosen's $S(m,n,q)$ and $H(M,n,q)$. We define the quantities:

$$X_i=\Sigma_{m,n}X_i(m,n,q)S(m,n,q)$$
$$Y_i=\Sigma_{m,n}Y_i(m,n,q)H(m,n,q)$$

and give the coefficients, $X_i(m,n,q)$ and $Y_i(m,n,q)$ in the Tables VII and VIII, respectively. The following integrals are then:

19. $L_{oo,oo}/z=(q^5/15)(X_1+Y_1)$

20. $L_{ss,ss}/z=L_3^{(0)}+L_3^{(2)}$

where:

$$L_3^{(0)}=q^9[(Y_2/10080)+(X_2/15120)]$$
$$L_3^{(2)}=q^9[(Y_3/10080)+(X_3/15120)]$$

21. $L_{oc,oc}/z=(q^7/420)(X_4+Y_4)$

22. $L_{cc,cc}/z=(q^4/16)L_{oo,oo}/z-(q^2/2)L'+L''$

where:

$$L'=(q^7/840)(X_5+Y_5)$$
$$L''=(q^9/15120)(X_6+Y_6)$$

23. $L_{cs,cs}/z=q^9\begin{bmatrix}[(X_7+Y_7)/23520]+[(X_8+Y_8)/211680]\\-[(X_9+Y_9)/25200]+[(X_{10}+Y_{10})/2400]\end{bmatrix}$

24. $L_{os,os}/z=q^7[[(X_9+Y_9)/6300]-[(X_{10}+Y_{10})/600]]$

25. $L(a_o,a_s;a_o,b_s)/z=L^{(1)}(a_o,a_s;a_o,b_s)+L^{(3)}(a_o,a_s;a_o,b_s)$,

where:

$$L^{(1)}(a_o,a_s;a_o,b_s)=(3/4)(-s_2+s_o)L_5^{(1)}+[s_4-(6/5)s_2+(1/5)s_o]A_1$$
$$L^{(3)}(a_o,a_s;a_o,b_s)=(-525/32)[s_6-(6/5)s_4+(1/5)s_2]L_5^{(3)}+(5/2)[-s_4+(6/5)s_2-(1/5)s_o]A_3,$$

where:

$$L_5^{(1)}=-(q^7/600)(X_{10}+Y_{10})$$
$$L_5^{(3)}=(q^7/6300)(X_9+Y_9)$$
$$A_1=-(q^7/32)(X_{11}+Y_{11})$$
$$A_3=(q^7/480)(X_{12}+Y_{12})$$

and

$$s_o=[\exp(q)-\exp(-q)]/q$$
$$s_2=q^{-3}[(q^2-2q+2)\exp(q)-(q^2+2q+2)\exp(-q)]$$
$$s_4=q^{-5}\begin{bmatrix}(q^4-4q^3+12q^2-24q+24)\exp(-q)\\-(q^4+4q^3+12q^2+24q+24)\exp(-q)\end{bmatrix}$$
$$s_6=q^{-7}\begin{bmatrix}(q^6-6q^5+30q^4-120q^3+360q^2-720q+720)\exp(q)\\-(q^6+6q^5+30q^4+120q^3+360q^2+720q+720)\exp(-q)\end{bmatrix}.$$

[16] N. Rosen, Phys. Rev. **38**, 2099 (1931).
[17] C. A. Coulson, Proc. Camb. Phil. Soc. **38**, 210 (1942).
[18] Hans Hellmann, *Einfuhrung in die Quantenchemie* (Franz Deuticke, Leipzig und Wien, 1937).
[19] J. H. Bartlett, Phys. Rev. **37**, 507 (1931).
[20] E. C. Kemble and C. Zener, Phys. Rev. **33**, 512 (1929).

II. Calculations of Energy for Normal H_2 Molecule

For computational purposes, it is convenient to rearrange the wave function for the normal hydrogen molecule into the form:

$$\Psi_{WIP}=\Psi_o+\alpha\Psi_s+\beta\Psi_c+\gamma\Psi_s,$$

where:

$$\Psi_o=a_o(1)b_o(2)+a_o(2)b_o(1)$$
$$\Psi_s=[a_s(1)b_s(2)+a_s(2)b_s(1)]\cos(\phi_2-\phi_1)$$
$$\Psi_c=a_c(1)b_c(2)+a_c(2)b_c(1)$$
$$\Psi_p=a_o(1)a_o(2)+b_o(1)b_o(2).$$

Then, since the Hamiltonian can be written:

$$H=-(1/2)\Delta_1-(1/2)\Delta_2-r_{a1}^{-1}-r_{a2}^{-1}-r_{b1}^{-1}-r_{b2}^{-1}+r_{12}^{-1}+R^{-1}.$$

It is easy to show that:

$$H\Psi_o=(-z^2+R^{-1})\Psi_o+a_o(1)b_o(2)\times[(z-1)(r_{a1}^{-1}+r_{b2}^{-1})-r_{a2}^{-1}-r_{b1}^{-1}+r_{12}^{-1}]+a_o(2)b_o(1)[(z-1)(r_{a2}^{-1}+r_{b1}^{-1})-r_{a1}^{-1}-r_{b2}^{-2}+r_{12}^{-1}]$$

$$H\Psi_s=(-z^2+R^{-1})\Psi_s+a_s(1)b_s(2)\cos(\phi_2-\phi_1)\times[(2z-1)(r_{a1}^{-1}+r_{b2}^{-1})-r_{a2}^{-1}-r_{b1}^{-1}+r_{12}^{-1}]+a_s(2)b_s(1)\times\cos(\phi_2-\phi_1)[(2z-1)(r_{a2}^{-1}+r_{b1}^{-1})-r_{a1}^{-1}-r_{b2}^{-1}+r_{12}^{-1}]$$

$$H\Psi_c=(-z^2+R^{-1})\Psi_c+a_c(1)b_c(2)\times[(2z-1)(r_{a1}^{-1}+r_{b2}^{-1})-r_{a2}^{-1}-r_{b1}^{-1}+r_{12}^{-1}]+a_c(2)b_c(1)[(2z-1)(r_{a2}^{-1}+r_{b1}^{-1})-r_{a1}^{-1}-r_{b2}^{-1}+r_{12}^{-1}]$$

$$H\Psi_p=(-z^2+R^{-1})\Psi_p+a_o(1)a_o(2)\times[(z-1)(r_{a1}^{-1}+r_{a2}^{-1})-r_{b1}^{-1}-r_{b2}^{-1}+r_{12}^{-1}]+b_o(1)b_o(2)[(z-1)(r_{b1}^{-1}+r_{b2}^{-1})-r_{a1}^{-1}-r_{a2}^{-1}+r_{12}^{-1}].$$

Thus it follows that the approximate energy is given as the lowest root of the secular equation:

$$|zU_{ij}+z(z-1)C_{ij}-(E+z^2-zq^{-1})N_{ij}|=0.$$

Here:

$U_{oo}=B_o+D_o$	$C_{oo}=2+Q_o$	$N_{oo}=1+S_o$
$U_{ss}=B_1+D_1$	$C_{ss}=4+Q_1$	$N_{ss}=2+S_1$
$U_{cc}=B_2+D_2$	$C_{cc}=2+Q_2$	$N_{cc}=1+S_2$
$U_{pp}=B_6$	$C_{pp}=2+Q_6$	$N_{pp}=1+S_o$
$U_{os}=(B_3+D_3)/2$	$C_{os}=0$	$N_{os}=0$
$U_{oc}=(B_4+D_4)/2$	$C_{oc}=Q_4/2$	$N_{oc}=-S_3/2$
$U_{op}=B_9/2$	$C_{op}=Q_9/2$	$N_{op}=S_9/2$
$U_{sc}=(B_5+D_5)/2$	$C_{sc}=0$	$N_{sc}=0$
$U_{sp}=B_7/2$	$C_{sp}=0$	$N_{sp}=0$
$U_{cp}=B_8/2$	$C_{cp}=0$	$N_{cp}=0,$

where:

$zB_o=-2G_o+K_{oo,oo}$	$zD_o=-2J_oI_{oo}+L_{oo,oo}$	$S_o=(I_{oo})^2$
$zB_1=-2G_s+K_{ss,ss}+2z$	$zD_1=L_{ss,ss}$	$S_1=I_{ss}$
$zB_2=-2G_c+K_{cc,cc}+z$	$zD_2=L_{cc,cc}$	$S_2=(I_{cc})^2$
$zB_3=2K_{os,os}$	$zD_3=2L_{os,os}$	$S_3=(I_{co})^2$
$zB_4=2K_{oc,oc}$	$zD_4=2L_{oc,oc}+4I_{co}J_{co}$	$S_9=4I_{oo}$
$zB_5=2K_{cs,cs}$	$zD_5=2L_{cs,cs}$	$zQ_o=2I_{oo}J_o$
$zB_6=-2G_o+(5/8)z-2I_{oo}J_o+L_{oo,oo}$		$zQ_1=4J_s$
$zB_7=4L(a_o,a_s;a_o,b_s)$		$zQ_2=4I_{cc}J_c$
$zB_8=4I_{co}G_{co}+4L(a_o,a_c;a_o,b_c)$		$zQ_4=-8I_{co}J_{co}$
$zB_9=-4I_{oo}G_o-4J_o+4L(a_o,a_o;a_o,b_o)$		$zQ_6=2I_{oo}J_{oo}$
		$zQ_9=4J_o+4I_{ooo}$

The best value of z to use in the secular equation is determined from the condition: $Z=-q(\partial E/\partial q)_z/(\partial E/\partial Z)_q$. Thus, at each value of q, the energy is calculated from the secular equation for each of a number of values of z from which the value of $(\partial E/\partial Z)_q$ can be estimated. Then comparing values of E calculated for the same value of z but for different values of q, we obtained estimates of $(\partial E/\partial q)_z$. An analytical curve fitting method was developed to simplify the work indicated above.

III. Calculations of Energy for First Excited State of H_2 Molecule

The wave function for the first excited ($^3\Sigma$) state of the hydrogen molecule can be written in the form:

$$\Psi_{WP}=\Psi_o'+\alpha\Psi_s'+\beta\Psi_c',$$

where:

$$\Psi_o'=a_o(1)b_o(2)-a_o(2)b_o(1)$$
$$\Psi_s'=[a_s(1)b_s(2)-a_s(2)b_s(1)]\cos(\phi_2-\phi_1)$$
$$\Psi_c'=a_c(1)b_c(2)-a_c(2)b_c(1).$$

The approximate energy is then given as the lowest root of the secular equation:

$$|zU_{ij}'+z(z-1)C_{ij}'-(E+z^2-zq^{-1})N_{ij}'|=0.$$

Here:

$U_{oo}'=B_o-D_o$	$C_{oo}'=2-Q_o$	$N_{oo}'=1-S_o$
$U_{ss}'=B_1-D_1$	$C_{ss}'=4-Q_1$	$N_{ss}'=2-S_1$
$U_{cc}'=B_2-D_2$	$C_{cc}'=2-Q_2$	$N_{cc}'=1-S_2$
$U_{os}'=(B_3-D_3)/2$	$C_{os}'=0$	$N_{os}'=0$
$U_{oc}'=(B_4-D_4)/2$	$C_{oc}'=Q_4/2$	$N_{oc}'=S_3/2$
$U_{sc}'=(B_5-D_5)/2$	$C_{sc}'=0$	$N_{sc}'=0.$

Here the B_i, D_i, Q_i, and S_i have the same meaning as in the case of the normal H_2 molecule.

THE JOURNAL OF CHEMICAL PHYSICS VOLUME 18, NUMBER 1 JANUARY, 1950

The Energy of the Hydrogen Molecule

E. F. GURNEE AND J. L. MAGEE
Radiation Chemistry Project, Department of Chemistry, University of Notre Dame,[1] Notre Dame, Indiana

(Received July 21, 1949)

A simple two-parameter variational function has been used to calculate the energy of normal H_2. The first parameter is the usual scale factor; the second parameter is a distance of displacement of the atomic orbitals (see Fig. 1). The best potential energy is obtained as approximately 96 kcal per mole for internuclear separation 1.45 a_0. The behavior of the new parameter as a function of internuclear separation is discussed.

A RECENT reinvestigation of the interaction of two hydrogen atoms by Hirschfelder and Linnett[2] has suggested that trial wave functions for H_2 may be improved by allowing the electrons to spend more time in the region between the nuclei. This idea has been tested with the simplest wave function for H_2 (the Heitler-London wave function) by shifting the atomic orbital centers closer together than the nuclei (see Fig. 1). The distance in Bohr radii that each center is shifted, x, is used as a variational parameter. It is easy to vary a scale factor z, so this has also been done.

[1] Supported by the AEC under contract number AT(11-1)-38.

[2] J. O. Hirschfelder and J. W. Linnett, J. Chem. Phys. 18, 130 (1950).

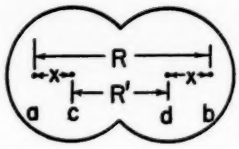

FIG. 1. The two nuclei are at a and b. The 1s orbitals have their centers at c and d.

TABLE I. Calculated values of the binding energy in Kcals./mole and the parameters x and z.

R	x	z	B.E.
1.00	0.06	1.275	59.6
1.20	0.03	1.23	85.3
1.40	0.06	1.185	94.7
1.50	0.08	1.16	95.1
1.60	0.10	1.13	92.2
1.80	0.130	1.07	82.2
2.00	0.115	1.03	67.8
2.41	−0.0158	1.0227	49.2
3.00	−0.0140	0.9925	26.3
4.05	−0.0048	0.9844	6.90
5.08	−0.0012	0.9932	1.49

The two-parameter wave function which we have used is thus:

$$\Psi=(z^3/\pi)^{\frac{1}{2}}[\exp(-zr_{c1}-zr_{d2})+\exp(-zr_{c2}-zr_{d1})].$$

Here r_{c1} is the distance in Bohr radii of the first electron from the orbital center c (which is not the position of a nucleus), etc.

Calculation of the energy involves only standard techniques and will not be discussed here. There is, however, a three-center integral in the energy expression which does not usually occur in diatomic problems.

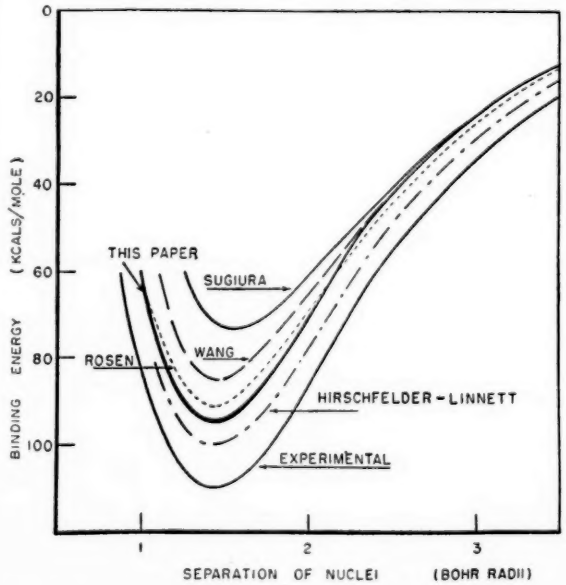

FIG. 2. Comparison of the energies of H_2 from several different calculations. At large distances the energy obtained in this work is always slightly lower than the Wang energy, which is slightly lower than the Sugiura energy, although the three are approximately equal.

TABLE II. Summary of H_2 calculations.

Calculation	Description of wave function used
Sugiura	Simple Heitler-London wave function used. No parameter varied.
Wang	Scale factor z varied (one parameter).
Rosen	Scale factor and polarization along molecular axis (two parameters).
Hirschfelder-Linnett	Scale factor, polarization along and perpendicular to molecular axis, ionic terms (four parameters).

This integral has been discussed by Hirschfelder and others.[3]

In Table I we list our calculated points. In Fig. 2 we compare the energies obtained in this work with several other calculations[4–6] and also with the experimental values.[7] These other calculations are described briefly in Table II. It will be recalled that the calculation of James and Coolidge[8] with a thirteen-parameter variational function led to substantially the experimental value at internuclear separation 1.4 a_0. The parameter x leads to an appreciable lowering of the energy for internuclear separations near the minimum energy, provided z is also varied.

A test which is sometimes applied to a wave function is whether or not the virial theorem is satisfied at the condition of minimum energy.[2,9] It is known[9] that the Wang function, which introduces the scale factor z into the Heitler-London wave function, brings agreement with this test, whereas the original function gave serious disagreement. The use of the parameter x maintains the agreement with the virial theorem.

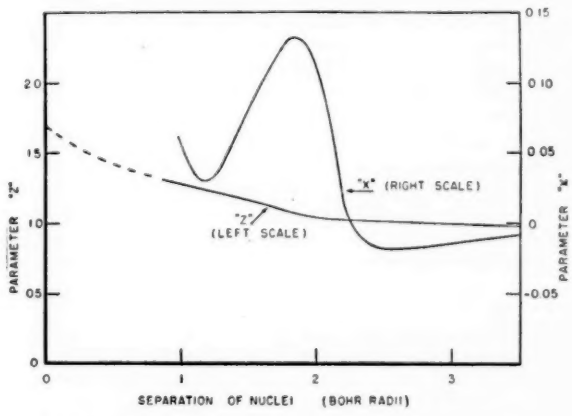

FIG. 3. Behavior of the parameters z and x as a function of distance.

[3] Hirschfelder, Eyring, and Rosen, J. Chem. Phys. **4**, 121 (1936); J. O. Hirschfelder and C. N. Weygandt, J. Chem. Phys. **6**, 806 (1938).
[4] Y. Sugiura, Zeits. f. Physik **45**, 484 (1927).
[5] S. C. Wang, Phys. Rev. **31**, 579 (1928).
[6] N. Rosen, Phys. Rev. **38**, 2099 (1931).
[7] R. Rydberg, Zeits. f. Physik **73**, 376 (1931).
[8] H. M. James and A. S. Coolidge, J. Chem. Phys. **1**, 825 (1933).
[9] J. O. Hirschfelder and J. F. Kincaid, Phys. Rev. **52**, 658 (1937).

The behavior of the two parameters z and x as a function of internuclear separation is indicated in Fig. 3. The variation of x has only a small effect on z and consequently the values of our parameter z are very close to those of the usual Wang variation. The effect of x is to increase z near the minimum. The fact that $(z-1)$ becomes negative for large values of internuclear separation is well known. In this work we found it interesting that the parameter x also changes sign for large values of R (i.e., in Fig. 1, R' becomes greater than R for large R). The dashed lines for z in Fig. 3 are interpolated. The value of z for $R=0$ is known to be 1.6875. The value of x for $R=0$ is zero. Since there are no calculated points in the internal $0<R<1$ and x apparently has a maximum value in this region, we have made no attempt to sketch the curve here.

The variation of the parameter x alone in the Heitler-London wave function for H_2 brings about only a slight improvement in the energy (about 2.5 kcal/mole). We have not shown this calculation in Fig. 2. It is only with the simultaneous variation of the scale factor z that a substantial lowering of the energy is obtained. It is seen in Fig. 2 that the improvement over the Wang energy on introduction of the parameter x is about 10 kcal/mole.

One of the authors (J.L.M.) would like to acknowledge discussions of this problem with Professor J. O. Hirschfelder. We appreciate the use of the Hirschfelder-Linnett paper[2] in advance of publication.

Letters to the Editor

THIS section will accept reports of new work, provided these are terse and contain few figures, and especially few half-tone cuts. The Editorial Board will not hold itself responsible for opinions expressed by the correspondents. Contributions to this section should not exceed 600 words in length and must reach the office of the Managing Editor not later than the 15th of the month preceding that of the issue in which the letter is to appear. No proof will be sent to the authors. The usual publication charge ($8.00 per page) will not be made and no reprints will be furnished free.

The Structure of Cerium at the Temperature of Liquid Air*

A. F. SCHUCH AND J. H. STURDIVANT
Gates and Crellin Laboratories of Chemistry, California Institute of Technology, Pasadena, California
November 9, 1949

IN a dilatometric investigation of metallic cerium Trombe and Foex[1] observed under certain conditions a transition at 109°K which was accompanied by a 10 percent volume decrease and a decrease in magnetic susceptibility. Professor Linus Pauling suggested to us in 1946 that this transition is caused by the promotion of a $4f$ electron to a bond-forming orbital, and that the dense phase be studied by x-ray diffraction. The investigation described below was completed in 1948. Lawson and Tang[2] have recently produced the transition at 15,000 atmospheres; they found there essentially the same structure which we found at the temperature of liquid air.

Cerium containing 0.2 percent calcium, 0.2 percent magnesium, and 0.04 percent beryllium was supplied by Dr. F. H. Spedding. To obtain the low temperature transition we found it essential to remove the calcium and magnesium by melting in vacuum.[3] In an argon atmosphere 200-mesh filings from the remelted cerium were collected in thin-walled glass capillaries 0.3 mm in diameter. The capillaries were then sealed with or without evacuation, and were heat treated in a variety of ways including both quenching and slow cooling to room temperature from as high as 575°C. X-ray diffraction photographs were taken with K radiation from a molybdenum target filtered through zirconium. The specimen tube was mounted on the axis of a cylindrical camera. For low temperature photographs the sample was surrounded by a cellophane tube 3 mm in diameter; a continuous stream of liquid air kept the cellophane tube full and overflowed to wash the outside free of ice.

The face-centered cubic structure with $a_0=5.140$A explained all diffraction maxima observed from both quenched and annealed cerium at room temperature. We observed no lines which required a hexagonal closest-packed structure.

TABLE I. Diffraction maxima from quenched cerium at 90°K.

Line	Intensity	d	Normal phase hkl	Normal phase a_0	Dense phase hkl	Dense phase a_0
1	Str	2.760			111	4.780A
2	Str	2.400			200	4.800
3	Str Wide	1.813	220	5.128A		
4	Str Wide	1.703			220	4.817
5	Str Wide	1.549	311	5.137		
6	Str Wide	1.457			311	4.832
7	Wk Wide	1.396			222	4.836
8	Wk	1.106			331	4.821
9	Wk	1.077			420	4.816
10	Str Wide	0.986	511	5.123	422	4.830
11	M Wide	0.927			511	4.817
12	Str Wide	0.860	531	5.088		
13	Str Wide	0.812	620	5.135	531	4.803
14	V Wk Wide	0.772	622	5.121		
15	M Wide	0.673			{711 / 640}	{4.806 / 4.853}
16	V Wk	0.644			642	4.819
17	Wk	0.628			731	4.824

Only with cerium which had been quenched by an air blast from at least 300°C to room temperature could we obtain a transition at the temperature of liquid air. Data from a typical photograph are given in Table I.

The data show the presence in quenched cerium at 90°K of two phases. One is the normally contracted room-temperature form. The other is an anomalously contracted phase which is also face-centered cubic. Its cell edge of 4.82A represents a 16.5 percent decrease in volume below that of the parent structure.

The new dense form was produced several times. In successive coolings of a specimen with liquid air, a smaller and smaller proportion of the new structure appears. This effect has also been observed by Trombe. Apparently mechanical stresses must be present in the metal if the transition is to occur.

* Contribution No. 1351 from the Gates and Crellin Laboratories of Chemistry.
[1] Felix Trombe and Marc Foex, Ann. d. chimie **19**, 417 (1944).
[2] A. W. Lawson and T. Y. Tang, Phys. Rev. **76**, 301 (1949).
[3] See Francoise Mahn, Comptes Rendus **223**, 78 (1946).

Rotational Isomerism in Substituted Ethanes

N. SHEPPARD
Department of Colloid Science, Cambridge University, Cambridge, England
AND
G. J. SZASZ
U. S. Office of Naval Research, London, England
November 28, 1949

THOMAS and Gwinn[1] have recently presented results on the configurations and relative energies of the rotational isomers in 1,1,2-trichloroethane and 1,1,2,2-tetrachloroethane derived from vapor phase dipole measurements. We wish to draw attention to the analogies and difference between these results and those obtained by us[2] from the study of the Raman spectra of the corresponding methyl derivatives of ethane (2-methylbutane and 2,3-dimethylbutane) in the liquid phase.

It was found that in both types of compounds the rotational isomeric composition remained approximately constant over a considerable temperature range, and further that in neither case could the 1,1,2,2 compounds consist solely of the centrosymmetric *trans*-isomer. The conclusions were all based on the observed qualitative behavior of the dipole moments and Raman spectra. The constant rotational isomeric composition was interpreted in both papers in terms of a very high or a very low energy difference between the rotational isomers. In the case of the chlorine compounds Thomas and Gwinn[1] concluded further from quantitative arguments that in 1,1,2,2-tetrachloroethane the energy difference is small (0 ± 200 cal. mole^{-1}) while in 1,1,2-trichloroethane it is large (>2300 cal. mole^{-1}). However, our tentative conclusion on the methyl derivatives was that the same explanation (of a high or a low energy difference) would apply to each hydrocarbon. As we stated before, accurate gas heat capacities would be well suited to choose between the alternative explanations.

Axford and Rank[3] have recently completed similar work on the infra-red spectra of the hydrocarbons in the liquid and solid states, and have confirmed our original conclusions. They find, moreover, that in the case of 2,3-dimethylbutane only one of the two strong, polarized Raman frequencies occurs in the infra-red spectrum in the 700–800 cm^{-1} region. This would be expected if one of these Raman lines was caused by the lowest skeletal stretching mode of the *trans*-molecule, but not if our alternative explanation of these two Raman lines in terms of Fermi resonance were correct. The combined infra-red and Raman results thus favor the presence of two rotational isomers with small energy difference in 2,3-dimethylbutane and, by analogy of the Raman spectra, very probably also in 2-methylbutane. In view of the conclusion of Thomas and Gwinn that steric rather than dipole repulsions are the more important factor determining the relative stabilities of the chloro-compound isomers also, 1,1,2-trichloroethane appears to be anomalous in having a large energy difference.

Some comments are also appropriate on the results of Langseth and Bernstein[4] on the energy difference in 1,1,2,2-tetrachloroethane in the liquid phase. They found that, in contrast to the small value in the gaseous state, there is an energy difference of *ca.* 1100 cal. mole^{-1} between the isomers in the liquid. A similar change in energy difference between the isomers of 1,2-dichloroethane in the liquid and gas is well known,[5,6] (ΔE is *ca.* 0 and 1200 cal. mole^{-1} respectively) and was explained by Watanabe, Mizushima, and Masiko[7] using an electrostatic model based on the Onsager internal field. Their results show that the more polar forms will always be stabilized in the liquid state due to dipole interactions. In the case of 1,1,2,2-tetrachloroethane, starting with the conclusion from Thomas and Gwinn's dipole moment data that the *trans-* and skew forms have equal stability in the gas phase, the observed change in energy difference on passing to the liquid can thus be explained as due to the extra stabilization of the skew form. This is consistent with the spectroscopic data of Langseth and Bernstein.[4] The alternative possibility, that the compound has a high energy difference between its isomers in the vapor—the stable form would have to be skew because of the observed dipole moment—would lead to an even greater energy difference in the liquid.

The view that in these simple branched paraffins the energy difference between the rotational isomers is approximately zero, would necessitate some change in the model used by Pitzer[8] in calculating their thermodynamic properties.

[1] J. R. Thomas and W. D. Gwinn, J. Am. Chem. Soc. **71**, 2785 (1949).
[2] G. J. Szasz and N. Sheppard, J. Chem. Phys. **17**, 93 (1949).
[3] D. W. E. Axford and D. H. Rank. personal communication, to appear shortly in J. Chem. Phys.
[4] A. Langseth and H. J. Bernstein, J. Chem. Phys. **8**, 410 (1940).
[5] H. Gerding and P. G. Meerman, Rec. Trav. Chim. **61**, 523 (1942).
[6] Morino, Watanabe, and Mizushima, Sci. Papers Inst. Phys. Chem. Res. Tokyo **39**, 396 (1942).
[7] Watanabe, Mizushima, and Masiko, Sci. Papers Inst. Phys. Chem. Res. Tokyo **40**, 425 (1943).
[8] K. S. Pitzer, J. Chem. Phys. **8**, 711 (1940).

Space Charge in Electrolytes

A. R. Gordon
Chemistry Department, University of Toronto, Toronto, Canada
November 16, 1949

In the October issue of this *Journal*, Reed and Schriever[1] report that a space charge exists in a column of electrolytic solution during electrolysis, and consequently state that Ohm's Law is invalid for such conductors. Their method consists in applying a potential of 8 volts to metal electrodes forming the ends of a cell 40 cm in length, the electrolyte being a 0.0024*N* solution of a salt of the metal (copper, zinc, nickel or aluminum) forming the electrodes. The potential between a probe of the metal in question and the anode or cathode is then determined as electrolysis proceeds. As might be expected, the probe potential was not a linear function of the distance x from the cathode, and Reed and Schriever then compute the space charge from the deviation of the measured potential gradient from 20 mv/mm.

(1) The usual test of Ohm's Law is to determine whether the resistance between two points in a conductor is independent of the current; moreover to obtain the true potential drop between two points in a solution, the conditions must be such that the two liquid-electrode potentials are equal and opposite in sign. Thus Jones and Bollinger,[2] in a classic research employing the a.c. bridge, showed that Ohm's Law was valid within a few thousandths of a percent. Measurements in this laboratory,[3] employing the direct current method in which the potential difference was measured between shielded, reversible probe electrodes remote from the anode and cathode, showed the same to be true. Finally, the results by both methods for a series of salts were in agreement within the precision of either set of data.

(2) "Hard" metals, such as those used by Reed and Schriever, are notoriously erratic in their behavior, and there is no evidence that the "chemical potential" between a probe and a current electrode will be the same when current is passing as when it is not.

(3) Reed and Schriever ignore electrode overvoltage; as is well known, this depends in a complicated way on the nature of the electrode surface, current density and the concentration of the solution in immediate contact with the electrode. See a recent Faraday Society symposium on electrode processes.[4]

(4) No account is taken of concentration changes in solution due to the electrode processes, migration and diffusion. For example, taking the transference number of sulfate ion in zinc sulfate solution[5] as 0.6, a concentration at a point near the anode twice that obtaining in the bulk of the solution, will of itself introduce a concentration e.m.f. of approximately 10 mv. To take the "five minute" curve of Fig. 2 as an example, the deviation is linear within the estimated precision of ± 4 mv for x between 2 and 32 cm, i.e. the results are consistant with an ohmic drop of approx. 7.87 volts and concentration e.m.f. plus overvoltage at the two electrodes of 0.13 volt—an entirely reasonable value.

(5) The slow changes in potential with time are much more reminiscent of slow processes such as migration and diffusion than of the electrostatic effect postulated. It would seem probable that Reed and Schriever have been studying the complicated effects of overvoltage and concentration changes in the liquid brought about by diffusion, migration, convection and the solution and deposition of the metal. In the opinion of the writer at any rate, their results do not demonstrate the existence of a space charge.

[1] C. A. Reed and W. Schriever, J. Chem. Phys. **17**, 935 (1949).
[2] G. Jones and G. M. Bollinger, J. Am. Chem. Soc. **53**,1207 (1931).
[3] H. E. Gunning and A. R. Gordon, J. Chem. Phys. **10**, 126 (1942); **11**, 18 (1943); G. C. Benson and A. R. Gordon, **13**, 470 (1945); **13**, 474 (1945).
[4] Faraday Soc., Discussions, **1947** No. 1.
[5] B. B. Owen and R. W. Gurry, J. Am. Chem. Soc. **60**, 3074 (1938).

Reply to "Space Charge in the Electrolytes"*

William Schriever
Physics Department, University of Oklahoma, Norman, Oklahoma
November 28, 1949

These replies to Professor Gordon's criticisms will be in the order given in his letter.

(1) Ohm made three important discoveries, two of which are usually called "Ohm's Law." The first may be written, the potential difference between the ends of a piece of conductor is directly proportional to the current through it. The second may be written, the current in a single-path complete circuit is proportional to the electromotive force in that circuit. The third may be written, the resistance of a piece of uniform conductor is directly proportional to its length and inversely proportional to the area of its cross section. A combination of the first and third leads to the statement that the potential gradient is the same at all points along a uniform conductor. Since the potential gradients were found *not* to be constant by Reed and myself we stated that Ohm's law was not obeyed. This appears to be an entirely proper deduction. Obviously we were not referring to the relatively thin layers next to the two electrodes.

Conductance measurements made by alternating-current methods need not be considered here because such electrical conditions are entirely different from those existing in direct-current methods.

Professor Gordon's cell for determining relative conductances by a direct-current method consisted of a Pyrex glass cylinder approximately 16 cm long by 5 cm in diameter with the current electrodes inserted in 5-cm long axial extensions 13 mm in diameter, at each end of the cylinder. The two probe-electrodes were inserted in lateral extensions 4 cm long and 13 mm in diameter, the centers of the two extensions being 10 cm apart. The axial distance from each current electrode to the nearest potential electrode was some 8 cm (distances were estimated from the drawing in his paper). According to his Table I the currents varied from 0.4 to 2 milliamperes, which lead to current densities in the cylinder to 2 to 10×10^{-5} amp/cm^2. The current through the cell

was reversed after each probe-potential measurement. The time interval during which the current passed through the cell in one direction was not stated. Since the potential probes were 8 cm in front of the current electrodes, and since the current was reversed regularly, it is entirely possible that appreciable space-charge effects never reached into that part of his cell between the potential probes.

(2) Let us grant that the "chemical potential difference" between the probe and the current electrode changed when the current passed. Our deviation-time runs were quite reproducible. Thus whatever change existed at the end of, say, 10 minutes for one run, also existed at the end of 10 minutes for every other run regardless of the position of the probe along the column. The net effect of this change, *if* it existed, would have been to raise, or lower, every point of our deviation-distance curve for 10 minutes, by the same amount. Thus the slope and curvature of the curve at every point would have remained unchanged (except very close to the electrodes where observation could not be made). Therefore the calculated potential gradient and space-charge distributions would have been unaffected.

(3) Overvoltage was not ignored even though it was never mentioned specifically. We did state specifically that in a relatively thin layer next to each current electrode there may have existed electrical double layers and other space-charge effects together with concentration changes which may have caused certain electromotive forces. These were intended to include any and all, known and unknown, complicated effects near these electrodes, including overvoltages. Again, since our deviation-time runs were reproducible, whatever complicated conditions existed near a current electrode at the end of, say, 10 minutes for one position of the probe, that same condition existed for all positions of the probe at the end of 10 minutes. These effects were specifically taken into account in the theory which we presented on page 936. Thus the shape of our potential distribution curves cannot be explained on the basis of "potentials" existing at or near the current electrodes; they must be explained by something taking place throughout the column of electrolyte.

(4) Concentration electromotive forces and all other processes which may have taken place at or near the current electrodes, have been taken into account in (3) above and therefore need not be discussed again. Concentration changes out in the column of electrolyte were considered in our paper on pages 937 and 943 and that material will not be repeated here. Since our current densities were only some 5×10^{-5} amp/cm^2 the resulting concentration changes very near the electrodes after the current had passed 15 minutes, must have been exceedingly small. Appreciable diffusion effects must have taken place only very close to the electrodes since diffusion is a very slow process. All such effects near the electrodes have been taken into account as was stated above. Additional evidence, that these current-electrode effects were properly allowed for, is that our observed deviations for points near the center of the column, were the same when measured with respect to the anode as when measured with respect to the cathode. The shapes of our potential distribution curves cannot be explained by phenomena at and near the current electrodes.

(5) The factors mentioned by Professor Gordon in his paragraph (5) have all been considered in (2), (3), and (4) above, except for "convection." Any stirring of the solution either by convection or otherwise made reproduction of data impossible. A thorough stirring removed all space-charge effects and other effects. Our data were reproducible. Therefore, I believe it is safe to say that "convection" cannot help to account for our observed potential distribution curves.

In Professor Gordon's first paragraph, in referring to our work, he stated, "As might be expected, the probe potential was not a linear function of the distance x from the cathode." All relative conductivity measurements by a d.c. method require an electrolyte standardized by an absolute determination of its conductivity by a d.c. method. The absolute determination requires the measurement of the length, the cross-sectional area and the resistance of a uniform column of the electrolyte, together with the assumption that the potential gradient in that column is constant. If the potential gradient in our work was "expected" to be variable, would not one also "expect" the potential gradient in the absolute determination apparatus to be variable? If so then the absolute determination would cease to be a measure of the actual conductivity.

* A. R. Gordon, J. Chem. Phys. **18**, 145 (1950).

Intramolecular Forces between Non-Bonded Atoms

D. F. Heath and J. W. Linnett
Inorganic Chemistry Laboratory, The Queen's College, Oxford University, Oxford, England
November 28, 1949

In a recent series of papers T. Simanouti[1] has applied the Urey-Bradley field[2] to a number of halogen derivatives of CH_4, C_2H_6 and SiH_4. The important conclusion reached by T. Simanouti is that, in molecules of the above type, repulsion forces between non-bonded atoms are not negligible compared with the valency forces. Terms to take account of such forces should, therefore, be included in functions giving the variation of molecular potential energy with changes of internal configuration. We had reached the same conclusion by considering the tetrahalides of the Group IV elements, the trihalides of boron and some analogous oxy-anions, and the hexafluorides of the Group VI elements.[3] We had found moreover, as T. Simanouti has done, that the force constants necessary to take account of these van der Waals' type repulsion effects are of the order of magnitude to be expected from a consideration of the known potential energy functions for the interaction between analogous inert gas atoms which have been deduced from equation of state studies[4] (see Table IV in Part III of Simanouti's series, and Table II in Part IV and Table II in Part V of our series). It seems to us that this is a most important conclusion concerning intramolecular forces. Moreover, it is confirmed by the calculations of F. H. Westheimer and J. E. Meyer,[5] those of T. L. Hill,[6] and by other observations.[7]

It is noteworthy that this general conclusion regarding the magnitude of the forces between non-bonded atoms has been reached independently by T. Simanouti and by us even though the two sets of calculations are made using rather different force fields. T. Simanouti has used a simple valency force field plus these repulsion terms, whereas we have used, as our basic field, one which is based more closely on modern ideas of directed valency. We have called it the orbital valency force field.

In silicon tetrafluoride T. Simanouti found that the ratio of F to F′ for F···F repulsion is very different from what would be expected from a consideration of Ne···Ne repulsion (see Table IV of his Part III). We had come to the same conclusion and commented on this fact in Part II of our series (see also Table II in Part II). On the other hand the behavior of carbon tetrafluoride seems to be quite normal. It would be interesting if the vibration frequencies of the tetrafluorides of the other Group IV elements could be determined to see whether they behave normally like CF_4 or abnormally like SiF_4.

Our calculations and those of Simanouti show clearly that, in a variety of molecules, it is important to take account of the repulsion between non-bonded atoms in constructing force fields to account for their vibration frequencies.

[1] T. Simanouti, J. Chem. Phys. **17**, 245, 734, 848 (1949).
[2] H. C. Urey and C. A. Bradley, Phys. Rev. **38**, 1969 (1931).
[3] D. F. Heath and J. W. Linnett, Trans. Faraday Soc. **44**, 561, 873, 878, 884 (1948); *ibid.* **45**, 264 (1949).
[4] See R. H. Fowler and E. A. Guggenheim, *Statistical Thermodynamics* (Cambridge University Press, London, 1939), p. 285.
[5] F. H. Westheimer and J. E. Meyer, J. Chem. Phys. **14**, 733 (1946); *ibid.* **15**, 252 (1947).
[6] T. L. Hill, J. Chem. Phys. **16**, 399, 938 (1948).
[7] See references in E. H. Hughes, Quart. Rev. Chem. Soc. **2**, 132 (1948); see also, J. R. Lacher, J. Am. Chem. Soc. **69**, 2067 (1947).

Mass Spectrometric Measurement of Low Vapor Pressures

A. W. TICKNER* AND F. P. LOSSING
Division of Chemistry, National Research Laboratories, Ottawa, Canada
November 29, 1949

VAPOR pressure measurements for hydrocarbons in the region below 1 cm are subject to large errors due to the presence of traces of volatile impurities. At temperatures where the vapor pressure is small, the gas phase may contain large amounts of a volatile impurity, even though the hydrocarbon as a whole is extremely pure. Because of the prohibitive degree of purity required, no reliable vapor pressure data exist below a few millimeters, and the only data below 0.1 mm is that of Delaplace[1] who made use of the dependence of thermal conductivity on the pressure.

The above difficulty would be avoided if the partial pressure of the hydrocarbon in question, rather than the total pressure of the sample, could be measured. Partial pressures can be readily measured by the mass spectrometer since a linear relation exists between the peak height due to a given substance and the pressure of that substance behind the mass spectrometer leak. This relation is linear up to a certain limiting pressure where viscous flow through the leak begins to be important.[2] For the leak used, the upper limit of linearity was a pressure of about 40 microns. To keep all measured pressures well within this limit, vapor pressures larger than 30 microns were measured by expanding the sample into the leak chamber from suitable calibrated volumes. The peak used for measuring purposes must of course be free from interference by the impurities present. In most cases the parent peak is suitable.

The temperature of the sample was controlled and measured by means of a trap which consisted of a vertical Pyrex tube with the lower end closed. The tube was surrounded by a spiral heater and enclosed in a vacuum jacket, the latter being immersed in liquid nitrogen.[3] The heater winding was spaced to provide a slight temperature gradient, so that the coolest point was at the bottom of the trap, where a copper-constantan thermocouple was located. By this means the temperature of the sample could be maintained and measured within about 0.2°C.

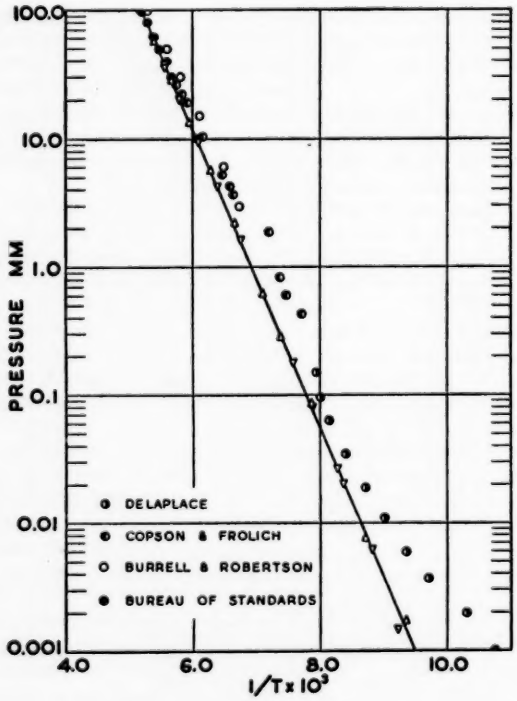

FIG. 1. Vapor pressure of propane.

In Fig. 1, the results obtained by this method are compared with the values previously determined by other methods for propane. It can be seen that the values reported here coincide with the values adopted by the U. S. Bureau of Standards[4] which have been reported only in the pressure range above 10 mm. All previously available data below 10 mm would appear to be too high, and become progressively worse with decreasing vapor pressures as would be expected if volatile impurities were present.

It can be seen from the above example that this method of measuring low vapor pressures is capable of much greater accuracy than previously available methods.[5,6] Furthermore, the method is rapid and convenient and should be capable of wide application. In this laboratory the vapor pressures of a number of light hydrocarbons are being measured over the same range. Results will appear in a forthcoming publication.

* Holder of National Research Laboratories Post-Doctorate Fellowship.
[1] R. Delaplace, Comptes Rendus **204**, 493 (1937).
[2] R. E. Honig, J. App. Phys. **16**, 646 (1945).
[3] G. L. Lee, unpublished work, University of Toronto, 1949.
[4] "Selected Values of Properties of Hydrocarbons," National Bureau of Standards, A.P.I. Project 44 (1949).
[5] G. A. Burrell and I. W. Robertson, J. Am. Chem. Soc. **37**, 2188 (1915).
[6] R. L. Copson and Per K. Frolich, Ind. Eng. Chem. **21**, 1116 (1929).

The Scintillation Counter. II. The Preparation of Transparent Inorganic Phosphor Screens*

LAWRENCE B. ROBINSON, CHARLIE S. COOK, AND DONALD E. JEFFERSON
Department of Physics,† Howard University, Washington, D. C.
November 10, 1949

IN this note, a description is given of an attempt at the preparation of phosphor screens having the desirable characteristics of both organic and inorganic phosphors without the undesirable characteristics of either. These phosphor screens were used with the scintillation counter. Organic phosphors have a low physical light yield (i.e., fraction of the absorbed radiation transformed into light), a high technical yield (i.e., the amount of light obtainable from a given intensity of radiation of a particular type, choosing the optimum thickness of phosphor), and high transparency to their own radiation. Inorganic phosphors usually have a high physical yield and a low practical yield because they are quite opaque to their fluorescent radiation. This method yields screens which are easily prepared, readily duplicated, and composed entirely of commercially available materials. The screens were prepared by dispersing suitable inorganic phosphor powders in a transparent plastic. The phosphors selected were recommended by the manufacturers as suitable for the counting of alpha-particles. The counting of alpha-particles was undertaken first because this problem is more simple than counting beta- and gamma-radiation. The phosphors used were zinc sulfide (ZnS) and barium-lead sulfate ($BaSO_4$:$PbSO_4$) which were obtained from E. I. du Pont de Nemours, Towanda, Pennsylvania, and zinc oxide (ZnO) and zinc sulfide-silver (ZnS:Ag) from the Radio Corporation of America (RCA), Harrison, New Jersey. All of these phosphors show good emission in the region of maximum absorption of the 931A photo-multiplier tubes. The requirement for the plastics were that they should be liquid and transparent, and should solidify in reasonably thick layers without too many technical operations. Two plastics were found which had practically identical spectral characteristics. They were Polyweld "912" coil dope (obtainable from American Phenolic Corporation, Chicago) and Bio-Plastic (obtainable from Ward's Natural Science Establishment, Rochester, New York).

The shape of the counting rate-concentration curves can be predicted, or at least accounted for, on elementary considerations. One would expect that the number of light pulses would be increased as the concentration of the phosphor powder increased. However, one should not expect that the counting rate should increase in the same fashion because the phosphor screen becomes

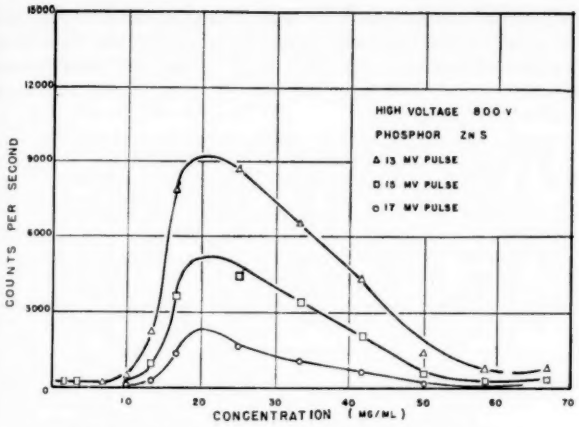

FIG. 1. Counting rate *vs.* concentration for the ZnS screens.

more opaque. Hence, elementary considerations would suggest that all of the counting rate-concentration curves should show maxima. Figures 1, 2, 3, and 4 show such curves. Figures 3 and 4

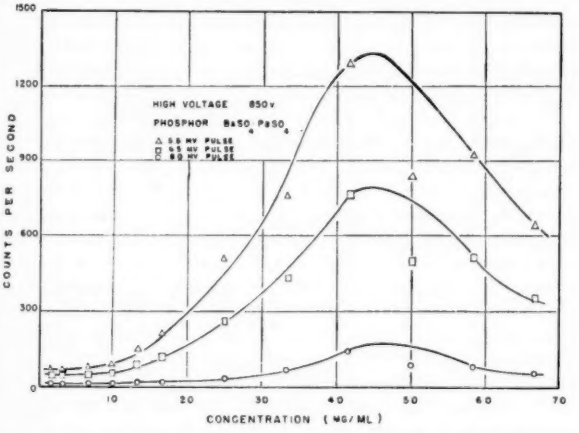

FIG. 2. Counting rate *vs.* concentration for the $BaSO_4$:$PbSO_4$ screens.

also show the percentage transmission of the phosphor screens for the wave-length for which the phosphor powder has the maximum emission. All of these curves were obtained under almost identical counting conditions. A polonium source of about 0.75 millicurie was used. The geometry was such that only a relatively small percentage (about 1 percent) of the total number of counts

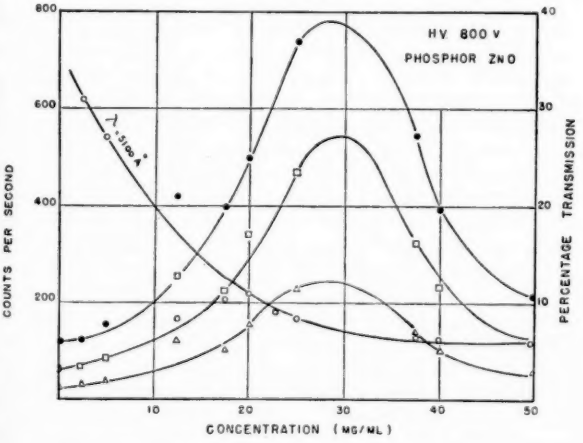

FIG. 3. Counting rate *vs.* concentration for the ZnO screens.

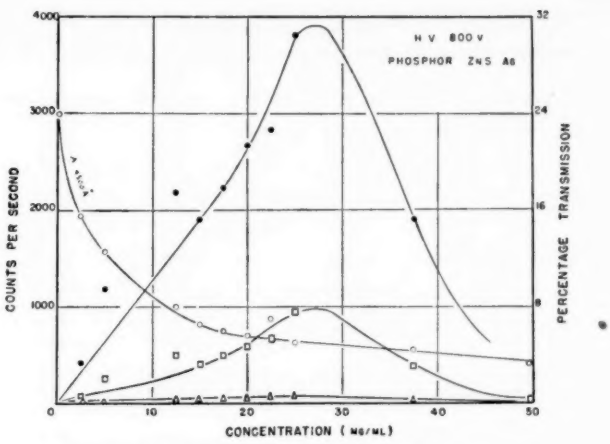

FIG. 4. Counting rate *vs.* concentration for the ZnS:Ag screens.

was intercepted. This arrangement was made purposely so that the mechanical recorder could follow the counts. The alpha-particles had about 4 Mev energy upon arrival at the screen. The scaler used was a Nuclear Instrument and Chemical Corporation model 162. The operating voltages are given in the graphs.

In general, it can be observed that a phosphor screen (about 0.5 mm thick) of about 30 mg/ml (30 mg of powder in 1 ml of plastic) gives best results. For the readers who are looking for a formula relating the counting rate to the concentration and spectral characteristics of the phosphor powder, the following relation is given:

$$\text{Counting rate} = f(A)\left[\int_0^\infty g(\lambda)g'(\lambda)d\lambda\right]\left[j(c)e^{-\mu c}\right].$$

If the above relation, $f(A)$ means some function of the activity (more than likely a constant fraction which considers the geometry). $g(\lambda)$ and $g'(\lambda)$ give the spectral characteristics of phosphor and cathode respectively and the integral $\int_0^\infty g(\lambda)g'(\lambda)d\lambda$ gives the extent to which these two overlap. The function $j(c)$ takes care of the conversion efficiency and the effect of concentration on number of light pulses. If one divided the counting rate curve in Fig. 3 or 4 by the transmission curve, the result would be a curve showing the number of light pulses *vs.* concentration; this latter curve is essentially $j(c)$. The absorption of the screens for their own radiation is essentially exponential. This accounts for the presences of $e^{-\mu c}$ in the formula percentage transmission curves in Figs. 3 and 4, also. Hence, it is possible to define each term in the equation (graphically) in terms of the data obtained.

* Part I in this series is the article by L. B. Robinson and J. R. Arnold [Rev. Sci. Inst. **20**, 549 (1949)].

† This research has received partial support from a grant by the Research Corporation of New York and from the joint program of the AEC and ONR.

Transport Properties of Gases

K. E. GREW
University College, Exeter, England
November 18, 1949

IN two valuable papers,[1,2] the second of which has only recently come to my notice, Hirschfelder, Bird, and Spotz have given theoretical values of the transport coefficients for gases whose molecules have force fields represented by

$$E(r) = 4\epsilon\left[\left(\frac{r_0}{r}\right)^{12} - \left(\frac{r_0}{r}\right)^{6}\right],$$

where E is the potential energy of interaction of two molecules at distance r apart, r_0 is the separation when E is zero, and ϵ is the minimum energy. It is perhaps desirable to point out an error which appears in their comparison of those theoretical and experimental results relating to thermal diffusion.

TABLE I. Values of R_T calculated for the (12, 6) model compared with experimental values.

Gas mixture	Temp. °K	R_T HBS†	R_T corrected	R_T experimental
He−Ne, 53.8% He	585.2	0.71	0.68	0.64
	233.2	0.70	0.67	0.64
	117.2	0.68	0.65	0.58
He−A, 51.2% He	585.2	0.73	0.67	0.66
	233.2	0.71	0.65	0.63
	117.2	0.63	0.58	0.55
He−Kr, 55.0% He	585.2		0.67	0.67
	233.2		0.63	0.67
	117.2		0.50	0.55
He−Xe, 53.6% He	585.2	0.75	0.71	0.66
	233.2	0.70	0.66	0.66
Ne−A, 51.2% Ne	585.2	0.66	0.61	0.57
	233.2	0.52	0.48	0.48
	117.2	0.27	0.25	0.28
Ne−Kr, 53.0% Ne	585.2		0.61	0.64
	233.2		0.43	0.47
	117.2		0.16	0.30
Ne−Xe, 54.2% Ne	585.2	0.66	0.61	0.66
	233.2	0.44	0.41	0.46
A−Kr, 53.5% A	585.2		0.50	0.61
	232.2		0.18	0.18
A−Xe, 56.4% A	585.2	0.51	0.48	0.45
	233.2	0.15	0.14	0.15
H_2−He, 53.6% H_2	284	0.53*	0.62	0.41,*,[a] 0.60[b]
H_2−D_2, 50% H_2	333	0.63	0.63	0.50,*,[a] 0.52,[c] 0.61[d]

† HBS: values given by Hirschfelder, Bird, and Spotz.
* For mixtures containing 80% H_2.
[a] See reference 3.
[b] See references 7, 8, and 9.
[c] See reference 4.
[d] See references 5 and 6.

The quantity used in the comparison is the thermal separation ratio R_T. Now the experimental values of R_T are calculated as the ratio $\alpha(\text{exp})/[\alpha(\infty)]_1$, where $\alpha(\text{exp})$ is the value of the thermal diffusion factor determined experimentally and $[\alpha(\infty)]_1$ is the theoretical value, in first approximation, for a mixture of molecules of the same masses, diameters and relative numbers as in the experimental mixture, but which interact as rigid elastic spheres. The diameters used in calculating $[\alpha(\infty)]_1$ are those found from the viscosity and the relation between viscosity and molecular diameter *appropriate to rigid spheres*. The corresponding theoretical value of R_T is the ratio $\alpha(12, 6)/[\alpha(\infty)]_1$ where $\alpha(12, 6)$ is the exact value of the thermal diffusion factor for the above model and $[\alpha(\infty)]_1$ is as just defined. It appears, however, that Hirschfelder, Bird, and Spotz, in calculating $[\alpha(\infty)]_1$ have used the "diameters" $2r_0$ found from the viscosity assuming that the molecular fields are of the (12, 6) type—and not rigid spheres, as should be done. The error introduced into R_T is in some cases appreciable, as can be seen in Table I. For isotopic mixtures the point does not arise, of course.

It may be pointed out too that some of the experimental values of R_T given by Hirschfelder, Bird, and Spotz are questionable. The values quoted for hydrogen-deuterium and hydrogen-helium mixtures—$R_T=0.50$ and 0.41 respectively—are those found by Murphey.[3] There is some uncertainty about both. For hydrogen-deuterium Waldmann's[4] results lead to $R_T=0.52$, while Heath, Ibbs, and Wild[5] agree with Grew[6] in finding $R_T=0.60\pm0.01$. For hydrogen-helium mixtures the results of Elliott and Masson,[7] of v. Itterbeek, v. Paemel, and v. Lierde,[8] and of Grew,[9] all indicate a value $R_T=0.60$. For hydrogen-carbon dioxide mixtures there are several independent measurements giving $R_T=0.44$ at 300°K and 0.57 at 600°K (Lugg,[10] Blüh, Blüh, and Puschner,[11] Bastick, Heath, and Ibbs[12]).

The effect of these corrections is in most cases to bring the theoretical and experimental values nearer to each other. It must be remembered, however, in drawing conclusions as to the suitability of the (12, 6) model that the theoretical values of $\alpha(12, 6)$ actually used in the calculation of R_T are first approximations only, and not exact values. It would be interesting to have the error of the first approximation determined, for then thermal diffusion measurements could, it seems, give rather precise information about molecular fields of force.

[1] Hirschfelder, Bird, and Spotz, J. Chem. Phys. **16**, 968 (1948).
[2] Hirschfelder, Bird, and Spotz, Chem. Rev. **44**, 205 (1949).
[3] B. F. Murphey, Phys. Rev. **72**, 834 (1947).
[4] Waldmann, Zeits. f. Physik **124**, 2 (1947).
[5] Heath, Ibbs, and Wild, Proc. Roy. Soc. **178A**, 380 (1941).
[6] K. E. Grew, Proc. Roy. Soc. **178A**, 390 (1941).
[7] Elliott and Masson, Proc. Roy. Soc. **108A**, 378 (1925).
[8] v. Itterbeek, v. Paemel, and v. Lierde, Physica **13**, 231 (1947).
[9] K. E. Grew, Proc. Phys. Soc. **62**, 655 (1949).
[10] Lugg, Phil. Mag. **8**, 1019 (1929).
[11] Blüh, Blüh, and Puschner, Phil. Mag. **24**, 1103 (1937).
[12] Bastick, Heath, and Ibbs, Proc. Roy. Soc. **173A**, 543 (1939).

The Crystal Structure of Urea-Hydrocarbon and Thiourea-Hydrocarbon Complexes

A. E. SMITH
Shell Development Company, Emeryville, California

November 14, 1949

THE formation of crystalline complexes of urea with straight chain hydrocarbons, fatty acids and other compounds was first reported by Bengen[1] and was further discussed by Zimmerschied[2] and co-workers. It is the purpose of this communication to report the results of an x-ray investigation of the crystal structure of both urea and thiourea complexes and to describe their molecular configuration and its relation to their stability.

Complete Weissenberg data were taken for single crystals of cetane-urea and 1, 10-dibromodecane-urea complexes. Powder patterns were also taken of urea complexes of $C_{10}-C_{50}$ hydrocarbons and various straight chain alcohols, acids and esters. All gave essentially identical powder patterns. The unit cell is hexagonal; $a_1=8.24$A, $c=11.0$A, space group $C6_12$, six urea molecules per unit cell. The urea molecules form spirals with the hydrocarbon molecules situated at the center (Fig. 1). Spirals of hydrogen bonds between the O and NH_2 groups of adjacent urea molecules account largely for the stability of the structure (Fig. 2). The shorter N−H−O bonds are about 2.93A in length and are planar with the urea molecule; the longer H bonds are about 3.03A General factors determining the stability of molecular complexes have been discussed by H. M. Powell.[3]

The hydrocarbons are at the special positions $(0, 0, Z)$ in a zigzag planar configuration with the long axis of the molecule parallel to Co. The molecules are randomly distributed with the plane of the molecule at positions perpendicular to the a axis and at multiples of 120° to this position. The Z positions of the carbon

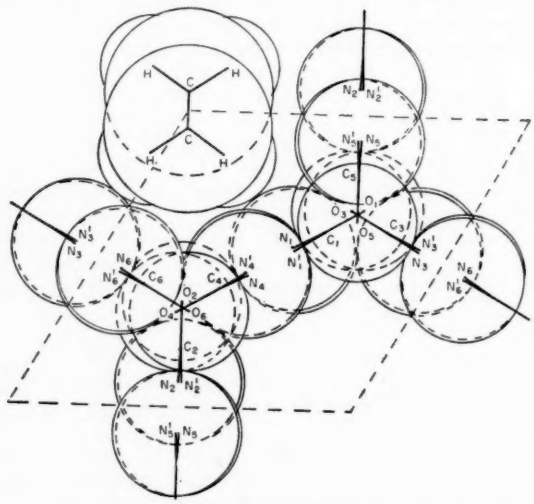

FIG. 1. Centane-urea complex, contents of unit cell projected onto (001) plane showing packing arrangement.

atoms are not fixed except in those cases in which the length of the straight chain is a multiple (or very close to a multiple) of the urea spiral repeat. In the latter cases the true unit cell has its c repeat increased by multiples of this quantity (e.g., for the centane-urea complex $c=22.0$A).

The general features of the structure were obtained directly from an implication diagram[4] or Patterson-Harker section $P(xy\frac{1}{6})$ (Fig. 3). Buerger[4] has shown that for space group $C6_12$ the implication diagram is equal to the Patterson-Harker section $P(xy\frac{1}{6})$, i.e., no ambiguities or satellitic peaks occur. $P(xy\frac{1}{6})$ is therefore essentially equivalent to a Fourier projection of the electron density onto the a_1a_2 plane. Approximate nitrogen x, y parameters were directly determined from a sharpened section $P(xy\frac{1}{6})$ but the oxygen and carbon atoms were not resolved because of overlapping. An electron density projection on the a_1a_2 plane obtained with the 1,10-dibromodecane-urea complex confirmed the results from the Patterson-Harker section $P(xy\frac{1}{6})$. The projection could be made directly since it has a center of symmetry and the electron density of the 1, 10-dibromodecane molecules in projection was sufficient to make all the significant F_{hkl} values positive.

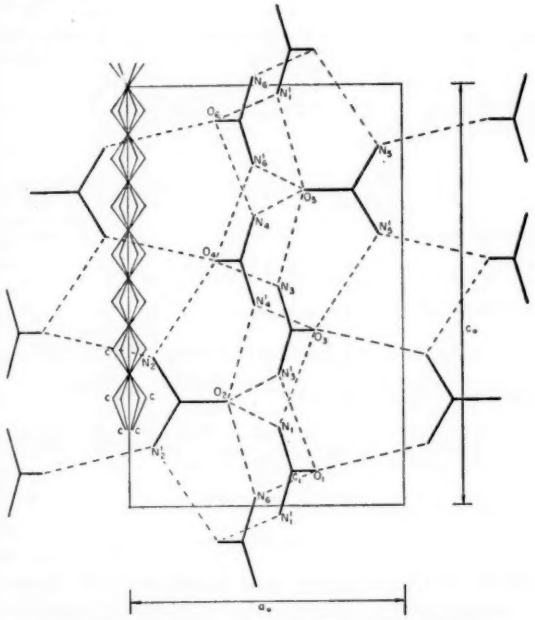

FIG. 2. Centane-urea complex, contents of unit cell ($\frac{1}{2}$ true unit cells projected onto the (010) plane of orthohexagonal cell. The N $-$H $-$O bond) are shown by dotted lines. The projection of the statistically possible C $-$ positions in the cetane molecule are also indicated.

Satisfactory agreement between calculated and observed intensities for the (*hko*) reflections was obtained using a temperature factor $e^{-B(\sin\theta/\lambda)^2}$ with $B\simeq 2.0$ for urea and $B\simeq 6$ for cetane. Contributions for hydrogen were included up to $\sin\theta/\lambda=0.30$. In addition to averaging the contribution of the carbon atoms of the cetane over the statistically possible positions for the (*hol*) reflections an anisotropic temperature factor is required. Consideration of the Fourier transform of the molecule shows, however, that the contribution of the cetane molecule to the structure factor is small unless 1 is about 9. Although the agreement between calculated and observed intensities for the (*hol*) reflections is satisfactory, further refinement by Fourier methods is in progress.

The composition of the complexes as a function of chain length can be readily calculated. Taking the alternate carbon-carbon distance $=2.54$A and the van der Waals radius of the CH_3 group $=2.0$A, the urea carbon atom ratio is approximately $[0.6925(n-1)+2.18]/n$ where n is the number of carbon atoms in the straight chain.

Measured values of the composition[5] are in excellent agreement with the theoretical values. It is also possible to predict from the structure and from the van der Waals packing radii whether or not substituted straight chain molecules will form stable complexes.

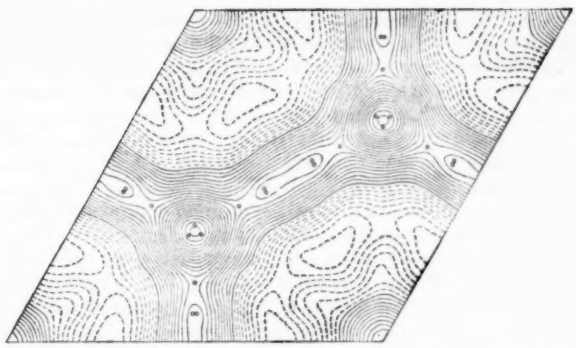

FIG. 3. Patterson-Harker section $P(xy\frac{1}{6})$. Positions of the oxygen, nitrogen and carbon atoms in the urea molecules indicated.

Thiourea forms crystalline complexes[6,7] with cyclohexane, triptane, and certain other branched chain hydrocarbons. Incomplete x-ray work on these complexes indicates that although the unit cell is rhombohedral, the arrangement of the thiourea molecules is similar to that of the ureas in the urea complexes. The larger radius of the sulfur atoms results in a larger channel into which cyclohexane, hexachlorethane, triptane, etc., just fit. The composition of the complexes could be calculated approximately and the relative stability of the complexes formed by thiourea and various branched chain molecules[5] predicted from the crystal structure in most cases. A more detailed account of the structures of the urea and thiourea complexes will be reported later.

[1] F. Bengen, U. S. Tech. Oil Mission Film No. 6, Item II-7 German Pat. Application O.Z. 12438 (March 18, 1940).
[2] Zimmerschied, Dinerstein, Weitkamp, and Marschner, J. Am. Chem. Soc. **71**, 2947 (1949); Symposium on Adsorption, ACS Meeting, Atlantic City, September, 1949, p. 225.
[3] H. M. Powell, J. Chem. Soc. 61 (1948).
[4] M. J. Buerger, J. App. Phys. **17**, 579 (1946).
[5] O. Redlich *et al.* (to be published).
[6] Angla, Comptes Rendus **224**, 402, 1166 (1947).
[7] L. C. Fetterly, (to be published).

A Theoretical Calculation of the Resonance Energies and Ultraviolet Spectra of Benzene and Naphthalene

J. VAN DRANEN AND J. A. A. KETELAAR
Laboratory for General and Inorganic Chemistry, University of Amsterdam, The Netherlands
November 29, 1949

IN our publication on the molecular orbital parameters[1] we have calculated the resonance energy (R.E.) of benzene using the second approximation method with the theoretical value of $\beta_{12}'=-2.42$ ev calculated there and the exchange integrals between non-neighboring atoms were estimated as proportional to the lack of orthogonality integrals S_{ik} with $S_{12}=0.260$; $S_{13}=0.04$ and $S_{14}=0.02$.

The M.O. method in the usual L.C.A.O. approximation gives for the resonance energy: R.E. $=1.040\beta_{12}'-0.849\beta_{13}'-2.087\beta_{14}'$, and for the first excitation energy: $\Delta E=2.222\beta_{12}'+0.560\beta_{13}'-2.222\beta_{14}'$. If we now compute also the values of β_{13}' and β_{14}' in the same purely theoretical way as β_{12}', we obtain: $\beta_{13}'=-0.703$ ev and $\beta_{14}'=-0.268$ ev as compared with the former estimates of -0.372 ev and -0.186 ev, respectively.

We thus obtain the theoretical values of R.E. equal to 1.37 ev (32 kcal) and $\Delta E=5.18$ ev (λ2400A), whereas with the former method R.E. 1.80 ev (42 kcal) and $\Delta E=5.17$ ev (λ2410A) were obtained. It would seem that the values of β_{13}' and β_{14}' thus calculated are rather surprisingly large. To put β_{ik}' proportional to

S_{ik}, as is done in the second approximation method is however useful, for with only a little more arithmetical work the numerical results are better than in the zero or first approximation method.

The procedure of calculation $V\pi(\nu)$ can be improved. To compute $V\pi(\nu)$ we now localize in each ρ_z-orbital one π-electron. So we avoid the great Coulomb-interaction of π-electrons in the same ρ_z orbital: for the theoretical values of α became so low, when we distributed each π-electron among all ρ_z-orbitals as done formerly. Instead of the average position of each π-electron, we take now the momentary position of all π-electrons. So α for a certain atom is equal to the sum of the ionization-energy ($W2\rho$) for this atom and the interaction-energy of a π-electron in its ρ_z-orbital with the other neutral atoms. Because this interaction-energy is low this method justifies to a certain extent the procedure of taking for α the ionization energy. As β_{12}' (in good approximation) is independent of $V\pi(\nu)$, this method of calculating $V\pi(\nu)$ does not change our conclusion or values of β_{12}'.

With the values for the integrals of Parr and Crawford[2] we find for the α of benzene and ethene respectively -12.56 ev and -11.82 ev ($W2\rho=-10.82$ ev[1]).

We now apply our method to naphthalene and take the following distances and angles between the C atoms.[3]

$$\begin{aligned} r_{12}&=1.358\text{A} & \angle(r_{12},r_{19})&=119°35' \\ r_{23}&=1.395\text{A} & \angle(r_{12},r_{22})&=120°50' \\ r_{19}&=1.421\text{A} & \angle(r_{19},r_{910})&=119°35' \\ r_{910}&=1.395\text{A} & & \end{aligned}$$

For the calculation of α_j we compute $V\pi(\nu)$ by again localizing the π-electron (ν) in the jth$-\rho_z$-orbital and we fill each other ρ_z-orbital with one π-electron (μ). This gives: $\alpha_1=-12.59$ ev; $\alpha_2=-12.67$ ev and $\alpha_9=-13.26$ ev.

For the β's of naphthalene we find (in ev's):

$$\begin{aligned} &\beta_{12}'=-2.76; \quad \beta_{23}'=-2.43; \quad \beta_{19}'=-2.10; \quad \beta_{910}'=-2.26 \\ &\beta_{13}'=-0.779; \quad \beta_{18}'=-0.199(!); \quad \beta_{14}'=-0.233; \quad \beta_{15}'=-0.062 \\ &\beta_{17}'=-0.061; \quad \beta_{27}'=-0.005; \quad \beta_{16}'=-0.013; \\ &\beta_{29}'=-0.727; \quad \beta_{110}'=-0.520; \quad \beta_{210}'=-0.233. \end{aligned}$$

For the exchange-integrals $\beta_{ij}'=\beta_{ij}-s_{ij}\alpha$ of C atoms, which have not identical positions in the molecule, we take for α the average value of α_i and α_j. The six lowest energy states of the π-electron in naphthalene are:

$$\begin{aligned} &E_1=\alpha+1.63\beta_{12}'; \quad E_2=\alpha+1.23\beta_{12}'; \quad E_3=\alpha+0.68\beta_{12}' \\ &E_4=\alpha+0.40\beta_{12}'; \quad E_5=\alpha+0.33\beta_{12}'; \quad E_6=\alpha-1.17\beta_{12}'. \end{aligned}$$

[It is convenient from an arithmetical point of view to take β_{12}' as unit; $\alpha=\frac{1}{2}(\alpha_1+\alpha_2)$.]

The R.E. of naphthalene is $0.98\beta_{12}'=62$ kcal (with the R.E. we mean the decrease in energy of naphthalene with regard to the energy of the Erlenmeyer structure with five localized double bonds between C_1-C_2, C_3-C_4, C_5-C_6, C_7-C_8 and C_9-C_{10}). Experimental value 75 kcal.[4]

The first excitation energy ΔE is $1.50\beta_{12}'=4.14$ ev. This value gives for λ2980A. (Compare experimental value 2750A.[1])

It should be emphasized that in these calculations as empirical values we have here only used the distances of C atoms and the effective nuclear-charge $Z=3.18$.[1]

Mathematical Appendix.—We call: the exchange penetration integral:[2]

$$\int\varphi_i(\nu)\varphi_j(\nu)H_j(\nu)d\tau=Ae(r_{ij})$$

the Coulomb penetration integral:

$$\int\varphi_i^2(\nu)H_j(\nu)d\tau=Ad/(r_{ij})$$

the hybrid Coulomb-exchange integral:

$$\int\varphi_i(\nu)\varphi_j(\nu)e^2/r_{\gamma\mu}\varphi_j^2(\nu)=Be(r_{ij})$$

the Coulomb-integral:

$$\int\varphi_i^2(\nu)e^2/r_{\gamma\mu}\varphi_j^2(\nu)=Bd(r_{ij})$$

the overlap-integral:

$$\int\varphi_i(\nu)\varphi_j(\nu)=S_{ij}.$$

For

$$Ad(r_{ij})+Ad(r_{il})\cdots$$

we write

$$Ad(r_{ij},r_{il},\cdots)$$

or

$$\sum_j Ad(r_{ij}).$$

We give a few examples: β_{13}' of benzene (m is a point midway between C_1 and C_3 with a virtual charge equal to S_{13} e).

$$\begin{aligned} \beta_{13}'=&S_{13}Ad(r_{m1},r_{m2},r_{m4},r_{m6},r_{m5}) \\ &-S_{13}Bd(r_{m1},r_{m2},r_{m4},r_{m6},r_{m5}) \\ &-s_{13}Ad(r_{12},r_{16},r_{13},r_{15},r_{14}) \\ &+S_{13}Bd(r_{12},r_{16},r_{13},r_{15},r_{14}). \end{aligned}$$

It is of course possible to "symmetrize" this expression in $m1$ and $m3$ by replacing: $Ad(r_{m1})\rightarrow\frac{1}{2}Ad(r_{m1},r_{m3})$ etc.

β_{12}' of naphthalene (n is a point midway between C_1 and C_2 with a virtual charge equal to S_{12} e)

$$\begin{aligned} \beta_{12}'=&Ae(r_{12})-Be(r_{12})+S_{12}\sum_{j=3}^{j=10}Ad(r_{nj})-S_{12}\sum_{j=3}^{j=10}Bd(r_{nj}) \\ &-\tfrac{1}{2}S_{12}\sum_{j=2}^{j=10}Ad(r_{1j})+\tfrac{1}{2}S_{12}\sum_{j=2}^{j=10}Bd(r_{1j}) \\ &-\tfrac{1}{2}S_{12}\sum_{j=1,j\neq2}^{j=10}Ad(r_{2j})+\tfrac{1}{2}S_{12}\sum_{j=1,j\neq2}^{j=10}Bd(r_{2j}). \end{aligned}$$

The term

$$\int\varphi_i(\nu)W_{2p}\varphi_j(\nu)d\tau$$

cancels exact; and the term

$$\int\varphi_i(\nu)V\pi(\nu)\varphi_j(\nu)d\tau$$

cancels in good approximation.

[1] J. van Dranen and J. A. A. Ketelaar, J. Chem. Phys. **17**, 1338 (1949).
[2] R. G. Parr and B. L. Crawford, J. Chem. Phys. **16**, 1049 (1948).
[3] Abrahams, Monteath-Robertson, and (in part) White, Acta Cryst. **2**, 238 (1949).
[4] L. Pauling, *Nature of the Chemical Bond* (Cornell University Press, Ithaca, New York, 1945).

Heats of Combustion and Formation of Some Organic Compounds Containing Oxygen

GEORGE S. PARKS, JOHN R. MOSLEY, AND PETER V. PETERSON, JR.
Department of Chemistry, Stanford University, Stanford, California
November 9, 1949

As one step in the development of a comprehensive table of free energy data for organic compounds containing oxygen, we have recently had occasion to measure the heats of combustion of six such substances (*viz.*, maleic anhydride, furoic acid, furfuryl alcohol, cyclopentanol, cyclohexanol, and benzophenone), for which combustion data have hitherto been either uncertain or non-existent, and to revise the earlier values for five other substances.

Our new measurements were made upon highly purified materials in accordance with the calorimetric bomb procedures which have been described in earlier papers[1,2] from this laboratory. They are based upon Jessup's recent value of 26,429.4 international joules per gram mass for the standard benzoic acid.[3] The resulting molal heats of combustion at 25°C and 1 atm. constant pressure, expressed in terms of the *defined* kilocalorie (=4.184 absolute kilojoules), are given under the heading $-\Delta H_R$ in the third column of Table I. Each value represents the average of four to seven combustion measurements and, in our judgment, should not involve an over-all uncertainty in excess of 0.05 percent. The

corresponding values for the heat of formation from the elements ($-\Delta H_f°$) in the last column have been computed by use of -68.3174 kcal. and -94.0518 kcal.[4] for the $\Delta H_f°$ of $H_2O(l)$ and $CO_2(g)$, respectively.

TABLE I. Molal heats of combustion and formation at 25°C.

Substance and state (l=liquid; s=solid)	Mole wt.	$-\Delta H_R$ kcal.	$-\Delta H_f°$ kcal.
Isopropyl alcohol (l)	60.094	479.24	76.18
Maleic anhydride (s)	98.056	332.29	112.23
Methyl ethyl ketone (l)	72.104	582.80	66.68
Fuoric acid (s)	112.082	487.75	119.14
Furfuryl alcohol (l)	98.098	609.16	66.05
Cyclopentanol (l)	86.130	740.07	71.77
Cyclohexanol (l)	100.156	890.77	83.45
Phthalic anhydride (s)	148.112	779.02	110.03
Phthalic acid (s)	166.128	770.49	186.88
Benzophenone (s)	182.210	1556.40	7.86
Cetyl alcohol (s)	242.432	2502.67	163.55

Included also in this table are our revised values for five other oxygen-containing substances which have been previously studied by Parks and co-workers.[1,2,5] The original data have now been corrected for a change in the accepted combustion value of the standard benzoic acid,[6] for a small change in the atomic weight of hydrogen, and for a small alteration in the measured heat capacity of our calorimetric system, resulting from an increased number of calibrations. In the case of isopropyl alcohol, an arithmetical error entering into the previously published result has here necessitated an additional correction of $+0.04$ percent.

[1] J. W. Richardson and G. S. Parks, J. Am. Chem. Soc. **61**, 3543 (1939).
[2] Moore, Renquist, and Parks, J. Am. Chem. Soc. **62**, 1505 (1940).
[3] R. S. Jessup, J. Research Nat. Bur. Standards **36**, 421 (1946).
[4] Wagman, Kilpatrick, Taylor, Pitzer, and Rossini, J. Research Nat. Bur. Standards **34**, 143 (1945).
[5] G. S. Parks and G. E. Moore, J. Chem. Phys. **7**, 1066 (1939).
[6] R. S. Jessup, J. Research Nat. Bur. Standards **29**, 247 (1942).

Light-Scattering Measurement of Interactions between Unlike Polymers

W. H. STOCKMAYER AND H. E. STANLEY
Department of Chemistry, Massachusetts Institute of Technology, Cambridge, Massachusetts
November 28, 1949

MEASUREMENTS of osmotic pressure or light scattering have been extensively used to evaluate thermodynamic coefficients characterizing polymer-solvent interactions. However, there have been no systematic investigations of interactions between different polymers. Such studies would have both theoretical and practical interest. Here we describe a preliminary light-scattering study of polymethyl-methacrylate-polystyrene interactions in butanone at 25°C.

From fluctuation theory, the turbidity τ (excess over pure solvent) of a multi-component fluid is given[1] by

$$\tau/H'' = \Sigma_i \xi_i^2 M_i c_i - 2\Sigma_{ij} \xi_i \xi_j B_{ij} M_i M_j c_i c_j + \cdots, \qquad (1)$$

with

$$H'' \equiv 32\pi^3 n^2/3N_0\lambda_0^4,$$
$$\xi_i \equiv (\partial n/\partial c)_{T,p,c},$$

where n is refractive index, λ_0 wave-length in vacuum, c_i solute concentration in mass per unit volume, M_i solute molecular weight, N_0 Avogadro's number, and B_{ij} a virial coefficient defined by the osmotic pressure expansion

$$\Pi/RT = \Sigma_i (c_i/M_i) + \Sigma_{ij} B_{ij} c_i c_j + \cdots. \qquad (2)$$

The sums go over all solutes. In terms of Flory-Huggins constants,[2]

$$B_{ij} = (1 - \mu_{1i} - \mu_{1j} + \mu_{ij})/2V_1\rho_i\rho_j \quad (\mu_{ii} \equiv 0), \qquad (3)$$

subscript 1 denoting the solvent, ρ_i solute density, and V_1 solvent molar volume. All quantities in Eq. (1) are accessible from studies of each solute separately, except for the coefficients B_{ij} with $i \neq j$. Thus, the latter are obtainable from turbidities of solutions containing two solutes.

The turbidities reported herein were evaluated from measured intensities of unpolarized green light (λ546 mμ) scattered at right angles, with apparatus constructed in this laboratory and broadly resembling that of Zimm.[3] The turbidity standard was a polystyrene sample[4] (in toluene) extensively calibrated elsewhere. The polymethylmethacrylate fraction[5] had molecular weights of 126,000 (number average[6]) and 138,000 (weight average), and the polystyrene fraction[7] had a weight-average molecular weight of 133,000. Hence, angular dissymmetries were low; moreover, according to theory,[8] dissymmetry affects calculation only of molecular weights, not of interaction coefficients. Cabannes' depolarization factor was applied throughout; this is probably valid only at infinite dilution, but the correction is small. Refractivity measurements give $\xi_2 = 0.114$ and $\xi_4 = 0.210$ ml/gram, subscripts 2 and 4 denoting polymethylmethacrylate and polystyrene, respectively.

In Fig. 1, the experimental results are plotted as $H''c/\tau$ against *total* solute concentration, $c \equiv c_2 + c_4$. Each line denotes a series of solutions with a fixed value of c_2/c. Quantities calculated from these data with Eqs. (1) and (3) by least-squares methods are given in Table I, and the solid lines of Fig. 1 are calculated from

TABLE I. Interactions at 25°C in the Ternary System: (1) Butanone, (2) Polymethylmethacrylate, (4) Polystyrene.

M_2	138,000[a]	M_4	133,000[a]
$B_{22}\times10^4$	3.2 ± 0.1[b]	$B_{44}\times10^4$	1.1 ± 0.2[b]
μ_{12}	0.460 ± 0.001	μ_{14}	0.489 ± 0.002
	$B_{24}\times10^4$	2.9 ± 0.3[b]	
	μ_{24}	0.014 ± 0.010	

[a] Molecular weights corrected for dissymmetry.
[b] Units: g^{-2} cm^3 mole.

these parameters. The polymer-solvent interactions obtained from the binary mixtures (series I and V) agree well with reported values for polymethylmethacrylates[6] and polystyrenes[3,9] of similar molecular weights. In computing the polymer-polymer interaction, the data of series II were rejected, since they give a limiting value of $H''c/\tau$ (see Fig. 1) markedly lower than that predicted by Eq. (1) from the binary data. Series III and IV, however, give the right intercepts, and their slopes lead to nearly identical values of B_{24}. The low value of μ_{24}, 0.014 ± 0.010, indicates similar cohesive energy densities for the polymers and negligible deviation from the Flory-Huggins entropy of mixing.[2]

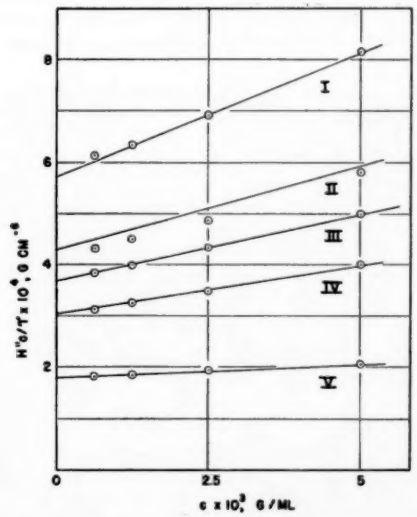

FIG. 1. Turbidities of polymethylmethacrylate—polystyrene solutions in butanone at 25°C, $\lambda = 546$ mμ. Each series corresponds to a constant weight-ratio of the two polymers. In series I to V, the weight fractions of polymethylmethacrylate in the total solute are 1, 0.850, 0.750, 0.600, and 0, respectively. The lines are calculated from constants of Table I.

A rough independent estimate of μ_{24} is available from compatibility measurements[10] on solutions of these polymers in benzene. With Scott's theory,[11] these yield $0.008 < \mu_{24} < 0.015$, the range resulting from uncertainties in molecular weights. Since butanone and benzene have equal molar volumes, μ_{24} should be the same in these solvents, hence agreement is remarkably good.

We thank Swift and Company for a grant supporting this work, and E. F. Casassa for experimental assistance. Measurements in other solvents and with other polymers are now in progress.

[1] (a) F. Zernike, Dissertation, Amsterdam (1915); (b) H. C. Brinkman and J. J. Hermans, J. Chem. Phys. **17**, 574 (1949); (c) J. G. Kirkwood and R. J. Goldberg, J. Chem. Phys. **18**, 54 (1950); (d) W. H. Stockmayer, J. Chem. Phys. **18**, 58 (1950).
[2] (a) P. J. Flory, J. Chem. Phys. **12**, 425 (1944); (b) M. L. Huggins, Ann. N. Y. Acad. Sci. **41**, 1 (1942); see also reference 11.
[3] B. H. Zimm, J. Chem. Phys. **16**, 1099 (1948).
[4] Obtained from Dr. P. M. Doty, Harvard University.
[5] Obtained from Dr. F. W. Billmeyer, Jr., Polychemicals Department, E. I. du Pont de Nemours and Company.
[6] H. G. Lauterbach, osmotic measurements in this laboratory.
[7] Obtained from Dr. E. H. Merz, Monsanto Chemical Company.
[8] B. H. Zimm, J. Chem. Phys. **16**, 1093 (1948).
[9] Doty, Zimm, and Mark, J. Chem. Phys. **13**, 159 (1945).
[10] A. Dobry and F. Boyer-Kawenoki, J. Polymer Sci. **2**, 90 (1947).
[11] R. L. Scott, J. Chem. Phys. **17**, 279 (1949).

Some Observations of the Epitaxy of Sodium Chloride on Silver*

GERALD W. JOHNSON
Brookhaven National Laboratory, Upton, New York
November 9, 1949

IN the classical work of Royer[1] on the growth of alkali halide crystals over various substrates, primarily ionic, it was concluded that parallel growth does not occur between differently bonded substances, i.e. between ionic crystals and covalent crystals. Beukers,[2] however, observed excellent orientation of sodium chloride when it was crystallized from solution on a freshly cleaved crystal of galena. This constitutes a departure from Royer's conclusion in that while galena is a semiconductor, sodium chloride is a purely ionic crystal. Sloat and Menzies,[3] looking for epitaxy between silver and various alkali halides, concluded that it would take place only if the difference of lattice parameter between the halide and the metal was small (~1 percent) for a particular relative orientation. It is now well established[4–6] that certain metals condensed in a vacuum on ionic substrates under proper conditions take up preferred orientations. Of particular interest for our purposes was the observation of Brück that silver oriented completely on cleaved rocksalt with the (100) planes parallel and the (100) direction of silver along the (100) of rocksalt, even though the difference in parameters in this orientation is 27.6 percent. The inverse case of the epitaxy of sodium chloride or other ionic crystals on metals does not seem to have been investigated extensively. In this communication are given examples of strong epitaxy of sodium chloride on oriented films of silver and on polycrystalline silver sheet.

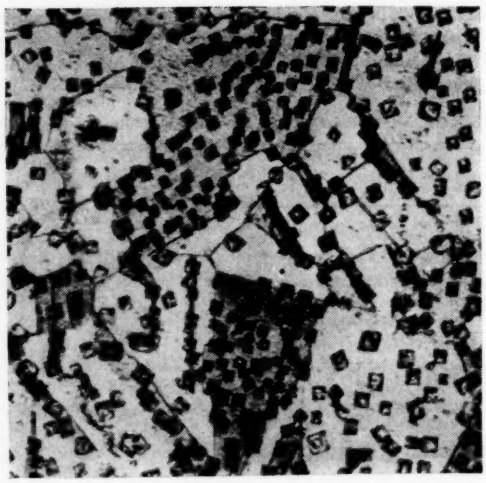

FIG. 2. Epitaxy of sodium chloride on polished and etched polycrystalline silver plate. 440×

A silver film was grown by the method of Brück.[4] The film was then floated off the rocksalt in water, picked up on a polished silver plate, and dried. On rinsing the film in saturated sodium chloride, almost complete orientation resulted (Fig. 1). The cube edges of the sodium chloride crystallites are parallel to the 110 direction of silver.

A polycrystalline sheet of high purity silver after recrystallizing at 700C was electropolished and lightly etched to reveal the grain boundaries. When this specimen was rinsed in sodium chloride, strong orienting effects were noted on some grains, which presumably then were those with the most favorable orientations (Fig. 2). It is noted that crystallization is much more profuse on those grains which show the greatest epitaxy. This is an expected result since the attractive forces between the substrate and crystals must be greatest when orientation results. This observation is consistent with that of Finch and Sun[7] who found that electroplated films were much more adherent to the substrate when the plated deposit followed the orientation of the substrate closely. In the photomicrograph presented here we have a graphic illustration of this effect.

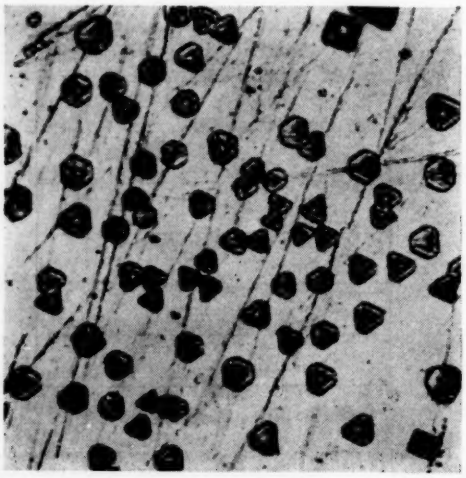

FIG. 1. Epitaxy of sodium chloride on film of silver oriented on rocksalt. 400×

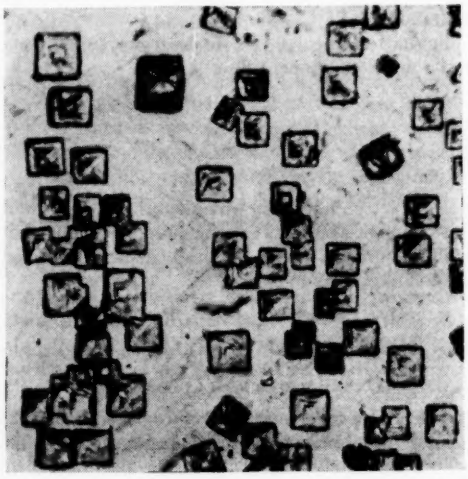

FIG. 3. Epitaxy of sodium chloride on film of silver oriented on mica. 400×

Although many cubic alkali halides orient when deposited on freshly cleaved mica, sodium chloride does not.[8] It is known that silver deposited on mica in a vacuum, under suitable conditions, is oriented with its (111) plane parallel to the substrate, and also is oriented in a particular azimuth.[6] We prepared such a film and rinsed it in sodium chloride solution as with the other surfaces, and found that the (111) planes of sodium chloride were in the plane of the surface. The triangular pyramids thus produced all have the same orientation within 180° (Fig. 3).

Thus strong epitaxy has been found between an ionic crystal and a metal. This observation provides a means of readily checking the degree of orientation of thin silver films without resorting to electron diffraction. At the same time one can distinguish between the (100) and the (111) orientation in the films. At the present time this method can be regarded only as a rough check as it is not yet known to what extent the surface may depart from the (100) or (111) orientation before epitaxy fails to appear.

* Research carried out at Brookhaven National Laboratory under the auspices of the AEC.

[1] L. Royer, Bull. Soc. Franc. Mineral **51**, 7 (1928).
[2] M. C. F. Beukers, Rec. Trav. Chim. **58**, 435 (1939).
[3] C. A. Sloat and A. W. C. Menzies, J. Phys. Chem. **35**, 2005 (1931).
[4] L. Brück and H. Lassen, Ann. d. Physik. (Leipsig) **22**, 65 (1935).
[5] L. Brück, Ann. d. Physik. (Leipsig) **26**, 233 (1936).
[6] O. Rudiger, Ann. d. Physik. (Leipsig) **30**, 505 (1937).
[7] G. I. Finch and C. H. Sun, Trans. Faraday Soc. **32**, 852 (1936).
[8] L. Royer, Comptes Rendus **194**, 620 (1932).

Carrier-Free Radioisotopes from Cyclotron Targets V. Preparation and Isolation of Se^{75} from Arsenic*

WARREN M. GARRISON, ROY D. MAXWELL,** AND JOSEPH G. HAMILTON
Crocker Laboratory, Radiation Laboratory, and Divisions of Medical Physics, Experimental Medicine, and Radiology, University of California, Berkeley and San Francisco, California

November 28, 1949

DEUTERON bombardment of arsenic produces 127-day Se^{75} by the nuclear reaction,[1] $As^{75}(d, 2n)Se^{75}$. This paper reports a radio-chemical isolation of carrier-free Se^{75} from an arsenic target bombarded with 19 Mev deuterons in the 60-inch cyclotron at the Crocker Laboratory. The possible[2] radio-isotopes of germanium (from n, p reaction) and gallium (from n, α-reaction) were allowed to decay out prior to the separation.

A 2-mm layer of C.P. arsenic powder, supported on a grooved water-cooled copper plate by a 0.25 mil tantalum foil, was bombarded for 100 microampere hours at a beam intensity of 8 microamperes. After aging for 24 hours, the bombarded arsenic was dissolved in a minimum volume of aqua regia. 12N HCl was added to destroy excess HNO_3 and the solution was adjusted to 3N. Ten mg of tellurous acid were added and precipitated as elemental tellurium with SO_2; approximately 95 percent of the Se^{75} carried. The supernatant showed the 26.8-hour period of As^{76}. The tellurium precipitate containing the carrier-free radio-selenium was dissolved in 16N HNO_3 and reprecipitated from 3N HCl in the presence of arsenic hold-back carrier. Two additional precipitations removed traces of carrier arsenic.

The tellurium precipitate was washed dissolved in a minimum volume of 16N HNO_3 and transferred to an all-glass distilling flask.[3] Fourteen percent HBr was added dropwise while a stream of N_2 carrier-gas was bubbled through the solution at 200°C. Under these conditions, selenium forms the volatile tetrabromide while tellurium is quantitatively retained in the residue. The distillate, containing the carrier-free Se^{75}, HBr and Br_2 was collected in a water trap cooled with ice. HBr was removed with HNO_3 and the solution was evaporated to dryness on 40 mg of NaCl after the addition of excess HCl. The activity, presumably as selenate, was quantitatively soluble in 5 ml of water. The resultant isotonic solution of carrier-free radio-selenium was used in subsequent biological experiments.

The Se^{75} was identified by the assigned[4] 120-day half-life and by the 0.45 Mev gamma-ray.[5] Chemical separations with added arsenic and selenium carriers further identified the activity as Se^{75}.

We are grateful to Professor G. T. Seaborg for checking the manuscript, to the staff of the 60-inch cyclotron for bombardments, and to Mrs. Alberta Mozley and Mrs. Helen Haydon for technical assistance.

* This document is based on work performed under the auspices of the AEC, Contract No. W-7405-eng-48-A.

** Lieutenant Colonel, U. S. Army, now stationed at Walter Reed Hospital, Washington, D. C.

[1] Kent, Cork, and Wadey, Phys. Rev. **61**, 389 (1942).
[2] G. T. Seaborg and I. Perlman, Rev. Mod. Phys. **20**, 585 (1948).
[3] J. A. Scherrer, J. Research Nat. Bur. Stand. **21**, 95 (1938).
[4] H. H. Hopkins, Jr. and B. B. Cunningham, Phys. Rev. **73**, 1406 (1948).
[5] Cowart, Pool, McCown, and Woodward, Phys. Rev. **73**, 1454 (1948).

The Infra-Red Spectrum of $ClC^{12}N$ and $ClC^{13}N$*

W. S. RICHARDSON AND E. BRIGHT WILSON, JR.
Mallinckrodt Chemical Laboratory, Harvard University, Cambridge, Massachusetts

November 15, 1949

THE Raman spectrum of cyanogen chloride has been reported by West and Farnsworth[1] and by Wagner,[2] and the infra-red spectrum has been observed by Nixon.[3] The infra-red spectra of $ClC^{12}N$ and $ClC^{13}N$ were observed in this laboratory as part of a general program of study of isotopic effects other than those involving deuterium.

Potassium cyanide containing 63 atom percent C^{13} was converted to ClCN by bubbling Cl_2 through a water suspension of the zinc potassium double cyanide formed with $ZnSO_4$.[4] The product was frozen down in an acetone-dry ice trap and separated from liquid chlorine by bulb to bulb fractionation in vacuum.

The spectrum was observed with a Baird Associates, Inc., Model B (NaCl prism) Infra-Red Recording Spectrophotometer in the region 2μ to 16μ. A 5 cm cell with NaCl windows was used with a total pressure of the isotopic mixture of 10 cm of Hg. Table I summarizes the results. The C≡N stretching frequencies

TABLE I. Observed and calculated vibrational frequencies of $ClC^{12}N$ and $ClC^{13}N$.

Designation	$ClC^{12}N$ frequencies (vac.) obs. (cm^{-1})	calc. (cm^{-1})	$ClC^{13}N$ frequencies (vac.) obs. (cm^{-1})	calc. (cm^{-1})
ν_1	714	714	708	708
ν_2*	—	—	not obs.	—
ν_3	2213	2212	2157	2158
$2\nu_2$	783	—	765	—

* ν_2 is reported at 397 cm^{-1} by West and Farnsworth (see reference 1).

(ν_3) for the two isotopic species were well separated, showing almost no overlap; but the C−Cl stretching modes (ν_1) and also the overtones of ν_2 overlapped seriously. To overcome this difficulty a sample of ClCN containing the normal abundance of C^{13} was prepared and was run in the comparison beam of the spectrograph. Its pressure was adjusted so that it just canceled ν_3 for $ClC^{12}N$, the resulting spectrum being only that of $ClC^{13}N$. At the pressures involved this did not seriously lower the sensitivity of the spectrograph in the regions of $ClC^{12}N$ absorption.

As a check on the observed isotopic shifts the Teller-Redlich product rule may be applied:

$$\frac{\omega_1\omega_3}{\omega_1^i\omega_3^i}=\left(\frac{M\cdot m^i}{M^i\cdot m}\right)^{\frac{1}{2}}=1.033$$

$$\frac{\nu_1\nu_3}{\nu_1^i\nu_3^i}=1.035,$$

where ω is the zeroth-order normal frequency, ν is the corresponding observed frequency, M is the molecular weight, m the mass of the carbon atom involved, and the superscript i denotes $ClC^{13}N$. While the product rule applies rigorously only to the zeroth-order frequencies, it is seen to fit the observed frequencies in this case to well within experimental errors. Here the anharmonic effects that lead to deviations from the product rule cancel

out very closely, as opposed to hydrogen-deuterium isotopic pairs where the observed frequency ratio is generally a few percent smaller than the mass term.

In other cases the spectra of the two species permit a calculation of the three force constants in the most general quadratic potential function

$$2V = f_1\Delta r_1^2 + f_2\Delta r_2^2 + 2f_{12}\Delta r_1\Delta r_2.$$

However, it was found that no *significant* value for the interaction term, f_{12}, could be calculated for ClCN. The isotopic shifts are not sensitive to the value of f_{12} in this case. The values of the principle force constants which reproduce the observed frequencies as shown in Table I are given in Table II. The frequencies are recalculated from the average values.

TABLE II. Force constants for $ClC^{12}N$ and $ClC^{13}N$ ($f_{12}=0$) in units of 10^5 dynes/cm.

	From $ClC^{12}N$	From $ClC^{13}N$	Average
f_1(C−Cl)	4.931	4.926	4.928
f_2(C≡N)	17.03	17.00	17.01

While it was not possible to calculate an exact value for f_{12}, calculations indicate that it is small and probably positive. A value for f_{12} of 1×10^5 dynes/cm probably represents a reasonable upper limit consistent with possible errors in the frequency measurements. Values of the principle force constants consistent with various values of f_{12} between 0 and 1×10^5 dynes/cm were calculated. It was found that f_1 varied between 4.7 and 5.0×10^5 dynes/cm and f_2 varied between 16.8 and 18.2×10^5 dynes/cm. These probably represent reasonable limits to the true values of f_1 and f_2 in the observed frequency approximation. The value of 4.9×10^5 dynes/cm for the carbon-chlorine force constant represents a considerable stiffening over the "normal" value. This is almost certainly due to resonance of the pure covalent structure with the double-bonded chlorine structure $\dot{Cl}=C=\bar{N}$, and if the latter structure is important, we should expect a positive value for the interaction term.

* The research reported in this paper was made possible by support extended Harvard University by the ONR under ONR Contract N5ori-76, Task Order V.

[1] W. West and M. Farnsworth, J. Chem. Phys. 1, 402 (1933).
[2] J. Wagner, Zeits. f. physik. Chemie **B48**, 309 (1941).
[3] E. Nixon, Brown University, private communication.
[4] C. Mauguin and L. J. Simon, Comptes Rendus **169**, 383 (1919).

Mass Spectra of N_2^{14}, $N^{14}N^{15}$ and N_2^{15}

VERNON H. DIBELER, FRED L. MOHLER, AND ROBERT M. REESE
National Bureau of Standards, Washington, D. C.
November 23, 1949

WE have recently had an opportunity to analyze a sample of nitrogen gas from Eastman Kodak Company containing approximately 65 atom percent N^{15}. The mass spectrum of this material permits an accurate calculation of the relative amounts of doubly charged N_2^{++} ions and a calculation of the dissociation patterns of the three isotopic nitrogen molecules.

The mass spectra were obtained with a model 21-102 Consolidated mass spectrometer using conventional techniques. The temperature of the ionization chamber was about 245°C.

The doubly charged ion at $m/e=14.5$ has an intensity relative to the 29^+ ion of zero for 20 v electrons, 0.99 percent for 50 v, 2.62 percent for 70 v, and 3.78 percent for 100 v electrons. Table I summarizes the calculations and the mass spectra for 50 v electrons. Columns 1 and 2, respectively, give the mass and relative abundance of all ions observed in the mixture spectrum. The peak at $m/e=14.5$ is entirely $(N^{14}N^{15})^{++}$. The contributions of the isotopic ions, $(N_2^{14})^{++}$ and $(N_2^{15})^{++}$ to $m/e=14$ and 15 are computed by multiplying the intensity of the 14.5 peak by the ratios 26.3/100 and 94.6/100. The resulting values appear in column 3.

TABLE I. Mass spectra of N_2^{14}, $N^{14}N^{15}$ and N_2^{15} for 50 v electrons.

		Doubly	Singly charged ions			Patterns	
m/e	Mixture pattern	charged ions	N_2^{14}	$N^{14}N^{15}$	N_2^{15}	N_2^{14}	N_2^{15}
14	5.36	0.26	1.77	3.33		6.73	
14.5	0.99	0.99					
15	10.0	0.94		3.33	5.73		6.06
28	26.3		26.3			100	
29	100			100			
30	94.6				94.6		100

The contribution to $m/e=14$ of the singly charged ion $(N^{14})^+$ from N_2^{14} can be computed from the 28 peak by correcting the $m/e=14$ pattern coefficient of normal nitrogen obtained under identical conditions for a 1 percent contribution from the doubly charged molecule ion as determined above. The contributions of N_2^{14} appear in column 4. The remaining contribution at $m/e=14$ is from the $(N^{14})^+$ dissociation of $N^{14}N^{15}$. Equal probability of formation of the $(N^{15})^+$ ion from $N^{14}N^{15}$ is now assumed. This is reasonable since Friedel and Sharkey[1] have shown H^+ and D^+ from HD to be of nearly equal probability. Thus, the dissociation pattern of $N^{14}N^{15}$ is given in column 5. The remaining contribution to $m/e=15$ is due to the $(N^{15})^+$ dissociation of N_2^{15} and is given in column 6. The normalized dissociation patterns of N_2^{14} and N_2^{15} corrected for doubly charged ions are given in columns 7 and 8.

A significant difference in the dissociation probability of N_2^{14} and N_2^{15} is observed. This is undoubtedly of the same origin as that observed for H_2 and D_2.[2,3] A similar effect is to be expected in the dissociation of $C^{12}O_2$ and $C^{13}O_2$. This would result in ambiguity in the observed isotopic abundance if for some reason the abundance is measured for a dissociated ion rather than the molecule ion. We are at present investigating this possibility.

[1] R. A. Friedel and A. G. Sharkey, Jr., J. Chem. Phys. **17**, 584 (1949).
[2] N. Bauer and J. Y. Beach, J. Chem. Phys. **15**, 150 (1947).
[3] D. P. Stevenson, J. Chem. Phys. **15**, 409 (1947).

Absolute Configuration of Optically Active Molecules

E. E. TURNER
Bedford College, London, England
AND
KATHLEEN LONSDALE
University College, London, England
November 18, 1949

FOLLOWING Fischer, the usual convention[1] is that the molecule of *d*-tartaric acid shall be written as the "projection formula" A, this implying that particular disposition B of the spatial

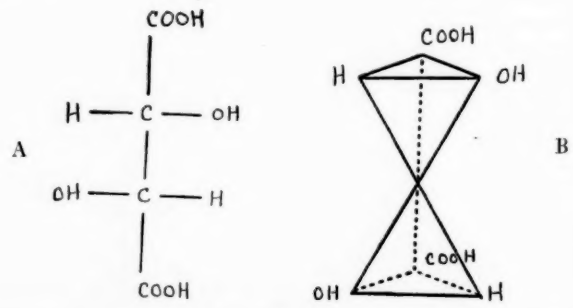

configuration in which for convenience one-half of the molecule has been rotated about the main axis in order to bring the two carboxyl groups below the plane of the paper and the two hydrogen atoms and the two hydroxyl groups into that plane. This

process does not imply hindrance of free rotation within the molecular configuration, insofar as tartaric acid in *solution* is concerned, and does not predicate any particular disposition within the molecular configuration which might have to be adopted in order that from molecules the *crystal* could be built.

The recent preliminary analysis of the crystal structure of *d*-tartaric acid[2] in fact indicates that in the crystalline state, if (in any one molecule) the two hydrogen atoms and the two hydroxyl groups are all in, or approximately in, the same plane (e.g. that of the paper), then one carboxyl group is above and the other below that plane, the planes of the acid groups themselves being steeply inclined the one to the other. The two possibilities for the molecule in the crystal are thus the enantiomorphic configurations:

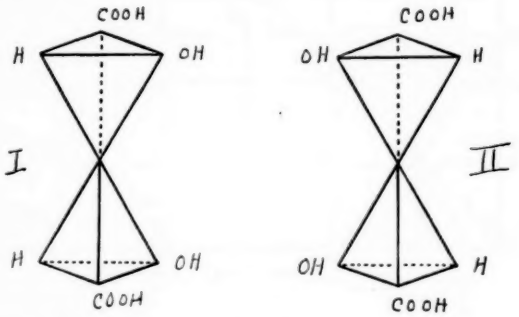

Between these, x-ray methods cannot distinguish.

Recently, however, J. Waser[3] has claimed that it is possible to make the distinction if crystal structure is considered in relation to crystal habit; that is, in relation to growth. He argues that, given the structure determined by Beevers and Stern,[2] the known habit of *d*-tartaric acid crystals would only be formed for molecules of the type II and that the Fischer convention is therefore incorrect. His argument is based on an examination of the ease with which hydrogen bonds may form, and persist, in various directions at the crystal surface as new molecules are deposited. He suggests, in fact, that a polar crystal grows differently at opposite ends simply because if the molecules themselves are asymmetric, *ab*, then the ease of attachment of an *a* end to a *b* face

will be different from that of a *b* end to an *a* face, and that it is possible to judge which event is the more likely.

Now we question very strongly whether such a judgment is possible on the basis of bond formation alone, and we do not think, therefore, that Waser's conclusion is valid. There is no *a priori* reason why the attachment *ba*→*ba* should form more readily than that of *ab*→*ab*. The bond is mutual.

Nevertheless it is true that polar crystals *do* often grow differently at the opposite ends of the uniterminal axis, and various causes may contribute to this otherwise curious phenomenon.

It may be that a face *b* is more easily "poisoned" than a face *a*, possibly by the occasional attachment of solvent molecules *c*.[4] Or again the solvent molecules may form temporary attachments more readily with the *a* end than with the *b* end of the "free" molecule and prevent its adherence to the crystal surface. But it would surely be much more difficult to put forward any convincing argument for the probability of a particular habit formation in an actual case on this kind of basis, and yet that, it seems, is what would be required for a determination of absolute configuration by such means.

At present, therefore, there is no sound evidence either for or against the correctness of the Fischer convention.

[1] Freudenberg, *Stereochemie*, p. 662–3; Werner, *Lehrbuch der Stereochemie*, p. 31, 92.
[2] Beevers and Stern, Nature **162**, 854 (1948).
[3] Jürg Waser, J. Chem. Phys. **17**, 498 (1949).
[4] Wells, *Crystal Growth* (Gurney and Jackson, London, 1949), Faraday Society Discussion No. 5, p. 200.

Isomer Distribution in Fischer-Tropsch Hydrocarbons

SOL WELLER* AND R. A. FRIEDEL*
Central Experiment Station, Bureau of Mines, Pittsburgh, Pennsylvania
November 10, 1949

A STATISTICAL derivation of the isomer distribution observed in Fischer-Tropsch products has recently been given.[1] This derivation involved the implicit assumption that the various isomers of a given molecular weight cut add carbon atoms (to form the next higher molecular weight cut) in proportion to their concentrations. Dr. R. B. Anderson has pointed out[2] that the calculation can also be made on the basis of the assumption that the isomers of a given cut add carbon atoms in proportion to the number of (weighted) ways that addition can occur to the individual isomers. The rules for addition given in reference 1 may be maintained unchanged. This may be illustrated by a particular example: The distribution of C_4 isomers is unchanged; that of *n*-butane remains $2a/(a+1)$ and that of *i*-butane, $b/(a+1)$. *N*-butane can react to form *n*-pentane in $2a[2a/(a+1)]=4a^2/(a+1)$ ways, or to form *i*-pentane in $2b[2a/(a+1)]=4ab/(a+1)$ ways; *i*-butane can react to form *i*-pentane in $3a[b^2/(a+1)]=3ab/(a+1)$ ways. The total number of (weighted) ways in which all of the C_4 isomers can react is $(4a^2+7ab)/(a+1)$, of which $4a^2/(a+1)$ give *n*-pentane and $7ab/(a+1)$ give *i*-pentane. The fraction of *n*-pentane in the C_5 cut is, therefore, $4a^2/(4a^2+7ab)=4a/(4+3b)$, and the fraction of $7ab/(4a^2+7ab)=7b/(4+3b)$.

Extension of the calculation to the remaining molecular weight fractions leads to the data of Table I. The table is simplified in the sense that the computation has been made only for those isomers experimentally observed; this does not materially affect the results. It is clear that use of this alternate basis of calculation

TABLE I. Alternate calculation of isomer distributions.

Isomer	Formula	Mole percent in cut Calculated ($a=0.975$, $b=0.025$)	Observed
n-pentane	$\frac{4a}{4+3b}$	0.957	0.950
i-pentane	$\frac{7b}{4+3b}$	.043	.050
n-hexane	$\frac{8a}{8+21b}$	.911	.896
2-methyl pentane	$\frac{15b}{8+21b}$	.044	.057
3-methyl pentane	$\frac{14b}{8+21b}$	.041	.047
n-pentane	$\frac{16a}{16+73b}$	.876	.877
2-methyl hexane	$\frac{31b}{16+73b}$	.043	.046
3-methyl hexane	$\frac{58b}{16+73b}$	.081	.077
n-octane	$\frac{32a}{32+209b}$	.838	.845
2-methyl heptane	$\frac{63b}{32+209b}$	.042	.039
3-methyl heptane	$\frac{120b}{32+209b}$	.081	.072
4-methyl heptane	$\frac{58b}{32+209b}$	.039	.044

also leads to isomer distributions which closely duplicate the observed distributions. For the particular choice of $a=0.975$ and $b=0.025$ the average deviation of the calculated from the observed isomer concentrations is again 0.7 percent.

The excellent agreement with experiment which is possible in both cases comes about because the same set of fundamental rules for addition of carbon atoms is used. In the absence of further information one has to consider each of the independent assumptions concerning weighting as reasonable; the almost exact comparability of results is, perhaps, encouraging in indicating the correctness of the fundamental procedure.

* Physical chemists, Bureau of Mines, Research and Development Branch, Pittsburgh, Pennsylvania.
[1] S. Weller and R. A. Friedel, J. Chem. Phys. **17**, 801 (1949).
[2] Private communication.

The Pyrolysis of *n*-Propyl Bromide

P. Agius and Allan Maccoll
Sir William Ramsay and Ralph Forster Laboratories, University College, London, England
November 29, 1949

THE organic bromides form an interesting series of compounds because of the widely diverse kinetic behavior shown in their pyrolyses. Although all the substances so far investigated have been reported to give first-order kinetics, the evidence suggests that different mechanisms are involved. Thus the work of Daniels and his collaborators[1] on ethyl bromide has led him to postulate a free-radical non-chain mechanism for its pyrolysis. In the case of allyl bromide[2] a different type of free radical mechanism has been suggested. Again for *t*-butyl bromide, Kistiakowsky and Stauffer[3] have been led to the view that the rate controlling step is the elimination of molecular HBr. It is the purpose of the present note to show that a fourth type of mechanism operates in the case of *n*-propyl bromide.

In his preliminary survey of the field of organic halides, Lessig[1] calculated a number of first-order coefficients for *n*-propyl bromide and observed that they were strongly pressure dependent. He also showed that the reaction was predominantly homogeneous, could be represented by the equation,

$$C_3H_7Br \rightarrow C_3H_6+HBr,$$

and was appreciably catalyzed by oxygen. The present note deals with an investigation of the reaction in the temperature range 300–380°C. In confirmation of Lessig's results, the reaction has been shown to be homogeneous, to follow the same equation, and to be catalyzed by oxygen. However, it soon became apparent that the first-order rate coefficients did not tend to a limiting value as the initial pressure was increased. Further, a plot of the first-order coefficients as a function of the square root of the initial pressure led to a straight line, passing through the origin, as shown in Fig. 1. This suggested the calculation of 1.5-order coefficients, which were found to show no trend with initial pressure. So it was concluded that the reaction was of the 1.5 order. The variation of the rate constants with temperature was represented by the equation

$$k=7.2\times10^{10}\exp(-33{,}800/RT)$$

k being expressed in $(\text{g/mole})^{-\frac{1}{2}}(\text{cc})^{\frac{1}{2}}(\text{sci.})^{-1}$. The energy of activation is thus much lower than that for ethyl bromide (53.0 kcal.).

The 1.5-order constants were only calculated for the early stages of a run, as they were found to fall as the reaction proceeded. As propylene, one of the products of reaction, is a well-known

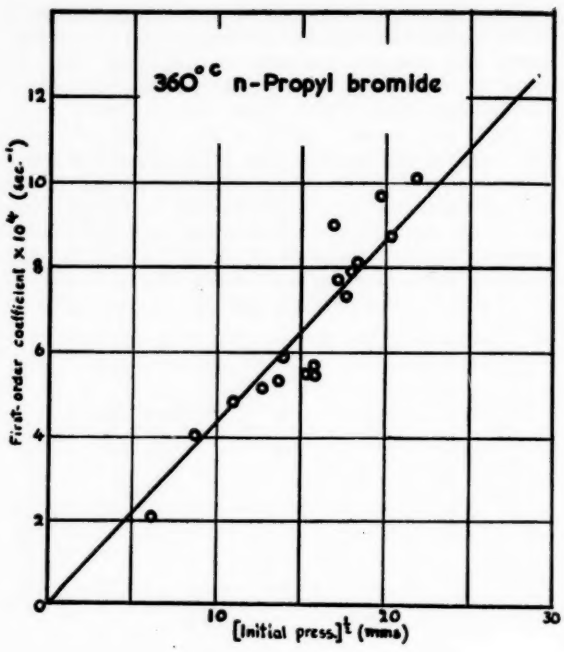

FIG. 1.

inhibitor of chain reactions, the effect of propylene on the rate was investigated. It was found strongly to inhibit the rate, but with increasing propylene pressure, the rate approached a limiting value. The limiting rate is believed to be that of a heterogeneous reaction, as it was found to be dependent on the surface-volume ratio.

The effect of oxygen and propylene, and the 1.5-order character of the reaction are all in favor of a chain mechanism. The following mechanism is put forward for the early stages of the decomposition

$$C_3H_7Br \rightarrow C_3H_7+Br, \quad (1)$$
$$Br+C_3H_7Br \rightarrow CH_3-CH-CH_2Br+HBr, \quad (2)$$
$$CH_3-CH-CH_2-Br \rightarrow CH_3-CH=CH_2+Br, \quad (3)$$
$$Br+Br+M \rightarrow Br_2+M. \quad (4)$$

The 1.5-order kinetics of the reaction follows from the nature of the chain-ending step, namely the recombination of bromine atoms. Assuming reasonable values for the rates of the elementary reactions, the observed rate can be satisfactorily accounted for. Further, a mechanism for the propylene-inhibited reaction, in which (2) is in competition with

$$Br+CH_3-CH_2=CH_2 \rightarrow CH_2-CH_2-CH_2+HBr \quad (5)$$

leads to general agreement with the form of the inhibition curve.

The present work raises the question as to whether any higher members of the series also show 1.5-order behavior. For preliminary measurements suggest that *i*-propyl bromide behaves in the same fashion.

A fuller account of this work will be published in due course.

[1] Lessig, J. Phys. Chem. **36**, 225 (1932). Vernon and Daniels, J. Am. Chem. Soc. **55**, 922 (1933). Fugani and Daniels, *ibid.* **60**, 721 (1938). Daniels and Veltman, J. Chem. Phys. **7**, 256 (1939).
[2] A. Maccoll, J. Chem. Phys. **17**, 1350 (1949).
[3] Kistiakowsky and Stauffer, J. Am. Chem. Soc. **59**, 165 (1937).